Sedimentology, diagenesis and geochemistry of the Great Limestone, Carboniferous, northern England.

GALLAGHER, JAMES

Sedimentology, diagenesis and geochemistry of the Great Limestone, Carboniferous, northern England.

James Gallagher

Abstract

Yoredale type cyclothems of the Mid-Carboniferous of north east England were deposited as a result of glacio-eustatic fluctuations arising from waxing and waning of the Gondwana ice sheets present in the southern hemisphere. Rhythmic alternations of areas of maximum cyclothem thickness have been recognised in the Scar to Little Cyclothems which are attributed to localised differential subsidence, flexuring and uplift of the Alston Block of the northern Pennines.

A detailed study of one cyclothem, the Great Limestone Cyclothem of the Alston Block, reveals that within the transgressive carbonates, the beds form two and a half thinning-upward to thickening-upward bed-sets with the individual beds and the bed-sets being correlatable across the region. Inevitable diagenetic alteration of the Great limestone has occurred and resulted in resetting of some initial geochemical values. However, it is proposed that in the case of $\delta^{18}O$ and several trace elements their trends through the limestone do in fact track an original pattern, namely that of the bed-thickness pattern.

It is suggested here that the cyclothems are attributable to the short eccentricity Milankovitch rhythm, the bed-sets, within the Great Limestone, to the range of either the obliquity and precession rhythms, with the beds in the Great Limestone being deposited in periods of the sub-Milankovitch millennial time-scales.

The biostromes within the Great Limestone, the *Chaetetes* band, Brunton band and the Frosterly band are typical of shallow-marine environments as are all grains seen in thin-section analysis. All limestone beds are a similar bioclastic wackestone to packstone with no observable changes in the proportions of the various elements throughout the thickness of the Great Limestone.

Sedimentology, diagenesis and geochemistry of the Great Limestone, Carboniferous, northern England.

James Gallagher

A thesis submitted in partial fulfilment of the degree of Doctor of Philosophy at the Department of Earth Sciences, Durham University.

2011

Contents

5.0 Bioclast analysis and palaeoecology of the Great Limestone

8.0 Major and trace element geochemistry of the Great Limestone

9.0 Stylolites, acid insoluble material and bedding planes.

10.0 Summary of conclusions.

Appendices

Table of Figures

Table of Tables

No part of this thesis has been previously submitted for a degree in this or any other University. The work described in this thesis is entirely that of the author, except where reference is made to previous published or unpublished work.

Acknowledgements

I would like to thank Maurice Tucker, for his supervision and kind support throughout the research period at the University of Durham.

I would like to thank Jim Gordon (I think) for putting the idea in my head in the first place.

This thesis has greatly benefited from discussions with various people, both members of academic staff in the department and professionals external to the University. I would like to thank Kirstin Lemon for her devoted time at the NERC Isotope Geochemistry Labs in Keyworth, with Melanie Leng, analysing the samples for the isotopes. Sincere thanks go to Dave Sales, Alan Carr and Janice Oakes, who all helped enormously.

There are various people external to the department who also provided encouragement and helped with this project. Thanks go to Brian Young, Dave Millward and Charlotte Vye at the British Geological Survey in Edinburgh who gave encouragement and provided me with access to borehole data for Northumbria. A special thank you also goes out to Angela Coe from The Open University for her help in the analysis and Dr. Daniel Vachard, University of Lille, for his help in fossil recognition in the Great Limestone.

My fieldwork was made enjoyable by the trips with Ray Fairbairn and his tongue in cheek “whimsical” and very funny explanations for the formation of the Great Limestone, Colin Scrutton usually put a more down to earth slant on proceedings. Ray’s provision of personal data was very instructive. Colin must be thanked for his expert and very helpful comments on Chapter 5 as must Howard Armstrong of the department.

I would like to say a big thank you to Pam Denton for her help with the initial fieldwork and her provision of help in bioclast/grain identification for the Great Limestone.

Last, but by no means least, my most sincere thanks and love go to Rose who put up with me and listened to me whinging, thank you for just being there, Richard, your apparent confusion as to why! is warranted, and finally my love goes out to Andrew who we miss dearly.

This thesis is dedicated to

the memory of Andrew who

we will always love and

painfully miss

Chapter 1.0 Introduction

1.1 Introduction

The middle Carboniferous was a time of major global environmental upheaval ranging from greenhouse to icehouse conditions. England was passing over the equator during this time and together with changing sea levels, due to the greenhouse to icehouse fluctuations, the thermal equator varying significantly around $10^0 – 15^0$ north, (Coe *et al.,* 2003) and variations in solar irradiance, this resulted in major changing sedimentary depositional environments and the formation of the 'Yoredale' cycles (also referred to as cyclothems).

1.2 Aims of Study

The aim of this study has been to assess the Asbian to Namurian sedimentation patterns and specifically the sedimentary mechanisms and time-scales of one such 'Yoredale' cycle, the Great Limestone cyclothem in greater detail.

The study tests the hypothesis that sedimentary controls of the mid-Carboniferous strata of the Alston Block of northern-England are, together with some local controls, attributable to orbital forced mechanisms related to Milankovitch and sub- Milankovitch rhythms and that trends seen within the bed architecture, oxygen isotopes and trace elements reflect the depositional environment.

This assessment has been carried out by:-

- Presenting details of the sedimentology of the 'Yoredale' cyclothems of the Alston Block of Northern England, including assessing the structural features of the Alston block.
- Discussing the thickness variations of each cyclothem between the Asbian and early Namurian, with particular emphasis on how the thickness of each cyclothem changes across the Alston Block and how cyclicity is presented within the bedding architecture.
- Examining the palaeoecology of the Great Limestone with regard to facies and revealing sub-facies and grain association changes through the limestone.

- Analysing the isotope and trace element geochemistry of the Great Limestone and comparing trends and cycles against those seen in the bed architecture.

1.3 Location of research

The Great Limestone cyclothem has been examined across the Alston Block and in the neighbouring Stainmore and Northumberland Basins (Figures 1.1 and 1.2). However, for the detailed, often bed-by-bed analysis of the Great Limestone, the accessible outcrops at Hudeshope beck near to Middleton in Teesdale has been studied in detail. A complete section of the limestone can be found there between O. S. Grid reference 394784, 527610 (Jacks Scar), and 394916, 527276 (Skears Quarry).

1.4 Sampling techniques

Two techniques were used for sampling of the Great Limestone and these are discussed in detail in Chapter 7 and 8. A total of 309 samples were collected for this research.

1.5 Cyclothem thickness analysis

Cyclothem thicknesses were analysed using published data. These data were transferred to the computer program ArcView™ which was used to construct isopach and contour maps. Cross section line data were then transferred to the computer program AutoCAD™ for construction of the cross-section lines.

1.6 Thin Sections

149 thin sections from the Great Limestone were studied for this research. Thin-section analysis was carried out to assess facies, textural classification, grain-size analysis, sedimentary structures, abundance and description of grains, biodiversity and grain associations. Published palaeobathymetric indicators were used within the analysis. Samples for the thin section analysis were collected from Hudeshope Beck at Middleton in Teesdale (OS 394784 527610 and OS 394916 527276) and the positions are shown in Figure 1.2.

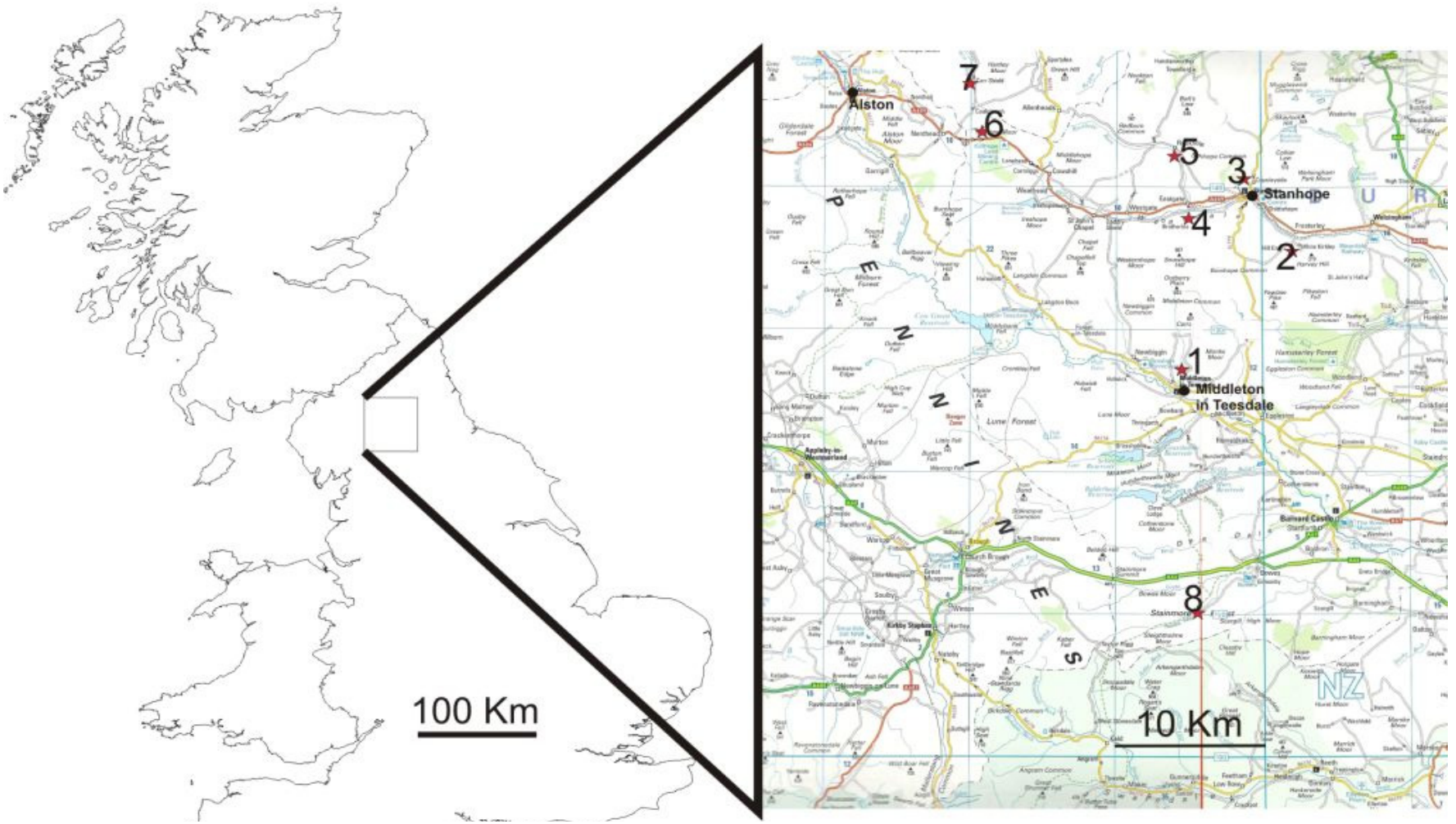

Figure 1.1Research location map. 1=Hudeshope Beck, Middleton in Teesdale (OS 394784 527610 and OS 394916 527276). 2=Bollihope Beck (OS 3010 5351). 3=Lanehead quarry, Stanhope (OS 39885 54052). 4= Weardale Cement Works, Eastgate quarry (OS 3949 5365). 5= (Chestergarth Quarry, Rookhope, Weardale OS 39410 54220). 6= Killhope, Weardale (OS 3822 5433). 7= Barney Cragg, Weardale (OS 3803 4675). 8= Sleightholm Beck (OS 953 105).

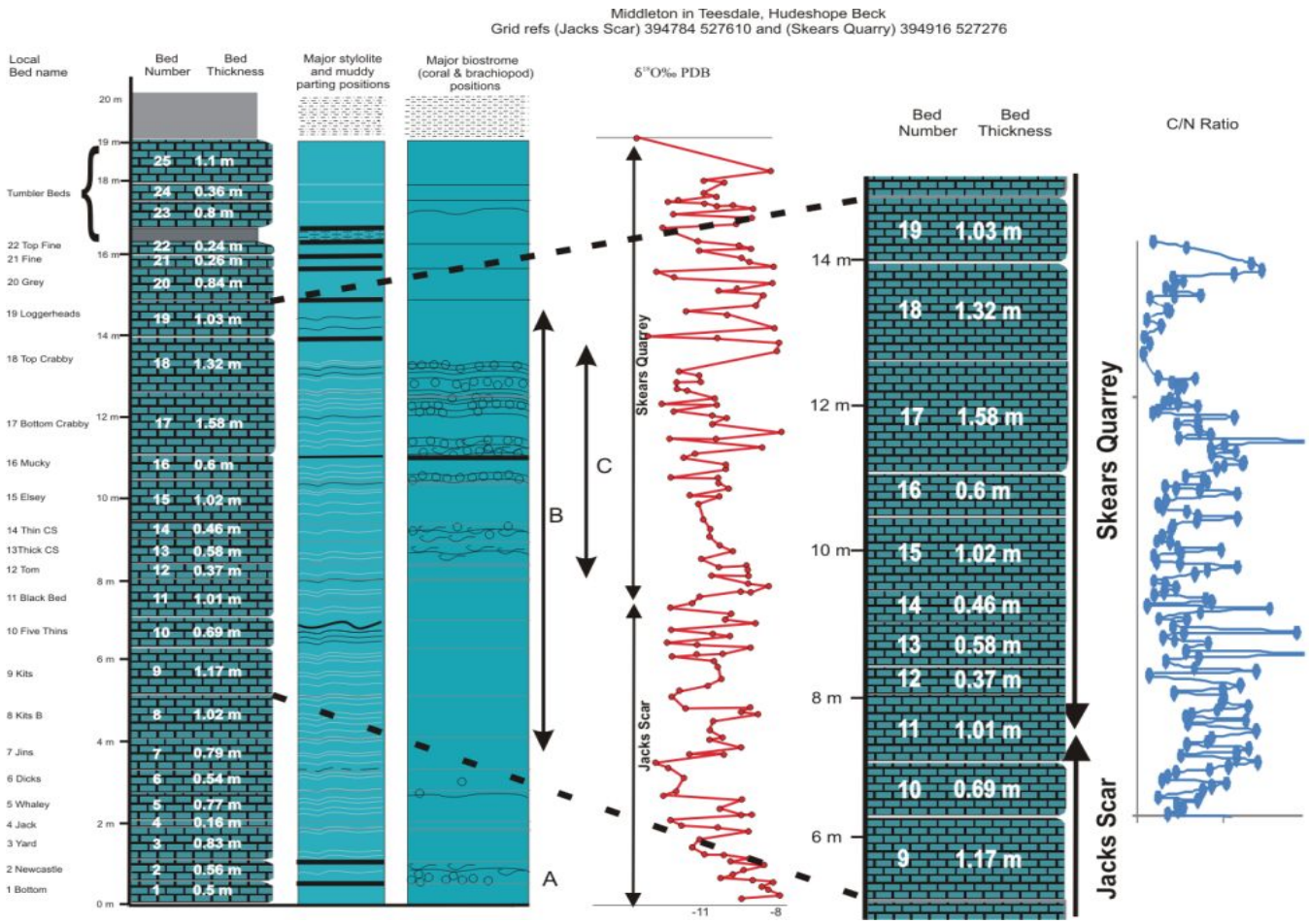

Figure 1.2 Log of the Great Limestone at Hudeshope Beck. Bed numbers (1–25), bed thicknesses, the names of the individual beds (correlated from Fairbairn's sections 1978), the occurrence of stylolites and pressure dissolution planes, and the location of the fossil bands ('biostromes'). A = Chaetetes Band, B = Brunton Band and C = Frosterley band. Sample positions for thin sections (Chapter 5), isotopes (Chapters 6 and 7) and trace elements (Chapters 6 and 8) shown on $\delta^{18}O$ plot, sample positions for CSN shown on C/N Ratio plot (Chapter 8).

1.7 Stable isotope analysis

149 Oxygen and carbon stable isotopes were analysed from the Great Limestone and these were used to assess the degree of diagenetic alteration and to contribute to the determination of the factors controlling deposition. Cyclicity within the data has been assessed and compared to a Fischer Plot of bed thickness to assess associations of bed thickness and geochemistry, again with a view to understanding deposition. The results of the analyses were compared with published data. The samples were collected from Hudeshope Beck at Middleton in Teesdale (OS 394784 527610 and OS 394916 527276) and the positions are shown in Figure 1.2.

1.8 Trace element geochemistry

149 samples of the Great Limestone have been analysed for Al, Ca, Fe, Mg, Mn, Si, Zn, Pb, Ba, Sr, S and Na. The sample positions were the same as those used for the thin-section and isotope studies and their positions are shown in Figure 1.2. The results of the analyses were compared with those from published data and used to assess cyclicity within the Great Limestone and make comparisons with the bed thickness patterns, all with the aim of determining the controls on deposition. The samples were collected from Hudeshope Beck at Middleton in Teesdale (OS 394784 527610 and OS 394916 527276) and the positions are shown in Figure 1.2.

1.9 Carbon- Sulphur-Nitrogen analysis

160 samples have been analysed for CSN analysis covering 8 metres of the Great Limestone from approximately 6 metres above the base to approximately 14 metres above the base, each sample was the result of collecting drill powder from sample positions at 5 centimetre intervals throughout the 8 metres. The results of the analyses were used to assess cyclicity within the Great Limestone and make comparisons with the bed thickness patterns with the aim of determining the controls on deposition. The samples were collected from Hudeshope Beck at Middleton in Teesdale (OS 394784 527610 and OS 394916 527276) and the positions are shown in Figure 1.2.

1.10 Outline of Thesis

Chapter 1 is a brief introduction to the thesis, the areas studied and methods.

Chapter 2 is a brief introduction to the regional and global depositional history of the Mid-Carboniferous of Northern England.

Chapter 3 discusses the structure of the Alston Block of Northern England including the fluvio-deltaic and shallow-water carbonate sedimentation referred to as the Yoredale cycles, of the Late Viséan and early Namurian.

Chapter 4 considers thickness variations of the Carboniferous cyclothems including the Great limestone Cyclothem using previously published data.

Chapter 5 presents the palaeoecology of the Great Limestone with regard to facies and proposes various sub-facies and associations.

Chapter 6 considers the geochemical data and whether these can be used for interpretations of the chemostratigraphic history of the Great Limestone. The integrity of the data with regard to the diagenetic history of the Great Limestone has also been considered.

Chapter 7 presents the results of oxygen and carbon stable isotope analysis of the Great Limestone, and makes interpretations in terms of the deposition and origin of to the beds and bed-set cycles, and environmental considerations.

Chapter 8 assesses the major and trace element geochemical and CSNdata as a record of the palaeoceanographic and depositional history and determines how these data can be used to understand the controls on limestone deposition. Data are also compared to published results of similar limestones.

Chapter 9 considers the occurrence of stylolites within the limestone and the possible controls on their formation.

Chapter 10 summarises the conclusions of this research.

2.0 Carboniferous palaeogeographical/geological and tectonic history of Northern England

2.1 Introduction

This chapter aims to set the scene with regard to the regional and global depositional history of the Mid Carboniferous of Northern England. To a certain extent the Mid Carboniferous palaeogeographic landscape of the area cannot be fully understood without a very brief discussion of the Cambrian to the Devonian and early Carboniferous Palaeogeographical/geological history and this is touched upon below.

The Closing of the Iapetus Ocean from the Cambrian to the Ordovician/Silurian and the resulting Caledonian Orogeny in the Silurian to early Devonian resulted in the formation of the Laurasian continent and the Caledonian mountain belt of North America, Greenland, Britain and Norway with Britain laying on the European, southern, side of the continent; contemporaneously the Tornquist Ocean between Avalonia and Baltica also closed. Caledonian Mountain building events and faulting and the emplacement of granites in northern England during the post Caledonian tectonics were of major importance to the structural and sedimentary evolution of the Carboniferous of Britain; Caledonian faults being reactivated during basin formation and mountain ranges supplying much of the non-marine sediment.

During the closing of the Iapetus Ocean the Rheic Ocean, formed between Gondwana and Avalonia, began to close in the Devonian and by the early to middle Carboniferous (Mississippian) , Figure 2.1, the eastern part of the ocean had already closed substantially due to the eastern United States colliding with the Meguma Terrain, a fragment of Gondwana. The resultant Variscan/Hercynian Orogeny involved a complicated assembly of different terrains, micro plates and collisions and this continued to develop until Gondwana and Laurasia were fully connected and the super continent Pangea was formed by the late Carboniferous to early Permian. This continent to continent collision, well developed within the Iberian-Amorican-Massif Central Region, resulted in the formation of back arc

basins and basins located behind island arcs on the overriding plate (Leeder 1987) and involved clockwise rotation of the continents resulting in strike slip faulting, crustal thinning and extension and major displacement (Redfern, 2000). Leeder (1987 and 1988) and Lemon (2006) referred to Britain as being on a wide shelf of a closing Hercynian marginal sea during the Carboniferous. Leeder (1987) found no evidence for a wide ocean to exist during the Visean between Britain and Gondwana due to limited oceanic crust development; however, he did suggest evidence pointed towards a Rheno-Hercynian zone acting as a back arc seaway, suggesting that the Rheic Ocean had already closed at this time south of Britain. The closure of the Rheic Ocean and the resultant crustal extension created by subduction of the plates was, together with the emplacement of granites in northern England during the post Caledonian tectonics, instrumental in the formation of a series of east-west orientated block and trough/basin structures in the North of England.

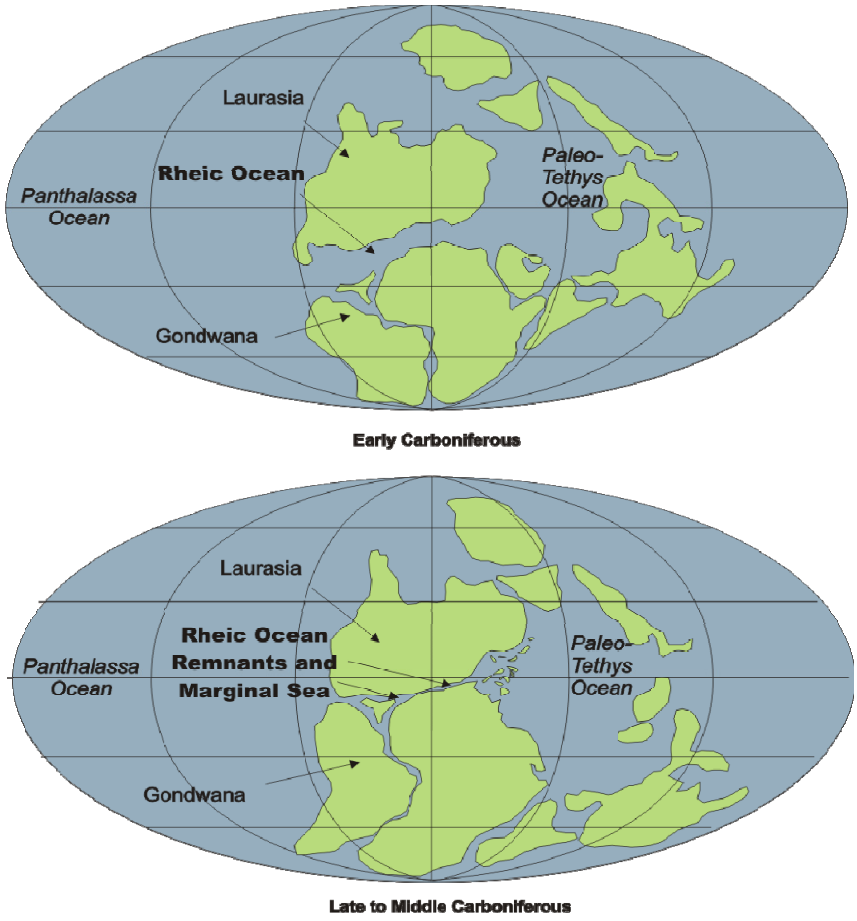

Figure 2.1. palaeogeographic reconstruction of major continents during the Carboniferous. After Grossman (1994), Lemon (2006) and Scotese (2008).

The closing of the Rheic Ocean would have been instrumental in major changes to climatic patterns throughout Gondwana and Laurasia; there is evidence for monsoonal circulation in palaeoequatorial regions with semi-arid conditions and seasonal rainfall indicative of monsoonal circulation (Wright, 1990; Falcon-Lang, 2000, Wright and Vanstone 2001). The closure of the Rheic Ocean would have resulted in the end of monsoonal circulation within Gondwana and Laurasia. Seasonal changes between semi-arid and high rainfall are characteristic of modern monsoonal circulation regions such as in south east Asia (Chao and Chen, 2001; Dettman *et al*., 2001).

As discussed above, during the Carboniferous, Britain was on a wide shelf of the closing Hercynian marginal sea, a possible remnant of the Rheic Ocean, with low land swamps to the north-east. The continuing development of the shelf-sea and land areas in north east England was dependent upon localised differential subsidence superimposed upon regional subsidence. Deposition occurred slightly below or above sea level with siliciclastic input from the Caledonian mountains in the north to north east. Generally, true marine conditions lay to the south west, while sedimentation became more terrigenous to the north east.

A major period of glaciation existed in Gondwana which could have commenced as early as the Late Devonian (Caputo and Crowell, 1985). By the Asbian stage of the Carboniferous this was well established (Wright and Vanstone, 2001) evidence of which can be found in Antarctica, Africa, India and Australia. Due to the North Pole being nearly devoid of ice while glaciation existed in Gondwana this resulted in the thermal equator being some 10^0 to 15^0 north of the geographical equator (Coe *et al*., 2003) Palaeoclimatic indicators, polar wandering curves and palynological assemblages (Van Der Zwan, 1981: Van Der Zwan *et al*., 1985), are supportive of the Laurasian continent having moved north eastward from approximately 15^0 south to a few degrees north of the palaeoequator from the late Devonian to late Carboniferous passing over the equator in the late Viséan to early Namurian; Britain had migrated into an equatorial forest and coal swamp environment during the Namurian.

2.2 Geological time scale

To place this research into the correct geological time context table 2.1 is provided using the Carboniferous time scale of Western Europe. This is divided into two epochs, and 5 stages. The North American Epochs, Mississippian and Pennsylvanian are also shown due to their use by some referenced authors.

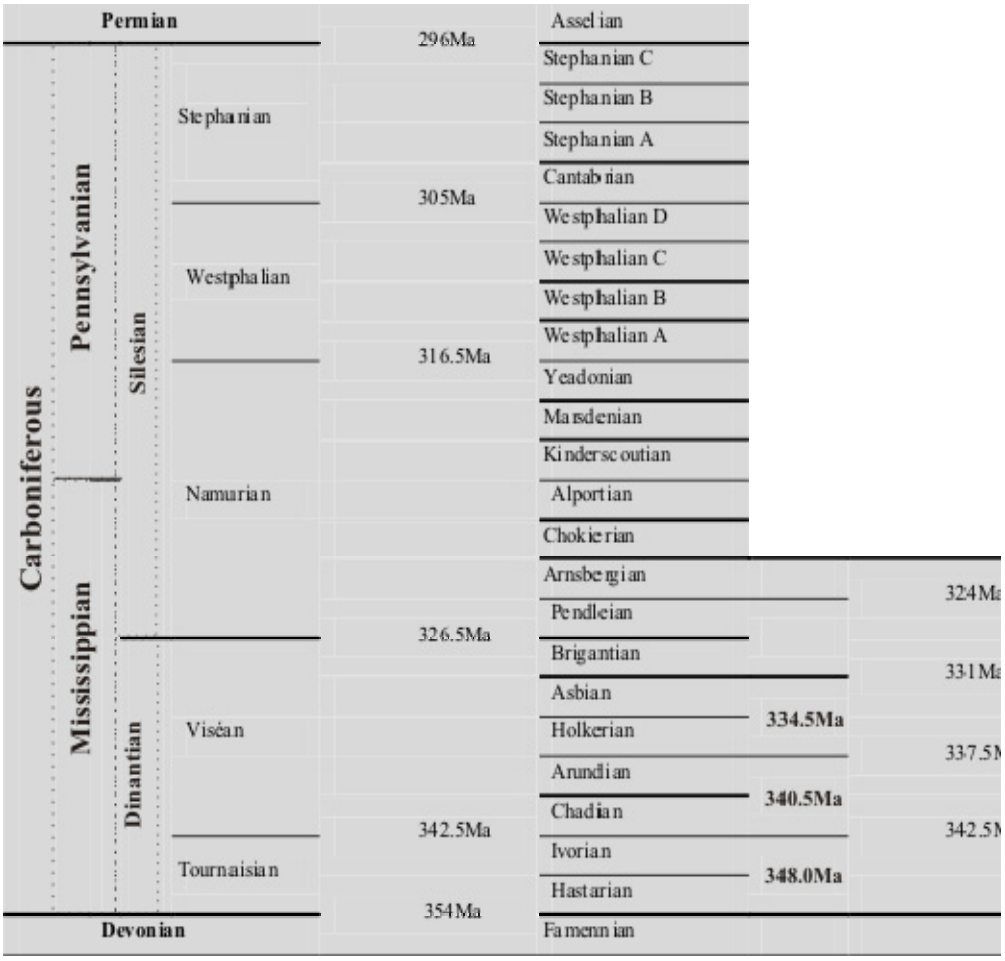

Table 2.1 Classification of Carboniferous rocks and approximate time scales. After Ramsbottom et al., 1978p; Harland et al., 1982. Approximate time Scale after Scale B, Menning et al., 1999

Using a combination of stratigraphic ages from Belgium, Britain, Spain and France, Menning *et al*., (1999) carried out the most recent work on radiometric dating on the Carboniferous. Using Time Scale B (Menning *et al*., 1999) the beginning of the Carboniferous occurs at approximately 354Ma and ends at 296Ma. The Dinantian period is shown to extend over approximately 27.5Ma and the duration of the Silesian period as approximately 30.5Ma. The Asbian is shown

to extend between 334.5Ma to 331Ma; the Brigantian between 331Ma to 326.5Ma and the Namurian commences at 326Ma and ends at 316.5Ma. These, together with other approximate time periods, are shown in Table 2.1.

The long history of geological research in the north east of England has resulted in regional variations in lithostratigraphical nomenclature and table 2.2 is used to present the history of this research and the main changes of lithostratigraphical nomenclature through geological research.

			Fowler (1936)		N. Pennines North *Young (1998) and Frost & Holliday (1980)*	N. Pennines West *Arthurton & Wade (1981)*	N. Pennines East *Mills & Holliday (1998)*	N. Pennines South *Dunham (1990)*
Silesian	Namurian	Cho	Millstone Grit		Morpeth Group	Millstone Grit	Quarterburn Marine Band	Quarterburn Marine Band
		Arnsbergian	Carboniferous Limestone Series	Upper Limestone Group			Stainmore Group	Stainmore Group
		Pendleian						
Dinantian	Viséan	Brigantian		Middle Limestone Group	Upper Liddesdale Group	Upper Alston Group	Upper Liddesdale Group	Upper Alston Group
		Asbian		Lower Limestone Group	Lower Liddesdale Group	Lower Alston Group	Lower Liddesdale Group	Lower Alston Group

Table 2.2. History of the Lithostratigraphy nomenclature of Carboniferous strata of northern England After Johnson, 1995 and Lemon 2006.

2.3 Glaciation of Gondwana

Uncertainty still remains with regard to the exact timing of the onset of the Gondwana glaciation (Wright and Vanstone 2001); however, evidence for major glaciation in Gondwana can be found within many of the continents including South America, Antarctica, Africa, India and Australia (Crowell 1978). Evidence from western South America and Southern Africa suggest major glaciation of Gondwana commenced in the Middle to Late Viséan and in particular within the early Asbian (Wright and Vanstone 2001); however, isolated occurrences of glacial deposits in South America point towards relatively small ice sheets commencing within the Late Devonian to early Mississippian (Crowell, 1983; Caputo and Crowell, 1985; Veevers and Powell, 1987).

Direct evidence for the commencement of glaciation in Gondwana is not always preserved as deposits generated in any first glaciation are likely to be reworked by further major glacial advances and consequently there is little direct evidence for the timing of the initial event (Langhorne *et al*., 2000). Crowell (1978) and Smith and Read (2000) suggest that indirect evidence, gained from Cyclothems deposited in lower latitudes, may prove to be the key to the timing and detail of early glaciation whereas Bruckschen and Veizer (1997) considered stable isotopes as an indirect method to identify the onset of glaciation. The commencement of the glaciation within the early Asbian is suggested by Wright and Vanstone (2001) to have occurred abruptly and been associated with a change to regular orbitally forced glacio-eustatic sea level oscillation with a periodicity of approximately 100 Ka and a consensus appears to suggest that the driving mechanism for the periodicity is Milankovitch insolation variations. High-amplitude sea level changes have often been linked to the glaciation on Gondwana (Wanless and Shepard, 1936; Heckel;, 1994; Veevers and Powell, 1987) and high-amplitude glacio-eustatic sea level changes and associated climate fluctuations have long been associated with Cyclothem development (Leeder, 1988; Veevers and Powel, 1987; Wright and Vanstone, 2001). Evidence would suggest that pre-Asbian climates were relatively stable whereas major climatic changes became more frequent in the Asbian and Brigantian. In the Asbian and Brigantian the Gondwanan ice sheet had also become highly sensitive to orbitally forced variations in solar insolation resulting in the high-amplitude variation of sea level.

The abrupt increase in the magnitude of glaciation could well have been produced by several mechanisms such as uplift in Australia and South America acting as a loci for glaciation (Powell and Veevers 1987), or it may reflect a threshold response for a more gradual change in atmospheric CO_2 and/or albedo feedback (Crowley and Baum, 1991; Langhorne *et al*., 2000) or changes to oceanic and atmospheric circulation due to the closure of the seaway between Laurasia and Gondwana (Rowley *et al*,. 1985, Raymond *et al*., 1989, Smith and Read 2000, Wright and Vanstone 2001). The interaction of these mechanisms, either on their own or in combination, are highly complex (Denton 2000) and as such make the precise dating of the major glaciation difficult to pin point. The closing of the

seaway between Laurasia and Gondwana, occurring in the mid to late Viséan, would have resulted in major atmospheric and oceanic circulation changes that likely resulted in warm air circulating towards the southern polar region providing increased water vapour necessary for precipitation to build significant ice sheets (Raymond *et al*., 1989; Langhorne *et al*., 2000; Smith and Read 2000); Figure 2.2 shows how equatorial currents may have changed as the closing of the seaway between Laurasia and Gondwana progressed.

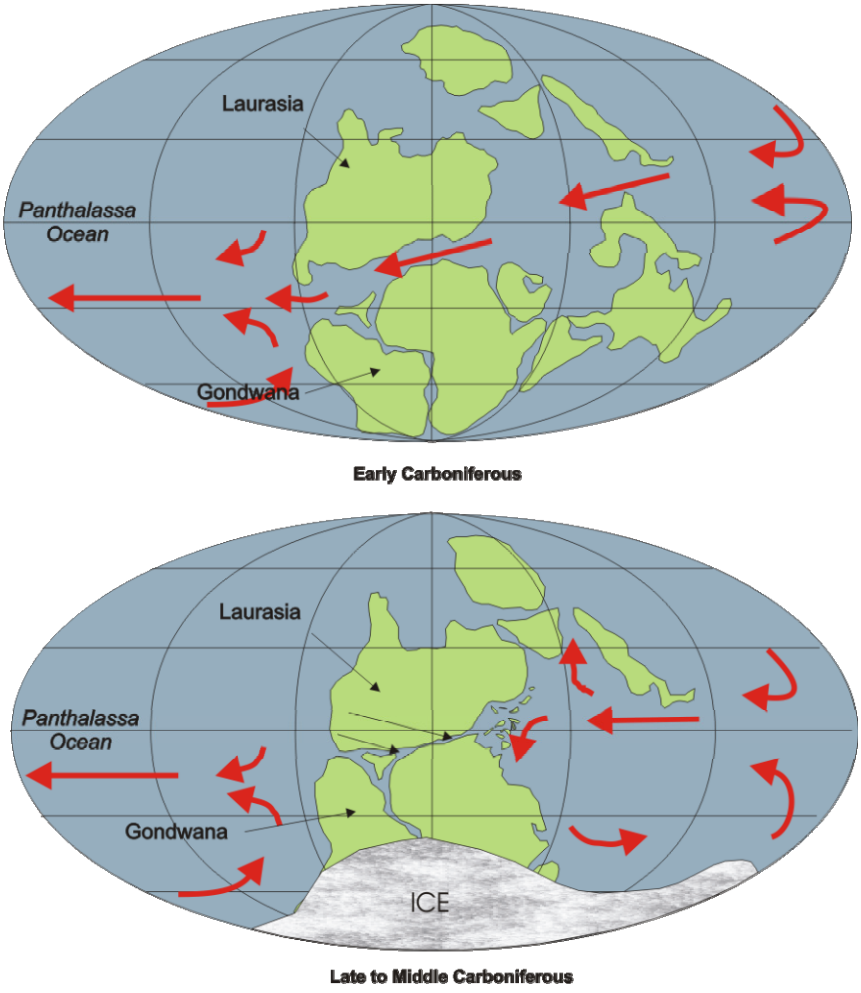

Figure 2.2. Schematic oceanic trends in Carboniferous showing trends after the seaway between Laurasia and Gondwana closed. After Langhorne, 2000. Base Map after Grossman (1994), Lemon (2006) and Scotese (2008).

2.4 Formation of the Blocks and Troughs in Northern England

Bott (1987) proposed that during the closure of the Rheic Ocean, Britain was attached to the subducting slab of southern Laurasia, with Gondwana on the

overriding slab. Leeder (1988), on the other hand, took the view that Britain was on the overriding slab and Gondwana on the subducting slab. Whichever model is correct, differential and regional subsidence from north-south tensional stresses caused by stretching and thinning of the lithosphere in response to the collision of terrains and the continents during subduction to the south, resulted in the formation of a series of east-west orientated block and trough/basin structures in northern England (Bott, 1984). This northern England extensional province is some 500 Km north of the Rheno-Hercynian back arc and due to the northward direction and migration of the extension the northern England province is younger (Fraser and Gawthorpe 1990).

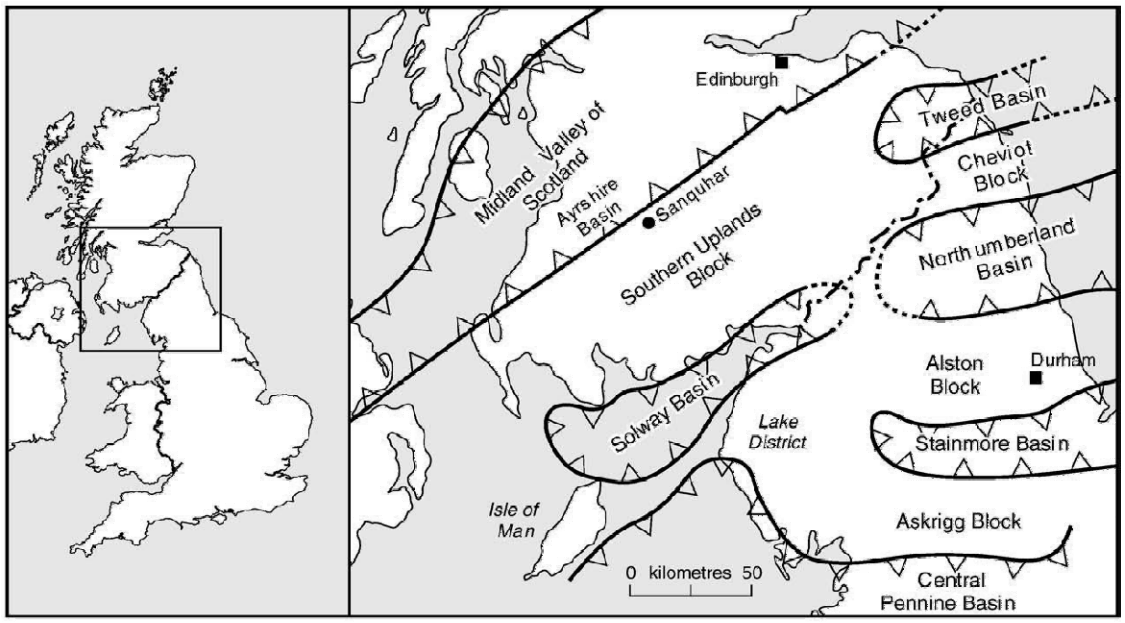

Figure 2.3. Location map for northern England showing the blocks and basins. After Johnson, 1984 and Tucker el al., 2009

A number of east-west orientated block and trough/basin structures (Figure 2.3) formed within northern England i.e. Northumberland Trough, Tweed Basin, Carlisle Basin, and the Stainmore Trough; the Northumberland Trough being further subdivided into the Solway Basin and the Northumberland Basin, the Tweed basin also merged into the Northumberland Basin (Johnson 1984; Turner *et al*., 1995). Initially differential subsidence existed between the blocks and the basins, due to the inherent buoyancy of the post Caledonian granites below the

blocks, and this resulted in the basins subsiding before the blocks. This differential subsidence stopped by the Namurian whereas regional post rift subsidence continued with the Blocks and Troughs subsiding at similar rates. This post rift subsidence was predominantly unfaulted thermal subsidence (Turner 1995; Bott 1987); however some reactivation of faults during the early Namurian did reoccur (Fraser and Gawthorpe 1990).

The block and trough structures of Northern England were originally detected by geological mapping where they were shown to be separated by relatively narrow hinge belts (Marr, 1921; Trotter and Hollingworth, 1928). The blocks initially formed regions of elevated topography, either emergent, as with the Alston and Askrigg blocks, or acting as shoals as the Cheviot block, until the late Asbian to Brigantian when they became fully submerged. The distribution of the post Caledonian granites was of great importance, giving buoyancy to the blocks. The Cheviot granite underlies the block adjoining the southern uplands; the Weardale granite underlies the Alston block and the Wensleydale granite the Askrigg block. Other highs exist to the south between the Askrigg block and the Wales Brabant Massif however these are fault controlled and not thought to be associated with granite bodies. Note, Kimbell, *et al.* (2010) refer to the Weardale Granite as the North Pennine batholith, due to new evidence regarding the placement of the batholiths. Within this research; however, the granite will be referred to as the Weardale Granite and not the North Pennine batholiths.

Differential subsidence within the basins, in some cases delineated by the reactivation of Caledonian faults, formed as grabens and half grabens, between the blocks, with a rate of settlement of approximately twice that of the blocks. Basin initiation commenced in the late Devonian to Tournaisian with reactivation in the Chadian to Asbian and some localised inversion during the Brigantian (Fraser *et al*., 1990; Gawthorpe *et al*., 1987).

2.5 Carboniferous syn-rift and post-rift sedimentation of Northern England

Four main phases of syn-rift sedimentation has been recognised in northern England, late Devonian to early Tournaisian, late Chadian to early Arundian,

mid/late Asbian and Brigantian; these phases were separated by relatively tectonic quiescence (Gawthorpe *et al*., 1987). In the Northumberland Basin basalts were erupted during the initial rifting stage in the Hastarian and early sedimentation was mature siliciclastics from the southern uplands hanging wall, the Visean, Arundian to Holkerian, saw the advance from the north-east of a major braided fluvial system, the Pennine system (Figure 2.4). Marine carbonate, from the South West and deltaic conditions, from the north east, then prevailed up until the Asbian when Yoredale type deposition dominated (Gawthorpe *et al*., 1988).

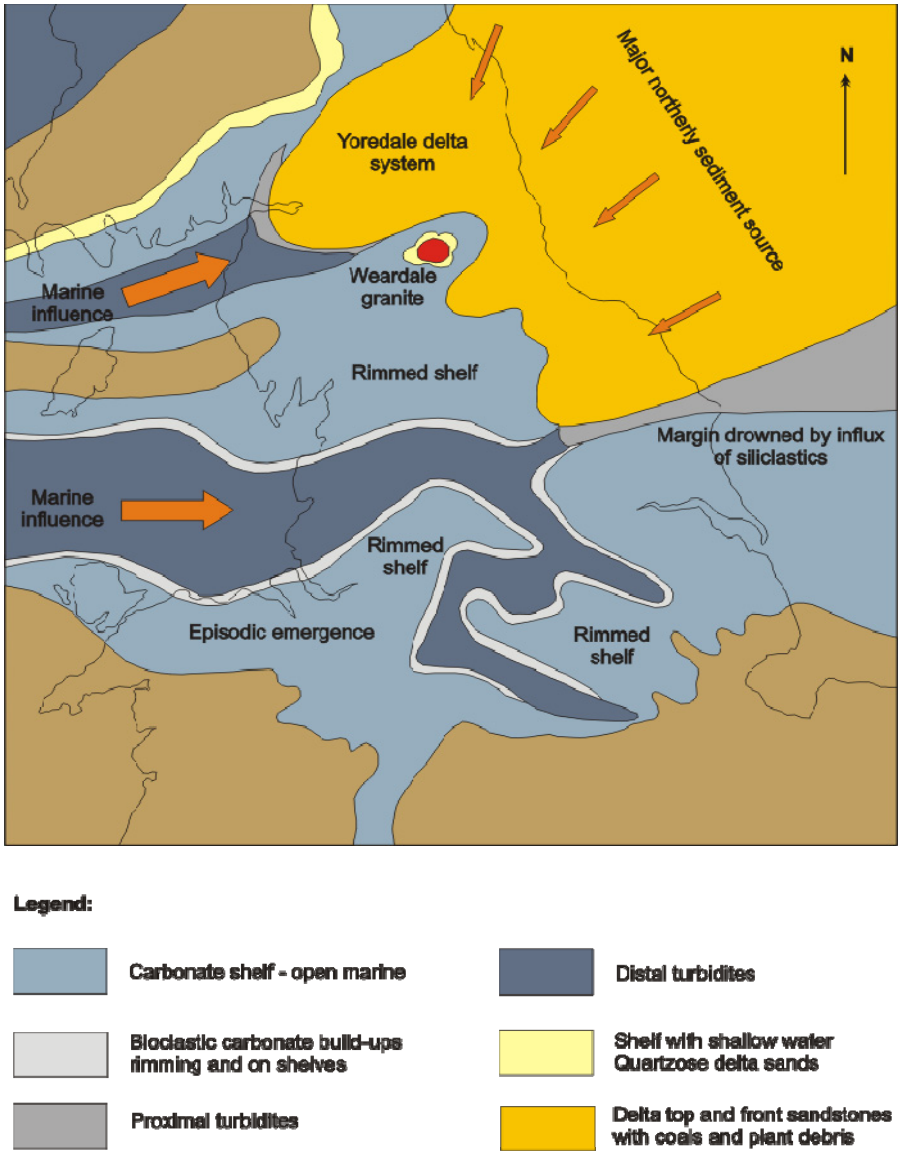

Figure 2.4 Facies map for late Dinantian to early Namurian. After Lemon (2006)

Clastic deltas prevailed in the north of the region whereas carbonate platforms existed to the south (Fraser and Gawthorpe 1990) with the main marine influence from the Craven Basin region (George *et al*., 1976). Tectonic subsidence generally exceeded sedimentation rates to basins and this subsidence resulted in thickening of sediments within basins whereas, until the late Asbian to Brigantian, the blocks were either emergent or just below sea level. Late Asbian marine sediments upon the Alston Block were therefore much thinner than found within the basins. Syn-rift sedimentation was, therefore, generally confined to the fault bounded basins within the area until the late Asbian to Brigantian. During the Namurian a transition occurred from differential settlement of the Blocks and Basins to a post-rift thermal sag stage; sedimentation rates on the Blocks and Basins resulted in similar bed thickness.

Post-rift sedimentation in northern England, between the Brigantian to Westphalian C, was not confined to the basins as the blocks became submerged during this time resulting in what could be regarded as an epeiric platform covering an area from north Yorkshire to southern Scotland of approximately 10,000 Km^2 (Holliday *et al*., 1975). The inherent nature of an epeiric type platform such as this may well have result in a low tidal range i.e. less than 10 centimetres (Wells *et al*, 2005) which in itself could promote poor mixing and stratification affecting carbonate productivity (Allison and Wright, 2005).

The advancement of the Pennine fluvial system, in the Namurian, due probably to changes to a humid climate in the hinterland (Cliff *et al*., 1991), resulted in sediment deposition exceeding subsidence and even though the area was effectively a flat shallow platform, differences in basin depths, with the Central Pennine Basin being a deep water basin, and differing heights of blocks, resulted in sediment thickness variations existing throughout northern England. The continuing southward movement of the Pennine fluvial system during the late Carboniferous eventually resulted in thinning of the marine limestone's and the eventual loss of limestone's and increase in fluvial sediment (Fraser *et al*., 1990). Changes from humid to arid conditions due to changes in palaeolatitude and in particular to the waxing and waning of the Gondwana ice sheet would have had a

profound effect upon the advancing and decreasing Pennine fluvial system and ultimately upon the mixing, stratification and salinity of the shallow epeiric sea (Wells, 2005).

2.6 Yoredale Cycles

As found in most parts of the world, the Carboniferous of the UK is mostly cyclic in nature (George *et al*., 1976; Ramsbottom 1973). In northern England, this commonly involves carbonate cycles in the Lower Carboniferous and clastics in the Upper Carboniferous with the Coal Measure Cyclothems of the Westphalian being classic examples. The Yoredales, first named by Phillips in 1836, are typically of mixed Clastic and carbonate facies (Figure 2.5); Johnson (1984) referred to them as Yoredale Cyclothems and Tucker (2003) Yoredale Cycles. The cyclicity involved in the deposition of the Yoredale Cycles is usually attributed to glacioeustic changes in sea level and particularly to orbital forcing and variations in solar insolation (Veevers and Powel, 1987; Wright and Vanstone, 2001); neither cyclic climate changes, autocyclicity, nor local tectonics could produce the cyclic nature of cyclothems on their own (Smith and Read, 1999). However, notwithstanding the dominance of orbital forcing, local tectonic and sedimentary controls on deposition would also be important on any cyclicity. Leeder (1988) suggested that the asymmetric nature of the cycles i.e. the slow shallowing and rapid deepening strongly mimics the slow ice growth and rapid meltdown associated with glacial formation, he also suggested that a glacioeustatic origin is inferred due to the fact that the cycles date from around the period suggested by evidence for Gondwana ice sheets in Eastern Australia and South America.

The Yoredale cycles vary in thickness from around 5 metres to 50 metres with the Great Cyclothem, studied in detail in this research, averaging 39 metres in thickness. The cycles generally consist of a lower carbonate part up to 30 metres thick overlain by a clastic section which are broadly deltaic i.e. shallowing up-ward, coarsening upward units (Figure. 2.5). In some cases the cycles are capped by a thin coal seam and rarely an incised valley filled with coarse clastics cuts down into the cycle top, even reaching the limestone in some cases; the Pre-High Coal Sill or Allercleugh Channel being an example where the top of the Great

Limestone (base of the Namurian) is known to be cut into; the Rogerly Channel being another example of a course clastic distributory channel (Hodge and Dunham, 1991). Shoreline or marine sandbar facies are not unknown throughout the block (Leeder and Strudwick, 1987; Tucker *et al*., 2003) with the White Hazel thickening above the Great Limestone being a classic example of a marine sandbar facies (Dunham, 1990; Hodge and Dunham, 1991).

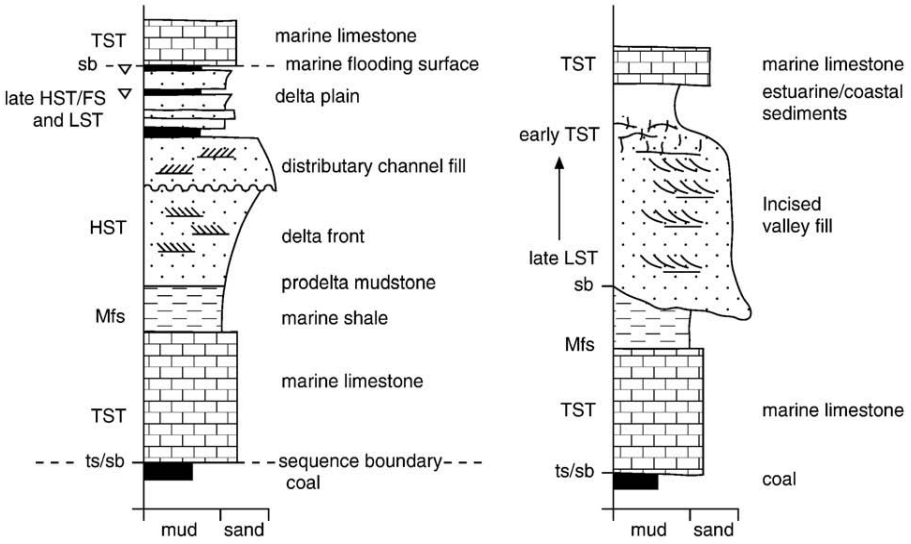

Figure. 2.5.. Schematic graphic logs for 2 types of Yoredale cycle with sequence stratigraphic interpretations: a) with deltaic clastic facies in the upper part and several minor cycles at the top, and b) with an incised-valley fill in the upper part. After Tucker el al., 2009.

Dunham (1950) suggested a standard Cyclothem as consisting of the following members (1) marine limestone; (2) Marine shale; (3) unfossiliferous (? Non marine) ferruginous shale; (4) sandy shale, shaly sandstone or "grey beds" (interbedded shales, siltstones and sandstones); (5) sandstone; (6) ganister or under-clay; (7) coal. This is a very general description of the Cyclothems; however, various members can often be missing i.e. the coal is not always present; nevertheless the description does prove to be generally consistent throughout the Alston and Askrigg Blocks. It is worth noting that loss of any members is frequently gained by another member resulting in a uniform thickness being maintained; Westgarth Forsters rule (1809) also referred to this continuity of thickness in strata. The top of the limestone and/or marine shale member relates to

the limit of marine conditions and the termination of the sandstone deposition approximately coincides with the maximum advancement of the shoreline; between the shoreline limit and the limit of marine conditions lays the region of deposition of the Yoredale Cyclothems (Johnson, 1959).

2.7 Summary

The Carboniferous sedimentary history of northern England is strongly influenced by a sequence of events which can be traced back to at least the Cambrian to the Ordovician/Silurian. The Closing of the Iapetus Ocean and the resulting Caledonian Mountain building events, faulting and the emplacement of post Caledonian granites were of major importance to the structural and sedimentary evolution of the Carboniferous of Britain; Caledonian faults being reactivated during basin formation, mountain ranges supplying much of the non-marine sediment to basins and granites providing buoyancy to blocks. The subsequent closing of the Rheic Ocean in the late Devonian to middle Carboniferous resulted in north-south tensional stresses and together with the emplacement of post Caledonian granites was instrumental in the formation of a series of east-west orientated block and trough/basin structures in the North of England and the formation of a Rheno-Hercynian zone acting as a back arc seaway. Differential settlement, created by the buoyancy of the granites, generally ceased by the Namurian whereas regional post rift, predominantly un-faulted thermal subsidence continued with the Blocks and Troughs subsiding at similar rates.

Changes within the relative positions of continents resulted in changes to climatic belts which in turn fed the advance from the north-east of the major braided Pennine Fluvial System. This system, which prevailed through both the syn-rift and post-rift periods, spread over the Rheno-Hercynian back arc seaway with clastic deltaic conditions in the north east and marine carbonate being deposited in the South West and this prevailed up until the Asbian when Yoredale type deposition dominated. Syn-rift sedimentation was punctuated by periods of relatively tectonic quiescence and tectonic subsidence generally exceeded sedimentation rates within basins whereas, until the late Asbian to Brigantian,

some of the blocks were either emergent or just below sea level and therefore lacking in sediment deposition. Syn-rift sedimentation was, therefore, generally confined to the fault bounded basins. During the Namurian a transition occurred from differential settlement of the Blocks and Basins to a post-rift thermal sag stage where sedimentation rates on the Blocks and Basins were similar.

3.0 Sedimentology of the Yoredale Cycles of Northern England

3.1 Introduction

The Carboniferous of Northern England, as found in most parts of the UK and indeed most of the world, is mostly cyclic in nature (George *et al*., 1976; Ramsbottom, 1973). As a result of the wealth of the mineral deposits contained in the Late Viséan to early Namurian successions of the area, these cyclic deposits have been extensively studied for many years. Westgarth Forster (1809) was probably the first to describe the cyclothem sequences on the northern Alston Block and later in 1836 John Phillips described the cycles on the Askrigg Block and named them "Yoredale Beds". During the initial geological survey of part of the Northumberland Basin, the rhythmic nature of the cycles was first recognised by Hugh Miller Jr. (1887), where he recorded them as limestone, shale, sandstone and coal units, repeated many times over. This simple description is very similar to what is now regarded as being the standard Yoredale cyclothem described by Dunham (1950), i.e. (1) marine limestone; (2) marine shale; (3) unfossiliferous (?non-marine) ferruginous shale; (4) sandy shale, shaly sandstone or "grey beds" (interbedded shales, siltstones and sandstones); (5) sandstone; (6) ganister or under-clay; and (7) coal. As can be seen in Chapter 2, Figure 2.5, the standard Yoredale Cycles in northern England are dominated by terrigenous sediments whereas the limestone units form a proportionately smaller part of the cycle.

This general cyclothem sequence can be found on the Askrigg and Alston Blocks and within both the Northumberland Basin and Stainmore Trough of northern England, but there are regional variations. Within the Northumberland Basin, as the limestones are traced from the south-west to the north-east, many become thinner, split or disappear altogether (Johnson, 1959) The proportion of siliciclastic sediments to limestone increases towards the north-east and the limestone thickness increases to the south-west (Figure 3.2); the thick terrigenous sediments imply continuous erosion and transport from land masses to the north-east through the Pennine fluvial system.

3.2 The structure of the Alston Block of Northern England

Figure 2.3, Chapter 2, illustrates the locations of the east-west oriented block and basin structures formed within the Carboniferous of northern England; this study relates specifically to the Alston Block of northern England. Major fault systems, some acting as hinge lines during the Carboniferous, separate the Alston Block from the Northumberland Basin to the north, the Stainmore Trough to the south and the lower Palaeozoic sediments to the west. The block tilts to the east and is obscured by Permian sediments. However, evidence from the Harton Borehole (NZ 396 656) near South Shields reveals a much thicker Carboniferous succession than on the Alston Block and this area may therefore be designated as more basin-ward in location (Ridd *et al*., 1970; Dunham, 1990).

The northern hinge line of the Alston Block corresponds to the Stublick and Ninety Fathom fault system and the southern edge of the block is delineated by the Swindale Beck, Closehouse, Lunedale, Staindrop and Butterknowle group of faults, with the Swindale Beck fault acting as a hinge line during the Carboniferous (Dunham, 1990). The western edge is marked by the Pennine fault system. The northern and southern faults and hinge lines have been associated with syn- and post- rift sedimentation during the Carboniferous; the Pennine fault system on the other hand is more complicated with later Hercynian and Tertiary reactivation (Shotton, 1935; George, 1958). Figure 3.1 shows the locations of the main boundary faults associated with the Alston Block, together with the veins and main faults, and the Burtreeford Disturbance which is a major east-facing monocline that winds its way north to south, approximately through the middle of the Alston Block.

The dominant NW and ENE direction of the faults and veins on the Alston Block are very apparent from Figure 3.1 and these are thought to be associated with the grain of the lower Palaeozoic basement developed during the Caledonian Orogeny. The Burtreeford disturbance has a maximum down-throw of 76 metres and easterly thrusts and displacements of up to 152 metres (Dunham, 1990). The monocline is a late Carboniferous compressional feature and as such did not have

any effect upon the thickness of individual units or cyclothems examined in this work.

Doming of the Alston Block is known to have occurred in the early Tertiary and many of the faults were reactivated during this movement. It has been suggested by Dunham (1990), however, that the doming probably originated during the Hercynian and that many of the dominant faults, such as the Great Sulphur Vein, originated at this time and were active, but diminishing in their movement, during the Carboniferous. It can be expected therefore that they will have had some affect upon sedimentation patterns.

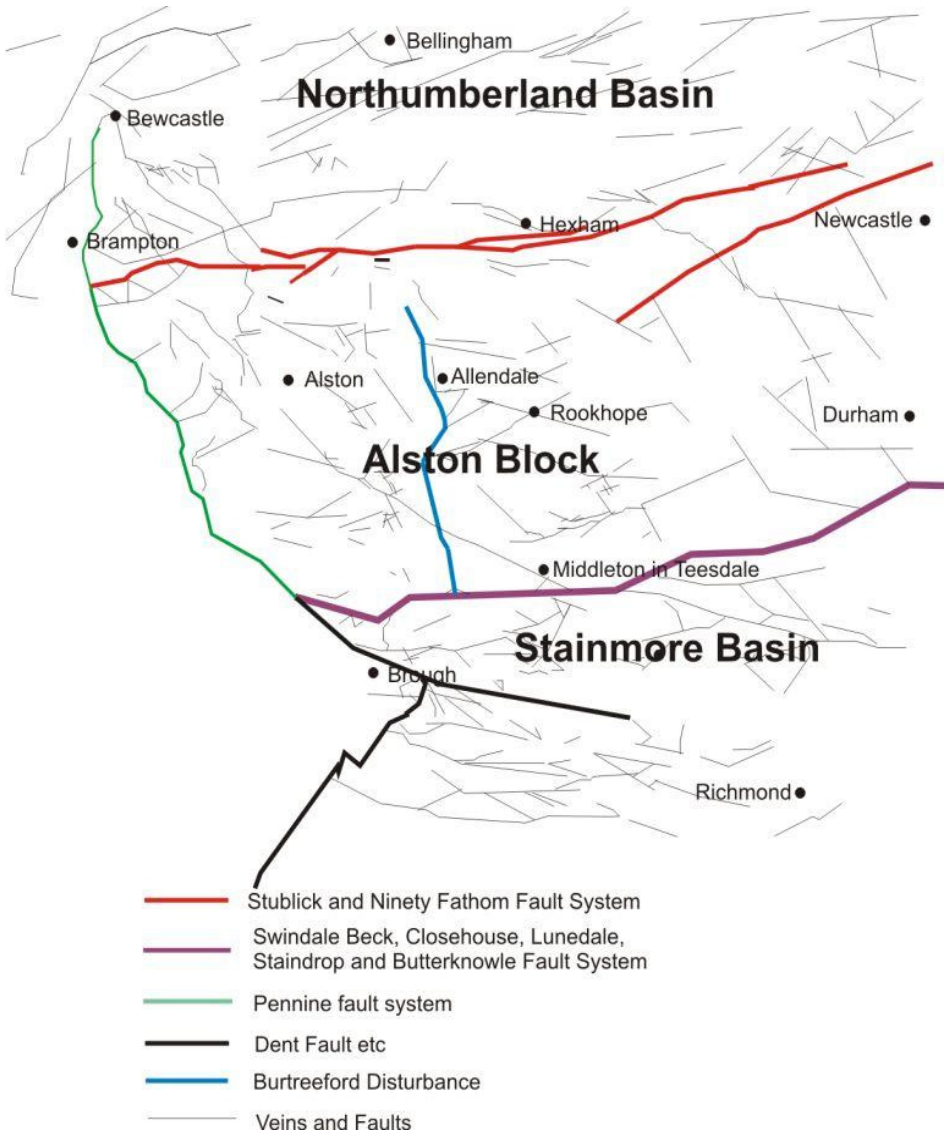

Figure 3.1 Structure of the Alston Block and surrounding area

3.2.1 The Great Whin Complex, Little Whin Sill and Whin Dykes

The Great Whin Complex is present in most of the area under discussion, extending from near the Lunedale, Closehouse and Butterknowle faults, north up to Holy Island. The Great Whin Complex varies from a few metres thick at Scoredale Mine (763 227) to nearly 100m in the central area of the Alston Block. The intrusion, however, is not concordant in that it cuts through many of the cyclothems and ranges from below the Melmerby Scar in the Asbian, up to its highest in the Coal Measures near to Brampton (Dunham, 1990; Johnson *et al*., 2001). Previously the term Whin Sill was used for the intrusion; however, due to the discordant nature of the complex Johnson *et al*. (2001)) referred to the Whin Sill as the Great Whin Complex, a name which is used here.

The Little Whin Sill covers a much smaller area, being exposed only in the vicinity of Stanhope and Eastgate (Dunham, 1990; Johnson *et al*., 2001)). The sill is 11.7m thick in Greenfoot Quarry and probably thickens to the east (Creeney, 1980). Both the Whin complex and the Sill, together with various Whin dykes, are dated to the late Westphalian or Stephanian, with the Little Whin Sill pre-dating the Great Whin Complex and the Whin dykes post-dating it. Even though the Whin complexes are important to the geological history of the Alston Block and adjoining areas, they obviously post-date the depositional episodes discussed here and so are not discussed further.

3.3 Transgressions and regressions on the Alston Block

The alternating cyclothems of limestone, shale and sandstone had commenced on the Alston Block by the end of the Asbian with the Birkdale cyclothem and by the start of the Brigantian the typical rhythmic series of the Yoredale beds was well established. The submergence of the Alston and Askrigg Blocks in the late Asbian resulted in marine carbonate conditions prevailing with terrigenous sediment encroaching on to the northern margins of the Alston Block only by the end of the Asbian. The initial marine transgressions extended into the Northumberland Basin; however, siliciclastic/deltaic sedimentation prevailed over much of that area as the subsiding basin was filled.

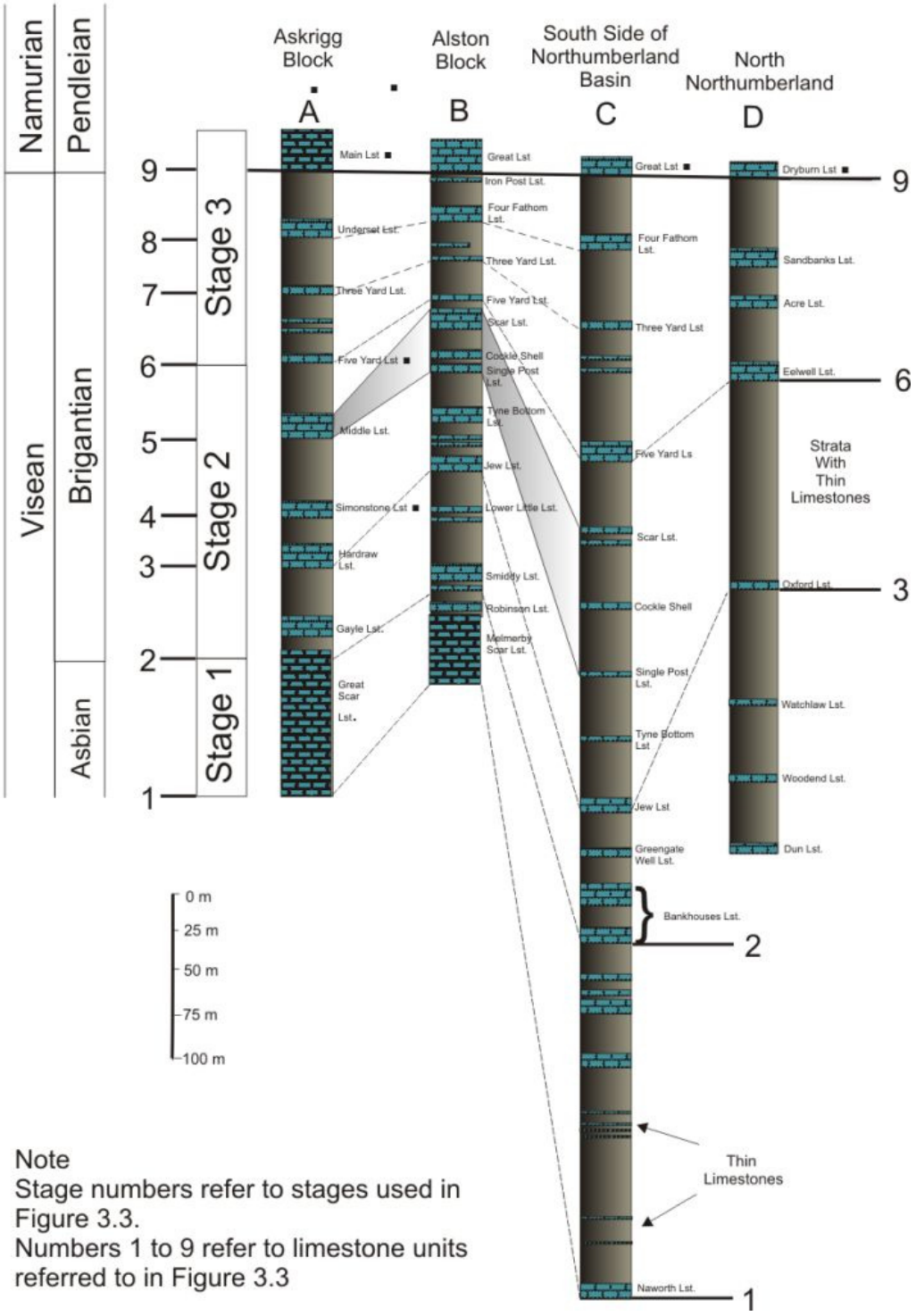

Figure 3.2 Generalised sections, from the south-west to the north-east, of the Askrigg Block, Stainmore Basin, Alston Block and the Northumberland Basin. After Johnson (1960).

Figure 3.2 includes generalised sections of the Askrigg Block, Stainmore Basin, Alston Block and the Northumberland Basin. These are an amalgamation of recorded data, first presented in a paper by Johnson (1959), and used to

illustrate thickness changes, of both carbonates and deltaics, in a south-west to north-east direction. It is worth noting the difficulty in comparing and correlating many of the limestones between the blocks and this becomes even more tenuous when considering the Northumbrian Basin succession.

Figure 3.3 illustrates how the sedimentation patterns change from the south-west to the north-east. This figure is useful in visualising the changing shorelines, limits of siliciclastic sedimentation and the extent of marine transgressions. The thickness changes and draping of limestones are highlighted as the Stublick fault-line is approached and crossed into the basin succession.

Stage 1, up to the Asbian/Brigantian boundary, shows how marine conditions prevailed on the blocks while only intermittently reaching into the Northumberland Basin. The shoreline and deltaic sediments encroached on to the northern margin of the Alston Block by the end of the Asbian. Marine carbonate sedimentation did not reach across the full width of the Northumberland Basin during this stage and the Great Scar and Melmerby Scar limestones of the Askrigg and Alston Blocks can be seen to split within the basin into at least five thin limestones. To summarise stage 1, during this stage it can be seen that marine deposition was extending north into the Northumberland Basin and the shoreline eventually moved south onto the northern region of the Alston Block.

During Stage 2 marine sedimentation continued to extend in area and the Yoredale cyclothems commonly split in the direction of the Northumberland Basin due to the movement on the Stublick fault system and associated compaction. The shoreline can be seen to extend further in a south-west direction on to and over the Askrigg Block and marine conditions extended even further into the Northumberland Basin. Only one cyclothem, the Hardraw/Jew/Oxford limestone (No 3), continues without splitting or disappearing and is persistent throughout the basin. The persistence of this limestone is significant in that, the marine transgression at the base of the limestone was far more extensive than had previously occurred; the limestone extends throughout the whole of the Mid-Northumberland Basin.

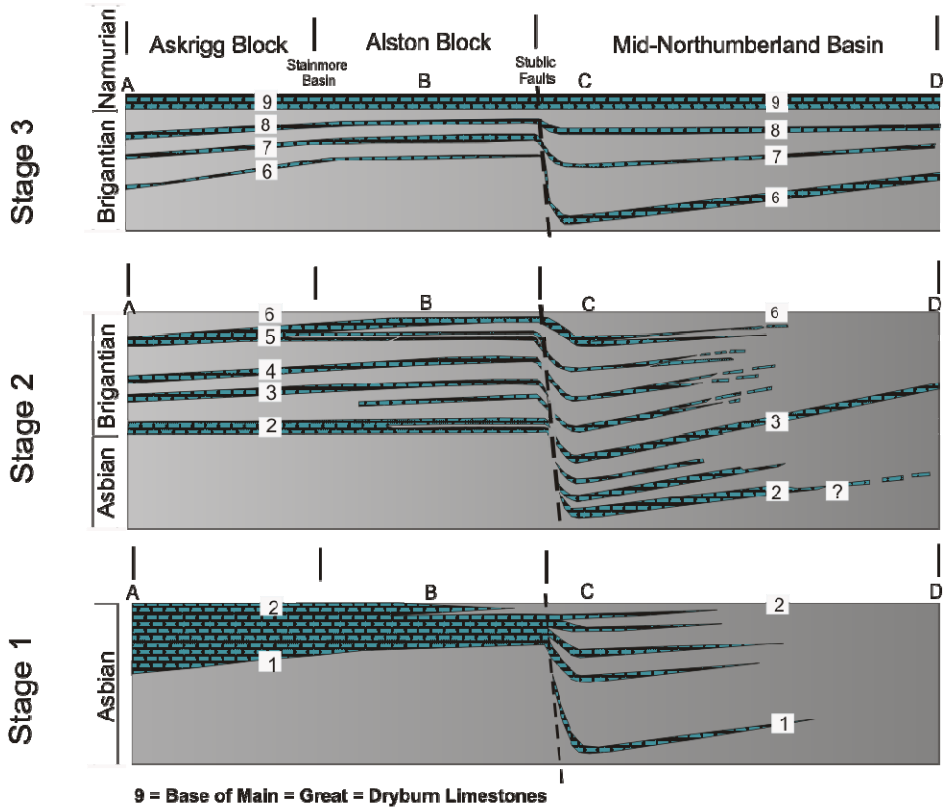

Figure 3.3, illustration of the changing sedimentation patterns from the south-west to the north-east. After Johnson (1960). Note that not all limestones shown in Figure 3.2 are included in this figure.

The Middle Limestone (5) of the Askrigg Block can be seen to split during the later part of Stage 2. On the Alston Block, this is seen as the Single Post, Cockleshell and Scar limestones, which continue into the southern side of the Northumberland Basin before splitting further and eventually dying out. Neither of these beds is recognised within the northern part of the Northumberland Basin (Johnson, 1959). Siliciclastic and therefore, the shoreline limits are shown to

extend south over the Askrigg Block in this stage while marine transgressions are seen to extend further into the Northumberland Basin. Only one limestone extends over the full area of the Mid-Northumberland Basin.

By Stage 3 the marine transgressions extend over the whole of the Mid-Northumberland Basin and deposition of Johnson's perfect "Major Cyclothems" occurred (Johnson, 1959). These cyclothems, the Five Yard, Three Yard, Four Fathom and Great Cyclothems, extend far to the north beyond the margins of the Northumberland Basin and the shoreline extended beyond the southern margin of the Askrigg Block (Johnson, 1959).

Figures 3.2 and 3.3 are useful in visualising and assessing the extent of the changing shoreline and marine transgressions throughout the area. The range of the transgressions increased from the late Asbian (Stages 1 and 2) and into the Namurian as did the extent of the shoreline. As a result of the inherent nature of a shallow epeiric sea, a few metres rise or fall in sea-level would have resulted in major changes to the coastline and hence the large transgressions and regressions over the blocks and basin. Ramsbottom (1979) suggested that the lowering of sea-level would be small in relation to the rises which preceded them and therefore subsidence would be required to accommodate the accumulating thickness changes.

3.4 Cycle lithology

As a result of several centuries of lead mining, the Carboniferous strata of the Alston Block comprise one of the first well-documented stratigraphic successions in Britain. The limestone beds in particular, due to their economic importance and lateral persistence, were individually named and recognised over a wide area (Holliday *et al*., 1975). The term Yoredale series or Yoredale cyclothem was originally proposed by Phillips (1836), after the older name of Uredale for the Wensleydale valley, and specifically related to the strata between the Scar Limestone and the Millstone Grit; however, this is now used as a more general description for rhythmic interbedded repetitions of marine limestone, mudstone, siltstone and sandstone.

The products of fluvio-deltaic and shallow-water carbonate sedimentation, the Yoredale cycles of the Late Viséan and Namurian, are mixed clastic-carbonate high frequency sequences varying from 5 to 50 metres in thickness. The limestones are characteristically marine limestones, typically dark blue-grey in colour with the darker hues due to increased organic content. The majority of the limestones are fine grained and mainly thin bedded and comprise biogenic packstones to wackestones with abundant bioclasts including crinoids, brachiopods, corals, calcareous algae, foraminifera, bivalves, gastropods and bryozoans. Girvanella/Osagia nodules are persistent within many of the lower limestones of the Brigantian of the area. The matrix is generally a lime mudstone/micrite, but this has commonly recrystallised to microspar (Tucker, 2003). Peritidal and nearshore carbonate facies occur within the cycles of the Lower Dinantian in the Northumberland Basin (Leeder, 1975; Leeder and Strudwick, 1987). The continuity of the limestones within the Yoredale cyclothems was recognised by Forster, 1809; Phillips, 1836; Dakyns *et al*. (1891); Gunn, 1895; Garwood, 1913 and Fairbairn, 1978.

The absence of transgressive lags at the base of many of the limestones would suggest that marine conditions, on the whole, were established without the passage of an erosive shoreface; the lower delta-plain sediments were gradually flooded (Reynolds 1992). The limestones are overlain by coarsening up fluvio-deltaic shoreline siliciclastic members; the succeeding calcareous shales are usually fossiliferous and these give way to dark grey or black unfossiliferous, usually non-marine shales, which are often ferruginous. Interbedded shales, siltstones and sandstones ("grey beds") commonly underlie or replace the sandstone. The sandstones are micaceous, usually fine grained (0.1mm to 0.3 mm) and locally are siliceous and workable as ganister (Dunham, 1990). Coal is found locally but this is usually thin, rarely exceeding a few tens of millimetres and in many cases is represented by a smut.

Many of the clastic members associated with the Yoredales are products of prograding deltas, the majority of which are river-dominated elongate types (see Moore, 1958; Elliot, 1974, 1975, 1976(a),(b),(c); Leeder, 1974; Leeder and

Strudwick, 1987; Ainsworth and Crowley, 1994). Eight marine shoreline lithofacies were recognised by Lemon (2006) related to prograding shorelines, Lemon also recognised eleven deltaic lithofacies within the cyclothems of the area, i.e. deltaic lithofacies such as prodelta and delta front, floodplain and interditributary bay, distributary channels, crevasse splay, levee deposits and palaeosoils. The onset of the deltaic clastic muds and shifting shoreline are markedly diachronous from proximal to distal areas, being in younger beds to the south on the Askrigg Block and in the older beds to the north in the Stainmore Basin and the Alston Block (Burgess and Mitchell, 1976).

Many of the cycles within the Brigantian of the Alston Block are named after their limestone at the base of each cycle. However, as discussed above not all limestones are named and they are not always obviously related to a full cyclic sequence. They may, however, still record actual cycles or alternatively they may be associated with localised depth or environmental changes.

3.5 Palaeontology of the cyclothems of Northern England.

Coral and brachiopod zones proposed by Vaughan (1905) and Garwood (1913) are commonly used for the correlation of the Lower Carboniferous strata of Southern Britain. Their use in Northern Britain; however, is difficult due to the lack of corresponding thick marine limestone bands and biostratigraphic units, therefore Armstrong and Purnell (1993) proposed foraminifera, conodont zones and palynology for correlation throughout the area. The Viséan-Namurian (Serpukhovian/Lower Bashkirian) boundary of the area was based upon the presence of the Ammonoids/ goniatites *Eumorphoceras* and *Cravenoceras*. Ammonoid biostratigraphy is available for the whole of the Namurian of Western Europe; however, they cannot be used as time unit's per se due to the significant changes of environment and the evolutionary rates of the species that can occur over the very long time periods in question.

3.6 The Great Limestone Cyclothem

The Great Limestone Cyclothem occurs at the Viséan-Namurian boundary (Serpukhovian/Lower Bashkirian) based upon the presence of the goniatites

Eumorphoceras and *Cravenoceras* which have been found within the beds below the cyclothem. The Great Limestone, the basal limestone of the cyclothem, was decided upon as the base of the Namurian as it is the nearest mapable limestone to the occurrences of the goniatites (Johnson 1958). Currie (1954) also suggested that the boundary lies at the base of the Top Hosie in Scotland, previously correlated with the Great Limestone by Trotter (1952). The Great Limestone has also been correlated with the Main Limestone south on the Askrigg Block and north into Northumberland where it is correlated with the Dryburn Limestone (Gunn, 1895).

Figure 3.4. Tuft sandstones directly below the Great Limestone at Hudeshope Beck. Note the thin immature coals and smuts within the beds.

The Great Limestone sits upon the sandstones of the Iron Post Cyclothem. These sandstones, locally referred to as the Tuft, vary lithologically from fine-grained brown micaceous sandstone to a coarse grit. Coal seams in the Tuft were worked at both Meldon Hill (770 290) and Knock Fell (720 300); however, the coals are usually immature and thin and in places are evident only by a smut. Figure 3.4 is a photograph taken in Hudeshope Beck near to Middleton in Teesdale (394784 527610) where many immature, thin seams are evident below and within the Tuft sandstone directly below the Great Limestone.

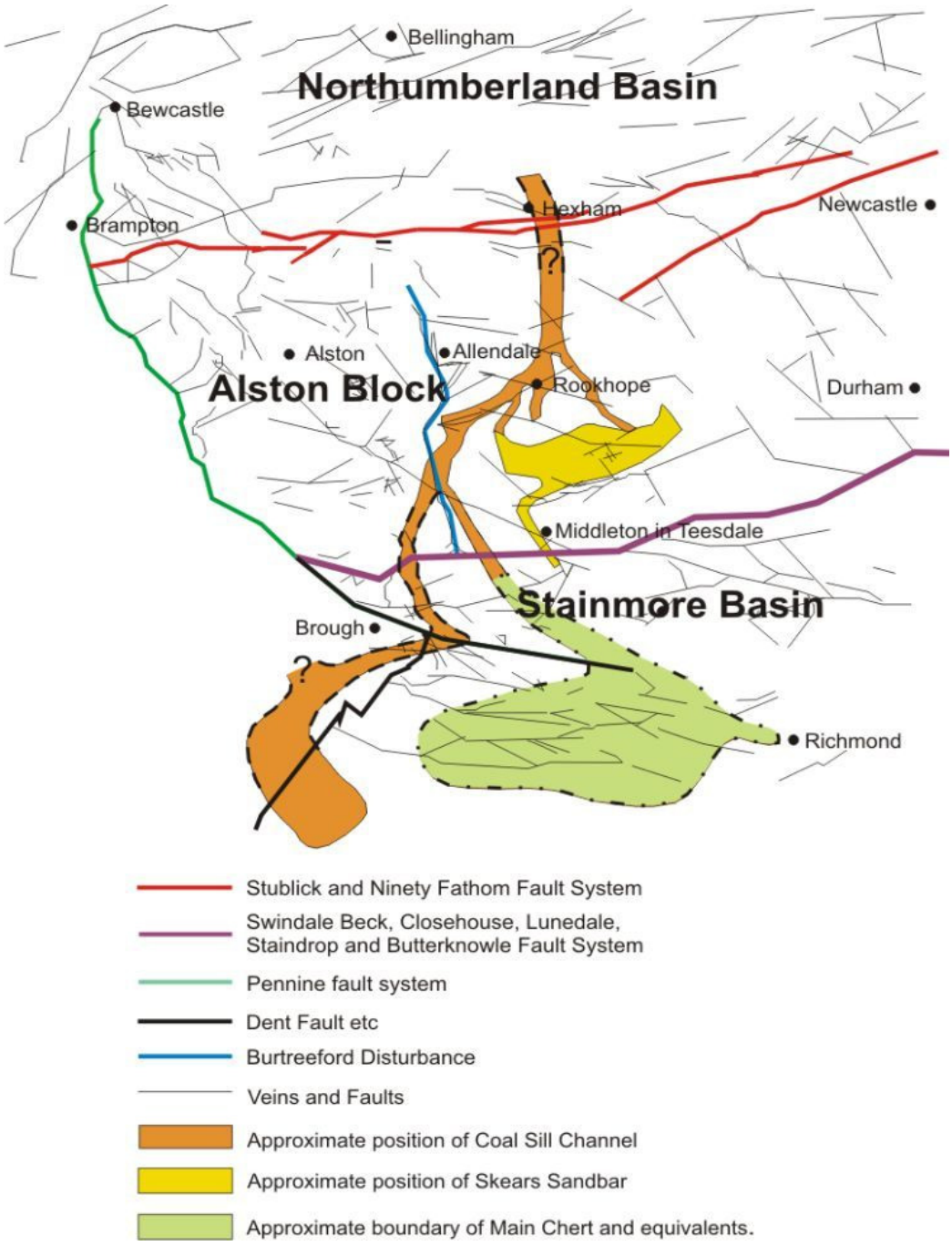

Figure 3.5 Approximate positions of Hodges Coal Sill Channel and Skears Sandbar. After Hodge and Dunham (1991).

The Great Limestone Cyclothem is the second thickest of the cyclothems looked at in this thesis, having an average thickness of 39.1 metres, the Little Cyclothem which lies directly above the Great Limestone Cyclothem is, despite its name, the thickest of the Cyclothems at approximately 45 metres thick. The mudstone/shale of the Great Limestone Cyclothem averages 9 metres and in some areas of the block this has been removed by channelling within the overlying

sandstones (Hodge 1965), referred to as the High Coal Sill, which is also known to cut down to the limestone in a large distributory channel known as the Coal Sill or Allercleugh Channel (Figure 3.5). The uppermost of the sandstones, the White Hazle, varies considerably in thickness; in Skears Mine (395700 523080), it is up to 22m thick and it is thought to be a remnant of a barrier island or sandbar (Dunham and Hodge 1991) (Figure 3.5).

3.6.1 The Great Limestone

The Great Limestone is the thickest limestone in the area averaging 20 metres but being slightly thinner than this within Hudeshope Beck at Middleton in Teesdale, where it is around 19 metres thick. The Great Limestone is more like the limestones within the Brigantian/ Viséan, as the Namurian limestones are usually much thinner with the cyclothem more clastic dominated; in places the Namurian limestones are represented by marine shales only. The Brigantian/ Viséan cyclothems on the other hand are more carbonate dominated, very much like the Great limestone. As with many of the limestones within the Brigantian/ Viséan, the Great Limestone is blue grey in colour and breaks into posts (beds), varying from a few tens of millimetres to a couple of metres thick (Dunham, 1990).

Westgarth Forster (1809) recorded that the Great Limestone comprises three mineralised flats, known as the lower, middle and upper flats. The flats are areas of limestone which are often highly mineralised by hydrothermal deposits replacing the limestone adjacent to mineralised faults. Johnson (1958), based on a section at Brunton Banks, Chollerford (928 570), suggested the limestone was divisible into three parts: a lower dark-coloured limestone up to 1 metre thick, a central division, referred to as the main posts, of light-coloured limestone 6 to 10 metres thick and an upper division of dark coloured limestone with intercalated shales called the Tumbler Beds. Fairbairn (1978) referred to five divisions; The Bench Posts, 1.7 to 2.8 metres thick, the Main Posts, 4.2 metres thick, the Fossil Posts, 6.5 to 10 metres thick, the Top Posts, 1.7 to 2.5 metres thick and the Famp Posts or Tumbler Beds, 2 to 9 metres thick. A post here is defined as a limestone bed or a limestone split by strong stylolites. Fairbairn's descriptions were based

on many measurements throughout the Alston Block, most of which were based in Weardale. Correlation of Fairbairn's Top Posts and Tumbler Beds with measurements at Hudeshope Beck near Middleton in Teesdale proved to be difficult and unproductive; nevertheless, the lower beds were correlated with Fairbairn's sections successfully using thickness changes and fossil assemblages. Figure 1.2 is constructed from measurements at Hudeshope Beck and includes the local bed names correlated from Fairbairn's sections (1978).

Figure 1.2 demonstrates how well bedded the Great Limestone is and significantly many of these beds can be correlated throughout much of the Alston Block (Fairbairn, 1990) and have been recognised in the Main Limestone within the Stainmore Basin and on the northern edge of the Askrigg Block. The beds at Hudeshope Beck vary between 0.16 to 1.58 metres with an average thickness of 0.75 metres. The beds are delineated by thin shale partings, most only millimetres thick, and pressure dissolution seams (Chapter 10), with the thickness of the shale partings increasing towards the top, as the Tumbler Beds are approached. Dolomitisation is not uncommon within the lower beds throughout the Alston Block and chert nodules are also common within the Main Posts.

3.6.2. The Great Limestone facies

Wilson (1989) divided the Yoredale cyclothems for the Brigantian and the Asbian into five broad sedimentary and ecological facies which are described in Table 3.1. The Great Limestone, even though it falls within the Namurian and not the Brigantian or Asbian, fits within Facies 5, i.e. being formed within a shallow, marine, clear-water offshore carbonate platform environment. To assess the Great Limestone facies with those suggested in Table 3.1 the description of facies 5 has been split into its various components.

1) *Offshore carbonate platform, shallow-water marine clear-water environment.* The Great Limestone facies and geochemistry imply a clear shallow- marine environment; calcium carbonate content is mostly around 90 to 97%. Mud partings at bedding planes suggest a change in environmental conditions as occasional and periodic incursions of prodelta mud occurred.

2) *Pale-grey and dark-grey bioclastic limestone with thin partings of calcareous mudstone.* The Great Limestone is pale to dark grey in colour and the limestone varies from a bioclastic wackestone to packstone with a dark micritic-microsparite matrix (from patchy neomorphism); a peloidal structure is frequently also seen in thin-section. Bedding planes, Chapter 3.6.6, are defined by thin partings of calcareous mudstone.

3) *Open-water marine fauna with colonial corals and large thick shelled brachiopods.* The fauna of the Great Limestone is typically marine consisting of brachiopod fragments, foraminifera, crinoidal, bryozoans and calcareous algal material (Figure 3.7). Other less common fossil debris includes that of gastropods, bivalves, nautiloids, serpulids, ostracods and trilobites many of which are recognised from fragments in thin-section, the typical fauna of *Diphyphyllum* and *Syringopora* mentioned within Table 3.1 are present. Productids and gigantproductids, spiriferids and crinoid columnals are common throughout the limestone and many major coral-brachiopod biostromes are present. There is significant bioclastic hash, probably derived from the comminution of skeletal material by scavenging organisms; overall, the biota, as preserved, was dominated by calcitic skeletal organisms. The majority of the bioclasts are less than a few millimetres in size although larger, commonly silicified whole fossils include the corals (rugose and tabulate) and productid and spiriferid brachiopods are also often found, all typical of open-marine conditions (Figure 3.8).

The petrographic examination of thin-sections from the Great Limestone indicates that there is no discernible systematic change in the composition of the microfacies up through the Great Limestone (Chapter 5). There is also no indication of any gradual change throughout or across the individual beds; however geochemically there are small changes towards the bedding planes Chapter 9). Mud partings at bedding planes suggest that a change in environmental conditions did occur and therefore a change in facies may be implied; however, to all intents and purposes, it seems clear that the limestone beds were all deposited under similar conditions, i.e. an offshore carbonate

platform in a shallow clear-water marine environment with occasional incursions of prodelta muds, although, presumably, specific local conditions also allowed the coral-brachiopod biostromes to form.

Facies 1	**Subaerial delta plain. A low emergent land surface colonised by land plants. Rare coal seams are formed with many seatearths (palaeosoils) composed of shale, siltstone and sandstone. Common fossils are rootlet beds and *Stigmaria in situ*. Angular shale, mudstone and limestone clasts are occasionally present in the sediments and indicate local emergence and erosion.**
Facies 2	**Shoreline, littoral and estuarine environments. Interbedded sandstone, micaceous siltstone and mudstone. Often carbonaceous and containing many derived fragments of land plants. Salinity-tolerant fauna with forms capable of surviving emergence, mainly composed of molluscs and track, trail and burrow-forming creatures. Common fossils include: tracks, trails, burrows and bioturbated beds, *Chondrites, Tormaculum, Planolites, Rugosochonetes hardrensis, Palaeoneilo, Bucanopsis, and Euphemites.***
Facies 3	**Relatively high-energy near-shore marine environment. Interbedded mudstone, siltstone and sandstone with thin bioclastic limestone bands composed of broken shell debris. Fauna dominated by molluscs with inshore tolerant brachiopods. Common fossils include: *Lingula, Orbiculoidea,* productids, *Pleuropugnoides pleurodon, Aviculopectin, Myalina, Palaeoneilo, Poledevcia, Wilkingia, Bucanopsis, Euphemites* and *Glabrocingulum.***
Facies 4	**Shallow-water muddy marine environment outside the zone of wave and current action. Mudstone and siltstone with bands of fine-grained sandstone and argillaceous limestone. Extensive muddy-bottom marine fauna of small simple corals, bryozoans, numerous and varied brachiopods, trilobites and many molluscs. Common fossils include: *zaphrentids, Fenestella,* productids, bivalves, gastropods and nautiloid cephalopods.**
Facies 5	**Offshore carbonate platform, shallow-water marine clear-water environment. Pale-grey and dark-grey bioclastic limestone with thin partings of calcareous mudstone. Open-water marine fauna with colonial corals and large thick shelled brachiopods. Particularly *Siphonodendron, Diphyphyllum* and *Syringopora* with productids, gigantproductids, spiriferids and crinoids columnals.**

Table 3.1. Brigantian and Asbian facies. After Wilson (1989) and Johnson and Nudds (1996). Note that not all facies may be present within a cyclothem.

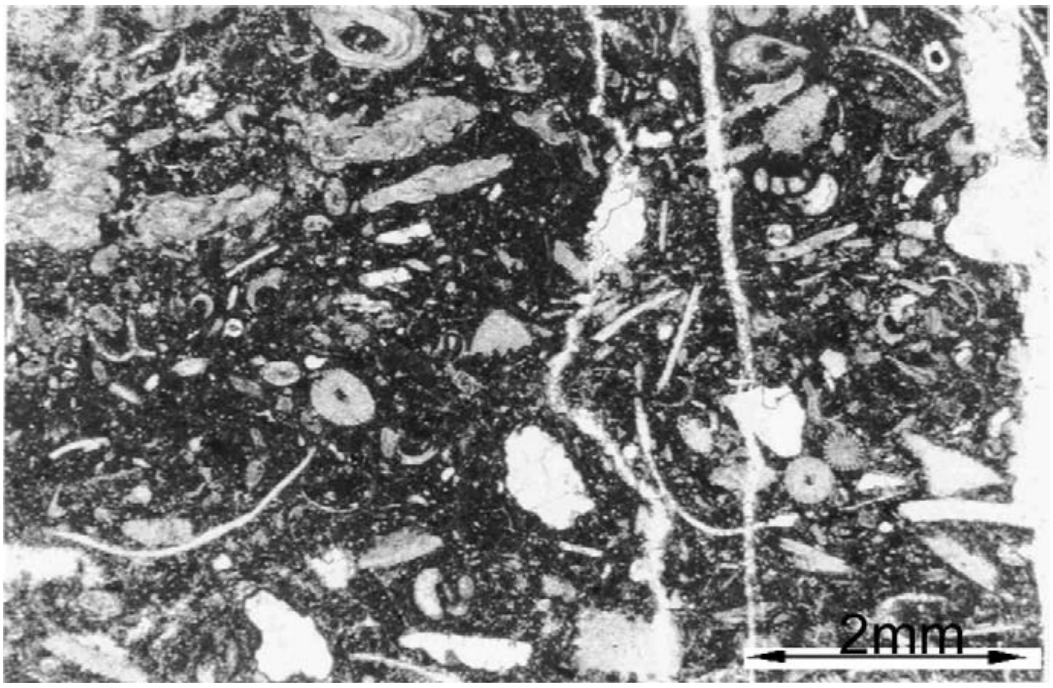

Figure 3.7. Photomicrograph of a typical Great Limestone sample showing abundance of bioclastic debris, including brachiopod, crinoid and replaced aragonitic skeletal material in a dark micritic–microsparitic matrix. Scale bar 2 mm.

Figure 3.8. Silicified rugose corals and brachiopods Field of view approximately 150 millimetres by 100 millimetres. (Hudeshope Beck).

Figure 3.9. Fallen block of Great Limestone containing symmetrical ripples. Size of block approximately 2.5 metres by 1.5 metres by 0.75 metres thick. (Hudeshope Beck).

The depth of deposition of the Great Limestone is interpreted as being in the outer shoreface/transition to offshore environment with water depths varying from below 5 metres to approximately 50 metres but generally below fair-weather wave-base. Localised symmetrical ripples are occasionally found (Figure 3.9), thought to be associated with water depths of a few metres or of deeper water and formed through storm reworking of sediments. There are locally sedimentary structures indicating current activity and Fairburn (1999) deduced preferred orientations and palaeocurrent patterns at some localities from the orientation of larger fossils such as corals, crinoids and brachiopod shells.

Bioclast lenses, 10–30 centimetres across and several centimetres in thickness, are commonly found and areas of densely packed coarse bioclastic material, interpreted as cross-sections through burrows, usually 0.5–3 centimetres in diameter can be seen on polished surfaces. There is abundant evidence of bioturbation both in the field and within thin-section. Burrows, simple straight to curved structures, 0.5 to 2 centimetres across, and up to 10 centimetres in length

are found upon bedding planes, mainly within the Tumbler Beds (Figure 3.10) and these can be attributed to the general group *Planolites*. The trace fossil *Zoophycos*, with the distinctive concentric burrow system reaching 15 cm across, also occurs on some bedding planes; again these are more prevalent within the Tumbler Beds (Figure 3.11). A crude lamination, defined by the grain size of the fossil fragments, is locally seen within some beds; however, cross-lamination or cross-bedding is only very rarely seen within the beds.

Planolites is placed within both the *Cruziana* and *Zoophycos* Ichnofacies where it is usually attributed to shallow water. The *Zoophycos* Ichnofacies has an extremely broad palaeobathymetric range (MacEochern *et al*., 2007) and it was previously ascribed to the continental shelf where lowered oxygen levels existed in quiet waters; however, re-evaluation by Frey and Seilacher (1980) who suggested the Ichnofacies could also be assigned to shallow-water, epeiric deposits where organic contents may have resulted in lowered oxygen levels (MacEochern *et al*., 2007).

To conclude, the facies and microfacies of the Great Limestone are typical of a shallow-water marine environment, i.e. outer shoreface/transition to offshore environment. The environment is suggested by the geochemistry, sedimentary structures and fossil assemblages, to be very stable and clear with only occasional storm reworking and incursions of prodelta mud before the final advancement of true delta conditions. It could be argued that there are two facies present within the Great Limestone, one being the clear shallow-marine facies and the second being a facies associated with changing environment where prodelta mud is dominant and carbonate production is reduced; however, to all intents and purposes, it seems clear that the limestone beds were all deposited under very similar conditions.

Figure 3.10 *Planolites* on underside of bedding plane. Field of view approximately 650 millimetres by 450 millimetres. (Eastgate Quarry Weardale OS 3940 5368)

Figure 3.11 *Zoophycos* on underside of bedding plane. Field of view approximately 250 millimetres by 200 millimetres. (Eastgate Quarry Weardale OS 3940 5368)

3.6.3. Biostrome and fossil assemblages within the Great limestone

The fauna of the Carboniferous Limestones has been discussed by many authors (Garwood, 1913; Hudson, 1925; Turner 1956). Cumings (1932) described the term Biostrome as "a purely bedded structure, such as shell beds, crinoid's beds, and coral beds etcetera consisting and built mainly by sedentary organisms"; the distinction between biostromes and bioherms was also made; a bioherm being a structure that is mound like or lens like. It was not until Johnson (1958) that the palaeoecology of the Great and Main limestone was fully considered in detail where he described three such biostromes in these limestones the *Chaetetes* Band, the Brunton Band and the Frosterley Band.

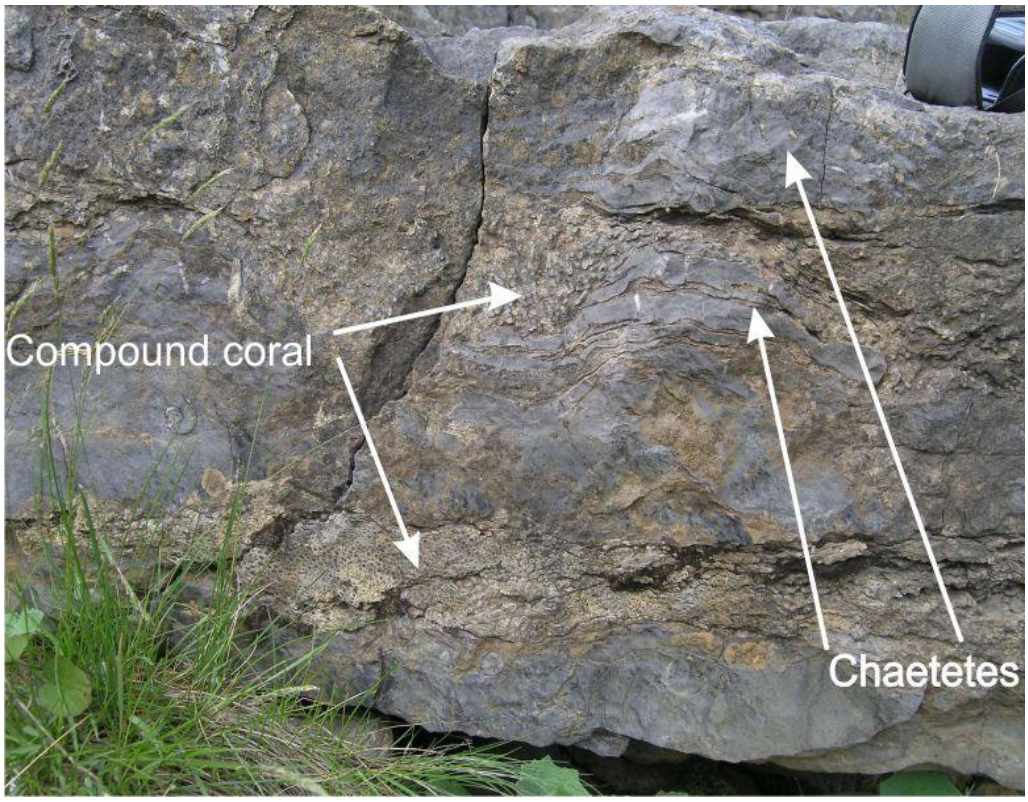

Figure 3.12. Chaetetes and compound corals within the "Chaetetes Band" of the Great Limestone. Field of view approximately 1.3 metres by 0.8 metres. (Chestergarth Quarry Rookhope, Weardale OS 39410 54220)

Within many areas of the Alston Block, and reported by Johnson (1958) at Brunton Bank Quarry, Chollerford (928 570), the *Chaetetes* Band is to be found within the bottom 1 metre, usually within either of the bottom two beds of the Great Limestone (Figure 1.2), and it consists of the sclerosponge *Chaetetes depressus*. Where *Chaetetes depressus* is not found on the block it is usually

replaced with compound corals such as *Diphyphyllum* or *Lonsdaleia laticlavia* and occasionally both *Chaetetes* and compound corals are found together (Figure 3.12). Within Hudeshope Beck; compound corals only are to be found; however, even these are patchy and not very abundant within this locality. Small lenses a few centimetres across of *Chaetetes* can also be found throughout the height of the Great Limestone (Figure 3.16).

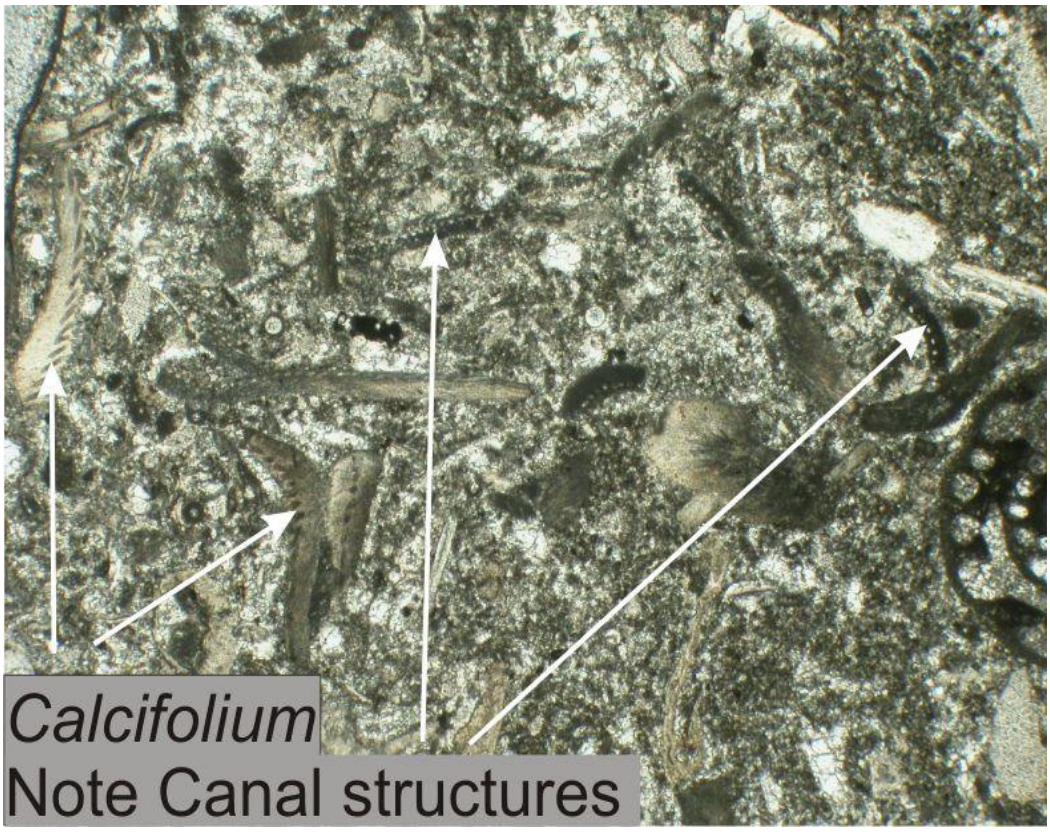

Figure 3.13. Calcifolium within the Great limestone. Field of view approximately 4 millimetres by 2.5 millimetres.

The Brunton Band lies within the centre of the Great Limestone and Johnson (1958) referred to the band commencing within approximately 5.5 metres of the base and varying between 3.6 metres and 6 metres thick. Within Hudeshope Beck the band commences at approximately 2.5 metres above the base within bed 5 and continues to approximately Bed 18, some 11 metres thick. The Brunton Band consists of the alga *Calcifolium bruntonense* sp. nov. and can only be recognised in thin-section. *Calcifolium* is restricted to only a few of the northern

limestones (Johnson, 1958). The limestone where the band occurs is generally lighter in colour than the rest of the limestone, suggesting that carbonaceous or other river borne minerals are reduced; however, this is not necessarily always borne out by the geochemistry (Chapter 9). The presence of the algae is recognised in thin-section by the partial sections of the branches and stems showing definite and obvious canal structures (Figure 3.13).

The Frosterley band of Weardale is famous for its use as columns in the 11th-Century (Norman) Durham Cathedral. It is locally referred to as the Frosterley 'marble'; however; the band is not actually a true marble. The band commences approximately 7 metres above the base (8 metres at Hudeshope Beck) and varies in thickness from less than a metre to over 5 metres in thickness; at Hudeshope Beck it is also approximately 5 metres thick. The band is surprisingly continuous throughout the Alston Block where it can be seen either as a single biostrome or several individual biostromes separated by thin limestone. At Hudeshope Beck the band is split into up to 5 individual biostromes by limestones, the thickest of which is nearly 1.5 metres thick (Figure 3.14). Johnson (1958) reported the band as being a persistent, though lenticular coralline biostrome, or biostromes, characterised by abundant remains of simple rugose corals, particularly *Dibunophyllum bipartitum* (McCoy), which is particularly abundant in the biostromes at Hudeshope Beck (Figure 3.15).

Apart from the biostromes there is no observable change in the proportions of the various bioclastic elements throughout the Great Limestone at Hudeshope Beck; all samples are similar — bioclastic wackestone–packstone with a range of skeletal fragments. There are localised accumulations, lenses and beds of *Chaetetes* (Figure 3.16) and the brachiopod *Gigantoproductus*, often seen in growth position (Johnson, 1958; Fairburn, 1999) and other quite rare local accumulations of specific fossils, such as beds of *Girvanella* nodules, *Sphaerocodium*, and spiriferids can be found. To all intents and purposes, it seems clear that the limestone beds were all deposited under similar conditions, although, presumably specific local conditions allowed the coral-brachiopod biostromes to form. Microfossil assemblages are further discussed in Chapter 5.

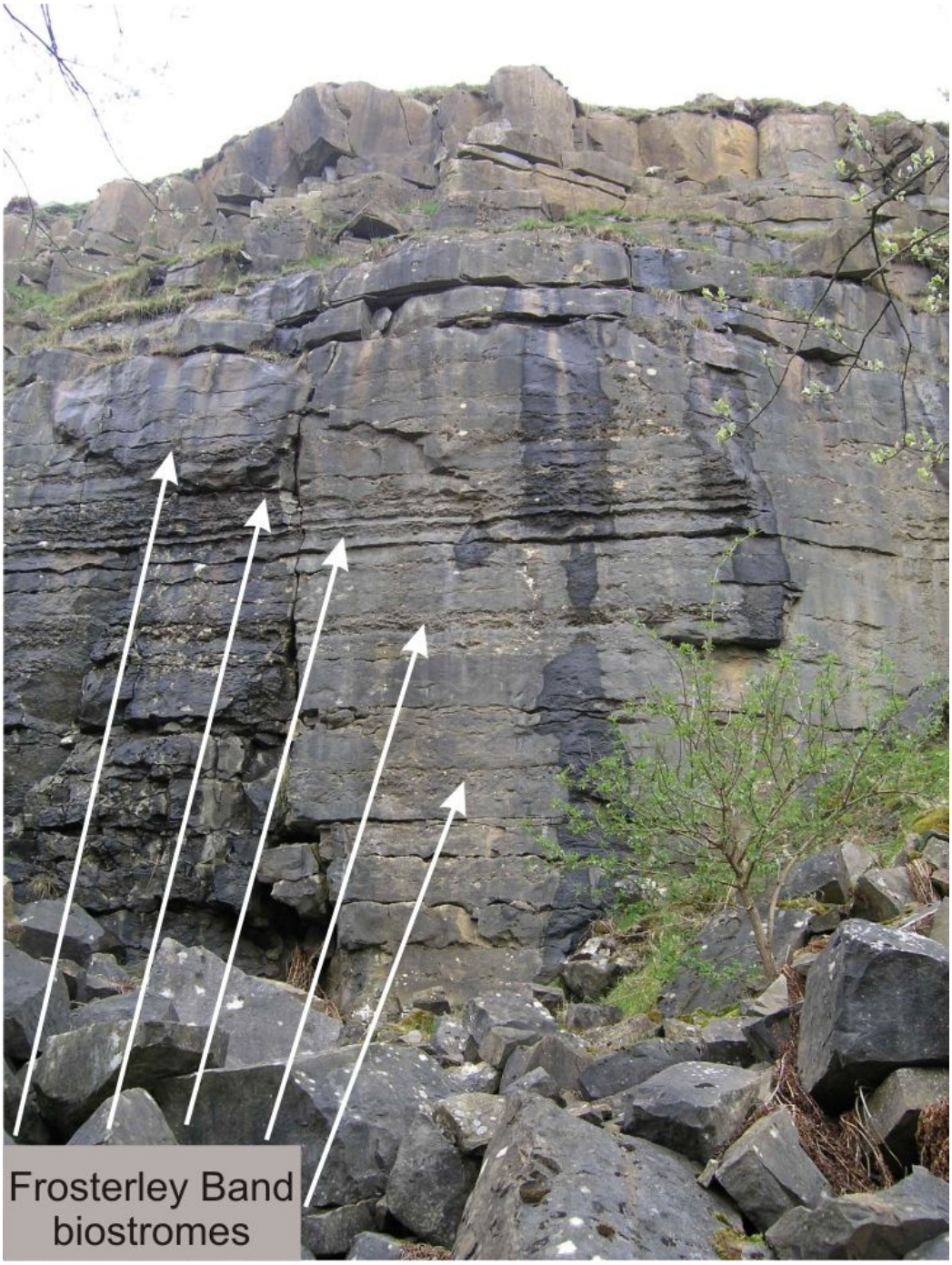

Figure 3.14. Frosterley Band biostromes within the Great Limestone at Hudeshope Beck Middleton in Teesdale. 5 individual biostrome picked out by arrows. Field of view approximately 18 metres by 11 metres.

Figure 3.15. Rugose corals, mainly *Dibunophyllum bipartitum* (McCoy) within one of the biostromes at Hudeshope Beck Middleton in Teesdale. Field of view approximately 200 millimetres by 120 millimetres.

Figure 3.16. Individual Chaetetes together with rugose coral (middle left) and brachiopod top left. Field of view approximately 110 millimetres by 100 millimetres. Hudeshope Beck, Middleton in Teesdale.

3.6.4. Taphonomy

The question must be approached as to whether the fossil assemblages and components are locally derived or exotic species from adjoining areas. The critical question posed is how valid is the variation in species shown in the fossil record of the Great Limestone; can it be regarded as a true representation of the environment of deposition.

The composition of shelly remains in any sedimentary succession depends upon many complex factors including the rate of shell supply, rate of sediment deposition and the conditions that the shells are exposed to during accumulation. The individual beds of the limestone and their thicknesses are correlatable over much of the platform which would suggest that the same depositional conditions were operating over the whole platform and; therefore, the large scale redistribution of sediment throughout the platform is unlikely to have occurred. The large scale redistribution of sediments would be expected to result in irregular bed thicknesses and patterns. Many macro-fossil assemblages such as corals are not in life position and fragmented, then again many of the brachiopods are in life position whereas the general background "hash" contains fragments of many different kinds of fossil suggesting current or storm activity was prevalent.

The background bioclastic "hash" within the Great Limestone probably consists of a mixture of comminuted skeletal material from both scavenging organisms and mechanical damage. Within shallow-marine environments, boring organisms can be a major cause of shell destruction (Driscoll, 1970; Cutler and Flessa, 1995) with cyanobacteria, sponges, bivalves and fungi being major contributors (Cobb, 1969). Repeated borings by endolithic cyanobacteria result in micrite envelopes forming around grains which are evident within most sections of the Great Limestone; micrite envelopes are indicative of deposition within the photic zone. It is obvious from thin-sections of the Great Limestone (Chapter 5) that many moulds exist within the sediment which are considered to highlight the positions of original bioclasts which have been dissolved within the sediment due to the instability of formerly high-magnesium calcite and aragonite at normal temperatures and pressure. In particular molluscan fragments are depleted within

the fossil assemblage, probably due to dissolution of shells and, therefore; it is probable that any discussion regarding the fossil environment will be biased towards fauna with original low-magnesium calcite shells. See Cherns and Wright (2000) for further discussion on the dissolution of aragonitic bioclasts.

Fragmented bioclastic remains can also be due to high-energy environments where wave action or current activity can cause mechanical damage resulting in fragmenting of the bioclasts. Bioclastic lenses, 10–30 centimetres across and several centimetres in thickness are commonly found within the Great Limestone, suggesting sorting by wave or current activity or even storm deposition, and areas of densely packed coarse bioclastic material are interpreted as cross-sections through burrows. Many bioclasts became disarticulated after death suggesting rapid burial did not occur; corals within the Great Limestone are very rarely in life position or articulated.

During life the skeletons of rugose corals are surrounded and supported by the soft sediment, but they may still be toppled over by storms or waves; however, not all toppled corals died, many were able to re-grow. Many corals within the Great Limestone are curved which is thought to indicate re-growth after falling over. Figure 3.17 is a picture of a polished slab of Frosterley “marble” where curved (geniculate) corals are evident on the left-hand side. This re-growth is suggestive of the coral toppling over, possible due to current or wave action removing the supporting sediment. The Frosterley biostromes show very little articulation and therefore they could be the result of accumulation due to currents, even so, the mass of corals present do suggest that the environment was conducive to coral “thicket” growth.

The epitheca of many corals is also damaged, some show loss of the epitheca on one side only while others have a total loss of the epitheca. Rolling from one side to another could account for the abrasion of the epitheca on one side and transportation over longer periods of time could result in total loss. This damage to the epitheca, disarticulation and sign of regrowth is suggestive of damage created by current, wave or storm action. It is worth considering that loss

of the epitheca could also be the result of dissolution in an acidic water/sediment interface, possibly as the result of the breakdown of organic components. Ainsworth and Crowley (1994) suggested that the shoreline orientation on Stainmore was predominantly east to west and Fairbairn (1999) found that many bioclasts, mainly corals fragments, on the Alston block were orientated indicating a current direction generally from the south-south-east indicating currents were prevalent and running very near to straight towards the shoreline.

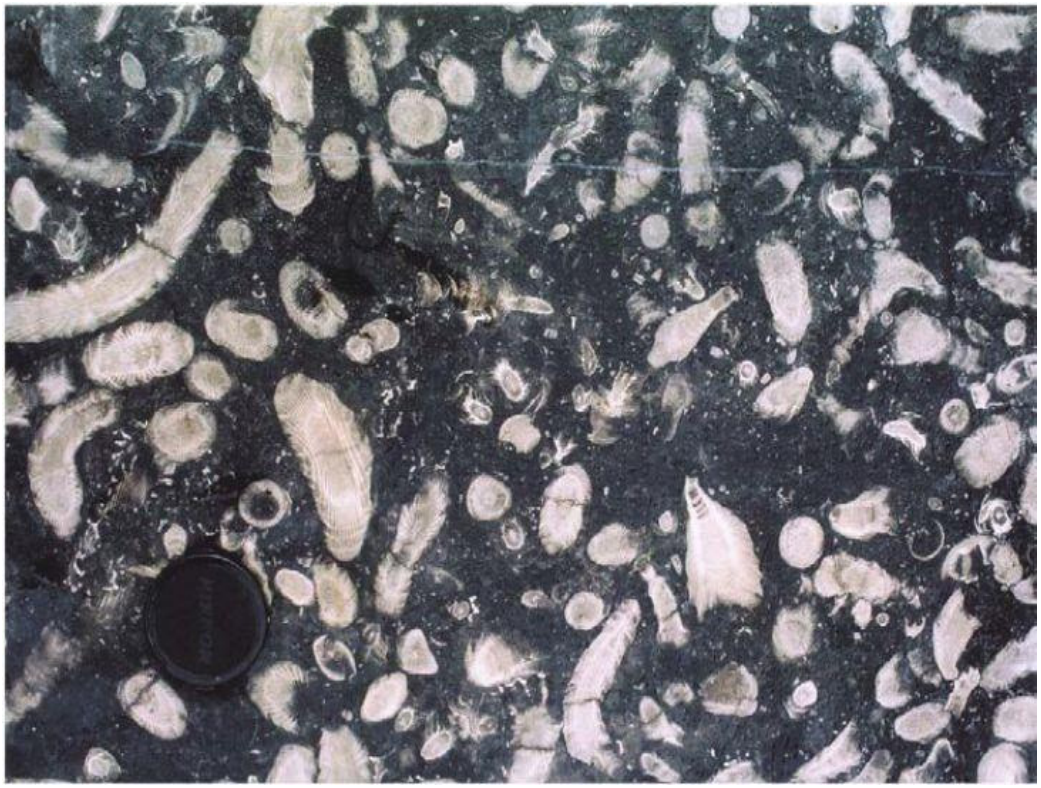

Figure 3.17. The coral *Dibunophyllum* within the Frosterley 'marble', of the Great Limestone. Note geniculate corals on the left hand side. Field of view 30×50 cm. Courtesy of M. E. Tucker.

On the whole there is little evidence of compaction within the limestones, some bioclasts undoubtedly did undergo breakage at both the sediment surface and after burial and an inspection of Figure 3.17 does reveal various breakages within corals. Pressure dissolution and grain to grain contacts are seen but they are limited and only significant adjacent to shale partings (Figs 3.7, 3.13 and 3.17).

Encrusting of skeletal parts during life and after death is not uncommon in the marine environment and where prevalent would suggest that encrusted

bioclasts were not covered by sediment straight after death. As it is not uncommon for skeletal parts to be encrusted during life and as sediments are often reworked then the use of encrustation as a true representation or proxy for an environment is difficult (Scoffin, 1992; Scoffin and Bradshaw, 2000).

To summarise, there is evidence for current activity and movement of the bioclasts and grains within the Great Limestone; however, the evidence does not necessarily suggest that the bioclasts have been transported over large distances. It is very unlikely that no bioclasts will have been transported from adjoining areas; however these may have been few and only small grains such as foraminifera. Storm reworking and deposition is also found in many places. Taphonomic evidence does support the probability that dissolution, mechanical damage and bio-erosion was prevalent as was encrustation, again not suggestive of long term transport. The evidence does suggest; therefore, that the fossil record of the Great Limestone; can be regarded as a true representation of the environment of deposition with the proviso that there is a bias against molluscan and other high magnesium calcite and aragonitic fragments.

3.6.5. Cementation within the Great limestone

Diagenesis of the Great limestone would have commenced almost immediately after deposition with major processes such as compaction, cementation, microbial micritisation, neomorphism and dissolution occurring. The magnitude of compaction would have depended upon the extent of cementation. The initial compaction, before cementation, would have resulted in porosity reduction and in some cases the change from an original lime mudstone or wackestone to packstone could also occur.

Photomicrographs of the Great Limestone at Hudeshope Beck show very little sutured grain to grain contacts and as such it is probable that lithification occurred early after sedimentation; however some grain to grain contact and chemical compaction can be seen (Figs 3.18 and 3.19). Stylolites and micro-stylolites are abundant showing chemical compaction of previously lithified

grains occurred (Figs 3.18 and 3.19); however, examination of micro-stylolites in photomicrographs suggests that loss of material is probably not substantial.

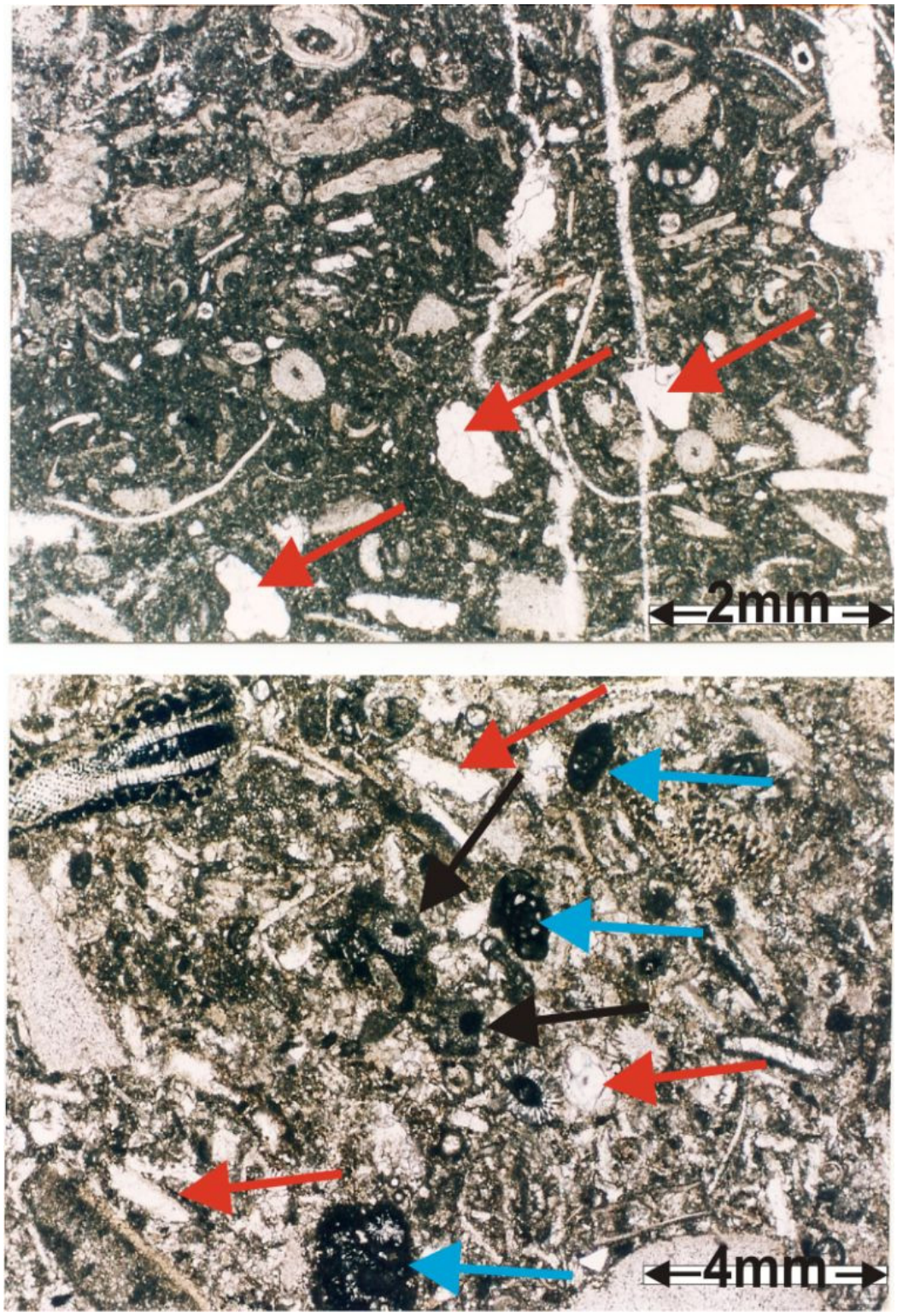

Figure 3.18. Photomicrographs of the Great Limestone. Note heavy micritisation of grains in bottom photomicrograph (blue arrows) whereas there is very little in the upper photomicrograph. Suture line running 'jaggedly up through the centre of the lower photomicrograph showing some loss of material on the sub-millimetre scale (black arrows) and mould of dissolved grains (red arrows). Scale bar 4mm on lower photomicrograph and 2mm on upper photomicrograph.

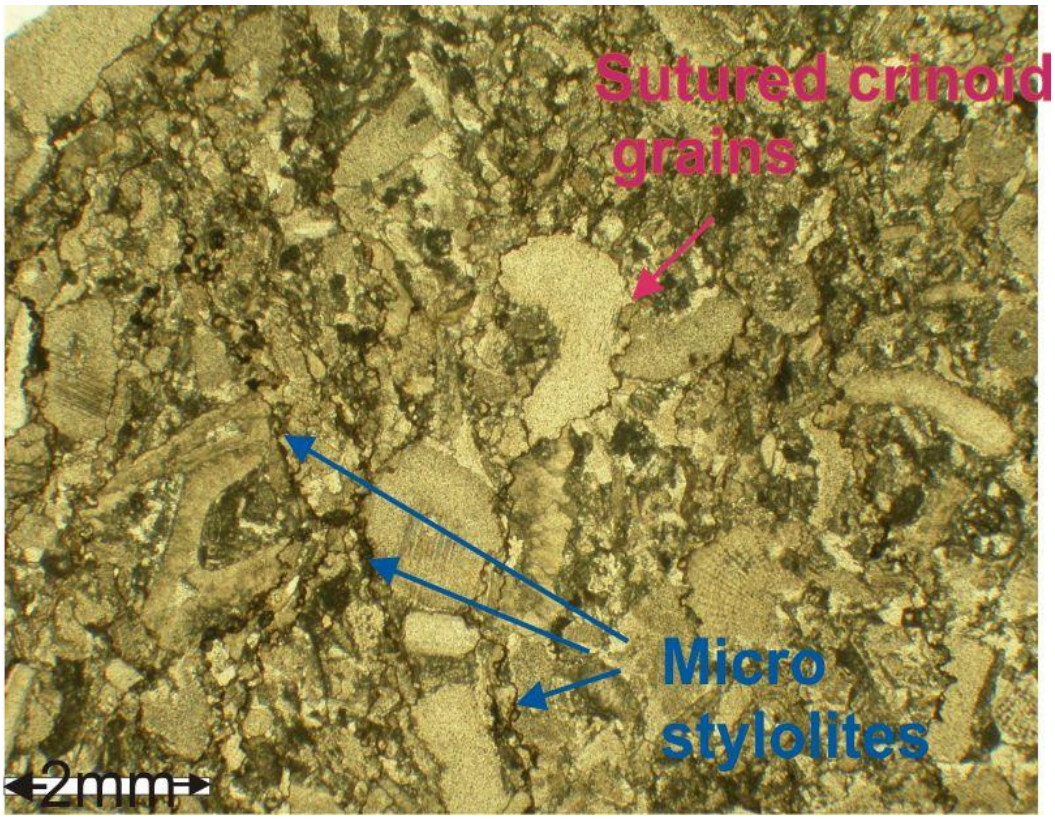

Figure 3.19. Photomicrograph showing micro-stylolites and sutured crinoid grains. Scale bar 2mm.

Due to the micritic nature of the sediment it is difficult to resolve any cement from the sediment itself; however, cement is visible within some large rugose corals (Fig. 3.20). It can be seen from Figure 3.20 that both isopachous and drusy calcite spar cements are visible within the corals, it also worth noting that the loss of the epitheca from the coral in the lower photomicrograph has resulted in filling of the septa with peloids. Peloidal structures are associated with many origins such as algal, replacement texture, and detrital sediment, product of pelletizing organisms or in situ precipitate (Tucker and Wright 1990).

Isopachous fringes of fibrous calcite are attributable to marine phreatic precipitation and as they are delicate in nature this suggests an environment where mechanical abrasion could not occur, hence the formation within the intraskeletal part of the coral. For the cement to form there must be an adequate exchange of seawater supersaturated with respect to calcium carbonate and to ensure this can occur an active pumping system would be required through the septa of the coral (Tucker and Wright, 1990). Growth of the cement would be slow with long

accumulation rates; therefore, the energy for this continuous exchange of supersaturated seawater would be due to currents or wave action rather than the occasional storm movement of water. The slow accumulation rate of the cement and the need for an active pumping system would suggest the corals were uncovered on the sea bed for a long period of time which in turn would require a slow sedimentation rate for the bed itself. The epitheca in the top coral is present even so; movement through the skeleton by supersaturated seawater would be required, suggesting mechanical damage to the coral must have occurred on the sea bed. Microbial micritisation is also visible upon the walls of the septa of the coral in the top of Figure 3.20.

Drusy calcite spar, seen within the corals in Figure 3.20, is a characteristic pore-filling cement of both burial and near-surface meteoric environments and it is recognised by the general increase in crystal size towards the centre of the void. It can be difficult to ascertain whether the drusy calcite is associated with burial rather than meteoric environments; however, if there is clear evidence for the spar to have been precipitated after mechanical or chemical compaction then a burial origin can be confirmed. Within Figure 3.20 it can be seen that the drusy calcite spar was precipitated after breakage of the walls of the septa, some of which are micritised, in both the top and bottom of Figures 3.20 which is suggestive of a burial origin for the cement.

Syntaxial overgrowths are not uncommon within the Great Limestone and are seen as echinoderm overgrowths. Syntaxial overgrowths can be associated with burial diagenesis, however they can also occur within near-surface marine as well as meteoric environments. Neomorphic coarse and micro spar is visible within various thin sections of the Great Limestone (Fig. 3.21) and this can be associated with either meteoric or burial diagenesis. Tucker and Wright (1996) discussed neomorphic coarse and micro spar and suggested that this can be recognised in thin-section by:

- Irregular, embayed to curved intercrystalline boundaries of spar cement.

- An irregular crystal size distribution and patchy development.
- Gradational and irregular boundaries to the areas of neomorphic spar.
- The presence of skeletal and other grains floating in coarse spar

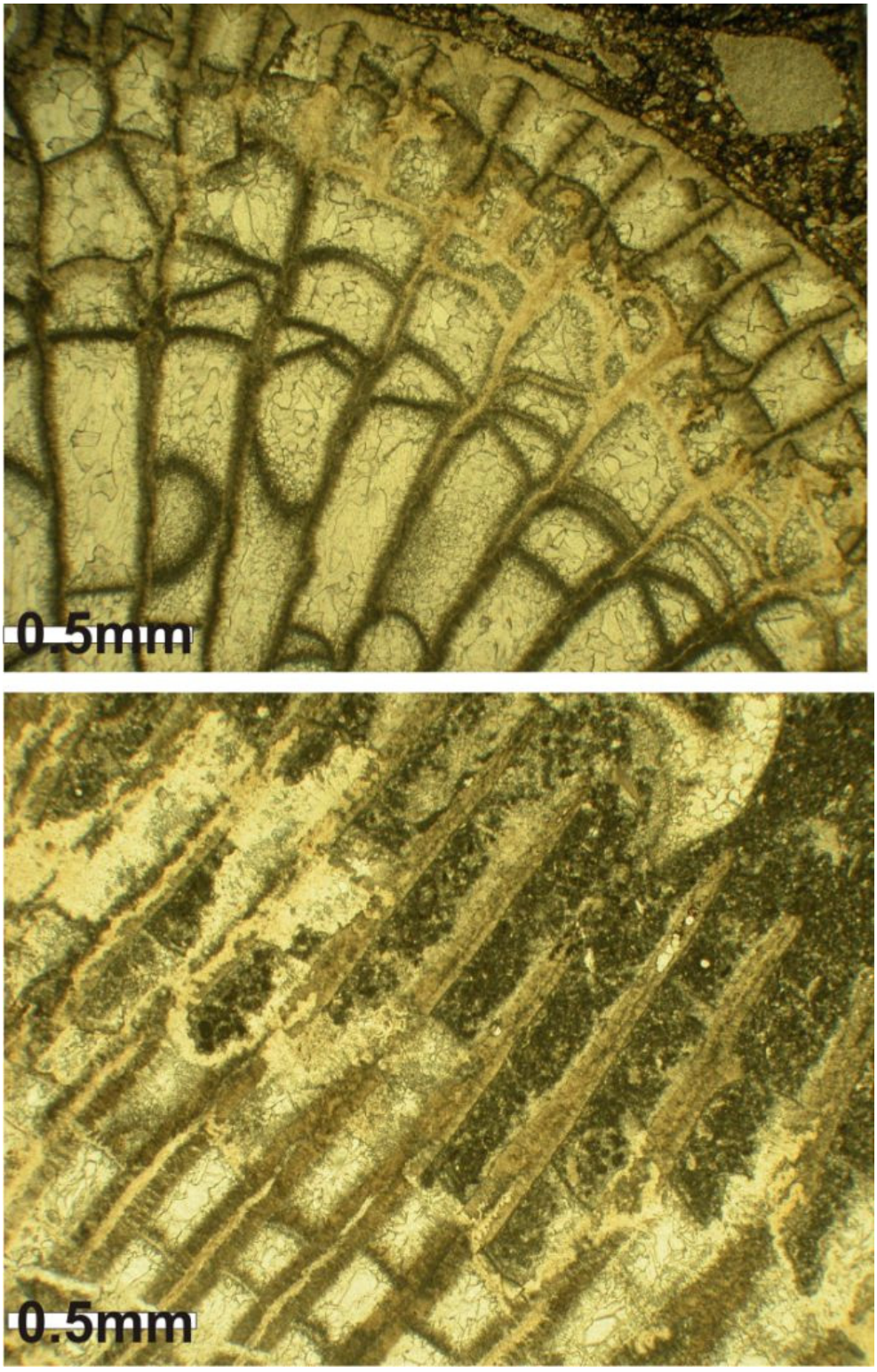

Figure 3.20. Photomicrographs of rugose corals. Peloidal infill can be seen within the bottom photomicrograph together with isopachous and equant cement. Isopachous and equant cement is visible within the top photomicrograph. Scale bars 0.5 mms.

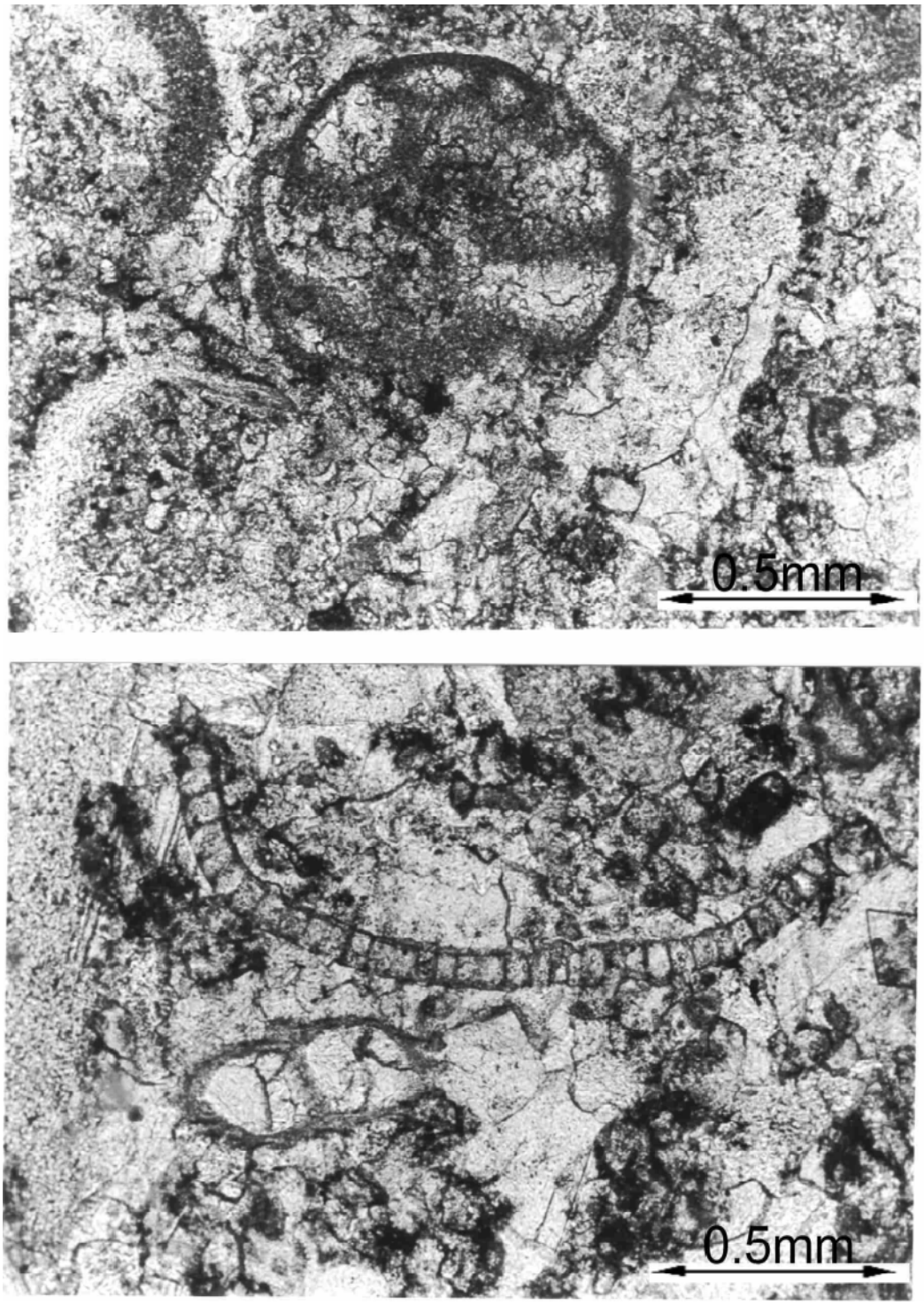

Figure 3.21 Coarse neomorphic spar and microspar.

It can be seen within Figure 3.21 that all the above points are visible confirming the presence of neomorphic spar. This aggrading neomorphism probable took place by the dissolution of grains and bioclastic fragments during early meteoric or burial diagenesis. Clay content is known to restrict the formation

of neomorphic spar; however, an assessment of the photomicrographs throughout the height of the Great Limestone at Hudeshope Bed does not suggest there is any clear relationship between the geochemical content of the limestone, or even the position of bedding planes, and the occurrence of neomorphic spar. It may be expected that as the bedding planes are approached and clay content increases then the occurrence of neomorphic spar should reduce; however this is not the case, possibly suggesting the clay content does not reach a limiting content; Bausch (1968) suggested that a limestone with more than 2% clay will not contain neomorphic spar.

3.6.6. Mudstone partings/bedding within the Great limestone

The Great Limestone, as with all of the mid-Carboniferous shelf limestones of northern England, have well-developed bedding (Figs 3.6 and 3.14). There are between 25 to 27 beds within the Great Limestone which vary in thickness from a few centimetres to a metre or more but generally they are in the range of 0.3 meters to 1 metre and an average thickness of 0.75 metres. The bedding is defined by thin shale partings 1–5 millimetres in thickness to thin mudstone inter-beds (generally less than 200 millimetres thick). Within the beds there may be a transition from the purer limestone to the mudstone parting over a few millimetres, but normally the contact is sharp. The bedding planes are generally planar (Fig. 3.22.) to undulating (Fig. 3.23.), and black from attached dark shale. Thin, millimetres thick calcareous units can be seen within some mudstone partings (Fig. 3.23) related to short increases in carbonate productivity. On inspection of Figure 3.23, even though the bedding is undulating, it can be seen that the mud bedding and the thin calcareous beds generally follow the undulating surface of the limestone bedding and this suggests that the undulating bedding surface is created through differential compaction of the bedding planes. Figure 3.24 shows a bedding plane with a high angle of repose. It is very likely that the angle of the bedding plane in Figure 3.24 is not an original deposition feature as it may be expected that the angle of repose of the deposited mud would have been exceeded resulting in slope movement which is not visible within the field, this again suggests that many of the undulating bedding planes are enhanced

by or are created by differential compaction of the limestone bed possibly due to differential cementation.

Figure 3.22. Planer bedded mudstone parting. Bedding plane approximately 60 millimetres thick. (Lanehead Quarry Weardale OS 39885 54052)

Figure 3.23. Undulating mudstone parting. Note thin calcareous units within bedding plane. Bedding plane approximately 20 millimetres thick. (Lanehead Quarry Weardale OS 39885 54052)

Figure 3.24. Undulating mudstone parting. Bedding plane varying between 10 millimetres and 30 millimetres thick. (Lanehead Quarry Weardale OS 39885 54052)

The bedding planes have commonly been affected by pressure dissolution and in some cases the bedding plane is a clear pressure dissolution seam with some anastomosing and dark clayey insoluble residue within the seams. There may also be stylolites parallel to the bedding, sutured and generally with less than 2 centimetres of relief along the surface. The general vertical distribution of the major stylolites is shown in Figure 1.2. The issue of pressure dissolution enhancing bedding planes, as well as creating them, has been addressed by Simpson (1985) and Bathurst (1987, 1991). Both of these studies actually involved Carboniferous limestones from the UK, and so the conclusions presented there are directly applicable to the rocks discussed here, namely that bedding planes were commonly enhanced by pressure dissolution, and indeed in some cases formed in that way; this is discussed further in Chapter 10. In the upper beds of the Great Limestone, the partings become a little thicker reaching 2–5 centimetres and this is regarded as being the transition from the limestone into the overlying marine mudstone (Fairbairn, 1978; Tucker *et al*., 2009).

For the mudstone partings/bedding planes to form a change in the marine environment is required resulting in carbonate production being reduced either with clastic deposition in a steady state or an increases in clastics resulting in the muddy bedding plane. Varker (1968) and Leeder and Strudwick (1987) suggested that the increase of mudstone and subsequent reduction in carbonate production within beds on the Askrigg Block was controlled by deepening of the marine environment and encroachment of the pro-delta mud plume. Carbonate deposition could have been interrupted or terminated by either a sea-level fall or sea-level rise, both resulting in an influx of clay into the environment to generate the shale partings and mudstone layers which define the beds (Fig. 3.25). During a sea-level rise, mud would be expected to be reworked from coastal mudflats in proximal areas, whereas, during a sea-level fall increased mud input to the shelf would result from increased river activity and down-cutting into floodplains and coastal mudflats. A decrease in carbonate production, not a total termination, is evident at bedding planes within the Great Limestone and this is also associated with increases in silica, aluminium and other river borne or re-worked sediment elements (Chapter 9). Figure 3.25 suggests that carbonate productivity increases with shallowing of sea-level and reduces with a sea-level rise; this would suggest that the increased input of clay and reduction of carbonate deposition required to form a bedding plane is more likely to have taken place through a sea-level rise, rather than a sea-level fall.

The individual bedding planes and partings could be the result of arid humid climate cycles (Fig. 3.25). A change in climate to a more humid phase could lead to increased clay input from increased river activity generating the shale partings. The influx of clay generating turbid water and increased freshwater runoff, reducing salinity, would both have a detrimental effect on carbonate productivity. Thus, it could be that the limestones were deposited during times of a more arid climate, with humid pulses leading to the deposition of the bedding planes and clay interbeds. Since the shale partings and mudstone layers are thin compared to the limestone beds this would suggest that the humid phases were short-lived; however, they could be horizons of condensation representing long periods of time. Fairbairn (2001) suggested that the supply of mud to the region

remained fairly constant throughout the deposition of both the Great Limestone and the bedding planes, with the thickness of the mudstone partings occurring at a rate of up to 100 times slower than the deposition of the limestone itself, i.e. the mudstone partings represent a considerable time span. In this scenario then, each unit of shale parting–limestone–shale parting would represent a humid–arid–humid climate cycle (Tucker *et al*., 2009). This possibility could very well have occurred without the need for a sea-level change occurring.

Up to a certain point, temperature can be a major control on carbonate productivity (Fig. 3.25); many organisms such as corals are dependent upon their environment experiencing only very small temperature changes. The individual bedding planes and partings could be the result of carbonate productivity being reduced through lower sea-water temperature. This reduction in temperature and a steady-state input of mud would allow shale partings or mudstone layers to accumulate to define the bedding. Changes to sea-water temperatures can be due to changes in sea-level or to regional weather patterns and could very well; therefore, have occurred without a sea-level change occurring. Fossil assemblages; however, do not show any systematic changes as the bedding planes are approached and corals are often seen at bedding planes. Even though temperature was important to the environment, the lack of any changes to fossil assemblages as bedding planes are approached would tend to rule out temperature changes being a major influence to bedding plane formation.

It is usual to assume that mud-size material is deposited within an environment of weak currents, hence the possible suggestion by Varker (1968) and Leeder and Strudwick (1987), discussed above, of deepening prior to formation of the bedding planes. Schieber *et al*. (2007); however, suggest that bedload transport and deposition of "flocculated muds" can occur at current velocities that would also transport sand sized material i.e. current velocities of 10 to 26 cm/s. This suggests; therefore, that a quiet environment is not always a prerequisite for mud deposition; flocculation of mud is the important factor. Either way it is obvious that environmental changes occurred to such an extent that the production of the bedding planes was possible.

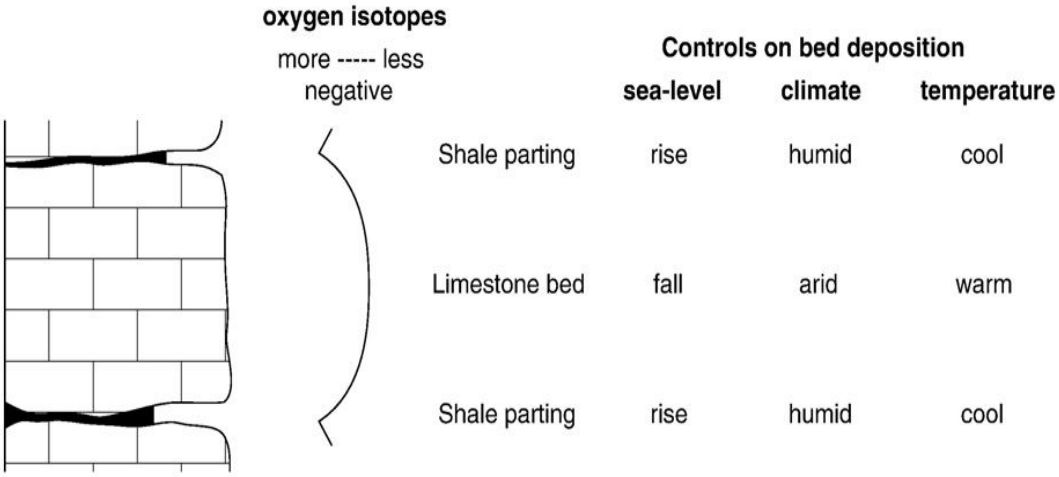

Figure 3.25 Possible explanations for the origin of the bedding planes and partings/mudstone interbeds which define the beds in the Great Limestone. The limestone beds themselves are discussed within section 3.6.7. The bedding planes and partings/mudstone interbeds could be the result of lower carbonate productivity in deeper water, with the clay input from reworking of mudflats, or a more humid climate (increased fluvial input) for the influx of the clay, or cooler water reducing carbonate productivity allowing clay to be deposited, The pattern of the δ18O data suggests that temperature itself is not the control, but does support a depth/sea-level and/or salinity (arid-humid climate) explanation and this will be discussed further in Chapter 7. See Tucker *et al*. (2009).

In conclusion, the bedding planes of the Great Limestone are generally sharp and planar; however, some can be seen to have undergone differential compaction resulting in undulating forms. Pressure dissolution features are common throughout the Great Limestone and in some cases the bedding plane is a clear pressure dissolution seam. The origin of the mudstone partings/bedding planes was assessed and three scenarios discussed; sea-level, climate and temperature, with regard to their ability to affect the formation of the bedding planes (Fig. 3.25). Carbonate productivity tends to increase with shallowing of sea-level and reduces with a sea-level rise suggesting that the increased input of clay and reduction of carbonate deposition seen at bedding planes, if sea-level changes are assumed, is more likely for the bedding planes to have formed during a sea-level rise rather than a sea-level fall. Climate and in particular changes between humid and arid conditions were also assessed and concluded with the possibility that each unit of shale parting–limestone–shale parting could represent a humid–arid–humid climate cycle occurring; a sea-level change was not a necessity for this scenario. The final assessment considered the impact of temperature on the formation of bedding planes. Even though temperature

changes are important upon carbonate production, it was felt that fossil assemblages did not support this scenario.

3.6.7 Bed thickness patterns

The continuity of the bed thicknesses within the Yoredale cyclothems has been recognised by many authors since Forster (1809) and Phillips (1836) and more recently Fairbairn (1978). Figure 3.26 is a Fischer Plot of bed thickness changes throughout the Great Limestone at Hudeshope Beck, Middleton in Teesdale where it can be seen that a pattern of thinning and thickening upwards through the limestone occurs, referred to here as bed-sets. Figure 3.27, constructed from data by Fairbairn (1978), shows that remarkably these bed-sets are also seen within the limestones throughout Teesdale and Weardale showing they are genuine widely developed patterns. Two full bed-sets are visible within the patterns of Figures 3.26 and 3.27, consisting of thinning-upwards and thickening-upward beds. Each bed-set consists of around 10 beds.

The widely set pattern of thinning-upward and thickening-upward bed thicknesses on a regional scale would suggest that a purely sedimentary (autocyclic) control is unlikely as this would be expected to result in anirregular bed thickness pattern. The well-organised nature of the patterns must; therefore, be created by some regular increasing-decreasing changing parameter(s) (allocyclic controls) (Tucker *et al*., 2009). The individual beds of the limestone and their thicknesses are correlatable over much of the platform which would suggest that the same depositional conditions were operating over the whole platform, and as discussed above, redistribution of sediment on a large scale throughout the platform is unlikely to have occurred.

Facies types would suggest that deposition of the Great Limestone took place within a mid-shelf environment; accommodation space was not being totally filled by the carbonate sediments and shallowing upward to peritidal carbonate facies and erosion of bedding planes through exposure is not evident except at the very top of the Great Limestone (see Section 3.6.8). As discussed in Section 3.6.6 sea-level changes could result in changes to carbonate production, with higher

rates and thicker beds at shallower depths and lower carbonate production resulting in thinner beds during deepening (Fig. 3.28). The same could also be true for the formation of the bed-sets with the thinning-up bed-sets occurring during sea-level rise and thickening-up bed-sets during a sea-level fall. The mechanism for these cycles could vary between Milankovitch rhythms to shorter time-scale sub-Milankovitch rhythms; these possibilities will be explored later in this thesis.

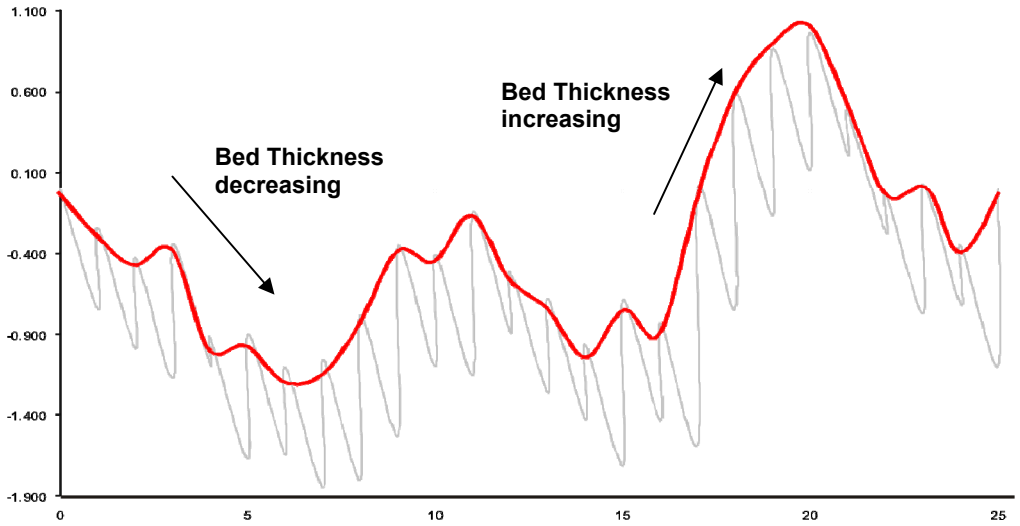

Figure 3.26. Bed-thickness pattern for the Great Limestone at Middleton in Teesdale. Data displayed showing the thickness of each bed (vertical line) successively through the limestone compared with the average thickness (diagonal line). Where there is an upward trend (rising arrow), beds are thicker than the average, and where there is a downward trend (falling arrow), beds are thinner than the average.

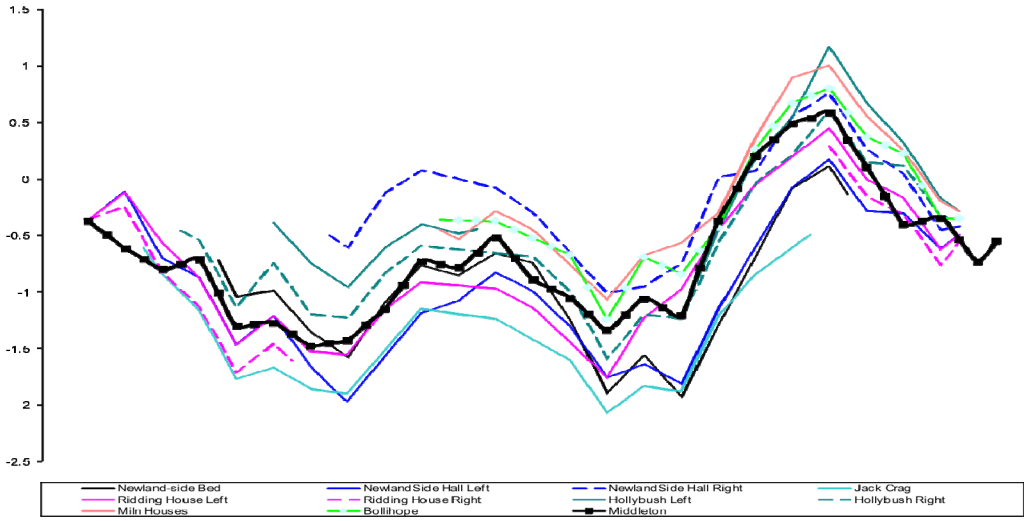

Figure 3.27. Bed-thickness patterns for the Great Limestone at 11 localities in Weardale and Teesdale displayed as cumulative deviations of bed thickness from the average through the succession, constructed from data by Fairbairn (1978). Where there is an upward trend, beds are thicker than the average, and where there is a downward trend, beds are thinner than the average.

As with the formation of bedding planes discussed in Section 3.6.6 climatic variations of arid to humid (dry to wet), with or without sea-level changes, could also explain the changes in bed thickness (Fig. 3.28), The influx of clay generating turbid water and increased freshwater runoff, reducing seawater salinity, during humid conditions would have a detrimental effect on carbonate productivity resulting in bed thicknesses and the bed-sets thinning. During more arid times, less rainfall, normal to slightly hypersaline seawater and clearer, less turbid seas would have led to higher productivity and so the trend to thicker beds and bed-sets.

Temperature changes, again not necessarily connected with changes in sea-level, are a further possibility (Fig. 3.28); temperature is a major control on carbonate productivity. Regional or global perturbations of temperature would be expected to affect carbonate productivity with higher temperatures leading to increased carbonate productivity which would give the trend to thicker beds, whereas lower temperatures would lead to the trend towards thinner beds.

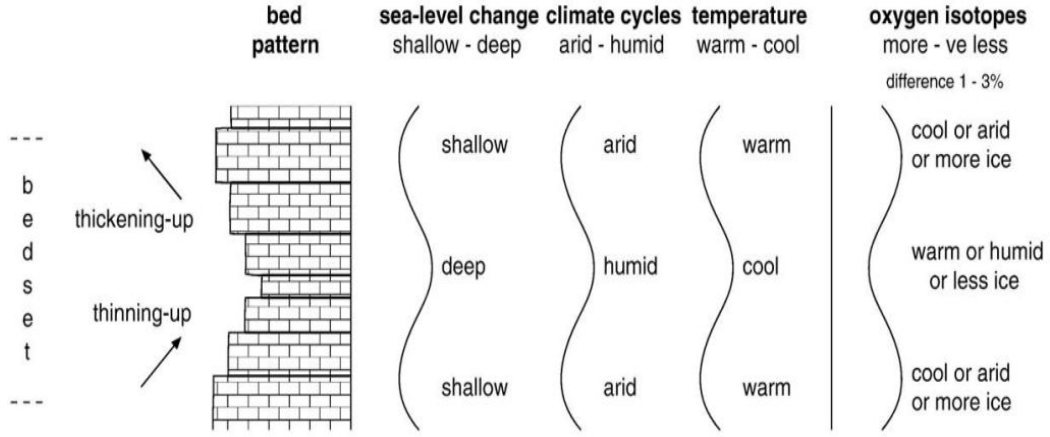

Figure 3.28. Possible explanations for the origin of the bed-sets in the Great Limestone, together with the generalised pattern of trends in the δ18O data to be discussed later in this thesis. Zones of thicker beds in the bedsets could be the result of higher carbonate productivity due to shallower water, clearer seas/lower rainfall (more arid climate) or higher temperature. Zones of thinner beds in bedsets could be the result of lower carbonate productivity due to deeper water or more turbid seas/higher rainfall (more humid climate) or lower temperature. The pattern of the δ18O data suggests that temperature itself is not the control, but does lend support to a depth/sea-level/ice-cap size control and/or a salinity-turbidity (arid-humid climate) explanation and this is to be discussed later. See Tucker *et al*. (2009).

In conclusion, there are three possibilities which could account for the formation of the bed-sets, sea-level changes, arid to humid cycles or temperature

changes. Carbon and oxygen isotope and geochemical variations within beds are considered in later sections within this thesis and will explore further the causation of the beds and bedset cycles.

3.6.8 Siliciclastic and minor cycles of the Great Limestone Cyclothem.

The sediments between the Tumbler Beds of the Great Limestone and the Little Limestone Cyclothem are of fluvio-deltaic lithologies consisting of at least three minor cycles of mudstone and sandstone and in some areas of the Alston Block 4 cycles of mudstone and sandstone are visible (Tucker *et al*., 2009). The mudstone generally coarsens up into the sandstone and these coarsening-upward packages are regarded as being minor cycles in their own right. Westgarth Forster (1809) described three sandstones within the minor cycles as the Low Coal Sill (average 3.0 metres thick), High Coal Sill (average 3.7 metres thick), and the White Hazel (average 2.1 metres thick). The mudstones, averaging up to 2 metres in thickness, usually contain a thin marine band at the base and the sandstones are commonly overlain by coal or a smut. The term sill, used here for the sandstones, must not be confused with the same term used today for a concordant minor igneous intrusion.

The coal formation at the top of the Great Limestone cyclothem is terminated by a marine transgression, the Little Limestone Cyclothem, considered by Dunham (1950) and Hodge and Dunham (1991) to be "... an apparently sudden event with little destruction of the sediment invaded". Elliot (1974) introduced the term abandonment stage for the cessation of clastic sediment supply and Hodge and Dunham (1991) suggested that Elliott's abandonment coal was the High Coal with a post-abandonment phase above this. It could be argued; however that the coals present in the Low Coal Sill and White Hazel are also abandonment stages with the marine incursions, above the coals of the Low Coal Sill, being regarded as a post- abandonment phase. In the case of the post-abandonment phases above the High and Low Coal Sills these are to a certain extent short lived and are dominated by terrigenous mud before returning to sandstone and a further abandonment phase. These short lived post-abandonment phases do not usually include a limestone phase; however, a sandy limestone has been reported in

Eastgate Cement Works in Weardale (949 365), but not witnessed by myself or seen on any available borehole logs, which may be correlated with the Low Coal and the Snope Burn Band of Trotter and Hollingsworth (1932).

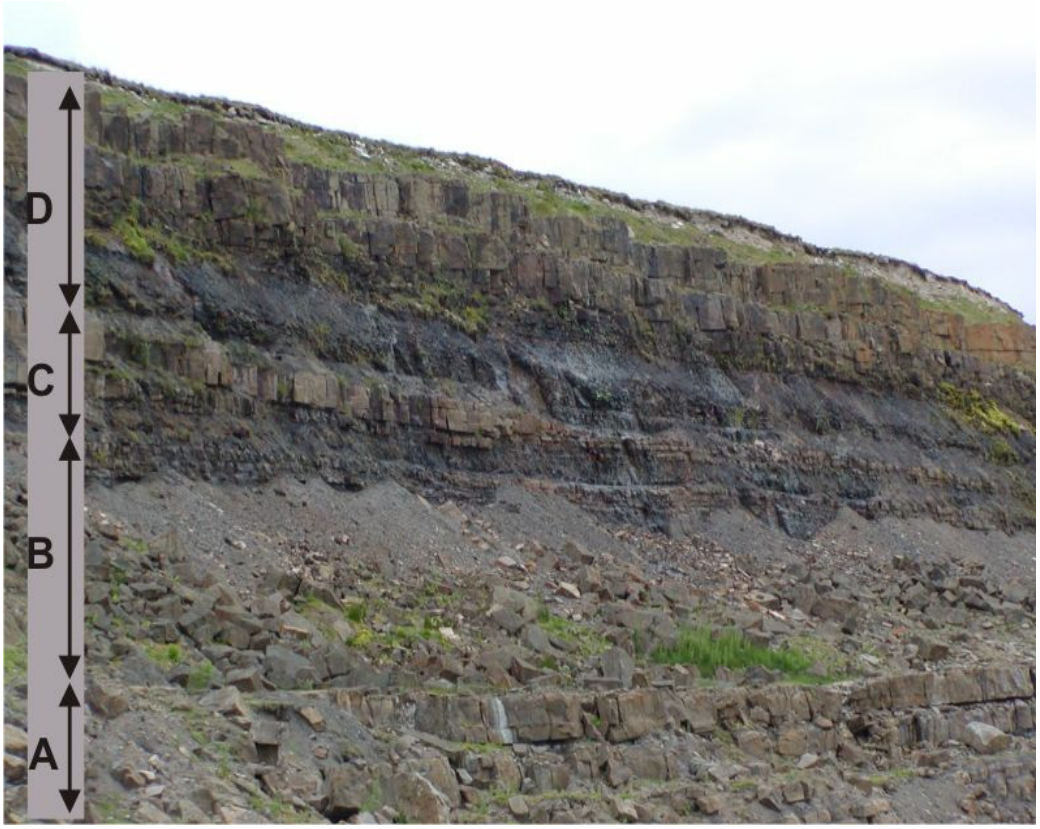

Figure 3.29 Eastgate quarry. A = top of Great Limestone. B = Low Coal Sill minor cycle. C = High Coal Sill minor cycle. D = White Hazel minor cycle. Height between top of the Great Limestone to the top of the White Hazel approximately 25 metres

In general the termination of deposition of the Great Limestone was preceded by deposition of prodelta mud, as would be expected in a standard Yoredale lithological sequence; however a further coal is seen within many of the borehole logs from Eastgate Cement Works in Weardale (949 365) lying directly on top of the Great Limestone itself, suggesting emergence of the Great Limestone occurred; Elliot (1975) found evidence for this coal at Crawleyside quarry in Weardale (998 399). Hodge and Dunham (1991) also found evidence for emergence of the Great Limestone at Stotfield Burn Mine (944 424) Boltsburn Mine and Jeffries Engine Shaft Hunstanworth (960 478). Hodge and Dunham (1991) found that this emergence episode was limited to the Weardale and Teesdale area, covering approximately 100 Km^2 and was probably the result of an

area of peat forming swamp; the coal was named by Hodge and Dunham (1991) as the Blackband. The Blackband at Eastgate Cement Works is associated in some cases with a band of chert possibly a continuation of the Main Chert within Swaledale on the Askrigg Block (Fig. 3.5); however, one log description from Eastgate Cement Works referred to the chert containing black wispy stylolites suggesting this is in fact a silicified limestone.

The position of the marine bands within the post-abandonment mudstones above the sandstones and coals of the minor cycles is not always evident within the many borehole logs from Eastgate Cement Works; however, Hodge and Dunham (1991) considered the marine bands to be reasonably continuous throughout much of the Alston Block. In many of the boreholes inspected at Eastgate Cement Works, the mudstones, siltstones and sandstones, are described as being non-calcareous and containing no fossils, whereas, in other boreholes, still described as non-calcareous, fossil debris such as brachiopods and crinoids are found within these post-abandonment phases. One sandstone bed, approximately 1 metre thick, within the High Coal Sill is also seen to contain fossil debris.

Where the fossiliferous mudstone facies occurs within the post-abandonment stage directly above the Great Limestone, or the Blackband, this varies from a few centimetres thick to around 4 metres in thickness. Within Snaisgill Sike (395415 526952), a few hundred metres east from Skears Quarry in Hudeshope Beck this mudstone is approximately 2 metres thick; fossil debris was not found. Within the post-abandonment mudstones above the High and Low Coal Sills on the Alston Block, the beds with fossiliferous debris is usually only a few centimetres in thickness; the fossils usually consist of brachiopods and crinoid debris. The occurrence of marine fossils, even though sparse, and the mud size sediment, are suggestive of deposition in a low energy environment below storm wave base; however, as discussed above, Schieber *et al*. (2007) suggested that bedload transport and deposition of "flocculated muds" can occur at current velocities that would also transport sand-sized material, suggesting that a quiet environment is not always a prerequisite for mud deposition.

Above the fossiliferous mudstone the facies changes to a mudstone with greater silt content and plant debris marked by carbonaceous streaks. Marine fossils are extremely sparse throughout this facies and die out vertically, probably suppressed by the plant debris; Hodge and Dunham (1991) suggested this phase may also have been anaerobic. Alternations of mudstone and siltstone, with some fine sandstone, on the millimetre scale appear towards the top of the facies with typically sharp contacts in places. The preponderance of mudstone throughout this facies would suggest a similar environment to that for the fossiliferous mudstone facies, i.e. low energy environment below storm wave base; however, the increase in siltstone and sandstone towards the top would suggest a shallowing up and increase in energy, probably storm-generated.

Figure 3.30 Low-angle cross-stratified bedding with sharp contacts, Snaisgill Sike (395415 526952). Field of view approximately 480 by 350 millimetres. (Hudeshope Beck)

The change from the fossiliferous mudstone facies to a non-fossiliferous facies containing greater silt content is not distinct and in most cases this is difficult to ascertain in the field, or even within borehole logs. This change between facies can only be regarded as being gradual with a hardly perceptible

coarsening up. Above the non-fossiliferous facies silt increases towards thin centimetre thick sandstone beds; Ainsworth and Crowley (1994) recorded hummocky cross stratified beds up to 150 millimetres thick within these sandstones on the Alston Block and within the Stainmore Basin. Cross stratification is visible in Snaisgill Sike within the initial minor cycle (Fig. 3.30). The sandstones are erosively based and interbedded with mudstone and siltstone. The occurrence of mudstone, siltstone and fine sandstone still suggests a low energy environment very near to storm wave base with storm activity continuing to affect deposition creating the sandstones and cross-stratified beds.

Figure 3.31 Swaley cross-stratified bedding Sleightholme Beck (953 105). Field of View approximately 1.1 metres by 0.85 metres. (Sleightholme Beck OS 953 105)

The sandstones above these mud and siltstone layers have both transitional and erosive contacts and generally become thicker vertically. They have been described by Ainsworth and Crowley (1994) as consisting of swaley cross-stratified and hummocky cross-stratified sandstone, planer laminated sandstone, trough cross-bedded sandstone, inclined stratified sandstones and rooted sandstones. These sandstone facies can be interpreted to vary from deposition in the high-energy sediment-laden currents at or above fair-weather wave base in the

shoreface to foreshore zone. Swaley-bedded fine-grained sandstone is seen within Sleightholme Beck (953 105) where down-cutting into a very fine grained sandstone can be seen (Fig. 3.31); planar bedding is seen to return at the top with a two centimetre thick bed before thinning beds thin again. The occurrence of the swaley cross-stratification and planar bedding suggests it was deposited from sediment-laden currents in a high-energy environment. The thinning of the beds at the top is suggestive of a reduction in sediment load. It was not possible to ascertain an exact position in the sequence this exposure belonged to, however; it was thought to be within the High Coal Sill sequence.

Dunham (1948) recognised sandstones on the Alston Bock which were much thicker than the sheet sandstones of the Low and High Coal Sills. The sandstones were noted to generally consist of fining-up sandstone and in places a conglomerate is found. One sandstone in particular, was recognised as a large palaeodistributary channel with sandstones occupying up to 90 percent of the thickness between the Great and Little Limestones. The thickness of the channel varies with a maximum thickness of 29 metres. This large distributary channel is known as the Coal Sill or Allercleugh Channel (Fig. 3.5). The sandstones of the channel are known, in places, to cut down to the limestone and have been recorded by Hodge and Dunham (1991) to cut into the top of the limestone itself; however over much of the area a couple of metres of mudstone exist between the top of the Great Limestone and the sandstones. At Sunny Brow Mine (878 390), north-west of St John's Chapel, Weardale, the channel has an irregular eroded base which cuts 8 metres down into the Great Limestone. The channel is associated with the Low and High Coal Sills; however, as the High Coal can be found on top of the sandstone it must predate this (Hodge and Dunham, 1991).

The White Hazel minor cycle is the final phase of the Great Limestone cyclothem, i.e. the abandonment phase of the Great Limestone cyclothem. This phase is generally very similar to the abandonment phases of the Low and High Coal Sills; however, it differs in that the sandstones are more flat bedded and include a fossiliferous sandstone facies; a coal is seen to cap the cycle in places before the commencement of the Little Limestone cyclothem. The White Hazel is

seen to thicken towards the west and south west of the Alston Block and in particular within Skears Mine (396 523) near to the Hudeshope Beck area, where it is seen to thicken to 22 metres. In places the White Hazel replaces both the Low and High Coal Sills with only a few metres of mudstone between it and the Great Limestone (Hodge and Dunham 1991). The thick sandstones of the white hazel were reported by Dunham (1948) and first attributed to a late palaeodistributary channel; however, further investigation by Hodge and Dunham (1991) confirmed that the sandstones coarsen up and confirmed a sand-bar environment. This sand bar they named as the Skears Sandbar. Figure 3.5 shows the extent of the Skears Sandbar near to Middleton in Teesdale. The normal succession of at least 3 cycles returns very quickly off the edge of the bar as can be seen at Snaisgill Sike only a few hundred metre away from the location within Skears mine.

3.7. Conclusion.

This chapter described the Carboniferous "Yoredale Cyclothems" on the Alston Block of Northern England. The Structure of the Alston Block is constrained to the north, south and west by major fault systems, some acting as hinge lines during the Carboniferous, and the Block tilts to the east. The submergence of the Alston and Askrigg Blocks in the late Asbian in the form of a shallow epeiric sea resulted in marine carbonate conditions prevailing with terrigenous sediment encroaching on to the northern margins of the Alston Block only by the end of the Asbian. The initial marine transgressions extended into the Northumberland Basin; however, siliciclastic/deltaic sedimentation prevailed over much of that area as the subsiding basin was filled. By the Brigantian and early Namurian the marine transgressions extended over the whole of the Mid-Northumberland Basin and deposition of major cyclothems occurred, some extending far to the north beyond the margins of the Northumberland Basin, and the shoreline extended beyond the southern margin of the Askrigg Block.

Products of fluvio-deltaic and shallow-marine carbonate sedimentation, the Yoredale cycles of the Late Viséan and Namurian are mixed clastic-carbonate high frequency sequences varying from 5 to 50 metres in thickness with the standard Yoredale Cycles in northern England being dominated by terrigenous

sediments, whereas the limestone units form a proportionately smaller part of the cycle. The proportion of siliciclastic sediment increases to the north-east and the limestone thickness increases to the south-west.

The facies and microfacies of the Great Limestone are typical of a shallow-marine environment, i.e. outer shoreface/transition to offshore environment. The environment is suggested by the geochemistry, sedimentary structures and fossil assemblages, to be very stable with only occasional storm reworking and incursions of prodelta mud before the final advancement of true delta conditions.

Three biostromes exist within the Great Limestone; the *Chaetetes* Band is to be found within either of the bottom two beds and consists of the sclerosponge *Chaetetes depressus* or replaced with compound corals such as *Diphyphyllum* or *Lonsdaleia laticlavia*. Small lenses a few centimetres across of *Chaetetes* can also be found throughout the height of the Great Limestone. The Brunton Band lies within the central part of the Great Limestone and consists of the alga *Calcifolium bruntonense* sp. nov., only recognisable within thin-sections. The Frosterley band, characterised by abundant remains of simple rugose corals is surprisingly continuous throughout the Alston Block where it can be seen either as a single biostrome or many individual biostromes separated by thin limestone.

Apart from the biostromes there is no observable change in the proportions of the various bioclastic elements throughout the Great Limestone at Hudeshope Beck; all samples are similar — bioclastic wackestone–packstone with a range of skeletal fragments. It seems clear that the limestone beds were all deposited under similar conditions, although, presumably specific local conditions allowed the coral-brachiopod biostromes to form.

There is evidence for current activity and storm reworking of the bioclasts and grains within the Great Limestone; however, the evidence does not necessarily suggest that the bioclasts have been transported large distances. Dissolution, mechanical damage, bio-erosion and encrustation was prevalent and

it is suggested that the fossil record of the Great Limestone can be regarded as a true representation of the environment of deposition.

Isopachous and drusy calcite spar cements are visible within skeletal fragments which are attributed to marine phreatic conditions where the fragments were left uncovered by sediment for long periods of time. Neomorphic spar is visible within some thin-sections suggesting dissolution of grains and skeletal parts during shallow burial diagenesis.

The bedding planes of the Great Limestone are generally sharp and planar; however, some can be seen to have undergone differential compaction resulting in undulating surfaces and pressure dissolution features are also common throughout.

Fischer Plots of bed thickness changes at Hudeshope Beck, and Weardale were constructed which showed that there is a pattern of thinning and thickening upwards through the limestone and remarkably these bed sets are genuine widely developed patterns created by some regular increasing-decreasing changing parameter(s) (allocyclic controls). Two full bed-sets, consisting of around 10 beds, are visible within the Fischer Plots consisting of thinning-upwards and thickening-upward beds. The individual beds of the limestone and their thicknesses are correlatable over much of the platform suggesting that the same depositional conditions were operating over the whole platform.

4.0 Thickness Variations of Carboniferous Cyclothems and the Great limestone

4.1 Introduction

There are significant thickness variations within the Great Cyclothem and these are well documented (Fairbairn, 1978; Hodge, 1965). The relationships of these changes to thickness variations within other cyclothems above and below the Great Cyclothem; however, are not as well documented. A comparison of thickness variations within the Great Cyclothem with other cyclothems was therefore carried out to ascertain whether or not any major local controls were in action on the block during deposition. It was not deemed essential, or indeed possible, to include the full thickness of strata from the Asbian to the Westphalian in the investigation. In fact for simplicity in the display of cross sections and due to the lack of thickness data for many cycles, the following cross sections commence with the Scar Cyclothem in the Brigantian and cover the cycles up to the Little Cyclothem in the lower Namurian.

Each cyclothem is laterally persistent over an area exceeding 10,000km^2 and as discussed in Chapters 2 and 3 usually consists of a limestone unit overlain by coarsening-up clastics and locally topped by a palaeosoil or coal. The cyclothems vary between 5 to 50m in thickness and generally the limestone units are thinner in the Northumberland Basin to the north of the Alston Block and the siliciclastics are generally thicker. Various records and data sets exist which reveal thickness variations within the cyclothems and even within individual beds on the Alston Block (Dunham, 1990; Fairbairn, 1978; Hodge, 1965). Major channels, washouts and sheet sandstones are also well known on the Alston Block, These include washouts in the Iron Post cyclothem which, in places, has removed the argillaceous and limestone units; the Pre-High Coal Sill (Allercleugh) palaeodistributory channels, sheet sandstones (High and Low Coal Sills), the Skears Sandbar in the Great Cyclothem and the Rogerly channel in the higher cycles at and below the Lower Felltop Cyclothem; for clarity the position of the Pre-High Coal Sill (Allercleugh) palaeodistributory channel and the Whin Sill are excluded from the sections.

The following average thicknesses, isopachs and contours were constructed using data from a Memoir of the British Geological Survey (Dunham, 1990), records from the British Geological Survey collection at Edinburgh, and a PhD thesis (Hodge, 1965).

4.2 The Cyclothems

Table 4.1 gives average thickness data for the seven cyclothems on the Alston Block studied in this Chapter, i.e. from the Scar Cyclothem in the Brigantian to the Little Cyclothem in the lower Namurian. A brief account follows giving general descriptions of the limestones and the terrigenous units. Where known the description of minor cycles within the cyclothems are also discussed. Minor cycles are defined here as a coarsening up from a mudstone of marine facies to a sandstone (Dunham, 1996), the sandstones would be expected to be topped by a coal or smut. However these are not always visible in the field or described in logs; nevertheless, the simple coarsening-up sequence is assumed to indicate a minor cycle. Figure 4.1 is a generalised section through the cyclothems discussed in this chapter and it may be noted that the Iron Post Cyclothem is included within the Four Fathom Cyclothem; this is discussed further in the text.

Cyclothem name	Average cyclothem thickness/m	Average combined sandstone thickness/m	Average combined mudstone thickness/m	Average limestone thickness/m	Number of minor cycles
Little	44.8	25.6	21.5	3.0	3
Great	37.1	9.0	9.0	19.1	4+
Iron Post	8.1	2.8	4.8	0.5	} 4
Four Fathom	24.9	7.4	11.0	6.5	
Three Yard	27.6	9.5	18.1	2.9	0
Five Yard	18.2	9	4.5	4.7	0?
Scar	22.8	7.8	6.0	11.0	3

Table 4.1 Average thickness data in metres for the cyclothems studied. After Dunham, 1990.

The cyclothems discussed within this chapter were, as discussed in Chapter 3, deposited in the shadow of a large Deltaic System and in a time of rising and falling

sea levels. Advancement of distributory channels cutting down into the deposited sediments is not unexpected in this type of environment and as such all cyclothems discussed here have resulting channels, ranging from large to small channels, the larger channels only are noted within the following text.

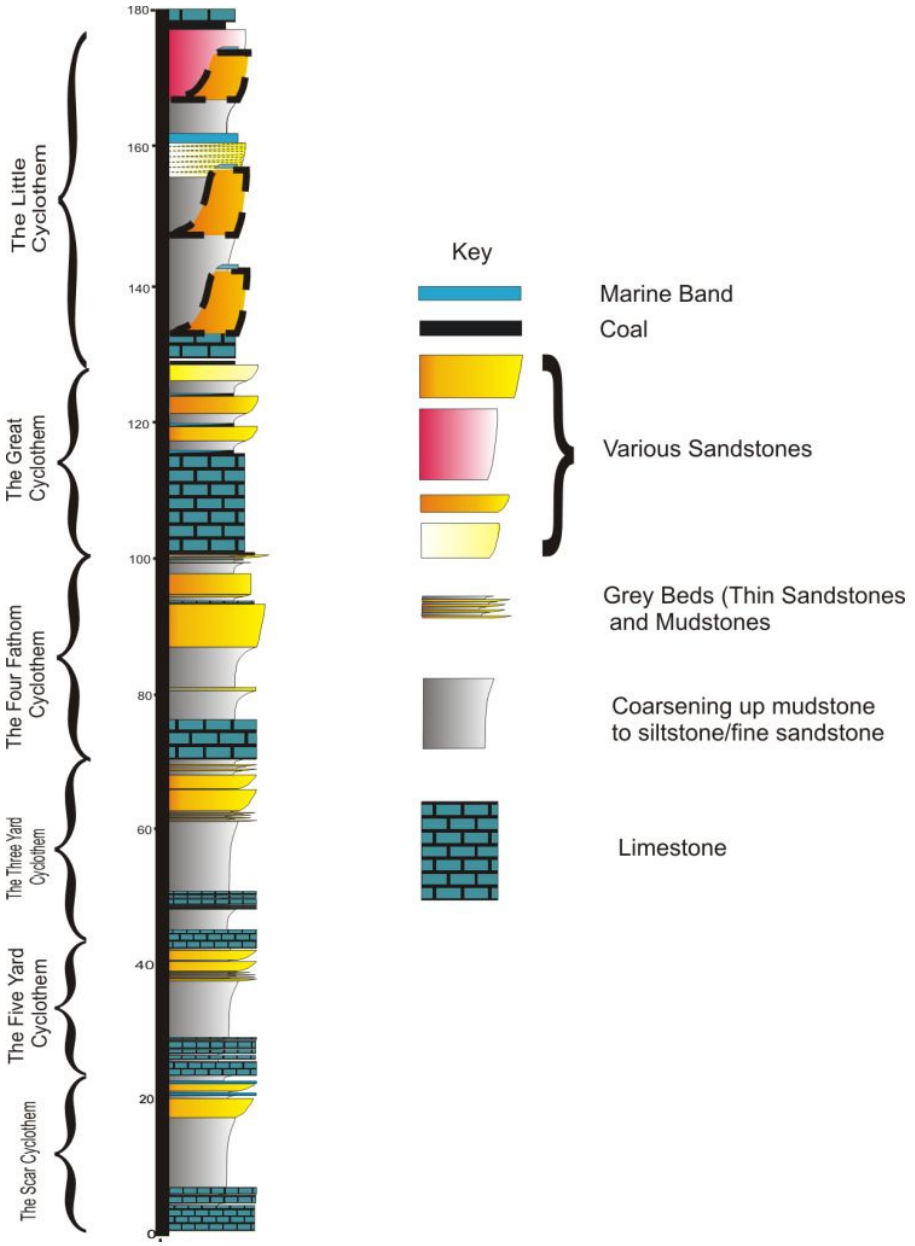

Figure 4.1. Generalised sections through the cyclothems discussed in this chapter.

4.2.1 Little Cyclothem

The Little Limestone is a relatively pure crinoidal limestone and despite its name this is often recorded as the thickest of the cyclothems investigated in this chapter at an average of approximately 45 metres thick; see section lines and statistics in Appendices A, B and C. The limestone itself is thin in comparison to the actual cyclothem averaging only 3 metres but reaching 6.4 metres in thickness at Harehope Gill Mine (004 349). Within north Yorkshire on the Askrigg Block and Stainmore Basin, Wells (1957: 1960) reported chert filled vertical borings within the limestone. A mudstone, up to 24 metres thick locally succeeds the limestone and above this, are sandstones consisting of three individual horizons; the Pattinson Sill (average 10.1m), the White Sill (average 5.4m) and the Firestone Sill (average 10.1m); south on the Askrigg Block 2 sandstones only are seen separated by a thick mudstone. In Dunn Fell Hush the Pattinson Sill and the White Sill are unrepresented; however the 30 metres of mudstone between the Little Limestone and the Firestone Sill contains 3 marine bands (Dunham, 1990). A coal is usually present on top of the Firestone Sill. Marine bands are usually present above both the Pattinson Sill and the White Sill; the post-abandonment phases.

4.2.1.1 The Pattinson Sill

The first sandstone within the Little Cyclothem is named as the Pattinson Sill. This sandstone very often appears directly above the limestone whereas other occurrences of the sandstone begin up to 9 metres above the limestone; the sandstone very often contains marine fossils. Dunham (1990) suggested that the so-called Pattinson Sill is actually several different lenticular sand bodies and their correlation throughout the block may actually be flawed. A sandstone 24 metres above the limestone, at Hunstanworth, which is 9 metres thick is called the Pattinson Sill; however, Dunham (1990) suggested this probably corresponds to the White Sill. Marine shales and even thin limestones have been recorded above various sandstones referred as the Pattinson Sill; however, it is difficult to correlate these throughout the block. The individual relationships and changes to the Pattinson Sill throughout the block are therefore complicated (Figure 4.2).

4.2.1.2 The White Sill

The White Sill is separated from the Pattinson Sill by 6 to 12 metres of shale. The sandstone itself varies between 1.5 and 7.6 metres thick and is often seen as alternations of sandstone and shale.

4.2.1.3 The Firestone Sill

Overlying the White Sill is a shelly sandstone or mudstone and above this a mudstone varying between 1.5 to 15 metres thick lies below the sandstone of the Firestone Sill. The Firestone Sill varies from a coarse sandstone in the south of the block around Weardale and Teesdale to a medium-grained sandstone elsewhere and in some areas this is overlain by a ganister. The Firestone Sill is quite often overlain by a coal, which can reach up to 0.45 metres thick, and this underlies the limestone of the Crag Cyclothem.

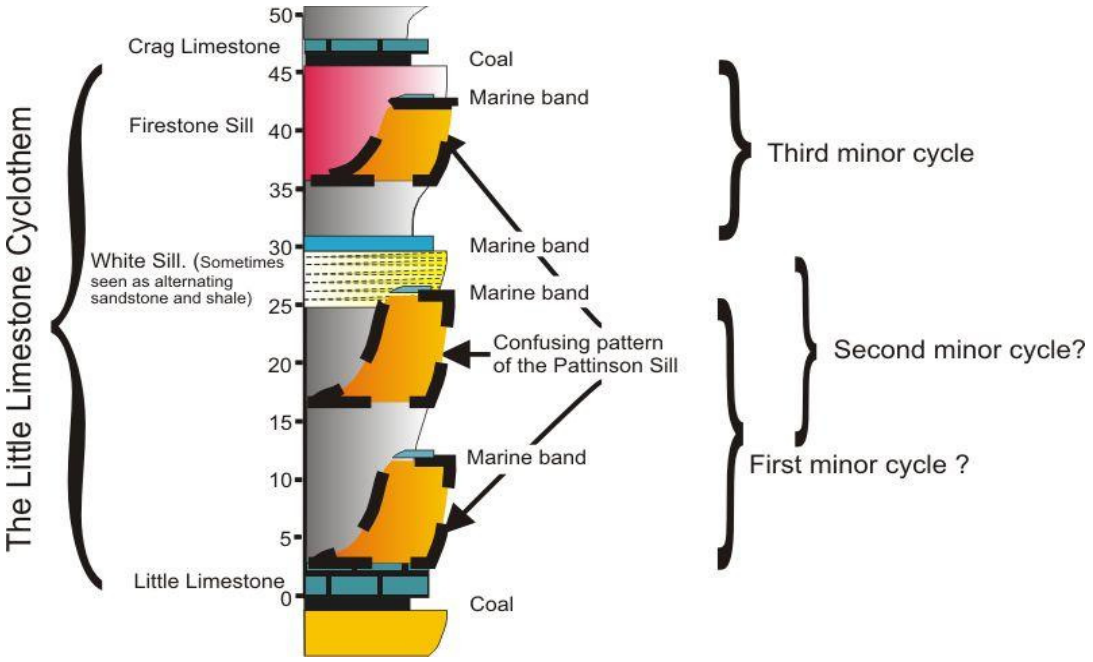

Figure 4.2 Generalised section of the Little Cyclothem and minor cycles. Note confusing pattern of the Pattinson Sill minor cycle.

4.2.2 Great Cyclothem

The Great Cyclothem (Figure 4.3) has been described in detail within Chapter 3 and, therefore, the following description will summarise the points only. The Great

Cyclothem is the basal member of the Namurian and underlies the Little Cyclothem. Whereas the Great Cyclothem varies considerably in thickness on the Alston Block it has an average thickness of 37.1 metres with the limestone taking up approximately 50% of the thickness. The limestone is thicker than most in the Carboniferous of the area at around 19 metres and is more like the Brigantian limestones rather than the other limestones in the Namurian. The Great Cyclothem sits upon the Iron Post Cyclothem and beneath the limestone of the Little Cyclothem.

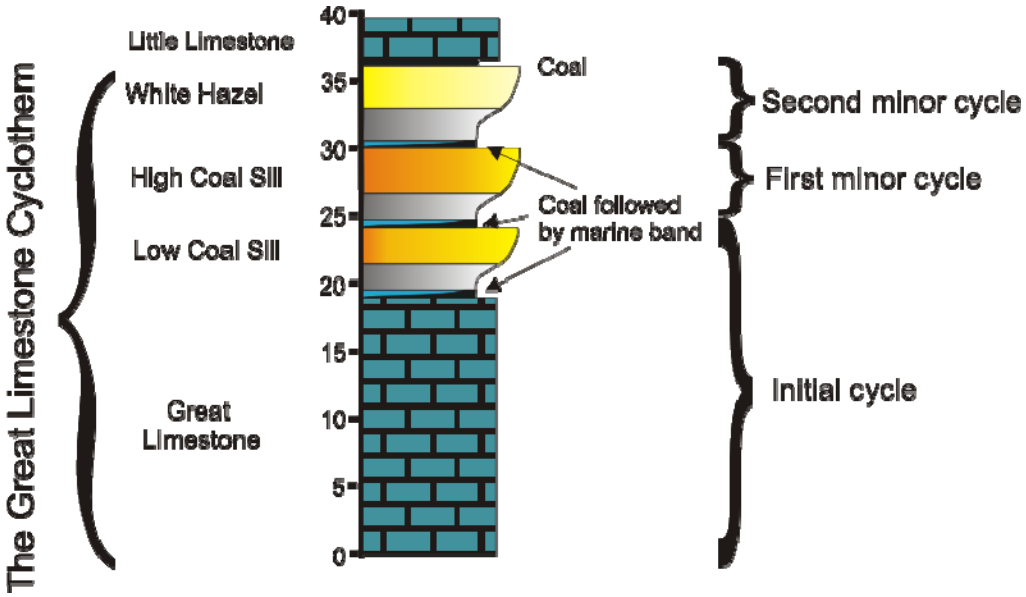

Figure 4.3 Generalised section of the Great Cyclothem and minor cycles.

The siliciclastics of the Great Cyclothem average 18 metres thick with the average combined thickness of the sandstones being 9 metres and the mudstone 9 metres. There are three main and some minor sandstones, the main sandstones being the Low Coal Sill (average 3.0 metres), the High Coal Sill (average 3.7 metres), and the White Hazle (average 2.1 metres). These sandstones are separated by mudstones with the mudstone above the limestone averaging 5 metres in thickness, the mudstone above the Low Coal Sill averaging 2.5 metres and the mudstone above the High Coal Sill averaging 1.5 metres. In some areas, the sandstones have completely removed the mudstones and in others, the Low Coal Sill is absent giving a thicker mudstone.

The High Coal Sill, as discussed in Chapter 3, is known to cut down to the limestone in a large distributory channel known as the Coal Sill or Allercleugh Channel (Figure 3.5). The uppermost of the sandstones, the White Hazle, varies considerably in thickness; in Skears Mine (395700 523080), it is up to 22 m thick and it is thought to be a remnant of a barrier island or sandbar (Hodge and Dunham, 1991) (Figure 3.5).

Coals can be found on top of all the 3 main sandstones which are usually only a few centimetres thick and are very often represented by a smut. The coals, however, are not persistent throughout the block and are often missing. Unusually, a coal is present directly on top of the Great Limestone within parts of Weardale and Teesdale and this is attributed to emergence of the limestone in this area and the formation of a peat-forming swamp (Hodge and Dunham, 1991). Above the sandstones, or the coals if present, a marine band is often present as the commencement of the next cycle, the post-abandonment phase occurs. Hodge (1965) showed various fossiliferous marine band horizons within the siliciclastics phases; however, they are not continuous throughout the Block.

4.2.3 Iron Post Cyclothem

The Iron Post Cyclothem (Figure 4.4) is the highest in the Brigantian lying directly below the Great Cyclothem. The average thickness of the Iron Post Cyclothem is 8.1 metres with the limestone averaging 0.5 metres and the siliciclastics 7.6 metres. The sandstone, the Tuft, averages 2.8 metres thick and the mudstone 4.8 metres thick; immature coals are not uncommon throughout the thickness of the sandstone beds, often seen as smuts (Figure 3.4). Above the initial Iron Post Cyclothem there are 3 minor cycles consisting of marine bands, mudstones, fine and medium grained sandstones, thin coals and smuts. Architecturally, this cyclothem is an anomaly due to its very thin limestone and overall thickness.

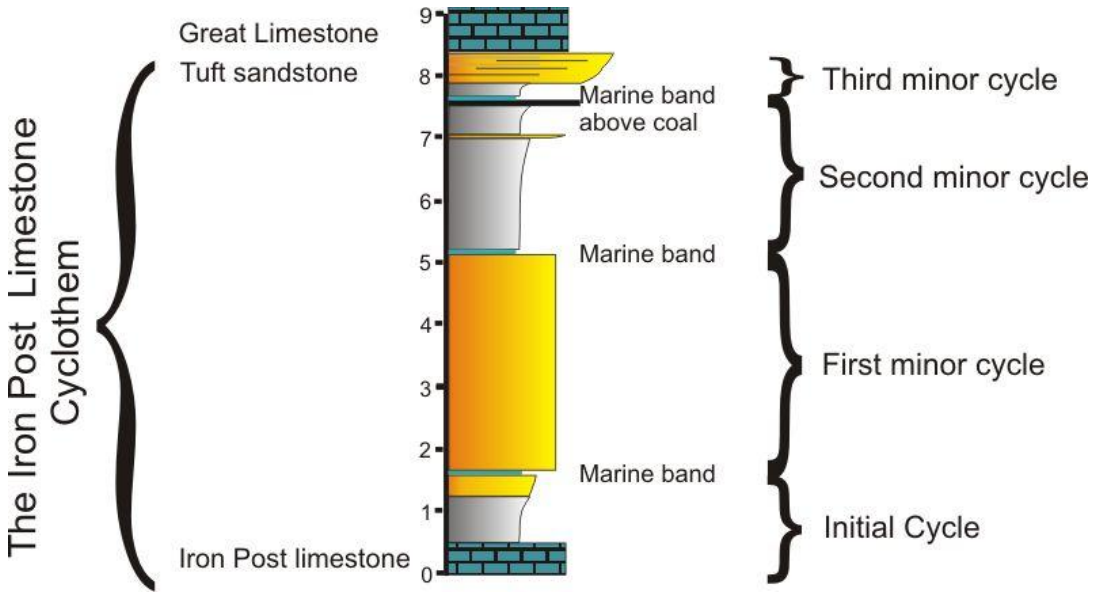

Figure 4.4 Generalised section of the Iron Post Cyclothem

The Iron Post Limestone is not laterally persistent on the Alston Block as it is missing in many of the mine sections, e.g. Killhope Mine (816 432) and Sedling Mine (860 411). In most areas where the limestone is missing it is replaced by a metre or so of highly fossiliferous shale overlying the Quarry Hazel sandstone of the Four Fathom Cyclothem below. Within Stanhopeburn Mine, Weardale (986 413) the Tuft sandstone lies directly upon the Quarry Hazel sandstone of the Four Fathom Cyclothem; the Iron Post limestone and mudstone are not present; here the combined thickness of sandstone reaches some 29 metres in thickness (Dunham, 1990). Dunham (1990) regarded this sandstone as a channel sandstone.

The Iron Post Cyclothem and the Great Cyclothem are situated each side of the boundary between the Brigantian and Namurian which have been designated as the boundary between the D6b and N1 Mesothems of Ramsbottom (1979). In his paper, Ramsbottom refered to the short duration at the end of a Mesothem (the regression) and a long duration at the start (the transgression). Whether the move from a thin cyclothem to a thick cyclothem, either side of the Mesothem boundary,

can be attributed to the time differences at the regression and transgression stages of the Mesothems is not clear and is difficult to assess with the data available.

4.2.4 Four Fathom Cyclothem

Johnson and Nudds (1996) regarded the Iron Post Cyclothem and the minor cycles above it as being minor cycles of the Four Fathom Cyclothem that underlies the Iron Post Limestone (Figure 4.5)

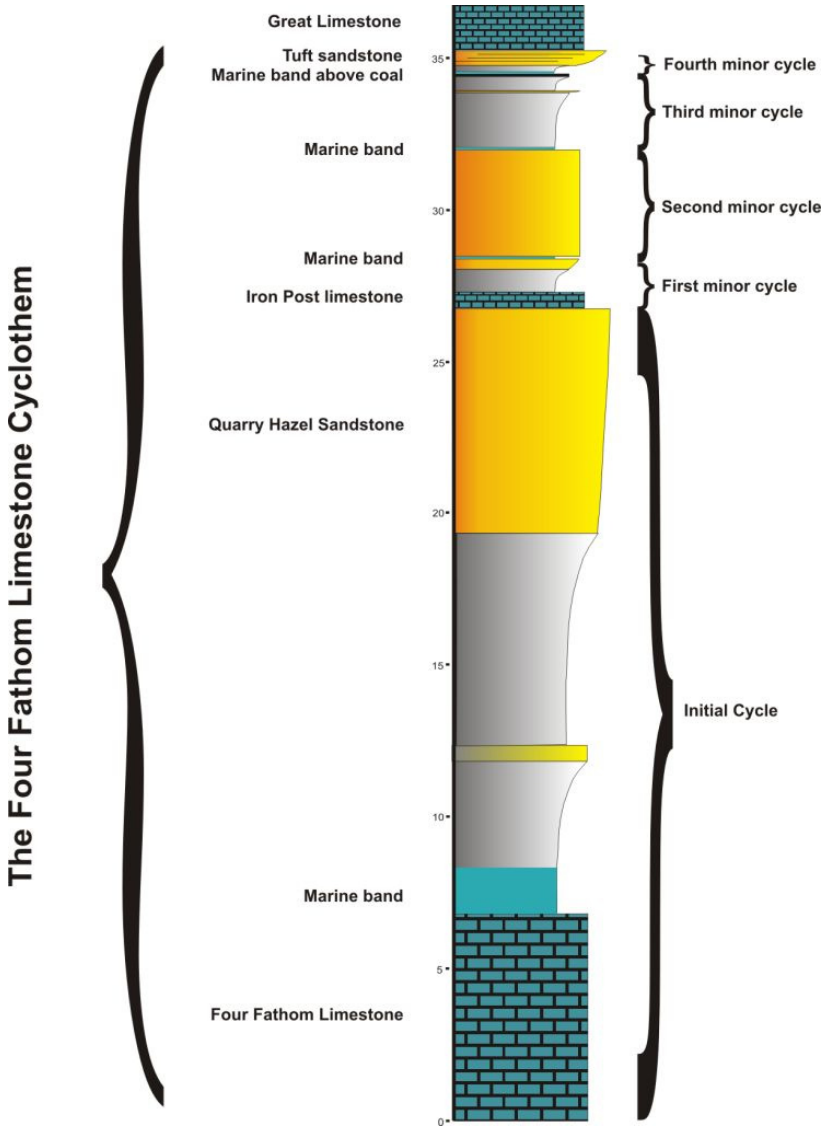

Figure 4.5 Generalised section of the Four Fathom Cyclothem. After Johnson and Nudds (1996).

If the Iron Post Cyclothem is included within the Four Fathom Cyclothem, as suggested by Johnson and Nudds (1996), the cyclothem is the thickest in the Brigantian succession with an average thickness of 33 metres. The limestone of the Four Fathom cyclothem has an average thickness of 6.5 metres and the mudstones, of both the Four Fathom and Iron post Cyclothems, average 16 metres. The Quarry Hazle sandstone varies considerably in thickness throughout the area from 1.8 metres to 23 metres with an average thickness of 7.4 metres. The large variation in thickness of the sandstone is due to the formation of channel sandstones which are known to remove the mudstones. As discussed in Chapter 4.2.3 the Tuft sandstone, above the Iron Post Limestone, can also be seen to lie directly upon the Quarry Hazel sandstone, giving a combined thickness of sandstone reaching 29 metres in thickness (Dunham, 1990).

4.2.5 Three Yard Cyclothem

The limestone of the Three Yard Cyclothem averages 2.9 metres, a thickness similar to that suggested by its name. The mudstone at 18.1 metres thick is unusually, for the cyclothems discussed, more than 50% of the total cyclothem thickness. The sandstone, the Nattrass Gill Hazle, varies in thickness from 4.0 metres to 26.0 metres throughout the area. A palaeosoil and sometimes a thin coal or carbonaceous mudstone is common at the top.

The Three Yard Cyclothem usually commences with a single limestone at the bottom; however, within Hudeshope Beck there is a second limestone bed separated from the lower limestone bed by a calcareous and fossiliferous shale approximately 2 metres thick (Figure 4.6); both limestone units are 2 to 2.5 metres thick. The second limestone consists of thin limestones intercalated with thin fossiliferous shales. The mudstone above the second post is fossiliferous which changes to a non-calcareous and non-fossiliferous shale and eventually into thin sandstones separated by mudstone known as the grey beds. Above the grey beds, the Nattrass Gill Hazle is split into at least three sandstones by mudstone and above the sandstone, directly below the Four Fathom Limestone, is a prominent palaeosoil with rootlets. The top of

the palaeosoil is split and contains smuts. Apart from the two limestone posts within the Three Yard Cyclothem there is only one general coarsening-up sequence with no minor cycles present.

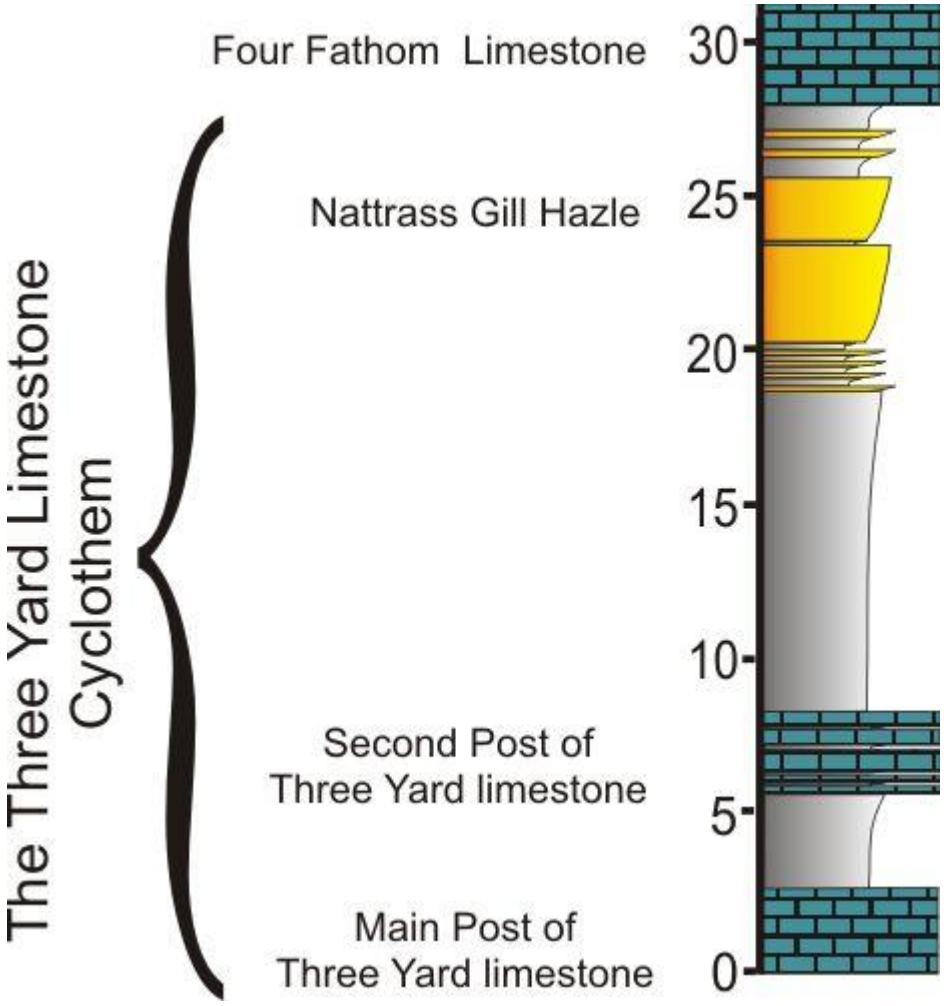

Figure 4.6 Generalised section of the Three Yard Cyclothem.

4.2.6. Five Yard Cyclothem

The Five Yard Cyclothem has an average thickness of 18.2 metres with the Five Yard Limestone averaging 4.7 metres and the sandstone, the Six Fathom Hazle or High Brig Hazle averaging 9.0 metres in thickness; a thin coal, up to 0.4 meters thick tops this cyclothem in places. As with the Three Yard Cyclothem above, this

cyclothem does not usually contain minor cycles; however, Johnson (1959) reported minor cycles within the cyclothem in the southern Northumberland Basin. The Five Yard Limestone is the lowest of Johnson's "perfect Major Cyclothems" (Johnson, 1959) discussed in Chapter 3, section 3.3, and covers an area from the Craven faults on the Askrigg Block to the Scottish Borders.

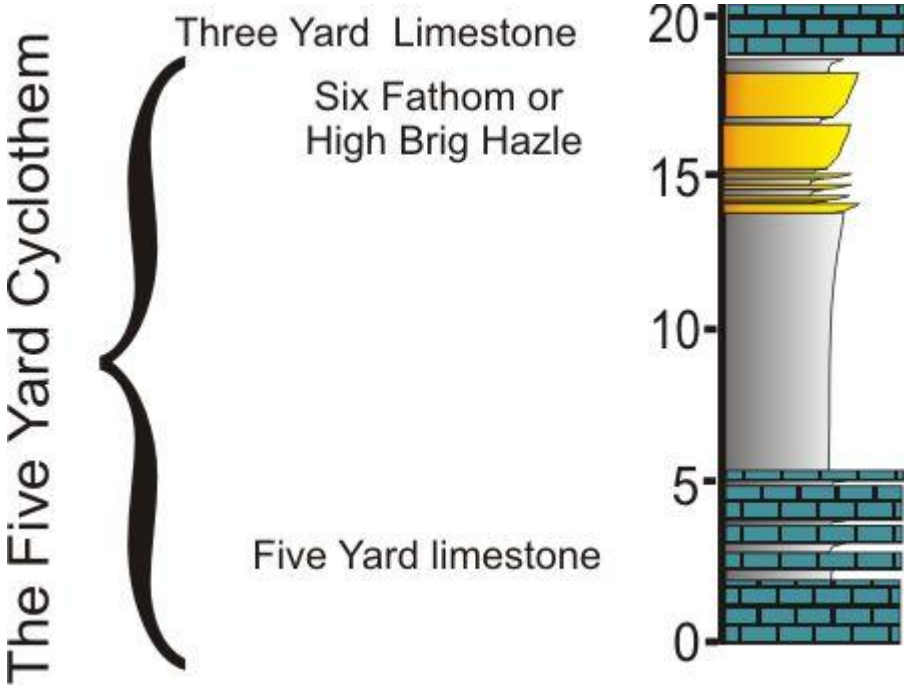

Figure 4.7 Generalised section of the Five Yard Cyclothem.

4.2.7 Scar Cyclothem

This is the lowest of the Cyclothems studied in this Chapter. The limestone is the second thickest of those studied in this Chapter at 11.0 metres. The sandstone, the Slaty Hazle or Low Brig Hazle, averages 7.8 metres, and this generally tops the cyclothem in the field.

The siliciclastics commence with a marine shale which is followed by non-marine mudstone. The non-marine mudstone coarsens up into the sandstones, which in Teesdale are more massive than those seen in the Weardale area which are often

seen as split sandstone and mudstone beds. Two minor cycles can often be seen above the initial cycle; the minor cycles commence with marine mudstone bands and coarsen up to and terminate with sandstone.

A large channel sandstone can be seen within the cyclothem at the waterfall upstream of the Bow Lees picnic area within Teesdale (907, 283). This channel can be seen to cut down to within a few metres of the Scar Limestone itself.

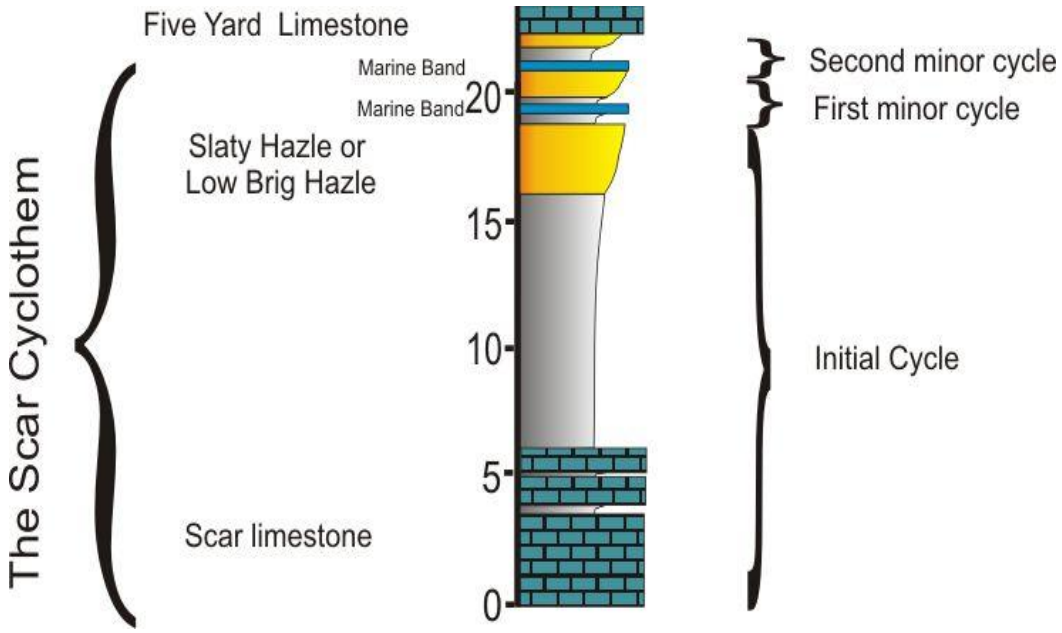

Figure 4.8 Generalised section of the Scar Cyclothem.

4.3. Isopachs, contours and section lines.

For the comparison of thickness variations within the cyclothems, isopachs and section lines were constructed from available data. The positions of the data points for section lines 1 to 15 are shown in Figure 4.9 (and Appendix A), using data from a Memoir of the British Geological Survey (Dunham, 1990) and records from the British Geological Survey collection at Edinburgh. The positions of the data points for section lines 16 to 28 are shown in Figure 4.10 (and Appendix A) and the section lines were constructed from an amalgamation of data from measurements (Appendix A) of figures given in a PhD thesis (Hodge, 1965). Isopach contours were

constructed in ArcView™ (sample shown in Figure 4.11) and the contour data were then used manually to identify thickness changes at the section positions and these were then transferred to AutoCAD™ for the final construction of the section lines. Section lines are provided in Appendix B and the positions of each section line is shown in Figures 4.14 and 4.15.

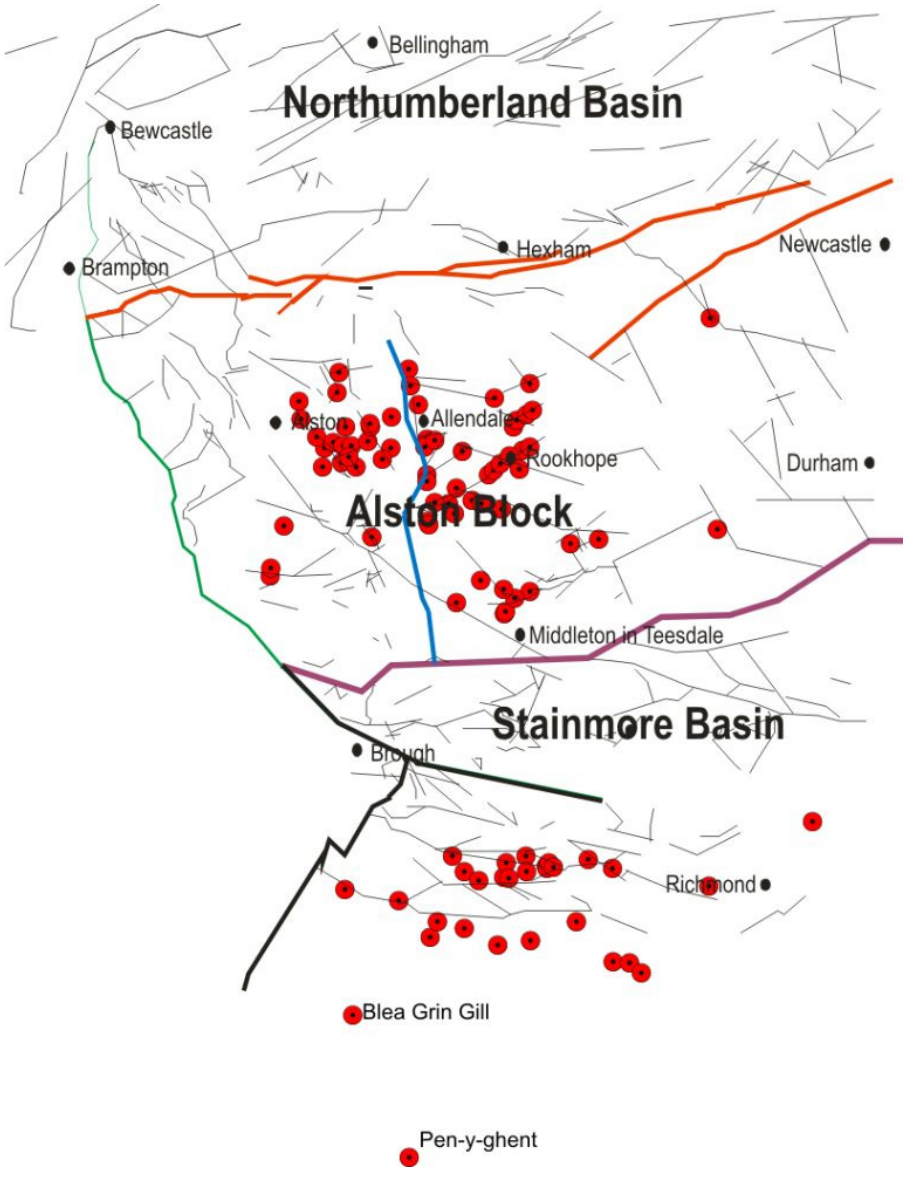

Figure 4.9 Locations of points for the construction of isopachs for Section Lines 1 to 15 (See also Appendix A)

Section lines 1 to 15 represent bed-thickness changes throughout the Alston Block from the Brigantian (Scar Cyclothem) up to and including the lower Namurian

(Little Cyclothem). Section Lines 16 to 28 are of the Great Cyclothem only and cover an area from the Northumberland Basin in the north to the Stainmore Trough to the south of the Alston Block.

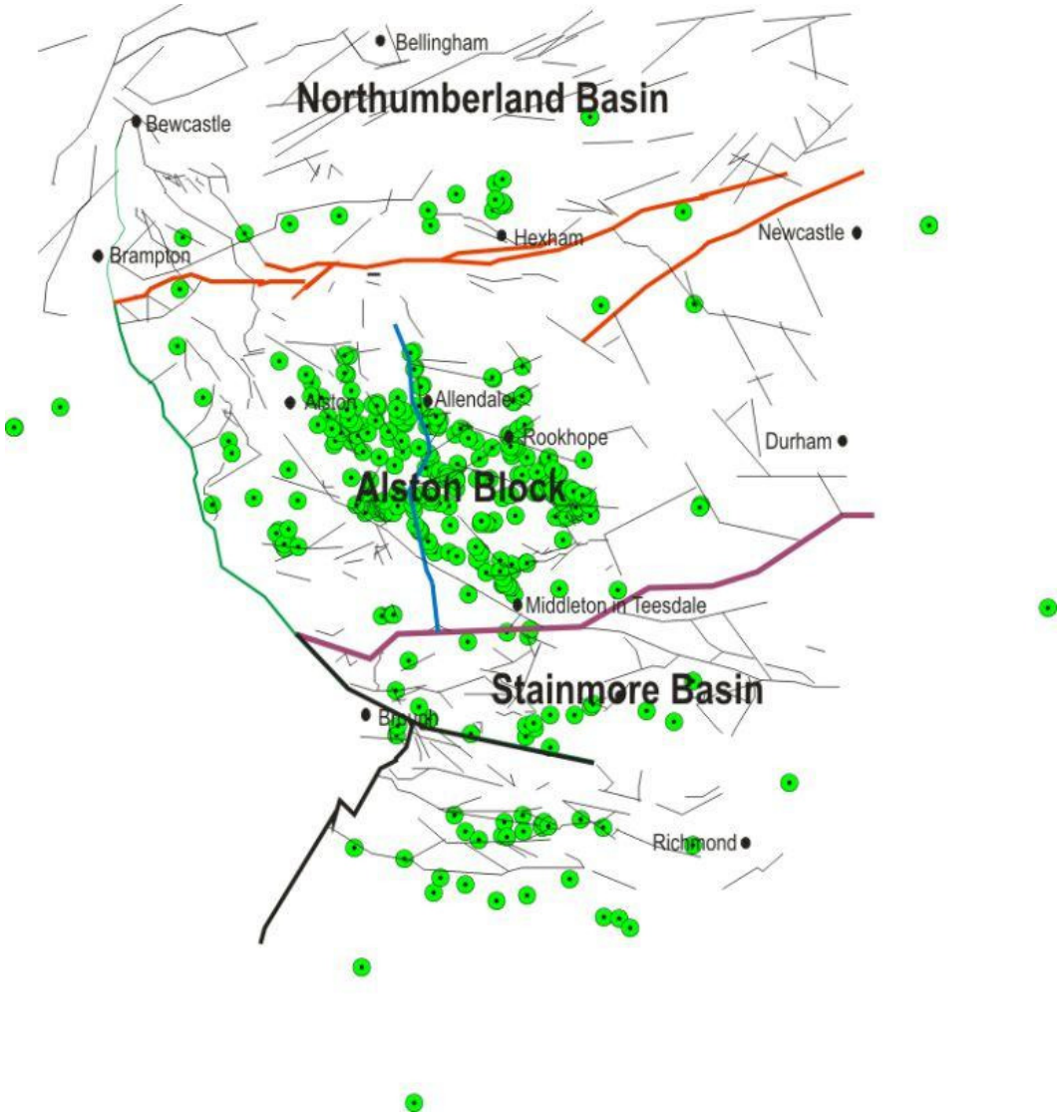

Figure 4.10 Locations of points for the construction of isopachs for Section Lines 16 to 28

Section lines 1 to 15 are not intended to be a true indicator of the actual cyclothem architecture; they are only to be used as an indication of overall thickness of each lithological unit in the cycle. Each cycle is shown in the sections to consist of three lithologies, i.e. limestone followed by mudstone followed by sandstone.

Whereas this would be an idealised progression, in the field the section may actually be far more complicated as some units may be repeated or absent. Figure 4.12 is a schematised section, as it may appear in the field, and Figure 4.13 shows how the section lines would represent the combined lithological thicknesses. This may appear to be an unusual and possibly unhelpful method to use; however, this has become necessary due to the way information is presented in many documents such as the British Geological Survey Memoirs. This combined information however, is still useful in representing the amount of marine to terrestrial material being deposited in the time-frame of the cyclothems.

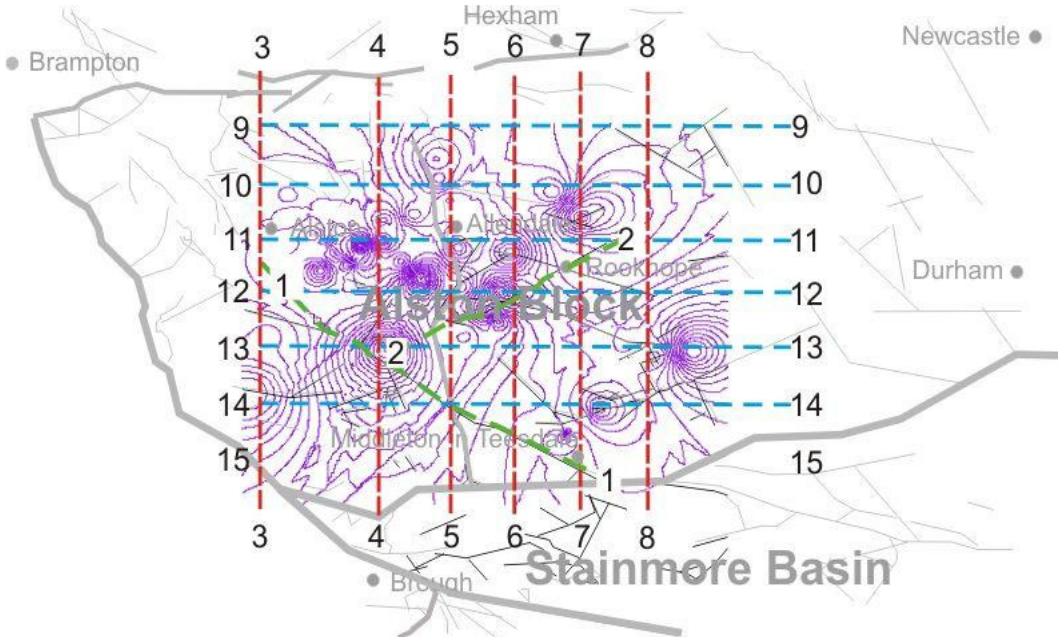

Figure 4.11 Example Isopachs for the base of the Great Limestone. See discussion for explanation

The construction and accuracy of the isopach contours can only ever be as good as the information collected and the number of data points used. For section lines 1 to 15 (Appendix A and B), 24 data points were used for the Scar Cyclothem whereas 58 were used for section lines 16 to 28 (Appendix A and B) for the Great Cyclothem. As the area covered by the isopachs is 1200km^2, this gives an average

coverage for the Scar Cyclothem of 1 per 50 km^2 and 1 per 21km^2 for the Great Cyclothem (Table 4.2).

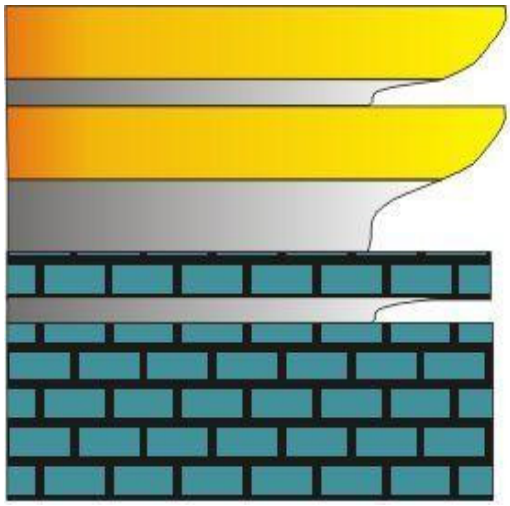

Figure 4.12
Schematised section showing relationships between beds as they may appear in the field.

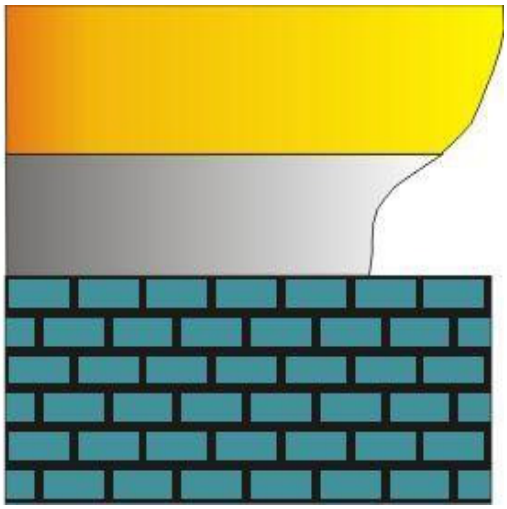

Figure 4.13
Section showing how the isopachs and sections would represent the lithology thickness relationships

Cyclothem	Number of Points	Coverage
Little Cyclothem	38	1 point per 31 Km^2
Great Cyclothem	58	1 point per 21 Km^2
Iron Post Cyclothem	36	1 point per 33 Km^2
Four Fathom Cyclothem	33	1 point per 36 Km^2
Three Yard Cyclothem	35	1 point per 34 Km^2
Five Yard Cyclothem	27	1 point per 44 Km^2
Scar Cyclothem	24	1 point per 50 Km^2
Total number of Points	**251**	

Table 4.2 Points used for constructing section lines 1 to 15

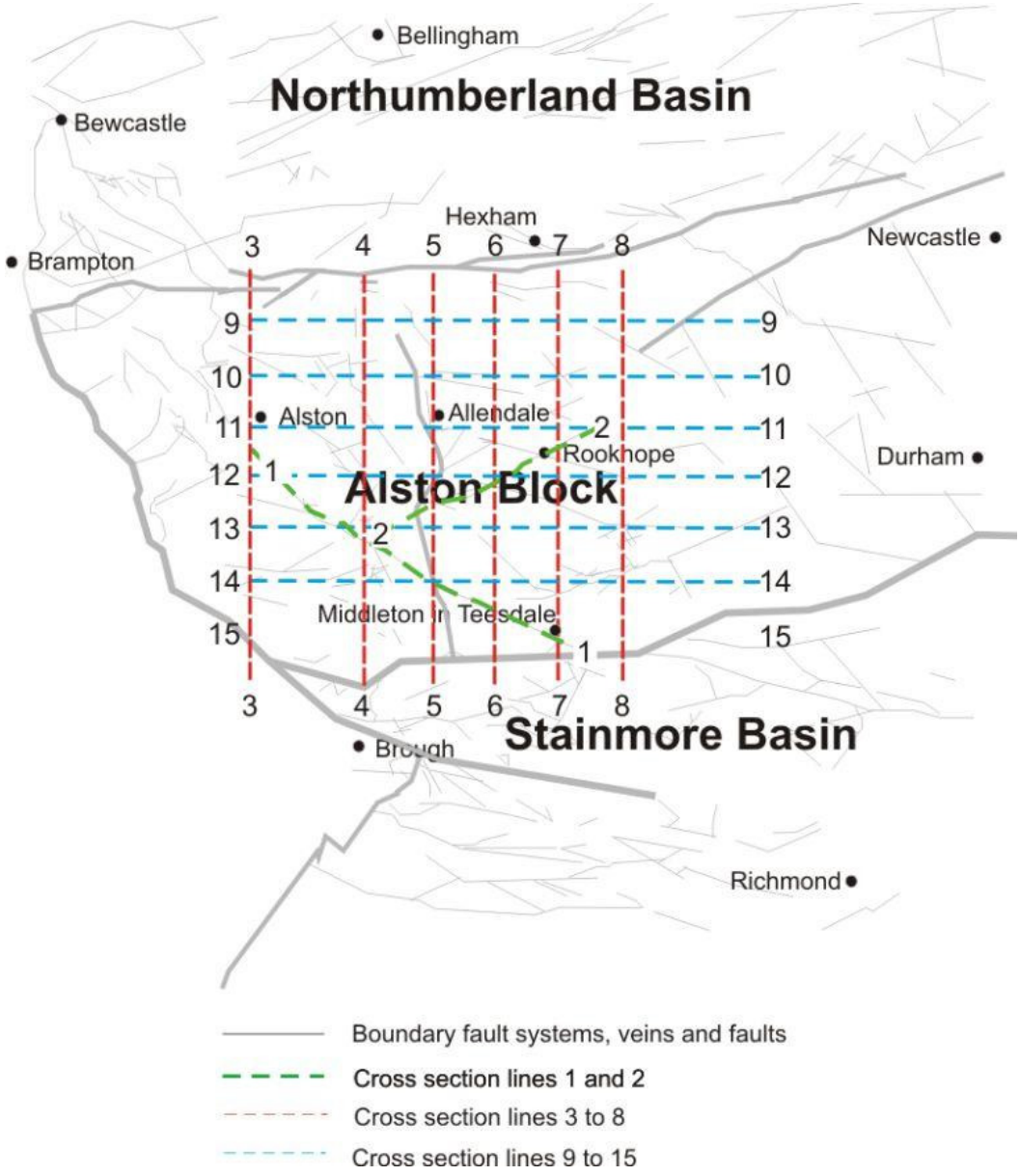

Figure 4.14 Position of section lines 1 to 15

The larger number of points used to construct section lines 16 to 28 (Appendix B) for the Great Cyclothem has undoubtedly resulted in the greater accuracy of changes being visible in these cross sections; however, this should not suggest that the isopachs for the other cyclothems are totally unrealistic. In fact, as can be seen in the section lines, similar thickness variations often occur throughout the different

cyclothems vertically above each other suggesting the number of data points, if not ideal, do give an acceptable, consistent picture.

Section lines 1 to 15 (Appendix B) are constructed as "hanging off" the flat top of the Little Cyclothem sandstone. This does not imply that the top of the sandstone is flat; it is used as a convenient starting point to draw all other units and cycles. Other methods were tried, such as drawing the Scar Limestone with a flat base and building everything up from this; however, the flat Little Cyclothem sandstone method was the easiest to construct and then interpret. The cyclothems in sections 1 to 15 are identified numerically on the right hand side from 1 to 7; Table 4.3 identifies the number and the corresponding cyclothem.

Number	Cyclothem
1	Little Cyclothem
2	Great Cyclothem
3	Iron Post Cyclothem
4	Four Fathom Cyclothem
5	Three Yard Cyclothem
6	Five Yard Cyclothem
7	Scar Cyclothem

Table 4.3 Corresponding number and cyclothem used in section lines 1 to 15.

Section lines 16 to 28 (Appendix B) are also constructed as "hanging off" the top of the upper-most sediment in the Great Cyclothem (usually the sandstone). They were constructed from scaling from previously constructed sections (Hodge, 1965). The isopachs for the Great Limestone itself used 321 data points covering, in part, the Northumberland Basin, the Alston Block and the Stainmore Trough. These section lines show the sandstones and mudstones in greater detail and as such this greater

accuracy has resulted in differences between calculated areas of each lithological unit. Even so the calculated areas in section lines 1 to 15 and 16 to 28, even though slightly different are still within the same magnitude and both are still instructive in their own way.

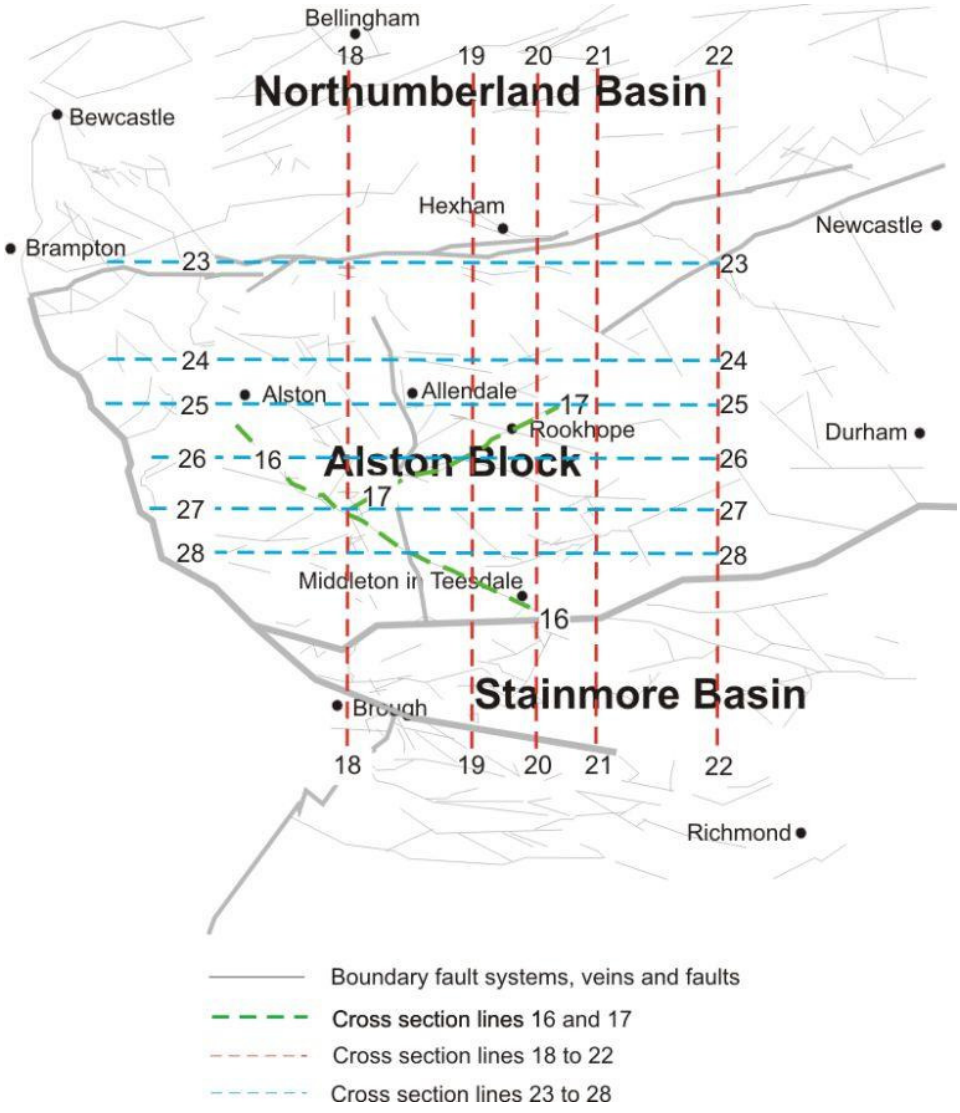

Figure 4.15 Position of Section Lines 16 to 28

The section lines 16 to 28 for the mudstone and the sandstones in the Great Cyclothem are a truer representation of the sediment succession throughout the Great Cyclothem of the Alston Block and adjacent areas. Sections 16 to 28 cover an

extended area of 3500 km^2, which is greater than those covered by Sections 1 to 15; this gives coverage of 1 point per 11 km^2.

The following Tables refer specifically to section lines 1 to 15 (Appendix A, B and C) and give computer calculated cross-sectional areas in km^2 of individual lithologies (limestone, mudstone and sandstone), in each cyclothem and totals for all seven cyclothems.

Cyclothem	(1) Area of limestone in the cyclothem		(1) Area of mudstone in the cyclothem		(1) Area of sandstone in the cyclothem		Total Area of cyclothem
	(2) % of Cyclothem	(3) % of Limestone in section	(2) % of Cyclothem	(3) % of mudstone in section	(2) % of Cyclothem	(3) % of sandstone in section	Percentage of All Beds
Little	(1) 0.07		(1) 0.60		(1) 0.50		1.17
	(2) 6.19	(3) 5.21	(2) 51.45	(3) 24.13	(2) 42.35	(3) 21.85	19.01
Great	(1) 0.56		(1) 0.26		(1) 0.52		1.34
	(2) 41.94	(3) 40.31	(2) 19.30	(3) 10.34	(2) 38.76	(3) 22.85	21.73
Iron Post	(1) 0.01		(1) 0.11		(1) 0.17		0.29
	(2) 3.47	(3) 0.72	(2) 37.66	4.33	(2) 58.87	7.45	4.67
Four Fathom	(1) 0.21		(1) 0.38		(1) 0.17		0.76
	(2) 27.91	(3) 15.17	(2) 49.57	(3) 15.03	(2) 22.53	(3) 7.51	12.29
Three Yard	(1) 0.10		(1) 0.61		(1) 0.23		0.94
	(2) 10.50	(3) 7.07	(2) 65.38	(3) 24.56	(2) 24.12	(3) 9.97	15.23
Five Yard	(1) 0.14		(1) 0.17		(1) 0.45		0.76
	(2) 18.95	(3) 10.27	(2) 21.88	(3) 6.62	(2) 59.17	(3) 19.68	12.26
Scar	(1) 0.30		(1) 0.38		(1) 0.24		0.91
	(2) 32.41	(3) 21.25	(2) 41.00	(3) 14.99	(2) 26.60	(3) 10.69	14.82
Totals	1.40		2.50		2.28		6.17

Table 4.4 Colour enhanced Section Line 1 Details, to be used for explanation of Tables B1 to B15 (Appendix C), see description below.

Table 4.4 is colour enhanced showing how the section line details are displayed and is a guide to the use of Tables B1 to B15 (Appendix C). The light grey cells, numbered 1, are the calculated area in km^2 of the individual lithological units, e.g. in the case of the Little Cyclothem, the calculated area of the limestone unit in section line 1 is 0.07 km^2, the calculated area of the mudstone unit in section line 1 is 0.60 km^2 and the calculated area of the sandstone unit in section line 1 is 0.50 km^2, giving a total area of the Little Cyclothem of 1.17 km^2.

The light orange cells, numbered 2, are the calculated percentage that the individual lithological units are of each cyclothem, e.g. in the case of the Little Cyclothem, the limestone is 6.2 percent of the cyclothem, the mudstone is 51.5 percent of the cyclothem and the sandstone is 42.4 percent of the cyclothem.

The blue cells, numbered 3 are the percentage that the lithological unit in each cyclothem is of all similar lithological units in the section line, e.g. in the case of the Little Cyclothem, the limestone is 5.2 percent of all limestones considered in section line 1, the mudstone is 24.1 percent of all mudstones in section line 1 and the sandstone is 21.9 percent of all limestones in section line 1.

4.4. Thickness variations in section lines 1 to 15

Figures 4.16 to 4.22, derived from the data in Tables B1 to B15 (Appendix C), illustrate how total and unit sectional areas change throughout the block in both a west to east and a north to south direction. The total thickness variations of the Scar to the Little Cyclothem are, as can be seen in section lines 1 to 15 (Appendix B), relatively small varying between 176 metres to 190 metres. Thickness variations of individual cyclothems are evident throughout the section lines and within section lines 1 to 8 changes can be seen in various cyclothems with the Little Cyclothem often thickening to the north and the Great Cyclothem thickening towards the centre and south of the block, probably due to the position of the Allercleugh Channel. The Three Yard and Five Yard Cyclothems can also be seen to thicken towards the centre and south of the block.

In section lines 9 to 12 (Appendix B) very little visual changes are obvious, whereas within section lines 13 to 15 (Appendix B) the main changes are seen within the Great Cyclothem, probably due to the Allercleugh Channel as discussed above.

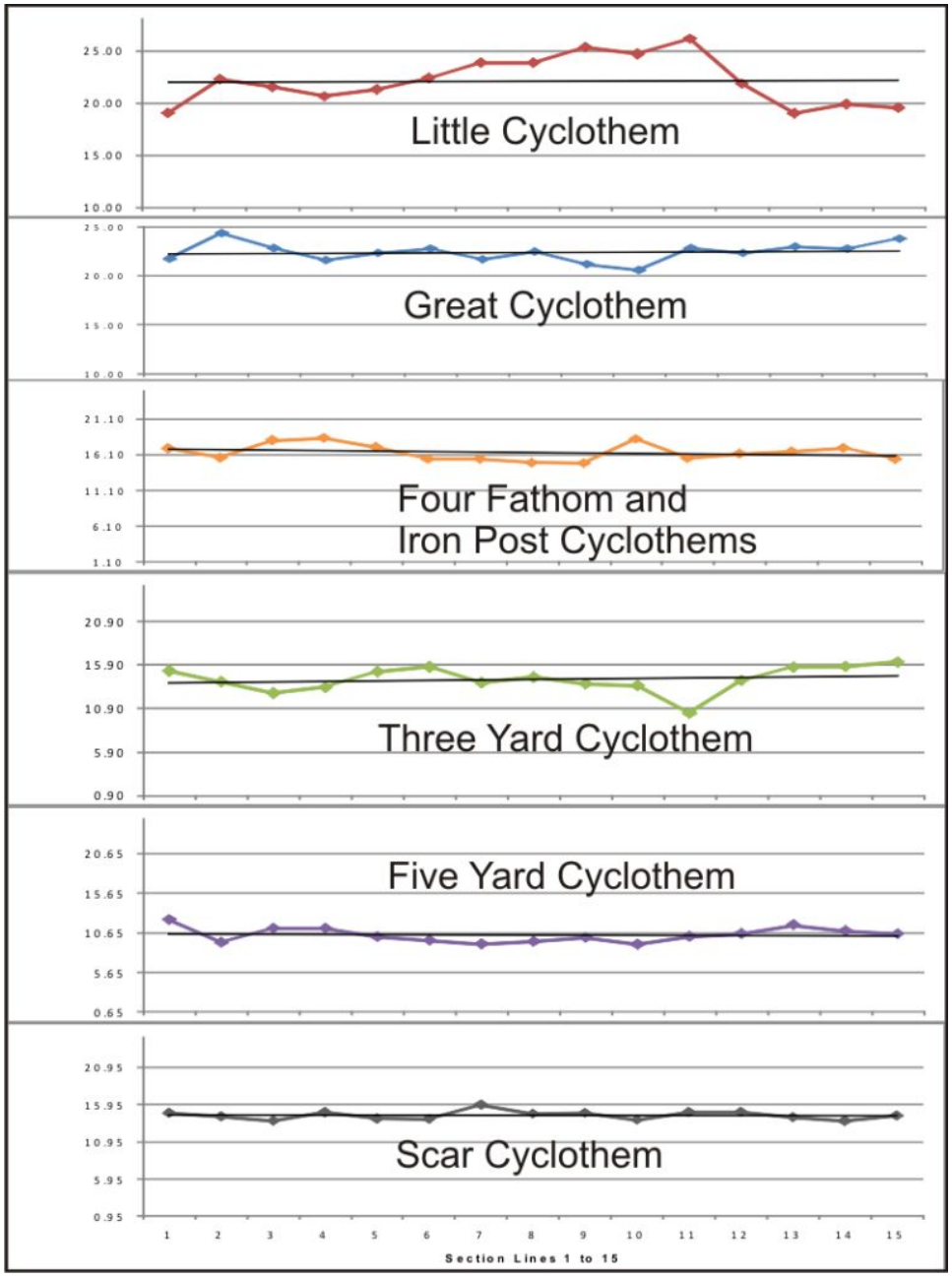

Figure 4.16 Percentage area of each cyclothem within section lines 1 to 15 together with trend lines

Section lines 1 and 2 cover shorter distances than do section lines 3 to 15 and therefore it is difficult to compare them easily, nevertheless, all section lines do show

relatively consistent thicknesses and vary by only a metre or so. A comparison of the percentage of each individual cyclothem within each section line is shown in Figure 4.16, where percentage changes can be seen to vary; however section lines 1 and 2 do fit within the general pattern.

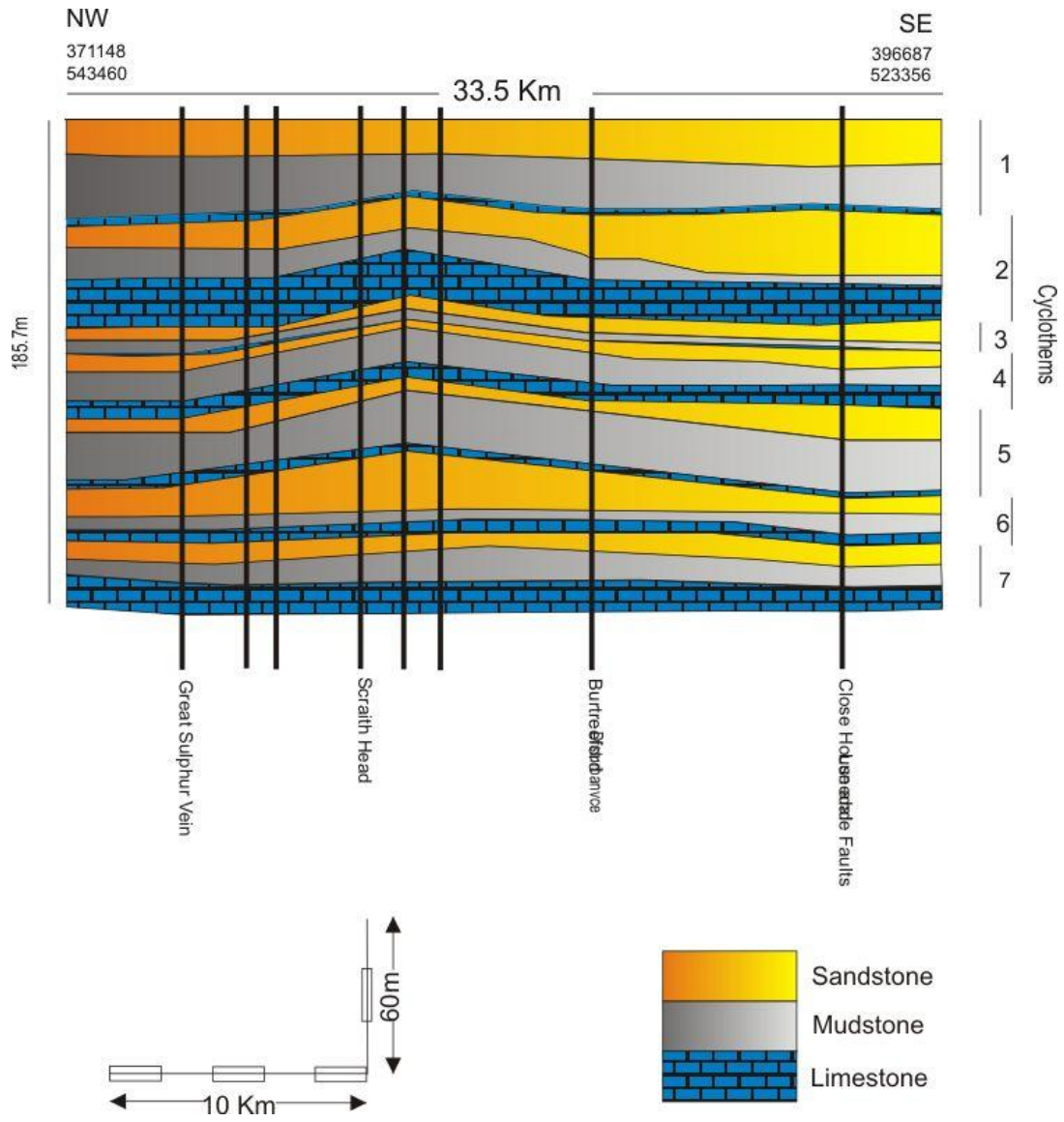

Figure 4.17 Section Line 1

Section line 1 (Figure 4.17), which runs 33.5 km in a south-east to north-west direction following the Teesdale fault system, Leehouse Well, Scar End and St John's veins, shows relatively little average change throughout; however, variation can be seen within individual cyclothems. The Scar and Great Limestones thicken towards the north-west and major changes can also be seen within the siliciclastics of the Scar and Five Yard Cyclothems near to the centre of the section. The sandstones of the Great Cyclothem are also seen to thicken towards the south-east of the section line, probably due to the position of the Allercleugh Channel.

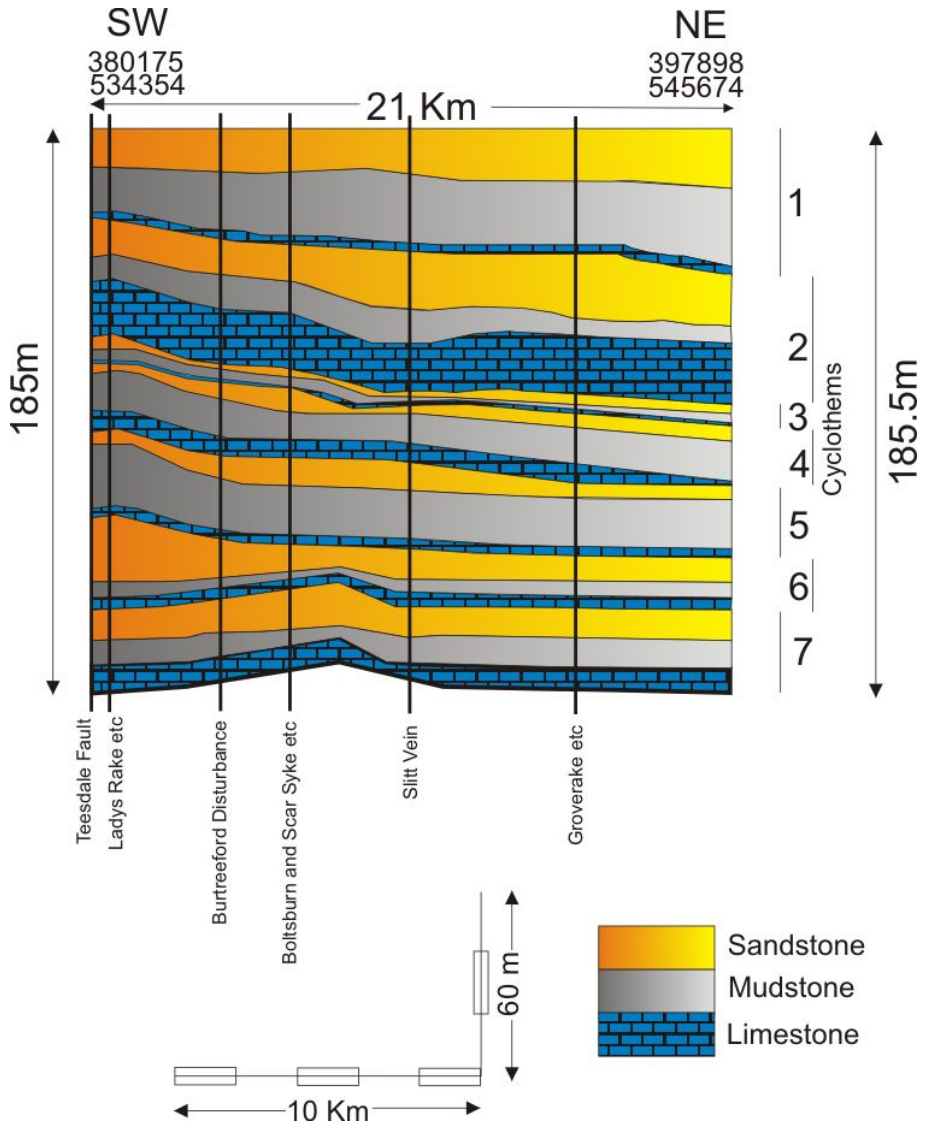

Figure 4.18 Section Line 2

Section line 2 (Figure 4.18), runs for 21 km in a south-west to north-east direction commencing near to the junction of the Teesdale Fault and Lady's Rake vein. Both the Little Cyclothem and Great Cyclothem can be seen to thicken towards the north-east whereas, the Five Yard thickens to the south-west; the Four Fathom Limestone also thins towards the north-east.

The areas of individual cyclothems and lithological units from section lines 3 to 15 (Appendix B) and Tables B3 to B15 (Appendix C) are used in the following paragraphs as a simple means of identifying area variations throughout the Alston Block. Even though this is a crude method, it is still thought to provide an interesting explanation of the changes occurring throughout the Alston Block. Figures 4.19 and 4.20 are constructed with the Iron Post and Four Fathom Cyclothems combined as discussed by Johnson and Nudds (1996) whereas, Figure 4.21 is provided to show how the splitting of these cyclothems affects the overall pattern.

Section lines 3 to 15 could be analysed in a similar way as to section lines 1 and 2; however as they are all of a similar length, i.e. 40 km they are considered in greater detail and in particular sectional areas are considered. Within section lines 3 to 15, the statistics within Appendices A and C show total areas of the section lines being around 7.3 to 7.4 km^2 with exceptions being in section lines 9 and 11 which are less than 7.0 km^2 and section lines 7, 14 and 15 which are 7.5 km^2 or greater.

The north to south sections (section lines 3 to 8, Appendix B) thicken from 181 metres to 187 metres in a west to east direction. The west to east section lines (section lines 9 to 15 Appendix B), show a thickening up to a maximum of 190 metres towards the centre and south of the area covered. The sectional areas show a steady increase in the total thickness of all the cyclothems to the east and to the south with a small increase near the centre of the block. Figures 4.19 and 4.20 illustrate how the cross sectional area of all 7 individual cyclothems change both in a west to east and a north to south direction.

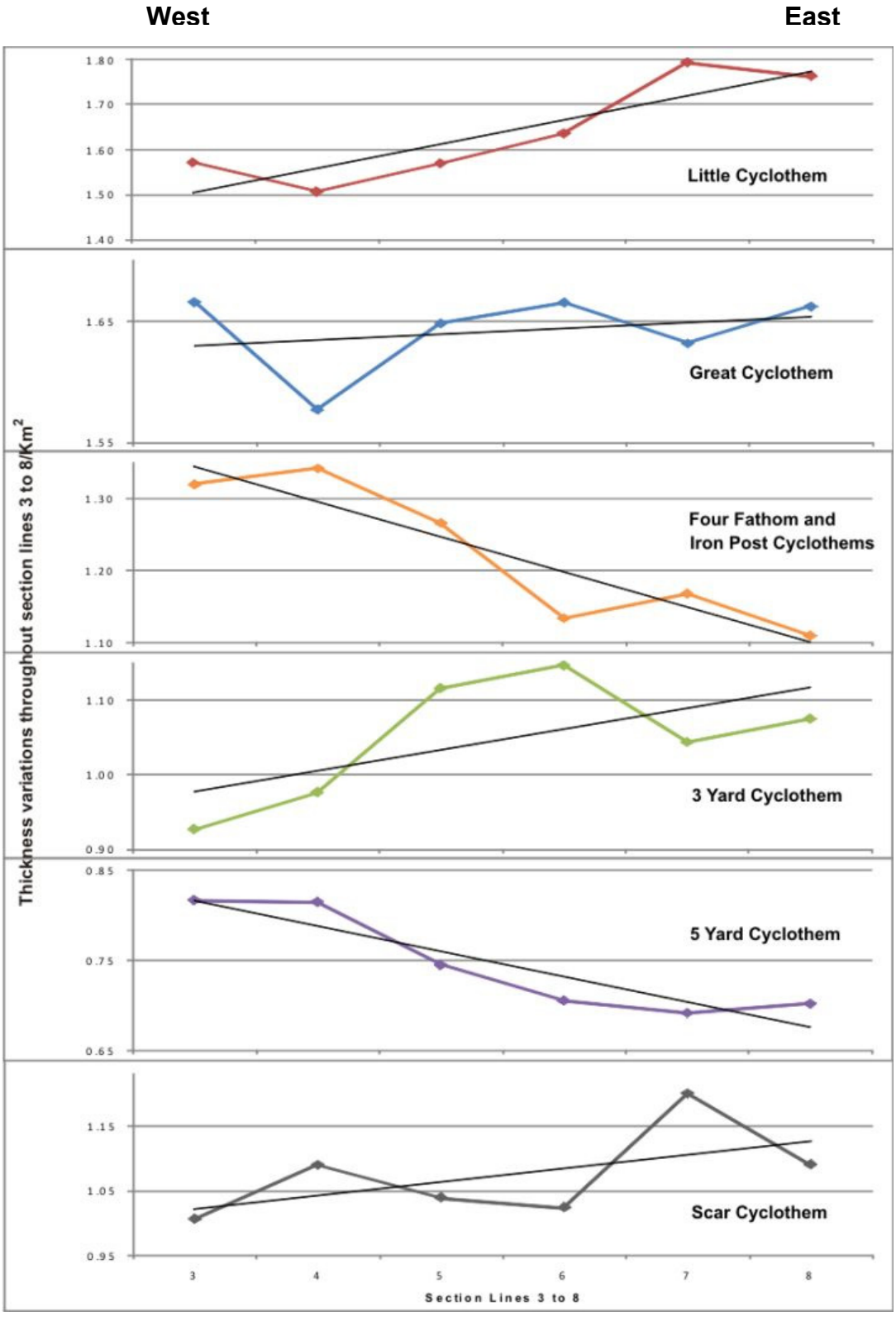

Figure 4.19 Thickness variations of individual north-south section lines 3 to 8 together with trend lines

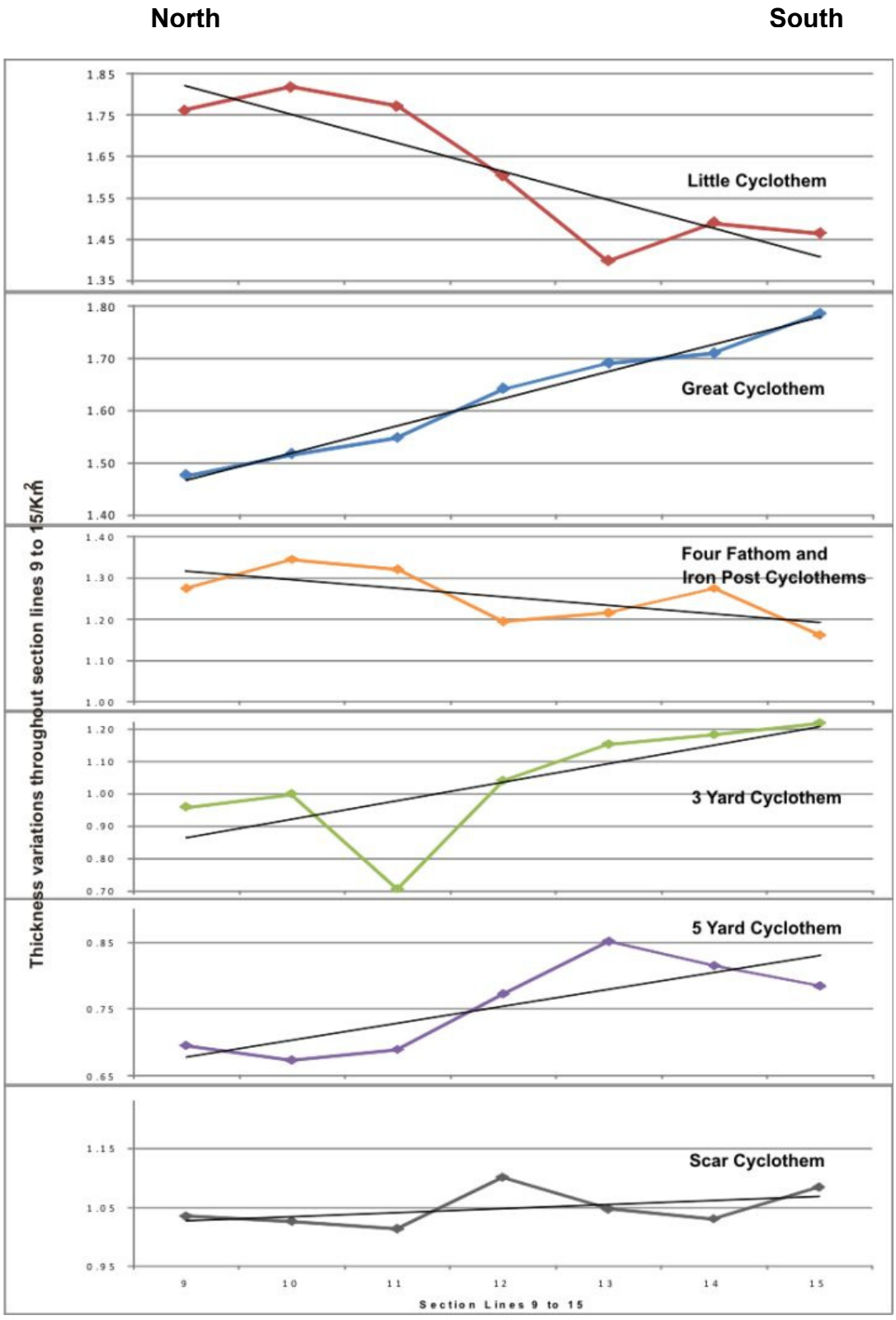

Figure 4.20 Thickness variations of individual west-east section lines 9 to 15 together with trend lines

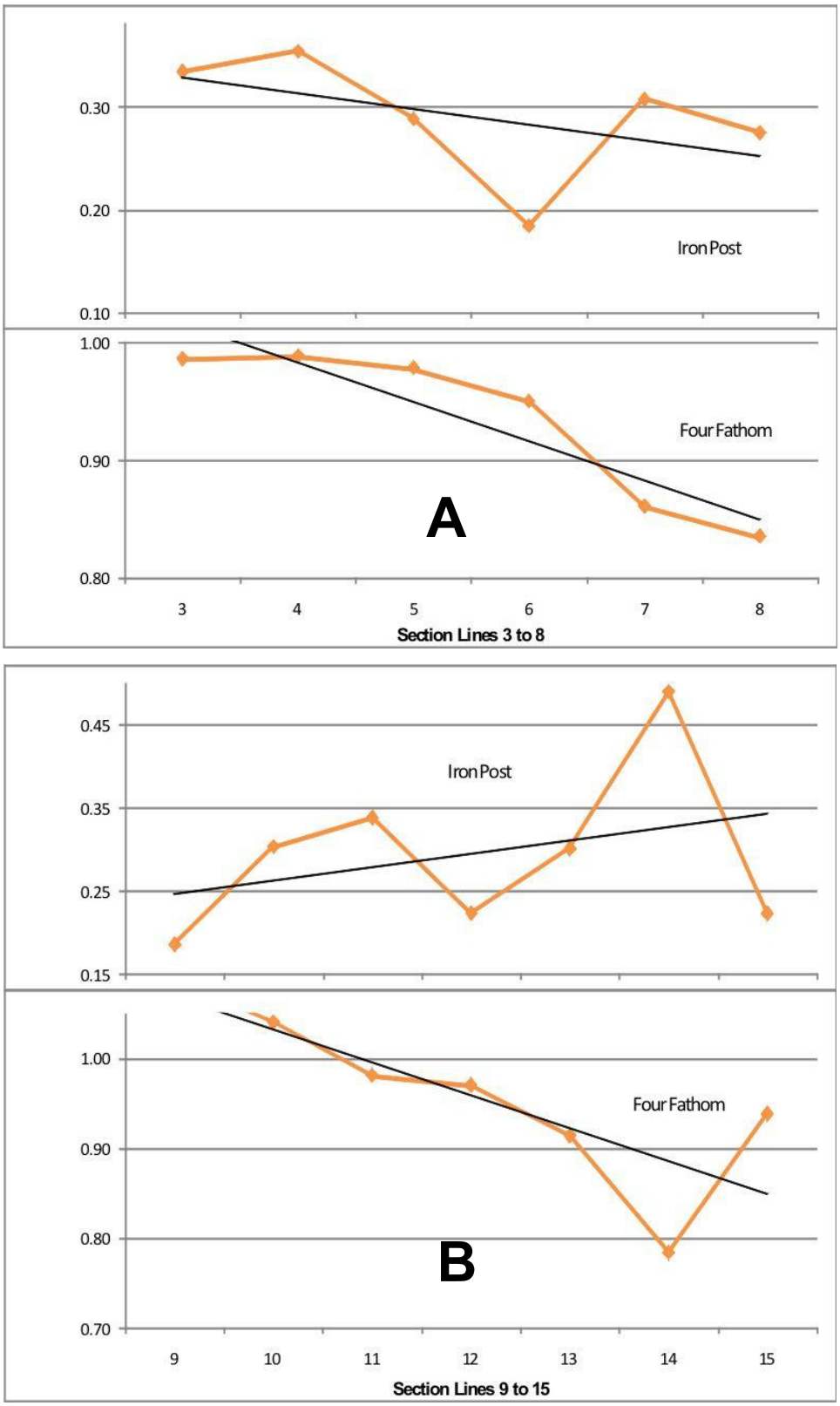

Figure 4.21 Iron Post and Four Fathom Cyclothem thickness variations provided for comparison purposes.

In Figure 4.19, in a west to east direction, the area of the Great Cyclothem is fairly constant with only a 5% rise, 0.08 km^2, between section lines 4 to 8, whereas the area of the Little Cyclothem increases by 14%, 0.22 km^2 between section lines 4 to 7. The Great Cyclothem can be seen to increase at section line 6 near to the centre of the block. Further area increases in a west to east direction can also be seen in the Three Yard Cyclothem of 0.15 km^2, a 16% increase, and the Scar Cyclothem 0.19 km^2, a 19% increase. A reduction in area of the Iron Post and Four Fathom Cyclothem of 0.23 km^2, a 17% reduction, and the Five Yard Cyclothem of 0.11 km^2, a 13.5% reduction can also be seen throughout the block.

Commencing with the Scar Cyclothem a simple alternation of cyclothem area increasing to the east and then to the west is evident in Figure 4.19 up to and including the Great Cyclothem after which the alternation fails with the Little Cyclothem area also increasing in a west to east direction, similar to the Great Cyclothem. The alternations are evident in both the plots of the areas of each individual cyclothem in the sections and their trend lines. It is interesting to note that the increase in area of the Scar and Three Yard together is 0.34 km^2 whereas the reductions in the Five Yard and Iron Post and Four Fathom is also 0.34 km^2, suggesting that by the bottom of the Great Cyclothem the alternations had somewhat been cancelled out. Figure 4.21 (A), shows the Iron Post and Four Fathom Cyclothems separated for comparison. If these cyclothems were considered individually then it would result in the failure of the alternation up through the sections at the Iron Post Cyclothem as it is shown to reduce in a west to east direction as the underlying Four Fathom Cyclothem.

In Figure 4.20, in a north to south direction, the area of the Little Cyclothem decreases by 20%, 0.36 km^2, while the Great Cyclothem increases by 20%, 0.3 km^2; a very similar area. From the Three Yard Cyclothem up to and including the Little Cyclothem a simple alternation of cyclothem area increasing to the south and then to the north is evident in Figure 4.20. The alternations are evident in both the plots of the areas of each individual cyclothem in the sections and their trend lines. It is

interesting to note that the increase in area of the Three Yard (0.26 km^2) and Great Cyclothems (0.3 km^2) together is 0.56 km^2 whereas the reductions in the Iron Post/Four fathom (0.18 km^2) and Little Cyclothems (0.36 km^2) is 0.54 km^2 suggesting that in this case by the top of the Little Cyclothem the alternations had somewhat been cancelled out.

Below the Three Yard Cyclothem the alternation is missing, the Five Yard and Scar cyclothems increase towards the south with a total increase in area of 0.13 km^2. Figure 4.21 (B) also shows the Iron Post and Four Fathom Cyclothems separated for comparison. This would show some alternation commencing with the Three Yard Cyclothem increasing to the south followed by the Four Fathom Cyclothem falling slightly to the south and then followed by the Iron Post Cyclothem increasing to the south. Continuation of the alternation then fails with the Great Cyclothem also increasing to the south as does the Iron Post Cyclothem.

In section lines 1 to 15 (Appendix B), Tables B3 to B15 (Appendix C) and Figure 4.22 the areas of limestone are generally consistent, with only minor variations seen throughout. Variations in the total limestone cross sectional area in Tables B1 to B15 (Appendix B) show a minimum of 1.59 km^2 and a maximum of 1.89 km^2, the greatest variations occurring in the Scar Limestone where the limestone area decreases in both a west to east and a north to south direction. The Great Limestone on the other hand is generally consistent in both an easterly and southerly direction with only a slight decrease; minor changes can also be seen in the other limestones.

Section lines 1 to 15 (Appendix B), Tables B3 to B15 (Appendix C) and Figure 4.22 show that terrigenous material makes up the majority of most of the cyclothems with mudstone generally being the principal component except where thick channels increase the sandstone area; exceptions to this can be seen in the Five Yard Cyclothem, where the sandstone is the greatest component throughout, and

within the Great Cyclothem, where sandstone also dominates in many section lines.

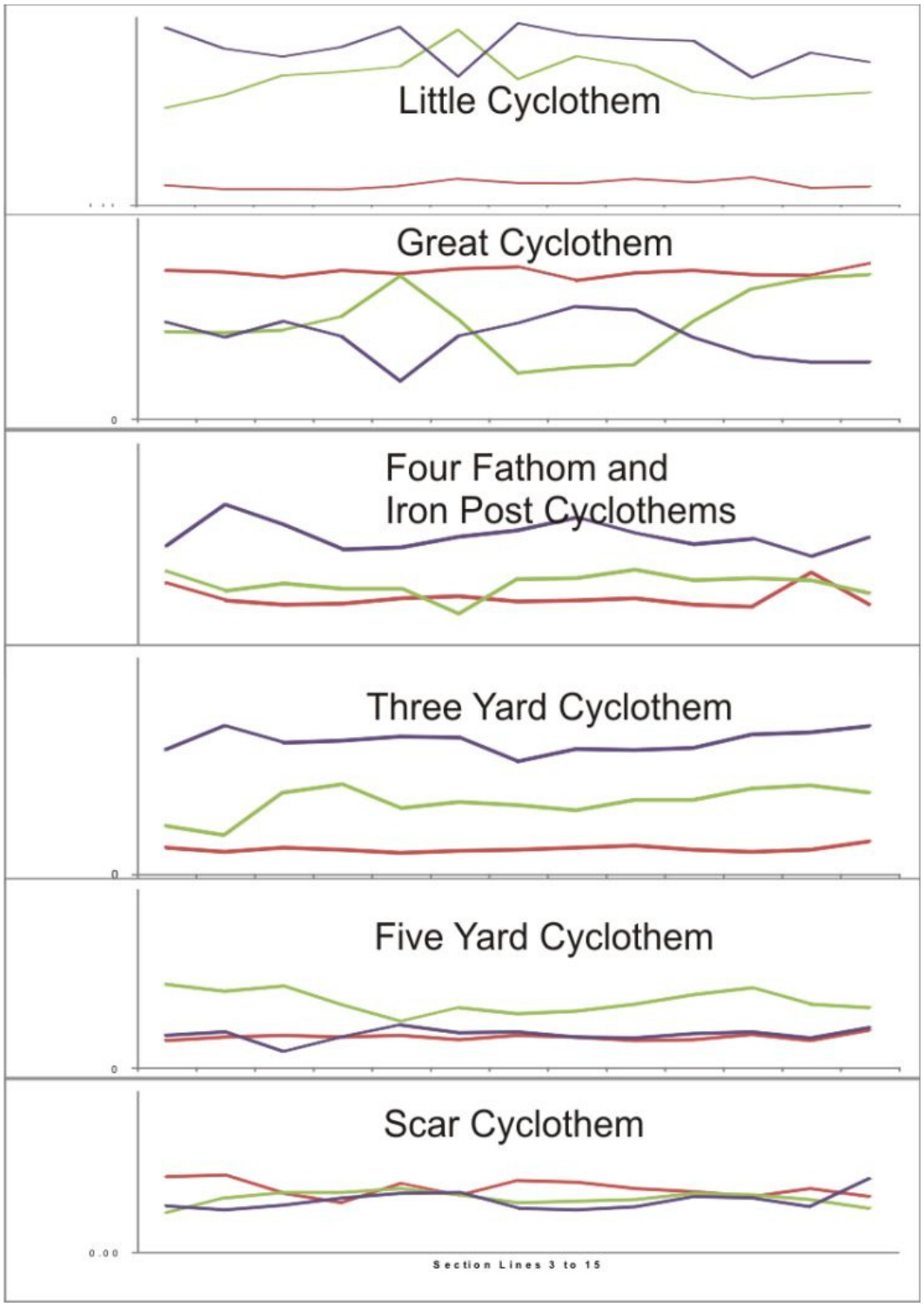

Figure 4.22 Thickness variations of lithological units within section lines 3 to 15 for each individual cyclothem. Red Line = limestone, green line = sandstone and purple line = mudstone.

The cross sectional areas of terrigenous material in all cyclothems vary between 0.01km^2 and 1.7 km^2 with the Little Cyclothem containing the greatest percentage of terrigenous sediment which increases in a west to east direction and decreases north to south.

It is difficult to ascertain whether the alternations in individual cyclothem areas are a direct consequence of a rhythmically changing sedimentation rate due to movement of the encroaching delta or to movement of the Alston Block itself. Dunham (1990) suggested however, that "A rhythmic rise and fall of the shelf, relative to the sea-level of the time took place throughout the Carboniferous, perhaps accompanied by very gentle warping"; presumably this gentle warping suggests movement of the Alston Block itself.

4.5 Thickness variations in section lines 16 to 28

It is difficult to compare section lines 16 to 28 with those for section lines 1 to 15 due to differences in length and the extension of some sections into the Northumberland Basin and Stainmore Basin; however, a direct comparison of section lines 16 and 17 with section lines 1 and 2 is possible. Table 4.5 gives areas in km^2 for each lithological unit within section lines 16 to 28 together with percentages of each lithological unit and Figure 4.23 shows how the percentage of each lithological unit changes throughout the section lines. Figure 4.23 shows how the percentage of each lithological unit changes throughout the sections; it is interesting to note how the percentage of limestone is shown to increase above section line 22 and the siliciclastics reduce where the section lines do not include the siliciclastics of the Northumberland Basin. The Great Limestone is consistently the greatest proportion of the sediments with sandstone being the greatest proportion of the siliciclastics.

Section line 16, as with section line 1 runs 33.5 km in a south-east to north-west direction following the Teesdale Fault system, Leehouse Well, Scar End and St John's veins. The section shows a slight thinning of the Great limestone towards the

north-west and a thickening of the siliciclastics near to the centre of the section. Overall the sandstone can be seen to be the greater proportion of the siliciclastics. Statistically, Table 4.5, the Great Limestone member is calculated at 0.6 km^2, the mudstone at 0.34 km^2 and the sandstone at 0.48 km^2. These are slightly different from those calculated for section line 1 previously, i.e. 0.56 km^2, 0.26 km^2 and 0.52 km^2, respectively, probably due to the greater number of points used for the construction of the section and the greater accuracy of the original data.

Sction Line	Area of limestone in the cyclothem/km^2	Area of mudstone in the cyclothem/km^2	Area of sandstone in the cyclothem/km^2	Length of section line/km	Total Area of cyclothem/km^2
	Percent of Cyclothem	**Percent of Cyclothem**	**Percent of Cyclothem**		
16	0.60	0.34	0.48	33.50	1.42
	42.25	**23.94**	**33.80**		
17	0.47	0.09	0.33	21.00	0.89
	52.81	**10.11**	**37.08**		
18	1.36	0.50	1.36	70.00	3.22
	42.24	**15.53**	**42.24**		
19	1.35	0.65	0.87	70.00	2.87
	47.04	**22.65**	**30.31**		
20	1.31	0.76	0.86	70.00	2.93
	44.71	**25.94**	**29.35**		
21	1.28	0.62	0.81	70.00	2.71
	47.23	**22.88**	**29.89**		
22	1.34	0.44	0.86	70.00	2.64
	50.76	**16.67**	**32.58**		
23	0.92	0.76	0.41	50.00	2.09
	44.02	**36.36**	**19.62**		
24	1.02	0.22	0.56	50.00	1.80
	56.67	**12.22**	**31.11**		
25	1.06	0.34	0.35	49.00	1.75
	60.57	**19.43**	**20.00**		
26	1.02	0.22	0.46	47.00	1.70
	60.00	**12.94**	**27.06**		
27	0.89	0.14	0.49	46.60	1.52
	58.55	**9.21**	**32.24**		
28	0.93	0.21	0.44	45.00	1.58
	58.86	**13.29**	**27.85**		

Table 4.5 Statistics for section lines 16 to 28

Section line 17, as with section line 2, runs for 21 km in a south-west to north-east direction commencing near to the junction of the Teesdale fault and Lady's Rake vein. The section shows a thickening of the siliciclastics near to the centre of the section and overall the sandstone can be seen to be the greater proportion of the siliciclastics. Statistically, Table 4.5, the Great Limestone member is calculated at 0.47 km^2, the mudstone at 0.09 km^2 and the sandstone at 0.33 km^2. These are different than those calculated for section line 2 previously, i.e. 0.33 km^2, 0.14 km^2 and 0.31 km^2, respectively, probably due to the greater number of points used for the construction of the section and the greater accuracy of the original data as discussed above.

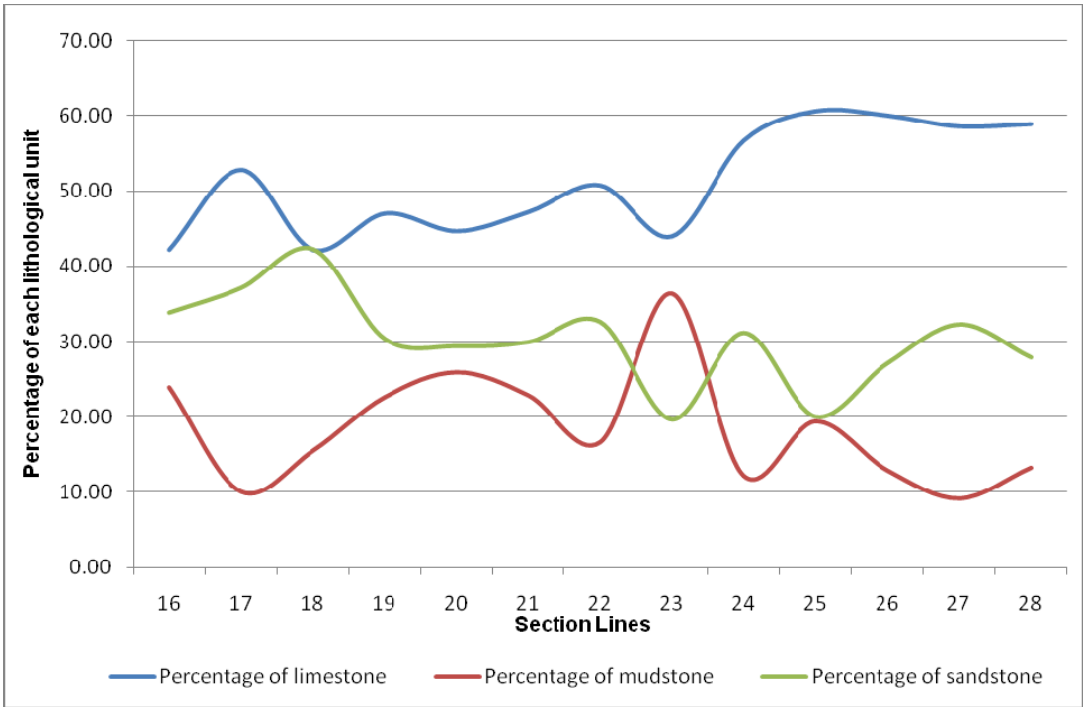

Figure 4.23 Percentages of each lithological unit throughout section lines 16 to 28

As discussed above section lines 18 to 28 cover the Alston Block and extend into the Northumberland Basin to the north and the Stainmore Basin to the south. Section lines 18 to 22 show clearly how the siliciclastics increase substantially as the section lines cross the Stublick Faults into the Northumberland Basin to the north,

whereas, apart from section line 18, little increase is seen in the siliciclastics as the Lunedale Faults are crossed and the Stainmore Basin entered to the south. These sections would imply that greater syn - rift sedimentation was occurring in the Northumberland Basin than the Stainmore Basin during the deposition of the Great Cyclothem. Chapter 2, section 2.2, suggested that by the Namurian, differential settlement between the Alston Block and Northumbrian Basin had terminated (Bott, 1987; Turner *et al*., 1995); however, section lines 18 to 22 show a greater thickness of siliciclastic sediment north of the Stublick and Ninety Fathom faults, suggesting differential settlement between the Alston Block and Northumbrian Basin was probably still active at this time.

Section lines 23 to 28 would suggest some movement was also occurring on the Pennine Fault system during deposition as can be seen by the increase of the siliciclastics towards the faults. The thickening of the sandstones is also easy to pick out as the Allercleugh Channel is approached and this is particularly noticeable in section lines 26, 27 and 28. Within section line 26 the channel can be seen to cut down into the Great Limestone near to the Slitt Vein.

Within section lines 16 to 28 a maximum of seven and a minimum of four sandstones are evident in the sections. Cycles of mudstone to sandstone are also evident within these section lines with at least three cycles and a maximum of five cycles being present. As marine cycles are not easily followed throughout the block and adjoining areas it is not clear whether these mudstone-sandstone cycles are true minor cycles as discussed by Dunham (1990). Minor cycles are defined by Dunham (1990) as a coarsening up from a mudstone of marine facies to sandstone, the sandstones would be expected to be topped by a coal or smut; however these are also not always visible within the field or described in logs

4.6 Sediment Compaction

The sediment thicknesses used in sections 1 to 28 are not necessarily a true representation of the original sediment as deposited; compaction would have occurred

as overburden increased during continued sedimentation. The amount of compaction that the sediments are subjected to during diagenesis is to a certain extent difficult, if not impossible to determine as this would depend upon many variables such as initial porosity, sorting of grains, facies, how quickly cementation occurred and overburden pressure. It is generally accepted, however, that significant reductions in porosity and therefore thickness of sediment can result during early diagenesis with only a few tens to hundreds of metres of sediment above (Goldhammer, 1997; Hillgartner and Strasser, 2003). Quantitative techniques are often used to analyse compaction of sediments (Baldwin, 1971; Perrier *et al*., 1974; Goldhammer, 1997; Hillgartner and Strasser, 2003) and decompaction is a useful technique used in back-stripping analysis; sediment thickness is decompacted by multiplying the present sediment thickness by a suitable decompaction number. This number is a ratio of the sediment thickness at a previous time (usually the original thickness at the time of deposition), to the present (compacted) thickness; the ratio usually depends upon overburden thickness.

There is some evidence in the thin sections of the Great Limestone examined in this study of preferred orientation of clasts and sutured contacts, suggesting that cementation occurred late in the initial stage of diagenesis; thickness reduction during physical compaction may therefore have been significant. Following the initial physical alteration and compaction, chemical compaction occurs as dissolution of the sediment is initiated through grain-to-grain contact and pressure dissolution. Chemical dissolution and in particular pressure dissolution can result in further reductions of thickness by up to 35% (Goldhammer, 1997).

Many micro-stylolites exist near to bedding and pseudo-bedding planes in the Great Limestone and even though it is difficult to determine exactly the loss of sediment due to the micro-stylolites, careful assessment of grains cut by them indicates loss is usually less than 0.1millimetres per micro-stylolite. There are in the region of 20 to 30 micro-stylolites at each bedding and pseudo-bedding plane,

suggesting losses of up to a few millimetres per bed. This minor loss could only have resulted in a 0.1% to 0.2% reduction in thickness of the limestone.

Larger stylolites also exist in many parts of the Great Limestone and it would not be difficult to imagine that losses here would be far larger than at the micro-stylolites; as yet however, it has proved impossible to estimate the sediment loss at these.

Sediment thickness reductions of 10% to 20% in carbonate sands, 50% in carbonate muds and 60% in terrestrial muds are possible by physical compaction at depths of only a few hundred metres (Baldwin, 1971; Perrier *et al*., 1974; Goldhammer, 1997). Creaney (1980) calculated a sediment thickness of 1km above the Great Limestone by the early Permian; a time span of approximately 30My. Using Goldhammer (1997) and Perrier *et al*. (1974) and overburden figures of 500m or even 1km, decompaction numbers in the region of 1.1 to 1.3 for carbonate sands, 1.6 to 2.1 for lime mudstones and 2.0 to 4.9 for terrestrial muds can be deduced. The carbonate figures are for physical compaction alone, higher ratios than this would suggest chemical as well as physical compaction had occurred (Goldhammer, 1997). Hillgartner and Strasser (2003) used decompaction figures of 1.2 for grainstones, 1.5 for packstones, 2 for wackestones and 2.5 for lime mudstones. Compaction to form coal not surprisingly depends upon the type of vegetation as well as overburden and temperature; Baldwin (1971) suggested decompaction numbers between 5.5 and 12 depending upon the age of the coal.

Both the compacted and de-compacted sections of the Great Cyclothem in Figure 4.24 are constructed from measurements taken at Hudeshope Beck (394751, 527633 and 394921, 527279) and Snaisgill Sike (395415, 526952) (and data from Hodge, 1965). Three sets of marker beds are shown on the section, which, from bottom to top, are, referred to locally as the ‘Jack Post’, ‘5 Thin Posts’ and the ‘Bottom Famp Mudstone’.

Thin-section analysis of the Great Limestone has revealed that the limestone is generally a packstone with small areas tending towards a packstone/wackestone In line with Hillgartner and Strasser (2003) a de-compaction value of 1.5 for the packstones and 1.75 for the packstones/wackestones have been used and where the facies is unknown or very recrystallised, a value of 1.5 has been used, i.e. a packstone has been assumed. A value of 3.5 (Perrier *et al*., 1974; Goldhammer, 1997) has been used for the mudstone partings between beds and for the thicker Bottom Famp Mudstone in the upper beds. A value of 1.1 has been used for the sandstone.

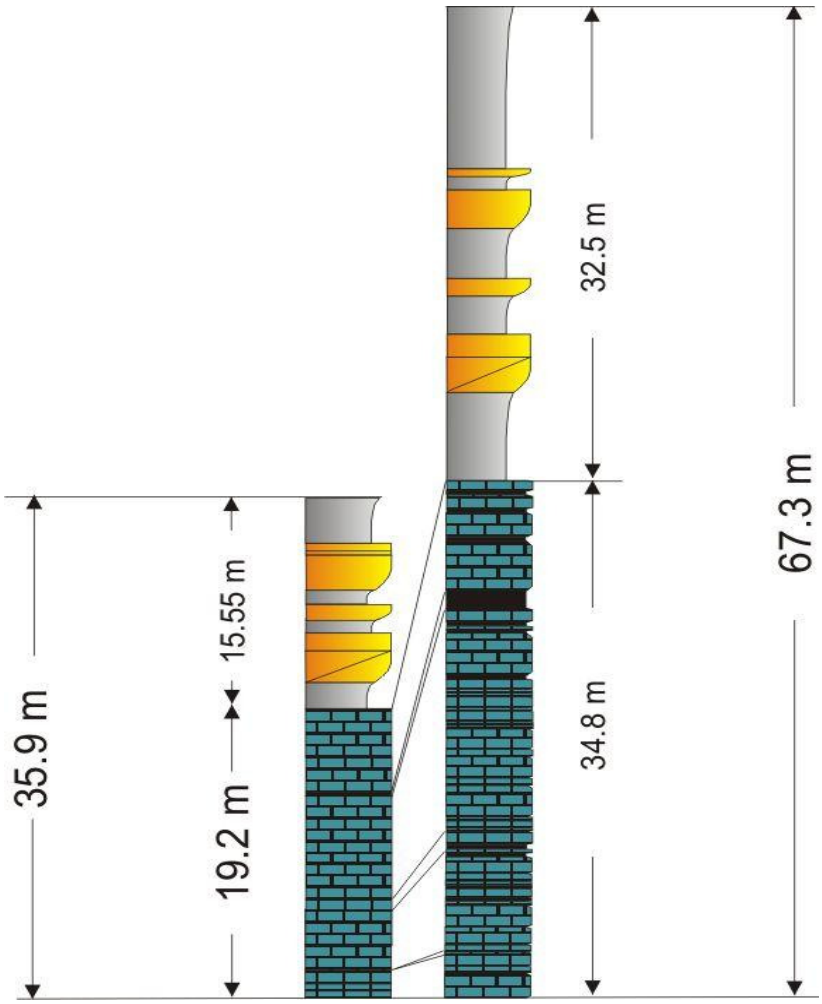

Figure 4.24 Compacted and decompacted cross sections. Data from Hudeshope Beck (394751, 527633 and 394921, 527279) and Snaisgill Sike (395415, 526952) and Hodge

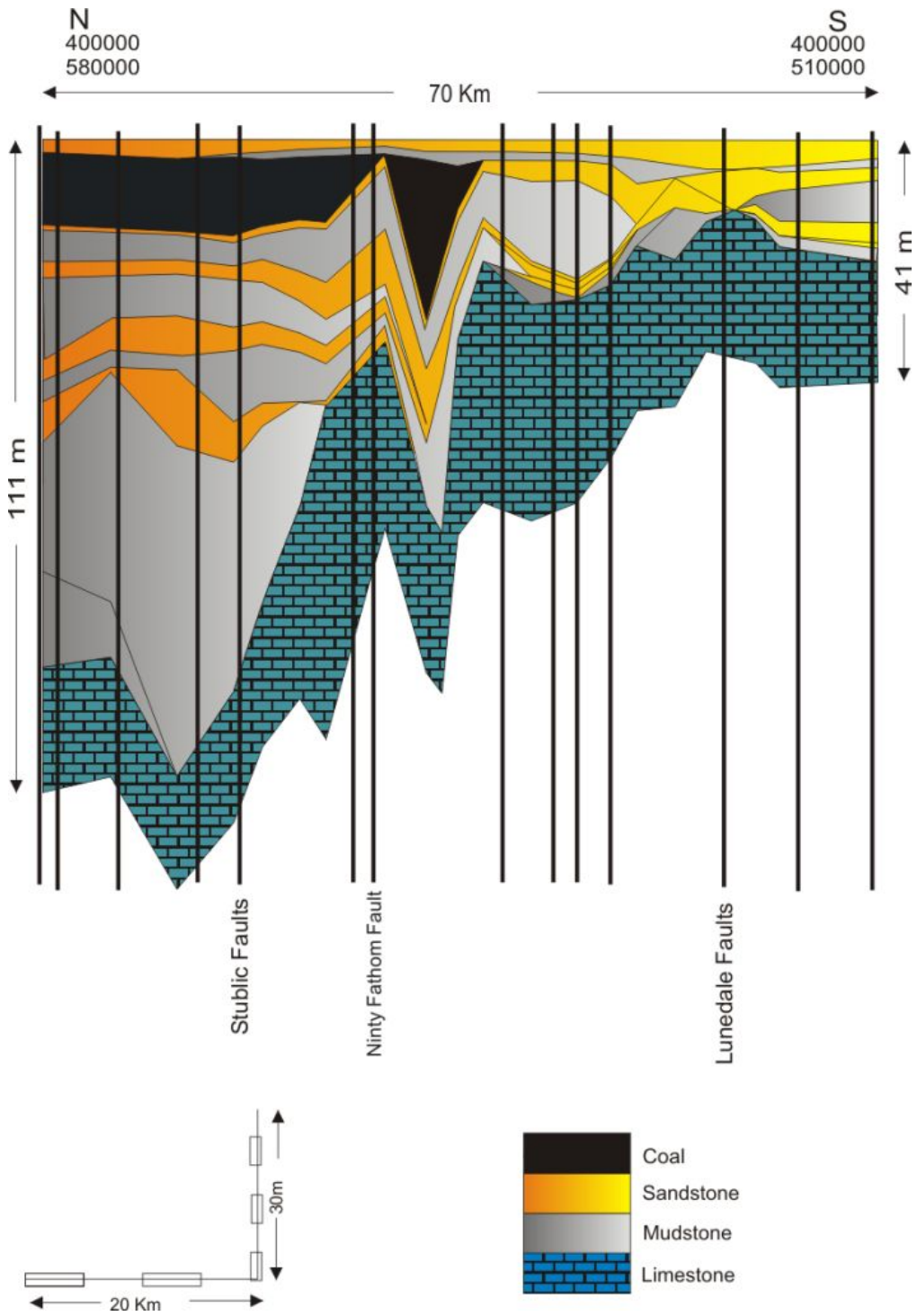

Figure 4.25 Decompacted section line 21 (Appendix A)

As expected from the decompaction figures used, the greatest decompaction occurs where the thickest terrigenous mudstone exists. Within the Great Limestone

this is at the positions of the 5 Thin Posts and in the Bottom Famp Mudstone in the top third of the limestone; the de-compacted section of the Great Limestone is approximately 1.75 times the compacted section. The de-compacted terrigenous sediments are approximately 2.1 times the compacted section, obviously due to the amount of mudstone present.

If a similar section were taken through the terrigenous sediments of Skears Mine, D or F Vein Rise, less compaction would be evident compared to Figure 4.24, as the Skears Sandbar has removed nearly all of the mudstones and thick sandstone remains (Hodge and Dunham 1991). At Skears Mine D or F Vein Rise, the compacted section has 25 metres of sandstone and 3.1 metres of mudstone giving a total of 28m of terrigenous sediment compared to 15.5 metres in Figure 4.24, de-compacting this gives a thickness of 38.4 metres which is very similar to the de-compacted section in Figure 4.24.

It becomes obvious from the de-compactions exercises how difficult it is to appreciate what the original sediment thickness may have been when looking at a compacted section. The percentage of mudstone and coal compared to sand within a compacted section makes a large difference in the decompaction. The decompaction given in Figure 4.24 and a comparison with Skears Mine D or F Vein Rise shows that in the Skears area the original deposited terrigenous sediment upper surface was surprisingly flat compared to the compacted sections; unfortunately this arrangement cannot be shown elsewhere on the block.

Figure 4.25 is a decompaction of section line 21 (Appendix B) using the decompaction values of 1.1, 1.5, 3.5 and 12 as discussed above. A comparison with the compacted section line 21 shows a substantial difference in thickness to the north, i.e. into the Northumberland Basin; the mudstones are very much thicker and as expected, the sandstones are only changed slightly. In Figure 25, the thickness of sediment north of the Ninety Fathom Fault is approximately 111 metres compared to

40 to 45 metres on the Alston Block and in the Stainmore Basin. The greater thickness of siliciclastic sediment north of the Stublick and Ninety Fathom faults suggests differential settlement between the Alston Block and Northumbrian Basin was probably still active as discussed in section 4.5.

The de-compacted thickness of the coal has to a certain extent distorted the section between the Ninety Fathom Fault and the faults to the south; however, a general thinning onto the block can be seen. Sediment thickness increases substantially into the Northumberland Basin, north of the Ninety Fathom Fault. The greater thickness of mudstone in the Northumberland Basin would have resulted in differential compaction occurring between the basin and the block.

Any discussion on the subject of decompaction could be regarded as being fraught with problems as decompaction figures cannot take into account every inconsistency and may ignore many factors such as early cementation, early or late dewatering (which may determine when compaction commences in mudstones, coal and peat), and calibration problems of converting experimental pressure into burial depths. These problems; however, are not thought to totally negate the results and the benefits gained from back-stripping techniques such as this and the resulting graphical representations of cross sections 21 and 29 and Figures 4.24 and 4.25 are useful in understanding the decompaction history of the Great Cyclothem and the differential compaction occurring at the time of deposition between the Alston Block, the Northumberland Basin and the Stainmore Trough.

4.7 Metasomatism and mineralisation

The cross sections and the decompaction discussed above do not take into account diagenetic factors such as alteration by mineralisation, i.e. metasomatism and famping.

Alteration of the limestones by mineralisation fluids is well known in the area with alteration to ankerite and siderite being common. This type of alteration can

result in up to a third reduction in thickness due to changes in density (Dunham, 1990); however it does not usually cover such large areas as to be visible at the scales used in the cross sections.

Mineralisation and weathering of limestone (mainly the Great Limestone) has, in places, resulted in the chemical deterioration to an ochreous clay known locally as famp (Hodge and Dunham, 1991; Burgess and Holliday, 1979). Famping has resulted in considerable thickness reduction down to a few metres in places (Burgess and Holliday, 1979). These alterations and the subsequent thickness reductions occur very locally and as such have not been included in any of the cross sections.

4.8 Condensation of the Great Limestone

Local thinning or condensation of the Great Limestone can be seen in places such as Ashes Quarries and Washpool Crags (398485, 535035 and 399958, 539711) where the thickness of the limestone units has reduced by up to a half. Substantial thinning of the Great Limestone is also reported in borehole logs by Blue Circle Cement for the East Gate Quarry Operation in East Black Hill, Weardale (390989, 534788).

Fairbairn (1978) reported significant variations of the Great Limestone, compared to the general Weardale succession, at East Ashes Quarry, Washpool Crags Quarry, Harrow Bank Quarry and within the ground to the west of Newlandside Quarry. Fairbairn's section of East Ashes Quarry shows the thinning commencing low in the Great Limestone section but there is a full development of the Tumbler Beds; he also noted the reduction in abundance of macrofossils in these areas. Fairbairn suggested the thinning of the Great Limestone beds occurs in a linear north-south trending belt, possibly associated with thick sandstones both above and below the limestone.

The thickness of the Great Limestone in the area of the Blue Circle works averages at around 24 metres, 4 to 5 metres thicker than at Middleton-in-Teesdale and

the thickness at "Area H" reflects this. Surprisingly, the thickness at "Area C" is somewhat thinner at 11 to 16 metres of which the Tumbler Beds account for up to 75 % of the section thickness, rather than the usual 25 % elsewhere in Weardale and Teesdale.

Approximately 2 metres above the base of the quarry at Washpool Crags, the beds thin substantially by up to 50 percent. This thinning occurs within a couple of hundred metres and can be seen easily wth the naked eye. On a close examination it can be seen that the thinning is associated with a marked decrease in macrofossils.

Hodge (1965) discussed various areas on the Alston Block where thinning of the Great Limestone occurs and he attributed the thinning to removal of the limestone through down-cutting of channels in the overlying sandstones or through famping, i.e. chemical deterioration of the limestone to ochreous clay. Hodge also noted a regional thinning of the Great Limestone in a north and north-west direction into and through the Northumberland Basin where the upper part of the limestone is replaced by shale.

The thinning at Area C still retains the Tumbler Beds, which are of average thickness for the area, and does not show any sign of down cutting by channelled sandstone or association with significantly thick sandstones within the terrestrial section of the cyclothem. The Tumbler Beds at Washpool Crags are not visible in the section; however, beds commence thinning a few metres above the base at bed 6 and it is possible to see the thinning of individual beds over a few hundred metres, suggesting that the thinning is not attributable to channel cutting; in neither case is chemical deterioration evident.

4.9 Conclusion

This chapter considered thickness variations of the Scar to Little cyclothems across the Alston Block and how these variations are reflected within adjoining cyclothems. These thickness variations reflect localised differential settlement and probably uplift on the block as well as a longer term flexing of the block in a west to

east and north to south direction creating rhythmic alternations of cyclothem areas. The thicknesses of limestones in the cyclothems are generally constant and change by a few percent only; however the thicknesses of the siliciclastics can be seen to change greatly. This movement of the block could have been an important control on sedimentation.

Further consideration of the Great Cyclothem, in isolation, suggests differential settlement was still active between the Alston Block and Northumberland Basin during the early Namurian. Decompaction of the Great Cyclothem sediment pile would suggest at least a two-fold increase in sediment deposition within the Northumberland Basin compared to the Alston Block. Differential compaction and settlement would have been a significant control on sedimentation resulting in the different rates seen between the blocks and troughs.

Localised thinning of the Great limestone have been associated with chemical alteration by mineralising fluids, channel sandstones in the cyclothem below the Great Limestone and large channels above the Great Limestone. Localised thinning of the Great Limestone is also known due to down-cutting by the Allercleugh channel.

5.0 Bioclast analysis and palaeoecology of the Great Limestone

5.1 Introduction

The fossil assemblages of the Great limestone have been partially discussed within Chapter 3 where the three major biostromes, the *Chaetetes* band, the Frosterley band and the Brunton band were considered. The *Chaetetes* band and the Frosterley band consist of macrofossil assemblages which are prevalent within the biostromes whereas the Brunton band consists of microfossils seen only in thin section.

This Chapter considers further the microfossil bioclastic assemblages prevalent within the Great Limestone and in particular it considers the environmental controls within the depositional environment. In Chapter 3 the Alston Block was shown to be submerged by the late Asbian to form a shallow epeiric sea with the depth of deposition of the Great Limestone, interpreted as being in the outer shoreface/transition to offshore environment with water depths varying between 5 to 50 metres but generally at or below fair-weather wave-base. Whether an epeiric ramp or aggraded platform model is most appropriate for the microfacies of the Great Limestone is not as such clarified by this research; nevertheless, both models share may similarities.

The Great Limestone lithofacies does not show any systematic changes throughout its stratigraphical thickness; however, at a sub-microfacies level some change can be seen within the bioclast communities. From a palaeoenvironmental point of view it is these changes that are considered here.

This Chapter tests therefore, the hypothesis that changes exist in the bioclast associations throughout the thickness of the Great Limestone and that these changes are related to depth or another palaeoenvironmental factor. To offer an alternative hypothesis would therefore be to accept that there are no obvious changes throughout the thickness of the Great Limestone with regard to bioclast associations and therefore environmental changes.

5.1.1 Abundance and data collection methods

Analysis of 62 thin sections from Middleton-in-Teesdale (O. S. 394784, 527610 and O. S. 394916, 527276, Figure 5.1) was carried out to assess the major carbonate contributing bioclasts within the Great Limestone and 45 of these were assessed further in greater detail. This analysis and fossil identification was carried out by myself with further help in fossil identification been provided by Dr. Daniel Vachard, University of Lille, and Pamela Denton, Open University PhD student. Abundance matrices of results of the thin-section analysis are given in Appendix D, Tables 5.1 and 5.2. The abundance matrices in Appendix D are shown with taxa in columns and samples in rows.

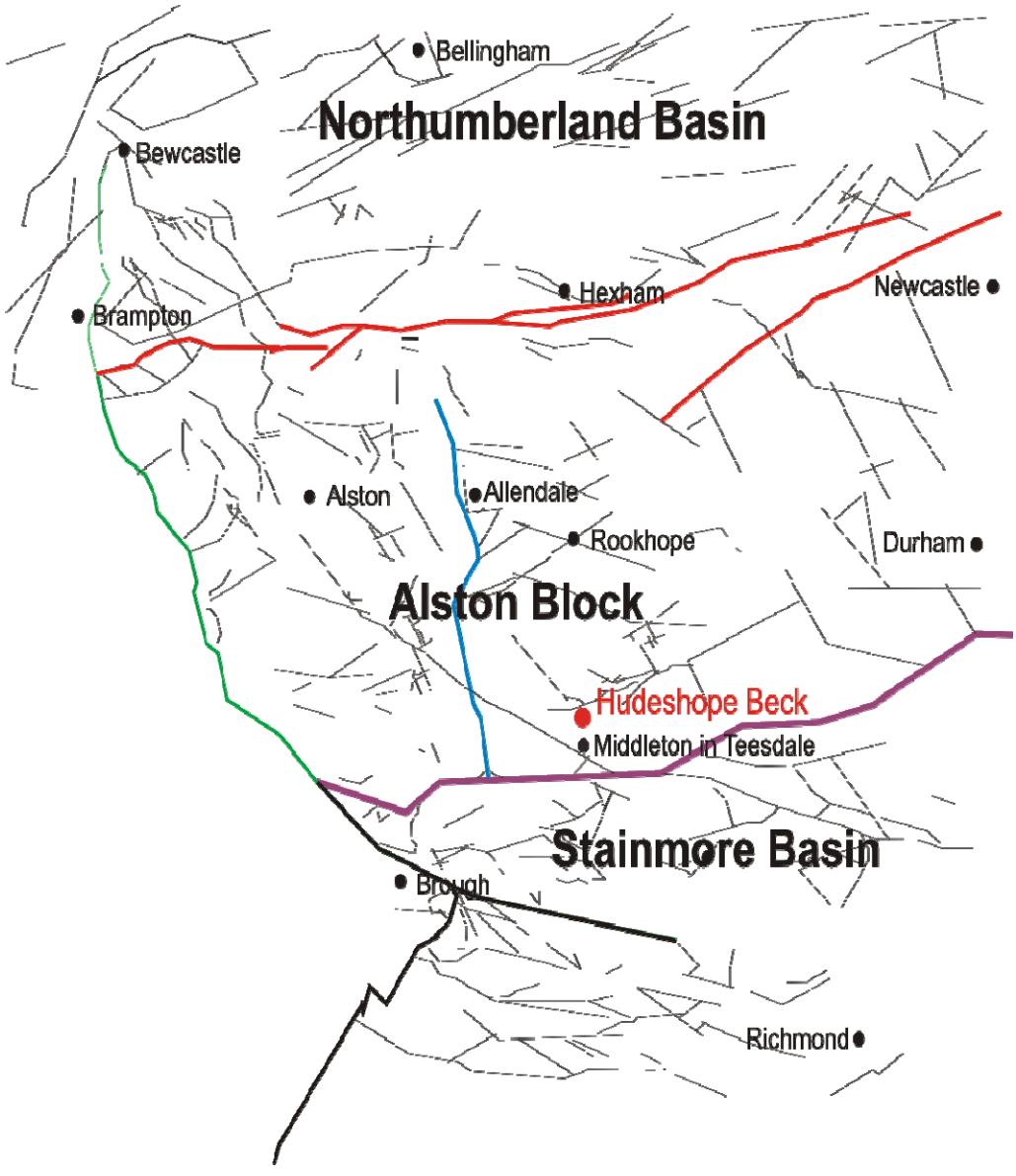

Figure 5.1. Sample Location, Hudeshope Beck
O. S. Grid reference 394784, 527610 (Jacks Scar), and 394916, 527276 (Skears Quarry).

The 62 thin sections from Middleton-in-Teesdale (Appendix D) were initially analysed for 7 dominant bioclasts: gastropods, brachiopods, crinoids, corals, bryozoans, ostracods and foraminifera. 45 of these 62 thin sections were then arbitrarily selected and analysed further for algae and foraminifera (Appendix D).

The abundance of grains was determined through the use of area counting; grains lying within the area of the thin-section were counted. The average size of thin sections analysed is 30 millimetres by 21 millimetres; where a thin-section was less than 30 millimetres by 21 millimetres the number of grains was recalculated to the average thin-section size.

It is obvious from the abundance matrices that all of the samples are dominated by fragments of brachiopods, crinoids, bryozoans and foraminifera, with minor constituents of the other grains; however, it must be remembered that many of the bioclast fragments are probably the result of fragmentation of larger specimens. Some bioclasts such as corals, brachiopods and *Chaetetes* are also seen in the field in growth position. Crinoids, mainly echinoderm fragments, are common in 99% of the thin sections, bryozoans in 91% and brachiopods in 55%.

5.1.2 Data analysis

Each grain type is considered in relation to published data to assess their importance with regard to palaeobathymetry. In order to assess any environmental gradients within the data various multivariate methods are used to assess the data including Biodiversity analysis, Seriation, Cluster Analysis and Correspondence Analysis. All analysis has been carried out using PAST (Hammer *et al.* 2001). Due to the disarticulation of some bioclasts, as discussed above, the techniques have been carried out using presence/absence data rather than absolute abundance unless otherwise stated.

5.2 Discussion of grain types

Each grain type recognised is described in the following section. The purpose of this section is to discuss the abundance of each grain and to assess any depth related environmental information from published data.

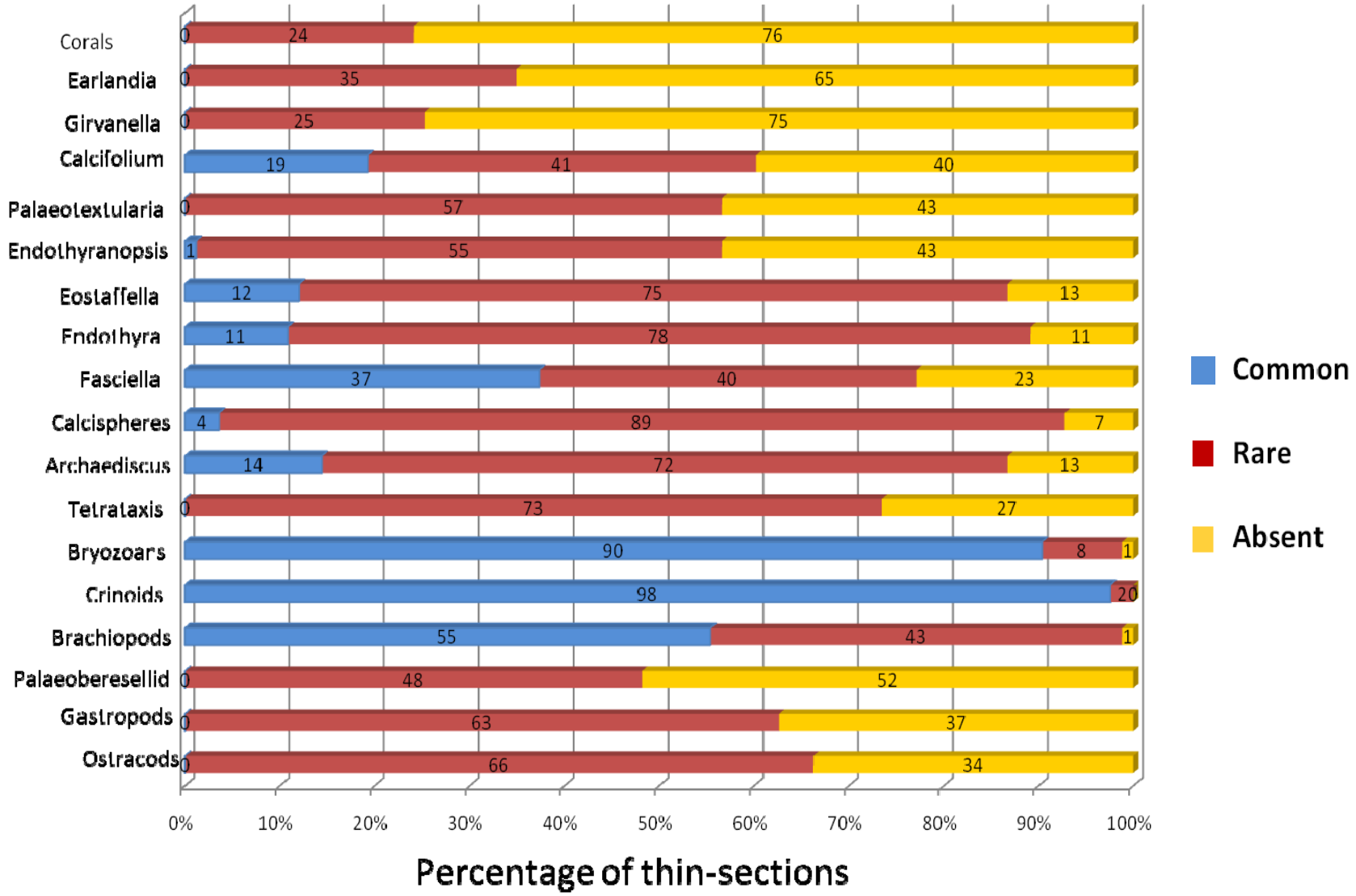

Figure 5.2 Percentages of grains within thin sections. Common = present in > 30% of thin sections and Rare = present in <30% and >0% of thin sections

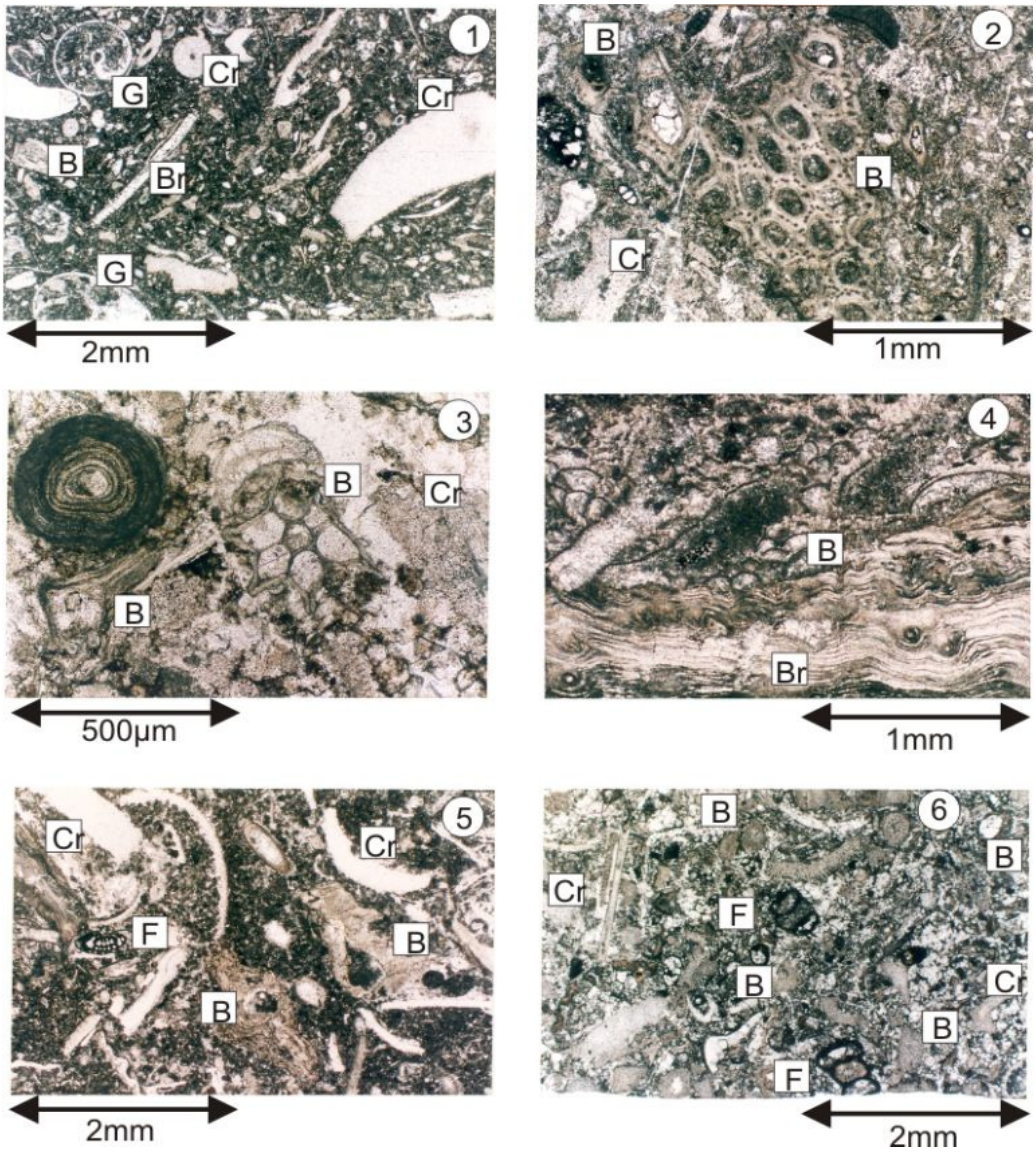

Figure 5.3 Crinoid (Cr) and bryozoan-rich (B) packstone thin sections 1=Crinoids, bryozoans, gastropods (G) and brachiopod fragments, 2=Stenoporid trepostrome (bryozoan) fragment, 3= Section through Rhabomeson (bryozoan), 4=Fistulipora (bryozoan) encrusting a pseudopunctate brachiopod (Br), 5 and 6= thin sections rich in crinoids, brachiopods, bryozoans and foraminiferans.

5.2.1 Crinoids and Bryozoans

Crinoids are common to abundant within 98% of the thin sections and rare in the remainder. Bryozoans are also common to abundant in 90% of thin sections, rare in 8% and absent in the remainder. Figure 5.3 shows thin sections consisting of crinoidal and bryozoan rich packstones where various bryozoan taxon are present. Gallagher (1998) and Madi *et al*. (1996) both interpreted crinoid and bryozoan thickets to accumulate at or below fair-weather wave base. Madi *et al*. (1996) found that ramose (branching) bryozoans were found at higher energy levels than fenestellid bryozoans; both ramose and fenestellid fragments

were found together within the thin sections analysed in this research. The crinoidal and bryozoan rich packstone is suggestive of the Great Limestone being deposited within environments at or below fair-weather wave base.

5.2.2Fasciella

Fasciella (Figure 5.4-1 and 2) is an encrusting red alga composed of irregular concentric layers of elongated hyaline cells (i.e. clear and containing no fibres or granular material) with yellowish walls. These algae are common in 37% of thin sections analysed, rare in 40% of thin sections and absent in the remainder (Figure 5.2).

All thin sections (except one) containing *Fasciella* also contain green algae indicating probable deposition within the euphotic zone. Flügel (2004) suggested *Fasciella* is common in both the euphotic and dysphotic zones and is also common within high-energy environments; Cózar (2005) also found *Fasciella* in both the deep-water and shallow-water facies of the early Serpukhovian of the Guadiato area southwestern Spain. The presence of *Fasciella* may not therefore be an ideal indicator of environmental changes.

5.2.3 Palaeoberesellids

Palaeoberesellids (Figure 5.4-3 and 4) are now regarded by workers as green algae belonging to the Dasycladaceans (Adams and Al-Zahrani, 2000; Flügel, 2004). They are seen in thin section as tubular, septate microfossils usually consisting of single crystal calcite plates with undulose extinction; however, a few large crystals may be present instead of a single crystal. These algae are rare in 48% of thin sections analysed and absent in the remainder (Figure 5.2). All thin sections containing Palaeoberesellids also contain other green algae and 85% of these also contain *Fasciella.* If Palaeoberesellids are to be accepted as dasyclads then the presence of dasyclad green algae will indicate the upper part of the euphotic zone (Flügel, 2004); Adam *et al.*, (1992), Horbury and Adams (1996) and Gallagher (1998) found Palaeoberesellids thrive in water depths of around 10 metres.

5.2.4 Calcispheres

Calcispheres (Figure 5.4-5 and 6) are regarded by most workers as being algal cysts (Flügel, 2004); however, Versteegh *et al.* (2009) considered that there is still confusion with respect to the nature and designation of these simple spherical calcareous microfossils of usually unknown biological affinity and proposed a new group called Calcitarcha to include all calcareous microfossils with a central cavity for which the biological affinities remain unknown. Calcispheres are seen in thin section as spherical or egg shaped, hollow microfossils with calcareous walls. These "algae" are common to abundant in 4% of thin sections analysed in this study, rare in 89% and absent in the remainder. Of all thin sections containing Calcispheres 82% contain other green alga and 83% also contain the red alga *Fasciella*. Calcispheres thrived in shallow-marine platforms and ramps during the Palaeozoic (Flügel, 2004).

5.2.5 Calcifolium

Calcifolium is regarded by many workers as being a problematic alga with assignment still in flux; Cózar and Vachard (2004) reported many morphotypes. *Calcifolium* has a pelotoid shape of tiny tubular filaments with tubes/canals (Figure 5.4-7 and 8). *Calcifolium* was found by Cózar (2005) in both deep-water and shallow-water facies of the early Serpukhovian of the Guadiato area southwestern Spain. *Calcifolium* is common in 19% of thin sections analysed, rare in 41% of thin sections and absent in the remainder (Figure 5.2). 94% of the samples containing *Calcifolium* also contain *Fasciella* and in approximately half of these samples both *Calcifolium* and *Fasciella* are common to abundant. The thin section analysis of the Great Limestone at Middleton in Teesdale shows *Calcifolium* occurring as two distinct groups around the middle of the limestone and always in the presence of green alga. This suggests occurrence within the euphotic zone rather than the dysphotic zone.

5.2.6 Earlandia

The foraminifera *Earlandia* are seen in thin section as a spherical proloculus (initial chamber) followed by a cylinder or flaring tube with a microgranular calcite cemented wall (Fewtrell *et al.*, 1981; Flügel, 2004). *Earlandia* is rare in 35% of thin sections and absent in the remainder (Figure 5.2). Gallagher (1998)

regarded Earlandia as surviving in a wide range of sub-tidal environments i.e. above and below fair-weather wave base; therefore this taxon is probably not an important environmental indicator.

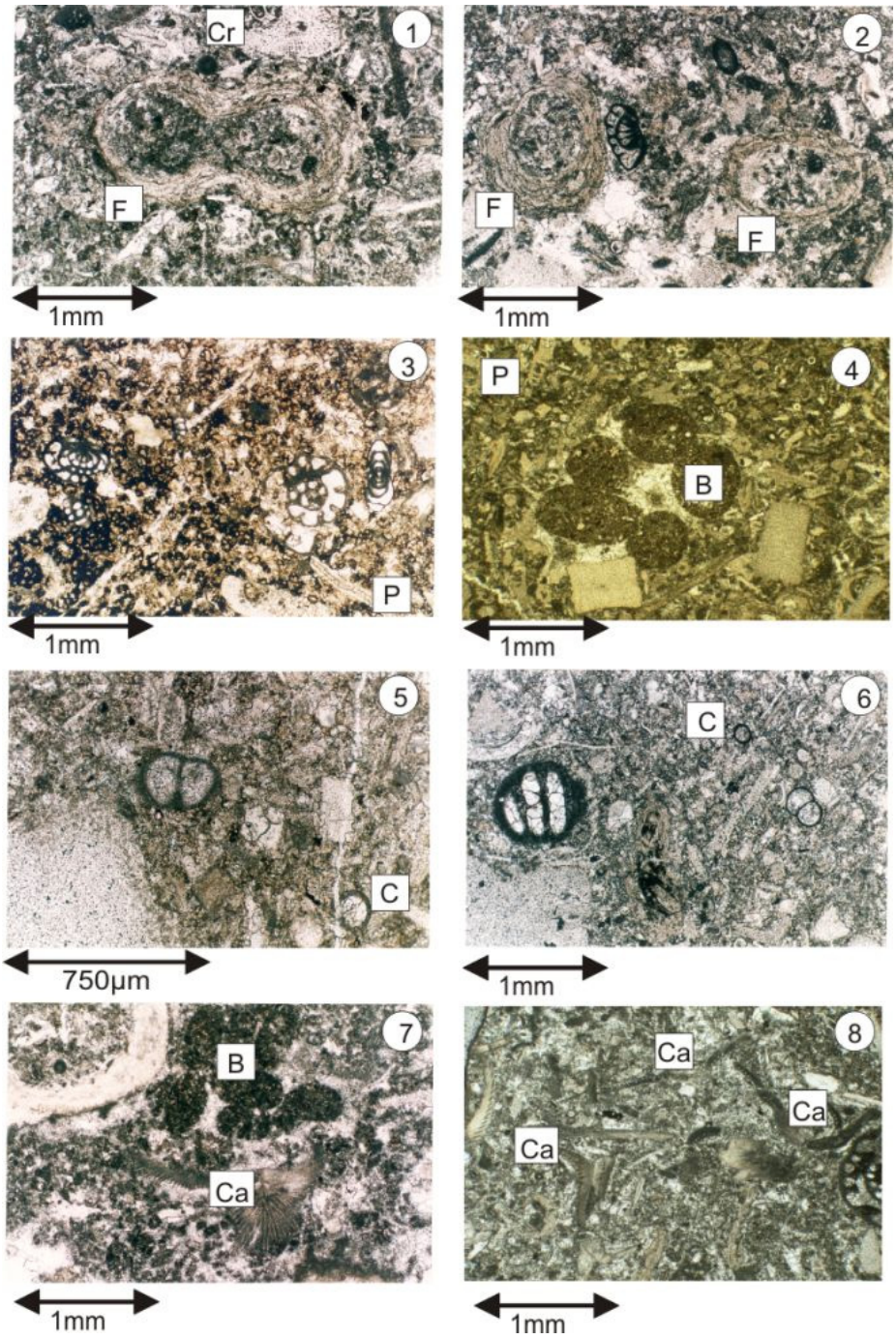

Figure 5.4 Alga contents of Great Limestone thin sections 1=*Fasciella* (F), 2=*Fasciella* (F), 3=small fragments of Palaeoberesellids *(P)*, *4*= small fragments of Palaeoberesellids *(P)* and burrows, 5=Calcispheres (C), 6=Calcispheres (C), 7= Calcifolium (Ca) and burrows (B), 8= Calcifolium (Ca)

5.2.7 Palaeotextularia

Palaeotextularia is rare in 57% of the thin sections analysed and absent within the remainder. *Palaeotextularia* is recognised within thin section as comprising 5 to 12 pairs of biserially arranged chambers with straight or gently arched tests (Hallett, 1970; Fewtrell, *et al.*, 1981; Gallagher, 1998; Flügel, 2004). Gallagher (1998) suggested that *Palaeotextularia* survived above fair weather base between 5 and 10 metres depth and Madi *et al.* (1996) also found *Palaeotextularia* in shallow water facies.

5.2.8 Endothyrids

The Endothyrids, *Endothyranopsis* and *Endothyra*, occur in 93% of thin sections analysed here. They are seen in thin section as multilocular (multi-chambered) foraminifera having microgranular/agglutinated walls containing secondary deposits within the base of the chambers. Haynes (1981) regarded these adaptations as providing sufficient strength to the walls to enable survival in high energy environments and Madi *et al.* (1996) also found Endothyrids in shallow-water facies. Gallagher (1998) suggested that *Endothyranopsis* and *Endothyra* may have been capable of inhabiting slightly different environments with *Endothyranopsis* inhabiting slightly deeper environments probably below fair-weather wave-base, between 10 metres and 20 metres.

The foraminifera *Endothyranopsis* is seen in thin section as planispiral multi-chambered and involute foraminifera with a microgranular calcite cemented wall (Fewtrell *et al.*, 1981; Flügel, 2004). *Endothyranopsis* is common in 1% of thin sections analysed here; rare in 55% of thin sections and absent in the remainder (Figure 5.2).

Endothyra is seen in thin section as planispiral to streptospiral multi-chambered foraminifera with a microgranular calcite-cemented wall (Fewtrell *et al.*, 1981; Flügel, 2004). This taxon is common to abundant in 11% of thin sections analysed, rare in 78% of thin sections and absent in the remainder (Figure 5.2).

5.2.9 Eostaffella

In thin section *Eostaffella* has involute, lenticular to nautiloid planispiral coiling tests which are laterally compressed. The walls are granular to microgranular calcite cemented (Fewtrell *et al.*, 1981; Flügel, 2004). *Eostaffella* is common to abundant in 12% of thin sections analysed, rare in 75% of thin sections and absent in the remainder (Figure 5.2). Gallagher (1998) found no apparent relationship between *Eostaffella* and diagnostic algal types in the Lower Carboniferous of Ireland, suggesting that this genus prevailed in a wide range of palaeoenvironments.

5.2.10 Archaediscus

Archaediscus is the most abundant of the foraminifera found in this study and is common to abundant in 14% of thin sections analysed, rare in 72% and absent in the remainder (Figure 5.2). The *Archaediscus* in this research has not been differentiated further in to genera. In thin section *Archaediscus* has micritic/prismatic wall structures composed of clear fibrous outer layers and microgranular inner layers, and non-septate tubular chambers coiled in various planes (Fewtrell *et al*., 1981; Gallagher, 1998). Madi *et al.*, (1996) found the shallow water facies of the Upper Viséan of the Béchar Basin, Western Algeria rich in *Archaediscus* numbers.

5.2.11 Tetrataxis

Tetrataxis is seen in thin section as trochospirally coiled with a concave base, flattened helically arranged chambers and bilayered walls (Fewtrell *et al.*, 1981; Gallagher, 1998: Flügel, 2004). *Tetrataxis* is rare in 73% of thin sections and absent in the remainder (Figure 5.2).

Gallagher (1998) suggested that *Tetrataxis* lived in depths exceeding 5 metres with an optimum depth of 10 metres and Madi *et al.* (1996) also suggested *Tetrataxis* is a common in shallow-water facies. Cossey and Mundy (1990), however, suggested that the limpet-like grazing nature may well have resulted in *Tetrataxis* being able to occupy other niches and not be restricted to any particular depth or lithofacies.

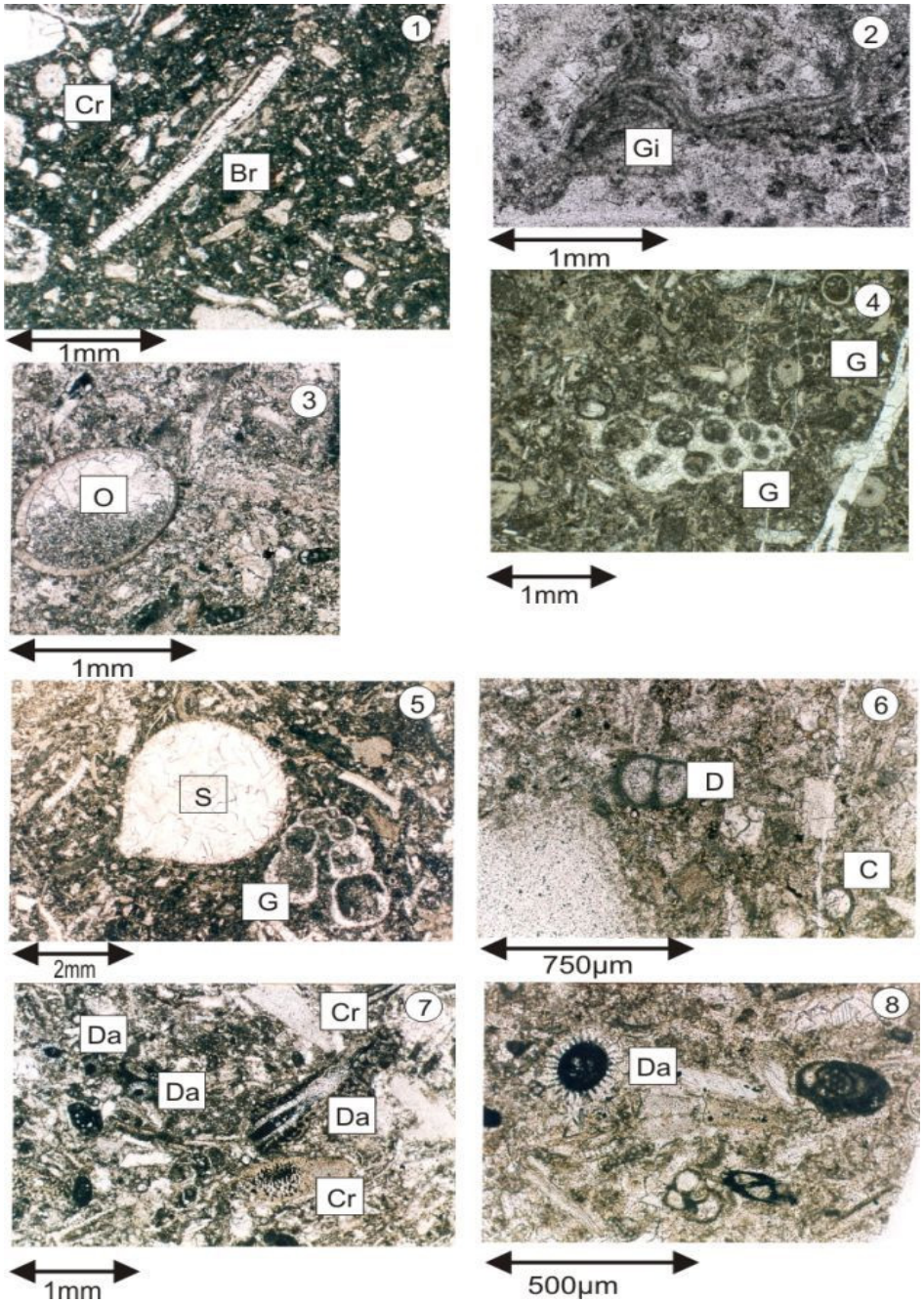

Figure 5.5 Thin section details of the Great Limestone 1=punctate brachiopod (Br), 2=*Girvanella* (Gi), 3=Ostracod (O), 4=Gastropod (G), 5=*Saccaminopsis* (S), 6=*Draffania* (D), 7=Dasyclad algae (Da) and crinoids (Cr) both cross section and longitudinal sections can be seen, 8=Cross section of dasyclad algae (Da).

5.2.12 Brachiopods

Modern brachiopods are common in all marine environments (Flügel, 2004) with palaeoenvironments for many fossil brachiopods suggested to range from the lower dysphotic zone to the upper euphotic zone around fair-weather wave base (Madi *et al.*, 1996). The brachiopod fragments found in the thin section analysis belong to the Class Articulata (hinged). Commonly fragments of pseudopunctate brachiopods are found; however, both punctate and impunctate

fragments are also rarely found. Pseudopunctate brachiopods such as Productids (*Gigantoproductus* and the smaller *Latiproductus*) are common throughout the Great Limestone and the small punctate *Dielasma* and impunctate spirifers can also be found. Brachiopods are common to abundant in 55% of thin sections and rare in 43% of thin sections (Figure 5.2).

5.2.13 Ostracods

Spence and Tucker (1999) regarded ostracods as being especially abundant in shallow hypersaline or brackish waters and in low-energy environments; however, Flügel (2004) and Bennett (2008) found ostracods within all aquatic environments. Ostracods (Figure 5.4-3) are rare in 66% of thin sections analysed in this research and absent in the remainder (Figure 5.2).

5.2.14 Gastropods

Gastropods are rare in 63% of thin sections analysed in this research and absent in the remainder. Gastropods live in terrestrial, freshwater as well as most marine environments and therefore may not be ideal environmental indicators.

5.2.15 Girvanella

Girvanella is an endolithic cyanobacteria, also known as calcimicrobes and blue green alga. It is seen in thin section (Figure 5.5-2) as thin walled sub-millimetre tubes which can form small nodules, be encrusting or sheet like. *Girvanella* is found in 25% of thin sections within this research and only as loosely tangled sheets.

Flügel (2004) regarded *Girvanella* to be most common within the upper photic zone above fair-weather wave base. Wolfenden (1958) recoded *Girvanella* in the reef and fore-reef complexes of a Mid-Viséan reef of northwest Derbyshire and Cózar (2005) found *Girvanella* in both the deep-water and shallow water facies of the early Serpukhovian of the Guadiato area southwestern Spain, as a depth indicator *Girvanella* may not; therefore, be ideal.

5.2.16 Saccaminopsis and the problematicum Draffania

Only two specimens of *Saccaminopsis* (Figure 5.5-5) were noted in the thin sections analysed. *Saccaminopsis* has had an uncertain past with it being

regarded as a foraminifera (Gutteridge, 1990) and then dasycladacean alga (Skompski, 1986; Poncert, 1989) and it is now again regarded as a foraminifera. Waters and Davies (2006) found *Saccaminopsis* together with *Girvanella* and attributed the deposition to be in comparatively shallow water; while Flügel (2004) regarded *Saccaminopsis* as being characteristic of the dysphotic bathymetric zone. The use of *Saccaminopsis* for environmental analysis could therefore be fraught with uncertainty.

The problematicum *Draffania* (Figure 5.5-6) was also noted within thin sections; however, this was limited to one specimen only. Somerville and Cózar (2006) discarded the affiliation of *Draffania* with foraminiferans, alga and crinoids and thought that it was related to fenestrate bryozoans and their palaeoecological constraints. Somerville and Cózar (2006) regarded the stratigraphic range of *Draffania biloba* to be the mid to late Viséan (Holkerian to Brigantian) and not the Namurian with most specimens being associated with abundant bryozoans and crinoids as is the case in the thin sections analysed here. Somerville and Cózar (2006) recognised *Draffania* as being found in shallow-marine water as well as in deeper, open-marine environments such as the typical deep-water, low-energy Waulsortian banks of the late Tournaisian. As with *Saccaminopsis,* the use of *Draffania* for environmental analysis may be uncertain.

5.2.17 Dasyclad alga

Dasyclad alga are marine green alga which are common within very shallow-water depths of only a few tens of centimetres down to depths of less than 10 metres (Flügel 2004; Madi *et al*. 1996). They are most common within the tidal to uppermost sub tidal zone. They are rare in thin sections analysed here and were only seen in a few thin sections as both cross and longitudinal fragments (Figures 5.5-7 and 5.5-8).

Figure 5.5-7 shows dasyclad alga together with crinoids, although according to Flügel (2004) and Madi *et al.* (1996) they did not co-exist within the same water depths or energy environments and are probably ecologically incompatible. This may suggest that the dasyclads found in this thin section analysis are allochthonous rather than autochthonous, having been transported by

wave or tidal currents to a deeper and less energetic environment or during remixing of adjacent facies.

5.2.18 Corals

Corals are generally seen within the Great Limestone as macrofossils rather than microfossils and, apart from their presence in the lower beds and the "Frosterly" biostromes, they are minor components within the limestone. Nevertheless, they are discussed here to facilitate estimation of environmental conditions and microfacies analysis.

The main factors affecting coral distribution, as with all other grain types discussed in this analysis, include substrate, turbidity, water energy, depth and light. Hubbard (1970) and Scrutton (1998; 1999) regarded the Palaeozoic corals as being unattached benthic organisms dominantly members of the orders Rugosa and Tabulata with Hetrocorallia being minor components. As the corals were dominantly unattached, stability of the organisms was gained from support by the sediment. As can be seen from Figures 5.6 and 5.7 coral support mechanisms varied between simply lying upon the sediment surface to support through burying by sediment. It may be expected that waters above soft muddy substrates would have been turbid, depending upon sedimentation rate, water movement and binding. This would suggest that Palaeozoic corals had some tolerance to turbidity (Scrutton, 1999)

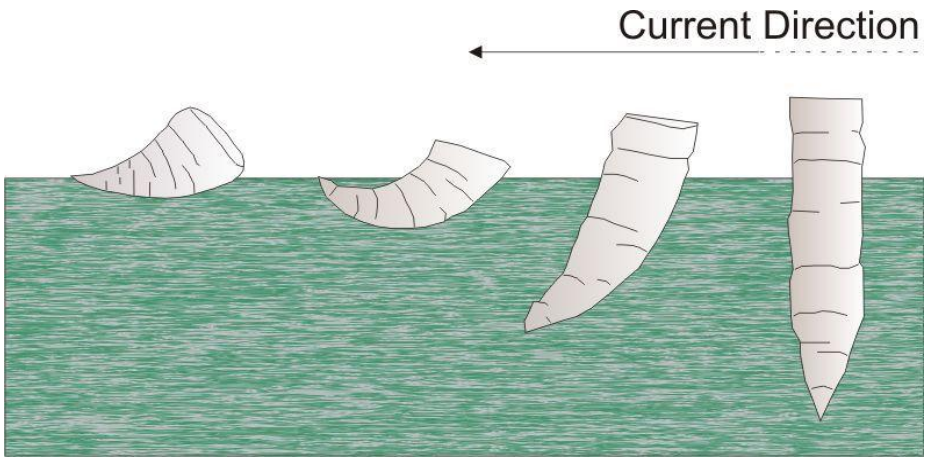

Figure 5.6 Solitary coral support adaptations. After Scrutton (1998; 1999).

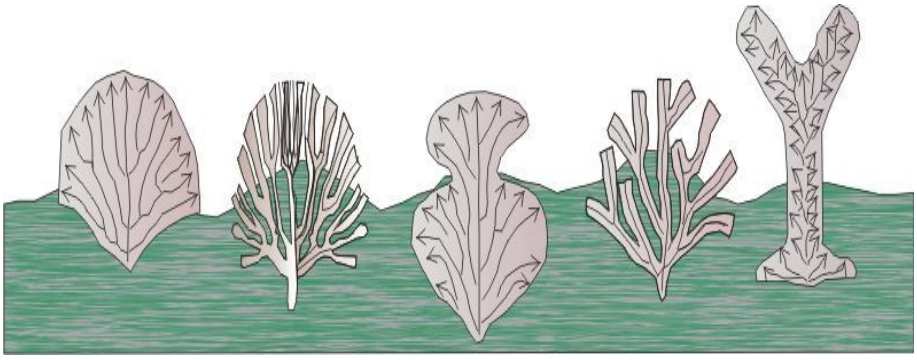

Figure 5.7 Tabulate coral support adaptations. After Scrutton (1998; 1999).

Figure, 5.6 shows coral fragments found within thin sections analysed in this research. The vast majority of the corals found within the Great Limestone are Rugose solitary corals, such as *Dibunophyllum bipartitim*; however, the Rugose fasciculate corals *Siphonodendron* and *Lonsdaleia* are also present. *Lonsdaleia* is often found near the base of the Great Limestone where it often replaces *Chaetetes*.

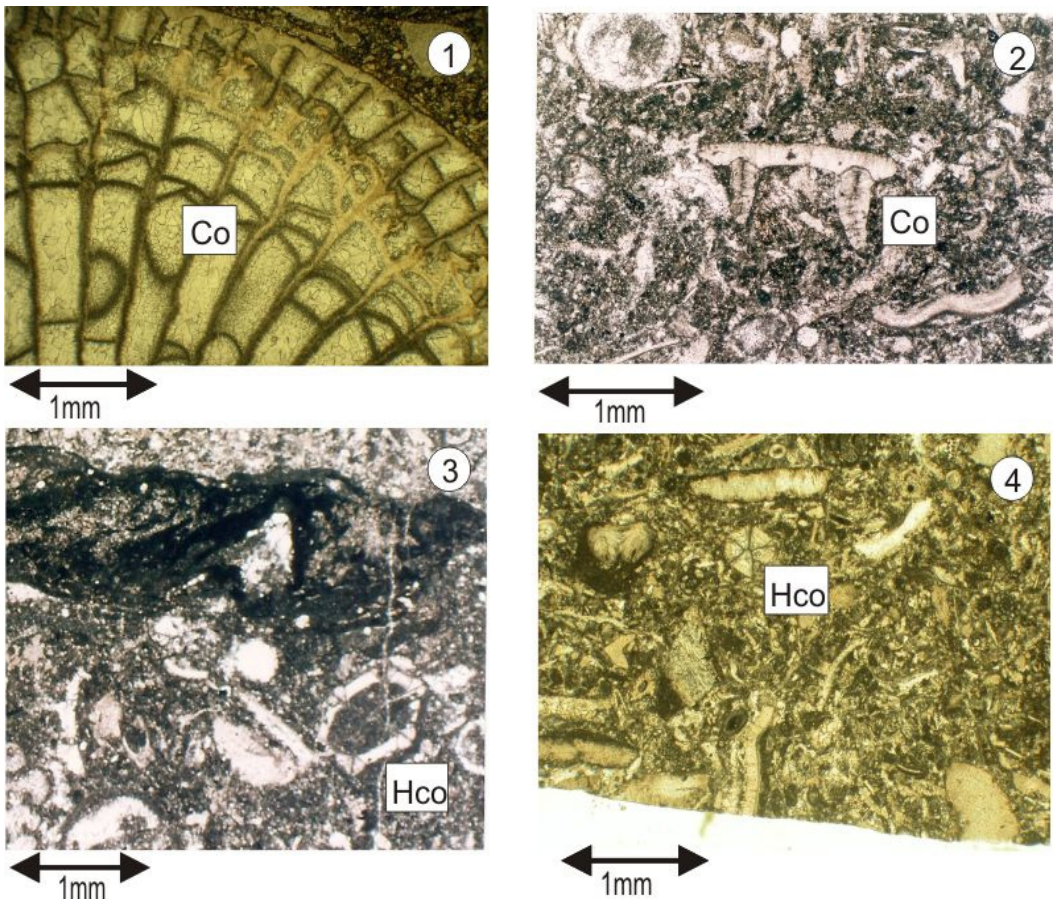

Figure 5.8 Coral fragments from the Great Limestone thin sections. 1=Coral fragment, 2=fragment of coral near to epitheca (Note similarity with upper, surface of coral in plate 1), 3and 4=Heterocoral fragments.

Dibunophyllum bipartitim is regarded by Scrutton (1999) as receiving support by being partly buried within the depth of the sediment, with possibly only a third of the coral protruding above the sediment surface (Hubbard, 1970). To ensure adequate support to the growing corals, sediment supply must have been sufficient to provide support without affecting development of the coral. Nudds and Day (1977) speculated that reduction in the growth rate of a studied *Siphonodendron* specimen was in response to a local increase in clastic sedimentation. Growth rates for Rugose corals have been estimated to be less than 27 millimetres per year for solitary corals, less than 32 millimetres per year for fasciculate corals and 2 to 10 millimetres per year for massive adaptations. Tabulate coral growth rates are much less than for rugose corals, being less than 20 millimetres per year (Scrutton, 1998). Within Chapter 3 it was proposed that sedimentation rates within the Great Limestone were between 100 and 750 millimetres per thousand years (0.1 to 0.7 millimetres per year) with an average of 370 millimetres per thousand years (0.37 millimetres per year), which is low compared to the expected coral growth rates. Coral growth rates may therefore suggest that, to ensure adequate support is maintained within the coral biostromes of the Great Limestone, sedimentation rates increased significantly from 100 to 750 millimetres per thousand years up to 3.2 metres per thousand years. Note that as the corals grew, their increasing weight would cause them to sink into the soft substrate to some extent. There would not have been a direct relationship between growth rates, non-geniculate length and rate of sediment accumulation. (Scrutton pers. Comm. 2010)

It has been noted that the epitheca of many of the corals found within the Great Limestone is damaged or totally missing. This has been attributed to rolling of the coral after death (Chapter 3 Section 3.6.4); however, it is also possible that the destruction of the epitheca occurred within acidic porewaters resulting from the breakdown of organic material. The latter is more likely as the rolling in soft mud is unlikely to have eroded the epitheca and in most cases the epitheca is usually missing only on one side of the coral. (Scrutton pers. Comm.). Most coral fragments in the Great limestone are found lying on their sides, suggesting gravitational instability or disturbance by scouring currents and storms; occasional

storms are thought to be the main cause of death in Palaeozoic corals. Geniculate growth of some corals in the Great Limestone (Figure 3.17) is suggestive of the corals being disoriented through loss of stability and then recovering growth. Both Scrutton (1998; 2000) and Hubbard (1970) regarded *Dibunophyllum bipartitim* as having the ability to survive repeated disturbances due to their re-growth ability.

Heterocorals are found within the Great Limestone as fragments and in thin section show the typical wall formation and corallite morphology (Figure 5.8). Heterocorals are typically solitary and rarely colonial (Cossey, 1997), and are well adapted to live in relatively quiet, low-energy environments. Their delicate wall and corallites would have been prone to fragmentation in shallow turbulent waters. As with many rugose corals Heterocorals also have the ability to survive repeated disturbances and therefore it is not unusual to find geniculate growth (Cossey, 1997); however, within the Great Limestone geniculate growth was not noted.

The biostromes on the Alston Block occur mainly in the south of the area between beds 10 and 19 with the coral biostromes occurring between beds 13 to 19 not as a single biostrome but as many thin ones. Within Skears Quarry at Middleton in Teesdale the coral biostromes are found between beds 14 and 18. Coral fragments can also be seen in thin section between these beds with minor fragments in lower beds.

Corals are rare in 24% of thin sections analysed in this research and absent in the remainder. Scrutton (1998) and Flügel (2004) suggested massive colonial corals dominated in shallow, higher energy environments while fasciculate Rugosa being more associated with quieter environments. The coral biostromes within the Great Limestone, dominated by the large rugose *Dibunophyllum bipartitim*, are therefore, suggestive of shallow, high energy environments with high sedimentation rates. Also, relatively undisturbed fasciculate corals (*Diphiphyllum lateseptatum*) are often a major component of the *Chaetetes* Band in the lower beds. In general the corals would live in quite environments, during

non-geniculate growth, with sporadic high energy episodes uprooting the solitary corals.

5.3 Bioclast analysis.

To test the Hypothesis that depth or other palaeoenvironmental changes exist in the bioclast associations throughout the thickness of the Great Limestone, microfacies interpretation was carried out through analysis of texture, composition and frequency of bioclasts and sedimentary structures.

5.3.1 Textural classification.

Using visual comparison charts from Baccelle and Bosellini (1965) and Mathew *et al*. (1991) for establishing and quantifying textural criteria, i.e. percentage of grains, would suggest that, for the Great Limestone, the grains seen in thin-section analysis exceed 10% and are generally less than 50%; the majority of the thin sections have around 20% grains (Figure 5.9). Using classifications by Dunham (1962) and Folk (1959, 1962), the first based on depositional textures and the second on grain composition, would suggest that the Great Limestone is classified as a wackestone to packstone with 10% to 50% grains (Dunham 1962) or a sparse biomicrite (Folk, 1959, 1962). There are no apparent patterns or cycles visible within the grain percentages or definitions of wackestone to packstone.

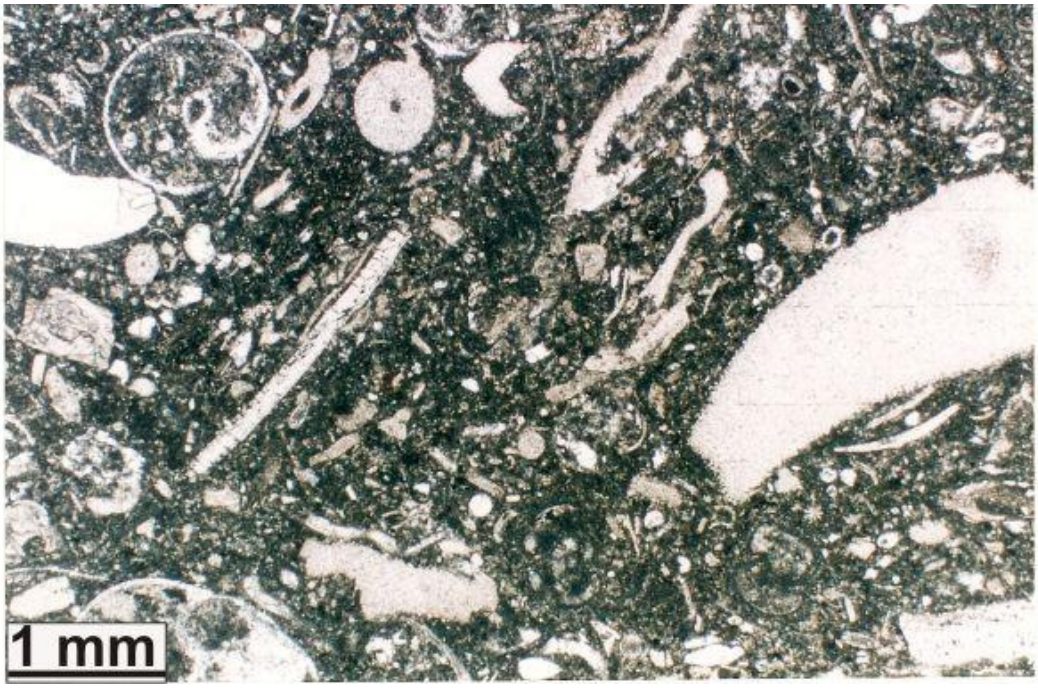

Figure 5.9 wackestone to packstone texture with approximately 20% grains

As discussed in Chapter 3, even though there is evidence for current activity and movement of the bioclasts and grains, i.e. breakage of brachiopods and loss of coral epitheca, evidence does not suggest that the bioclasts have been transported over large distances. Undoubtedly the limestones have undergone some compaction, which can be seen at some bedding planes, therefore, the packstone fabrics could be the result of compaction and dewatering of wackestones. Even so the micritic matrix with large skeletal fragments and angular to sub-rounded bioclast fragments does suggest accumulation in a low energy environment where large benthos existed. The bioclast/grain contents would suggest that the limestone is generally autochthonous i.e. it was deposited more or less within the place of origin of the grains/sediment; however see the discussion in section 5.2.17 and 5.6 regarding allochthonous deposition of Dasyclad alga.

5.3.2 Grain-size analysis.

Average grain size throughout the thin sections varies from 0.75 millimetres to 1.0 millimetre with the maximum grain size, a coral from the area of the biostromes, of 25 millimetres. Fragmentation of the larger grains is visible within most thin-sections and some degree of grain sorting is also obvious. In the field larger grains can be seen within the biostromes up to 40 millimetres diameter and a few centimetres long. Apart from the biostromes themselves, the thin sections do not reveal any obvious changes or grain-size patterns throughout the thickness of the Great Limestone.

The comparison charts of Pettijohn (1973) and Longiaru (1987) would suggest a moderate to poor degree of grain sorting within the analysed thin sections. Flügel (2004) regarded well to moderately sorted grains to reflect high energy environments whereas poor sorting of grains may be caused by weak tidal and bottom currents or reworking of larger grains into finer sediments. Wells *et al.* (2005) regarded the Namurian epeiric seas of NW Europe to be micro-tidal with tides of only a few centimetres and a maximum of 1 metre in estuaries created by indented coastlines. With a low tidal range and a large epeiric platform protecting the interior due to frictional effects, tidal energy and currents would have been small, resulting in a low energy environment. Therefore the moderate to poor degree of grain sorting within the sediments of the Great Limestone and

the probable low tidal affects would suggest that local sorting of the grains resulted from bottom and storm water currents rather than tidal action.

5.3.3 Sedimentary Structures.

Locally, there are sedimentary structures indicating current activity and Fairburn (1999) deduced preferred orientations and palaeocurrent patterns at some localities from the larger fossils such as corals, crinoids and brachiopod shells; occasional symmetrical ripples (Figure 3.9.) associated with water depths of a few metres or of storm reworking in deeper water are also found. The Great Limestone gets progressively muddier towards the top and bottom of individual beds and grain alignment, and compaction, is also visible at these positions within thin sections. Within Figure 5.10, a thin section near to the top of a bed, both grain alignment and imbrication can be seen suggesting that current action is responsible for the structure and probably not due entirely to compaction of the sediment surface.

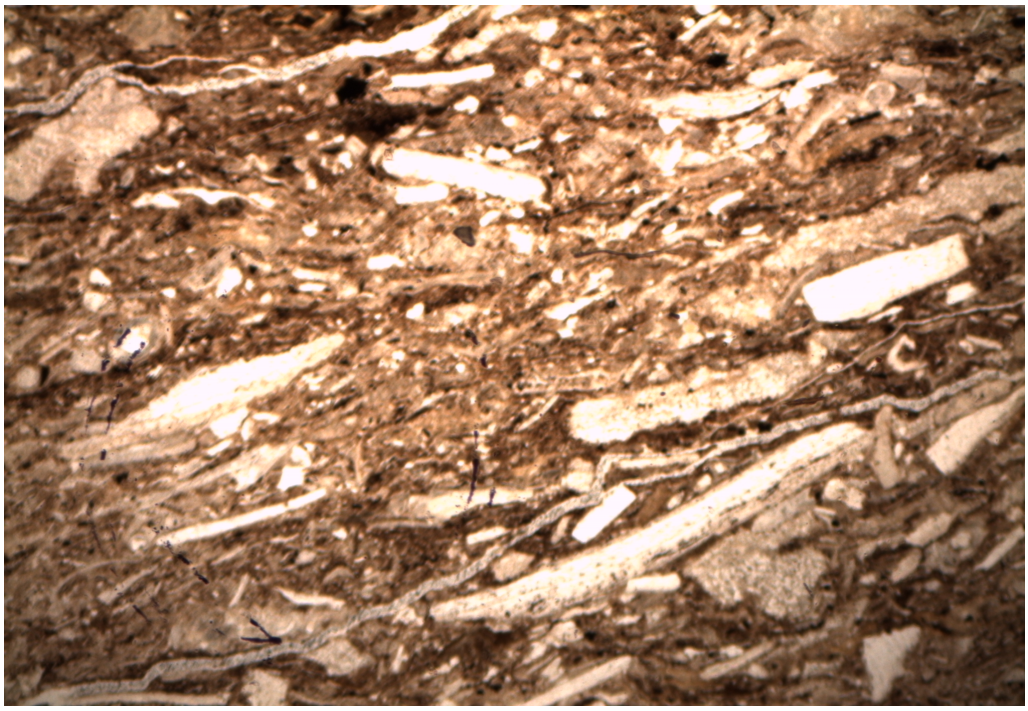

Figure 5.10 Alignment of grains and imbrication at bedding plane

Mottling of sediment is seen within most thin sections indicating micro burrowing and bioturbation; burrowing, however, is not as obvious in the field. The thin section analysis suggests that the majority of each bed has undergone

some bioturbation probably resulting in the destruction of many original sedimentary structures. Bioturbation may therefore have contributed to mixing and “unsorting” of some sedimentary structures.

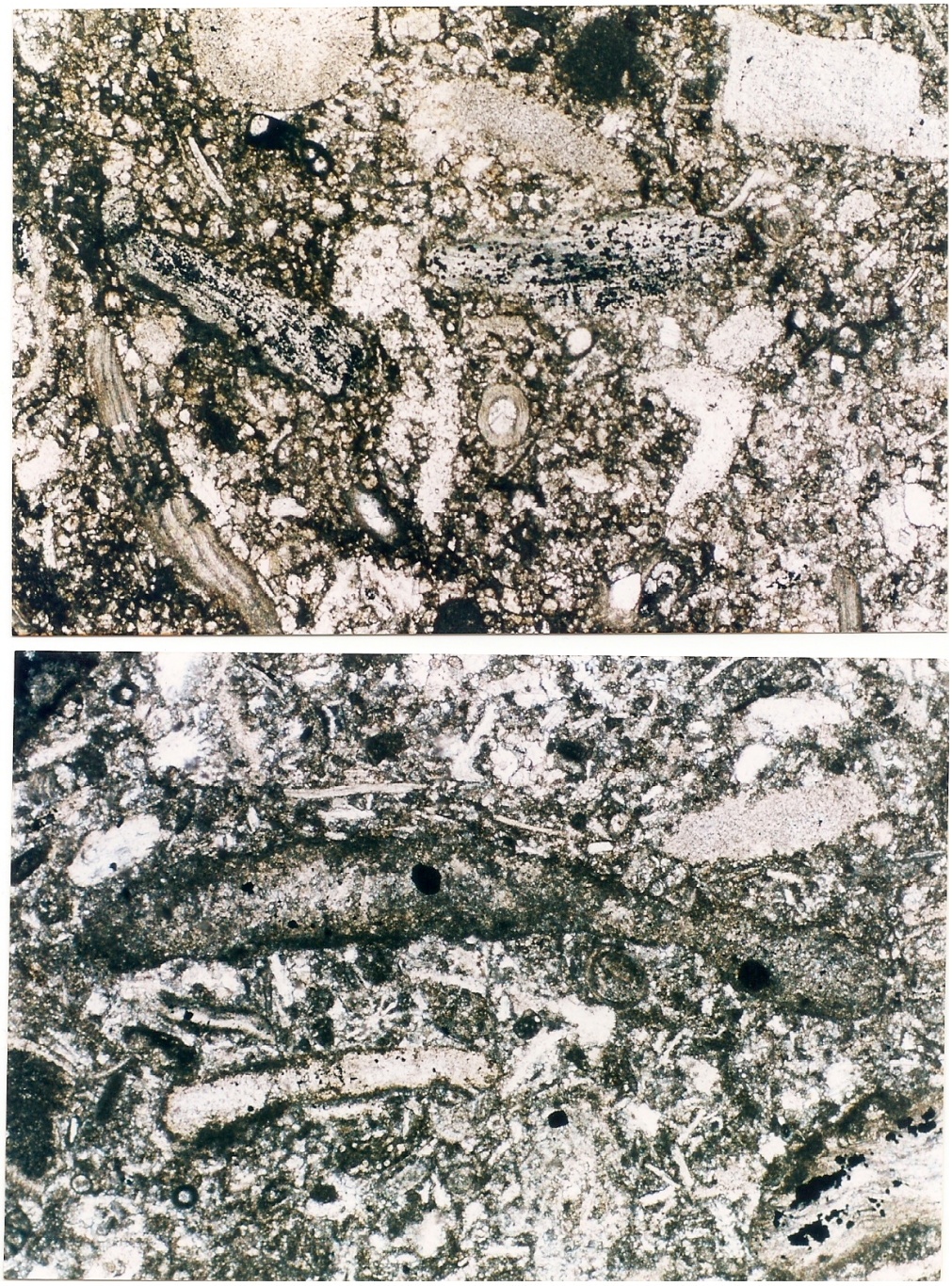

Figure 5.11 Micrite envelopes and microboring of grains

Fasciella encrusting organisms (Figures 5.4-1 and 5.4.2), microborings and micrite envelopes are not common within the thin sections analysed, but they can be seen on some grain fragments such as brachiopod, crinoid and algae (Figure 5.11). Micrite envelopes and boring are usually suggestive of microbial action in shallow marine environments; however, microboring endolithic organisms are also found in deeper marine environments (Flügel, 2004). Figure 5.12 shows encrusting bryozoan fragments on a coral fragment and Figure 5.3.4 show encrusting of a brachiopod by an encrusting bryozoan. It can be seen from Figure 5.12 that the epitheca of the coral is missing suggesting encrustation after the coral has been rolled or damaged by acidic sediment. These borings, encrusters and micrite envelopes are suggestive of action in a shallow marine environment.

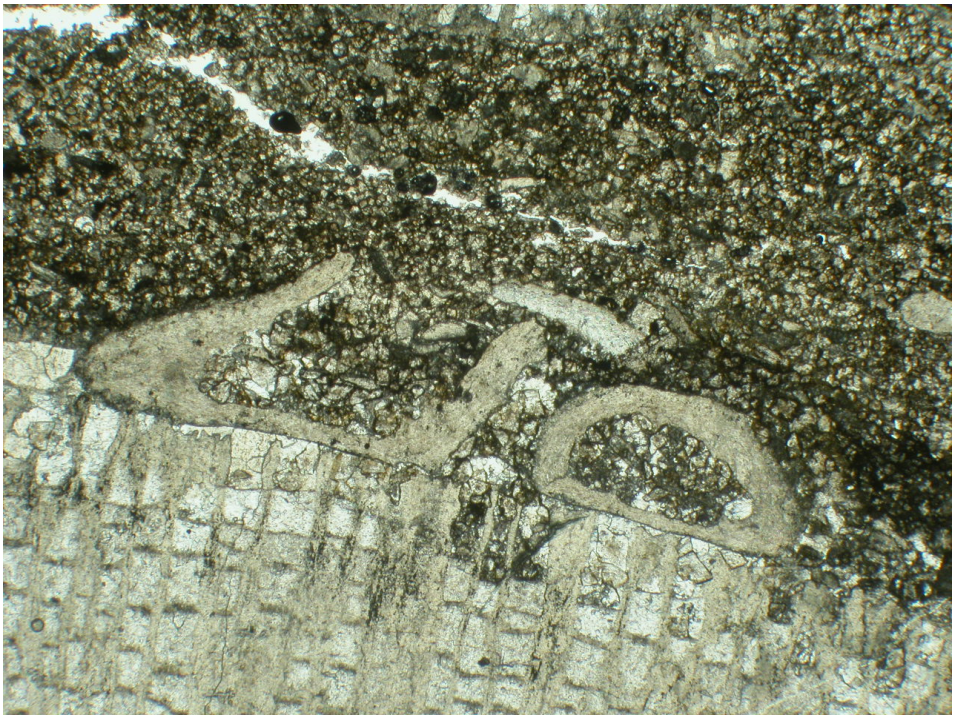

Figure 5.12 encrusting of coral fragment by bryozoans. Note loss of coral epitheca.

Apart from at bedding planes, discussed above, fracturing of grains through physical compaction is not obvious within the thin sections analysed suggesting early cementation of the sediment before compaction occurred. Figure 5.13 shows breakage of a brachiopod spine and therefore it is probable that this breakage is the result of current or storm action rather than compaction. Pressure

dissolution and grain to grain contacts are seen in the thin section analysis but is limited and only significant adjacent to shale partings (Figures 3.18 and 3.19). An analysis of the grains at grain to grain contacts and stylolites does not suggest that loss of material is substantial (Chapter 3.6.5)

5.4 Biodiversity and richness

Before moving onto the multivariate analysis and grain associations biodiversity and richness has also been considered with regard to the thinning and thickness patterns seen in the Fischer Plot of bed thickness changes. Biodiversity can be a useful indicator of changes and trends within environments such as climate and geochemical changes as well as local variations such as changes from brackish to marine conditions; stressed environments typically have low diversities. The simplest diversity index is the species richness, i.e. the number of species present. Figure 5.14 is a chart which shows how the species richness (blue line) changes throughout the thickness of the Great Limestone. As species richness is usually underestimated in counts of species, two other richness indices, Menhinick richness index and Margalef's richness index, which attempt to compensate for this underestimate (see Hammer and Harper, 1998 for a discussion), are also included within Figure 5.14. It can be seen that there is a close correlation between all three indices suggesting underestimation due to counting errors, even though, inevitable, it may not have greatly affected the taxon richness pattern.

Figure 5.13 breakage and microfracture of brachiopod spine

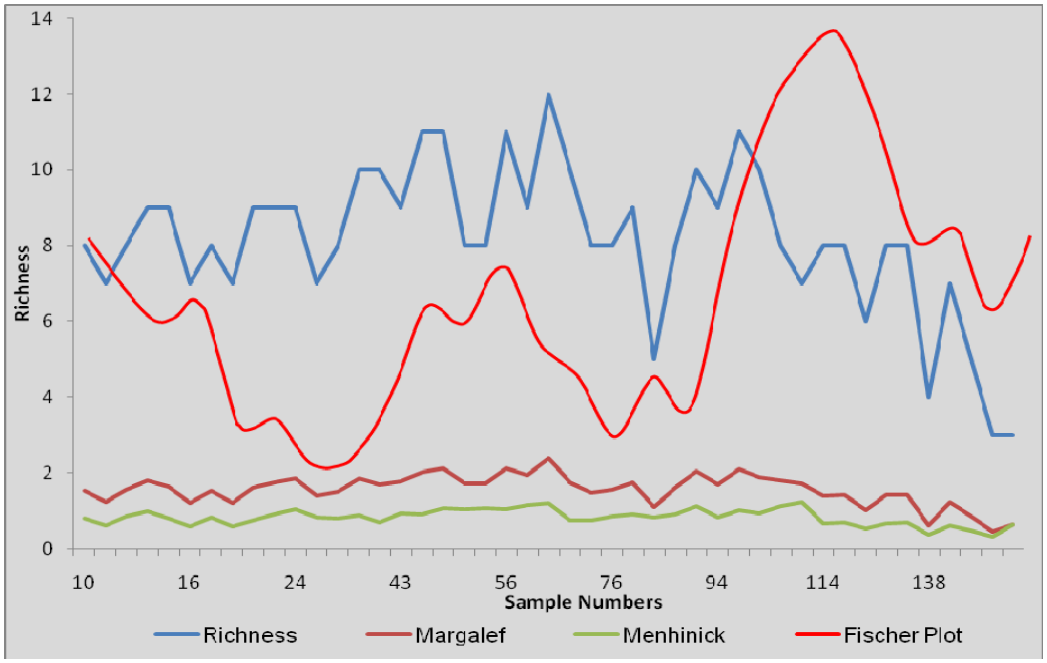

Figure 5.14 Taxon Richness through the Great Limestone

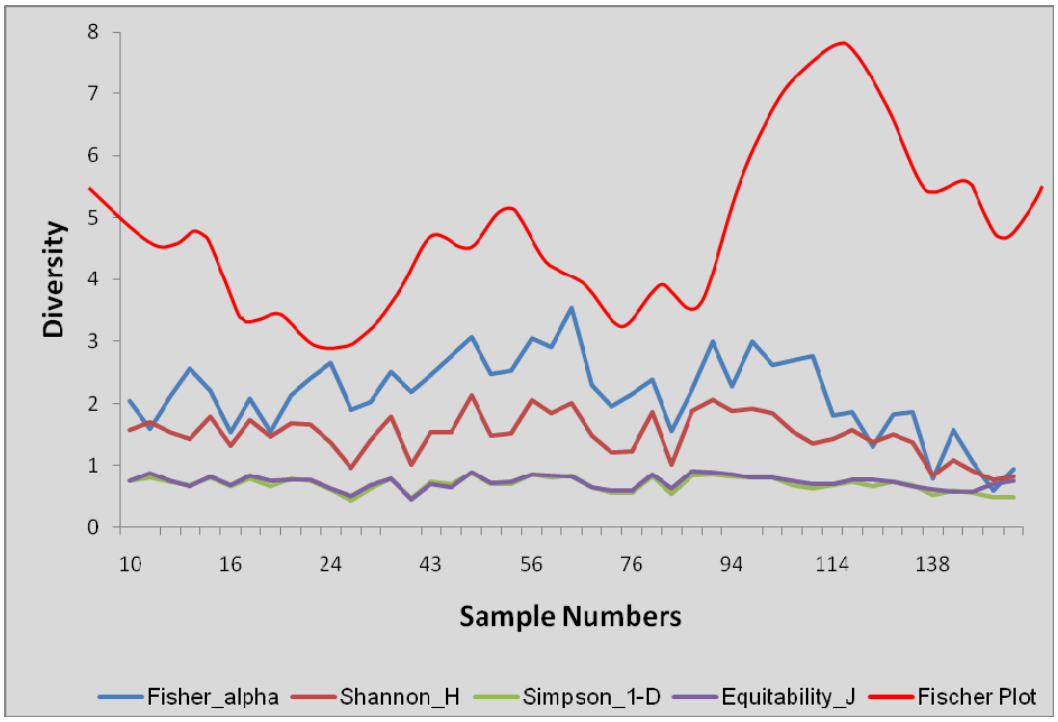

Figure 5.15 Diversity through the Great Limestone

The Fischer Plot of bed thickness in Figure 5.14 is included to assess whether there is a correlation between bed thickness taxon changes. Taxon Richness can be seen to increase throughout the lower half of the Great Limestone until around sample 72 where there is a large change to taxon richness. Generally,

until sample 45 there is little correlation between the richness and Fischer Plot; however, above sample 45, richness and the Fischer Plot do appear to correlate even though "lags" are visible between the plots.

To further assess diversity changes through the Great Limestone three diversity indices have been constructed in Figure 5.15 together with the Fischer plot of bed thickness. The three diversity indices support each other quite well and differ only in the small scale detail. The Fischer Plot can be seen to correlate quite well with the Fischer_alpha and Shannon indices; a drop in diversity can be seen around sample 57 corresponding to the thinning shown in the Fischer Plot.

Both the Richness and Diversity analysis are useful indicators of how the fauna within the Great Limestone have changed through time and when compared to the Fischer Plot correlations can be seen. This correlation between richness, diversity and part of the Fischer Plot suggests an environmental change could be the cause of both bed thickness, diversity and the richness of taxon. It is suggested that environmental changes enhanced or stressed taxon and diversity which in turn affected the calcium carbonate deposition/ production and therefore bed thickness.

5.5 Bioclast associations.

Figure 5.16 illustrates the absolute abundance of faunal grains throughout the stratigraphical thickness of the Great Limestone at Middleton in Teesdale. Whereas this chart is useful to assess the distribution of the grains it is important to remember that some grains such as crinoids, bryozoans and *Palaeoberesellids* will undoubtedly be from disarticulated specimens and other grains such as ostracods, brachiopods and gastropods and some alga could also be fragments of larger grains. Therefore the absolute abundances presented in Figure 5.14 could be misleading.

Even though Figure 5.16 could be misleading it is still instructive in the assessment of the spread of many of the bioclasts throughout the thickness of the Great Limestone, i.e. the persistence of bioclasts such as brachiopods, crinoids, bryozoans and *Endothyra*.

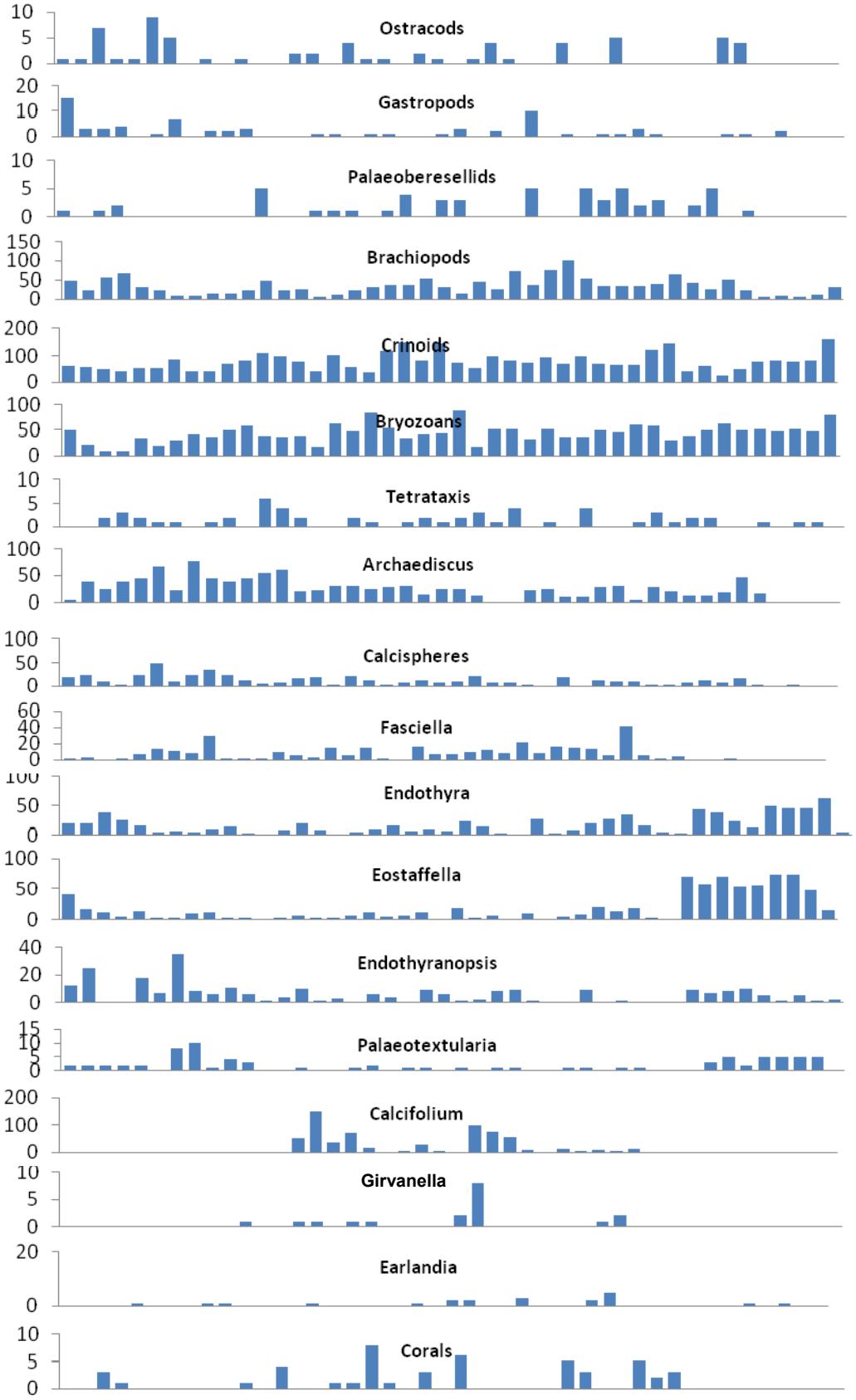

Figure 5.16 Bar chart illustrating abundance throughout the stratigraphical thickness of the Great Limestone at Middleton in Teesdale.

The abundance of many of the bioclasts suggest trends or cyclicity are present within the Great Limestone and this is explored in Figure 5.17 where the Fischer Plot (red line) of bed thickness is included with the bar chart for crinoids; there is some similarity in trends although this is not conclusive.

Seriation and Correspondence Analysis (CA) are ordination methods used to visualize trends and groupings with CA used to project multivariate datasets in two or three dimensions. Seriation is an ordination method used to order samples and or taxa in order to identify any environmental gradients. As there is no inherent ordering of the original data, unconstrained seriation is used leaving it possible for the columns to be randomly reordered (permutated); samples are placed in rows and taxa in columns.

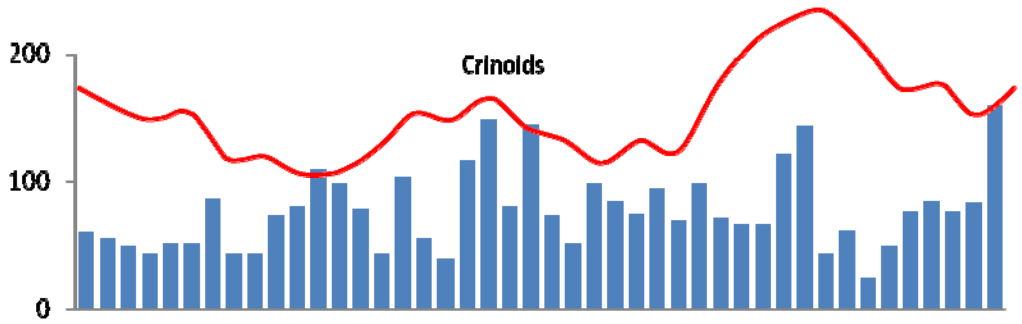

Figure 5.17 Bar Chart of crinoid data from Middleton in Teesdale together with Fischer Plot of bed thickness

Cluster Analysis assesses whether there is any group structure in the composition of the data and cluster groups are analysed to assess similarities using un-weighted pair- group averages. These are then joined based upon the average distance/similarity between members. Hammer and Harper (2006) referred to cluster analysis as not a typical formal statistical technique and being more related to data exploration and visualisation. Cluster analysis is a common method used in palaeoecology; however, it must be treated with caution due to its instability (Brenchley and Harper 1998). Cutting of the resulting dendrogram at the appropriate level is a problem that must be considered when carrying out Cluster Analysis (Sneath and Sokal, 1973; Milligan and Cooper, 1985; Jerram and Cheadle, 2000); however, even though there is an enormous amount of literature

on the subject, this is not a matter of statistics; therefore, clear meaningful answers to this problem do not appear to be available (Hammer pers. comm., 2010). This analysis has loosely cut the dendrograms according to branch lengths and known published palaeobathymetric indicators. Nevertheless Cluster Analysis is still a powerful tool, when used together with other multivariate methods, which can be used to clarify the clusters recognised.

In Correspondence Analysis, if there is a structure to the data set, then the positions of both taxa and samples are placed close together, maintaining the correspondence. Unfortunately Correspondence Analysis tends to compress the ends of the axis which results in the samples and taxa at the ends being squeezed together. A second problem associated with Correspondence Analysis is the so called "Arch" effect, which results from the bleeding of data between axes. However; CA is still a useful tool when used together with other analysis such as Seriation and Cluster Analysis.

Grain	Environment	Grain	Environment
Endothyra	High energy very shallow water	Calcispheres	Shallow water
Palaeotextularia	Very shallow water above FWB	Corals	Shallow above FWB
Endothyranopsis	shallow water	*Girvanella*	Shallow above FWB (or deep water)
Tetrataxis	Very Shallow water 5 to 10 metres deep	*Fasciella*	Shallow or deep water
Palaeoberesellids	Shallow water around 10 metres deep	Calcifolium	Shallow or deep water
Archaediscus	Shallow water		

Table 5.2 Grains analysed within the multivariate analysis

5.5.1 Q-Mode Multivariate grain analysis (constituent grains).

The Seriation Plot in Figure 5.18 is constructed using all data from Tables 5.1 and 5.2 and it can be seen that a crude gradient exists from the top left down to the bottom right. If this represents a palaeobathymetric profile then it may be interpreted as *Girvanella* and corals in the shallowest environment and *Tetrataxis* and *Endothyranopsis* in deeper environments. The majority of the grains are

placed within the centre columns of the plot and many of the samples cross over the environmental profiles suggesting either, these fauna thrive in a variety of environments or alternatively within environments between the two extremes.

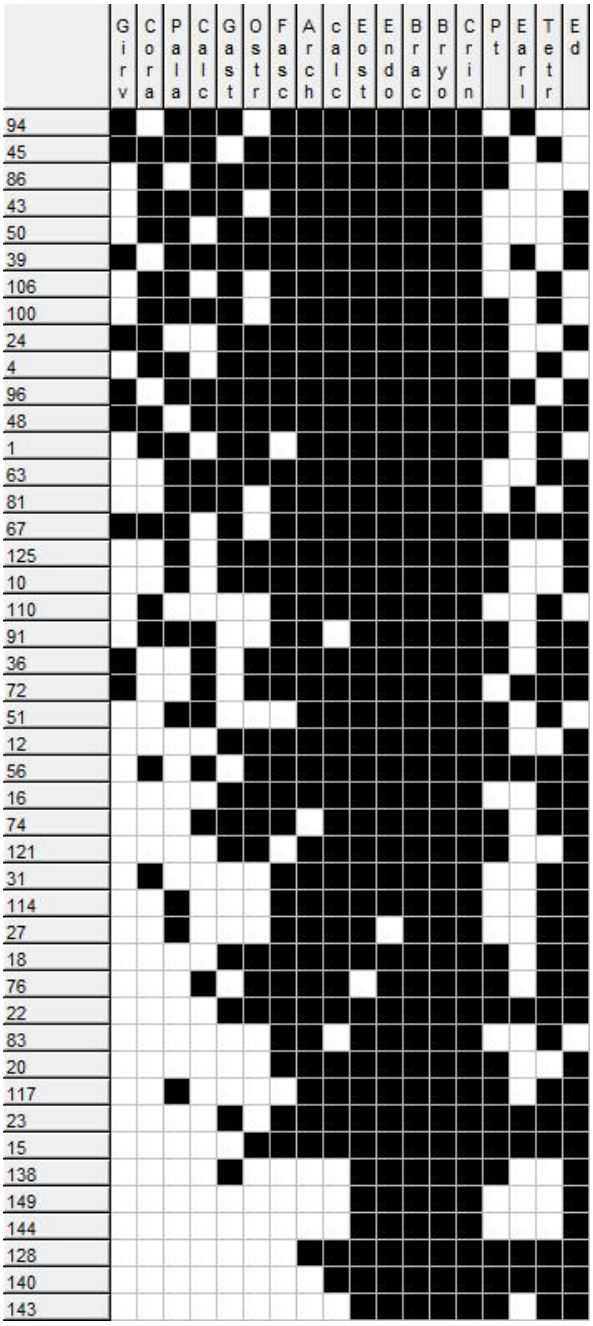

Figure 5.18 Seriation of data from the Great Limestone at Middleton in Teesdale. Grain types in columns and samples in rows.

As discussed above not all of the grains are useful as palaeobathymetric indicators and as many grains are persistent throughout the thickness of the Great Limestone, i.e. grains such as brachiopods, bryozoans' and crinoids, the number of grains used in the following analysis has been reduced to ensure only material

that will contribute to an assessment of the hypothesis will be used. Table 5.2 has been constructed to show which of the grain types are to be used in the assessment and multivariate analysis.

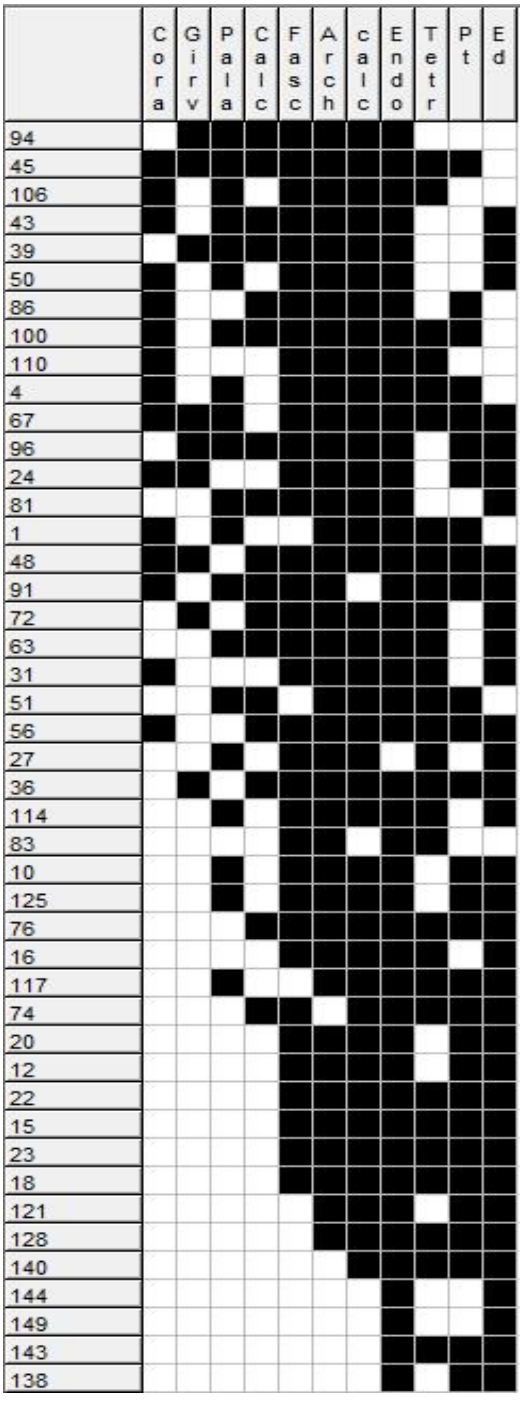

Figure 5.19 Seriation using data from Table 5.1. Grain types in columns and samples in rows.

The Seriation Plot in Figure 5.19 has been constructed using the grains with known palaeobathymetric usefulness (Table 5.2) and it can be seen that a slightly better constructed Seriation Plot is revealed still with a gradient from the

top left down to the bottom right; however, even this gradient is not ideal as many of the samples are still seen to be spread across different environments and many of the grains are placed within the centre columns of the plot. The success of the Seriation is quantified by a seriation index (also known as the criterion) which in this case is 0.82 suggesting some structure to the seriation exists and random distribution of the original data is unlikely; the fewer the influences such as water depth, salinity etc the better the clustering and the higher the seriation index. The plot shows corals and *Girvanella*, possibly the shallowest environment and *Palaeotextularia* and *Endothyranopsis* in the deeper environment.

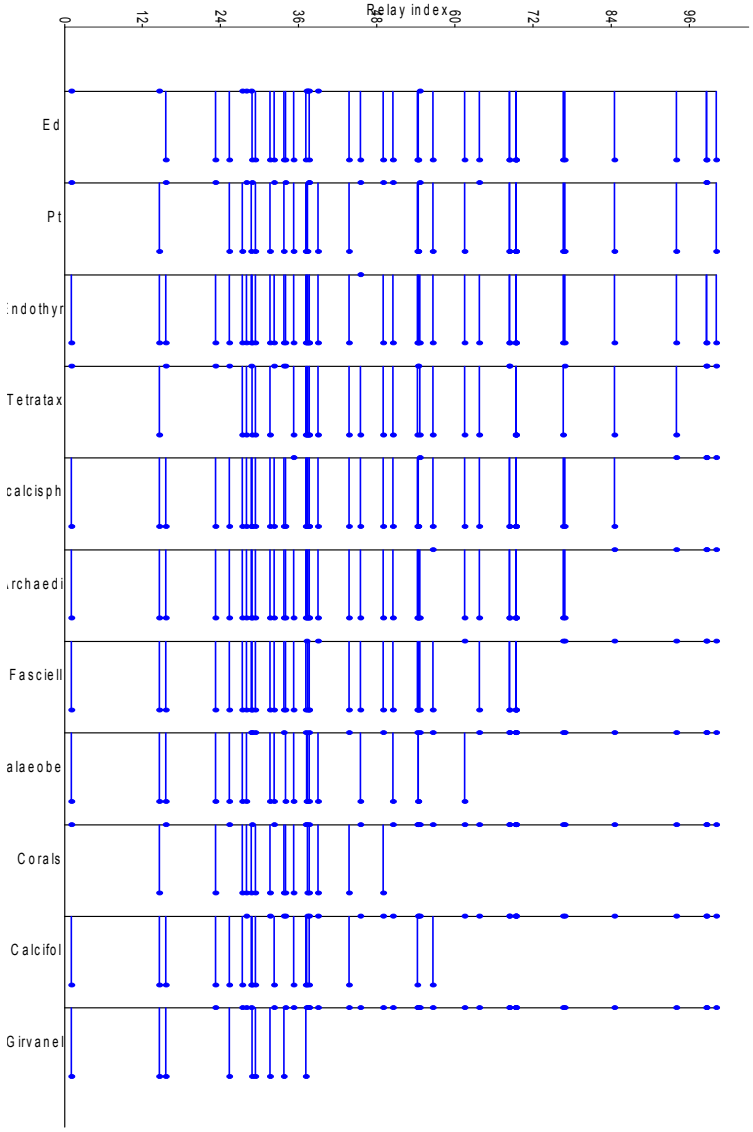

Figure 5.20 Relay Plot from Correspondence Analysis

Results from Figure 5.19		Results from Figure 5.20	
Grain	**Environment**	**Grain**	**Environment**
Corals	Shallow water	*Girvanella*	Shallow quiet above FWB (or deep water)
Girvanella	Shallow quiet above FWB (or deep water)	Calcifolium	Shallow or deep water
Palaeoberesellids	Shallow water around 10 metres deep	Corals	Shallow water
Calcispheres	Shallow water	Palaeoberesellids	Shallow water around 10 metres deep
Fasciella	Shallow or deep water	*Fasciella*	Shallow or deep water
Archaediscus	Shallow water	Archaediscus	Shallow water
Calcifolium	Shallow or deep water	Calcispheres	Shallow water
Endothyra	High energy very shallow water	Tetrataxis	Very Shallow water 5 to 10 metres deep
Tetrataxis	Very Shallow water 5 to 10 metres deep	Endothyra	High energy very shallow water
Palaeotextularia	Very shallow water above FWB	Palaeotextularia	Very shallow water above FWB
Endothyranopsis	shallow water	Endothyranopsis	shallow water

Table 5.3 positions of grains within gradients/relays from Figures 5.19 and Figure 5.20.

As Seriation did not provide a clear gradient Figure 5.20, a gradient/relay using Correspondence Analysis was constructed. Even though this relay is running from bottom (possible the shallowest environment) to top (deeper environment) it is still very similar to the Seriation Plot in Figure 5.19 although some grains are transposed, i.e. *Girvanella*, *Calcifolium* and corals are shown at the probable shallowest environment while *Endothyranopsis* and *Palaeotextularia* the deepest.

Figures 5.19 to 5.20 imply a weak gradient or relay exists within the R mode (grains) data from Middleton in Teesdale. Table 5.3 shows the positions of these grains together with expected depths from published data discussed in Sections 5.2.1 to 5.2.18. It can be seen from Table 5.3 that a clear gradient from shallow, possibly turbulent water into deeper water below fair-weather wave base is not proven with the Seriation and Correspondence analysis.

To assess whether any group structures are visible between the grains within the data, Cluster Analysis has been carried out. Many similarity measures have been used to assess clusters and as the Raup_Crick similarity measure was found to show clusters that loosely followed the discussions in Sections 5.2.1 to 5.2.18 with regard to palaeobathymetric indicators, this measure is shown in Figure 5.21. It is interesting to note that the use of absolute abundance in the analysis rather than presence/absence resulted in similar cluster associations.

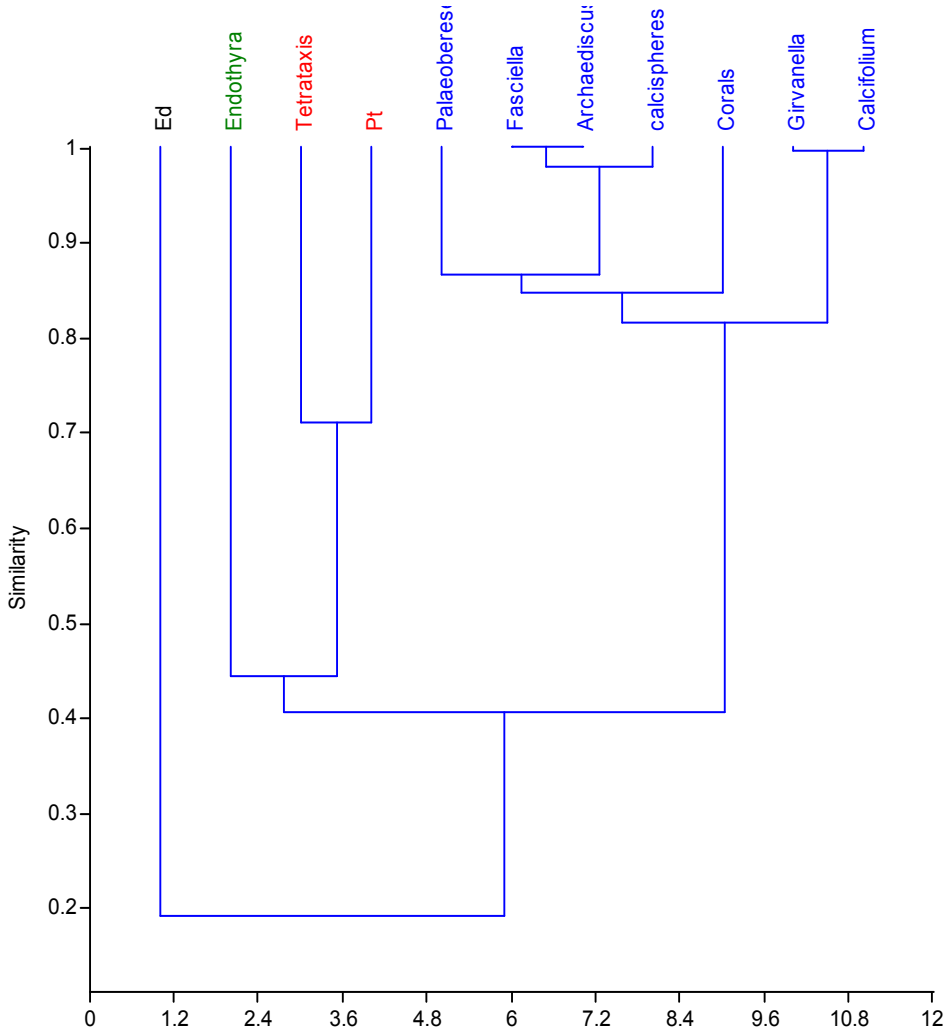

Figure 5.21 Cluster Analysis of grains using Raup_Crick similarity measure.

Within Figure 5.21 and using branch length to cut the dendrogram it is easily split into two coloured clusters, red and blue, with *Endothyra* and *Endothyranopsis* in separate groups or outliers i.e. very little similarity to the other grains. The clustering within Figure 5.21 suggests depth related grouping, when compared to published data used for palaeobathymetric indicators. The dendrogram splits off quite clearly with the Endothyrids, *Endothyranopsis* (Ed)

and *Endothyra* suggesting shallow high energy environments (Haynes, 1981) followed by *Tetrataxis* and *Palaeotextularia* (Pt), water depths of 5 metres to 10 metres deep (Gallagher, 1998; Madi *et al.*, 1996). Corals and Palaeoberesellids are shown to be somewhat separate from the blue cluster (longer branches) with corals still suggesting shallow water; Palaeoberesellids, due to association with dasyclads may however be suggestive of very shallow water. *Fasciella, Archaediscus* and calcispheres are shown to have similar associations (branch length) and are still suggestive of shallow water (Madi *et al.,* 1996; Flügel, 2004) *Girvanella* and *Calcifolium* are shown grouped together with very short branched associations and these are suggested by Wolfenden (1958) and Cózar (2005) to be associated with either shallow or deeper water.

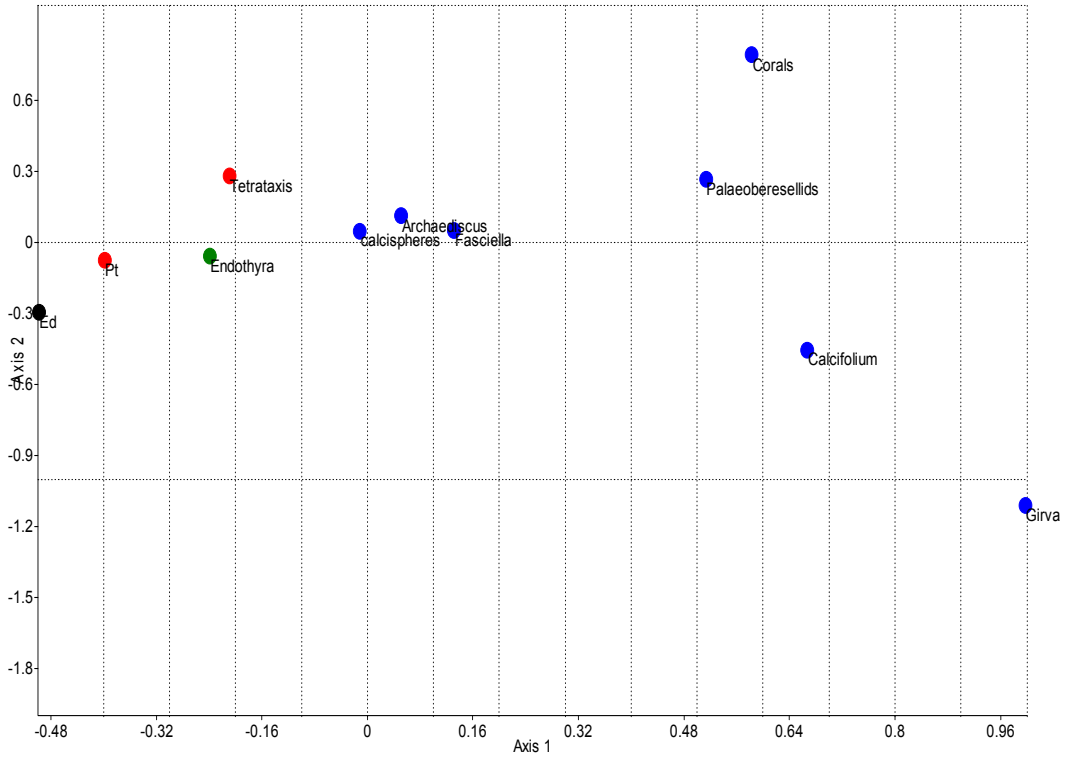

Figure 5.22 Correspondence analyses of grains from Middleton in Teesdale.

To consider further the possibility of these associations between grains Correspondence Analysis has also been carried out to assess the validity of the cluster analysis results and to provide a different view of the data set. Figure 5.22 shows the results of the Correspondence analysis where a grouping of *Archaediscus,* calcispheres and *Fasciella* are seen in the central upper half of the

point cloud and the remainder of the other grains are more diffuse than at first suggested by the Cluster analysis. *Girvanella, Calcifolium* and corals are seen to be separated, as in the cluster analysis and *Palaeoberesellids* also join this grouping. At the opposite end of the point cloud Endothyranopsis (Ed) and *Palaeotextularia* (Pt) followed by *Endothyra* and *Tetrataxis* are seen.

Axis 1 in Figure 5.22 explains the greatest variation with a total of 42% whereas Axis 2 and Axis 3 explain 25% and 10 % variation respectively. This would imply that any relay would be strongest on Axis 1; however, as seen in Figure 5.20 this relay is not convincing. Nevertheless a comparison between Figure 5.21 and Figure 5.22 do show some strong similarities. Moving along Axis 1, from left to right, the following relay is shown; *Endothyranopsis* (Ed), *Palaeotextularia* (Pt), *Endothyra* and *Tetrataxis* with *Palaeotextularia* (Pt) and *Endothyra* transposed in the Correspondence analysis compared to Cluster analysis. A small grouping of *Fasciella, Archaediscus* and calcispheres as in Figure 5.21, then *Palaeoberesellids* and Corals which are further down the relay than shown in the cluster analysis, however, are still suggestive of shallow water, and finally *Calcifolium* and *Girvanella* at the right of the relay. Even though there are some difference between Figure 5.21 and Figure 5.22 this is only in the detail as the basic depth related relay appears to still hold true.

From both the Cluster analysis and the Correspondence analysis four associations are implied, i.e. association A, *Endothyranopsis* (Ed), *Palaeotextularia* (Pt), *Endothyra* and *Tetrataxis;* association B, *Fasciella, Archaediscus* and calcispheres; association C, *Palaeoberesellids* and Corals and association D, *Calcifolium* and *Girvanella*.

5.5.2 R-Mode Multivariate analysis (samples).

The Seriation Plots in Figure 5.18 and Figure 5.19 also show the positioning of the samples in relation to the gradient/relay and as discussed above only a crude gradient exists from the top left down to the bottom right. It is necessary to consider the positioning of the samples within the figure to consider if sample positions are related to environmental constraints such as depth gradients. It was found within the Q_mode analysis that Seriation did not easily

differentiate the gradients within the grain analysis and as can be seen in Figures 5.18 and 5.19 this also holds true for the samples, therefore, the sample positioning will also be assessed by cluster and Correspondence analysis.

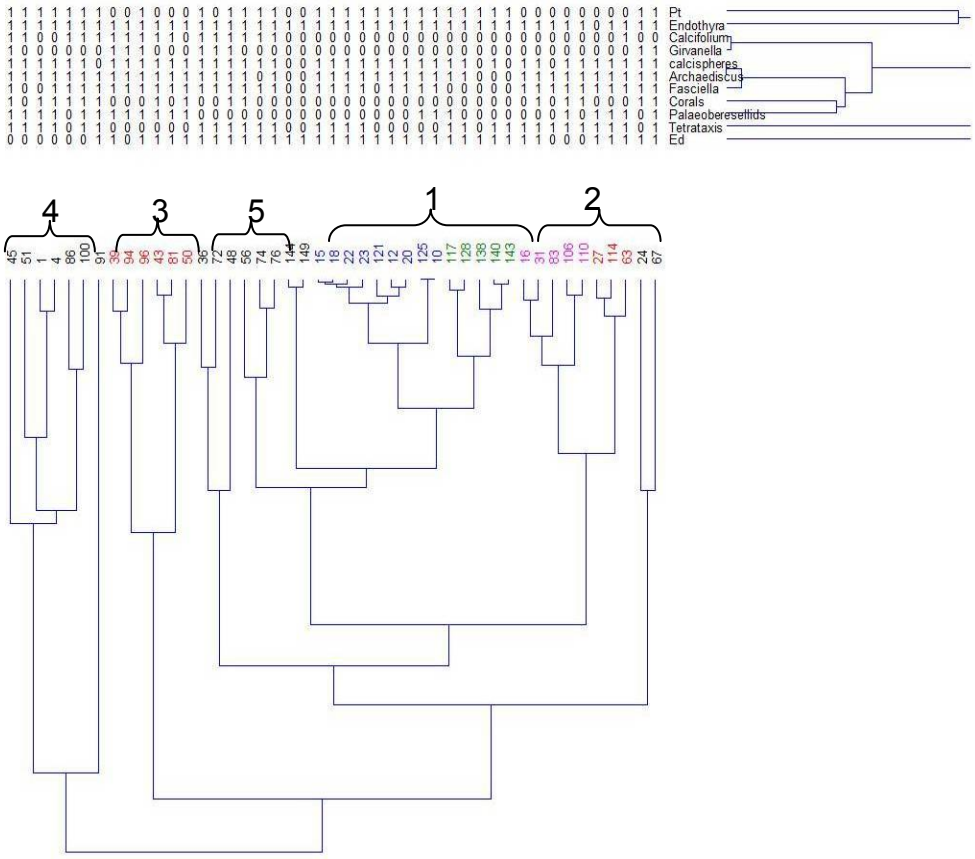

Figure 5.23 2 way Cluster analysis of samples and grains from Middleton in Teesdale using Raup_Crick similarity measure

An analysis of the Middleton in Teesdale samples using 2 way Cluster Analysis (samples and grains) is presented in Figure 5.23 and this suggests some similarities between the samples exists. Clusters which are easily differentiated are highlighted by colour coding and numbered 1 to 5; all associations are defined by the length of the branches and the similarity within the dendrogram. *Archaediscus* dominate many of the samples and calcispheres are present in all clusters; *Archaediscus* and calcispheres are found in most shallow water environments (Madi *et al.*, 1996). The associations are: (1) *Endothyra*-*Archaediscus* association, Table 5.4, (2) *Archaediscus*-calcispheres association,

Table 5.5, (3) *Calcifolium- Archaediscus* association Table 5.6, (4) *Archaediscus-Endothyra* association, Table 5.7, (5) *Calcifolium*-calcispheres association, Table 5.8.

Sample No	15	18	22	23	121	12	20	125	10	117	128	138	140	143	Total	% Fauna	Present %
Archaediscus	44	21	45	39	17	37	77	47	5	11	15	0	0	0	358	29	79
Endothyra	17	7	11	14	23	21	6	12	20	38	50	45	46	63	373	30	100
Calcispheres	24	9	36	24	8	24	24	16	18	13	3	0	3	0	202	16	86
Endothyranopsis	18	35	6	11	8	25	8	10	12	7	5	1	5	1	152	12	100
Fasciella	7	11	30	2	0	3	8	1	1	0	0	0	0	0	63	5	57
Palaeotextularia	2	8	1	4	5	2	10	2	2	3	5	5	5	5	59	5	100
Tetrataxis	2	1	1	2	0	0	0	0	0	2	1	0	1	1	11	1	57
Palaeoberesellids	0	0	0	0	0	0	0	1	1	5	0	0	0	0	7	1	21
Calcifolium	0	0	0	0	0	0	0	0	0	0	0	0	0	0	0	0	0
Girvanella	0	0	0	0	0	0	0	0	0	0	0	0	0	0	0	0	0
Corals	0	0	0	0	0	0	0	0	0	0	0	0	0	0	0	0	0

Table 5.4 *Endothyra-Archaediscus* association. Number of samples = 14, Total = total number of each grain type in the association. % Fauna = percentage of each grain type within the association. Present % = present within % of the association.

The *Endothyra-Archaediscus* association (Table 5.4) is dominated by *Endothyra* and *Archaediscus* with proportions of 30% and 29% respectively. *Endothyra* are present in 100% of these samples whereas *Archaediscus* are only present within 79% of the samples. *Endothyra, Endothyranopsis* and *Archaediscus* are at their greatest abundance within these samples and *Calcifolium, Girvanella* and corals are not present. The abundance of *Endothyr*a and *Endothyranopsis* in these samples is suggestive of high energy shallow water (Haynes, 1981). This association covers samples near to the bottom and top of the Great Limestone. *Archaediscus* and Calcispheres numbers are high in the lower samples and *Endothyra* numbers in the higher samples.

Sample No	16	31	83	106	110	27	114	63	Total	% Fauna	Present %
Archaediscus	67	61	24	27	19	55	11	23	287	50	100
Calcispheres	49	7	0	3	2	5	8	8	82	14	88
Endothyra	5	9	3	5	4	0	44	7	77	14	88
Fasciella	14	10	8	5	2	1	4	7	51	9	100
Endothyranopsis	7	4	0	0	0	1	9	6	27	5	63
Tetrataxis	1	4	1	3	1	6	2	1	19	3	100
Palaeoberesellids	0	0	0	3	0	5	2	3	13	2	50
Corals	0	4	0	2	3	0	0	0	9	2	38
Calcifolium	0	0	0	0	0	0	0	5	5	1	13
Palaeotextularia	0	0	0	0	0	0	0	0	0	0	0
Girvanella	0	0	0	0	0	0	0	0	0	0	0

Table 5.5 *Archaediscus-calcispheres*. Number of samples = 8, Total = total number of each grain type in the association. % Fauna = percentage of each grain type within the association. Present % = present within % of the association.

The *Archaediscus*-calcispheres association (Table 5.5) is dominated by *Archaediscus* being 50% of the fauna and present within all the samples. Calcispheres are 14% of the fauna and are found within around 88 % of samples. Palaeotextularia and *Girvanella* are absent from these samples with corals and *Calcifolium* being in small numbers. Compared to association 1 *Endothyra* and *Endothyranopsis* numbers have reduced by at least 50% in these samples; *Fasciella* fragments have also increased and are now present within all samples. The reduction in *Endothyra* and *Endothyranopsis* and increase in the red alga *Fasciella* is suggestive of movement away from a high energy environment; however, Cózar (2005) found *Fasciella* in both deep-water and shallow-water facies. *Archaediscus* and Calcispheres numbers are high within the lower samples and reduce in numbers in higher samples. *Endothyra* numbers are generally low throughout the association.

Sample No	43	81	50	39	94	96	Total	% Fauna	Present %
Calcifolium	35	9	0	150	10	7	211	34	83
Archaediscus	30	21	27	21	27	29	155	25	100
Endothyra	2	27	17	9	28	35	118	19	100
Fasciella	15	22	1	3	13	5	59	9	100
Calcispheres	3	4	4	18	12	11	52	8	100
Palaeoberesellids	1	5	1	1	3	5	16	3	100
Endothyranopsis	3	1	4	1	0	1	10	2	83
Girvanella	0	0	0	1	1	2	4	1	50
Corals	1	0	1	0	0	0	2	0	33
Palaeotextularia	0	0	0	0	0	1	1	0	17
Tetrataxis	0	0	0	0	0	0	0	0	0

Table 5.6 *Calcifolium-Archaediscus* association. Number of samples = 6, Total = total number of each grain type in the association. % Fauna = percentage of each grain type within the association. Present % = present within % of the association.

Calcifolium fragments in the *Calcifolium-Archaediscus* association (Table 5.6) is 34% of the fauna and are present within 83% of the samples; *Archaediscus* are 25% of the fauna and are present within 100% of the samples. Corals and *Girvanella* are present in low numbers within this association and *Palaeotextularia and Tetrataxis* are absent. *Endothyra* and *Endothyranopsis* numbers continue to reduce and *Fasciella* increase, suggesting a move towards deeper water at or below fair-weather wave-base (Flügel, 2004; Còzar, 2005).

Sample No	45	51	1	4	86	100	Total	% Fauna	Present %
Archaediscus	30	29	24	39	10	6	138	27	100
Endothyra	5	7	38	26	9	17	102	20	100
Calcifolium	70	1	0	0	13	13	97	19	67
Calcispheres	21	7	9	4	20	11	72	14	100
Fasciella	6	0	0	1	16	42	65	13	67
Corals	1	0	3	1	5	5	15	3	83
Palaeoberesellids	1	4	1	2	0	2	10	2	83
Palaeotextularia	1	1	2	2	1	1	8	2	100
Tetrataxis	2	1	2	3	0	1	9	2	83
Girvanella	1	0	0	0	0	0	1	0	17
Endothyranopsis	0	0	0	0	0	0	0	0	0

Table 5.7 *Archaediscus-Endothyra* association. Number of samples = 6, Total = total number of each grain type in the association. % Fauna = percentage of each grain type within the association. Present % = present within % of the association.

The *Archaediscus-Endothyra* association (Table 5.7) is similar to association 1 in that it is dominated by *Archaediscus* and *Endothyra* with proportions of 27% and 20% respectively. *Endothyranopsis* are absent and *Endothyra* percentages are lower in this association compared to association 1; *Calcifolium* are present, but only in low numbers. The abundance of *Endothyr*a in these samples is suggestive of high energy shallow water (Haynes, 1981); however, the percentage reduction in *Endothyra*, compared to association 1, the absence of Endothyranopsis and presence of *Calcifolium* may suggest a transition between high energy and lower energy environments.

Sample No	36	72	48	56	74	76	Total	% Fauna	Present %
Calcifolium	51	101	18	30	75	56	331	48	100
Calcispheres	17	21	12	13	8	7	78	11	100
Archaediscus	19	11	23	13	0	1	67	10	83
Fasciella	5	10	15	16	12	8	66	10	100
Endothyra	21	15	10	10	3	1	60	9	100
Endothyranopsis	10	2	6	9	8	9	44	6	100
Tetrataxis	2	3	1	2	1	4	13	2	100
Corals	0	0	8	3	0	0	11	2	33
Girvanella	1	8	1	0	0	0	10	1	50
Palaeotextularia	1	0	2	1	1	1	6	1	83
Palaeoberesellids	0	0	0	0	0	0	0	0	0

Table 5.8 *Calcifolium*-calcispheres association. Number of samples = 3, Total = total number of each grain type in the association. % Fauna = percentage of each grain type within the association. Present % = present within % of the association.

The *Calcifolium*-calcispheres association (Table 5.8) is dominated by *Calcifolium* which are present within all samples and 48% percent of all fauna. Calcispheres account for 11% of the fauna and are present in 100% of samples. *Palaeoberesellids* are absent within this association; *Palaeotextularia and Girvanella* in low numbers being only 1% of all fauna. The low numbers in both *Endothyra* and *Endothyranopsis* and the greatest number of *Calcifolium* is suggestive of deep water probably at or below fair-weather wave base.

Figure 5.24 brings together all associations stratigraphically together with the Fischer Plot of bed thickness. The *Endothyra-Archaediscus* association (green markers) can be seen to occur on the first and last falling legs of the Fischer Plot where beds are generally thinning. The greatest number of *Endothyra* occur near to the top of the Great Limestone where beds are near their thickest and if the Fischer Plot is accepted as a proxy for water depth, then this could be interpreted to be at a point where water is near to its shallowest.

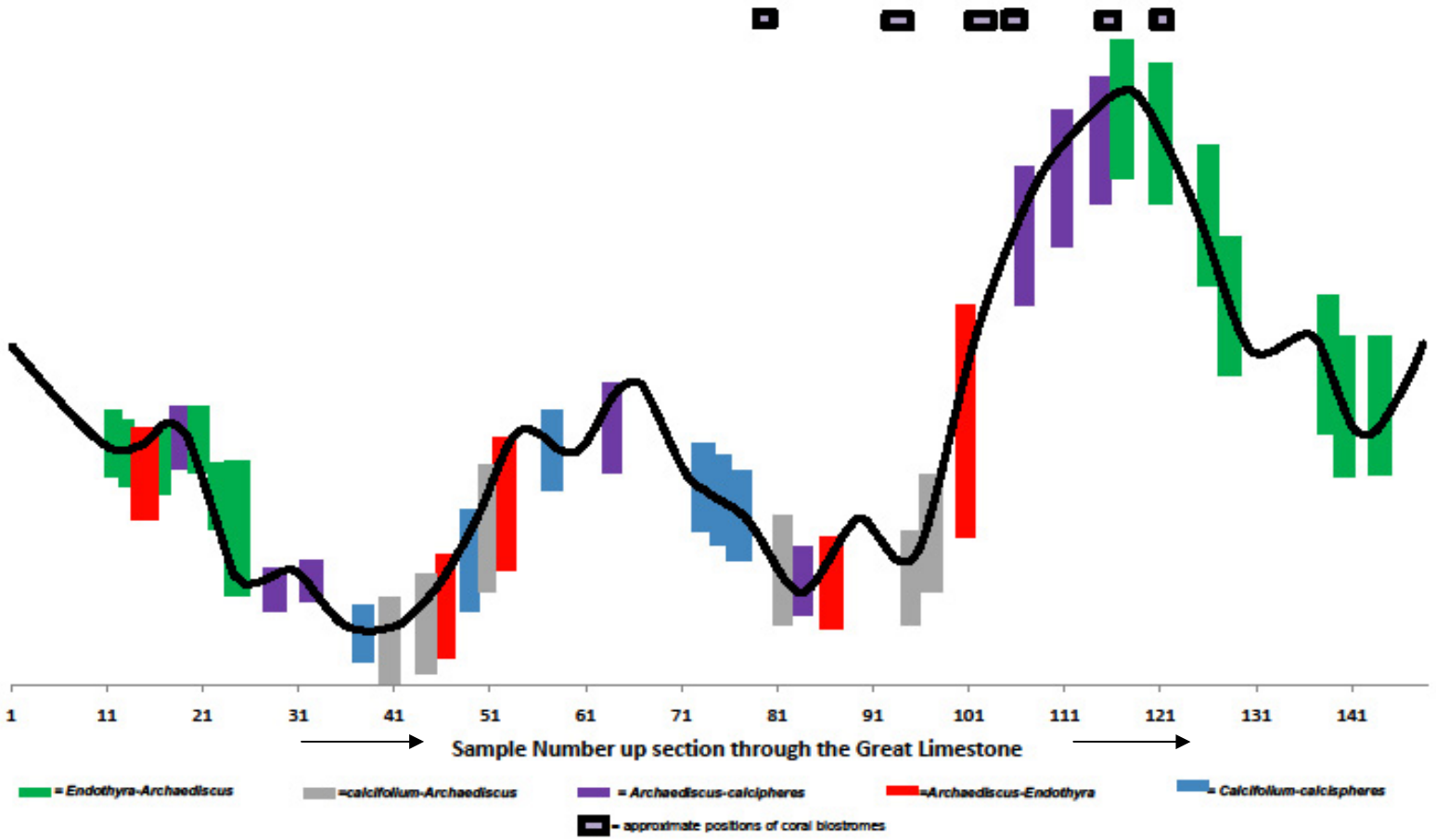

Figure 5.24 Stratigraphical positions of associations together with Fischer Plot of bed thickness (Black Line).

The *Calcifolium-Archaediscus* association (grey markers) generally appear where beds are thinnest and commence to thicken. Assuming that the Fischer Plot represents water depth then this shows *Calcifolium* fragments occurring at the deepest points. The greatest numbers of *Calcifolium* fragments, in sample 39, are seen at the lowest point of the Fischer Plot.

The *Archaediscus*-calcispheres association (purple markers) occurs on the rising limbs of the Fischer Plot, where the thicker beds occur. *Archaediscus* and calcispheres numbers are high within the lower samples and reduce in numbers in the higher samples of the association; *Endothyra* numbers are generally low throughout the association. The association is generally diffused throughout the thickness of the Great Limestone and is suggestive of a transition between high energy above fair-weather base to below fair-weather base.

The *Archaediscus-Endothyra* association (red markers) occurs on the rising limbs of the Fischer Plot where beds are thickening and *Calcifolium* fragments are usually still present. The comparison with the Fischer Plot and the presence of *Calcifolium* fragments is also suggestive of a transition between deeper to shallower water.

The *Calcifolium*-calcispheres association (blue markers) generally occur on the falling limbs of the Fischer Plot; however, they are also present in the deepest point of the Fischer Plot and on one rising limb. Calcifolium fragment numbers are at their highest in this association and *Endothyra* their lowest. This association would also suggest presence within the transition between the deep and shallowest water depths.

Figure 5.24 is instructive in that association changes can be seen to occur as the bed thickness changes; however, the figure does suggest some overlap of associations occurs. Figures 5.25 and 5.26 are the results of Correspondence Analysis for both Axes 1-2 and 2-3 which have been carried out to assess presence of any relays and the possible overlap of associations. Note the enclosing shapes around the samples are entirely arbitrary and used only to highlight the sample positions;

Figure 5.25 would suggest a comparative relay exists running from top left to bottom right. Overlap can also be seen between the associations in both Figures 5.25 and 5.26; however, the green and blue associations in Axes 1-2 show the least amount of overlap. It is probably not unexpected to see overlap between the associations due to the positions of each sample on the limbs of the Fischer Plot and this tends to confirm that the associations are interlinked and change slowly as environmental changes such as depth are changing.

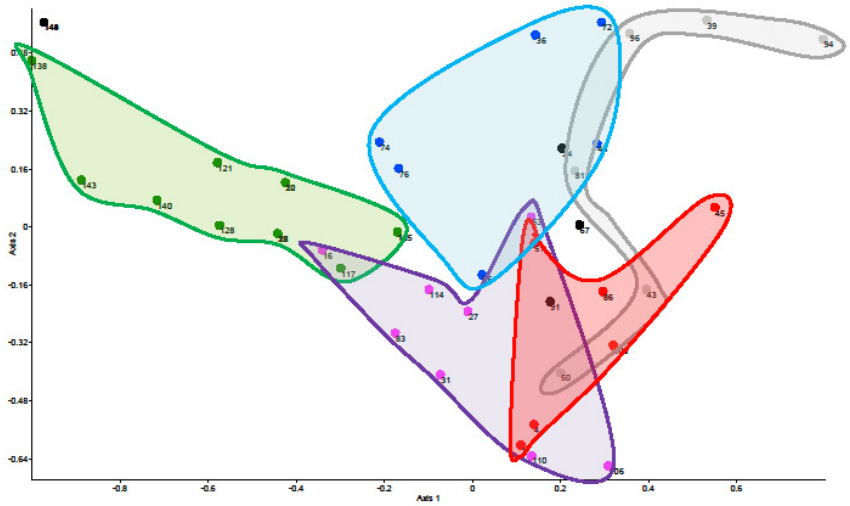

Figure 5.25 Correspondence analyses of samples, Axes 1-2

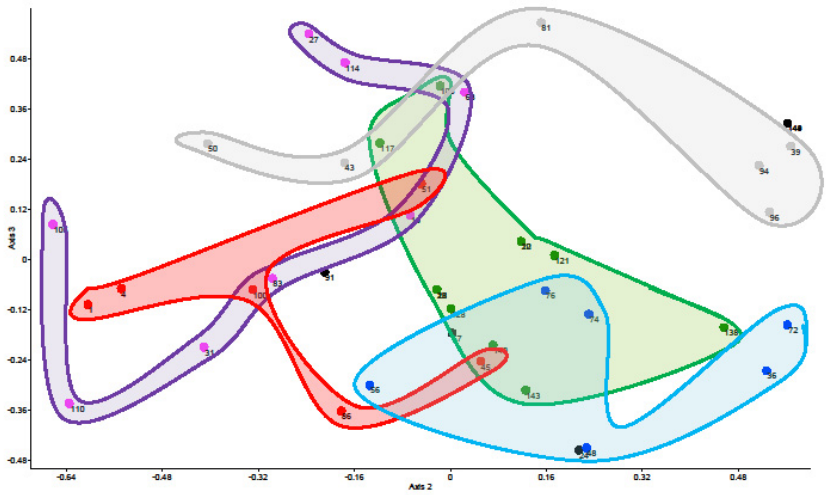

Figure 5.26 Correspondence analyses of samples, Axis 2-3

5.5.3 Biostromes

The Frosterley band of Weardale is also present within the Great Limestone in Teesdale (Chapter 3.6.3) between beds 14 and 18 where it is seen as multiple bands of *Dibunophyllum bipartitim* and brachiopods such as *Gigantoproductus, Latiproductus*, *Dielasma* and spirifers. Figure 5.24 shows the approximate positions of the individual coral biostromes in relation to the Fischer Plot. The figure suggests that the biostromes are generally spread over the rising limb of the Fischer Plot and either side of the purple and grey associations at the transitions between high energy above fair-weather wave base to around fair-weather wave base or just below. This fits in with Scrutton (1998) and Flügel (2004) who suggested Rugosa being more associated with quieter environments rather than high energy with high sedimentation rates.

5.6 Microfacies interpretation.

The previous sections have analysed and discussed the contents of thin sections which have been used to assess the palaeoecology and palaeodepositional environments of the Great Limestone. To assess the microfacies throughout the Great Limestone further, it is important to analyse specific changes in depositional settings or environments. On a basic level, the microfacies could be built around the dominant grains as other interpretational aspects such as lithology, texture and sedimentary structures etc, do not change substantially throughout the Great Limestone. Therefore, due to the strong echinoid (mainly crinoid)-bryozoan and brachiopod associations and the many foraminifers, the microfacies could be described as a bioclastic crinoid, bryozoan and brachiopod packstone with foraminifers. The previous sections also suggest there may also be specific, smaller scale environmental changes throughout the Great Limestone, which have affected bioclast associations and indicating a sub-microfacies level also exists. These sub-microfacies are suggested by the changes within the foraminifera and alga contents of the samples.

Sections 5.2 to 5.5 considers associations, clusters and affinities between grains and samples where depositional environments were also considered and found to vary between many of the grain and sample clusters. It was suggested in these sections that a small range of depositional environments existed and, apart from the

possible allochthonous dasyclads, these varied from just above fair weather wave base down to environments affected only occasionally by storm action.

5.7. Conclusions

The Great Limestone is classified as a wackestone to packstone with 10% to 50% grains (Dunham 1962) or a sparse biomicrite (Folk, 1959, 1962) and the microfacies could be described as a bioclastic crinoid, bryozoan and brachiopod packstone with foraminifers. Analysis of thin sections revealed moderate to poor sorting, fragmentation of larger grains and alignment and imbrication of grains at the top of beds suggestive of storm and wave action. The analysis of bioclast/grain contents and facies would suggest that the limestone is generally autochthonous i.e. it was deposited more or less within the place of origin; however the presence of dasyclads in the lower beds would suggest some allochthonous deposition or remixing due to the incompatibility of dasyclads and crinoids. The presence of some fossils in growth position such as corals, brachiopods and *Chaetetes* is indicative of long periods without major storm disruption and is suggestive of low energy environments, possibly below fair-weather wave base.

Biodiversity, Taxon Richness and Multivariate Analysis has been carried out to assess changes in the environments of deposition and grain associations. Biodiversity and taxon richness suggests some environmental changes, possible resulting in stressing of the bioclasts which is reflected in bed thickness shown in the Fischer Plot. Grain associations are suggested by the Multivariate Analysis and a comparison with published depth related data suggests these associations are linked to depth changes. The multivariate analysis clustered the grains in accordance with suspected depositional environments; however, the implied associations suggest only a small range of depositional environments varying from above fair-weather wave base to close to storm wave base, i.e. the communities generally changed very little with the greatest changes occurring where *Girvanella, Calcifolium* and coral fragments increased. The analysis would suggest that the communities were, in general, stable with palaeoenvironmental conditions, in particular water depth and energy conditions, varying little during deposition of the Great Limestone.

Using the epeiric platform model, (Irwin, 1965; Tucker and Wright, 1990; Flügel, 2004) this research suggests deposition of the Great Limestone occurred within and near to the boundaries of zones Y and Z, i.e. near fair weather wave base and down to zones with only periodic storm affects. Using the epeiric ramp model (Read, 1998: Lukasik *et al.,* 2000; Flügel, 2004) suggests deposition of the Great Limestone each side of the proximal/distal boundary. The characteristic burrowing suggested for this model (Flügel, 2004) is also extensive throughout the Great Limestone.

A discussion of coral growth and support adaptations show that the corals within the biostromes have undergone gravitational instability or disturbance by scouring currents and storms resulting in death or re-growth. Support mechanisms of the rugose solitary corals *Dibunophyllum bipartitim,* which are common in the biostromes, may suggest that sedimentation rates increased significantly to ensure adequate support was maintained; however, as the corals increased in size and weight they would have sunk into the soft sediments which would therefore mean that increased sedimentation rates would not be required.

The hypothesis tested in this Chapter, that changes exist in the bioclast associations throughout the thickness of the Great Limestone and that these changes are depth or other palaeoenvironmental related, has been proven; however, this is agreed on the proviso that, these environmental changes do not appear to have been substantial as the overlap of associations and individual grain types does suggest a stable environment existed, albeit with some stressing of bioclast communities.

6.0 Diagenesis and geochemistry of the Great Limestone

6.1. Introduction

A chemostratigraphic study of the Great Limestone has been carried out using major and trace element and stable isotope techniques. Before exploring in any detail the major and trace element and stable isotopes this Chapter is intended to carry out an assessment of the magnitude of diagenetic overprinting which was felt to be vital to ascertain the acceptability of the data. Geochemical analysis, together with petrography, can help in unravelling the diagenetic effects and this objective was regarded as being fundamental to the geochemical research.

6.2. Diagenesis and acceptability of results

Before the geochemical data can be used for interpretations of the chemostratigraphic history of the Great Limestone, the integrity of the data with regard to its diagenetic history needs to be determined. Petrography has shown that diagenesis has occurred in many parts of the Great Limestone and this can be seen as recrystallisation with the formation of microspar, dolomite rhombs and loss of some grains such as bivalves and gastropods (Figures 6.1 and 6.2). Meteoric diagenesis can lead to the increase of both iron (Fe) and manganese (Mn) and a decrease in strontium (Sr) and magnesium (Mg); the stable isotopes $\delta^{13}C$ and $\delta^{18}O$ can also be affected by diagenesis (Popp *et al*. 1986; Bruckschen *et al*., 1999; Brand *et al*., 2004) so it is important to ascertain at an early stage whether the geochemical results are representative of the original signal or trend, or have been altered through diagenesis to such an extent that further analysis would be untenable.

6.2.1 Iron and Manganese

Iron (Fe) and manganese (Mn) concentrations in modern carbonates are very low, being in the range of only a few tens of ppm (Mason, 1966; Milliman, 1974; Tucker, 1986; Morse and Mackenzie, 1990; Libes, 1992), reflecting their low concentration in seawater (Chapter 9 Table 9.1). These elements are in higher

concentrations, however, in diagenetic pore-waters, especially in the shallow to deep burial environment, where negative Eh normally exists (Tucker, 1986).

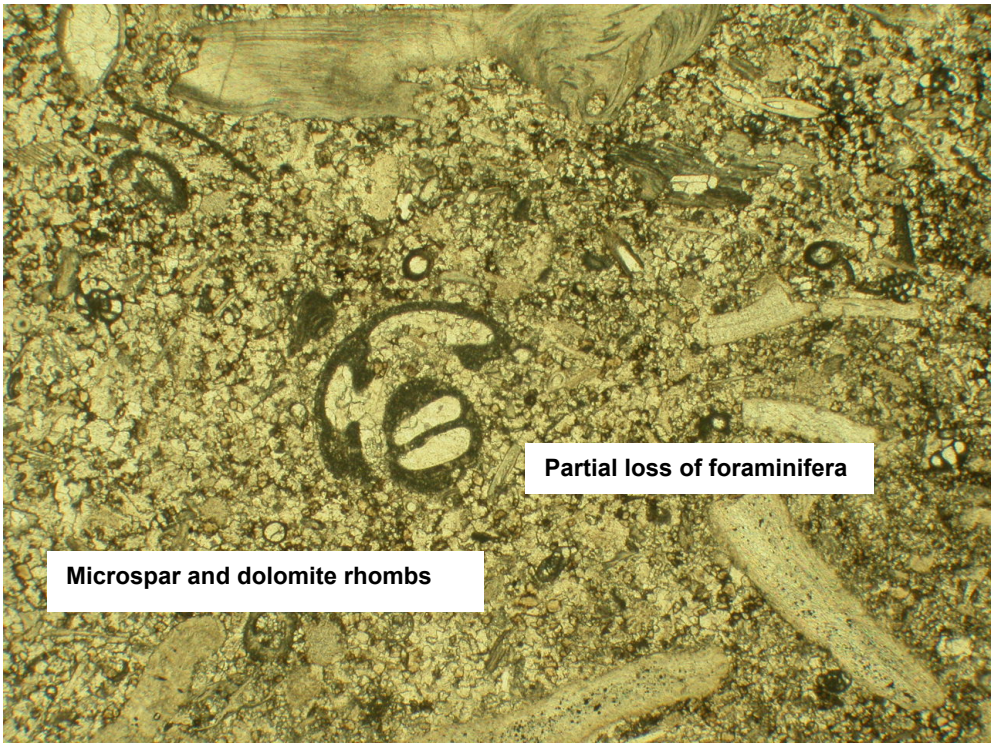

Figure 6.1 Coarse microspar and dolomite rhombs and partial loss of foraminifera.

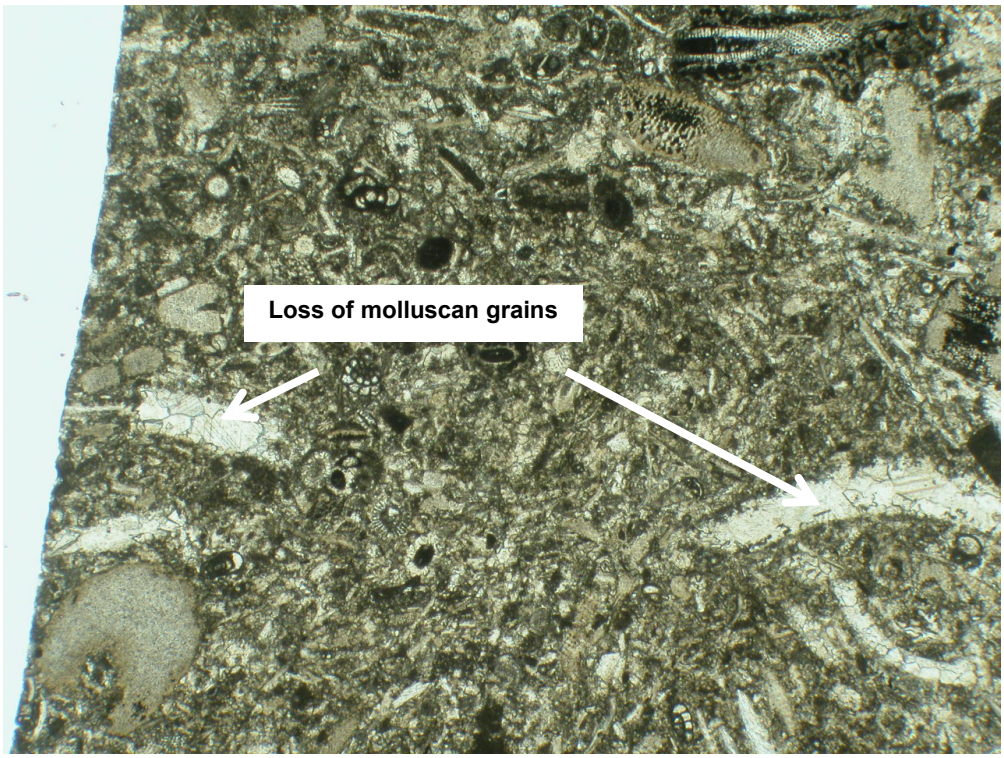

Figure 6.2 Loss of mollusc grains through dissolution of aragonite and replacement by low magnesium sparry calcite cement.

Values of Fe and Mn in Figure 6.3 are high compared to modern seawater concentrations with averages for Fe and Mn of 1620 ppm (maximum 2260, median 770) and 200 ppm (maximum 980, median 170) respectively. Wagner *et al*. (1979) gave values for five north-west Arkansas Mississippian and Pennsylvanian limestones of between 360 to 17,500 ppm for Fe and 170 to 2080 ppm for Mn, and "global" averages for Pennsylvanian limestones of 9600 and 830 ppm for Fe and Mn respectively (see also Brand and Veizer, 1980). The Fe and Mn values in Figure 6.3 fit well within the "global" and other limestone values in Wagner *et al*. (1979); however, these values are high compared to modern seawater carbonate. High Fe and Mn can be the result of several different processes:

- Fe and Mn derived from associated clay minerals or organic matter (Jenkyns *et al*., 2002).
- Fe and Mn from hydrothermal sources.
- Fe and Mn from diagenetic fluids.

Even though the cause of the high Fe and Mn could be any of the above it is more likely that the first and last processes are involved.

	Al	*Ca*	*Fe*	*Mg*	*Mn*	*Si*	*Ba*	*Sr*	$\delta^{18}O$	$\delta^{13}C$	*Insoluble Residue*	*CaCO3*	*MgCO3*	*Soluble Material*
Al	1.00													
Ca	-0.67	1.00												
Fe	0.68	-0.70	1.00											
Mg	0.21	-0.60	0.48	1.00										
Mn	-0.05	-0.07	0.39	0.25	1.00									
Si	1.00	-0.67	0.67	0.21	-0.06	1.00								
Ba	0.46	-0.33	0.36	0.01	-0.03	0.45	1.00							
Sr	0.52	-0.18	0.23	0.12	-0.23	0.52	0.38	1.00						
d18O	-0.23	0.29	-0.26	-0.19	-0.23	-0.22	0.03	0.07	1.00					
d13C	-0.32	0.45	-0.55	-0.48	-0.41	-0.31	-0.14	-0.11	0.34	1.00				
Insoluble Residue	0.71	-0.96	0.65	0.35	0.00	0.71	0.39	0.17	-0.28	-0.36	1.00			
CaCO3	-0.67	1.00	-0.70	-0.60	-0.07	-0.67	-0.34	-0.18	0.29	0.45	-0.96	1.00		
MgCO3	0.21	-0.60	0.48	1.00	0.25	0.21	0.01	0.12	-0.19	-0.48	0.35	-0.60	1.00	
Soluble Material	-0.71	0.96	-0.65	-0.35	0.00	-0.71	-0.39	-0.17	0.28	0.36	-1.00	0.96	-0.35	1.00

Table 6.1 Correlations between trace elements and isotopes

Apart from the one sample with very high Fe and Mn (2256 ppm and 982 ppm respectively), high Fe values do not closely track high Mn values. Correlation analysis of the Fe and Mn data shows little relationship between the two, with an index of only 0.37 (Table 6.1).

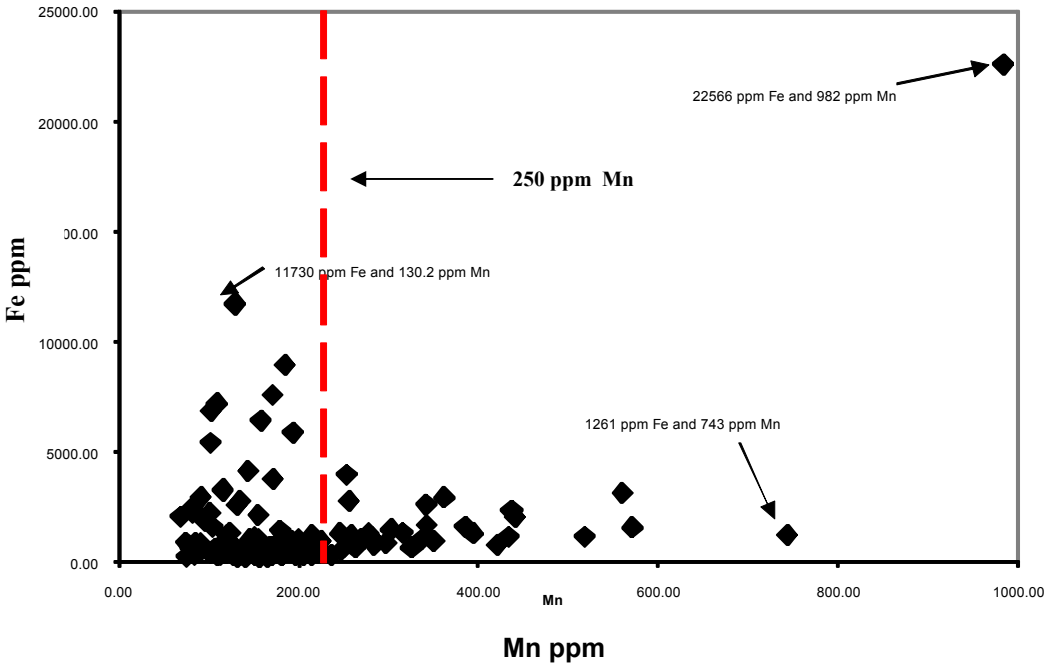

Figure 6.3 Comparison of Fe and Mn values

Bruckschen *et al*. (1999) referred to the preservation of non-luminescent brachiopods and recommended a value of 200 ppm Mn as the cut-off limit for considering brachiopod samples as being well preserved. Popp *et al*. (1986) considered a value of 250 ppm Mn as being acceptable. Even though it would not be expected that a whole rock sample, consisting predominantly of grains which originally would have been composed of a mixture of low Mg calcite, high Mg calcite and/or aragonite, is chemically comparable to brachiopods with near original composition of low Mg calcite (Bruckschen *et al*. 1999), the use of the 200 ppm, and in particular the 250 ppm, Mn limit is still a useful concept. As can be seen in Figure 6.3, the majority (71%) of the samples have a Mn content which falls below the 250 ppm limit, suggesting that extensive burial diagenesis of the samples has not occurred.

6.2.2 Strontium

The element strontium (Sr) is principally supplied to the oceans by rivers or hydrothermal systems (Jenkyns *et al*., 2002) and it is preferentially taken into the aragonite lattice (up to 10,000 ppm) compared with calcite (typically up to 1000 ppm). Ancient limestones have Sr values between 100 ppm and 1000 ppm (Wagner *et al*., 1979; Tucker, 1986), a range much less than that shown in Figure 6.4 where the minimum is 950 ppm and the maximum is 2210 ppm Sr (average 1440 ppm, median 1390 ppm). Veizer *et al*. (1999) suggested a cut-off at 800 ppm Sr to show the diagenesis of brachiopod shells before they could be regarded as being diagenetically altered. Diagenesis usually leads to a decline in Sr. Even though the Sr levels in whole rock will not be the same as in brachiopod shells, the Sr in the Middleton in Teesdale samples are above this minimum level, suggesting little alteration.

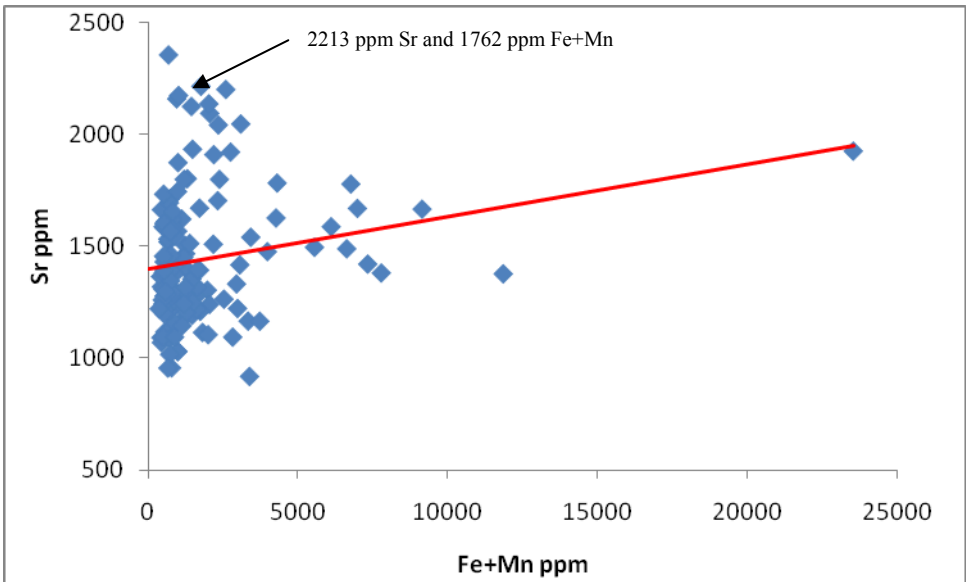

Figure 6.4 Plot of Fe + Mn against Sr

Tucker (1986) suggested that plotting Fe + Mn against Sr could be a useful tool in providing a broad sense of the extent of limestone diagenesis; a negative correlation would suggest that Sr has been lost during diagenesis. Figure 6.4 plots Fe + Mn against Sr and generally shows the points grouping around the 1000 ppm Fe+Mn with a maximum of 23550 ppm and minimum of 360 ppm (average 1820 ppm, median 9890 ppm). The high Fe+Mn values do not correspond strongly with

the high Sr values and correlation analysis gives an index of only +0.22 (Table 6.1). The positive correlation in Figure 6.4 implies that some Sr has been added during diagenesis, however, the partition coefficient of 0.14 for strontium would suggest that this is unlikely and thus the use of this plot in this case is inconclusive. The use of Fe and Mn therefore, does not give a true picture of events as concentrations depend upon many local conditions, such as the supply of elements and redox conditions (Tucker, 1986); nevertheless it is still thought to be a useful tool in assessing the diagenesis of the Great Limestone.

As a result of the differences in the Sr/Ca and Mn/Ca ratios, and the distribution coefficients, the Sr content should decrease and Mn content increase during progressive diagenetic alteration and therefore a negative correlation between Sr and Mn should be seen (Popp *et al*., 1986). Figure 6.5 is a plot of Mn and Sr, which shows the suggestion of a slight negative correlation between the two, implying that strontium reduces as manganese increases; however, statistical analysis gives a correlation index of only –0.19 (Table 6.1). Nevertheless, the negative correlation does imply that a diagenetic imprint exists for Sr and Mn.

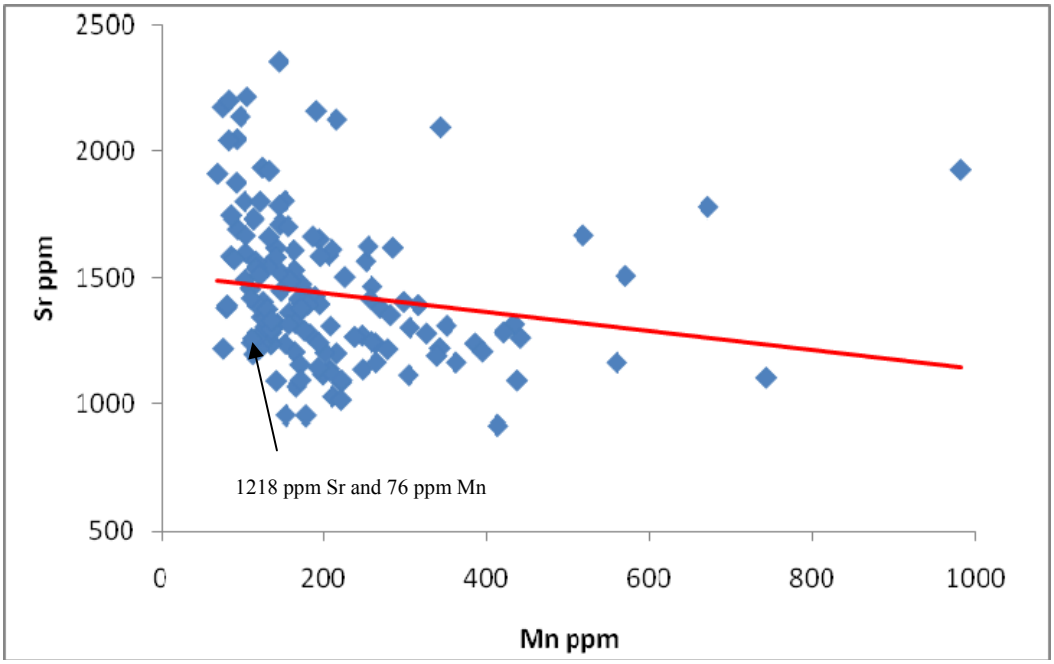

Figure 6.5 Plot of Mn against Sr

6.2.3 Magnesium and Strontium

Many ancient limestones were originally formed from a mixture of low Mg calcite, high Mg calcite and/or aragonite. Aragonite is by far the most dominant carbonate mineral in modern tropical and subtropical shallow-water carbonate-rich sediments (Morse, 2002). Modern aragonite grains generally have high Sr levels, with modern ooids containing 9000 to 10000 ppm, whereas modern high Mg calcite grains have lower values, in the range of 1000 ppm to 2000 ppm (Tucker, 1986).

Whether calcite and/or aragonite is precipitated in a marine regime is dependent upon temperature, pCO_2, pH and among other constraints, e.g. $[Mg^{2+}]/[Ca^{2+}]$ (Dietzel *et al*., 2004), as well as the organisms producing skeletal grains. Both high Mg calcite and aragonite are unstable and easily transformed to low Mg calcite during diagenesis. Once a limestone is stabilised to low Mg calcite its potential for further changes are reduced but not eliminated (Maliva, 1998; Veizer *et al*., 1999). An original aragonitic limestone can be transformed to low Mg calcite by either total dissolution of aragonite grains, which results in moulds which can be filled with cement (Figure 6.2), or the aragonite can be transformed by the simultaneous volume-by-volume dissolution of aragonite and precipitation of calcite, a process known as calcitization; this can be thought of as occurring across a thin film whereby dissolution of aragonite occurs on one side and precipitation of calcite occurs on the other (Tucker, 1986; Tucker and Wright, 1990; Maliva, 1998). Calcitization of aragonite and formation of pseudospar/microspar can result in Sr levels of several thousand ppm (Tucker, 1986).

Figure 6.6 is a plot of Sr against Mg together with equilibrium values for modern high Mg calcite and aragonite (after Tucker, 1986). The high Sr levels for the Great Limestone can be seen to be below the equilibrium value for modern marine aragonite and above and near to the expected value for modern marine high Mg calcite. It is most likely that these high Sr levels are due to stabilisation of an original aragonite-rich limestone to low Mg calcite, and not from an original marine, high Mg calcite-rich sediment. The reduction in Sr is consistent with the

expected effects associated with diagenesis and the low (0.14) distribution coefficient of Sr.

The higher solubility rates of aragonite compared to high Mg calcite would result in differential dissolution of aragonite grains relative to calcite, especially in an acidic setting, such as results from the decay of organic material, sulphate reduction and/or microbial effects (Wright *et al*., 2003). Cherns and Wright (2000) and Wright *et al*. (2003) have discussed the loss of at least 65%, and possibly up to 90%, of mollusc material from the fossil record, due to large-scale, early diagenetic dissolution of these formally aragonitic grains. Petrographic study in this research has also shown the loss of mollusc grains (Figure 6.2) and this loss of aragonitic fauna due to the stabilisation of the aragonite grains, could result in an increase of Sr in the pore-waters

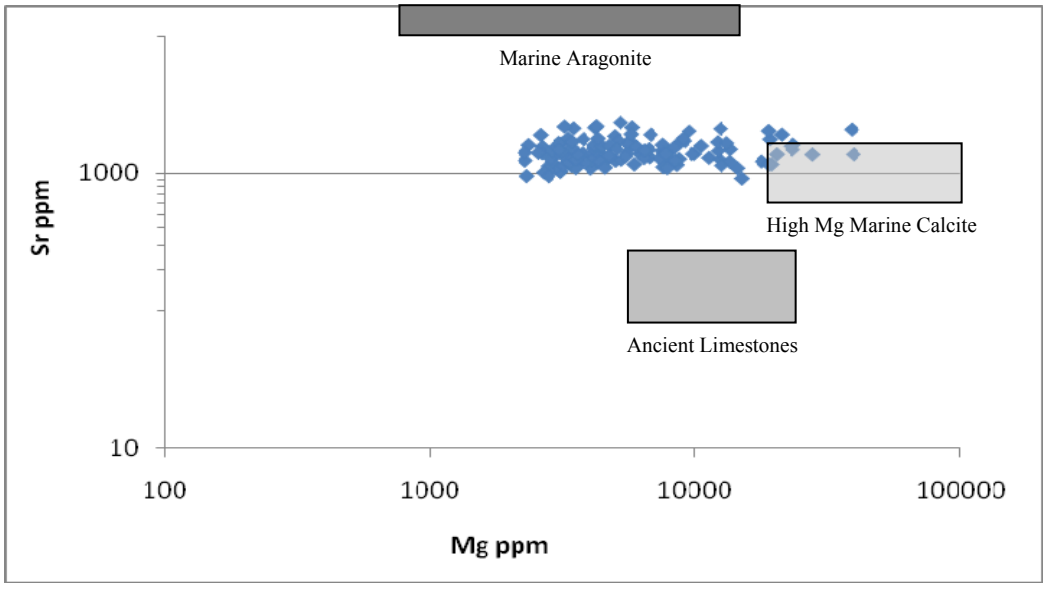

Figure 6.6 Plot of Sr against Mg together with "Equilibrium" values for ancient limestones, marine calcite and marine aragonite (after Tucker, 1986).

The Mg content of seawater largely depends upon the supply from rivers and the take-up into biogenic limestones. The Mg content of marine carbonates fluctuates within a wide range and therefore on their own are not necessarily helpful in determining diagenetic history (Bruckschen *et al*., 1999), however, a decrease in Mg could be expected due to diagenesis. With this in mind, Mg levels in Figure 6.6 can be seen to vary between 2300 ppm (0.23%) and 39000 ppm (3.9%) (average 7000 ppm (0.7%)). Even though these are not excessively high

values, marine aragonite would only be expected to have between 5000 ppm (0.5%) Mg and 15000 ppm (1.5%) Mg, values around 5000 ppm (0.5%) being typical (Tucker, 1986). The majority of the Mg values are lower than what may be expected in high magnesium marine calcite and nearer to those levels expected in marine aragonite (Figure 6.6). A reduction in Mg may also be expected due to diagenesis and; therefore, even though 3.5% HNO_3 at 120^0 C in the chemical analysis may not be expected to fully dissolve dolomite, the higher end of the Mg range in Figure 6.6 could be from Mg leached from the scattered dolomite rhombs which occur in some beds and not from an original marine calcite.

6.2.4 Diagenesis and dissolution in individual beds

Frank *et al*. (1999) showed that carbonate liberated from calcareous shales by dissolution could be transported over tens of centimetres to precipitate in bioturbated limestones as calcite cement: a move of carbonate from a less calcareous to a more calcareous unit. The progressive addition of calcite cement (low strontium) to the limestone from dissolution and pressure dissolution can provide enough $CaCO_3$ to account for all cement (Bathurst, 1991), resulting in a gradual decrease in bulk Sr/Ca ratios and a more negative $\delta^{18}O$ value for the limestone as a whole, and a gradual increase of bulk Sr/Ca ratios and a more positive $\delta^{18}O$ value in the carbonate shale (Frank *et al*., 1999).

Figure 6.7 illustrates calcium, strontium (times 100) and strontium/calcium ratios (times 1000) for beds 1, 20 and 27 of the Great Limestone; shale units of varying thickness delineate these beds: from a few millimetres each side of bed 1, 10 to 30 millimetres each side of bed 20, 5 to 10 millimetres at the bottom of bed 27 and several metres above bed 27.

It can be seen from Figure 6.7 that the strontium/calcium ratios in these beds are generally greater adjacent to the bed margins and the calcareous shale and reduce within the limestone as predicted by Frank *et al*. (1999).

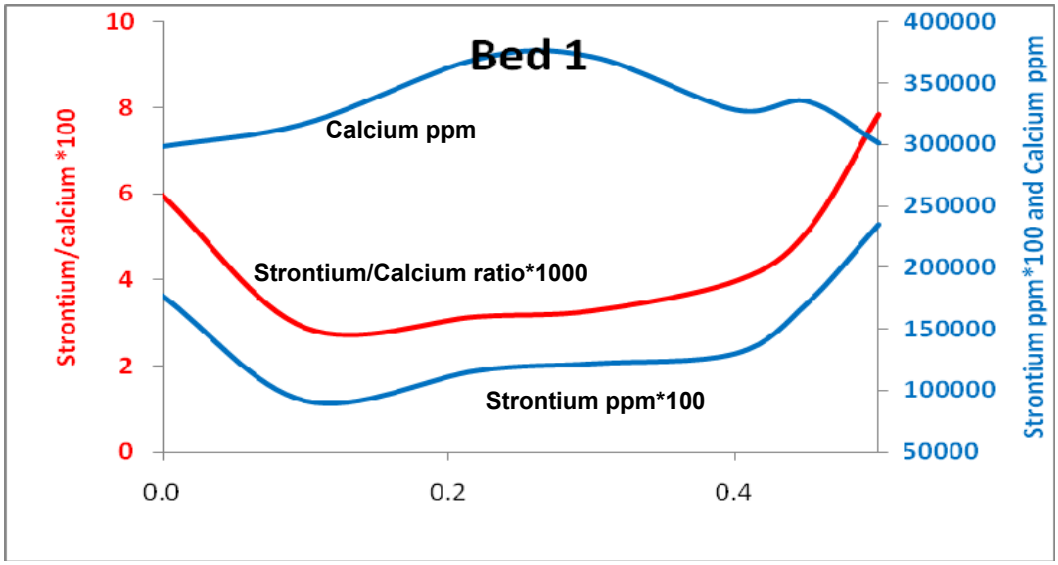

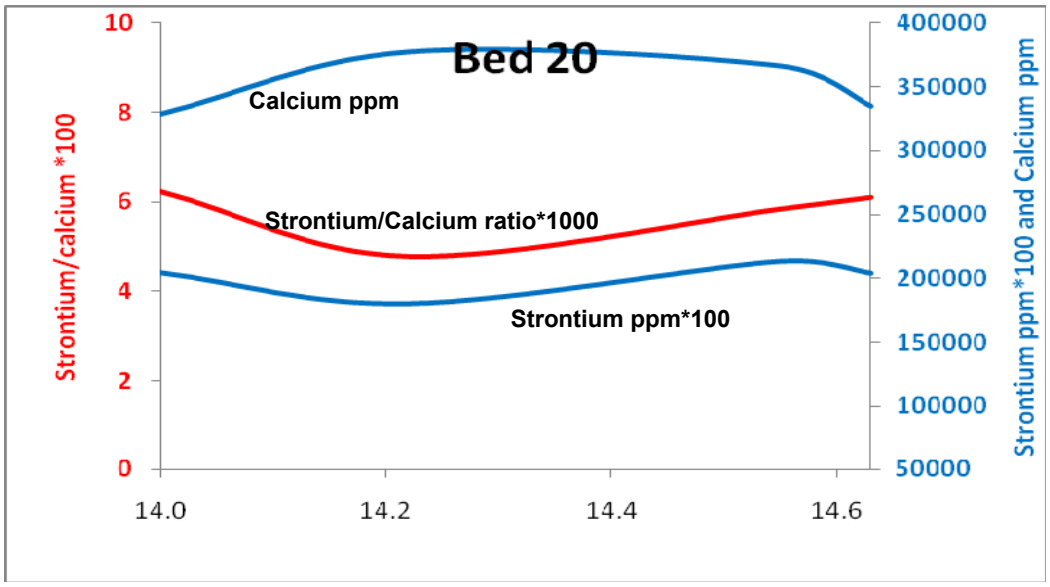

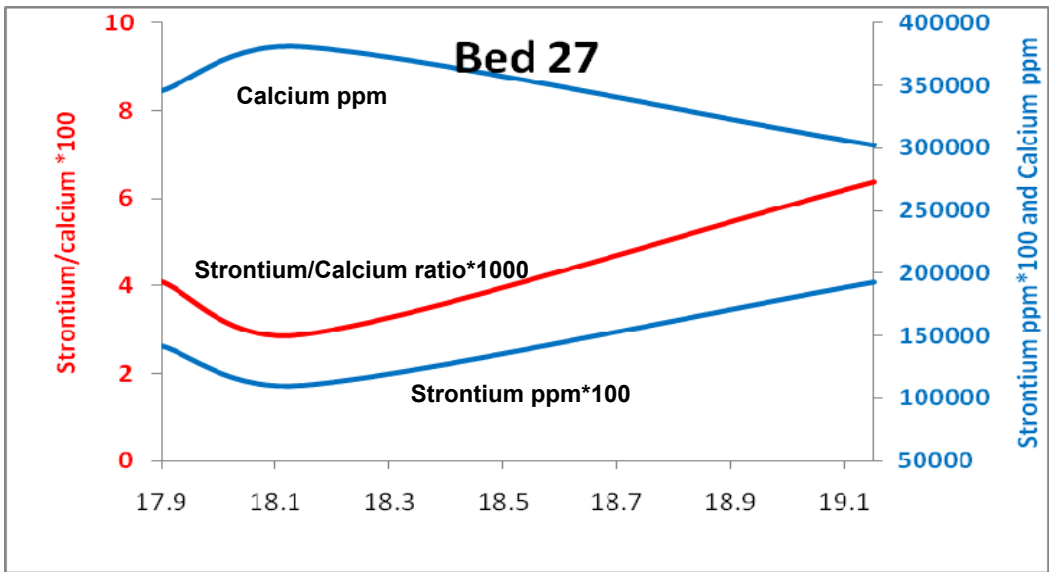

Figure 6.7 Calcium, strontium (times 100) and strontium/calcium ratios (times 1000) for Beds 1, 20 and 27.

Strontium, as expected, follows the same trend as the strontium/calcium ratio while the trend for calcium is opposite, confirming the discussion above with regard to increases within beds. However, it is interesting to note that the thickness of the shale/parting itself, does not seem to influence the degree of change within the strontium or magnesium trend of the limestone. The more positive $\delta^{18}O$ values as predicted by this model do not always occur within the Great Limestone and this is discussed further in Chapter 7.

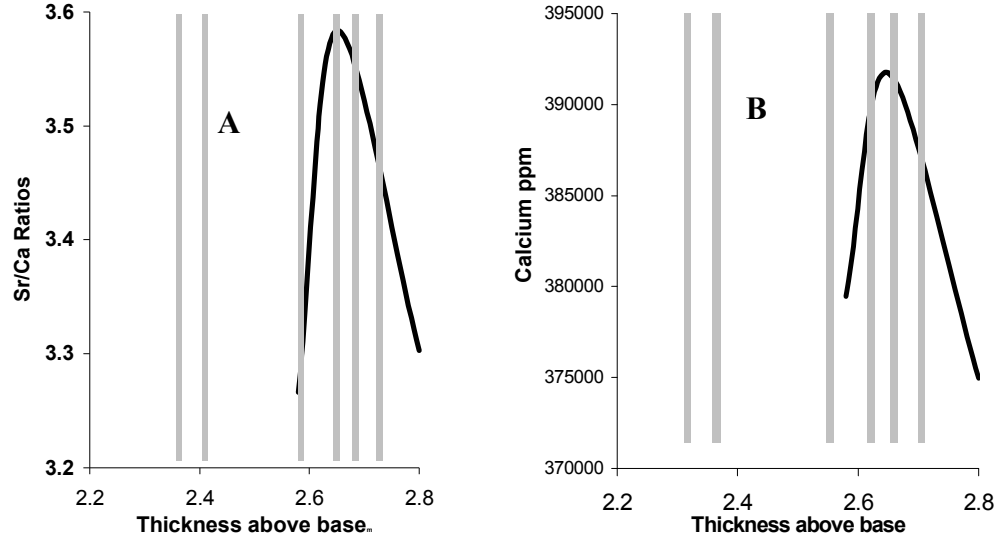

Figure 6.8 Sr/Ca ratios for bed 5 (A) and Ca concentration for bed 5 (B) (Note grey bands are the positions of stylolites)

Similar decreases and increases in strontium/calcium ratios, strontium and calcium can be seen in many of the other beds, e.g. 8, 12, 15, 17, 19, 22, 23 and 25. The remaining beds are either not bounded by mudstones or the trend is confused and difficult to establish.

The position of stylolites within many of the beds may be expected to be areas of low Ca and high Sr/Ca ratios due to the probable increased clay content and subsequent pressure. However, this is not always the case and in many beds a confused pattern arises where Sr/Ca ratios are rising at stylolites, as may be expected by the discussion above, even though the Ca levels are also rising (Figure 6.8).

6.2.5 Stable Isotopes

Modern marine carbonates have carbon and oxygen stable isotope values in the range of 0‰ to 4‰ $\delta^{13}C$ and –2‰ to +1‰ $\delta^{18}O$; and average ancient limestones have values between –2‰ and +2‰ for $\delta^{13}C$ and –10‰ to -2‰ for $\delta^{18}O$ (Tucker, 1986). There is also evidence for a secular variation through time with $\delta^{13}C$ becoming more positive by –1‰ to +4‰ VPDB during the Palaeozoic and $\delta^{18}O$ becoming more positive by -8‰ to 0‰ VPDB in the course of the Phanerozoic (Veizer *et al*., 1999; Mii *et al*., 1999).

Figure 6.9 is a plot of $\delta^{13}C$ and $\delta^{18}O$ values from the Great Limestone together with data by Tucker (1986), Mii *et al*. (1999) and Mii *et al*. (2001). The Great Limestone values can be seen to group tightly together with $\delta^{13}C$ varying between –0.7‰ and +1.9‰ (average +1‰, median +1.1‰) and $\delta^{18}O$ between – 13.6‰ and –7.8‰ (average and median -10.4‰). The $\delta^{13}C$ values fall generally within the expected range for ancient limestones (Tucker, 1986), non-luminescent brachiopods (Mii *et al*. 1999, Mii *et al*. 2001) and modern marine carbonates (Tucker, 1986); on the other hand 80% of the $\delta^{18}O$ values are much more negative than all of these projected ranges. These very negative $\delta^{18}O$ values could suggest there may have been large differences in sea-surface temperatures and/or SMOW at the time of deposition, compared to modern values, or that the values are due to either diagenesis by non-marine meteoric fluids and/or high temperatures during diagenesis.

Most recent research into $\delta^{13}C$ and $\delta^{18}O$ variations and values in sediments has revolved around the use of low Mg calcite brachiopods (e.g. Popp *et al*., 1986; Veizer *et al*., 1997; Bruckschen *et al*., 1997; Veizer *et al*., 1999; Mii *et al*., 1999; Bruckschen *et al*., 1999; Mii *et al*., 2001; Brand *et al*., 2004), and as such, much of the published $\delta^{13}C$ and $\delta^{18}O$ data, does not cover whole rock analyses, but is for brachiopods composed of original low Mg calcite. Original low Mg calcite brachiopods probably underwent little alteration during diagenesis; unaltered and non-luminescent brachiopods are therefore ideally suited to represent ancient seawater chemistry. Mii *et al*. (1999, 2001) reported $\delta^{13}C$ and $\delta^{18}O$ values from

non-luminescent mid-Carboniferous brachiopods ranging between -3.6‰ to +7‰ and -6‰ to -0.4‰ respectively.

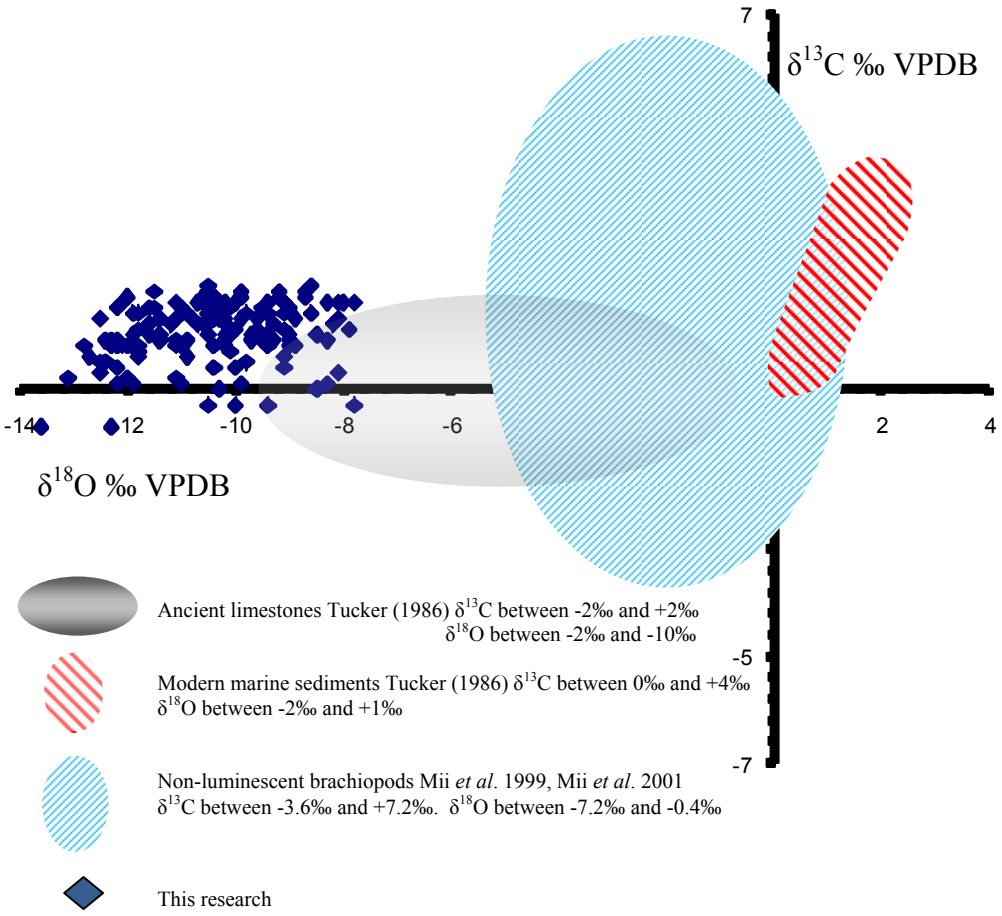

Figure 6.9 $\delta^{13}C$ and $\delta^{18}O$ variations within the Great Limestone. Shaded areas represent data specified by Tucker (1986), Mii *et al.* (1999) and Mii *et al.* (2001)

Veizer *et al.* (1999) considered the $\delta^{13}C$ and $\delta^{18}O$ variations in Silurian micritic matrix and early marine cement compared to low Mg calcite brachiopods and found the $\delta^{13}C$ mean values to be comparable, but for the $\delta^{18}O$ values of the whole rock to be generally depleted by ~2‰ relative to unaltered non-luminescent brachiopods (Figure 6.10). Interestingly, a convincing argument was also put forward by Veizer *et al.* (1999) that whole rock $\delta^{13}C$ and $\delta^{18}O$ data are, to a certain extent (albeit with the ~2‰ $\delta^{18}O$ depletion in mind) also a general proxy of the original seawater chemistry. The argument is built around the assumption that diagenetic stabilisation of shelf carbonates, i.e. alteration of metastable aragonite and high Mg calcite to low Mg calcite, occurs very early, when

diagenetic fluids still retain many seawater chemical signatures which therefore limit the whole rock $\delta^{18}O$ shift to ~2‰. This early stabilisation results in the limited resetting of the chemical, and in particular the $\delta^{18}O$ signal. Any further diagenetic alteration, after this initial re-setting, results in a much less pronounced $\delta^{18}O$ depletion (Maliva, 1998; Veizer *et al*., 1999).

Mii *et al*. (2001) reported mid-Carboniferous cement, matrix and luminescent brachiopods having $\delta^{18}O$ values of 1.6‰ to 4.4‰ more negative than non-luminescent brachiopods. Stoll and Schrag (1996) also argued that post-diagenetic $\delta^{18}O$ trends for carbonates could be regarded as following the primary signal. Frank *et al*. (1999) pointed out, however, that for this model to be true, bulk density, porosity and lithification from bed to bed must be very similar and that the assumption that "*the recrystallisation rate as a function of age can be envisaged as a smooth curve*" should therefore be used with caution, as it ignores the significance of variation in bulk density, porosity and lithification. These features in the Great Limestone have not been fully explored; however, thin-section analysis does show it comprises a generally homogeneous, wackestone/packstone to packstone texture throughout with a consistently low porosity. It is felt, therefore, that any variations between beds or throughout the limestone are insignificant and as such would not cause large shifts in the initial diagenetic stabilisation trend.

$\delta^{18}O$ values for recent red algae, corals, shallow-water molluscs, forams and green algae can be very negative compared to average modern marine sediments, because of the so called "vital effect", with $\delta^{18}O$ values for red algae and corals being as negative as -6‰ and shallow-water molluscs, forams and green algae -4‰ (Tucker and Wright, 1990). Petrographic studies of the Great Limestone show a mixture of bioclasts with, in some cases, abundant green and red algae with the ubiquitous crinoid segments; corals also dominate in some sections of the limestone. Whether these bioclasts had similar very negative $\delta^{18}O$ values is not known of course, nor whether they were sufficiently abundant so as to affect the overall $\delta^{18}O$ value of the whole rock.

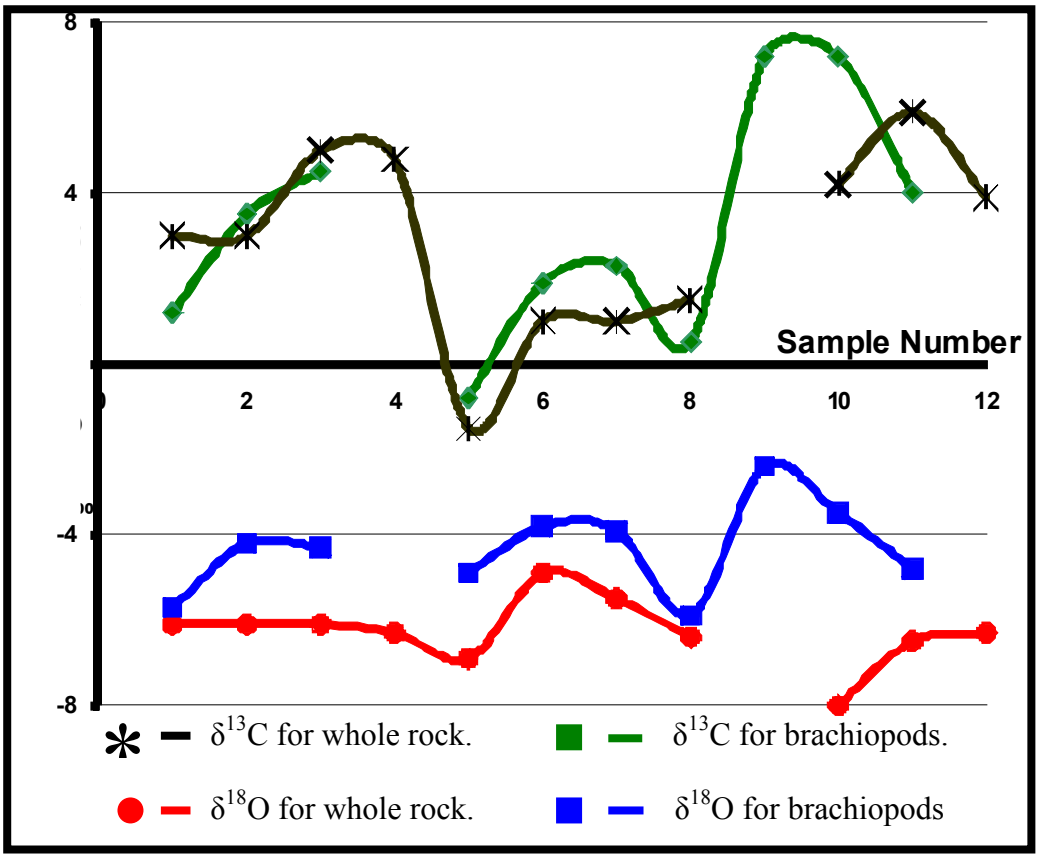

Figure 6.10 Comparison of Silurian whole rock and brachiopod $\delta^{13}C$ and $\delta^{18}O$ values (after Veizer *et al.*, 1999).

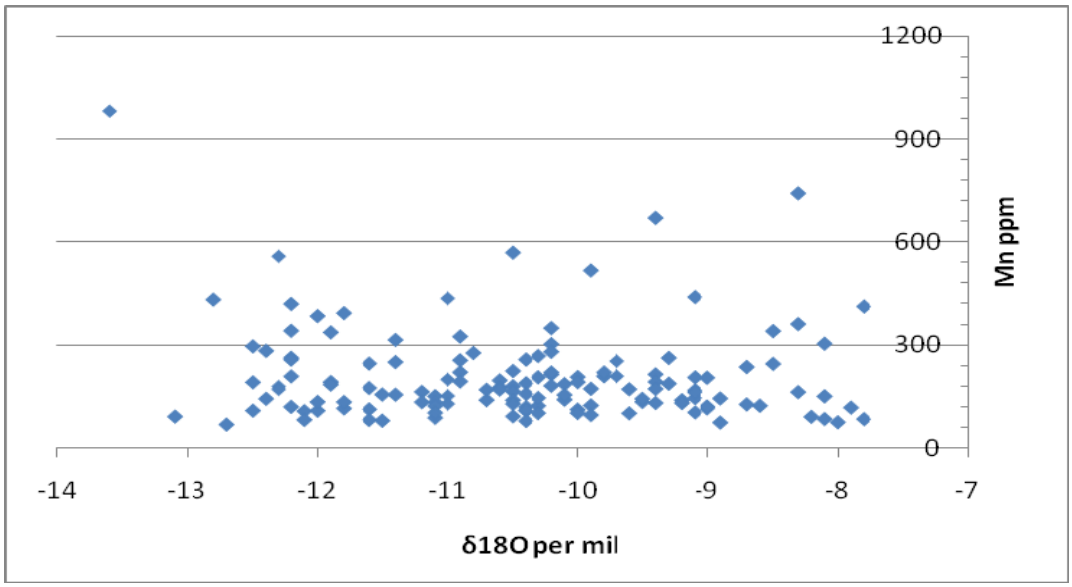

Figure 6.11 Plot of $\delta^{18}O$ and Mn

Figure 6.11 is a plot of $\delta^{18}O$ and Mn, which at first sight gives the impression that $\delta^{18}O$ and Mn values are closely linked, i.e. one of the least negative $\delta^{18}O$ values corresponds to the highest Mn level (-7.3‰ $\delta^{18}O$ and 980

ppm Mn) and the most negative $\delta^{18}O$ value corresponds to one of the lowest Mn (-13.1‰ $\delta^{18}O$ and 150 ppm Mn); however, this trend is in fact opposite to what would be expected from diagenesis (i.e. it would be expected to see high Mn with the most negative $\delta^{18}O$). Statistical analysis also gives a correlation of only -0.19 suggesting little relationship exists between the two.

Using the argument from Veizer *et al*. (1999), it may be expected that the $\delta^{18}O$ trend within the Great Limestone is likely to be partly due to the very early post-depositional resetting related to stabilisation of metastable polymorphs (aragonite, high Mg calcite) into stable low Mg calcite. This, however, would account for only a ~2‰ more negative value than the original trend, whereas the actual $\delta^{18}O$ values in the Great Limestone are much more negative than what would be expected using the values from an ancient limestone (see Figure 6.6 and Table 6.1) and this ~2‰ reduction.

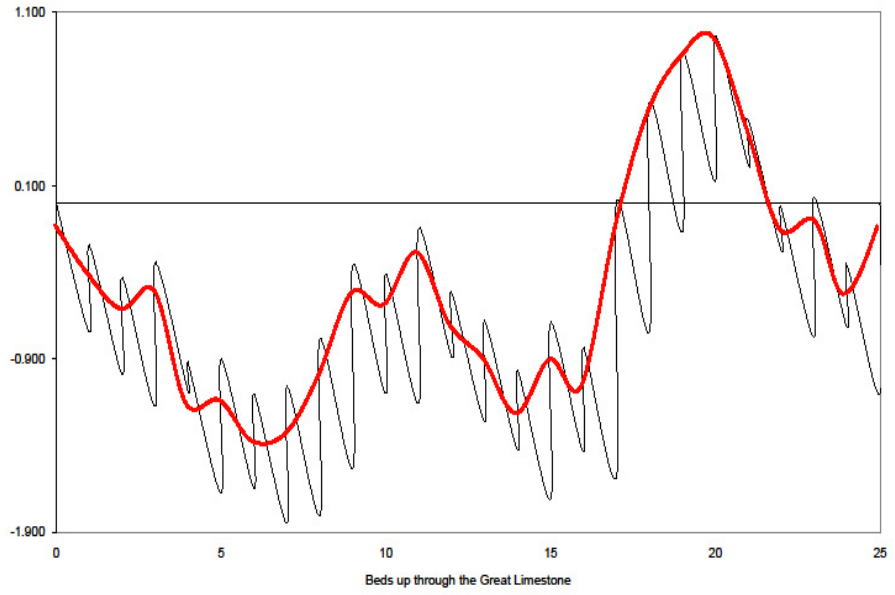

Figure 6.12 Fischer Plot of the Great Limestone

How early this stabilisation process occurs is difficult to ascertain; however, to a certain extent this is irrelevant; the important point as far as this research is concerned, is whether the original $\delta^{18}O$ trend is intact and therefore a

good expression of the patterns at the time of deposition. If the $\delta^{18}O$ trend is the result of sedimentological, geochemical or environmental changes during deposition, then it may be expected that the trend will be apparent in other data, e.g. bed-thickness variations, trace elements and petrographic data.

Figure 6.12 is a Fischer plot of bed thickness against bed number. A trend can be seen within the plot that traces out at least $2^1/_2$ cycles. Fischer plots calculated from Fairbairn's (1978) Great Limestone sections (Figure 3.27) which cover large areas of the Alston Block and parts of the Northumberland Basin, also reveal very similar trends, suggesting the control on bed deposition was not just local, but also covered a large area of what is now the north of England, some 10,000 sq km.

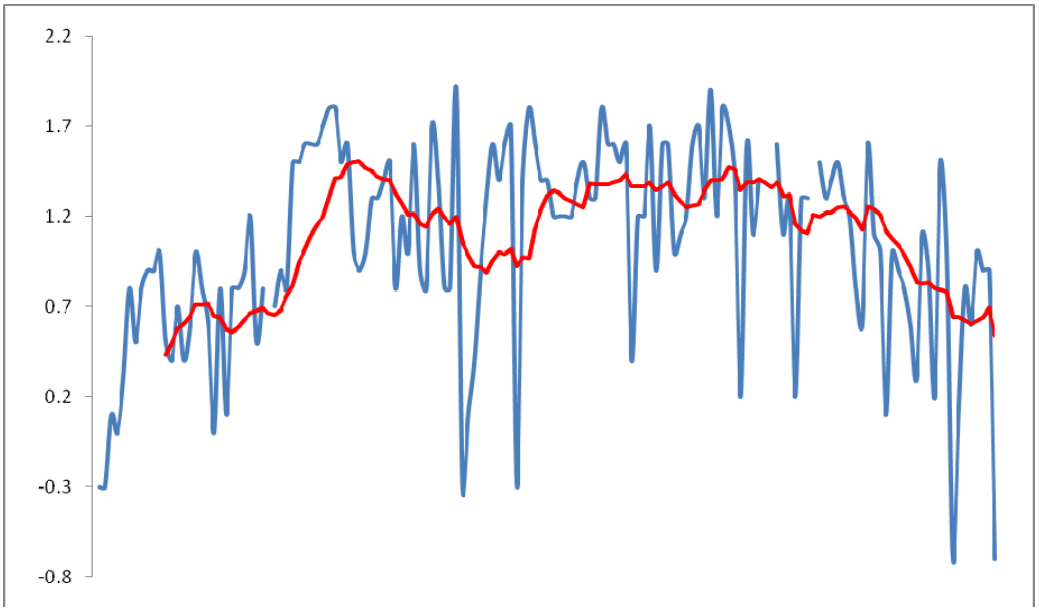

Figure 6.13 Carbon ($\delta^{13}C$) values plotted stratigraphically through the Great Limestone with 12 period moving average trend line (Red Line)

The $\delta^{18}O$ and possibly the $\delta^{13}C$ trends may be expected to show similar plots of $2^1/_2$ cycles if there is some sort of correlation and/or associated cause for the depositional trends. 12 period moving average trend lines for plots of $\delta^{13}C$ and $\delta^{18}O$ through the Great Limestone (Figures 6.13 and 6.14) do show some trends; however, these are not as clear as the trend shown in Figure 6.12 for the Fischer Plot. In an attempt to highlight any trends further, the same principle as used in the construction of Fischer plots has been used in the construction of Figures 6.15 and 6.16, i.e. the data have been plotted with cumulative deviation of the $\delta^{13}C$ and

$\delta^{18}O$ values from the average value through the Great Limestone (hereafter referred to as "AvPlots"). The "AvPlot" for the $\delta^{13}C$ (Figure 6.15) shows an initial fall followed by a gradual rise through the section with a drop off at the end. One small excursion can be seen near the middle of the plot. The "AvPlot" for the $\delta^{18}O$ (Figure 6.16) is similar but opposite to the $\delta^{13}C$ "AvPlot". Two and a half cycles are evident in both plots. Figure 6.16 is confusing at first sight as, due to the negative numbers, if $\delta^{18}O$ values are less negative than the mean, the limb of the Av Plot goes down, and if $\delta^{18}O$ values are more negative than the mean, the limb of the AvPlot will go up. Therefore the result is an opposite effect than what occurs with the positive number of the $\delta^{13}C$ AvPlot.

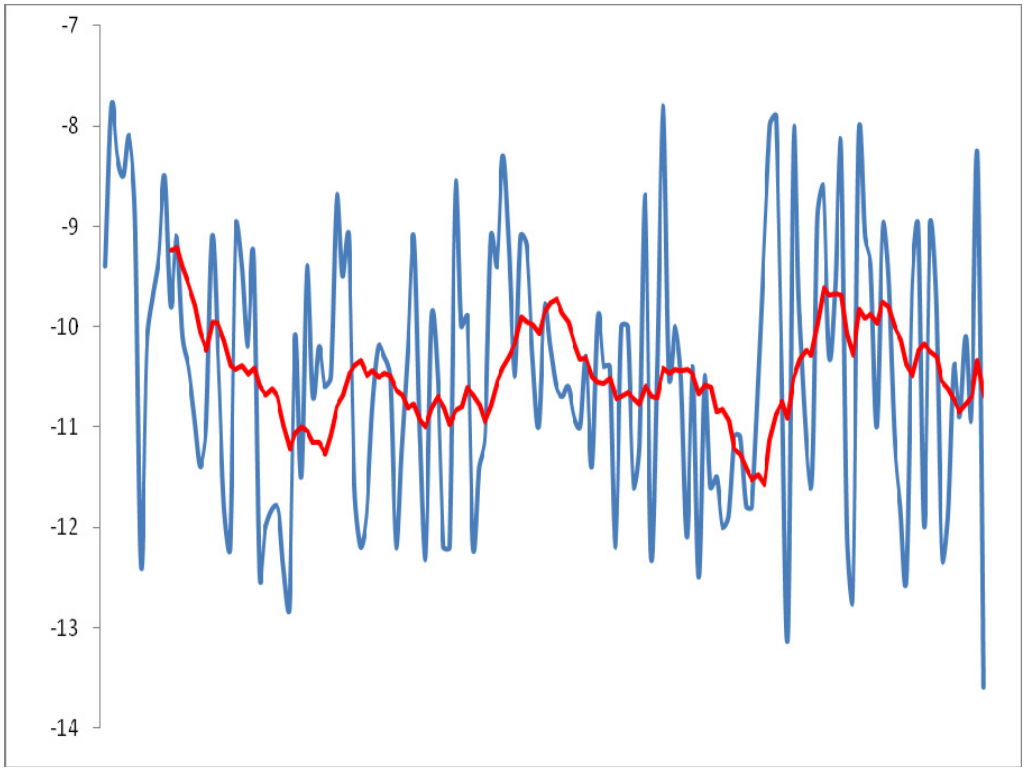

Figure 6.14 Oxygen ($\delta^{18}O$) values plotted stratigraphically through the Great Limestone with 12 period moving average trend line (Red Line)

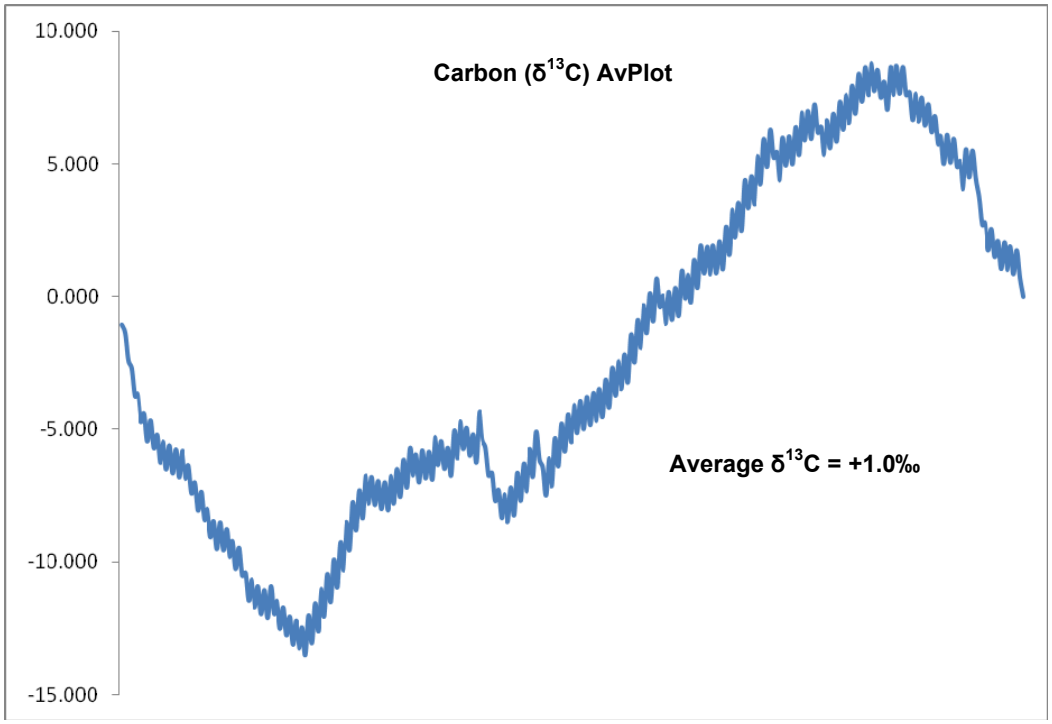

Figure 6.15 Carbon ($\delta^{13}C$) "AvPlot"

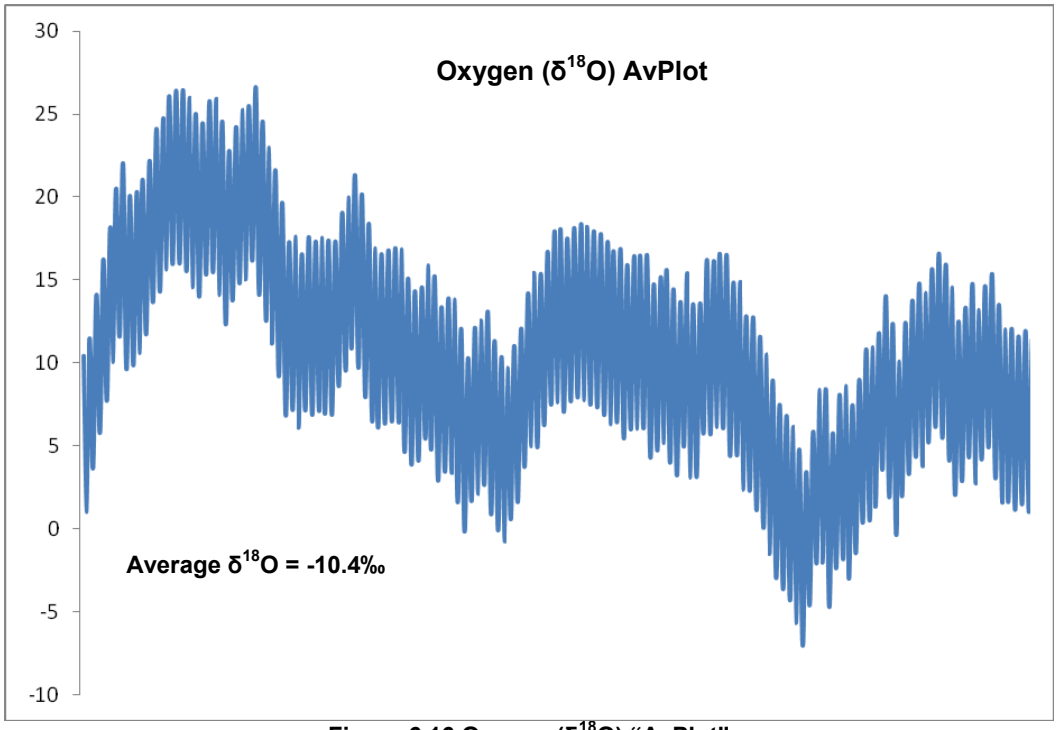

Figure 6.16 Oxygen ($\delta^{18}O$) "AvPlot"

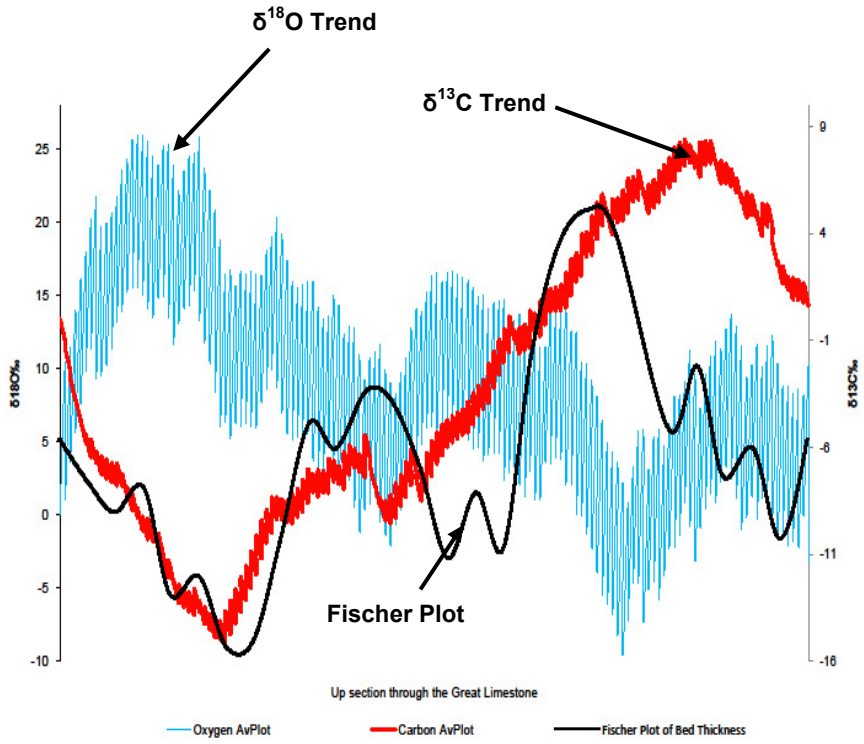

Figure 6.17 Combined $\delta^{13}C$ (red) and $\delta^{18}O$ (blue) "AvPlots" together with the Fischer plot (black line).

Figure 6.18, even though it appears to be a complicated plot, shows the combined $\delta^{13}C$ and $\delta^{18}O$ "AvPlots" together with the Fischer plot, for Middleton in Teesdale, for comparison. Even though there are 'lags' between the peaks, there are strong similarities between the individual graphs; this could suggest a possible common cause. These close similarities between the "AvPlots" and the Fischer plots would suggest some over-riding factor(s) controlling deposition, whether Sedimentological, geochemical or environmental. It could be argued that these close similarities of trends between the "AvPlots" and the Fischer Plot reinforce the principles adopted here that the $\delta^{13}C$ and $\delta^{18}O$ trends closely track the original palaeotrend. See also Chapter 7.

Figures 6.15 and 6.16 show the AvPlots for $\delta^{18}O$ and $\delta^{13}C$ and Figure 6.17 combines the $\delta^{18}O$ and $\delta^{13}C$ AvPlots and the Fischer Plot of bed thicknesses. There are some lags in the comparisons between the $\delta^{18}O$ and $\delta^{13}C$ AvPlots and the Fischer Plots, but generally the less negative $\delta^{18}O$ and $\delta^{13}C$ values occur in the zones of thicker beds whereas the more negative $\delta^{18}O$ and $\delta^{13}C$ values occur

within zones of thinner beds. The apparent increasing-decreasing bed thickness patterns revealed in the Fischer Plots and comparison with the $\delta^{18}O$ and $\delta^{13}C$ suggest some regular increasing-decreasing changing parameter(s) controlling deposition; this will be discussed further in Chapter 7.

Table 6.1 gives correlation values for all trace elements and isotopes. It can be seen that little relationship exists between the trace elements and the isotopes with the best correlation being between Fe and $\delta^{13}C$ at –0.54. Relationships between the trace elements themselves are not much better with the majority of the values being below 0.5; however, Al has a near perfect correlation with Si and good correlatıons with Fe and S. Si and Fe are probably linked to terrestrial input and S to organic matter decomposition, the source of which may also be associated with a terrestrial input. The link with S and organic matter is also suggested by the close correlation between S and Fe, suggesting the S is present in pyrite. Si correlates slightly with Sr, S and Na; the first two being linked to terrestrial input again; however, Na is usually associated with crystal growth rate rather than seawater chemistry (Tucker and Wright. 1990). The poor correlations between the majority of the trace elements, and between the isotopes and the trace elements, are possibly suggesting several phases of diagenetic alteration in fluids of different composition.

6.3 Intrusion of the Whin Sill and rejuvenation of the Weardale Granite.

Creaney (1980) and Ferguson (1984) studied the petrography and vitrinite reflectance of coals on the Alston Block and suggested that, as well as the expected temperature/burial changes to the vitrinite reflectance of coals; at least two major pulses of heat flow are also indicated. Creaney (1980) used vitrinite reflectance measurements from coals in the Great and Little Limestone Cyclothems to conclude that temperatures in excess of 185^0 C were attained at the level of the Great Limestone within parts of the Alston Block, and, importantly, that this was pre-Whin Sill intrusion and in response to rejuvenation of the Weardale Granite at depth, probably as a result of the Hercynian orogeny. This pulse was followed towards the close of the Carboniferous by the intrusion of the Whin Sill. The intrusion of the Whin Sill complex in the Late Carboniferous

(Johnson and Dunham, 2001) would undoubtedly have produced elevated heat flow through the country rocks; however, this heat flow may only have affected rocks immediately adjacent to the intrusion (Creaney, 1980), whereas the pre-Whin Sill heat flow pulse affected rocks at a greater distance than that associated with the Whin Sill.

Heating of the sediments on the Alston Block would undoubtedly have resulted in changes to the $\delta^{18}O$ values of the limestones and therefore should have resulted in greater changes, i.e. more negative values, in the area of greatest heating. As can be seen in Figure 6.18, Middleton in Teesdale is within the Group I Vitrinite Zone and therefore would not be expected to have undergone the greatest range of heating. The Group I Vitrinite zone would, no doubt, still have undergone some temperature/depth-related heating; however, this would not be expected to have been as great as in Zones II, III and IV. Petrographic study of the samples from Middleton in Teesdale does not reveal neomorphic degradation of grains such as crinoid fragments as may be expected through the effects of thermal alteration (Folk, 1965: Lemon, 2006).

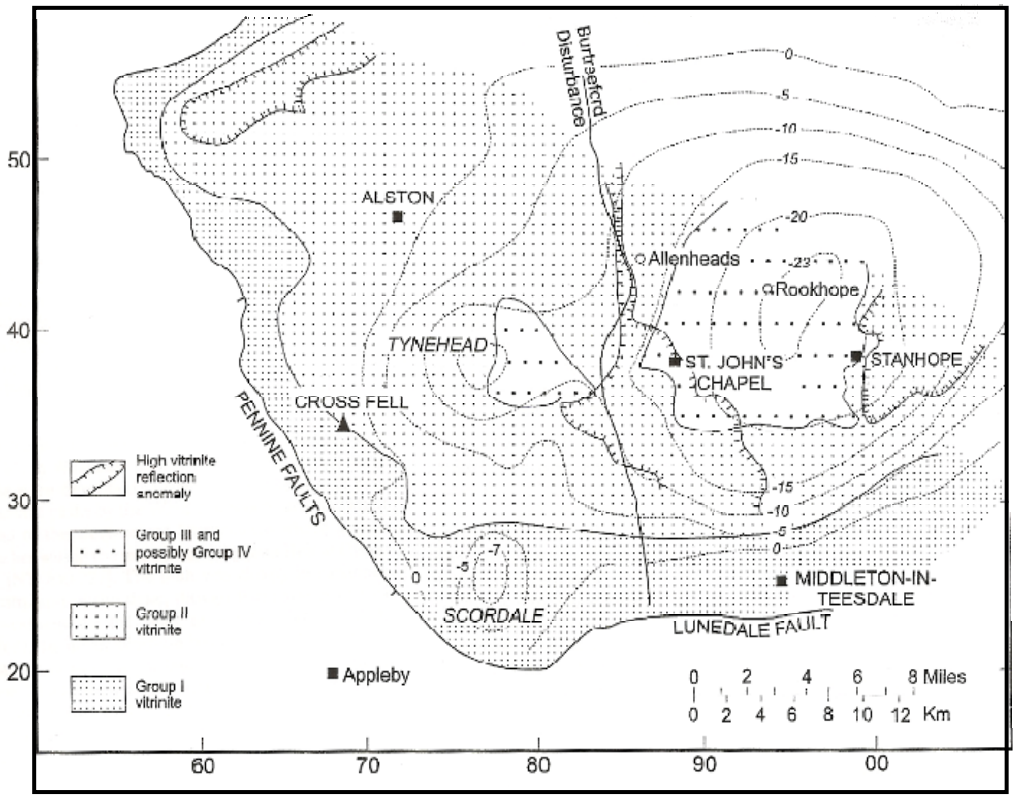

Figure 6.18 Vitrinite reflectance map of the Alston Block. After Creaney (1980) and Johnson and Dunham (2001).

6.3.1 Covariance of isotopes

Figure 6.19 shows the cross correlation between $\delta^{13}C$ and $\delta^{18}O$ values for Middleton in Teesdale where some covariance can be seen by the positive trend line, even though in Table 6.1 the correlation index is not very strong at 0.34; covariance is also discussed in Chapter 8. Coincidence of $\delta^{13}C$ and $\delta^{18}O$ trends are generally considered to reflect late diagenetic over-printing caused either by interaction with meteoric ground waters or by dissolution and recrystallisation at higher temperatures during burial diagenesis (Sakai and Kano, 2001; Keller *et al*., 2004). The low correlation index for $\delta^{13}C$ and $\delta^{18}O$ would suggest that $\delta^{13}C$ and $\delta^{18}O$ values were not affected in the same manner during diagenesis or that there may be other underlying causes for the trends and scatters seen in Figures 6.9, 6.15 and 6.16. These matters are considered further in Chapter 8.

The features of the Great Limestone at Middleton in Teesdale do not indicate that high temperatures were involved in its diagenesis; however, burial which resulted in the Group I vitrinite would undoubtedly have resulted in some heating of the sediments. The quite negative $\delta^{18}O$ values do suggest a meteoric diagenetic fluid or recrystallisation at a higher temperature and whether the high negativity of the $\delta^{18}O$ values is related to depth connected to heating or both is not certain. However, Nielsen *et al*. (2000) suggested that alteration due to elevated temperatures is indicated by very low $\delta^{13}C$ as well as negative $\delta^{18}O$, which is also indicated in this research.

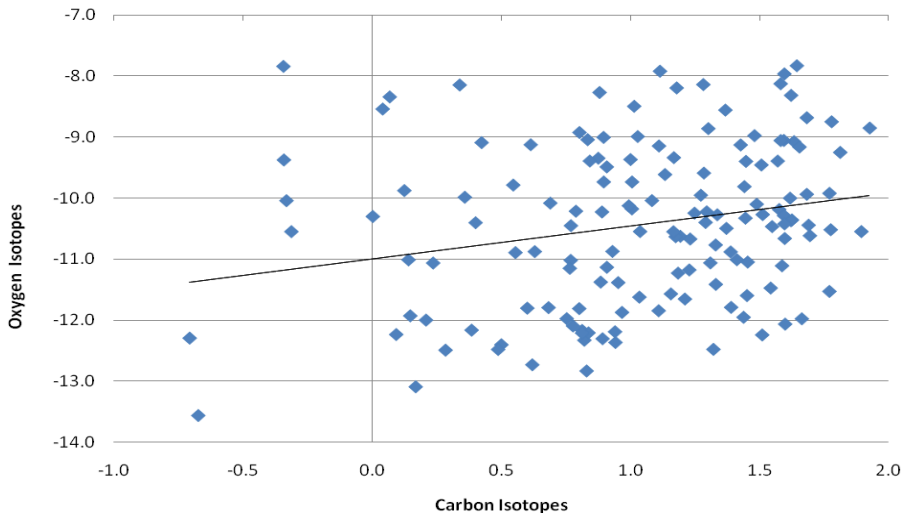

Figure 6.19 Cross correlation between $\delta^{13}C$ and $\delta^{18}O$.

6.3.2 Comparison of changes to $\delta^{13}C$ and $\delta^{18}O$ isotopes

$\delta^{13}C$ and $\delta^{18}O$ analyses were carried out by Lemon (2006) as part of her PhD and Figure 6.20 shows the sample locations for this work. Lemon's results are considered here to ascertain changes in relation to the vitrinite groupings. Unfortunately vitrinite reflectance data are not available covering all areas of Lemon's (2006) study; however, this hopefully does not pose a major problem with regard to the following discussion. The Rookhope borehole is sat directly over the high vitrinite reflectance anomaly shown in Figure 6.19 and, after the discussion above regarding alteration of $\delta^{13}C$ and $\delta^{18}O$ values due to re-activation of the Granite, it may be expected that the $\delta^{13}C$ and $\delta^{18}O$ values for the Rookhope borehole would become more negative with depth. Figure 6.21 are the plotted results of Lemon's (2006) $\delta^{13}C$ and $\delta^{18}O$ analyses for the Rookhope borehole limestones where it can be seen that both the $\delta^{13}C$ and $\delta^{18}O$ values do in fact become more negative with depth.

Figure 6.20 Location map for Lemon's (2006) $\delta^{13}C$ and $\delta^{18}O$ analyses

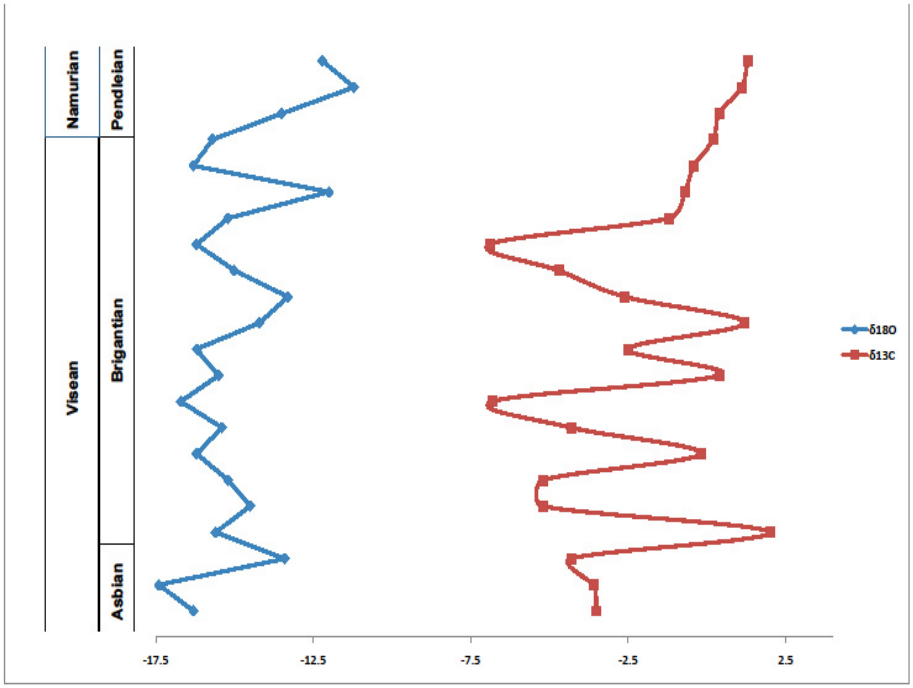

Figure 6.21 $\delta^{13}C$ and $\delta^{18}O$ analyses for Rookhope borehole limestones using values from Lemon (2006) Note the vertical axis is not to scale.

The top of the plot in Figure 6.21 has values of between -11‰ to -12‰ for $\delta^{18}O$ and this gets more negative towards the bottom where it is between -16.3‰ to -17 .4‰. This trend towards more negative values is in agreement with the discussion that alteration of $\delta^{18}O$ values will occur due to heating; the trend from top to bottom gets more negative as the borehole approaches the Weardale Granite at depth. It can also be seen in Figure 6.21 that the $\delta^{13}C$ values also become more negative from 1.3‰ to -3.5‰ as the plot moves from top to bottom. The $\delta^{13}C$ values are also very light compared to modern and ancient limestone values discussed in Section 6.2.5.

It can be seen within Figure 6.21 that both the $\delta^{13}C$ and $\delta^{18}O$ values have a large scatter and in many cases the trends correlate well and have a relatively strong correlation index of 0.4. Even though there is an obvious trend in both the $\delta^{13}C$ and $\delta^{18}O$ values from top to bottom, it must also be remembered that relatively large scatter of $\delta^{18}O$ values of up to 4.5‰ has been found in this research in various beds of the Great Limestone at Middleton in Teesdale.

Figure 6.22 shows the plotted $\delta^{18}O$ results from Lemon (2006) for five locations, two of which, Rookhope Borehole and Bowlees, are on the Alston Block, Haltwhistle is north of the Alston Block in the Northumberland Basin and Spittal and Beadnell are to the east on the coast (Figure 6.20). This figure shows that the values for each locality appear to form a trend moving northwards away from the block towards Spittal, the farthest from the block. However, due to the lack of sampling in comparable limestone units and beds, this pattern is not convincing. It is interesting to note that the trend for Haltwhistle becomes more positive towards the bottom of the Namurian, which is generally opposite to the other trends.

Figure 6.23 shows the plotted $\delta^{13}C$ results from Lemon (2006) for the same locations. There is a large spread of $\delta^{13}C$ values from 4.8 to -6.8 across the region, with Beadnell having the most positive values and Rookhope the most negative i.e. as distance from the Weardale Granite increases.

The Middleton in Teesdale values have also been added to Figures 6.22 and 6.23 and it can be seen that they cluster near to the least negative of the Namurian and late Brigantian values from the other locations values.

6.4 Conclusion and acceptability of trace element and isotope data

Both the trace elements and isotopic data for the Great Limestone demonstrate that, inevitably, diagenetic alteration has occurred which has resulted in the resetting of the initial values. Mn values are higher than expected for modern seawater precipitates; however, most of the values are below the threshold of 250 ppm Mn recommended by Popp *et al*. (1986) for brachiopods being analysed for isotope signatures. This therefore suggests the limestone can be regarded as "well preserved" as far as Mn is concerned.

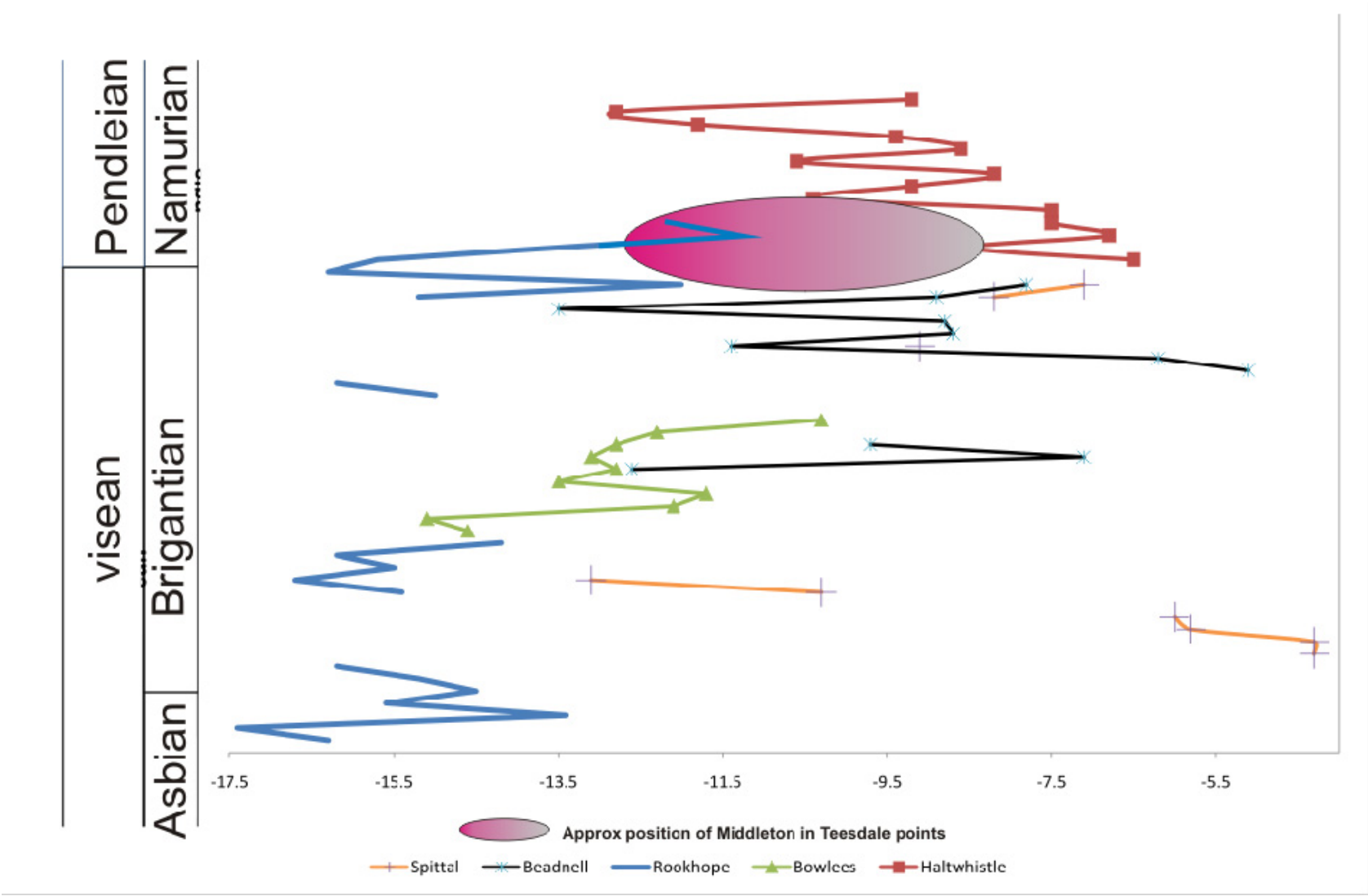

Figure 6.22 $\delta^{18}O$ analysis for five locations on and adjacent to the Alston Block using data from Lemon (2006) plus Middleton in Teesdale analysis. Note the vertical axis is not to scale

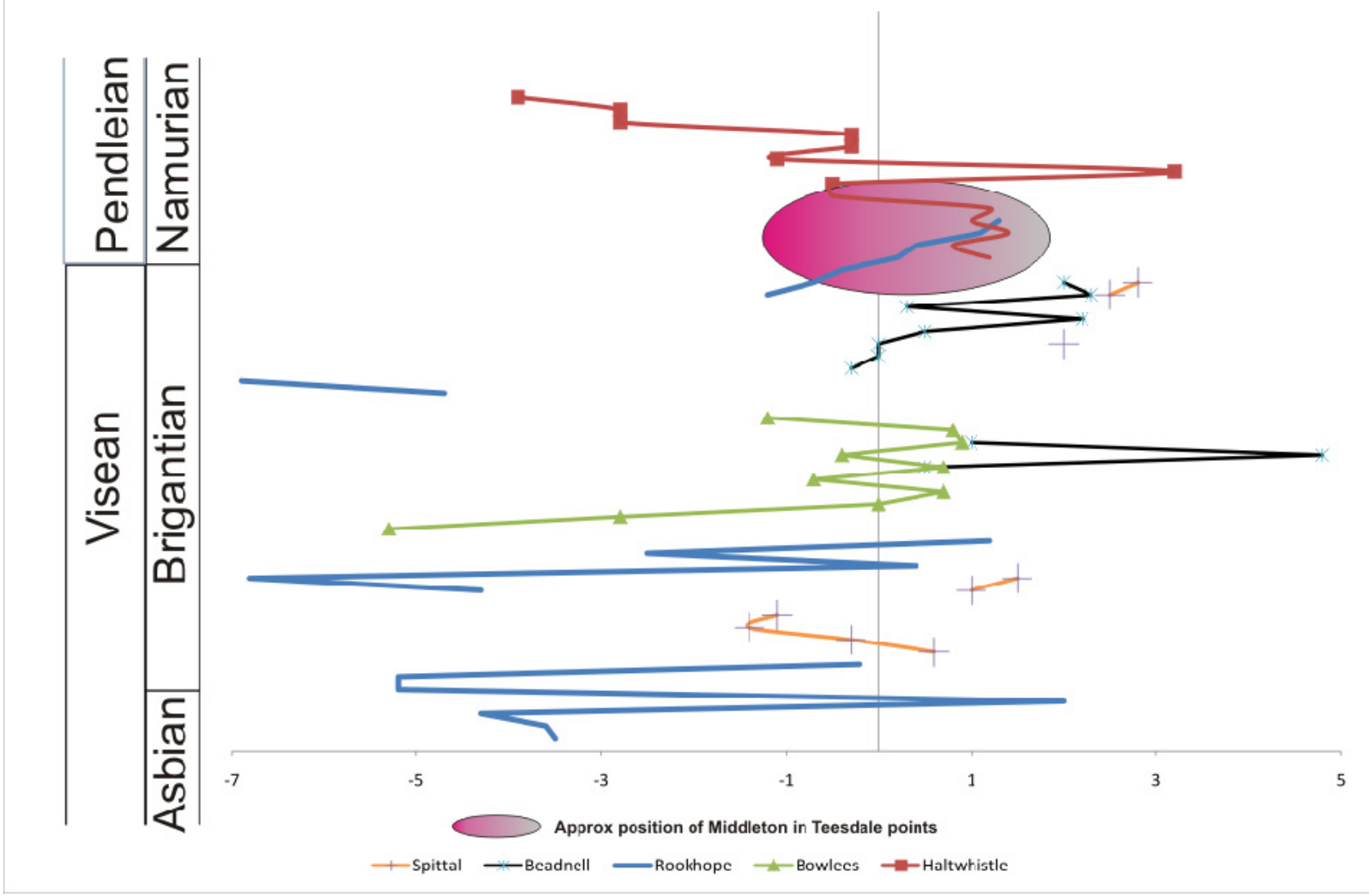

Figure 6.23 $\delta^{13}C$ analyses for five locations on and adjacent to the Alston Block using data from Lemon (2006) plus Middleton in Teesdale analyses. Note the vertical axis is not to scale

Fe values are high and this is very likely due to burial diagenesis. As both Mn and Fe are expected to increase with diagenesis, a close correlation between these elements may be likely; this, however, is not the case. It would appear therefore that even though the limestone can be regarded as being "well preserved" as far as Mn is concerned, the high Fe values suggest diagenetic alteration in fluids rich in Fe, probably derived from terrigenous clay, so Fe contents may not follow any original trend.

The Sr values fall near to marine calcite concentrations and below values for an aragonite precursor. Whatever the hypotheses for the formation of the limestone, the Sr values are high compared to average ancient limestones. This suggests that the original sediment had significant aragonite content.

Modern marine calcite would be expected to contain Mg levels around 15,000 – 100,000 ppm; however, the Mg levels for the Great Limestone are much less than these. These values could be due to an original marine calcite, losing Mg during diagenesis or, as also suggested by the Sr values, it is a relic of an original aragonite-rich limestone.

Changes within beds of strontium/calcium ratios, strontium and calcium also show that diagenesis has occurred and resulted in movement of carbonate liberated from calcareous shales by pressure dissolution being transported over tens of centimetres to precipitate within the limestone as calcite cement: a move of carbonate from a less calcareous to a more calcareous unit.

The $\delta^{13}C$ values are comparable to ancient limestones and only slightly more negative than modern marine calcite. The $\delta^{18}O$ values on the other hand are very negative with an average of -10.4‰ and most negative value of -13.6‰. These very negative values are nearly an order of magnitude less than modern marine carbonates, which would suggest that these values are partly due to resetting by a meteoric diagenetic fluid or recrystallisation at a higher temperature.

Changes in $\delta^{18}O$ and $\delta^{13}C$, at various locations and depths on and adjacent to the Alston Block, were assessed for comparison of values and trends in relation to the re-activation of the Weardale Granite. The Rookhope Borehole does show a negative trend towards the granite; however this negative trend reduces in localities farther away from the high vitrinite reflectance zone.

The question remains as to whether it is felt acceptable to use the data for further analysis. The trace elements (excepting Fe) and $\delta^{13}C$ data are thought to be acceptable in that values do not show excessive diagenetic alteration if compared to published data; the $\delta^{18}O$ values on the other hand are not comparable to published data for well-preserved brachiopods. There are strong arguments (Veizer *et al*. 1999) for a resetting of the original $\delta^{18}O$ signal during diagenetic stabilisation of shelf carbonates. These are convincing, and suggest that very early in diagenesis $\delta^{18}O$ values are set at ~2‰ more negative than the initial level and any further diagenesis results in a much less pronounced $\delta^{18}O$ change. These arguments would suggest that the resetting will result in new, more or less fixed values, which will contain an approximation of the original trend (~2‰ more negative than the original trend) and any further diagenesis will not destroy this trend to any large extent. An attempt has been made above to show that the $\delta^{13}C$ and $\delta^{18}O$ trends do in fact track an original pattern, namely that of the bed-thickness pattern. This was achieved by comparing a Fischer plot for the cumulative deviation of bed thickness from the average with similar graphical methods carried out on the $\delta^{13}C$ and $\delta^{18}O$ data (AvPlots).

Thus, even though the use of the actual $\delta^{18}O$ values may be in question and they are therefore probably unusable in any further analysis, the use of the trend is not. The trace element and the isotope values prove that diagenetic alteration has occurred; however, it is concluded from these discussions that the data for $\delta^{18}O$ in particular can, with caution, be used for further analysis to interpret the chemostratigraphic, palaeoceanographic, and the palaeoclimatic history of the Great Limestone.

7.0 Oxygen and carbon stable isotope geochemistry of the Great Limestone

7.1 Introduction

The global environmental changes during the Carboniferous, including the proliferation of land plants, led to increased rates of continental weathering (Algeo *et al*., 1995) and storage of organic carbon leading to a drawdown of atmospheric CO_2 and cooling. The Carboniferous climate was also entering icehouse conditions with glaciations (González, 1990; Frakes *et al*., 1992; Berner, 1994; Dickins, 1996) and sea-level oscillations (Ross and Ross, 1998). During this pivotal time in the Earth's history, many of the changes in temperature, palaeoceanography and carbon cycling/storage were recorded in the carbon and oxygen isotope compositions of marine carbonates. Analysis of stable isotopes is therefore a fundamental tool for the study of palaeoclimate and palaeoceanography.

Differing numbers of neutrons within isotopes results in similar, but not identical chemical properties that lead to variations in kinetic and isotope exchange processes or isotope fractionation. It is due to the fact that different isotopes of an element do have this variation in their physical-chemical properties that stable isotopes are so useful in the understanding of diagenesis and palaeoenvironmental issues. Many factors affect the chemical composition of a carbonate, including seawater chemistry, temperature, salinity, evaporation, freshwater influx, ice volume, continental weathering, hydrothermal activity and the so called 'vital effect' which organisms exert with regard to how elements, including the stable isotopes of oxygen and carbon, are concentrated within the hard and soft parts of their bodies; i.e. biogenic carbonate may be in isotopic disequilibrium with ambient seawater (McConnaughey, 1989).

The stable isotopes of carbon and oxygen have already been discussed in Chapter 7 where they were used together with trace elements to investigate the diagenetic history of the Great Limestone and to compare the concentrations to both modern and average ancient limestones. Chapter 7 concluded that the carbon isotopes of the Great Limestone had not undergone excessive diagenetic resetting

and compared favourably to modern and ancient values. It was also suggested that even though diagenetic alteration would have resulted in a change to the oxygen stable isotope values, this is not thought to have resulted in the loss of the isotope trends. The following section will not therefore revisit diagenesis to any great extent.

The purpose of this chapter is to assess the palaeoenvironment of the early Namurian environment and seawater with regard to chemistry, temperature, salinity, freshwater influx and ice volume.

7.2 Sample collection

149 whole-rock limestone samples were collected from two outcrops of the Great Limestone at Middleton-in-Teesdale (O.S. 394784, 527610 and O.S. 394916, 527276, Figure 5.1) which covered the full height of the limestone. The outcrops were sampled at between 100 millimetre and 150 millimetre intervals. The limestone samples were visually assessed for the presence of large grains or vein calcite which, if present, were rejected. All samples were powdered using a mortar and pestle.

7.3 Methodology

All geochemical analyses were carried out at the NERC Isotope Geoscience Laboratory (NIGL) by Dr Kirstin Lemon during her own PhD research at Durham University and Dr Melanie Leng of the BGS,. The following methodology is from Lemon's own description.

Whole rock limestone samples were visually assessed for the presence of excessive organic material by examining the overall colour of the limestone. Those with a very dark grey to dark grey coloration were interpreted as containing excessive levels of organic material. Samples with excessive levels of organic material were immersed in 5% NaOH.Cl overnight to remove any organic material that may influence the isotopic results by reflecting the isotopic values of organic carbon as opposed to marine carbon.

An aliquot of powdered sample (c. 10mg) was time-reacted with anhydrous phosphoric acid in vacuo at 16^{o}C for 2 hours. This low temperature / short

reaction dissolves the calcite but leaves any dolomite present un-reacted. The CO_2 liberated was separated from water vapour and collected for analysis.

Measurements were made on a VG Optima mass spectrometer. Overall analytical reproducibility for the samples was normally better than 0.1 for $\delta^{13}C$ and $\delta^{18}O$. Isotope values are reported as per mil deviations of the isotopic ratios ($^{13}C/^{12}C$ and $^{18}O/^{16}O$) from standards (VPDB for carbonates).

7.4 Great Limestone $\delta^{13}C$ and $\delta^{18}O$ isotope results

The whole-rock $\delta^{13}C$ and $\delta^{18}O$ results for the Great Limestone are summarised in Table 7.1. (Appendix E). The $\delta^{13}C$ values are within the range of 1.9‰ to -0.7‰ with an average of 1.0‰ and the $\delta^{18}O$ values within the range -7.8‰ to -13.6‰ with an average of -10.4‰. In Figure 7.1 both the $\delta^{13}C$ and $\delta^{18}O$ results are seen to have a wide scatter and some of the $\delta^{13}C$ and $\delta^{18}O$ values are covariant.

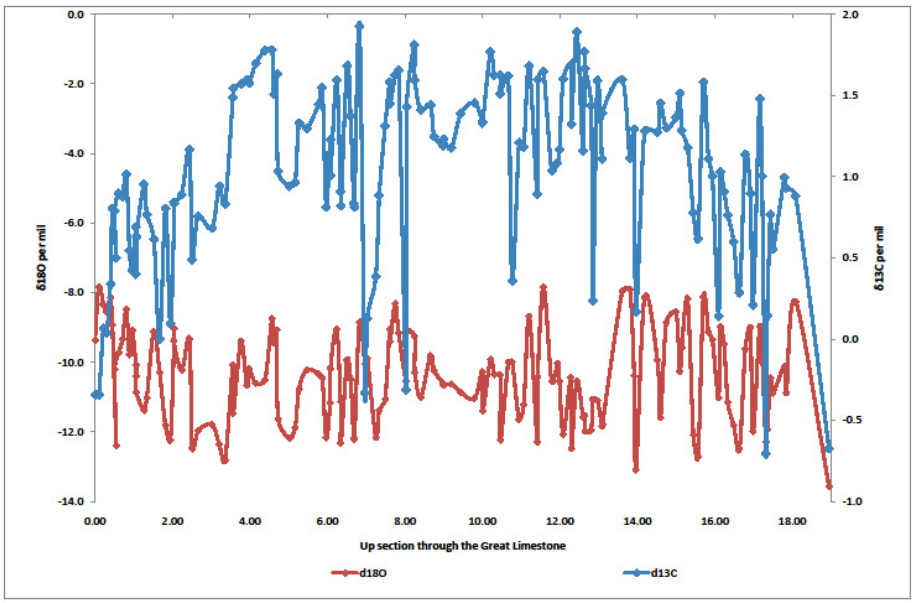

Figure 7.1 $\delta^{13}C$ (blue line) and $\delta^{18}O$ (red line) results for the Great Limestone at Middleton in Teesdale

Chapter 7 considered the $\delta^{13}C$ and $\delta^{18}O$ values and the patterns visible within the data. To assess these patterns further and the acceptability of the data, Runs Analysis has been carried out to assess whether these patterns can be regarded as being the result of random or non-random causes. The runs test is a non-parametric test for randomness in a sequence of values such as a time series. It is used to assess whether the pattern in the plot has arisen by pure chance (See Chapter 6 for a description of RUNS analysis). Both runs about the median (RAM) and runs up and down (RUD) have been applied to both the $\delta^{13}C$ and $\delta^{18}O$ data using the statistical program PAST and the results are shown in Table 7.3.

	$\delta^{13}C$		$\delta^{18}O$	
	RAM	**RUD**	**RAM**	**RUD**
N_1 (number of thick runs)	**69**	**79**	**69**	**80**
N_2 (number of thin runs)	**76**	**65**	**76**	**64**
Number of Runs	**35**	**91**	**64**	**88**
Z-Score	**-6.4**	**+3.15**	**-1.56**	**+2.69**

Table 7.3 Results of RUNS analysis for $\delta^{13}C$ and $\delta^{18}O$ from the Middleton in Teesdale beds

Table 7.3 gives the results of the RUNS analysis of the $\delta^{13}C$ and $\delta^{18}O$ data, where the z-values for $\delta^{13}C$ of -6.4 (RAM) and 3.15 (RUD) and for $\delta^{18}O$ of -1.56 (RAM) and 2.69 (RUD) are shown. Apart for the $\delta^{18}O$ RAM results, the figures suggest that the patterns are not due to chance and are non-random; Sadler *et al*. (1993) showed that z-scores between -2.1 and +2.1 are within the random field although Bosence *et al.* (2009) regarded these figures to be nearer -1.8 to +1.8.

7.5 Palaeo-seawater $\delta^{13}C$ and $\delta^{18}O$ composition

Increases in organic carbon burial, such as storage in coal, and increases in the amount of living biomass will affect the isotope composition of dissolved inorganic carbon in seawater; this causes an increase in $\delta^{13}C$ to more positive values through the preferential extraction of ^{12}C. Anoxic events or changes in organic carbon burial rates can occur relatively quickly and these can be reflected

as rapid excursions in the $\delta^{13}C$ trends. Chapter 3 suggested that the periodicity of the Great Limestone is the result of Milankovitch rhythms. The variations in intensity of the Milankovitch rhythms as discussed in Chapter 3 will affect sea level through glacial advances and retreats and through time this will also affect climate, in particular temperature, humidity and aridity.

The transition from the Viséan to the Namurian corresponds to a time of major cooling and glaciation and the onset of the Permian-Carboniferous glaciation which would have resulted in more positive $\delta^{13}C$ and less negative $\delta^{18}O$ values of marine carbonate. Glacial periods are characterised by greater productivity due to higher nutrient supply from erosion of exposed shelves during lowered sea-level and greater organic carbon burial in marine sediments. Greater ice volume and cooler water results in less negative seawater $\delta^{18}O$ values; decrease in $\delta^{13}C$ and more negative $\delta^{18}O$ suggests warming and less ice volume, as well as higher pCO_2. Waxing and waning of polar ice sheets would, due to strong oceanic currents, result in worldwide changes of temperature, salinity and sea level; however, changes at the equator in temperature will be less prominent than those at the poles.

The very negative $\delta^{18}O$ values were suggested in Chapter 7 as the result of diagenetic alteration and the scatter of depleted $\delta^{13}C$ and $\delta^{18}O$ does suggest post-depositional overprinting. However, it was argued in Chapter 7 that the original trend in $\delta^{18}O$ is preserved there, such that the variations can be interpreted in terms of changing temperature, salinity and ice-volume. High-frequency scatter and covariant $\delta^{13}C$ and $\delta^{18}O$ values are often attributed to the result of ice-house effects with possibly up to 2‰ due to ice mass or up to 4.3‰ due to combined ice mass and cooling (Bruckschen and Veizer, 1997). This would; however, be expected to result in a more positive $\delta^{18}O$ rather than a move to more negative values as seen in this analysis. Increases in both $\delta^{13}C$ and $\delta^{18}O$ suggest cooling with drawdown of atmospheric CO_2, decreases in both $\delta^{13}C$ and $\delta^{18}O$ suggest warming and higher pCO_2.

7.6 Diversity and $\delta^{18}O$ and $\delta^{13}C$ changes

Chapter 5 discussed biotic diversity changes throughout the thickness of the Great Limestone. Diversity was not seen to change substantially and changes did not suggest that any major stressing of the environment took place. Nevertheless, changes in diversity were evident and it is these changes that are considered here in relation to the $\delta^{18}O$ and $\delta^{13}C$ values. Figures 7.2 and 7.3 are compilations of $\delta^{18}O$, $\delta^{13}C$ and diversity changes through the thickness of the Great Limestone.

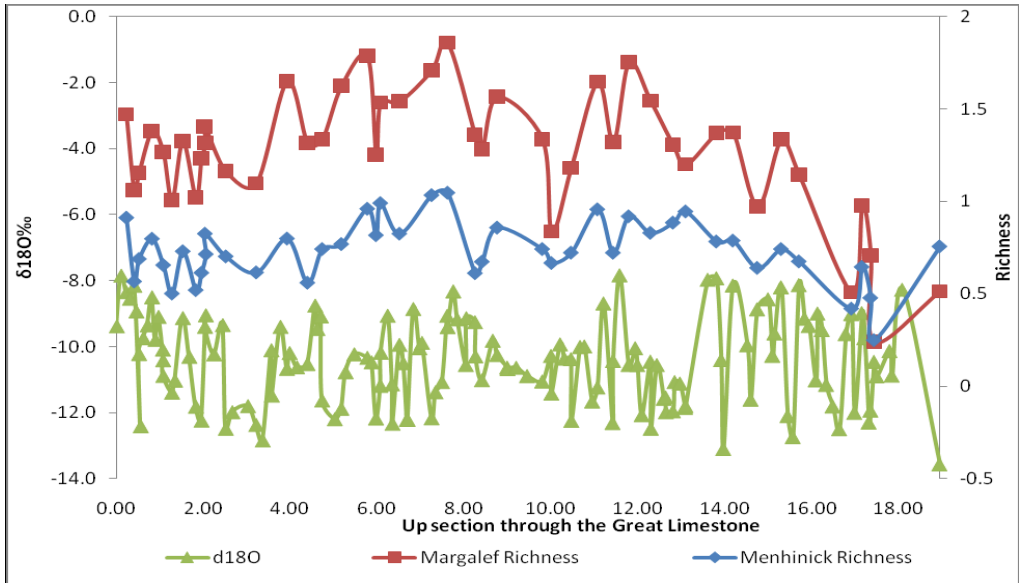

Figure 7.2 $\delta^{18}O$ and diversity changes throughout the thickness of the Great Limestone.

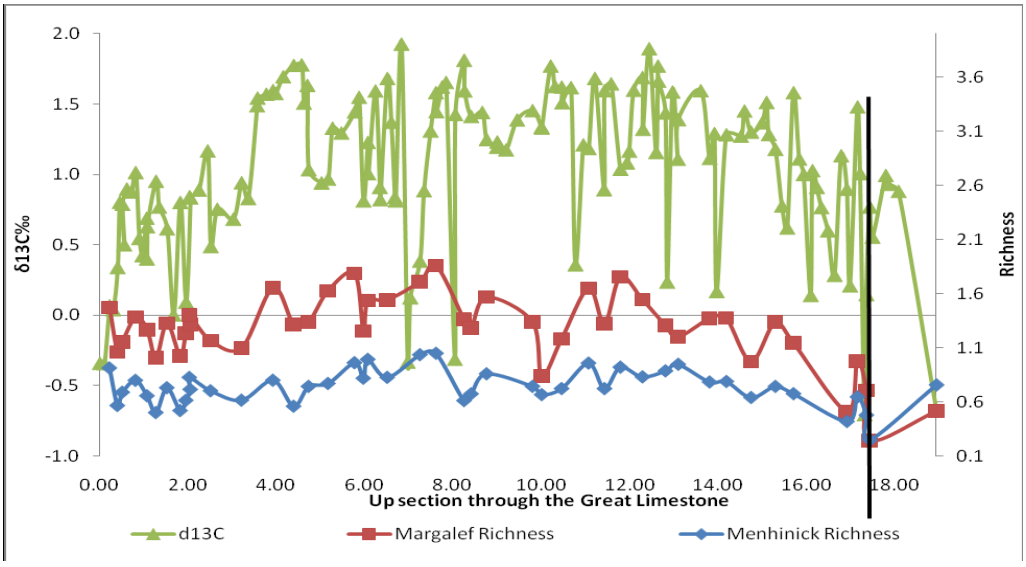

Figure 7.3 $\delta^{13}C$ and diversity changes throughout the thickness of the Great Limestone.

It can be seen in Figures 7.2 and 7.3 that there are remarkable correlations between $\delta^{13}C$, $\delta^{18}O$ and diversity. These changes in value appear to occur over time periods of only hundreds to a few 1000's of years (see Section 8.11). The number of thin sections analysed; however is only about a third of the samples analysed for the isotopes; therefore, it is difficult to attain a true comparison of values and plots. Nevertheless these correlations and the short time periods of the fluctuations, if they are true representations, would suggest a strong relationship between $\delta^{13}C$, $\delta^{18}O$ and biota, probably the result of short duration environmental changes, such as salinity or temperature, the two most important factors controlling productivity and biotic development.

7.7 Sea surface temperature

$\delta^{13}C$ values of carbonates are affected very little by changes in temperature, more by processes related to organic matter. Brand and Legrand (1993); Bruckschen and Veizer (1997) and Bruckschen *et al*. (1999) suggested that Namurian sea-surface temperatures was in the order of $20^0C \pm 5^0C$. Accepting these temperature thresholds, the calculated sea-water $\delta^{18}O$ values during deposition of the Great Limestone would be interpreted as shown in Figure 7.4, using the calculation method (1) of Epstein *et al.* (1953) modified by Craig (1965).

$$T(^0C) = 16.9 - 4.2\ (\delta c - \delta w) + 0.13\ (\delta c - \delta w)^2 \quad (1)$$

Figure 7.4 shows the temperature ranges calculated using formula (1) and the data from appendix E together with average temperatures (2 bed window), ± 2 times standard deviation (grey) and the 15^0C to 25^0C envelope as suggested for the Namurian seawater temperature by Bruckschen *et al* (1999) the results of the calculation shows seawater temperature would be far in excess compared to the acceptable 15^0C to 25^0C envelope. To achieve values that fit within the 15^0C to 25^0C temperature envelope, the Namurian seawater would require to have $\delta^{18}O$ values at the time of deposition of -8 SMOW.

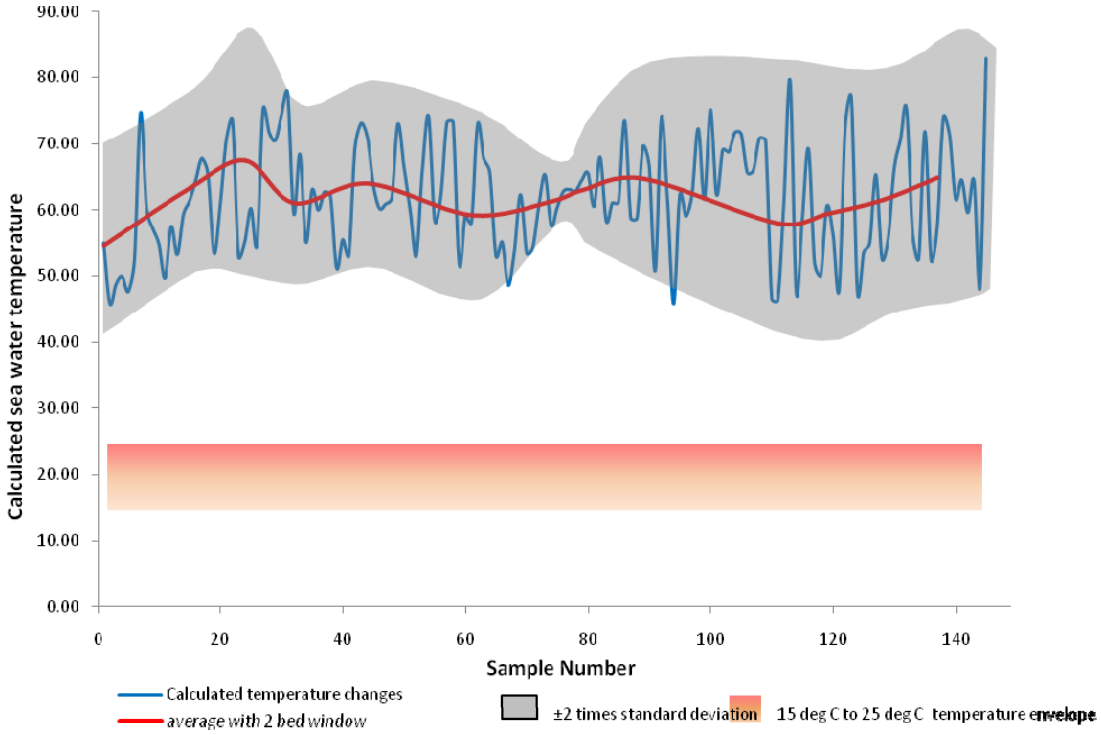

Figure 7.4 Calculated seawater temperatures using $\delta^{18}O$ values from Appendix E, together with average temperature (red line using 2 bed window) and ±2 times standard deviation (grey shading). The coloured envelope represents the 15^0C to 25^0C extent of the Namurian sea water temperature as suggested by Bruckschen *et al.* (1999)

Bruckschen and Veizer (1997) regarded seawater $\delta^{18}O$ during glacial periods as being around 0‰ SMOW; therefore, to invoke a seawater $\delta^{18}O$ value of -8‰ SMOW does not seem appropriate; however, expanding glacial waters may have been much lighter in $\delta^{18}O$ than this average suggests. It is not unusual to have seawater $\delta^{18}O$ values much lower than this and Froehlich *et al*. (1988) reported the brackish waters of the Baltic Sea to have $\delta^{18}O$ values as low as -8.2‰ SMOW. These very low $\delta^{18}O$ values of seawater are; however, found in much higher latitudes than the Carboniferous subequatorial oceanic gateway where the $\delta^{18}O$ decrease due to latitude would be stronger.

As the calculated temperatures represent a glacial ocean, maximal oceanic $\delta^{18}O$ values may have been up to 1‰ to 1.7‰ higher due to the glacial ice mass effect (see Shackleton, 1977: Bruckschen, *et al.,*1999 for discussion) and any proposed glacial ice mass effect, would not be expected to result in the very negative SMOW.

The result of upwelling and circulations patterns off the coast of modern West Africa results in a 9^{O}C difference in sea-surface temperatures compared to those off the coast of South East Asia, both at 20^{O}N (Bruckschen *et al*. 1999) which does show how large variations in sea-surface temperature can occur at similar latitudes, even so, considering the calculated SMOW it is unlikely that ambient seawater temperature is the only controlling factor in the variation of the Great Limestone $\delta^{18}O$.

7.8 Salinity effects

It was suggested by Keller *et al*. (2004) that covariance between $\delta^{18}O$ and $\delta^{13}C$ values could be the result of changes in salinity due to mixing of water masses or changes in precipitation-evaporation cycles (Wolff *et al*., 1999; Keller *et al*., 2004) and not just as a result of diagenesis. The subequatorial oceanic gateway (Chapter 2 Figure 2.1) between Tethys and Panthalassa and the assembly of Pangea occurred during the mid-Carboniferous and this resulted in enhanced poleward transport of heat and moisture (Veevers and Powell, 1987; Saltzman, 2003). This oceanic gateway closure would also have resulted in major changes to oceanic circulation patterns and nutrient supply to the remaining seaway. Water circulation may have been weaker before full closure of the seaway; however, near to or after closure deep-water circulation could have resulted in enhanced upwelling and lower $\delta^{13}C$ on the west coast (Russia) of Pangea, while promoting nutrient depleted and higher $\delta^{13}C$ on the East coast (North America) (Mii *et al*., 2001). Whether this closure also resulted in major changes to salinity is unclear; however Veizer *et al*. (1997) regarded shelf seas to have higher salinity than thermally stratified seas. However, this discussion must be considered in the context of the biota and biotic associations discussed in Chapter 5 where open, normal-marine environments were suggested.

Rohling (2000) regarded palaeosalinity as being one of the major unsolved variables in palaeoceanographic studies and is not convinced that it can be adequately determined from available proxy-data; even so salinity conditions of ancient environments are often described in rather general terms. Normal marine conditions are characterised by salinity in the range of 33‰ to 38‰, brackish

water covers a large range from less than 1‰ up to 33‰ and freshwater contains only small quantities of dissolved salts; hypersaline salinities cover values above 40‰. Interestingly the most common of the bioclasts found in this analysis, echinoderms, bryozoans, corals and some green algae inhabit normal-marine salinities, although some restricted tolerance may have been acceptable.

Sub-saline surface waters and negative $\delta^{18}O$ values are often the result of freshwater input from rivers and possibly in response to wet periods of higher temperature and high rainfall. If river water input is regarded as a major control on the salinity of the shelf seas then it may be expected that changes in salinity may also be accompanied by an increase in input of terrestrial elements such as aluminium and silicon; however, correlation indices between $\delta^{18}O$ and aluminium and silicon are not strong at around -0.23, and between $\delta^{18}O$ and aluminium and silicon around -0.32 also do not as such confirm input by freshwater from rivers. However, this will be considered further in Chapter 9.

7.9 Sea-level changes

Bruckschen and Veizer (1997) modelled lower Carboniferous sea level assuming that for a 10 metre sea-level rise the $\delta^{18}O$ ice mass effect is -0.1‰ and a temperature increase is $0.47^{O}C$. Whereas the greatest deviation between adjoining $\delta^{18}O$ values is around -5‰ this would equate to a 500 metre sea-level variation or a $23^{O}C$ temperature variation; both of which are probably untenable over very short periods of hundreds to a few thousand years. A large variation in temperature of $23^{O}C$ would result in the threshold temperature for most living marine invertebrates of $38^{0}C$ being far exceeded (Brand and Legrand, 1993; Bruckschen and Veizer, 1997).

7.10 Bed variations

The pattern of at least two cycles of thinning and thickening bed sets as well as a clear cyclicity with regard to $\delta^{18}O$ and $\delta^{13}C$ values has been discussed in Chapter 7 where it was suggested that they were the result of some well-organised regular changing parameters.

Within individual beds $\delta^{18}O$ and $\delta^{13}C$ values can be seen to covary both positively and negatively, i.e. the values of $\delta^{18}O$ move in a similar manner to $\delta^{13}C$ or alternatively $\delta^{18}O$ values move in an opposite manner to $\delta^{13}C$. Figure 7.5 shows both negative and positively covariation with generally negative coincidence in beds 1 to 3 and generally positive in beds 4 to 7. $\delta^{18}O$ and $\delta^{13}C$ in beds 8 to 13, Figure 7.6, are generally positively coincident, whereas within beds 14 to 20 (Figure 7.7) there can be seen both positive and negative covariation. Figure 7.8 again shows positive covariation of $\delta^{18}O$ and $\delta^{13}C$ within the top few beds.

Included in Figures 7.5 to 7.8 is the Margalef Richness Index (see Chapter 5) which can be seen to generally follow the $\delta^{18}O$ curve. However, as a result of the smaller number of samples used for the thin-section analysis compared to those used for the isotope analysis, this is not conclusive. It is interesting to note; however, that where two or more Margalef Richness values coincide with the isotope samples, such as between beds 3 and 4, 9 and 10, 14 and 15 and 16 and 17 there is a close similarity between the richness index and $\delta^{18}O$, and in many cases also with $\delta^{13}C$.

Figure 7.9 displays the positions of the groupings of the $\delta^{18}O$ and $\delta^{13}C$ from Figures 7.5 to 7.8 together with the Fischer Plot of bed thickness and shows how the $\delta^{18}O$ and $\delta^{13}C$ covariations change throughout the thickness of the Great Limestone. These groupings do not coincide exactly with the bed-sets discussed in Chapters 3 and 7; however, there is a close correlation. Changes in positive and negative covariation of $\delta^{18}O$ and $\delta^{13}C$ could be the result of many changing variables and these will be considered further later.

The Great Limestone, as with most mid-Carboniferous shelf limestones of northern England have well-developed bedding. There may be a transition from the purer limestone to the mudrock parting over a few mm, but normally the contact is sharp. The bedding planes have commonly been affected by pressure dissolution. Indeed in some cases the bedding plane is a clear pressure dissolution seam with some anastomosing and dark clayey insoluble residue within the seams. Many of the pressure dissolution seams can be recognised within individual beds

with a strong change in $\delta^{18}O$ and/or $\delta^{13}C$ being present, e.g. within bed 4 the major changes within both $\delta^{18}O$ and $\delta^{13}C$ are clearly seen in the field as pressure dissolution seam at these positions.

Numerous geochemical analyses have been made of the Great Limestone which will be the subject of Chapter 9 where it can be seen that patterns are evident within individual beds and patterns are also evident within the isotope analyses. Chapter 7, section 7.2.4 discussed the movement of carbonate from a less calcareous to a more calcareous unit, i.e. from adjoining shales at the margins of beds to the centre of the bed. Frank *et al*. (1999) suggested that this progressive addition of calcite cement to the limestone from dissolution and pressure dissolution resulted in a gradual decrease in bulk Sr/Ca ratios and a more negative $\delta^{18}O$ value for the limestone as a whole, and a gradual increase of bulk Sr/Ca ratios and a more positive $\delta^{18}O$ value in the calcareous shale and therefore at the margins of the bed.

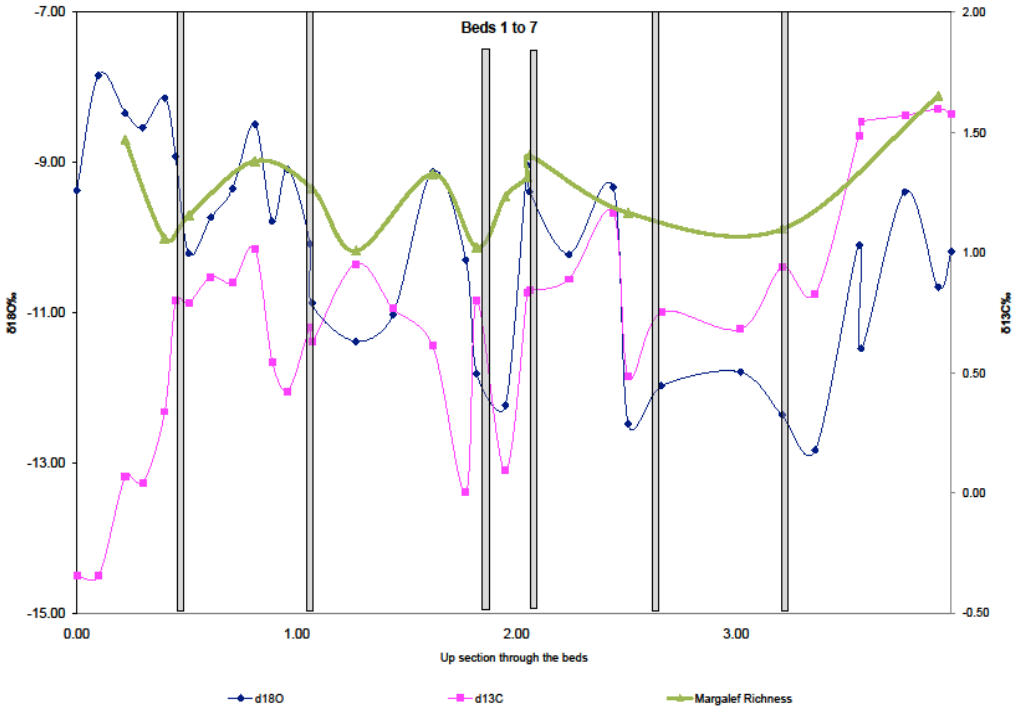

Figure 7.5 Predominantly negatively covariation of $\delta^{18}O$ and $\delta^{13}C$ through beds 1 to 7

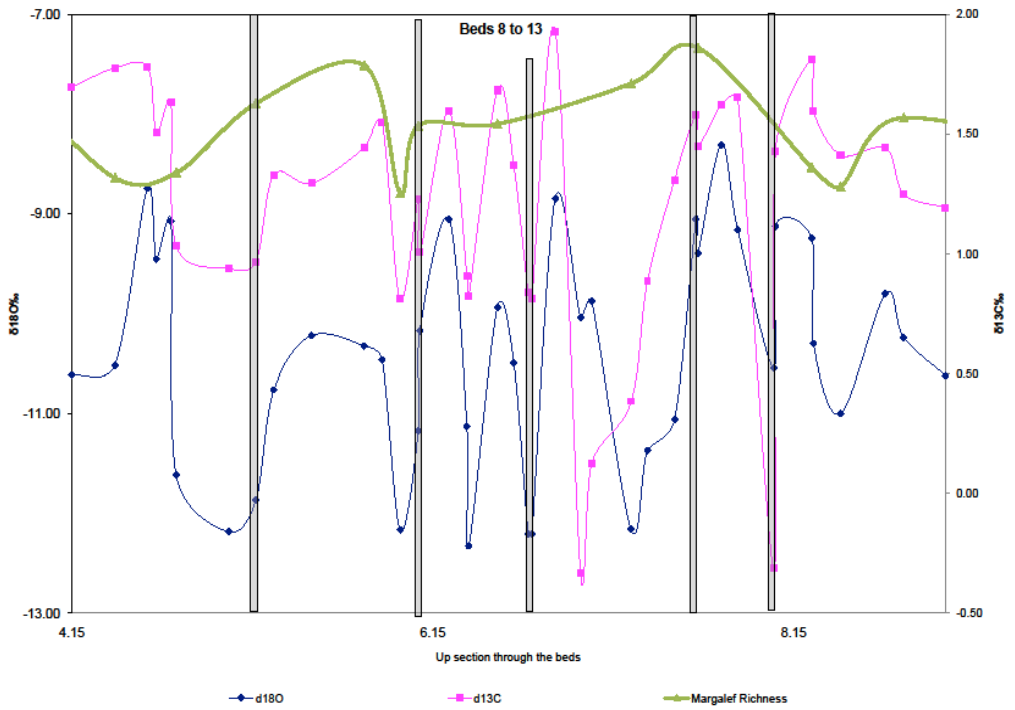

Figure 7.6 Positive covariation of $\delta^{18}O$ and $\delta^{13}C$ through beds 8 to 13

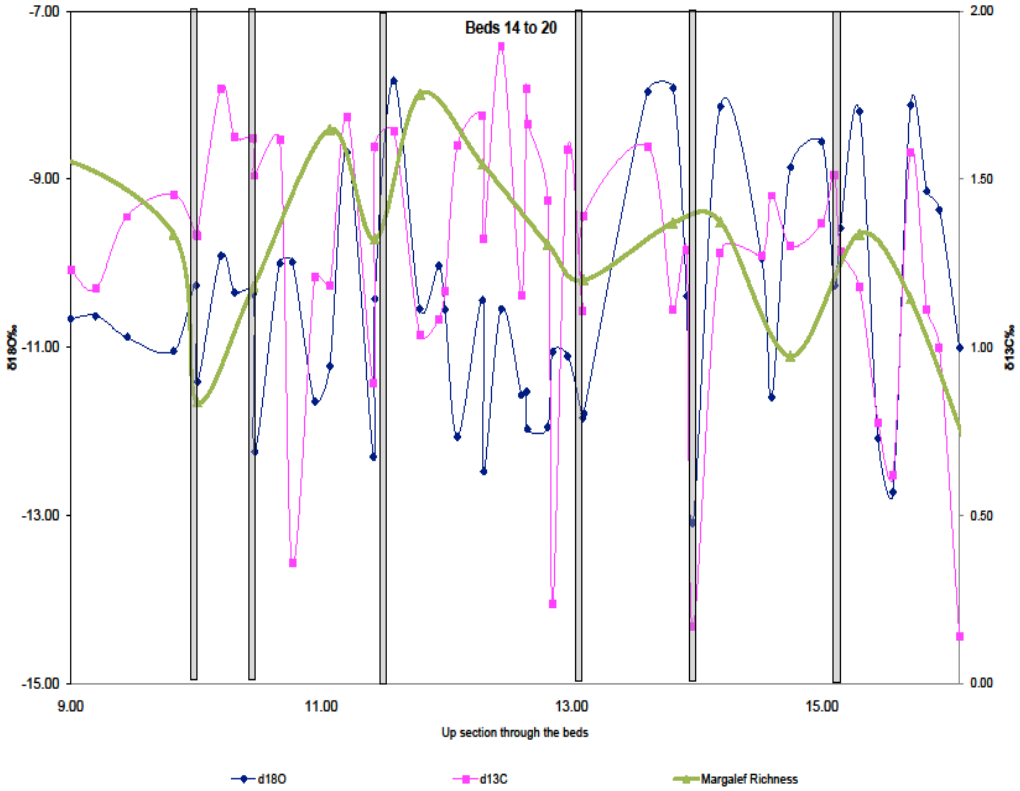

Figure 7.7 Positive and negative covariation of $\delta^{18}O$ and $\delta^{13}C$ through beds 14 to 20

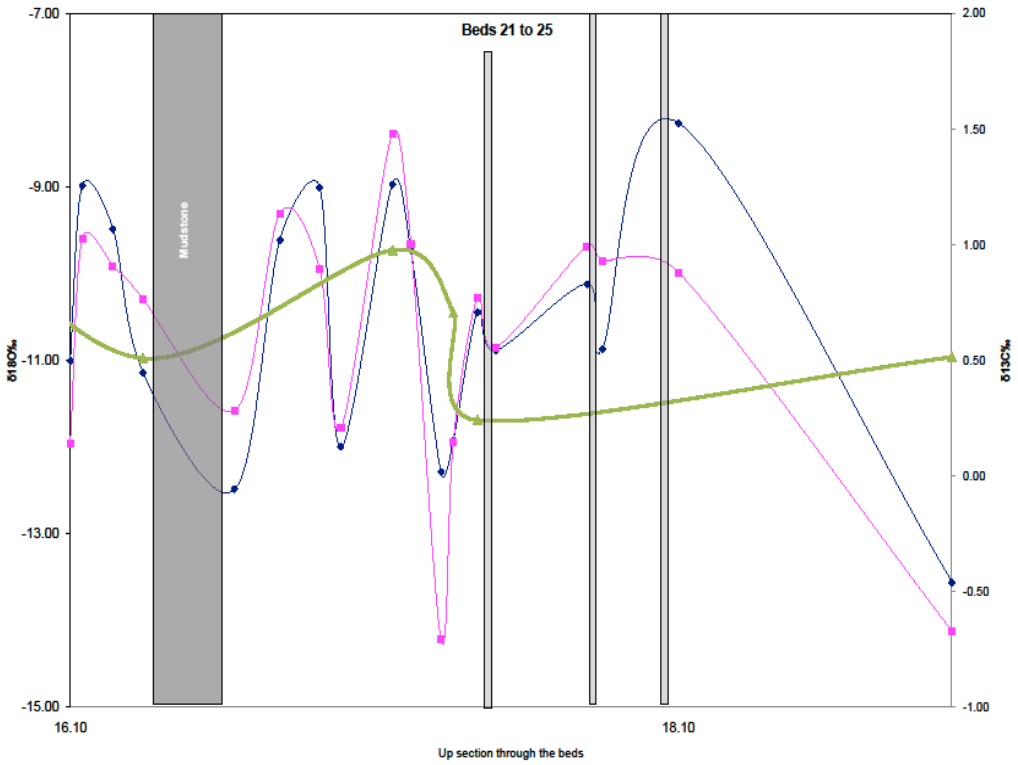

Figure 7.8 Positive covariation of $\delta^{18}O$ and $\delta^{13}C$ through beds 21 to 25

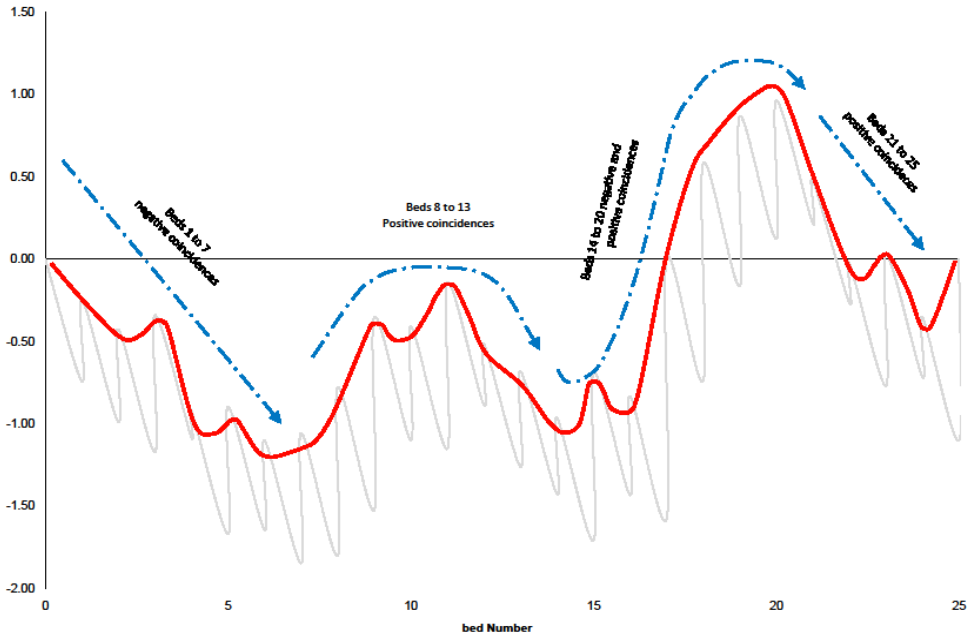

Figure 7.9 Fischer Plot of bed thickness together with $\delta^{18}O$ and $\delta^{13}C$ covariation changes

The $\delta^{18}O$ and $\delta^{13}C$ data for some individual beds show changes at the margins of the beds as well as within the beds themselves. $\delta^{18}O$ values in many beds are more negative towards the margins of a bed, and less negative within the central part of the bed (beds 1, 6, 8, 9, 10, 12, 15, 16, 18, 19, 21 and 22) which is opposite to the discussion in Chapter 7; see also Frank *et al*. (1999) for discussion. In some cases $\delta^{13}C$ values are less positive at the margins and more positive in the centre of a bed (beds 3, 4, 6 and 16).

7.11 Origin of the $\delta^{18}O$ and $\delta^{13}C$ variations within beds and bed-sets

The source of carbonate sediment on a platform is the result of both in-situ carbonate production and the influx of carbonate from a shallower-water factory, brought there by waves, tidal currents and storms. With deposition of the Yoredale limestones taking place at around 5–30 m water depth (Chapter 5), both in-situ carbonate accumulation and influxes of carbonate are likely. There is evidence of storm reworking within the beds, as noted above, but no evidence for the wholesale introduction of large quantities of sediment from a shallower-water source area, as would be provided, for example, by the presence of graded beds ('tempestites') of shallow water bioclastic material. In fact, there are no very shallow-water carbonate facies (such as tidal-flat limestones) present on the platform. This suggests that the flooding of the platform, after deposition of the siliciclastic delta-top/swamp facies at the top of the previous cycle, was very rapid indeed, so that moderately deep conditions were quickly and uniformly established across the region, and then that these conditions more or less lasted for the duration of carbonate deposition (Tucker *et al*., 2009).

The pattern of thinning and thickening bed-sets and $\delta^{18}O$ and $\delta^{13}C$ values within the Great limestone could be interpreted as indicating continued sea-level rise after the initial, rapid flooding of the platform followed by sea-level fall. A sea-level rise would be expected to result in more negative $\delta^{18}O$ due to rising temperatures and reduction of ice volume; $\delta^{13}C$ values would be expected to be more positive as a result of higher temperatures and greater productivity from increased shelf seas. However, $\delta^{13}C$ values could also be expected to be more positive during a sea-level fall due to increased riverine nutrient influx and

increased productivity together with less negative $\delta^{18}O$ due to falling temperatures and increase in ice volume.

Another explanation, not necessarily connected with sea-level change, is based on temperature changes through the precession rhythm. Higher temperatures, more negative $\delta^{18}O$, would lead to increased carbonate productivity, and more positive $\delta^{13}C$, which would give the trend to thicker beds. Lower temperatures, less negative $\delta^{18}O$, would lead to the trend towards thinner beds with less positive $\delta^{13}C$ due to decreased productivity.

Another possibility for the patterns within the bed-sets, beds and $\delta^{18}O$ and $\delta^{13}C$, with or without sea-level change, is a climatic explanation of arid to humid (dry to wet) climate change, i.e. effectively changes in salinity–turbidity, again driven by variations in solar irradiance as a result of the precession rhythm (Tucker *et al*., 2009). During more arid times, less rainfall, normal to slightly hypersaline seawater and clearer, less turbid seas would have led to higher productivity and so the trend to thicker beds. $\delta^{18}O$ would be expected to become less negative during more arid times, due to increased evaporation and salinity which would result in $\delta^{13}C$ being more positive from increased productivity.

Under more humid conditions, with increased rainfall, lowered seawater salinity (more negative $\delta^{18}O$), increased water turbidity and terrigenous clay influx, a trend towards thinner beds would have resulted from decreasing carbonate productivity (less positive $\delta^{13}C$). Increased rainfall could also result in greater productivity and diversity from an increase in river-borne nutrients; however, there must be a tolerance limit to which productivity and diversity will slow as a result of less salinity and increased turbidity. $\delta^{18}O$ would be expected to become more negative during more humid times due to the increase in temperature and freshwater input, while $\delta^{13}C$ would become less positive from decreased productivity. Increases of river-borne nutrients to oceans could also result in more positive $\delta^{13}C$ from increased productivity leading to greater orgC (^{12}C-rich) burial in marine sediments.

Salinity changes can occur over time periods of less than 10^3 years (Anderson and Arthur, 1983; Mii *et al*., 1999); however, tropical meteoric water has only a minor effect on seawater $\delta^{18}O$ of about 0.3‰ to 0.4‰ per 3ppt salinity decrease (Mii *et al*., 1999). Biota in Chapter 5, even though diversity does show rhythmic changes, does not suggest excessive stressing of communities due to major salinity changes. This would suggest that salinity on its own is unlikely to be the only case for the deviation in $\delta^{13}C$ and $\delta^{18}O$ values seen in Figure 7.1. Temperature fluctuations would result from waxing and waning of ice sheets; however, near to the equator this would not be as great as at the poles and a $1^{O}C$ change in temperature would only result in a change of $\delta^{18}O$ of just over a quarter per mil.

The origin of the $\delta^{18}O$ in the two and a half bed-sets could be considered with regard to sea-level fluctuations, climate and temperature and these are shown in Figure 7.10 together with the expected $\delta^{18}O$ changes. The pattern of the $\delta^{18}O$ data suggests that temperature itself is not the control on the bed-sets, but does lend support to a depth/sea-level/ice-cap size control and/or a salinity-turbidity (arid-humid climate) explanation (Tucker *et al*., 2009).

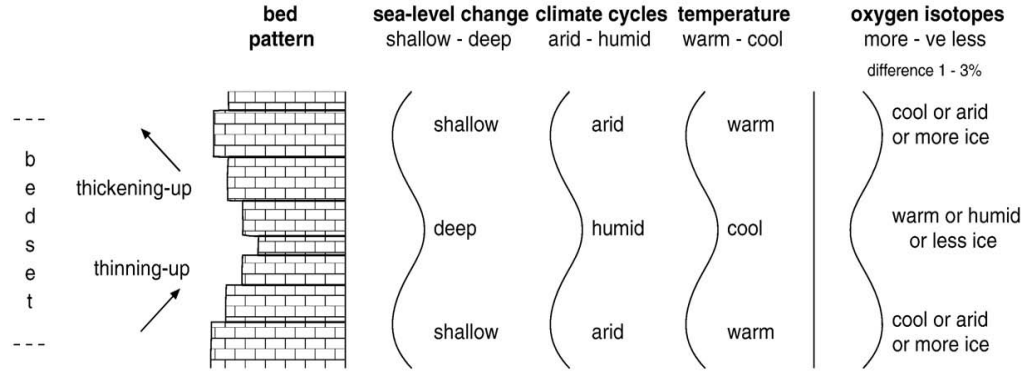

Fig. 7.10. Possible explanations for the origin of the two and a half bed-sets in the Great Limestone, together with the generalised pattern of trends in the δ18O data. Zones of thicker beds in the bed sets could be the result of higher carbonate productivity due to shallower water, clearer seas/lower rainfall (more arid climate) or higher temperature. Zones of thinner beds in bed sets could be the result of lower carbonate productivity due to deeper water or more turbid seas/higher rainfall (more humid climate) or lower temperature. The pattern of the δ18O data suggests that temperature itself is not the control, but does lend support to a depth/sea-level/ice-cap size control and/or a salinity-turbidity (arid-humid climate) explanation. See Tucker *et al*. (2009).

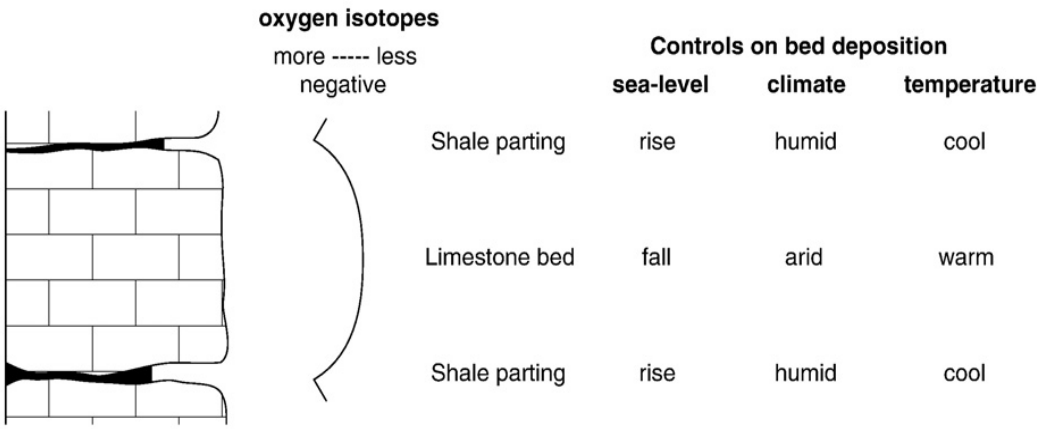

Fig. 7.11. Possible explanations for the origin of the beds in the Great Limestone. See Tucker *et al*. (2009)

Figure 7.11 shows a generalised explanation for the more negative $\delta^{18}O$ at bed margins and less negative within the beds There are at least three explanations for the limestone beds, as opposed to the partings/mudstone interbeds which define the beds: 1) they could be the result of higher carbonate productivity in shallower water, with the clay input through a sea-level rise (reworking of mudflats), or 2) warmer water promoting limestone deposition and cooler water reducing carbonate productivity allowing clay to be deposited, or 3) a more arid climate (clearer seas) during limestone deposition, then a change to a more humid climate (increased fluvial input) for the influx of the clay. Seawater temperature changes at low latitudes are generally only 1-2 degrees during glacial-interglacial periods, and these relatively small changes are unlikely to have had any major effect on carbonate productivity. Thus temperature changes are not regarded as the major control on limestone depositon. However, the pattern of the $\delta^{18}O$ data would support a depth/sea-level (through changes in ice volume) and/or arid-humid climate explanation (possibly through mirgrations of the intertropical convergence zone) (see Tucker *et al*., 2009 for further discussion).

The above discussions would suggest that assessing the origin of the beds and bedsets within the Great Limestone is fraught with difficulty when considering $\delta^{18}O$, and this is also the case when considering the grouped $\delta^{13}C$ and $\delta^{18}O$ covariations shown in Figures 7.5 to 7.9. However, this does present some possibilities for discussion. It may be difficult to assign a control of pure sea-level change for the resulting $\delta^{13}C$ and $\delta^{18}O$ variations and groupings; however, there is

no doubt that this would be a major control. Sea-level fluctuations and in particular the initial transgressive sea-level rise would be expected to result in more negative $\delta^{18}O$ due to higher sea surface temperatures which would have resulted in glacial melting, together with more positive $\delta^{13}C$ due to higher organic productivity and increased shelf-sea area. Figure 7.5 shows a generally negative covariation of $\delta^{13}C$ and $\delta^{18}O$ between beds 1 to 7. As well as sea-level fluctuations, temperature changes would result in negative coincidences between $\delta^{13}C$ and $\delta^{18}O$. The positive covariations within Figures 7.6, 7.8 and part of 7.7 could also be the subject of sea-level fluctuations as well as arid to humid variations in climate affecting salinity and turbidity; fluctuations in nutrient supply could also result from increased river input during humid conditions.

7.12 Periodicity of events

The cyclicity which so dominates Carboniferous sedimentary successions was largely produced by glacioeustatic changes in sea level as a result of orbital forcing and variations in solar irradiance (e.g. Veevers and Powell, 1987; Wright and Vanstone, 2001) and locally there would have been tectonic and sedimentary controls on deposition too (Tucker *et al*., 2009). The Milankovitch rhythms for the Carboniferous are thought to have been 21 and 17 kyr for precession (now 23 and 19 kyr), 34 kyr for obliquity (now 42 kyr) (Maynard and Leeder, 1992), and 112 kyr and 413 kyr for short and long eccentricity (as now, there was no change through the Phanerozoic). There have been numerous papers discussing the periodicity of Carboniferous cycles in Europe and North America, e.g. Walkden (1987); Maynard and Leeder (1992); Ross and Ross (1987); Heckel (1986); Goldhammer *et al*. (1994); Horbury (1989); Smith and Read (2000, 2001) and Wright and Vanstone (2001).

There are at least 70 cycles in the Asbian, Brigantian and Pendleian stages of the Yoredale cycles in northern England (Tucker *et al*., 2009), a period of around 12 m.y., which on a straight division, each cycle would have a duration in the order of 170 kyr. Taking into consideration the issue of missed beats, Tucker thus suggested that the actual duration of a cycle would be much less than 170 kyr and implicated the short eccentricity rhythm (112 kyr) for the cyclothems. Tucker

et al. (1999 considered that the apparent well-organised nature of the bed-thickness trends could only be interpreted in terms of allocyclic controls on deposition and could not have formed from a purely sedimentary (autocyclic) control.

If it is accepted, as argued by Tucker *et al*. (2009), that the Yoredale cycles as a whole are formed by the short eccentricity astronomic rhythm, which in the Carboniferous was 112 kyr, the bed-sets could be the product of a higher-frequency orbital rhythm. This could be either precession or obliquity and two possible interpretations are considered below.

The clastics in the upper part of the Yoredale cycles are broadly deltaic and in the Great Limestone Cyclothem, four minor cycles can be recognised in the clastics (Chapter 3) consisting of a thin (1–5 m thick) coarsening-upward unit of mudrock to fine to coarse sandstone, locally with coal. Thus with four minor cycles in the clastics and at least two bed-sets in the carbonates, there are around six to six and half high-frequency cycles within the one Great Limestone clastic-carbonate Yoredale cyclothem suggesting that the minor cycles are the order of around 17,000 to 18,000 years in duration which is within the timeframe of the precession rhythm (and not obliquity). If this is accepted, then with around ten beds in a bed-set, the duration of the Yoredale limestone beds themselves is the order of 1500–2000 years, which is millennial scale. The two to two and a half bed-sets in the carbonates of the Great Limestone itself would; therefore, be in the range of 34 kyr to 45 kyr which fit within the obliquity time frame.

The high frequency of the $\delta^{18}O$ and $\delta^{13}C$ variations, assuming beds-sets are deposited in periods of around 17,000 to 18,000 years, can be seen in Figure 7.1 to occur over short time periods of possibly only hundreds to a few thousand years, which is obviously far quicker than the proposed durations of the bed-sets. It is possible therefore that there are three underlying cycles in the Great Limestone itself, one of around seventeen to eighteen thousand years (the bed-sets), one of millennial scale (the beds) and the third of hundreds to a few thousand years (the cycles or fluctuations of $\delta^{18}O$ and $\delta^{13}C$ within the beds).

These highest frequency, millennial-scale cycles might possibly correlate with the Bond cycles and or Dansgaard–Oeschger (D–O) events, sub-Milankovitch, millennial-scale cyclicity which is well recorded from Quaternary strata (e.g. Clark *et al*., 1999; Sarntheim *et al*., 2002).

To assess this cyclicity further, Time Series Analysis has been carried out on the $\delta^{13}C$ and $\delta^{18}O$ data using the statistics program PAST (Hammer *et al*. 2001) and the results are shown in Figures 7.12 and 7.13. The time periods are calculated assuming the limestone was deposited in 34 kyr to 45 kyr as discussed above and the results of this analysis are shown in Table 7.2.

Figure 7.12 shows the Time Series for $\delta^{13}C$ and the p = 0.05 and 0.01 significance lines. It can be seen that only two peaks pass the significance lines, the first peak corresponds to time periods of 39.0 kyr and 51.6 kyr, depending upon the time period calculated (Table 7.2). The second peak corresponds to time periods of 15.2 kyr and 20.1 kyr, depending upon the time period calculated (Table 7.2). The remaining peaks do not reach the significance levels; however, it was still thought to be worth evaluating their periodicity. Table 7.4 shows the corresponding periodicities for the first twenty peaks.

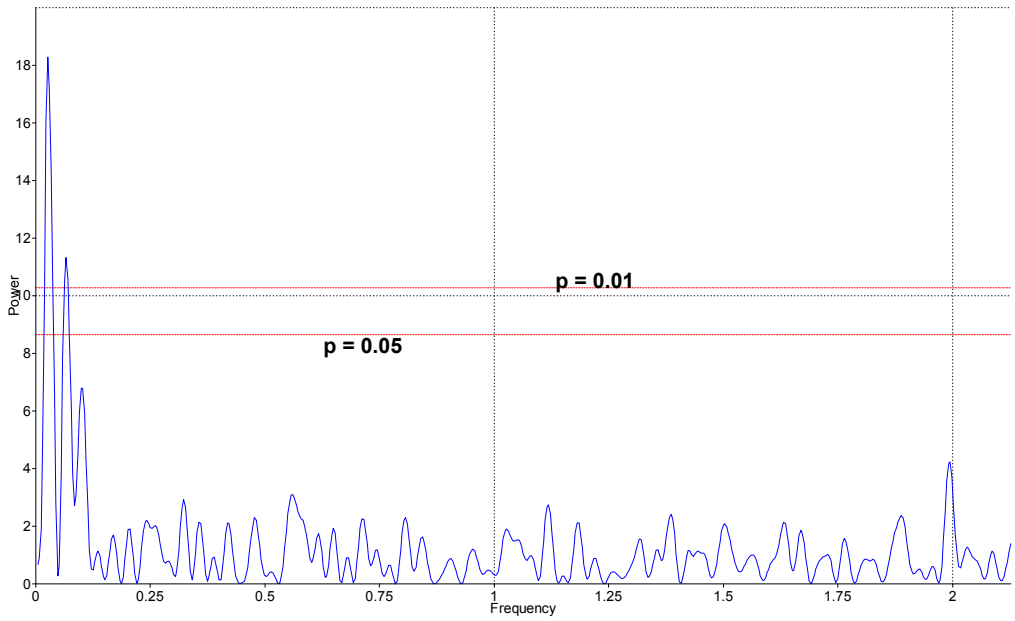

Figure 7.12 Time Series Analysis of $\delta^{13}C$ values using the statistical program PAST

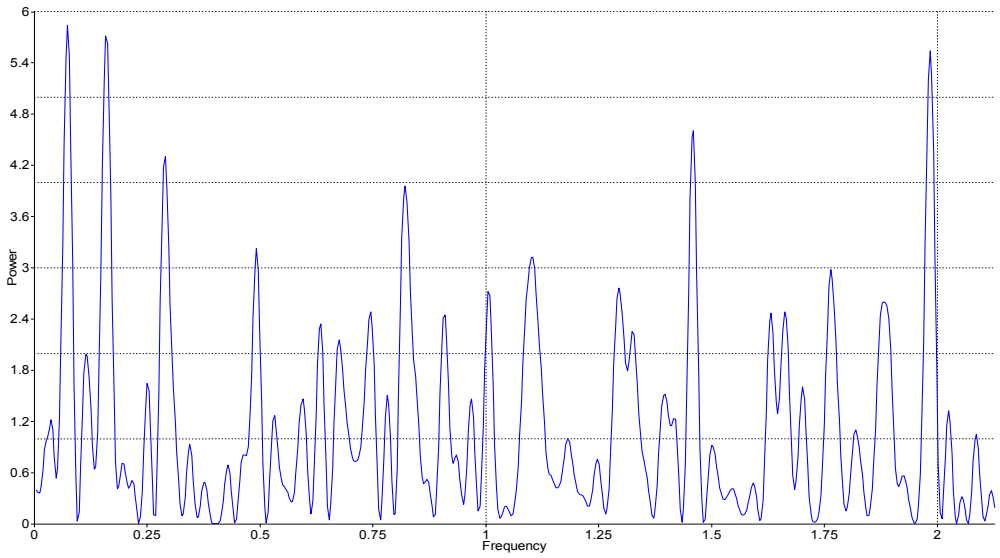

Figure 7.13 Time Series Analysis of $\delta^{18}O$ values using the statistical program PAST

Figure 7.13 shows the Time Series for $\delta^{18}O$, the p = 0.05 and 0.01 significance lines are not, in this case, visible, i.e. the peaks do not reach the significance lines. The p = 0.05 and 0.01 significance lines are above the peaks within the plot at power levels of 10.28 (0.01) and 8.64 (0.05). Even though the peaks do not reach the significance levels their periodicity has still been evaluated. Table 7.4 shows the corresponding periodicities for the first twenty peaks. The first peak corresponds to time periods of 27.3 kyr and 51.6 kyr, depending upon the time period calculated (Table 7.2). The second peak corresponds to time periods of 13.6 kyr and 36.1 kyr, depending upon the time period calculated (Table 7.2).

It is difficult to equate all of the peaks shown in Figures 7.12, 7.13 and Table 7.4 with Milankovitch rhythms. However, the first peaks within the $\delta^{13}C$ and $\delta^{18}O$ analysis are within the obliquity orbital rhythm time frame of around 34 kyr; the second peaks are nearer to the 17 kyr to 21 kyr year precession cycle and the remainder of the peaks less than this. Note that there is some controversy with regard to the time period of the Milankovitch rhythms. The last ten or so peaks shown in Table 7.2 show more rapid oscillations of sub-Milankovitch millennial time-scales. There is a large and rapidly growing literature on sub-Milankovitch, millennial-scale cyclicity recorded from Quaternary strata (e.g. Clark *et al*., 1999; Sarntheim *et al*., 2002). The mechanisms involved include: rapid warming/slow

cooling for Dansgaard–Oeschger (D–O) events, Bond cycles attributed to oceanic–atmospheric circulation and high-frequency climate changes, and the shedding of ice-rafted debris (Heinrich events) in the North Atlantic, controlled by ice-sheet dynamics. Bond *et al*., (2001) suggested a link between fluctuations in solar irradiance, climate and millennial-scale cycles; however, Foukal et al., (2006) found no significant evidence to link solar luminosity variations with climate variations on either a centennial, millennial or even million-year timescales.

Time Series Analysis of $\delta^{13}C$ and $\delta^{18}O$ using a time period of 34 kyr for the deposition of the Great Limestone		Time Series Analysis of $\delta^{13}C$ and $\delta^{18}O$ using a time period of 45 kyr for the deposition of the Great Limestone	
$\delta^{13}C$ peaks in kyr	$\delta^{18}O$ peaks in kyr	$\delta^{13}C$ peaks in kyr	$\delta^{18}O$ peaks in kyr
39.0	39.0	51.6	51.6
15.2	27.3	20.1	36.1
9.7	13.6	12.9	18.0
7.4	8.8	9.8	11.6
5.9	6.3	7.8	8.4
4.9	5.1	6.6	6.2
4.1	4.6	5.5	5.3
3.8	4.0	4.6	4.6
3.5	3.4	4.1	3.8
3.1	2.9	3.7	3.5
2.8	2.6	3.4	3.1
2.6	2.5	3.2	2.7
2.4	2.3	2.8	2.5
2.1	2.2	2.6	2.2
1.9	2.0	2.4	2.1
1.8	1.9	2.1	2.0
1.6	1.7	2.0	1.8
1.5	1.6	1.9	1.7
1.5	1.5	1.9	1.6
1.4	1.3	1.8	1.5

Table 7.4 First 20 peaks from Time Series Analysis using $\delta^{13}C$ and $\delta^{18}O$ for time periods of 34 kyr and 45 kyr duration of deposition of the Great Limestone

Modern delta systems such as the Mississippi tend to prograde and fill the available space relatively quickly (Coleman, 1988). Coleman (1988) found that large deltaic lobes having average thicknesses of 35 metres can be deposited in 1½ thousand years within the Mississippi system and bay-fills of 15 metres can be deposited in only 150 years. The modern Balize delta was also found to form 80 metre thick distributary mouth sand bars in a period of only 200 years. Hori *et al*. (2002) also recorded sediment accumulation rates of 1.1 metres per thousand years within the prodelta and 3½ metres per thousand years for the delta front of the Changjiang (Yangtze) River delta, China; the maximum accumulation rates

reached approximately 10 metres per thousand years. Amorosi (2005) assessed the predominantly silt, clay and sandstone high-frequency cycles of between 3 and 5 metres thick, within the Po Delta, Italy, and found these to be deposited on a millennial-scale, spanning intervals of about one thousand years. None of these figures appear to take into account compaction of the sediments.

It can only ever be a crude method to compare modern and ancient delta systems; nevertheless, these rates would point towards the delta/siliciclastic sedimentation occurring over a short-time period. Tucker *et al*. (2009) calculated carbonate sedimentation rates for the Great Limestone of the Alston Block being between 0.1 and 0.75 metres per thousand years with an average of 0.37 metres per thousand years. These large differences in the sedimentation rates for the carbonate and siliciclastic/deltaic members would suggest that the whole Great Limestone cyclothem may also not have been deposited evenly over the proposed 112 kyr rhythm. A further explanation for the periodicity and time frame for the beds and bed-sets of the Great Limestone is considered below.

As discussed, within the Great Limestone cyclothem, there is an average of 16 metres of deltaic/siliciclastic material and around 19 metres of limestone on the Alston Block; at least four cycles are evident within the deltaic/siliciclastic members (Chapter 3), and 2½ cycles within the limestone. Obviously these thicknesses do not take into account the original, as deposited thicknesses, i.e. the un-compacted thickness. An uncompacted stylised section has been provided within Figure 4.24 using decompaction figures of 1.5 for the limestone, 3.5 for the mudstone and 1.1 for the sandstone; see Chapter 4 for a discussion on decompaction of sediments. Table 7.5 shows compacted and decompacted thicknesses for the stylised section in Figure 4.24.

Table 7.5 shows that the deltaic/siliciclastic material is predominantly delta-front muds and distributary channel sands; only a small proportion has been attributed to prodelta muds. Therefore, if a conservative sedimentation rate of 3.0 metres per thousand years (Hori *et al*., 2002; Amorosi, 2005) is used for the delta-front muds and sands, and 1.1 metres per thousand years for the prodelta muds

then this would equate to approximately 12,000 years to deposit the full thickness of the deltaic/siliciclastic sediments in the Great Limestone. If an average of four mudstone sandstone packets are considered and these are regarded as cycles within their own right, then these would span intervals of around 3000 years, a much greater time period than suggested for the Po Delta, Italy (Amorosi, 2005) and possibly stretching the suggestion that they may be millennial-scale cycles; however, Mawson and Tucker (2009) reported millennial scale cycles of a quasi-periodic duration between 700 to 4300 years.

	Compacted thickness	Compaction ratio	Decompacted thickness
Limestone	19 metres	1.5	27 metres
Prodelta muds	1 metre	3.5	3.5 metres
Delta front muds	4.4 metres	3.5	15.3 metres
Sandstone	10.5 metres	1.1	11.5 metres

Table 7.5 Compacted and uncompacted sediment thicknesses

Assuming that the short eccentricity of 112,000 years is accepted for the full Great Limestone cyclothem, this would result in the limestone being deposited in approximately 100 thousand years which does not fit comfortably within any of the Milankovitch rhythms for the Carboniferous. A straight calculation, for the 27 metres of uncompacted limestone deposited over a period of 100 thousand years, would equate to an approximate carbonate sedimentation rate of 0.27 metres per thousand years. This figure is low; however it is still within the range suggested by Tucker *et al*. (2009) of between 0.1 to 0.75 meters per thousand years for the Great Limestone sedimentation rate.

There are, on average, 25 individual beds averaging 0.76 metres, which would equate to an uncompacted thickness of 1.14 metres, and assuming that each bed is continuously laid down at a sedimentation rate of 0.27 metres per thousand years then this would result in an average bed being deposited in around 4.2 kyr, greater to that suggested for the clastics of three thousand years as discussed above but within the quasi-periodic time scale of 700 to 4300 years reported by Mawson and Tucker (2009) for millennial scale cycles. It may be expected that the sedimentation rate within a bed is not at a continuous rate and Yang (2002)

found both vertical and horizontal changes in sedimentation rates within Holocene platform carbonates in Belize. Many of the beds of the Great Limestone show a decrease in calcium carbonate and increase in siliciclastic and insoluble material towards the bedding planes (Chapters 7 and 8). Input of siliciclastic material could result in a slowing down of carbonate production or even in certain circumstances an increase in carbonate production may occur due to the increase in nutrients. The sedimentation rate of 0.27 metres per thousand years can only ever be accepted as an average and sedimentation rates could conceivably have been much greater than this within parts of the bed.

Time Series Analysis of $\delta^{13}C$ and $\delta^{18}O$ using a time period of 100 kyr for the deposition of the Great Limestone	
$\delta^{13}C$ peaks in kyr	$\delta^{18}O$ peaks in kyr
114	114
46	80
28	40
22	26
17	19
15	14
12	12
10	10
9	9
8	8
8	7
7	6
6	6
6	5
5	5
5	4
4	4
4	4
4	4
4	3
4	3

Table 7.6 Time Series Analysis using $\delta^{13}C$ and $\delta^{18}O$ for a time period of 100 kyr duration of deposition of the Great Limestone

If the 2½ bed-sets within the limestone are related to the Milankovitch rhythms for the Carboniferous then a straight calculation for the limestone deposition of 100 kyr divided by 2½ would give an average cyclicity of 40 thousand years for each bed set which is very near to the obliquity rhythm of 34 kyr. There are approximately ten beds per bed set which would suggest each bed equates to approximately 4000 years per bed similar to the deposition suggested for the average bed thickness. The concept of missing beats discussed above should be considered with regard to how this would affect the relationship with

the obliquity rhythm. Figure 7.14 is a stratigraphical model using a periodicity of 34 to 45 kyr and Figure 7.15 using a periodicity of 100 kyr for the deposition of the Great Limestone.

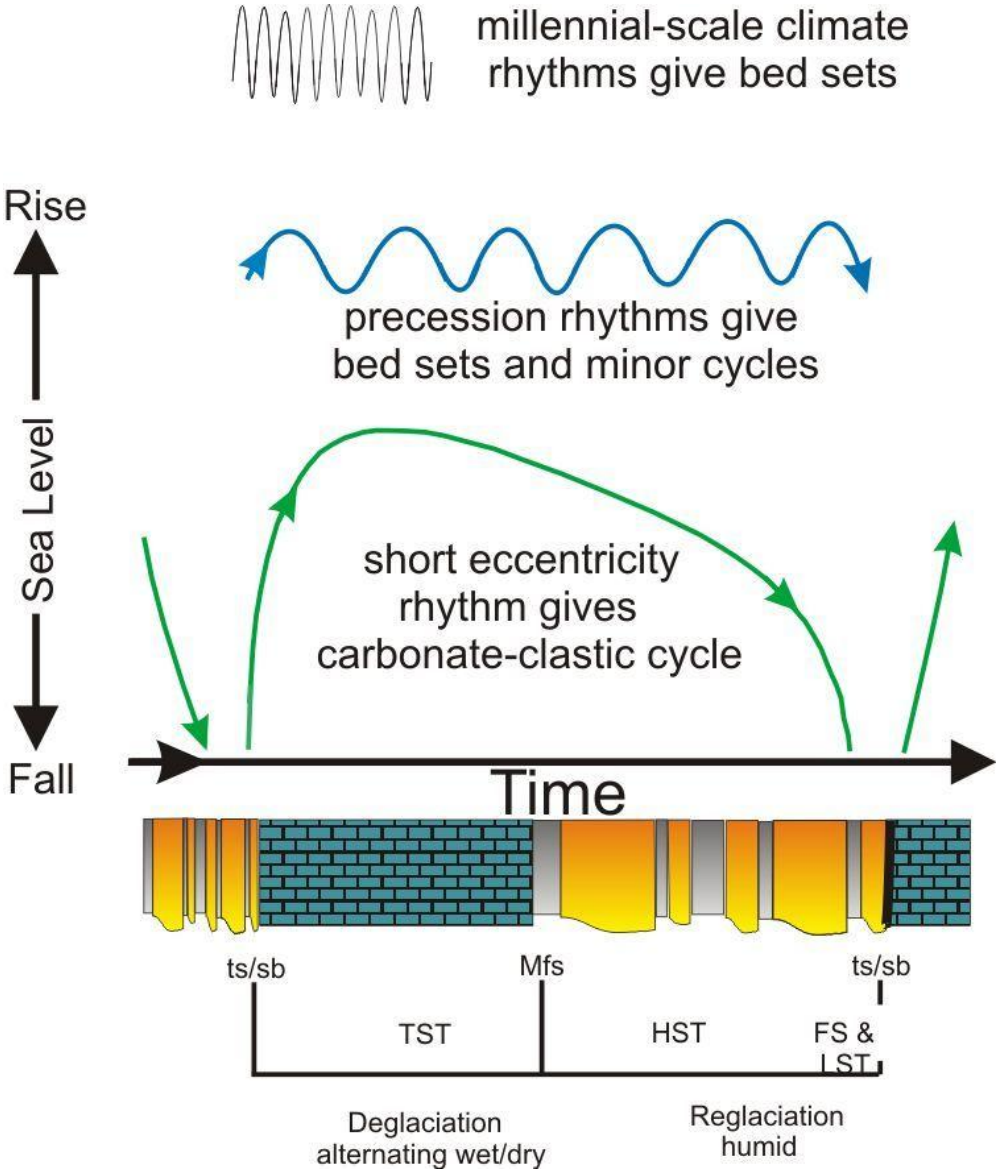

Figure 7.14. Sequence stratigraphic model for the Great Limestone based on orbital forcing and climate-forcing processes using a periodicity of 34 to 45 kyr. Idea from Tucker *et al.*, 2009

1 = Short eccentricity rhythm giving carbonate-clastic cycle
2 = Precession rhythms giving bed sets and minor cycles
3 = Millennial-scale climate rhythms giving limestone beds and siliciclastic cycles

Time Series Analysis using 100 kyr for deposition of the Great Limestone, Table 7.6, shows the first peaks within the $\delta^{13}C$ and $\delta^{18}O$ analysis are within the short eccentricity Milankovitch rhythms, the second peaks within the $\delta^{13}C$ Time

Series are near to the obliquity orbital cycle at 46 kyrs while the second peak for $\delta^{18}O$ at 80 kyr is more than double the obliquity orbital cycle. The third $\delta^{18}O$ peak, at 40 kyr is near to obliquity. Peaks 4 and 5 of both the $\delta^{13}C$ and $\delta^{18}O$ peaks are around the precession cycle and the remainder of the peaks are less than this. As with the Times Series Analysis using deposition of the cycles as 34 to 45 kyr it is difficult to equate all of the peaks shown in Table 7.2 to Milankovitch rhythms.

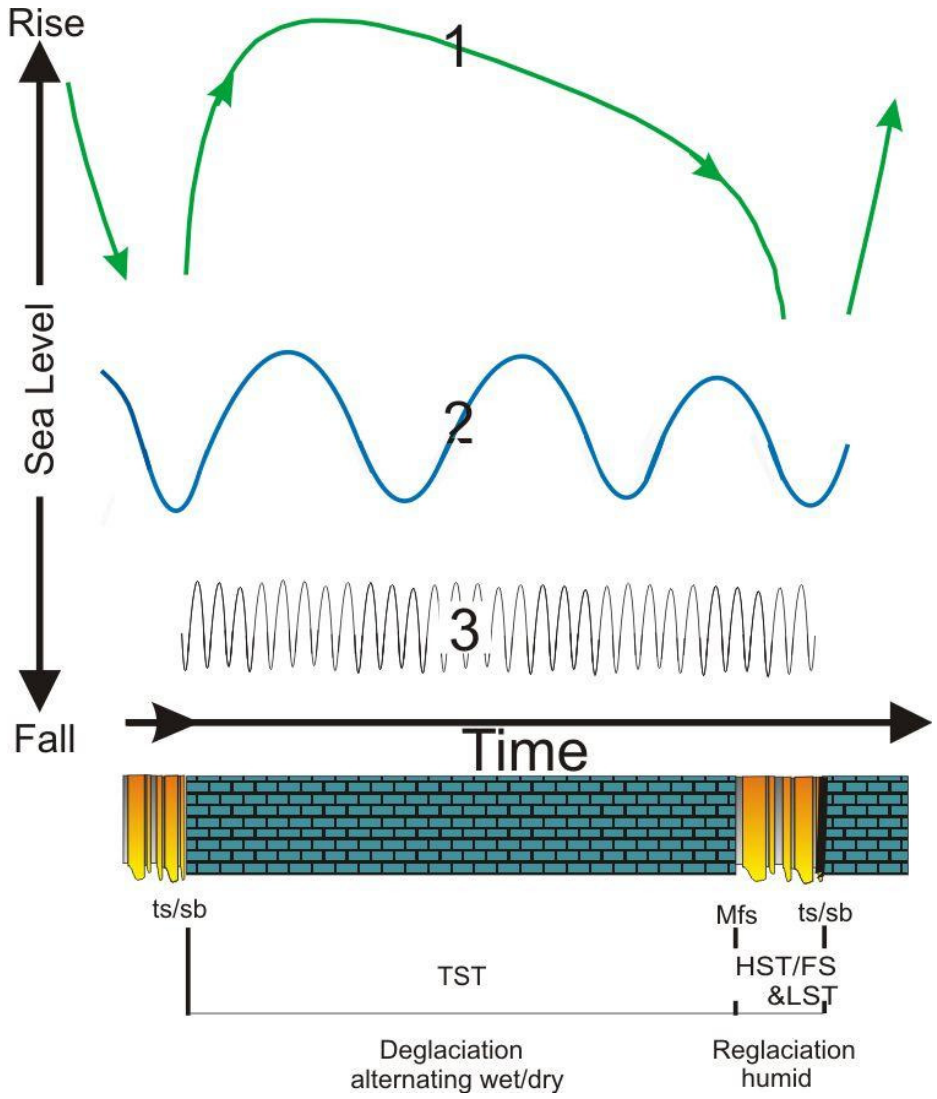

Figure 7:15. Sequence stratigraphic model for the Great Limestone based on orbital forcing and climate-forcing processes using a periodicity of 100 kyrs. Idea from Tucker *et al.*, 2009

1 = Short eccentricity rhythm giving carbonate-clastic cycle
2 = Obliquity rhythms giving bed sets and minor cycles
3 = Millennial-scale climate rhythms giving limestone beds and siliciclastic cycles

The Time Series analysis has not resulted in any clear periodicity for the deposition of the Great Limestone and it may be that further analysis may be undertaken in the future using different analysis methods such as the REDFIT algorithm (Schulz and Mudelsee, 2002), that may result in more acceptable estimates of the predominant frequencies.

7.13 Conclusion

The whole rock $\delta^{13}C$ and $\delta^{18}O$ isotope values show a wide scatter but patterns are seen within the underlying data. Chapter 7 showed a close relationship between $\delta^{13}C$ and $\delta^{18}O$ and the Fischer Plot of bed thickness and suggested that even though diagenesis has inevitably changed $\delta^{13}C$ and $\delta^{18}O$, some semblance of the original trend would have remained.

RUNS analysis of the $\delta^{13}C$ and $\delta^{18}O$ values was carried out to assess the patterns in the data and generally it was implied that the patterns are not random and are; therefore, probably the result of some external forcing. It was the search for this external forcing that was followed in this Chapter.

Sea level, temperature and salinity have been considered in this Chapter with regard to the origins of the beds, bed-sets and covariations of $\delta^{13}C$ and $\delta^{18}O$ and diversity. Although diversity showed some interesting comparisons with $\delta^{13}C$ and $\delta^{18}O$ throughout the thickness of the Great Limestone, it proved to be inconclusive, probably as a result of the lack of samples analysed for diversity compared to the number of samples analysed for $\delta^{13}C$ and $\delta^{18}O$. The $\delta^{13}C$ and $\delta^{18}O$ analysis suggests some groupings between $\delta^{13}C$ and $\delta^{18}O$, and possible origins of beds, bed-sets and covariations of $\delta^{13}C$ and $\delta^{18}O$ have been explored; nevertheless, these discussions and possibilities must always be considered with regard to the underlying diagenetic effects.

Time Series Analysis was carried out on the $\delta^{13}C$ and $\delta^{18}O$ data using time frames for the deposition of the Great Limestone of 34, 45 kyr and 100 kyr. The first larger peaks in the Time Series do suggest that periodicity in the range of

obliquity, of around 34 kyr, and the precession cycle, 17 to 21 kyr, with the remainder of the peaks much less than this and many of sub-Milankovitch millennial time-scales. The Time Series Analysis has; however, proven to be inconclusive.

8.0 Major and trace element geochemistry of the Great Limestone

8.1 Introduction

In Chapter 6, the geochemical data obtained in this research were assessed in terms of the amount of alteration that may have taken place during diagenesis and whether original trends through the Great Limestone may have been preserved. It was concluded that, even though the data had been altered, original patterns were still present and these patterns could be considered in terms of the conditions of deposition.

The objective of this Chapter is to assess the major and trace element geochemical data as a record of the palaeoceanographic history and to determine how these data can be used to understand the controls on limestone deposition and chemostratigraphic. This Chapter also compares the results with known published data of facies of a similar age, not as a chemo-correlation potential, as the time period covered is small compared to published data, but solely as a comparison of data.

Many of the elements are compared within the plots using 12 period moving average trend lines. However, it does appear to be an inherent problem within the calculation for the moving average trend lines that the peaks and troughs are moved to the right. Even though this apparent inherent problem exists within moving average trends, the results are still interesting and are still indicative of the elements analysed. Nevertheless, this movement of the trend line, sometimes up to 0.75 metres, must still be considered when assessing the plots.

The elements are also at times compared to a Fischer plot of bed thickness. The Fischer plot reveals a pattern of beds appearing to thin and thicken upwards, and this pattern is present not only in Teesdale but it can also be seen throughout much of Weardale, suggesting that it is a genuine widely developed pattern. However, as discussed in Appendix H the calculation of z-scores suggests that this pattern is not ordered, but is random. Nevertheless, it is still felt useful to use the patterns of the

Fischer plot with the geochemical analyses as it is felt that the patterns, albeit random, are the result of changes in the environmental controls on sedimentation.

8.2. Method

One hundred and forty nine samples from the full height of the Great Limestone at Middleton in Teesdale (See Chapter 5, Figure 5.1 for location) were collected at 100 to 250 mm intervals (average 150 mm) throughout the limestone. These samples were also sectioned for petrographic study (Chapter 5). A further 160 samples from the Great Limestone were obtained by drilling the rock face every 50 mm using a cordless drill and these samples were used for Carbon, Sulphur and Nitrogen (CSN) analysis. CSN analysis was carried out on samples covering a total of 8 metres commencing approximately 6 metres above the base of the Great Limestone to approximately 14 metres above the base of the Great Limestone.

A visual assessment of all samples was carried out and any organic and/or weathered material removed. Any samples containing large skeletal grains or obvious cement were also rejected before processing further. Enough material from the samples to produce 10 to 20 grams of powder per sample was chiselled from the original whole rock samples and this was then wrapped in thick paper before being crushed further using a hammer and anvil; taking care to ensure that the sample did not come into contact with the hammer or anvil. The crushed material was then placed in a mortar and crushed to a powder by use of a pestle. One problem with this method that became obvious from the beginning was the inclusion of pieces of paper within the sample during breaking with the hammer and anvil. It was important that the broken rock was inspected thoroughly to remove any traces of paper before it was put in the mortar. It is thought that, even though a close inspection of every sample was undertaken, contamination of samples by very small amounts of paper may have occurred. However, even though the chemical content of the paper is unknown, it is not thought that this method would have resulted in unusable data.

Vials to receive the samples for trace element analysis and a number of blanks were cleaned with 3.5% HNO_3 and 2 ml of 3.5% HNO_3 were placed in the vials and left overnight on a hot plate at 120^0C; the HNO_3 was then discarded and the vials rewashed. 100 µg of powdered sample were measured out (to 3 decimal places) and this was placed in the vials together with 10 ml of 3.5% HNO_3 which was then left overnight on a hot plate at 120^0C together with the blanks containing 10 ml of 3.5% HNO_3 only. The sample and acid was transferred to 50 ml flasks and the volume made up to 50 ml with 3.5% HNO_3 and left until the next stage.

The next stage involved preparation of the samples, blanks and standards for placing into the instrument, a Perkin Elmer Optima 3300RL ICP OES (Inductively Coupled Plasma Optical Emission Spectrometer). This and the previous stage were carried out under the direction of Dr C Ottley Senior Research Officer, Durham University. Before loading into the instrument, 10 ml test tubes were spiked with 10 ppm yttrium to act as an internal standard, and 10 ml of the 3.5% HNO_3 acid soluble sample were then added to the tubes and the contents mixed; acid insoluble material was left in the bottom of the flask undisturbed. The loaded samples, together with a number of blanks, were then analysed for Al, Ca, Fe, Mg, Mn, Si, Zn, Pb, Ba, Sr, S and Na. Appendix F shows the results of the trace element analysis.

The 160 samples analysed for Carbon, Sulphur and Nitrogen were obtained by first thoroughly cleaning the face of the exposure with a wire brush and then drilling out the samples; samples were drilled every 50 mm with an estimated measurement error of 2 millimetres (i.e. the thickness of the marker pen line). The drill dust from the first 5 mm of drill hole was discarded and then approximately 2 to 4 grams of drill dust were collected for each sample. Collection of the drill dust was achieved by fixing a small sample bag directly below the drill hole with tape. This method proved successful; however, collection of the drill dust was estimated to be as low as 60% at times due to the wind. The sample was discarded if any contaminants fell into the bag during drilling, i.e. pieces of soil and grass and insects from above. A note was taken of where each sample was drilled in relation to bedding planes, muddy partings or

large grains and fossils. These samples were then placed in small individual glass containers and dried in a domestic oven at a temperature of approximately 50^0C for 6 hours. The samples were then stored in a dry warm cupboard until the next stage.

The analysis for CSN was carried out at the Open University laboratories at Milton Keynes under the supervision of Dr A Coe. A Leco Instruments CNS-2000 elemental analyser was used to determine the weight percent (wt %) concentration of total carbon (TC), total organic carbon (TOC), total inorganic carbon (TIC), and total sulphur (TS). Using the Leco elemental analyser the dry rock powders were combusted in pre-conditioned inert ceramic boats at 1350°C and the evolved CO_2 and SO_2 gases were measured using infrared detectors.

For total carbon (TC) and total sulphur (TS) measurements, ~200 mg of dried, crushed rock powder were placed into the ceramic boats along with ~1 g of ComCat combustion catalyst, (a propriety catalyst manufactured by Leco). The ComCat and sample were thoroughly mixed to ensure complete combustion. For total inorganic carbon (TIC) measurements, ~300 mg of dried, crushed rock powder were weighed into the boats and transferred to a separate furnace at 450°C for 7-12 hours before the addition of ComCat and the analysis. This 'ashing' procedure burns off all organic carbon in the sample. Total organic carbon (TOC) was calculated by subtracting the wt% of TIC from wt% TC (TOC = TC-TIC) for a given sample. For most sedimentary rocks studied, all inorganic carbon measured in the samples is assumed to be in the form of calcium carbonate ($CaCO_3$).

The autoloader for the Leco takes 40 rock samples at a time, with the remaining 9 positions in the loader occupied by 2 empty boats (blanks) analysed at the start of a run, 2 ComCat blanks (just ~1 g of ComCat on its own) analysed after the blanks, and 5 intercalated samples of a rock standard with empirically known C and S concentrations (one positioned every 10 samples). The standard was prepared with ComCat as per the rock samples. The standard used was a powdered,

homogenised Oxford Clay sample (Open University in-house standard 'OXC-12'). Table 8.2 Appendix F shows the results of the CSN analysis.

8.3. Modern carbonates

Input of major and trace elements to river water and the degree and speed of removal of these elements from areas of erosion is dependant upon many variables, such as source rock, climatic conditions and elevation, all of which will influence river concentrations and the contribution of elements to the oceans. A comparison of both river and sea water major and trace element concentrations shows that they are generally chemically opposite in that Ca > Na > Mg and CO_3 > SO_4 > Cl in river water, whereas Na > Mg > Ca and Cl > SO_4 > CO_3 in sea water.

Marine organisms control the production of much of the modern carbonates; however, non-biogenic carbonates such as ooids and aragonite needle muds are still important contributors. Modern shallow-water carbonate sedimentation occurs in water depths up to 50 m and is restricted to tropical and sub-tropical climates, with the mineralogy dependent upon temperature and magnesium content; aragonite is the common phase to be precipitated inorganically.

The factors controlling whether calcite or aragonite is precipitated are still controversial to a certain extent. However, researchers have shown that the magnesium ion can inhibit calcite precipitation, resulting in the supersaturation necessary for aragonite precipitation (Morse and Mackenzie, 1990, see also Pytkowicz 1965; Berner 1975). The structure of aragonite permits substitution of the larger cations like strontium, barium and lead, whereas the smaller cations like iron, manganese and zinc are more likely to be substituted into calcite or dolomite (Mason, 1966; Milliman *et al*., 1974).

Component	% Org Matter	Mineral	Percentage				Parts Per Million				
			Ca	Mg	Sr	Na	Fe	Mn	Ba	Si	Al
Pelletoid	2.3-4.7	Aragonite		0.41-0.19	0.8-1	0.23	274-1290	10-80			
Ooids	0.3-2.5	Aragonite	37.8-38	0.05-0.69	0.94-0.99	0.24-0.44	14-350	3-7	9-65	376-730	100-300
Bahama mud samples		Aragonite		0.48-0.96	0.82-0.95	0.33-0.62	180-973	7-20			
Coccolith ooze	2.2-8.8	Calcite		0.11-0.17	0.15-0.21		1000-2000	265-1500	160-510		
Articulate and crustose coralline algae	2-23	MgCalcite	27-33	3.47-8.0	0.14-0.41	0.09-0.9	35-1132	24-113	8		
Green Algae	8 –24	Aragonite	32.9-39	0.09-0.37	0.8-0.9	0.21-0.9	160-3600	8-17			
Benthic Foraminifera	1.3-8.7	MgCalcite	31.6-35.4	1.25-3.75	0.15-0.2		10-1100	2-60	1-115	40-1350	
Corals	3-8.6	Aragonite and MgCalcite	33.2-39.4	0.07-0.32	0.28-0.95	0.34-0.44	12-300	2-6	8-85		
Bryozoan	5 –32	MgCalcite	35.7-39.2	0.16-2.99	0.19-0.87		0.1-1.3		21-98		
Echinoderms	35.8	MgCalcite	32.4-38.7	1.08-4.45	0.14-0.27	0.38-0.64	22-270	4.0-35	6	600-1440	
Bivalves	1.3-2.6	Aragonite and Calcite	2–39.2	0.01-0.43	0.01-0.32	0.2-0.57	10-1600	2-224	0-25		71-365
Gastropods	1.8-8.5	Mixed	32-40	0.27-1.4	0.21-0.37	0.21-0.55	4-1200	2-62	1-20		80-470

Table 8.1. Average composition of common non-skeletal and skeletal grains from modern carbonates. After Mason (1966), Milliman et al. (1974), Morse and Mackenzie. (1990) and Libes (1992). Note the compositions are an amalgamation of various research results and are for illustrative purposes only.

Major and trace element composition of carbonates depends upon mineralogy, temperature, magnesium content, partition coefficients and probably more importantly the "vital effect" or "enrichment factor" of individual organisms. Table 8.1 gives some major and trace element concentrations for various common components of modern marine carbonates and it can be seen that concentrations between components differ quite substantially, up to two orders of magnitude in some cases. The same can also be said within each faunal group where major and trace element concentrations between different species can also vary by similarly large

amounts; even individual parameters, such as age, can play a major role in how an individual preferentially concentrates elements and isotopes within its hard skeleton and soft parts of its body (Morse and Mackenzie 1990).

8.4. Major and trace elements in the Great Limestone

The purity of the Great Limestone is variable throughout its succession and, as will be seen from the following discussions, this variability is a direct consequence of the change in the concentrations of the elements and insoluble material. Chapter 6 discussed the comparisons between trace elements, isotopes and diagenesis, whereas stratigraphic trace element variations and correlations throughout the limestone were not considered. It is these variations that are the purpose behind this Chapter.

Temperature, salinity, light intensity and nutrient supply are among the major controls on the production of carbonate sediment, regulating the abundance of each type of carbonate producer. Light intensity is dependant upon water depth and turbidity, which is affected, quite significantly, by the input of terrigenous sediment, especially clays, the quantity of which will be a major control on the deposition rate and purity of the limestone. Changing faunal distributions within the Great Limestone (Chapter 5) could be the result of varying seawater depths from a few metres up to possibly 50 m or due to variations in climate (temperature, humidity) affecting carbonate productivity.

Climate has a strong influence on the type of terrigenous material supplied by rivers, with a humid climate providing more clay through chemical weathering, and an arid climate generating more sand and gravel-rich sediments, but with a lower frequency. Sediment deposition during sea-level change can also vary significantly; a falling sea level will increase river down-cutting therefore providing more sediment to the sea, and a sea-level rise will move sediment deposition to previously subaerial areas.

Mg^{2+} ions can distort the calcite lattice, which in turn increases its capacity for

trace element incorporation. Mg^{2+} ions also increase the proportion of aragonite to calcite formation (Wagner *et al*. 1979) and aragonite has a larger capacity for trace element inclusion than does calcite. Diagenetic alteration of the unstable aragonite to stable low Mg calcite results in the loss of strontium, magnesium and other trace elements to pore fluids, matrix and cement (Wagner *et al* 1979). As discussed in Chapter 6, high strontium levels within the Great Limestone point towards an original aragonite-rich composition, which was subsequently transformed during diagenesis and this, would have resulted in some trace elements being lost from the lattice. The assessment of strontium, magnesium and calcite concentrations from the Great Limestone supports the assumption of original mixed aragonite and calcite sediment and changes related to production rates.

Redox reactions, controlled by the amount of organic matter and the availability of electron receptors such as O_2, NO_3^- and SO_4^{2-}, can result in suboxic conditions being present within the sediment. Bioturbation usually results in re-oxidation of the sediment and the removal of any chemical gradients. Bioturbation is evident throughout much of the Great Limestone. Thus, any chemical gradients created by redox reactions, if they existed, may have been destroyed; however, the loss of the epitheca in some corals has been attributed to acidic porewaters (Chapter 5).

Trace elements within the Great Limestone may be present as inclusions in biogenic material, matrix or calcite cement, i.e. within the carbonate fraction, and also present within clays, POM or Fe-Mn oxides. The supply of much of the trace element content to the limestone is mainly dependant upon terrigenous input. However, diagenetic fluids may also have contributed significantly as trace elements are remobilised from both the carbonate and non-carbonate fractions and are made available for inclusion into cements and biogenic elements.

Even though any clay in the samples analysed would not be expected to have been dissolved in the HNO_3 acid during preparation, the remobilisation of adsorbed

elements and leaching from the clays is always a possibility. A study of total acid insoluble material shows a high percentage of carbonate material throughout the majority of the limestone and a low insoluble residue. Although the majority of the major and trace elements in the Great Limestone are expected to be from the carbonate fraction, the results from the analysis of the samples may also include some elements from remobilisation of adsorbed elements and leaching of the clays. For ease of comparison of the data from the analysis of the Great Limestone with those for average rock types, Table 8.2 is included from an amalgamation of data from Mason (1966), Wagner *et al*. (1979) and Libes (1992).

Rock Type	Percentage				Parts Per Million			
	Ca	Mg	Sr	Na	Fe	Mn	Al	Si
Shales	2.2	1.5	0.03	0.96	47,200	850	80000	47000
Sandstones	3.9	0.7	0.003	0.33	9,800		25,000	368,000
Carbonates	30.2	4.7	0.99	0.04	9,600	830	4,400	29,000
Igneous	3.6	2.4	0.03	2.2	50,000	950	81,300	277,200

Table 8.2 Comparison of major and trace elements for average rock types. After Mason (1966), Wagner et al. (1979) and Libes (1992).

8.4.1 Aluminium

Figure 8.1 shows the aluminium data plotted stratigraphically with the 12 period moving average trend line. The concentration of aluminium, up to approximately 14 m above the base of the limestone, is fairly constant at 300 ppm with brief excursions at about 10 m and 12 m above the base to around 1000 ppm. Major changes occur towards the top of the limestone near to 14 m above the base with peaks over 5000 ppm that are an order of magnitude above the background concentration. The background levels around 300 ppm are an order of magnitude less

than those shown for an average carbonate rock of 4400 ppm in Table 8.2. Even the large peaks of over 5000 ppm within the upper beds, are still within an acceptable range of the values in Table 8.2.

The high concentrations at 10 metres and 12 metres correspond to the obvious increases in thin shaley partings visible at outcrop. Bedding planes at these levels also become more shaley at around 14 metres where the amount of shale in both beds and partings between beds increases substantially as the "Tumbler Beds" are approached.

As stated above, the concentration within the lower beds is fairly consistent and this masks any possible trends within these beds. Within the 12 period moving average trend line in Figure 8.1, however, three and a half cycles are just discernable, i.e. cycles from the base up to approximately 5.5 metres, from 5.5 metres up to approximately 8.5 metres, 8.5 metres to 14 metres and then half a cycle from 14 metres up to the top.

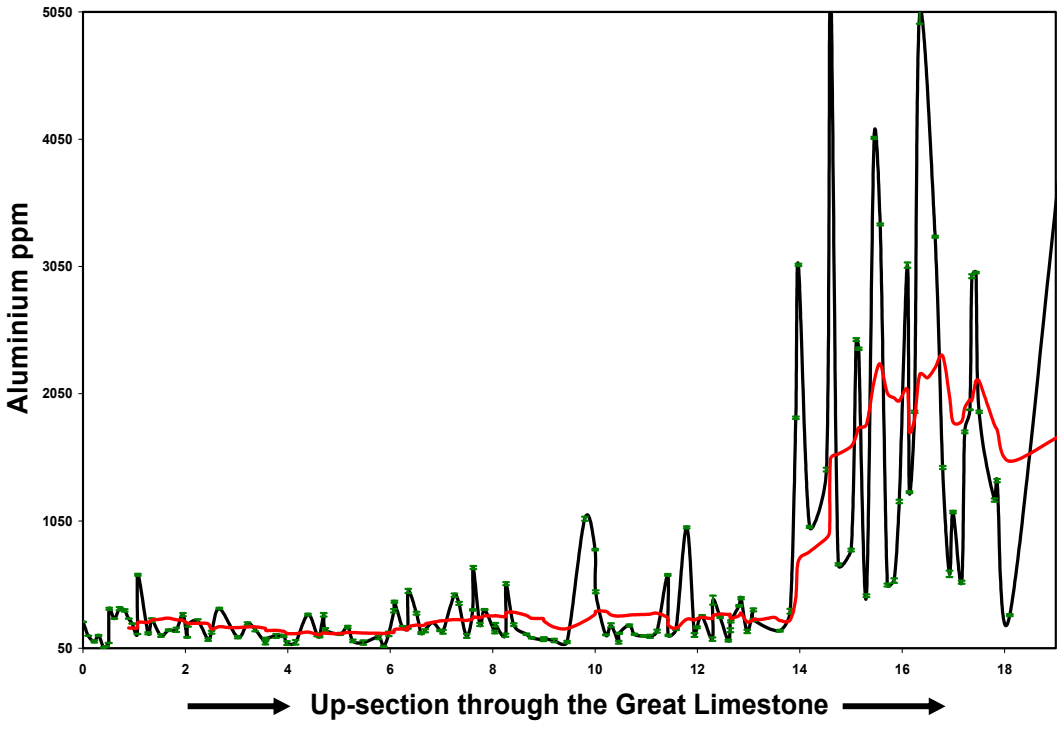

Figure 8.1 Aluminium (Al) data plotted with 12 period moving average trend line. 3 times the standard deviation error bars in green.

Within-bed changes in Al concentration throughout the majority of the beds vary by about 200-300 ppm. However, above bed 15 (10.5 metres) variations in concentration within beds reach 900 ppm and above bed 19 (14 metres) changes within beds are as much as 2000 ppm. As discussed above, these increases within individual beds follow the increase in occurrence of a shaly top and shaley bottom to many of the upper beds and the mudstone partings seen in the field as the Tumbler Beds and the mudstone above the Great Limestone are approached.

Aluminium can be present as minute inclusions within the calcite lattice or adsorbed to the carbonate. The similar size, in Angstrom units, between Mg^{2+} and Al^{3+} can result in the Mg^{2+} ion providing a proxy site within the lattice for Al^{3+}. Diagenesis during changes from oxic to suboxic conditions can result in aluminium, as well as many other elements, being released from both the carbonate and non-carbonate fraction to pore waters and made available for any cements being precipitated. However, as discussed above, there is no evidence for oxic conditions to have occurred at this locality.

The aluminium levels discussed above are low compared to values within Table 8.2. However, they do follow the scant data given in Table 8.1 for common skeletal and non-skeletal grains. A perfect correlation exists between aluminium and silica and a moderately negative correlation of -0.67 with $CaCO_3$ (Chapter 6, Table 6.1). The Al-$CaCO_3$ negative correlation reflects the terrigenous input reducing carbonate productivity. The Al-Si positive correlation is not surprising since they are both predominantly derived from terrigenous sources.

8.4.2. Iron

Figure 8.2 is a stratigraphical plot for iron, together with 12 period moving average trend lines for iron and aluminium. It can be seen that there is some resemblance between the trend lines. Figure 8.2 shows the concentration of iron, up to approximately 14 metres above the base of the limestone, to be fairly regular with

a background level of around 750 ppm. There is an initial concentration of 6000 ppm of iron at the base of the limestone and this increases at about 1.5 metres, 2.5 metres, 5 metres and 6 metres above the base to around 2400, 1700, 1500 ppm and 3000 ppm respectively. Major changes occur near to 14 m above the base of the limestone with peaks of 9000 to 12000 ppm and a maximum of 22500 ppm near the top; these are an order of magnitude above the background concentration. The increases in aluminium at 10 metres and 12 metres above the base of the limestone, which are evident in Figure 8.1, are not as apparent for iron in Figure 8.2. The background concentrations are generally well below those shown in Table 8.2 for average carbonate rocks (with values of 9600 ppm). However, some peaks are up to two and a half times the quoted value in Table 8.2 with concentrations of up to 22500 ppm.

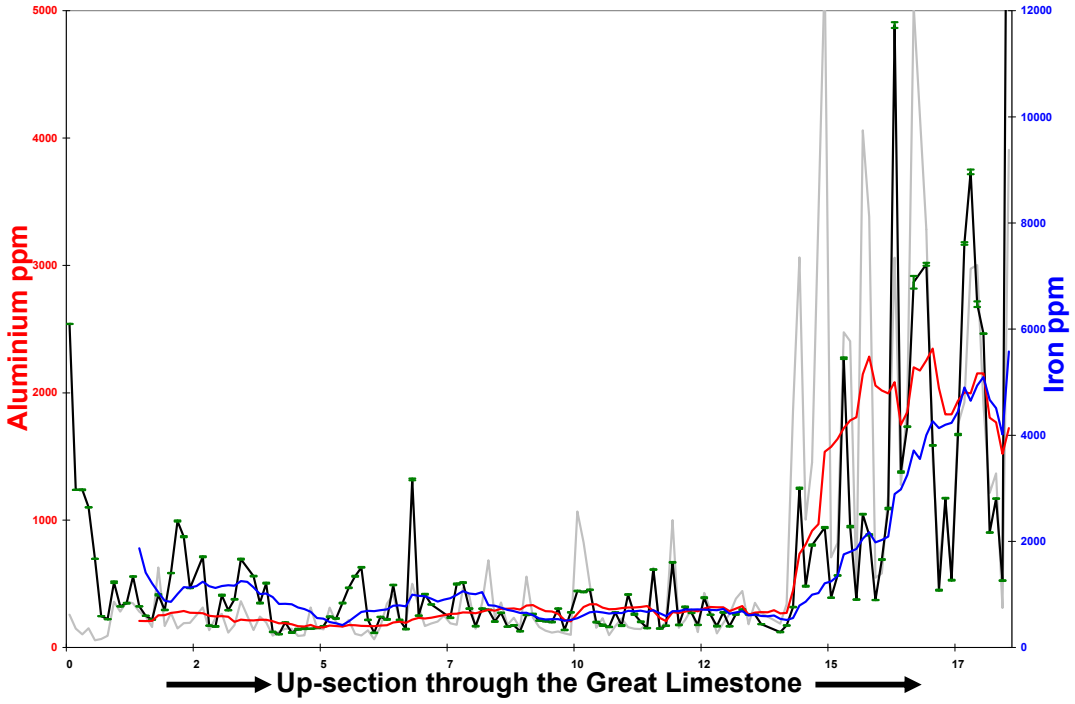

Figure 8.2 Comparisons of 12 period moving average trend lines for Al (red Line) and Fe (blue Line). 3 times the standard deviation error bars in green.

Similar patterns are evident within both the aluminium and iron plots of the 12 period moving average trend lines. However, an early trend, probably due to the initial spike at the bottom of the limestone, is also evident in the plot for iron. Nevertheless the resemblance of the plots and the correlation of 0.68 (Chapter 6, Table 6.1) between aluminium and iron reinforce the similarity of these element

concentrations throughout the limestone and points towards a similar terrigenous source for the elements. The initial iron concentration of 6000 ppm at the base of the limestone, and some of the other spikes, are possibly due to iron-rich pore-waters sourced from the sandstone below or from hydrothermal fluids.

Table 6.1 (Chapter 6) shows a moderately strong negative correlation of -0.7 between iron and $CaCO_3$ and a positive relationship of 0.68 with both aluminium and silica suggesting again a probable relationship with terrestrial input and productivity.

8.4.3. Silica

Silica can be present as minute inclusions within the calcite lattice, adsorbed to the carbonate, as an integral part of a clay lattice. In silica under-saturated waters, dissolution of any biogenic opaline silica detritus can occur and, over long periods of time, diagenesis can result in the majority of opaline silica and adsorbed silica being released and subsequently then converted to chert and quartz (Libes 1992). Small concentrations and nodules of chert can be found at some levels in the Great Limestone, but they are not common on the Alston Block. However, chert beds are common on the Askrigg Block to the south, at the level of the Tumbler Beds and above.

Figure 8.3 is a stratigraphical plot for silica, together with the 12 period moving average trend lines for both silica and aluminium. This bears a resemblance to the plots for aluminium and iron presented above; the similarity of the aluminium and silica 12 period moving average trend lines, points towards a probable similar source for the elements, namely terrigenous material.

The concentration of silica is fairly uniform up to approximately 14 metres above the base of the limestone, with a background level of around 200 ppm and increases at about 10 metres and 12 metres above the base to around 1500 ppm and 1350 ppm respectively. As in the previous plots, a major change occurs near to 14

metres above the base of the limestone with peaks around 8000 ppm, which are more than an order of magnitude above the background concentration. The increases at 10 metres and 12 metres are similar to those seen in Figure 8.1. All concentrations of silica within the Great Limestone are much lower than the values given for average carbonate rocks in Table 8.2 of 29000 ppm. As with aluminium, a moderately negative correlation of -0.67 exists between silica and calcium carbonate (Chapter 6, Table 6.1) suggesting a possible link between productivity and terrestrial input.

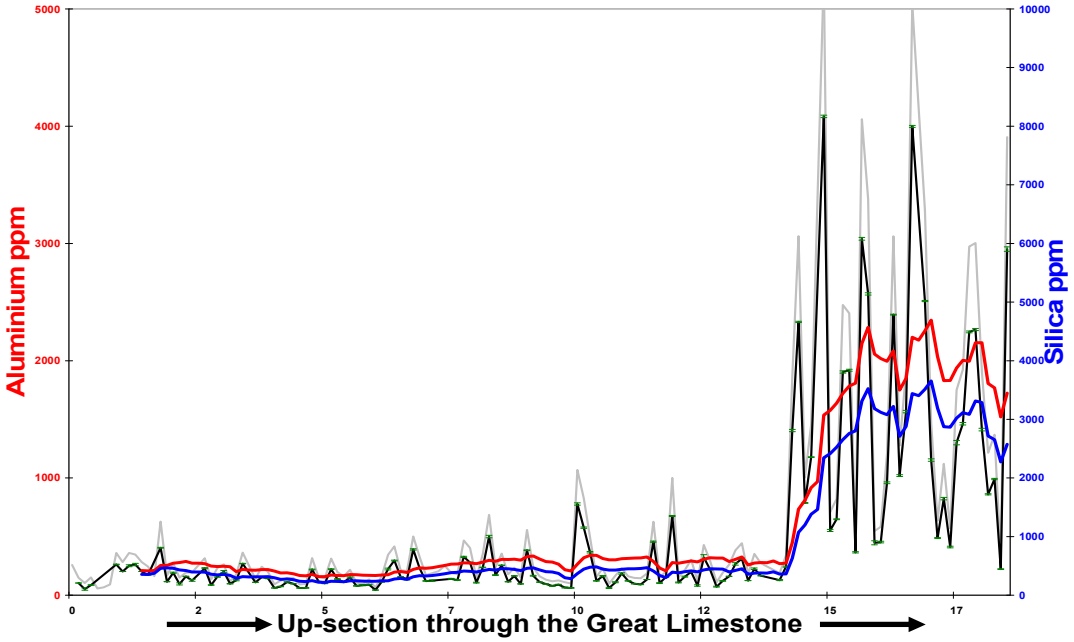

Figure 8.3 Comparisons of the 12 period moving average trend lines for Al (red Line) and Si (blue Line). 3 times the standard deviation error bars in green.

8.4.4. Barium

Figure 8.4 is a stratigraphical plot for barium, together with 12 period moving average trend lines for both barium and aluminium. There is a resemblance with the other river-sourced elements, aluminium, iron and silica mentioned above; however, the changes above 14 metres can be seen to be less intense.

The concentration of barium is fairly regular up to approximately 14 metres above the base of the limestone, with a background level of around 20 ppm and increases at about 3 metres, 6 metres, 10 metres and 12 metres above the base up to approximately 140 ppm, and at 7.5 metres with a concentration of 200 ppm. As in the

previous plots for aluminium, iron and silica, a change can be seen to occur near to 14 metres. However, the barium change is not as substantial as that for the others with an increase in background level up to approximately 120 ppm. Two spikes occur around 14 metres and 17 metres with concentrations of 380 ppm and 600 ppm respectively. A comparison of values with those for common skeletal and non-skeletal modern grains in Table 8.1 does show they are generally within the same order of magnitude with only the high concentrations above 17 metres moving towards more abnormal concentrations.

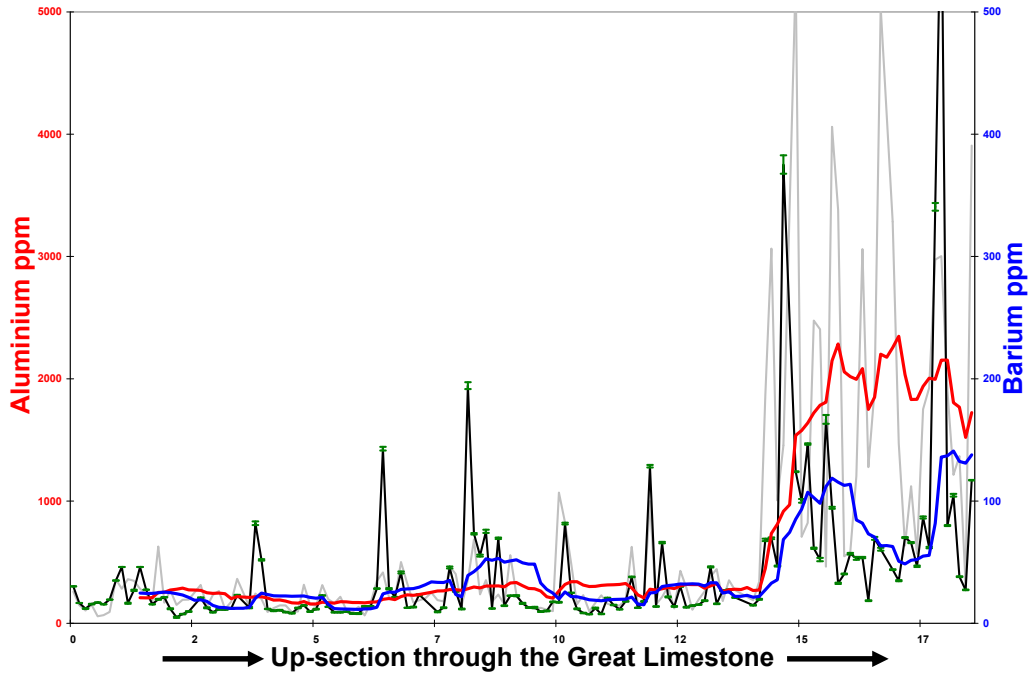

Figure 8.4 Comparisons of 12 period moving average trend lines for Al (red) and Ba (blue). 3 times the standard deviation error bars in green.

The 12 period moving average trend lines do demonstrate some similarity and many of the cycles below 14 metres can be seen in both barium and the plot for aluminium (and iron too, see above). The high content towards the top of the beds (15.5 m to 17.2 m) however, does not contain the continuous increase in concentration seen in the plots for aluminium and iron. There are some correlations of the positions of the main fossil beds within the limestone with the barium peaks which may indicate that barium in the Great Limestone is a proxy for productivity (see also section 8.4.7).

Alibert *et al*. (2003) found that Ba/Ca peaks in modern corals off the Burdekin River (Great Barrier Reef) corresponded to large flooding events and a relationship, at times, to high productivity. The use of barium as a proxy for productivity, however, is not thought to be reliable as Ba may be remobilised in anoxic conditions during sulphate-reducing reactions (McManus *et al.,* 1998; Alibert *et al.,* 2003, Eagle *et al*. 2003), resulting in lower values. McManus (1998) found that high concentrations of barium were coincident with high iron and/or manganese in modern seawater, possibly suggesting an interaction between barium and metal-oxide recycling in anoxic situations. Table 6.1, however, shows little relationship between iron, manganese and barium, with correlations of only 0.36 and –0.4 respectively suggesting that anoxic conditions, if they did exist, may only have been very localised and so not evident in the chemical signatures analysed here. It is also suggested by the bioclasts that water depths during deposition were in the range of a few metres up to approximately 50 metres maximum (Tucker *et al*. 2008). This would suggest that oxic conditions existed during deposition of the Great Limestone; however, anoxic conditions could have developed during shallow burial.

Dehairs *et al*. (1980, 1990) associated marine barite ($BaSO_4$) with decaying organic matter and Dymond *et al*. (1992) predicted a positive correlation between non- terrigenous barium accumulation and carbon export; this non-terrigenous barium has been variously referred to as Bio-Ba and Ba_{excess} (Dehairs *et al,*. 1980, 1990; Kasten *et al*., 2001; Eagle *et al*., 2003). Eagle however referred to Bio_{excess} as being difficult to calculate and suggested that in many cases it is location-dependant and may not always be a true representation of marine barium. Barium is contained within many phases with biogenic phases related to organic matter, biogenic silica and biogenic carbonate, and other phases related to terrigenous silicates, Fe-Mn oxides and hydroxides; therefore, a true determination of Bio_{excess} can be difficult to assess (Dymond *et al.,* 1992; Kasten *et al.,* 2001; Eagle *et al.,* 2003; Arrigo and Van Dijken, 2003). Calculations of Bio_{excess} also take into account Ba/Al ratios of terrigenous shale which have been found to change considerably and in addition, non-terrigenous

aluminium from diatom tests can confuse the assessments. Nonetheless, Eagle *et al*., (2003) considered that the discrepancy between Bio_{excess} and actual barite is of greater importance than calculations of the actual Ba/Al ratios. He was also of the opinion that barium as a proxy for productivity may only be applied in oxic sediments. To distinguish between the different sources of barium, the total barium has to be corrected for the biogenic (barite) and non-biogenic contents, and Ba/Al ratios. These calculations, however, are beyond the scope of this research.

Figure 8.5 is a plot of Ba/Ca times 10000 together with a Fischer plot of bed thickness; the 12 period moving average trend (blue) shows a close relationship with the Fischer plot (red). Whether this relationship is due to changes in river input, productivity or both is not clear; however, the similarity with aluminium, silica, iron and the Fischer plot may suggest that a relationship with terrestrial input and therefore nutrient input and/or productivity may exist. This is also confirmed by the correspondence with the 2 fossil bands, *Calcifolium bruntonense* commencing near to 5 metres above the base and the main brachiopod/coral band commencing around 9 metres above the base.

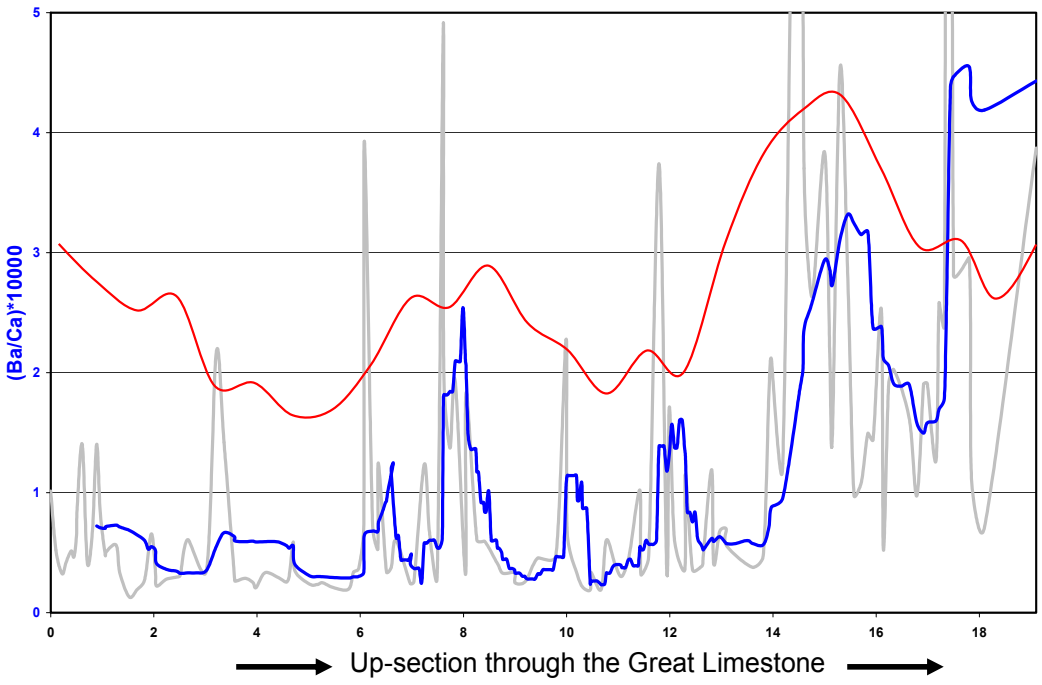

Figure 8.5. (Ba/Ca)*10000 (blue) together with a Fischer plot of bed thickness (red)

8.4.5. Strontium

Strontium can be incorporated into clays and importantly, into biogenic carbonate. The large ionic radius of Sr^{2+} permits it to substitute for Ca^{2+} within skeletal aragonite, so that aragonite has a Sr/Ca ratio of 2-6 times that of calcite (Lea *et al.* 1999; Jenkyns *et al.* 2002). Whether aragonite or calcite is deposited depends, as discussed above, upon the concentration of Mg^{2+} ions. Biogenic incorporation of Sr depends upon many variables such as salinity, pH, Sr/Ca ratio of seawater and productivity; however, it is probably not temperature dependent (Stoll *et al*., 2001; Lea *et al*., 1999).

Figure 8.6 is a stratigraphical plot for strontium, together with 12 period moving average trend lines for both strontium and aluminium. There is some resemblance to aluminium, except around 10 m to 12 m where the trends diverge. A moderate correlation of 0.52 exists between aluminium and silica, with a poor correlation of 0.23 existing with iron (Chapter 6, Table 6.1). The trend above 14 metres can be seen to correspond to the increases in shale seen in the aluminium trend; however, this falls after the initial increase. From Figure 8.6 various trends can be seen in the plot for strontium with a long-term increase from the base up to approximately 16 m, together with smaller trends. An increase is visible from the base up to approximately 2.5 metres, which is then followed by a negative trend up to approximately 6 metres. This is followed by a similar positive and negative trend at 6 metres up to 9 metres and 10.5 metres up towards the top. Cycles are picked out by the 12 period moving average trend line between 0 metres and 6 metres, 6 metres to 10.5 metres and 10.5 metres to the top. Large peaks occur throughout, with the most noticeable at 1 metre (2120 ppm), 2.5 metres (2100 ppm), 3.5 metres (1620 ppm), 7.3 metres (1670 ppm), 14 metres (2150 ppm), 18.5 metres (2213 ppm) and the top (2000 ppm).

As discussed in Chapter 6, strontium concentrations are high compared to those expected for ancient limestones (see Table 8.1), suggesting the original sediment had a significant aragonite content. The large peaks in Figure 8.6 could be

the result of changes in the primary signal due to environmental factors such as changes in sea level, seawater temperature or productivity etc. A drop in seawater temperature due to glacial periods of thousands of years can cause strontium depletions up to 2% (Lea *et al*., 1999); however, the fluctuations seen in Figure 8.6 are over very short time periods and therefore unlikely to be glacially related on their own.

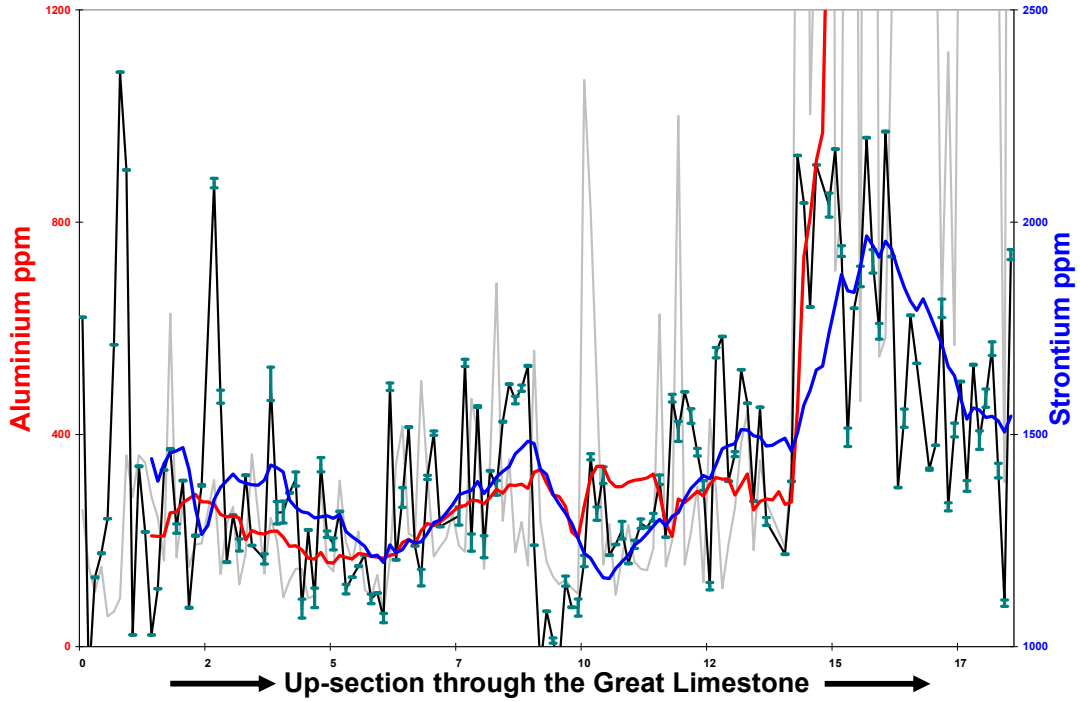

Figure 8.6 Comparisons of 12 period moving average trend lines for Al (red) and Sr (blue) 3 times the standard deviation error bars in green Note the high aluminium concentrations near the top of the limestone have been removed for clarity

Figure 8.7 shows that a slight negative correlation exists between strontium and $CaC0_3$, indicating that there may be some relationship between the strontium levels and the calcite lattice, possibly due to diagenetic effects. This poor correlation is also confirmed by a correlation index of -0.18 (Chapter 6, Table 6.1). Interestingly there is also a poor relationship between strontium and insoluble material with a correlation index of 0.17, suggesting little relationship with river input.

Variations in Sr/Ca ratios of seawater are sensitive to sea-level changes; rapid

increases in strontium can be interpreted as resulting from either a sea-level rise or fall (Frank *et al*. 1999). A rise in sea level can cause drowning of carbonate platforms, decreasing shallow-water aragonite precipitation and therefore increasing the seawater Sr/Ca ratio. A sea-level fall, on the other hand, could result in meteoric water diagenesis of aragonite, or erosion of exposed aragonitic limestone, and an increase in continental weathering, also resulting in a release of strontium and an increase in Sr/Ca ratios of seawater. Decreases in Sr/Ca seawater ratios can be associated with an increase in productivity and therefore increased $CaCO_3$ production and precipitation.

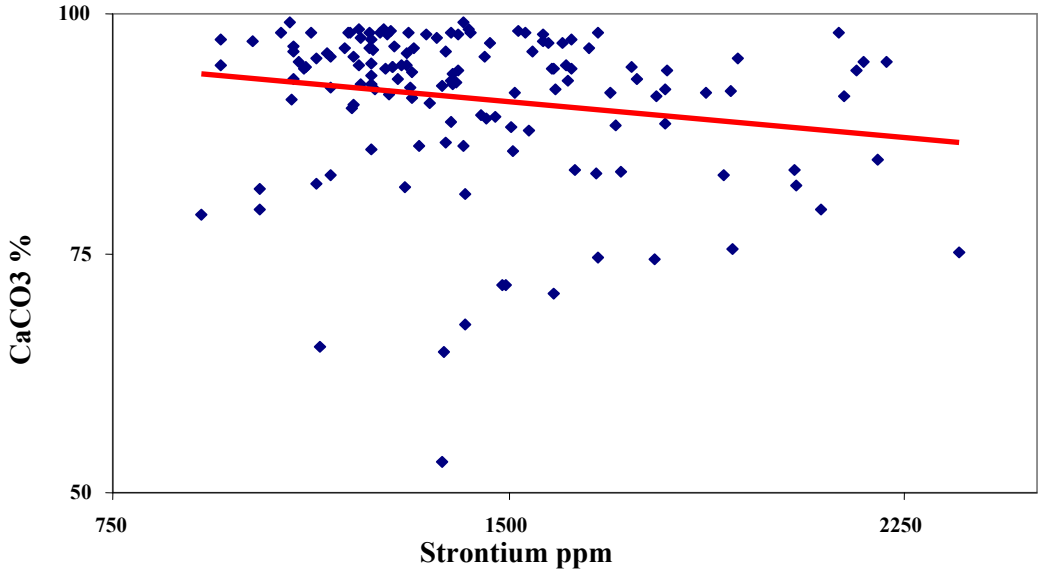

Figure 8.7. Comparison of strontium and $CaC0_3$ showing a slight negative correlation trend in red.

Figure 8.8. is a plot of the 12 period moving average trend line for strontium together with the Fischer plot of bed thickness. As can be seen, there is a remarkable correlation between the strontium trend line and the Fischer plot suggesting that a possible close relationship exists between strontium content and environmental factors controlling deposition. The Fischer plot shows thickness variations which could be related to carbonate productivity changes resulting from climate changes (humidity, temperature) with or without actual sea-level changes. Even though the strontium content of seawater is sensitive to sea-level perturbations, research has shown that Sr/Ca trends in ancient limestone usually correspond poorly to sea-level

plots and they are therefore difficult to use successfully as a sea-level proxy (Stoll *et al*., 2001). Primary trends are better preserved in carbonate-poor sediments, such as mudstones and marls, rather than limestone (Frank *et al*. 1999).

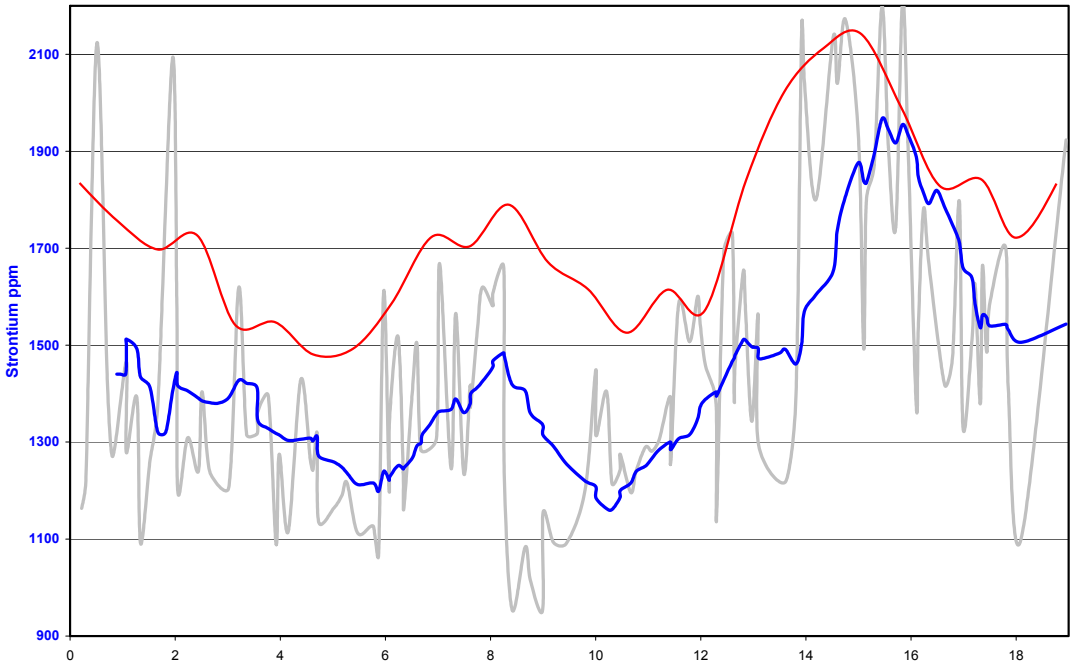

Figure 8.8. 12 period moving average trend line for strontium (blue) together with a Fischer plot of bed thickness (red). Note the Fischer plot is not to the same vertical scale.

Figure 8.9 is a plot of the 12 period moving average trend line for molar strontium/calcium together with the Fischer plot of bed thickness; the plots still show a close correlation between the trend lines. As discussed above, decreases in Sr/Ca seawater ratios can be associated with an increase in productivity and precipitation due to an uptake of strontium from seawater. It may be expected, therefore, that a decrease in seawater Sr/Ca, due to increases in productivity, may be associated with an increase in sediment Sr/Ca ratios and an increase in bed thickness. It is proposed, therefore, that the 12 period moving average trend line for molar strontium divided by molar calcium and the Fischer plot in Figure 8.9 are the results of increased aragonitic faunal production and therefore productivity rather than solely sea-level changes. This is also confirmed by the correspondence with the 2 fossil bands, *Calcifolium bruntonense* commencing near to 5 metres above the base and the main brachiopod/coral band commencing around 9 metres above the base.

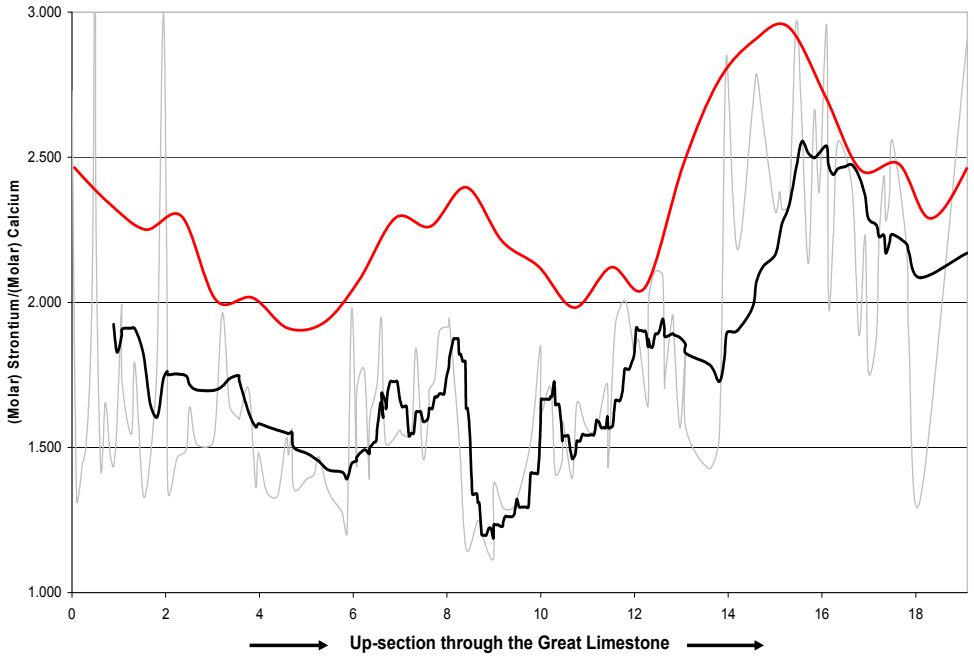

Figure 8.9. 12 period moving average trend line of (molar) strontium divided by (molar) calcium (black) together with a Fischer plot of bed thickness (red)

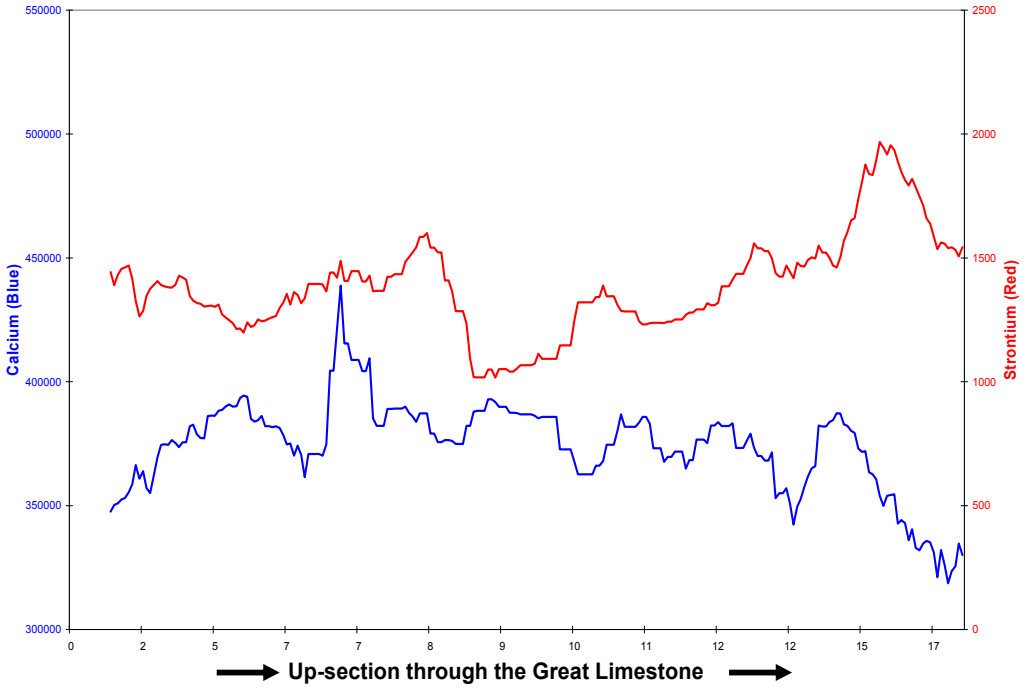

Figure 8.10. 12 period moving average trend lines for strontium and calcium through the limestone

Al-Hashimi (1976) found that dolomitisation of Carboniferous rocks within the Northumberland Trough, resulted in the removal of strontium from the calcite lattice. However, as can be seen by the poor correlation index of 0.12 in Chapter 6 and Table 6.1, little, if any, correlation exists between strontium and magnesium, possibly suggesting that removal of strontium during dolomitisation did not occur within the Great Limestone at this locality. However, it is also possible that the patchy, partial dolomitisation and recrystallisation of the Great Limestone may have resulted in a masking and partial loss of part of the original strontium trend.

Figure 8.10 shows the 12 period moving average trend lines for strontium and calcium concentrations stratigraphically through the Great Limestone. The discussions above together with a lack of correlation between the two elements in Figure 8.10 and a correlation index of –0.18 (Chapter 6, Table 6.1), would suggest that strontium and calcium are not strongly linked. However, I would propose that the general high background strontium levels are probably associated with an original aragonite composition as discussed in Chapter 6, and therefore carbonate precipitation rates. The actual changes in concentration of strontium throughout the Great Limestone may be associated with productivity or masked by diagenesis and/or association with terrigenous input.

8.4.6. Manganese

Figure 8.11 is a stratigraphical plot for manganese, together with 12 period moving average trend lines for both manganese and aluminium. The figure shows that above 12 metres to 14 metres above the base of the limestone there is little to no correlation with aluminium. There is a similarity of trend with aluminium up to approximately 8 m; however, the comparison stops there. In Chapter 6, Table 6.1 shows poor correlations with aluminium, iron, silica and barium of –0.05, 0.39 –0.06 and 0.03 respectively.

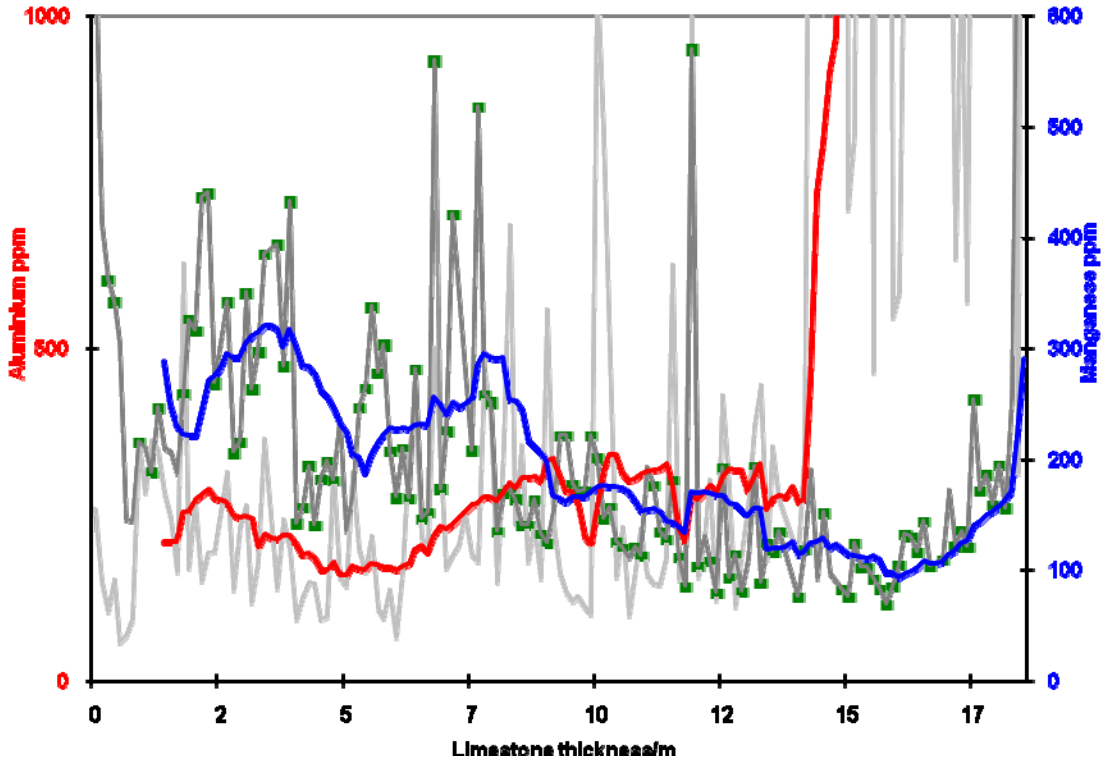

Figure 8.11 Comparisons of 12 period moving average trend lines for Al (red) and Mn (blue). 3 times the standard deviation error bars in green.

The manganese profile in Figure 8.13 generally decreases in concentration from the base to the top of the limestone with positive followed by negative trends around 0.5 metres to 3.5 metres (maximum 440 ppm) and 4 metres to 8 metres (maximum 550 ppm). There are 2 other large peaks at 11.5 metres (570 ppm) and at the top of the limestone (980 ppm). Cycles are visible within the 12 period moving average trend between 0 metres to 5 metres, 5 metres to 11.5 metres, 11.5 metres to 16.5 metres and 16.5 metres to the top. The manganese concentrations compare favourably with those for average carbonate rock types given in Table 8.2 with background concentrations being around half of the expected values and maximum values at or very near to the expected values given in the table.

McManus *et al*. (1998) suggested that a coincidence of manganese, iron and barium peaks might indicate that manganese/iron oxy-hydroxides could be contributing to barium recycling in anoxic conditions. Figure 8.12 shows the plots for

manganese, barium and iron concentrations and it can be seen that the peaks in manganese are not a good fit with those for barium and iron suggesting little association with barium recycling or anoxic conditions. Chapter 6, Table 6.1 also shows little correlation between manganese, barium and iron with indexes of –0.03 and 0.39 respectively. The high peaks therefore are more likely related to diagenesis in manganese-rich pore waters.

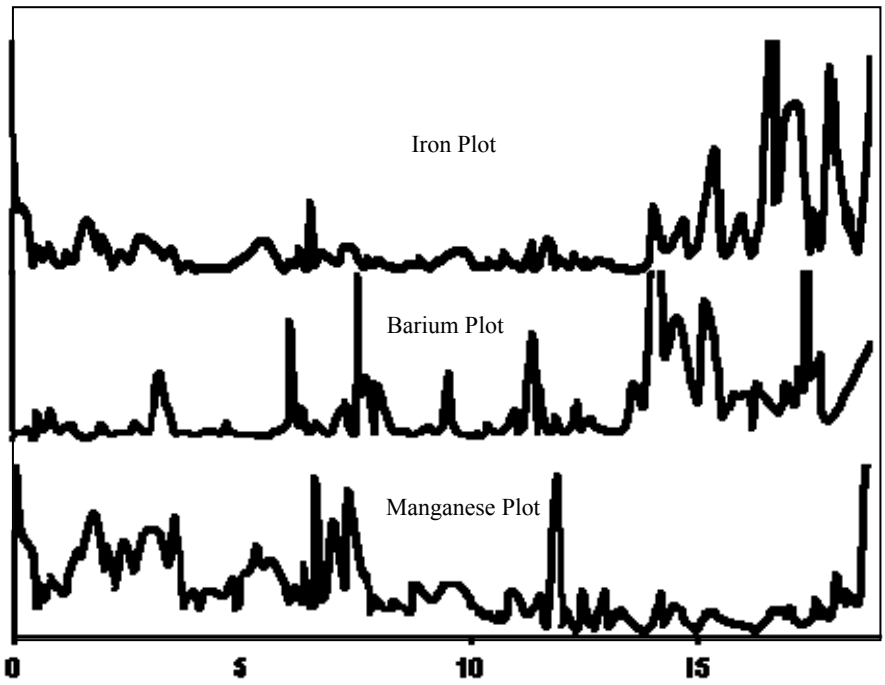

Figure 8.12. Manganese, barium and iron plotted for comparison. Note, not to same vertical scale.

If manganese concentrations were controlled by terrigenous influx it may be expected that the manganese trend would have a close correspondence to aluminium, silicon and total insoluble material (Jarvis *et al*., 2001). However, as can be seen in Chapter 6, Table 6.1, there are very poor correlations with these elements. The general lack of correspondence between these plots is consistent with manganese not being controlled by river influx and suggests the usual assumption that manganese is predominantly a carbonate-bound element (Jarvis *et al*., 2001); however, this is not substantiated by the poor correlation index of –0.07 (Chapter 6, Table 6.1).

8.4.7. Magnesium

Magnesium content of seawater is controlled by fluvial supply, the ratio of removal into carbonates and the removal during hydrothermal reactions (Jenkyns *et al*., 2002). The actual content within calcite is dependent upon the Mg/Ca ratio of the seawater and temperature. Studies by Lea *et al*. (1999) have shown that magnesium partition coefficients increase with temperature; original magnesium trends could therefore be expected to follow sea-surface temperatures; however this will depend upon the extent of diagenetic alteration.

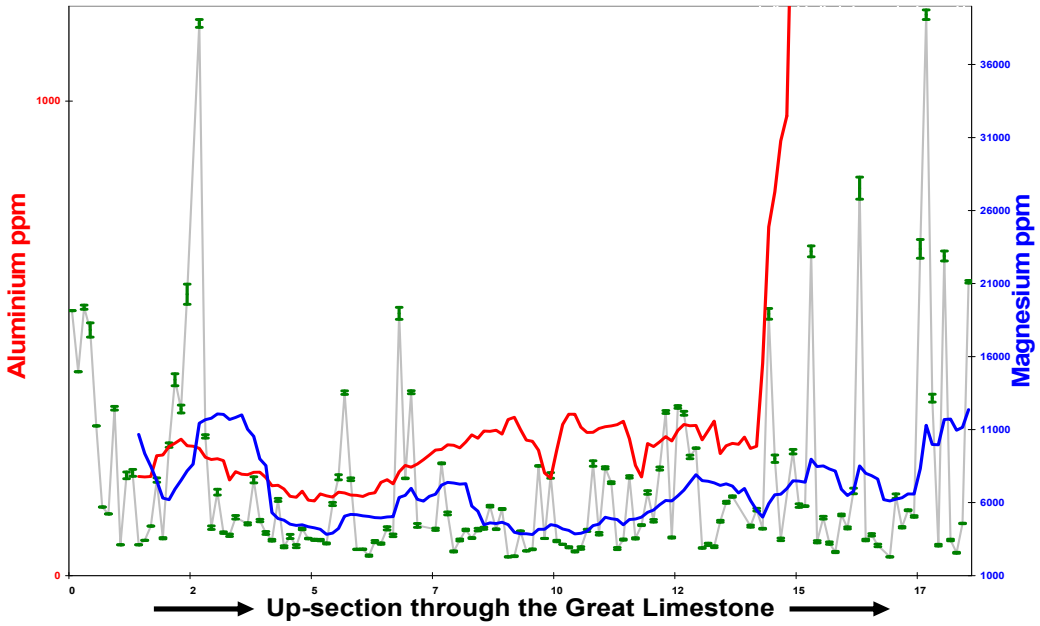

Figure 8.13 Comparisons of 12 period moving average trend lines for Al (red) and Mg (blue) 3 times the standard deviation error bars in green

Figure 8.13 is a stratigraphical plot for magnesium, together with 12 period moving average trend lines for both magnesium and aluminium. There is little comparison of trends with the other river-sourced elements, aluminium, iron, silica and barium mentioned above, with the greatest obvious difference being above 12 metres and 14 metres, where large increases seen in the other elements are replaced by individual peaks within the magnesium profile. Correlations (Chapter 6, Table 6.1) with aluminium, silica and barium confirm this with indexes of 0.21, 0.21 and 0.01 respectively; interestingly there is a slightly stronger correspondence with iron of 0.48 possibly suggesting some relationship with diagenesis.

Short-term trends, in Figure 8.13, similar to those seen in strontium, can be seen in the bottom few metres. However, high magnesium levels at around 2 metres probably correspond to the patchy dolomitisation in the lower beds and a correlation index of 0.21 suggests little association exists. A general increase in concentration can be seen above 10 metres from the base to the top of the limestone with peaks from 8000 ppm at 10 metres above the base to 40000 ppm at the top. Peaks within the profile correspond to both bedding planes and inter-bed intervals. A comparison with Table 8.2 shows the concentrations within the Great Limestone favourably compare to average values for carbonate rocks. The magnesium trend shows up to four and a half cycles, and this is comparable to many of the other trends above; however, the comparison stops there.

Within bed changes in concentration of up to 15000 ppm can be seen in the bottom beds and above this the concentration within beds varies by an average of 3000 ppm. Above bed 18, within bed concentration variations increase to 10000 ppm and peak at 35000 ppm at bed 25. These large within-bed variations in concentration coincide with local burial dolomitisation of the lower and upper beds.

Whether calcite or aragonite is precipitated can depend upon the Mg^{2+} ion concentration of seawater. High Mg/Ca ratios can result in aragonite precipitation resulting in low Sr/Ca ratios in seawater and high Sr/Ca ratios within the sediment. A low Mg/Ca ratio on the other hand favours calcite formation resulting in high Sr/Ca ratios in seawater and low Sr/Ca ratios in the sediment (Steuber and Veizer, 2002). As discussed above, the high strontium concentrations within the Great Limestone are likely to be a relic of an original aragonitic sediment; therefore, if it is assumed that the original Mg/Ca and Sr/Ca trends remained within the Great Limestone after diagenesis, and they are related to aragonite precipitation, using the findings of Steuber and Veizer (2002) and the discussion above, it may be expected that a close correlation may be seen within the Mg/Ca and Sr/Ca trends of the Great Limestone.

The correlation index between Mg/Ca and Sr/Ca at 0.42 is not strong; however, as can be seen in Figure 8.14, a plot of the 12 period moving average trend

lines for both Mg/Ca and Sr/Ca: even though there are some 'lags', there does appear to be a close relationship between the two trend lines. The close relationship between the 12 period moving average trend lines for Mg/Ca and Sr/Ca in Figure 8.14 would suggest that, even though some changes to magnesium concentrations may have resulted from diagenesis, the original trend may have remained.

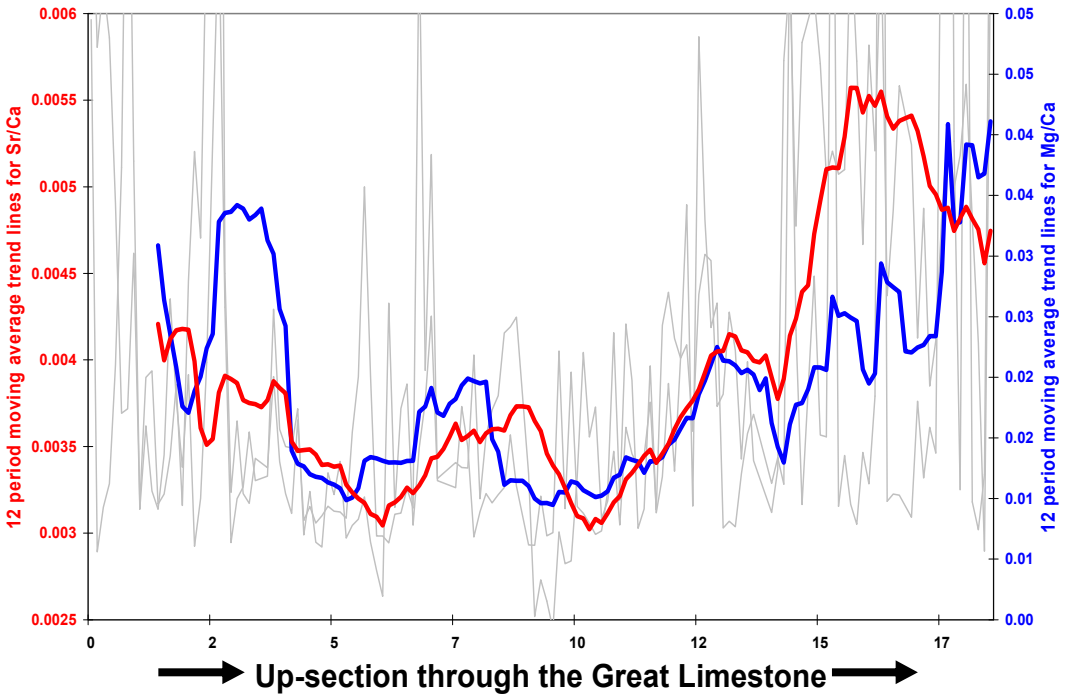

Figure 8.14. 12 period moving average trend lines for Mg/Ca and Sr/Ca

8.4.8. Sodium

Figure 8.15 shows the 12 period moving average trend lines for sodium and aluminium. There is some correspondence of trends between 13 metres and 15 metres otherwise there is little similarity between the plots or between the plots for the majority of the other elements discussed above. The sodium trend does show up to five cycles similar to those seen with the manganese trend discussed above. The error bars (green) shown in the sodium plot cover a large range, probably due to the actual concentrations being near to or below the detection limit of the equipment for sodium. Thus the results for sodium should be treated with caution.

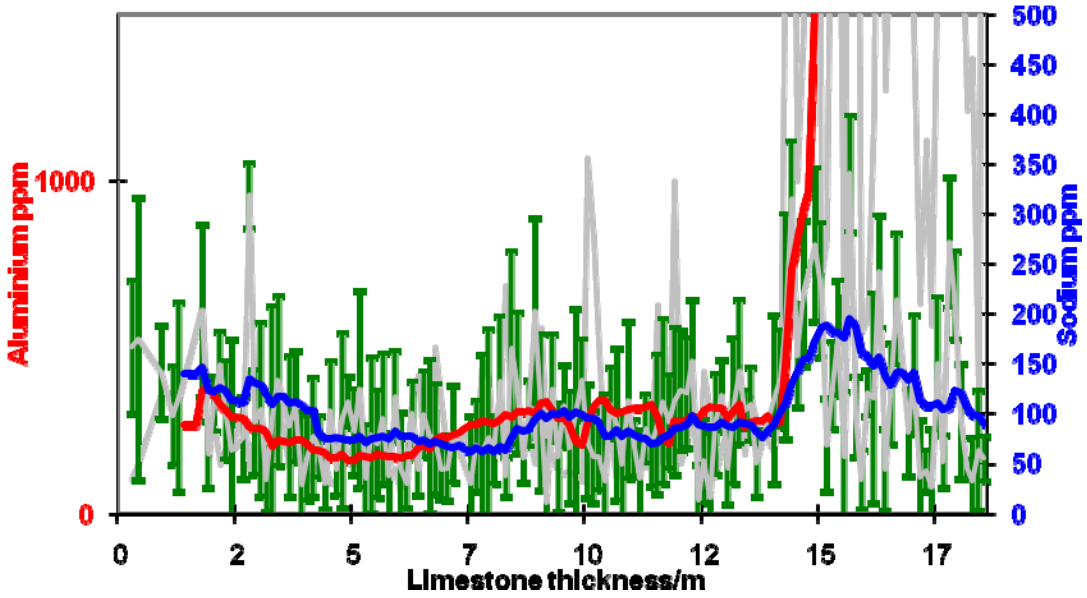

Figure 8.15 Comparisons of 12 period moving average trend lines for Al (red) and Na (blue) (3xStd deviation error bars in green)

8.4.9. Calcium and calcium carbonate.

Calcium is supplied to the oceans from weathering and river input and removed from the water column by direct carbonate precipitation, biological processes and subsequent loss to sediments. Remobilisation occurs at and just below the sediment surface by dissolution/decomposition of biological material. Deep-sea carbonates are generally homogeneous in terms of mineralogy, whereas shallow-water carbonates, such as the Great Limestone, are heterogeneous, reflecting the variety of organisms involved in carbonate deposition and the mineralogy of the matrix and cements.

The calcium concentration in Figure 8.16 varies from a minimum of 178,650 ppm to a maximum 397,000 ppm and this equates to a percentage calcium carbonate of 45% minimum and 98% maximum. The lower concentrations towards the base of the Great Limestone equate to the higher magnesium content and terrigenous concentrations in the lower beds. The other spikes throughout the limestone are at times consistent with proximity to bedding planes, stylolites and the Tumbler Beds.

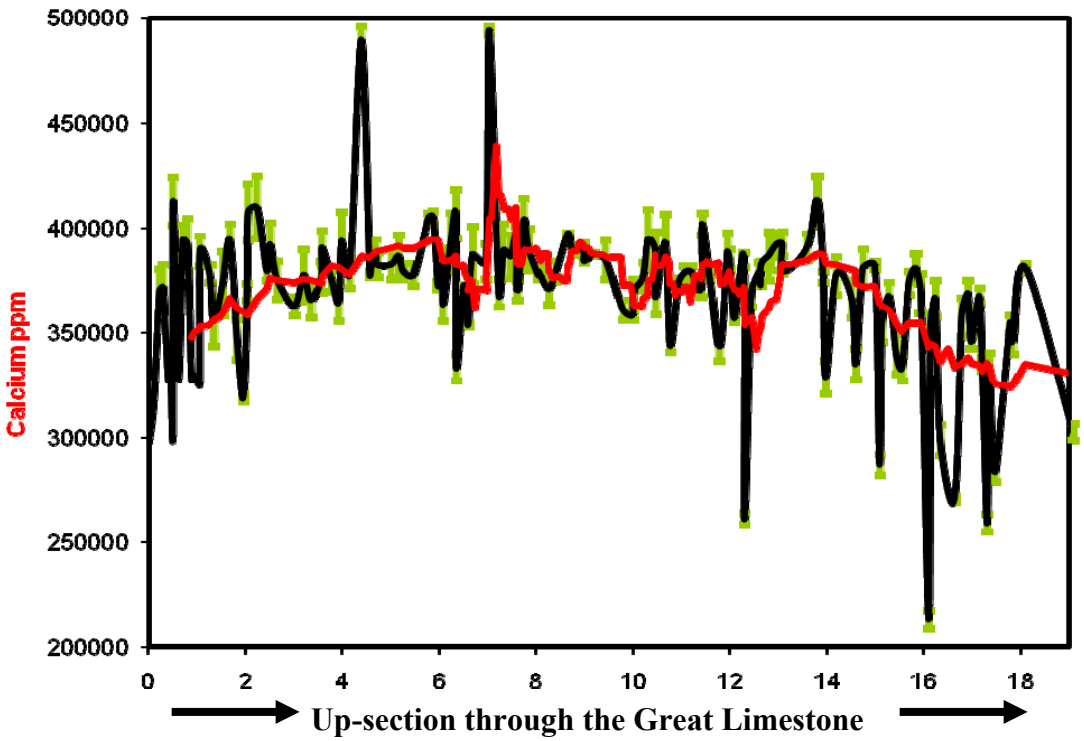

Figure 8.16 Calcium (Ca) data plotted stratigraphically. 3 times the standard deviation error bars in green. Note high peaks around 4.5 m and 7 m are regarded as being errors.

On a close examination of the 12 period moving average trend line for calcium carbonate in Figure 8.17, three cycles can be seen, one cycle up to approximately 7 metres, a second cycle up to approximately 13 m and a third cycle up to 18 m near the top of the limestone; these cycles are not, however, as obvious as those seen in other elements.

In previous sections many of the elements were compared to aluminium so as to ascertain any association between the elements and terrigenous sediment, and this has also been carried out in Figure 8.18 where aluminium and silica are compared to calcium carbonate. The 12 period moving average trend lines within Figure 8.18 do not show a close correspondence between the three elements; however, Chapter 6, Table 6.1, does show a moderate negative correlation of –0.67. This moderate negative relationship between the elements would suggest that silica and aluminium are probably linked to terrigenous input which in turn could be a control on productivity cycles. The aluminium and silica trends in the upper beds obviously

depart from that for calcium carbonate and show a negative relationship, which may suggest a control on the production of calcium carbonate. This could confirm the previous discussion that the aluminium and silica concentrations reflect a terrigenous source

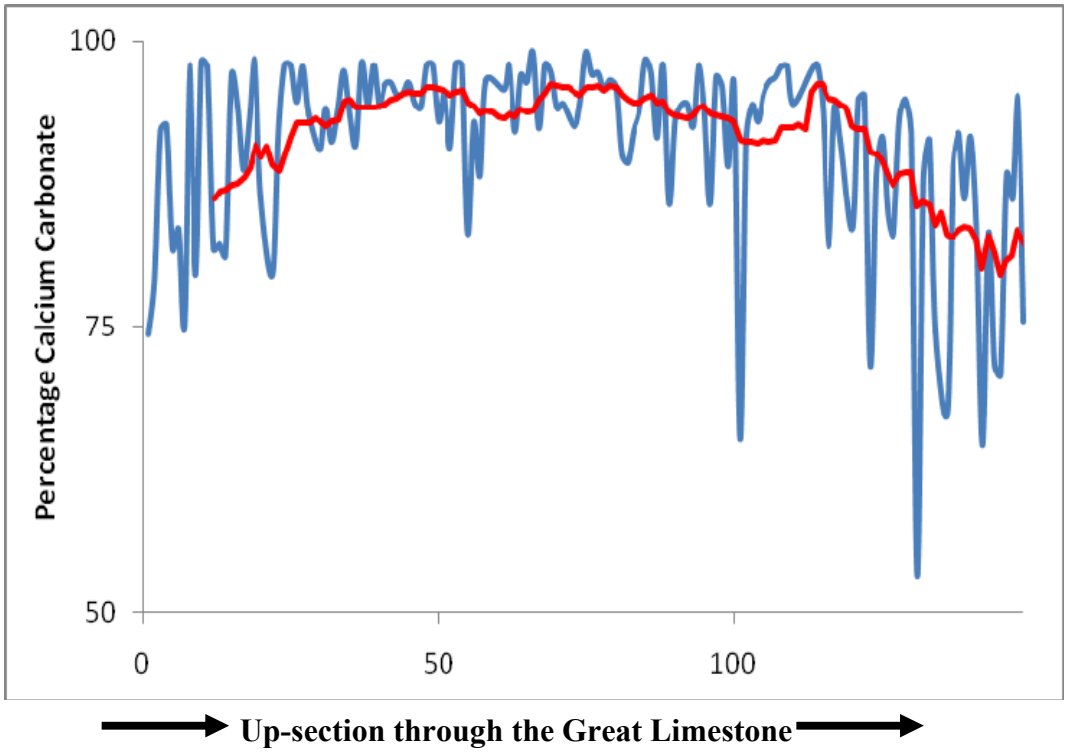

Figure 8.17. Percent calcium carbonate ($CaCO_3$) and 12 period moving average trend line.

Figure 8.19 shows percentage calcium carbonate throughout beds 7, 9 and 20 of the Great Limestone. As with many of the other elements, the calcium carbonate variations within many of the individual beds of the Great Limestone are confused and do not exhibit any obvious trends. Some beds have higher calcium carbonate levels near to bedding planes than within the centre of beds, whereas others have higher levels within the bed itself than towards the bedding planes. Within-bed calcium carbonate percentage variations fluctuate by a few percent within the lower beds rising to fluctuations of 35 percent within bed 23 and falling to a fluctuation of 20 percent within the top bed.

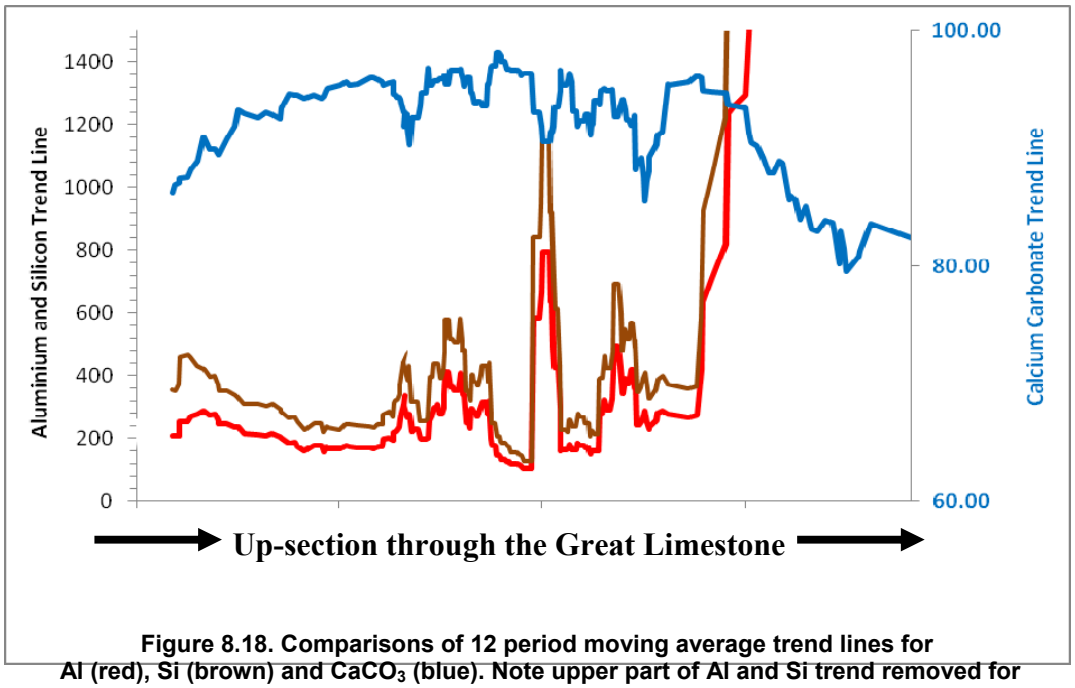

Figure 8.18. Comparisons of 12 period moving average trend lines for Al (red), Si (brown) and $CaCO_3$ (blue). Note upper part of Al and Si trend removed for clarity.

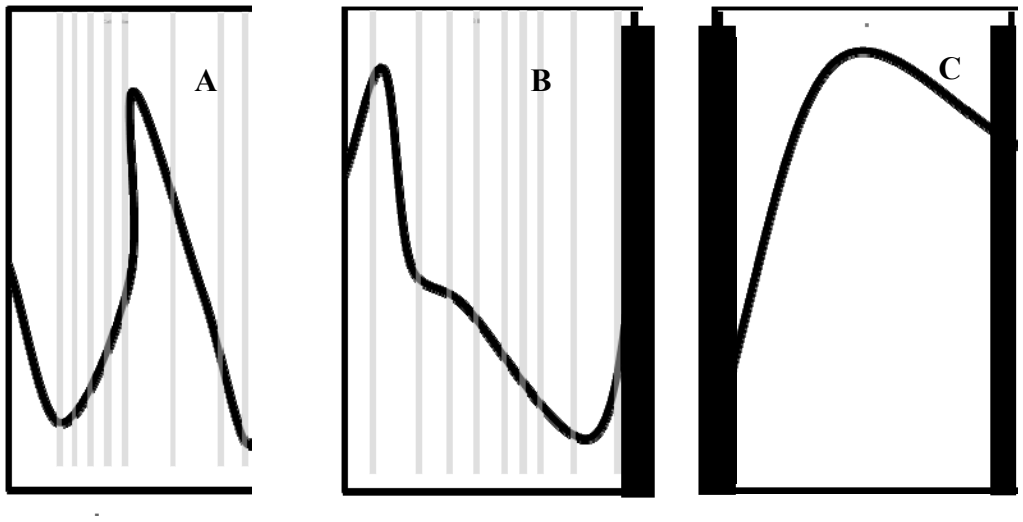

Figure 8.19. $CaCO_3$ concentrations for bed 7 (A), bed 9 (B) and bed 20 (C) (Note grey bands are the positions of stylolites; black bands the position of muddy partings.)

8.4.10. Lead and zinc

Lead and zinc are present in minute quantities in both river and seawater. Lead concentrations of seawater are in the region of 0.0003 ppm and 0.005 ppm in river water and zinc concentrations are in the order of 0.01 ppm in seawater (Mason,

1966). Lead concentrations in a typical carbonate are in the order of 9 ppm and zinc 20 ppm. The presence of lead within fluids favours aragonite precipitation, but whether this is due to it inhibiting calcite precipitation is unknown. Zinc in a fluid on the other hand favours calcite and dolomite precipitation (Mason, 1966; Milliman, 1974).

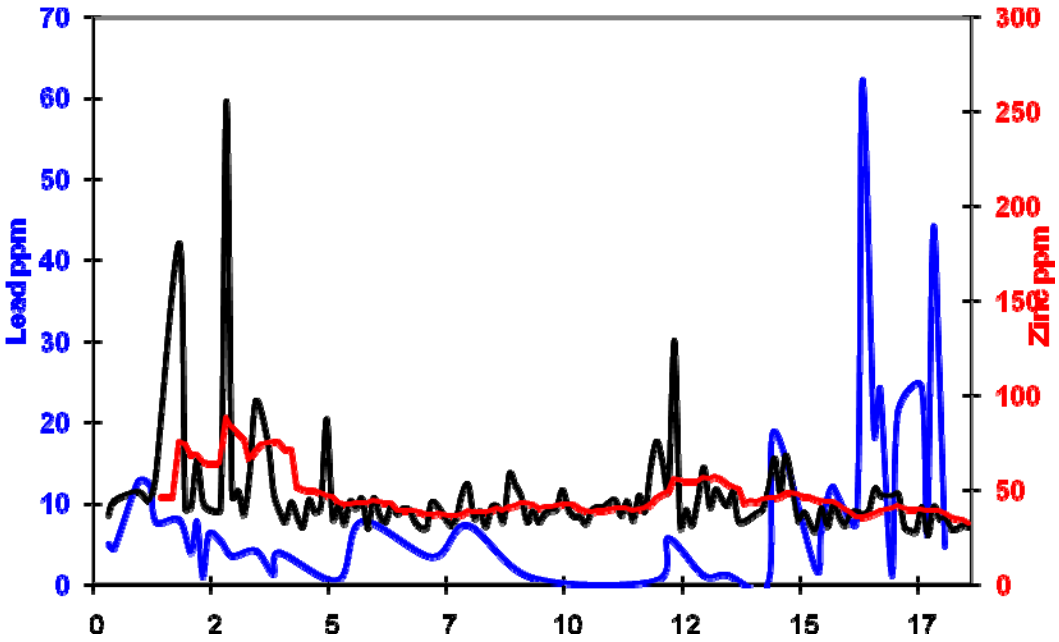

Figure 8.20. Concentrations for lead (blue Line) and zinc (black Line) in ppm. 12 period moving average trend line for zinc (red Line).

The concentrations of lead and zinc within the Great Limestone are generally very low and in many cases below the detection limit of the equipment. Apart from the high levels near to the bottom and at the top of the Great Limestone, background levels of both elements are at or below the concentrations discussed above for average carbonates of 9 ppm for lead and 20 ppm for zinc.

As can be seen in Figure 8.20, however, lead concentrations do increase within the upper beds. A 12 period moving average trend line for lead was found to be difficult to determine as it follows the concentrations closely and is therefore not shown in Figure 8.20. A 12 period moving average trend line for zinc is easier to follow and is therefore included. It is possible to pick out two and a half to three

cycles in the 12 period moving average trend line for zinc; however, it is not as convincing as for the other elements discussed above.

8.4.11. Carbon-Sulphur-Nitrogen (CSN) analysis.

Unlike the analysis for the previously mentioned elements, which were sampled throughout the full height of the Great Limestone, the CSN analysis covers only 8 metres of the limestone from approximately 6 metres above the base to approximately 14 metres above the base. The sampling method also differed in that each sample was the result of collecting drill powder from sample positions at 5 centimetre intervals throughout the 8 metres. For these reasons it has proven very difficult to compare the results of the CSN analysis with the results of the previously discussed elements and where this has been attempted the relevant sections of the 12 period moving average trend lines for $\delta^{13}C$, Ba/Ca and molar Sr/Ca have been used for comparisons with organic carbon and C/N ratios.

8.4.12. Total carbon

The total carbon analysis gives an average of 11.72 wt % with a range between 10.72 wt % and 12.51 wt % with a slight fall in concentration over the 8 metres. 2 large cycles and 1 small cycle are visible within the 12 period moving average trend in Figure 8.21 from approximately 6.8 metres to 9.4 metres, 9.4 metres to 10.5 metres and 10.5 metres to the top.

Within bed changes in concentration vary from 0.16 wt % to 1.6 wt % with the greatest change in concentration being at approximately 11.5 metres. Even though some large changes in concentration occur at bedding planes, stylolites and thin mudstones, they are not limited to these as a large increase in concentration also occurs away from bedding and stylolites at approximately 8.8 metres. Many rises in concentration occur just below and continue through the majority of the bedding planes and stylolites.

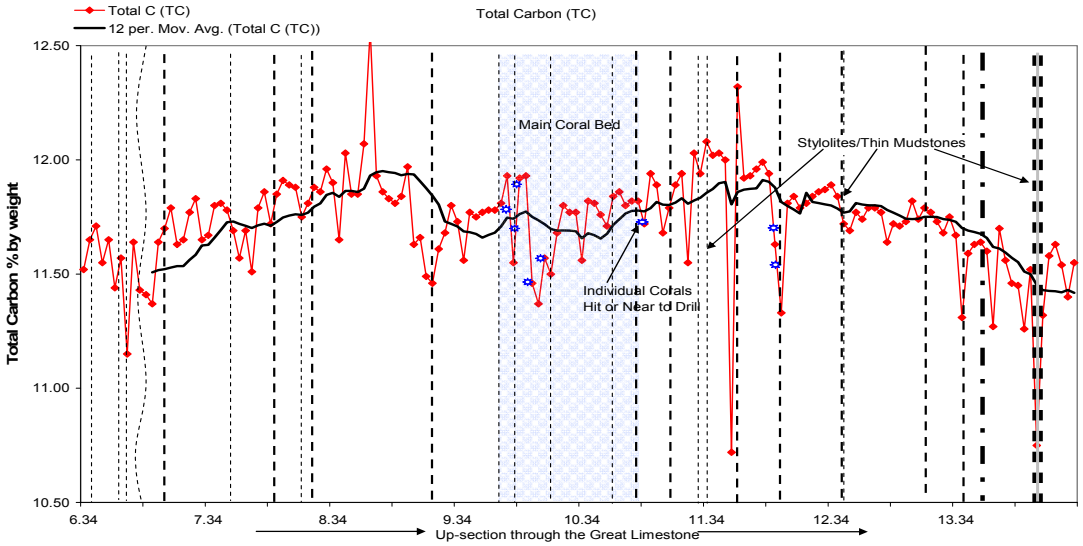

Figure 8.21. Total Carbon also showing the positions of bedding planes, stylolites, thin mudstones and the positions of individual corals hit by or near to the drill site.

Diester-Haass *et al*. (1992) and Meyers (1994) suggested that an inverse relationship between organic carbon and inorganic carbon reflected varying dissolution of $CaCO_3$ by dissolved CO_2 generated by oxidation of the organic carbon. A moderately negative correlation of –0.5 exists between organic carbon and inorganic carbon within the Great Limestone analysis, which may indicate that little $CaCO_3$ dissolution by CO_2 occurred. However, it would also be expected that diagenesis of organic material would have occurred in any bioturbated surface layers of the sediment and this would have affected organic carbon content.

8.4.13 Inorganic carbon

It is assumed in this analysis that all inorganic carbon measured in the samples is in the form of calcium carbonate ($CaCO_3$) sourced from dissolved bicarbonate. Inorganic carbon concentration averages at 11.55 wt % and ranges between 10.24 wt % and 11.94 wt %. It is apparent from a comparison of Figures 8.21 and 8.22 that the majority of the total carbon is, as to be expected in a limestone, consisting of inorganic carbon. The inorganic carbon concentration equates to an average of 96.24% $CaCO_3$ with a range of 85.3% to 99.46% which is close to that calculated above from the calcium concentrations.

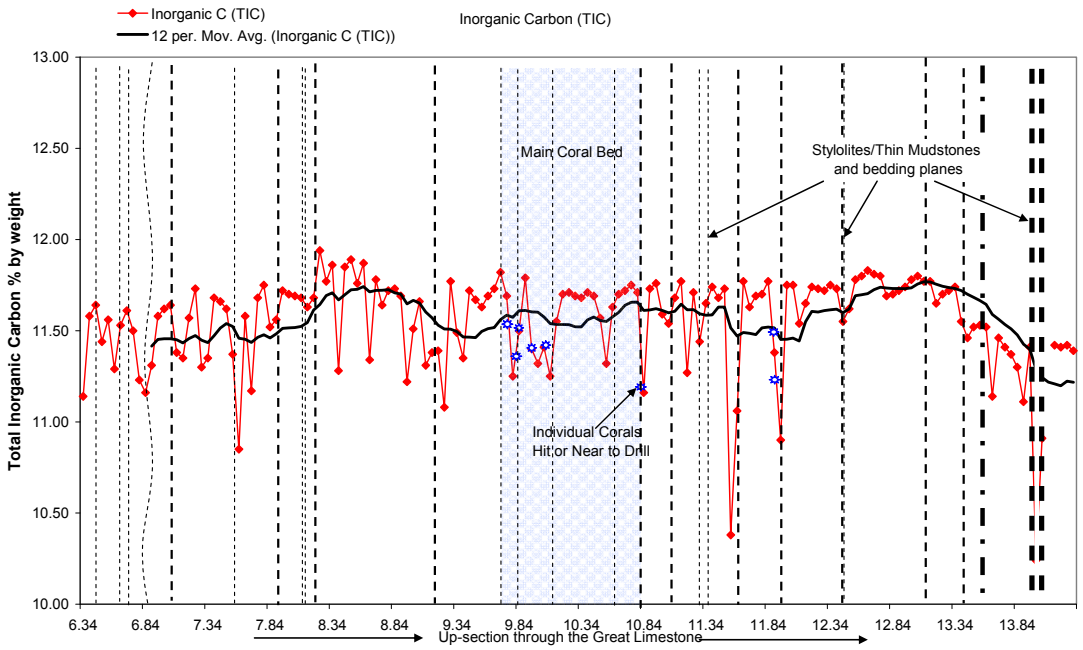

Figure 8.22. Inorganic Carbon also showing the positions of bedding planes, stylolites, thin mudstones and the positions of individual corals hit by or near to the drill site.

The 12 period moving average trend line in Figure 8.22 picks out 2 large cycles, between 7.5 to 9.4 metres and 11.9 metres to the top, and 2 smaller cycles between 9.4 to 10.4 metres and 10.4 to 11.5 metres. Within bed changes in concentration vary from 0.5 wt % to 1.59 wt % with the greatest change in concentration being at approximately 11.5 metres. Up to approximately 10.5 metres generally there is a rise from just below the top of a bed which continues through the bedding plane and continues into the lower section of the next bed. The upper beds, on the other hand, generally exhibit the opposite, i.e. a fall from just below the top of a bed which continues through the bedding plane and continues into the lower section of the next beds.

As the inorganic carbon is assumed to be in the form of $CaCO_3$, it is probable that the concentration changes are the result of productivity cycles; however, see Section 8.4.4. Interestingly, the greatest inorganic carbon concentrations do not correspond to the positions of the coral/brachiopod biostromes; they correspond closer to areas of increased bryozoans and the algae *Calcifolium bruntonense*.

8.4.14 Organic carbon

Organic carbon concentration averages at 0.2 wt % and ranges between 0.02 wt % and 1.26 wt %. The 12 period moving average trend line in Figure 8.23 picks out 3½ cycles, between 7.0 to 9.5 metres, 9.5 to 10.5 metres, 10.5 to 13 metres and 13 metres to the top. Within-bed changes to concentration vary from 0.13 wt % to 1.2 wt % with the greatest change in concentration being near to 12 metres. No obvious trends can be picked out within beds. However, many beds generally exhibit a rise in concentration towards the bedding planes possibly suggestive of increased marine organic matter production or alternatively an increase in land-derived organic matter, or an association with terrigenous material.

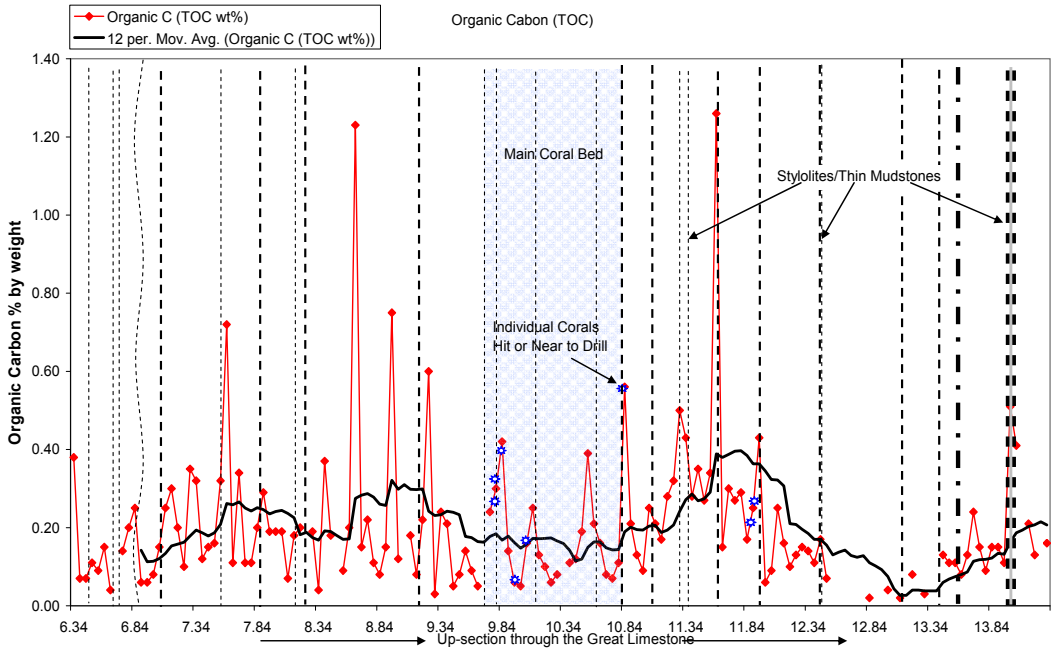

Figure 8.23. Organic Carbon also showing the positions of bedding planes, stylolites, thin mudstones and the positions of individual corals hit by or near to the drill site.

8.4.15 Sulphur

Sulphur concentrations are very low, averaging at 0.0042 wt % and range between 0.0003 wt % and 0.0152 wt %. Many gaps exist within the data due to levels below the detection limit of the instrument.

The 12 period moving average trend line in Figure 8.24 picks out 3½ cycles, between 7.0 to 9.75 metres, 9.75 to 11 metres, 11 to 13 metres and 13 metres to the

top. Within bed changes of concentration vary from 0.003 wt % to 0.013 wt % with the greatest change in concentration being near to 8.5 and 11.5 metres.

No obvious trends can be picked out within beds; however many beds generally exhibit a rise in concentration towards the bedding planes possibly suggestive of increased land-derived organic matter. There is very little correlation between sulphur and organic carbon with a correlation index of 0.05 and between sulphur and nitrogen with a slightly better, but still very poor, index of 0.11. The low levels of sulphur (and iron, Figure 8.2), together with the lack of evidence for anoxic conditions (Section 8.4.6), would suggest the formation of iron sulphide were unlikely to have occurred, and this is further confirmed by petrographic study.

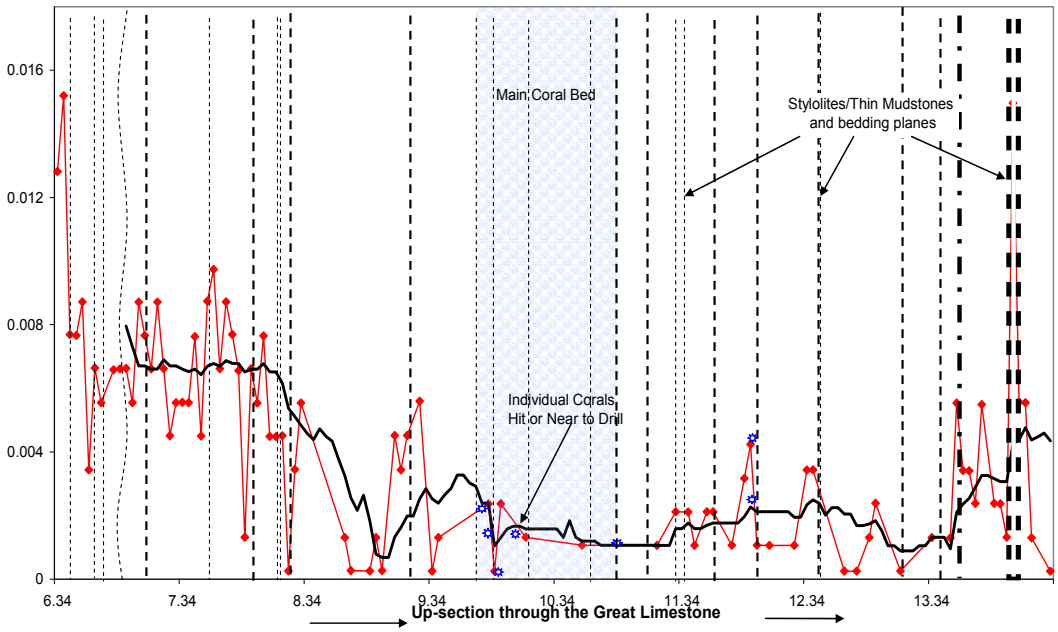

Figure 8.24. Sulphur also showing the positions of bedding planes, stylolites, thin mudstones and the positions of individual corals hit by or near to the drill site.

8.4.16. Nitrogen

Nitrogen concentrations are low, averaging at 0.028 wt % and range between 0.016 wt % and 0.086 wt %. Gaps exist within the data due to levels below the detection limit of the instrument or possibly errors in analysis.

The 12 period moving average trend line in Figure 8.25 picks out 3½ cycles, between 6 to 8.75 metres, 8.3 to 11 metres, 11 to 13 metres and 13 metres to the top. Within bed changes to concentration vary from 0.003 wt % to 0.034 wt % with the greatest change in concentration being at approximately 14 metres. It can be see that there is a close correlation between the 12 period moving average trend lines for nitrogen and organic carbon suggesting a probable similar source, i.e. river input; however, the source of the carbon and nitrogen could also be marine organic carbon from plankton.

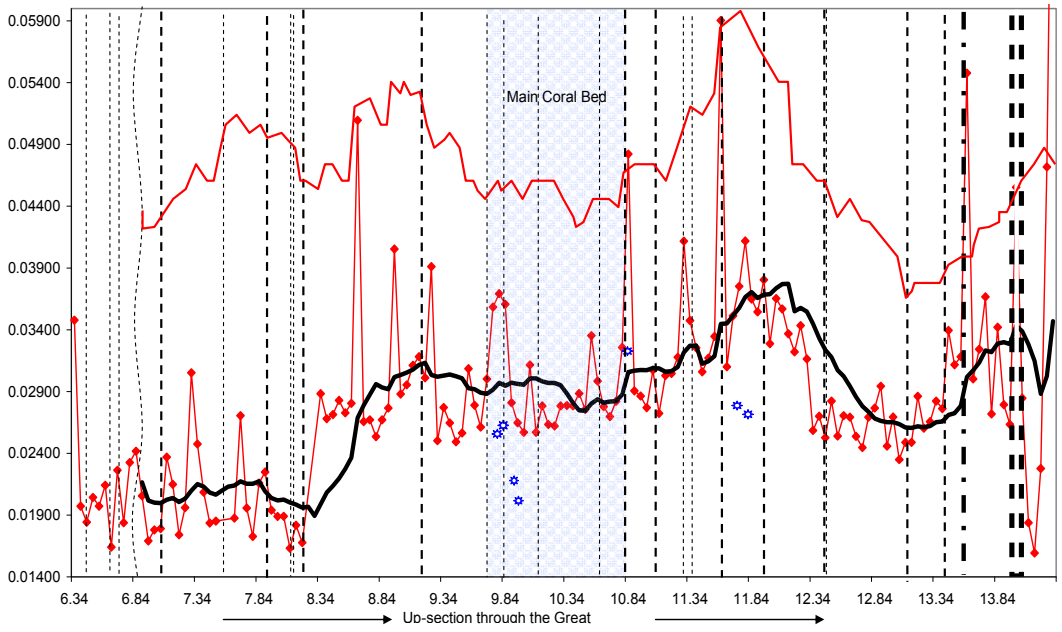

Figure 8.25. Nitrogen concentrations together with 12 period moving average trend lines for nitrogen (black) and organic carbon (red). Note organic carbon not to same vertical scale.

8.4.17. Carbon/nitrogen ratios

Preservation of organic carbon within sediments is dependant upon factors such as organic carbon concentration and sedimentation rate. Increased burial may enhance preservation but this is questionable (see Ricken, 1991 for discussion). Other factors are cementation and dissolution rates, water depth, oxygen content of the sediment and bacteria present within the sediment column. Despite any losses of organic matter during early diagenesis, bulk identifiers of organic matter sources such as C/N ratios and $\delta^{13}C$ appear to undergo little change (Meyers, 1994; Mackie *et al.*, 2005). The degree of diagenesis of organic matter in seawater and sediments depends,

to a large extent, upon the occurrence of lignin and cellulose, which are particularly susceptible to diagenetic alteration, and the marine fauna. In particular, algae contain no cellulose and have C/N ratios less than 20 and usually between 4 and 10. Sediments with organic content less than 3% are believed to undergo little diagenetic alteration (Meyers *et al*., 1993, Mackie *et al*., 2005). Therefore, with a maximum organic carbon concentration of 1.26%, it would be expected that diagenetic alteration of the organic content of the Great Limestone would be very small. However, as it is expected that the sediment was laid down under oxic conditions some oxidation of organic carbon would be expected within both the water column and at/within the sediment surface.

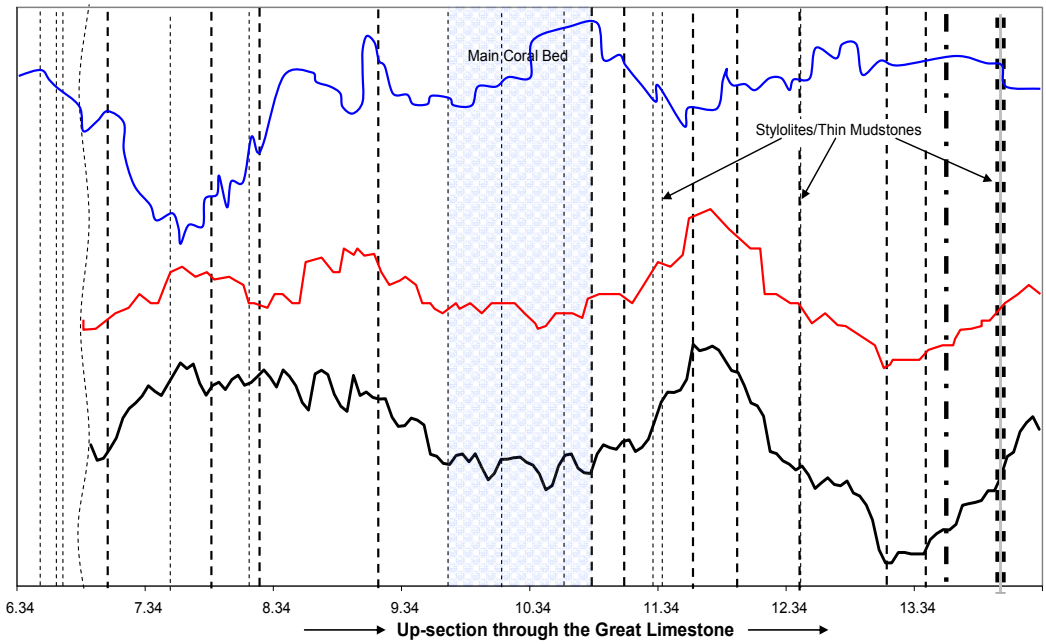

Figure 8.26. 12 period moving average trend lines for C/N (black), organic carbon (red) and $\delta^{13}C$ (blue). Note not to same vertical scale.

The analysis of the C/N ratios within the Great Limestone shows a large range between 0.1 and 24.1 with an average of 6.5 and median of 5.6 falling generally within the range for marine sources (Meyers 1994); interestingly there are only 2 points which exceed a C/N ratio of 20, one of which is near to 8.8 metres (ratio of 24.1) and the second is on a bedding plane (ratio of 21.3).

Figure 8.26 is an amalgamation of the 12 period moving average trend lines for C/N (black) and organic carbon (red) together with the relevant section of the trend for $\delta^{13}C$ (blue). The 12 period moving average trend line for C/N follows very closely that for organic carbon; however, it only contains 2½ cycles. An increase in marine productivity typically results in heavier (more positive) $\delta^{13}C$ values, and if under conditions of limited nitrogen availability, elevated C/N ratios may also be expected (Meyers 1992; Meyers 1994). However, increases in $\delta^{13}C$ (more positive) values and C/N ratios, may also be associated with increased river input.

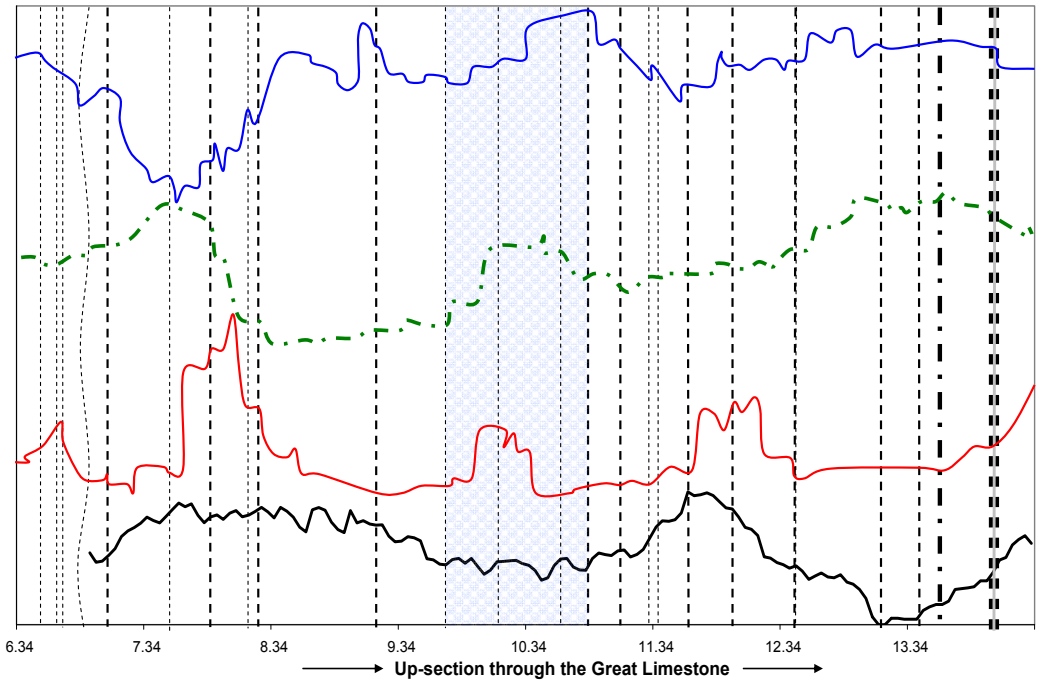

Figure 8.27. 12 period moving average trend line for C/N (black) together with the relevant sections of the 12 period moving average trend lines for Ba/Ca (red), molar Sr/Ca (green dashed) and $\delta^{13}C$ (blue). Note not to same scale.

Figure 8.27 is an amalgamation of the 12 period moving average trend line for C/N (black) and the relevant 12 period moving average trend lines for Ba/Ca (red), molar Sr/Ca (green dashed) and $\delta^{13}C$ (blue). In Sections 8.3.4 and 8.3.5, barium and strontium have been assessed with regard to their concentrations being related to marine productivity cycles and these are assessed further in this section together with C/N ratios and $\delta^{13}C$.

It is interesting to note that highs are visible in the trend lines for Ba/Ca, molar Sr/Ca and $\delta^{13}C$ within the area defined as the main section of the coral biostromes (note other smaller coral biostromes occur above this) and this would tend to confirm association with productivity. The C/N ratio on the other hand, shows a low in this area suggesting this is not associated with productivity and may in fact be associated with river input. However, a moderately high plateau is visible in the nitrogen trend in Figure 8.25 which may be resulting in a suppression of the C/N ratio.

Other highs in Ba/Ca and molar Sr/Ca are visible around 7.34 to 8.34 metres above the base which are associated with a move from a low to an increase in $\delta^{13}C$ and a high in C/N; these areas, and slightly above, are also associated with increases in bryozoans, *Calcifolium bruntonense*, *Girvanella*, and crinoids. Changes in productivity may be associated with changes in river and/or nutrient input and to a certain extent, these changes can be observed in the trends. However, it is also obvious, that the cause of the changes to productivity and the role of carbon, sulphur and nitrogen are in fact very complicated and not easy to distinguish in these plots.

8.5. Bed-by-bed concentration changes

Bedding architecture has been associated with rhythmic environmental changes on a millennial scale resulting from many different causes such as temperature changes (Huls and Zahn, 2000), freshwater/river run off and input (Noren *et al*., 2002, Tucker *et al*., 2009) and sea-level changes (Potter *et al*., 2004, Tucker *et al*., 2009). The trace element concentration and changes within beds and at bedding planes in the Great Limestone are complicated and difficult to assess.; However, it is thought that changes in humidity/aridity cycles, freshwater/river run off and input and sea-level fluctuations may be the cause of element changes within the beds of the Great Limestone.

Environmental changes such as sea-level rise and fall could both affect influx of terrestrial material to the marine environment with a sea-level fall cutting down into coastal sediments and transporting them sea ward, while a sea-level rise would

rework existing coastal deposits. Both could result in an increase in nutrient availability to the environment resulting in more advantageous conditions being available for carbonate production. Alternatively, a sea-level rise or fall may also result in turbidity changes disadvantaging carbonate production. Increases in aluminium, silicon, iron, manganese and barium could, therefore, result from both down cutting and transportation sea ward or reworking of coastal-plain sediments.

To visualise the changes throughout the beds they are presented in Figures 8.28 to Figure 8.34. At the base of many of the beds decreases can be seen in calcium carbonate and this generally increases towards the centre of the bed (see also Section 7.2.4 and the discussion from Frank *et al*., 1999). These decreases in calcium carbonate at bedding planes are in many cases associated with increases in aluminium, iron, magnesium, barium and strontium; this pattern follows evidence seen in the field such as the lower beds tending towards having shaley tops and bottoms. Nearly all beds, to a greater or lesser extent, show increases in calcium carbonate directly above the bedding plane and within the middle of the bed. However, there is not always a clear association with element input, whether this association between $CaCO_3$ and bedding is solely due to diagenesis as discussed in Chapter 6, Section 7.2.4 or is due to a primary cause is discussed further here.

Looking at the concentration of the elements on a bed-by-bed basis, there are no apparent continuous patterns. For many of the elements, within-bed changes in concentration vary by only a few ppm around the average; however, above bed 15 (11 metres) within-bed variations in concentration usually start to increase substantially (Sections 8.4.1 to 8.4.17). These within-bed increases in concentration above bed 15 follow the increase in occurrence of a shaley top and shaley bottom seen in many of the upper beds and the mudstone partings seen in the field as the Tumbler Beds and the mudstone above the Great Limestone are approached.

Analysis of the changes in elements throughout the thickness of the Great Limestone and in particular on a bed-by-bed basis shows a complicated number of

associations. The elements within the first 6 beds generally show a close positive relationship between Al, Mg, Ba, Sr and $CaCO_3$ with small increases in the elements being beneficial to $CaCO_3$ production. Above bed 6 $CaCO_3$ and Sr begin to react less positively with changes in the other elements; increases in Al, Mg and Ba can be seen, in some cases, to result in a reduction in $CaCO_3$ and Sr. This negative association becomes more obvious as you move up through the beds towards the top of the limestone.

Between beds 11 and 19, CSN analysis (Sections 8.4.11 to 8.4.17) has also been carried out which also shows a complicated pattern with the elements and $CaCO_3$. Within bed 12, near to the second stylolite, increases in TOC and N are associated with an increase in $CaCO_3$ while Al, Fe, Mg and Ba fall or remain fairly constant; this also occurs at the base of bed 14 and within the middle of bed 19. Within the middle of bed 17, however, an increase in all elements also results in a rise of $CaCO_3$. Above bed 20 the negative association of the elements and $CaCO_3$ is seen to be the strongest.

To a certain extent the patterns visible within the data are dependant upon the general random method used for the sampling. Nevertheless, there are remarkable visual positive and negative correlations between the geochemical data and the position of many of the bedding planes and stylolites within beds. Considering Bed 1 in Figure 8.28, visually it can be seen that calcium carbonate is both negatively and positively correlated with the other elements. However, up to approximately 0.3 metres, the elements are generally negatively correlated with calcium carbonate, probably due to the initial. Where calcium carbonate and all elements rise rapidly at the bedding planes above 0.5 metres this could imply an association with an input of beneficial nutrients during an increase in river input and/or temperature changes.

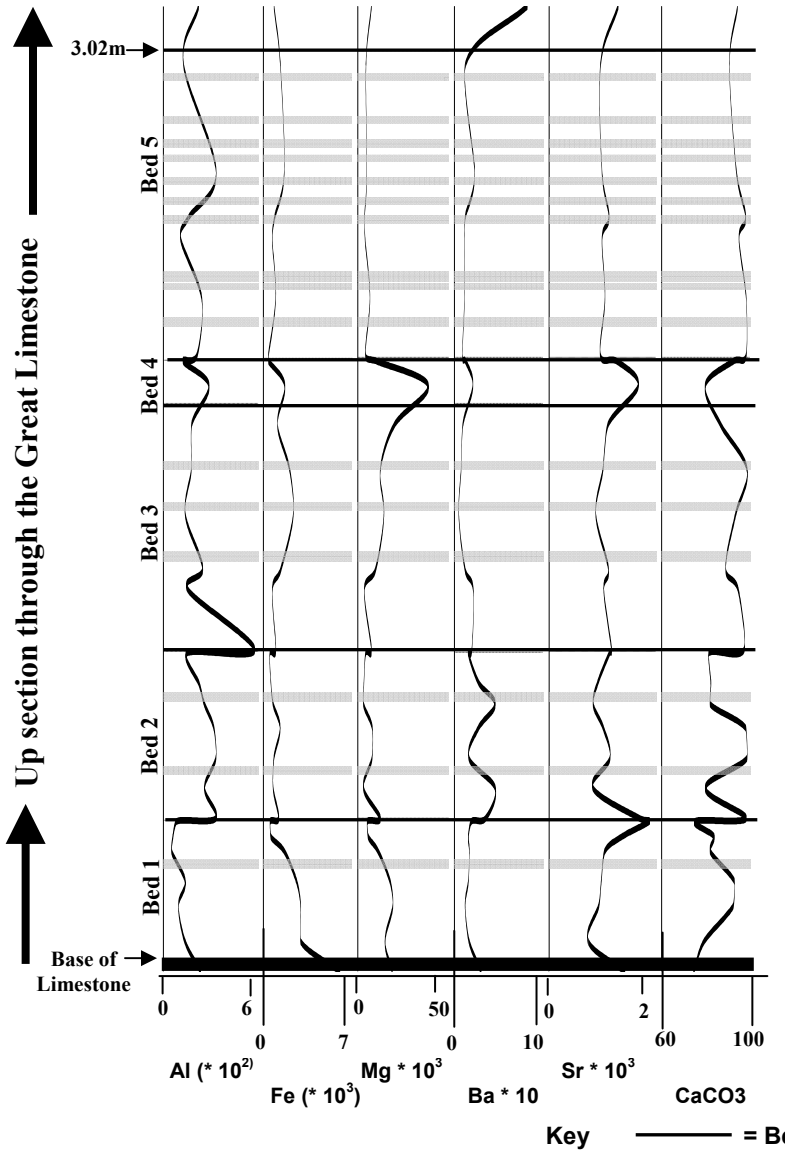

Figure 8.28. Geochemical changes within Beds 1 to 5

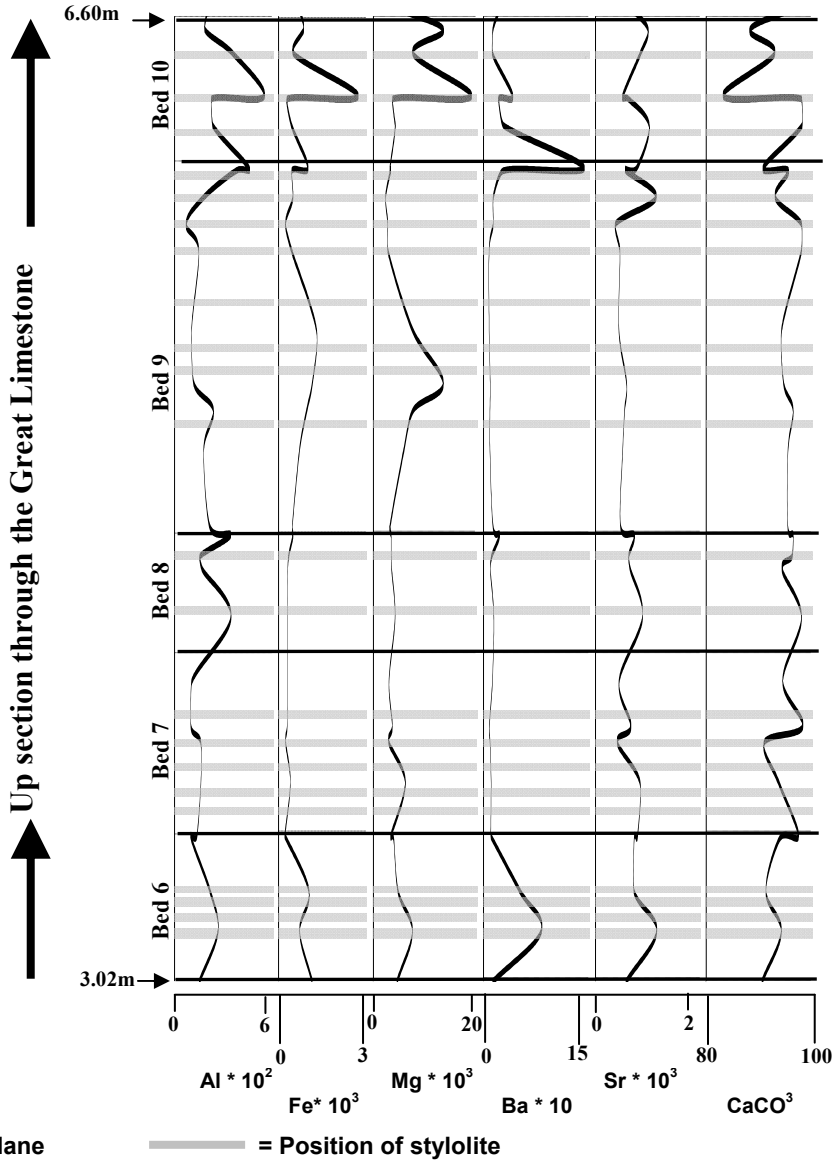

Figure 8.29. Geochemical changes within Beds 6 to 10

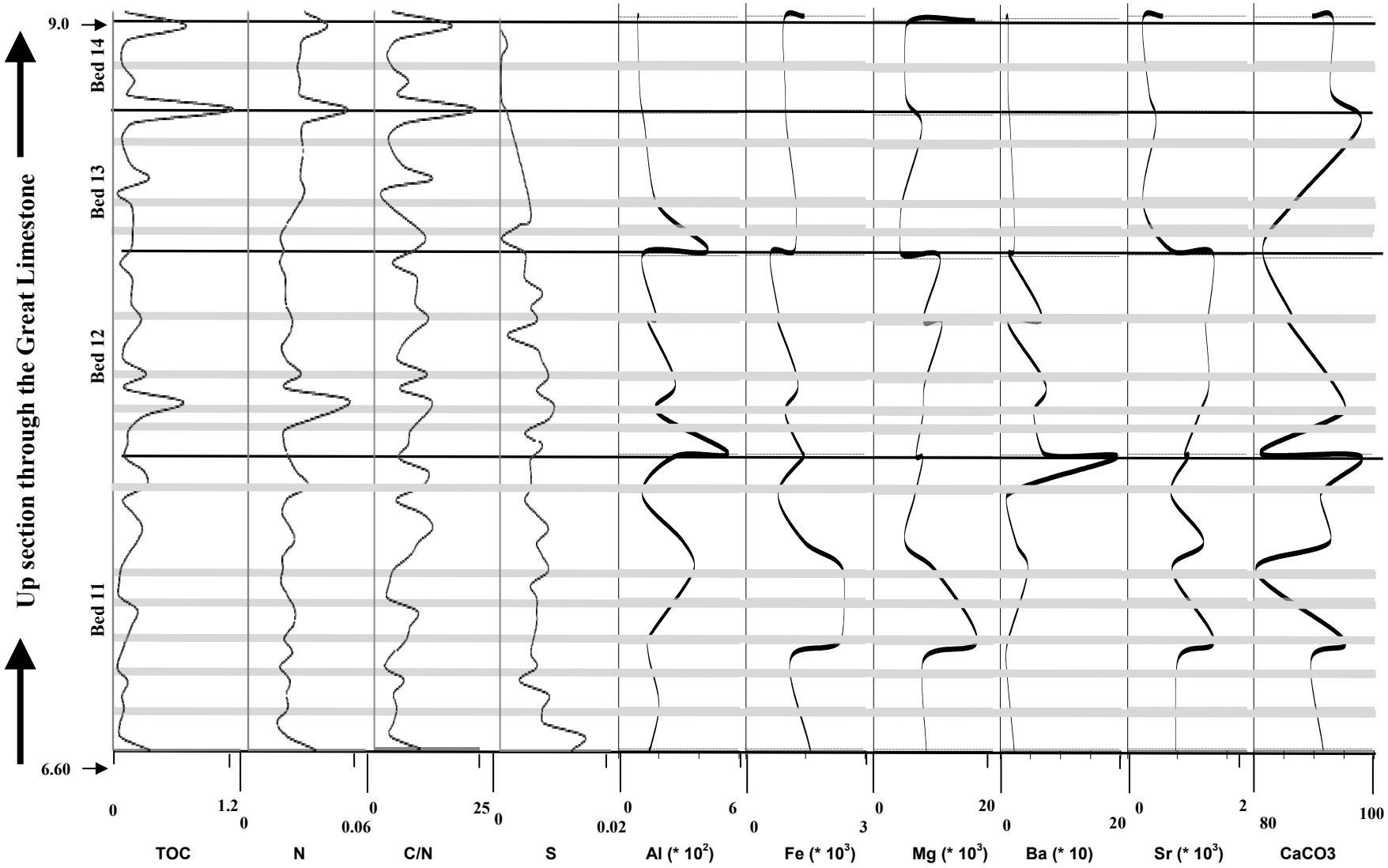

Figure 8.30. Geochemical changes within Beds 11 to 14

Key ——— = bedding plane = position of stylolite

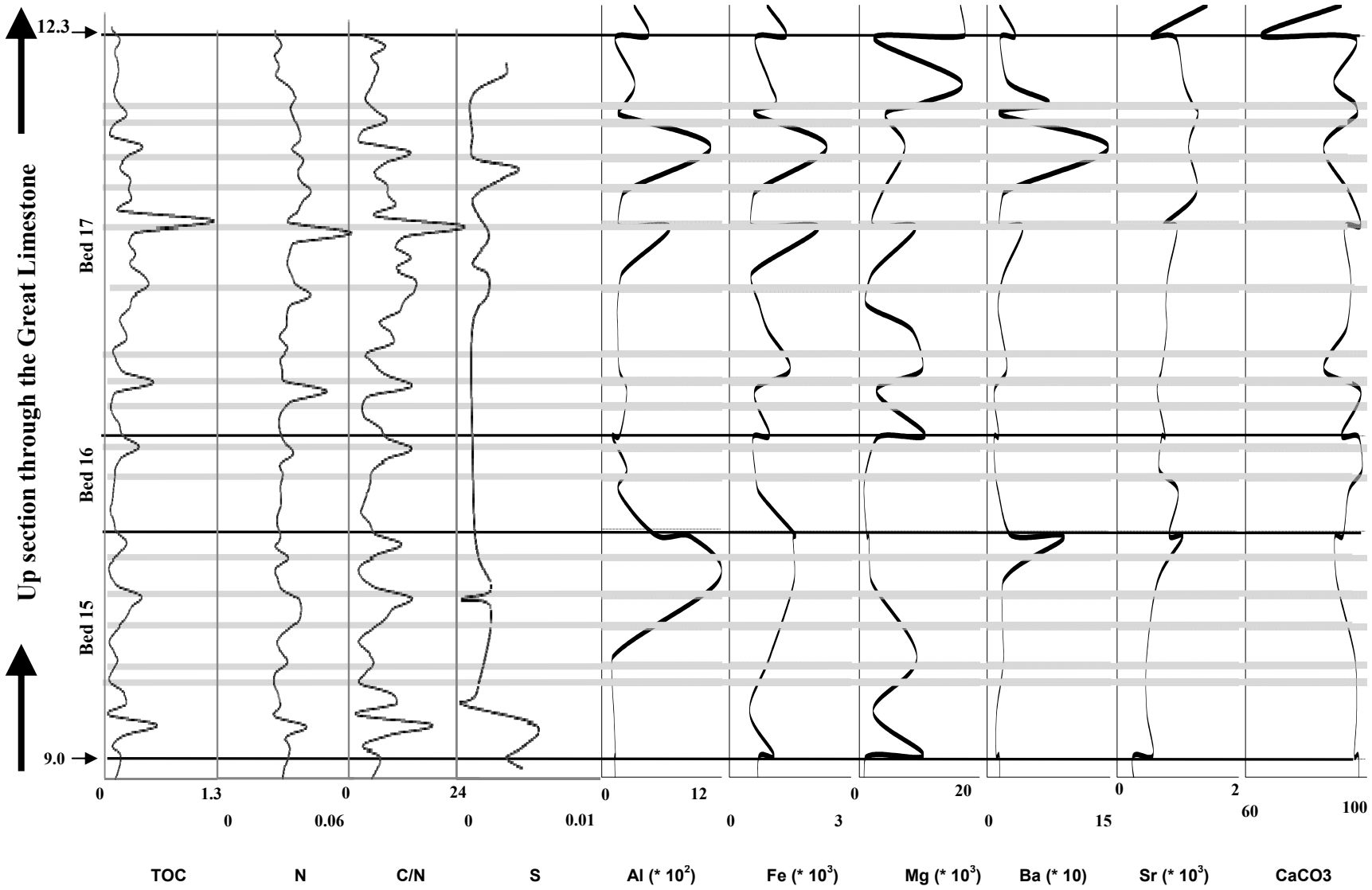

Figure 8.31. Geochemical changes within Beds 15 to 17

Key ——— = bedding plane ▬ = position of stylolite

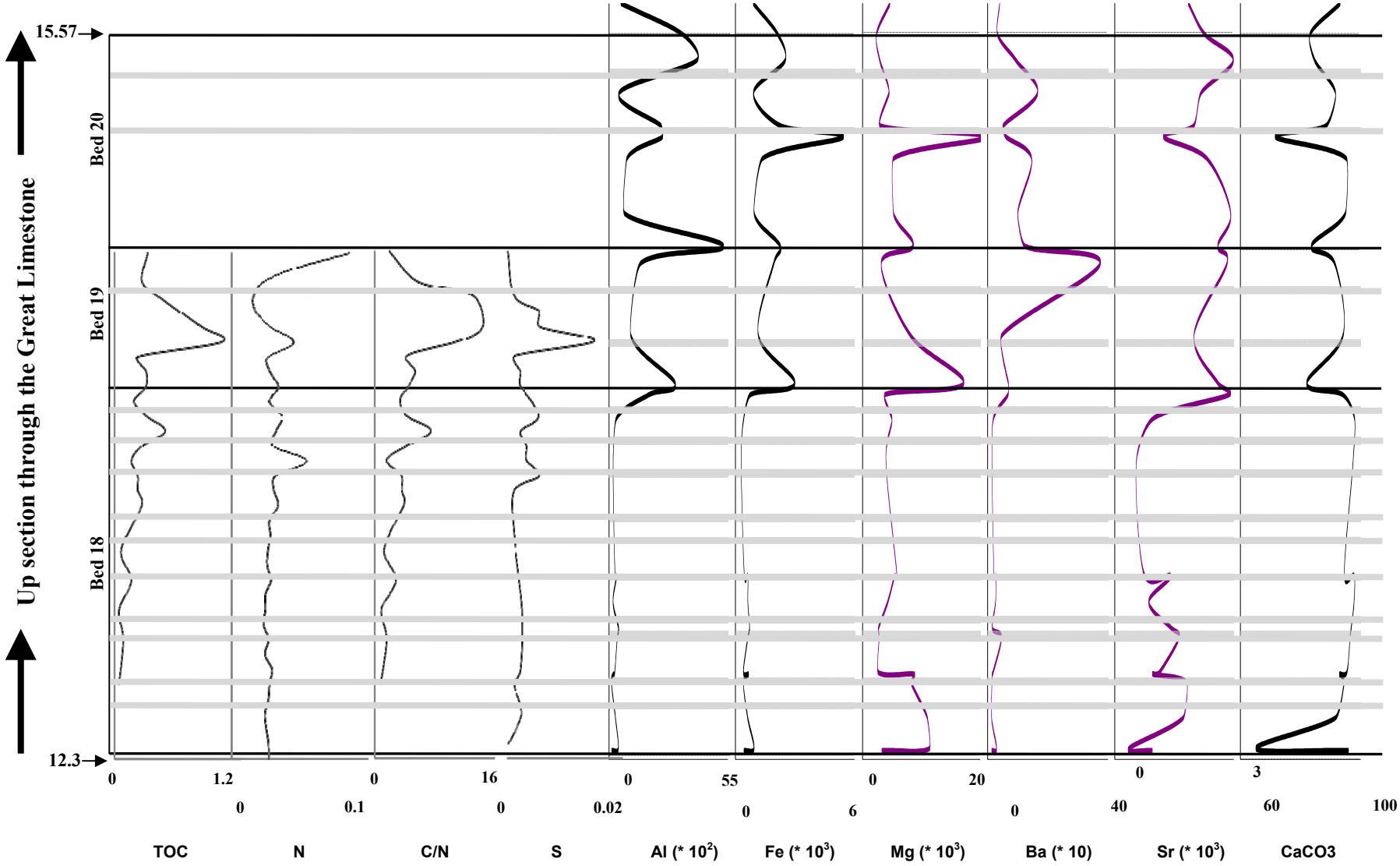

Figure 8.32. Geochemical changes within Beds 18 to 20

Key ——— = bedding plane ▬ = position of stylolite

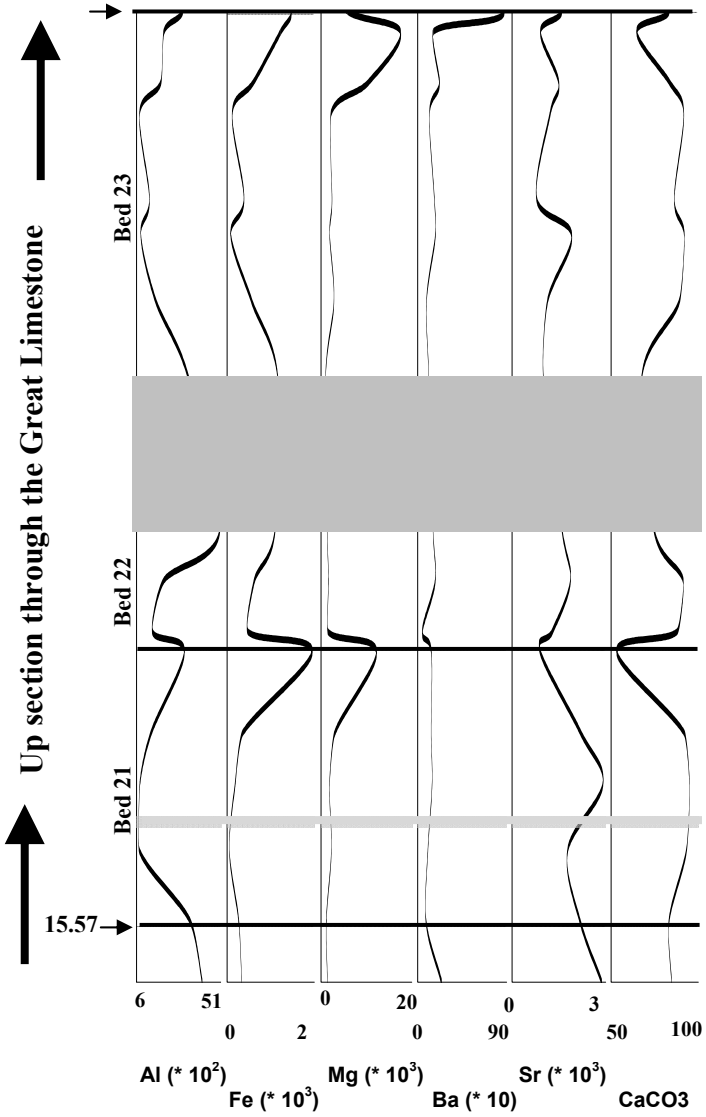

Figure 8.33. Geochemical changes within Beds 21 to 23

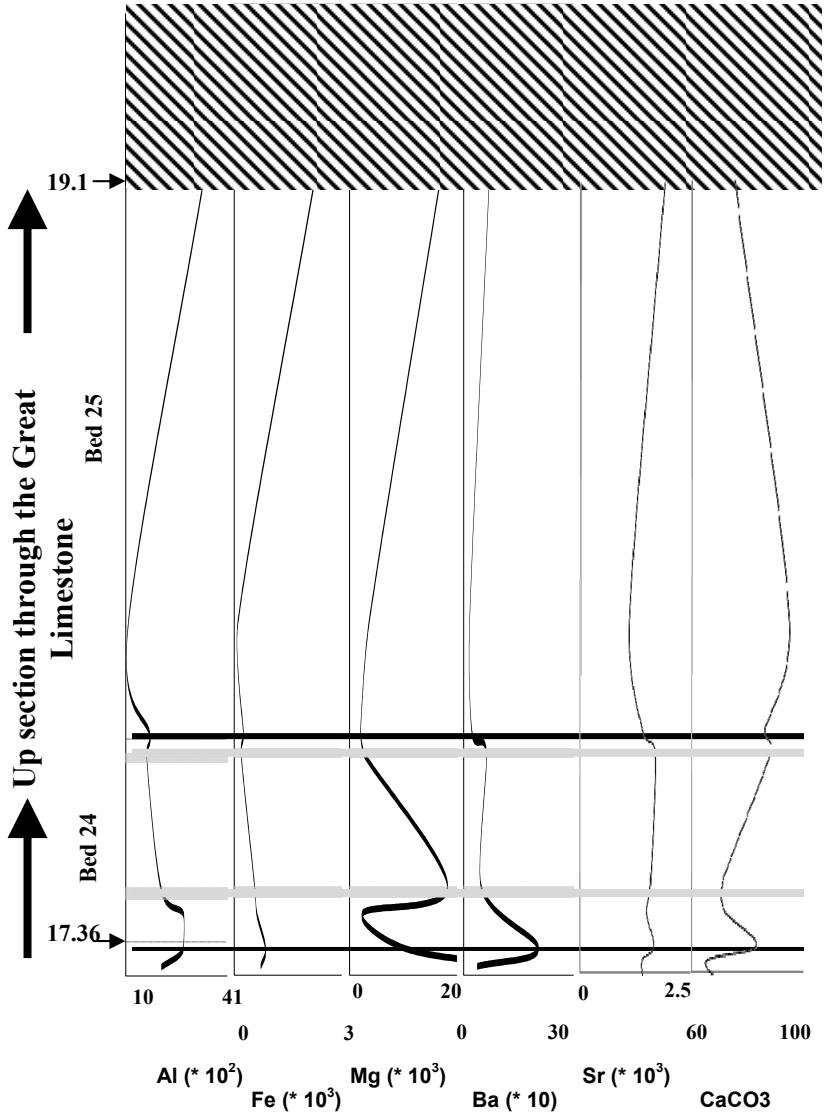

Figure 8.34. Geochemical changes within Beds 24 to 25

Key = Bedding Plane = Stylolite = Large Mudstone = Mudstone above Great Limestone

If the changes within concentrations of Al, Si, Fe, Mn and Ba within beds and at bedding planes are associated with increased freshwater/river input this may be expected to result in changes to carbonate productivity through nutrient, salinity and turbidity alterations; increased terrigenous material at bedding planes, as seen in Figure 8.28 to Figure 8.34 may therefore be expected. An alternative to the freshwater/river causation, is increases and reductions in calcium carbonate sedimentation together with a steady state input of terrigenous material (Ricken, 1991; Fairbairn, 2001; Tucker *et al*. 2009), i.e. there is a steady background deposition of terrigenous material while carbonate production varies due to environmental factors such as sea-level rise or fall and/or temperature fluctuations. Therefore, even though a bed by bed correlation of calcium carbonate against the other elements may prove to be instructive the actual causation may be difficult to assess.

There does not appear to be any simple patterns visible within the major and trace element analysis of individual beds and calcium carbonate production. It does become apparent, however, that approximately 14 metres above the base of the Great Limestone (beds 18-19), major and trace elements increase substantially which results in changes to calcium carbonate production.

Interestingly strontium appears to have a close affinity with Al, Fe, Mg, Ba and calcium carbonate at bedding planes throughout the limestone. This could be regarded as being at variance with Chapter 6 where it was suggested that the Sr changes at bedding planes could be associated with diagenesis rather than original deposition. The close correlation of Sr with Al, Fe, Mg, Ba and calcium carbonate at bedding planes would therefore imply changes are more likely to be associated with original deposition rather than diagenesis.

8.6 Periodicity of events

Within Chapter 7 cyclicity of the $\delta^{13}C$ and $\delta^{18}O$ results was assessed using depositional time periods of 34, 45 and 100 kyr for the Great Limestone and this has

also been carried out for the major and trace elements Al, Fe, Sr, Mg and $CaCO_3$ using the statistics program PAST (Hammer *et al*. 2001). Table 8.3 gives the time periods of the major peaks within each Time Series

Al 34 kyrs	Al 45 kyrs	Al 100 kyrs	Fe 34 kyrs	fe 45 kyrs	fe 100 kyrs	Sr 34 kyrs	Sr 45 kyrs	Sr 100 kyrs	Mg 34 kyrs	Mg 45 kyrs	Mg 100 kyrs	CaCO3 34 kyrs	CaCO3 45 kyrs	CaCO3 100 kyrs
45	60	133	45	60	133	39	51	114	39	51	114	39	51	114
17	23	50	17	23	50	14	19	42	4	6	13	15	20	44
11	15	33	10.4	14	32	7	10	22	4	5	11	2	3	7
1	1.31	2.92	2.4	3.2	7	1.3	1.8	4	3	5	10	2	2.4	5.3
0.54	0.71	1.57	1	1.3	3	0.9	1.2	2.6	3	4	9	1	1.3	3
						0.5	0.6	1.4	3	4	8	0.9	1.1	2.5
									3	3	7	0.8	1.1	2.4
									2	3	7			
									2	3	6			

Table 8.3 Time periods for the spectral analysis of Al, Fe, Mg, Sr and $CaCO_3$ using depositional time periods of 34, 45 and 100 kyr for the Great Limestone.

It is difficult to equate all of the peaks shown in Table 8.3 with regard to Milankovitch cycles. However, the first peaks within the analysis using 34 kyr are near to the obliquity orbital cycle time frame of around 34 kyr; the first peaks using 45 kyr are nearly double the obliquity orbital cycle. The second peaks using 34 and 45 kyrs are nearer to the 17 kyr to 21 kyr year precession cycle. Using the 100 kyr deposition period gives the first peaks of around the short eccentricity cycles and the second peaks near to obliquity. The remainder of the peaks shown in Table 8.3 are much less than the precession cycle values and some are near to the sub-Milankovitch Dansgaard–Oeschger (D–O) events and Bond cycles discussed in Chapter 7 of around 1.4 kyrs.

As discussed in Chapter 7, Time Series analysis has not resulted in any clear periodicity for the deposition of the Great Limestone. It may be that further analysis

may be undertaken in the future using different analysis methods such as the REDFIT algorithm (Schulz and Mudelsee, 2002), that may result in more acceptable estimates of the predominant frequencies.

8.6. Major and trace element geochemistry: Conclusion

The history of the Great Limestone has been assessed in this Chapter using major and trace element geochemistry and the data are shown to compare favourably with those for average carbonate rock types. The concentrations of the major and trace element data point towards the Great Limestone being relatively 'clean' with little terrigenous input and a high calcium carbonate concentration averaging around 92% with deviations from this level mainly within the lower beds, at the commencement of carbonate production after the initial flooding, and in the upper beds where river borne elements increase substantially. There is little sign of anoxic conditions prevailing. However, Chapter 5 did suggest acidic porewater conditions resulted in damage to the epitheca of some corals.

Correlations and comparison of trends imply a close relationship between the elements and river supply with temperature, humidity/aridity cycles being prevalent; however associations appear to change continuously throughout the thickness of the Great Limestone.

Increases of terrigenous material such as aluminium silicates (clays etc) to the area of deposition, possibly from prograding delta fronts, would have resulted in an increase in availability of many of the elements within the water column for substitution into the calcite lattice (though, perhaps, released later during diagenesis). The correlations between calcium carbonate and many of the elements point towards a likely source for the elements being from clays and POM. Increases in the concentrations of many of the major and trace elements above 14 metres and the negative correlations with calcium carbonate at bedding planes could be indicative of an effect of the higher clay content; this may well have led to lower carbonate production.

The manganese spikes and the lack of any correlation between iron, manganese and barium could be suggestive of the Great Limestone being deposited in oxic water conditions and this is further reinforced by the fossil content and diversity. The very high manganese spikes and high magnesium concentrations are likely, however, to be associated with diagenesis rather than from primary signals.

Whereas some trends are visible in the lower and upper beds on a bed-by-bed basis, commonly, within-bed concentration changes are confused. Within-bed concentration changes vary within a relatively few ppm of the average for the majority of the limestone; however, as the upper beds are approached the within-bed concentration changes generally show significant increases. Concentration spikes are visible throughout the Great Limestone for many of the elements and some correspond to pressure-dissolution seams, stylolites, swarms and bedding planes (discussed further in Chapter 9). Large concentration spikes show a general increase in number and amplitude as the upper beds are approached.

CSN analysis suggests little diagenesis of organic carbon may have occurred and therefore the results probably show an original signal. The low C/N value of 6.5 points towards the organic carbon being of a marine origin and not particularly influenced by terrigenous carbon input. Comparisons of CSN with $CaCO_3$, Ba and molar Sr/Ca with regard to productivity was generally inconclusive; whereas, comparisons with the major and trace elements and calcium carbonate, on a bed-by-bed basis, show both negative and positive correlations and suggest a complicated relationship with productivity and element source.

Time Series Analysis was carried out on some major and trace elements; however this proved to be inconclusive. It may be that further analysis using different analysis methods such as the REDFIT algorithm may prove to be more informative.

High strontium levels are regarded as being a relic of an original aragonitic sediment (Chapter 6); however, the close correlation between Mg/Ca and Sr/Ca ratios would suggest a mixed aragonite and high Mg calcite sediment.

A moderate negative relationship exists between $CaCO_3$ and some of the terrigenous major and trace elements suggesting, either, through nutrient supply, salinity or turbidity, some control existed over $CaCO_3$ production from the external terrigenous input.

To conclude, the major and trace element analysis points towards the Great Limestone developing within a relatively 'clean' and oxic marine environment with periods of increased terrigenous input throughout its formation. The majority of the major and trace elements discussed here show both negative and positive relationships to calcium carbonate suggesting a link between carbonate production and river input due to environmental changes in either temperature, humidity or aridity. The major and trace element analysis suggests; therefore, that control on carbonate production is linked to terrigenous input and subsequently to turbidity, temperature and/or humidity/aridity cycles.

9.0 Stylolites, acid insoluble material and bedding planes.

9.1. Introduction

Stylolites are thought to be an important part of the story with regard to the Great Limestone, especially in terms of determining the source of trace elements. As discussed below, stylolites are closely associated with changes in both the organic and inorganic geochemistry and the acid insoluble material, present within the limestone. The majority of the beds within the Great Limestone are punctuated by muddy bedding planes and partings, pressure-dissolution seams, stylolites and stylolite swarms, many of which are continuous over long distances, particularly within Teesdale and Weardale (Fairbairn, 1978, 1990, 1999) and many can be recognised within the area of the Stainmore Basin at Sleightholme Beck (953 105). Due to the continuous nature of some pressure dissolution seams within Teesdale and other areas of the Alston Block and Stainmore Basin, their presence can make the identification of some individual bedding planes extremely difficult and this is particularly true with regard to beds 13 to 14 and 17 to 18 where the boundaries can be particularly ill-defined in some locations.

With regard to the relationship between pressure dissolution features and bedding planes, it is a distinct possibility that in many cases the bedding planes have been enhanced by the effects of pressure dissolution, i.e. the limestone becomes more stylolitised as the bedding plane is approached. Simpson (1985) and Bathurst (1987) addressed this possibility in detail using studies of Carboniferous limestones in the UK.

9.2. Total acid insoluble material.

The acid insoluble material within the Great Limestone includes magnetite, clay minerals, particulate organic matter (POM), iron and manganese oxides. The insoluble residue does have a moderately strong correlation with iron at 0.65 (Table 6.1, Chapter 6). Thus the insoluble residue may be a proxy for the input of terrestrial material and the location of zones of high insoluble residue may have controlled the position of many of the stylolites in the limestone.

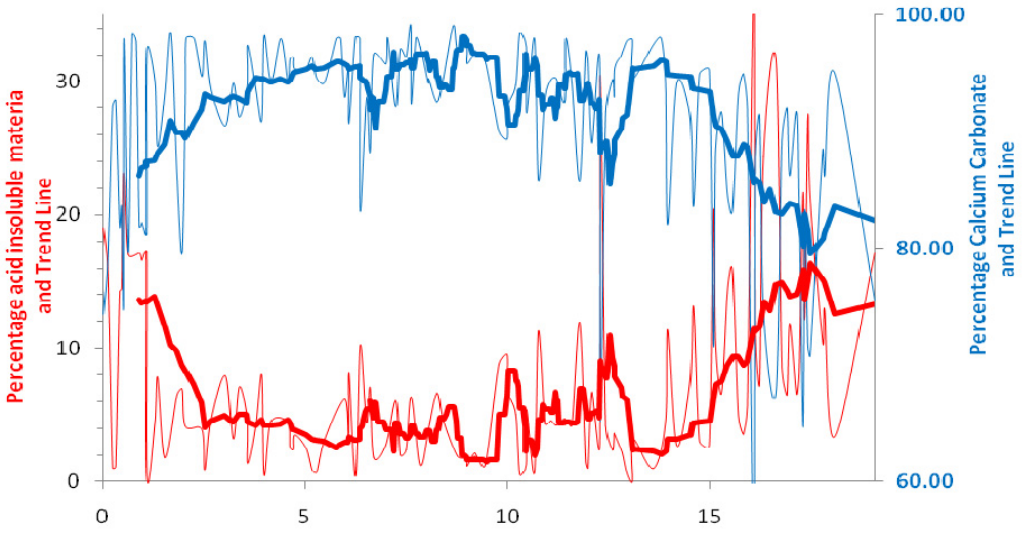

Figure 9.1. Comparisons of 12 period moving average trend lines for Total acid insoluble material (blue Line) and $CaCO_3$ (red Line).

Table 6.1 in Chapter 6 unsurprisingly shows a near-perfect negative correlation of -0.96 between calcium carbonate and acid insoluble material. As can be seen in Figure 9.1, the 12 period moving average trend lines are a near mirror image of each other. This near-perfect negative correlation together with the correlations between aluminium, silica and iron, and the acid insoluble material, of 0.71, 0.71 and 0.65 respectively, are suggestive of a close link existing between calcium carbonate production and river input, as discussed in Chapter 8.

9.3. Pressure-dissolution features and/or bedding planes.

As discussed above, the Great Limestone is punctuated by muddy bedding planes and pressure-dissolution features, many of which are continuous over large distances. The vertical distance between these features varies considerably between 0.03 metres and 1.1 metres throughout the thickness of the Great Limestone (Appendix G). Figure 9.2 is a plot showing how the distance between these features changes throughout the limestone, together with a 12 period moving average trend line. At least 4½ cycles of increasing and decreasing distances between stylolites are visible within the 12 period moving average trend line, with the first cycle up to approximately 3 metres from the base, the next

cycle up to approximately 6 metres, then up to 12 metres above the base, a very small cycle up to approximately 14 metres above the base and the last half cycle up to the top.

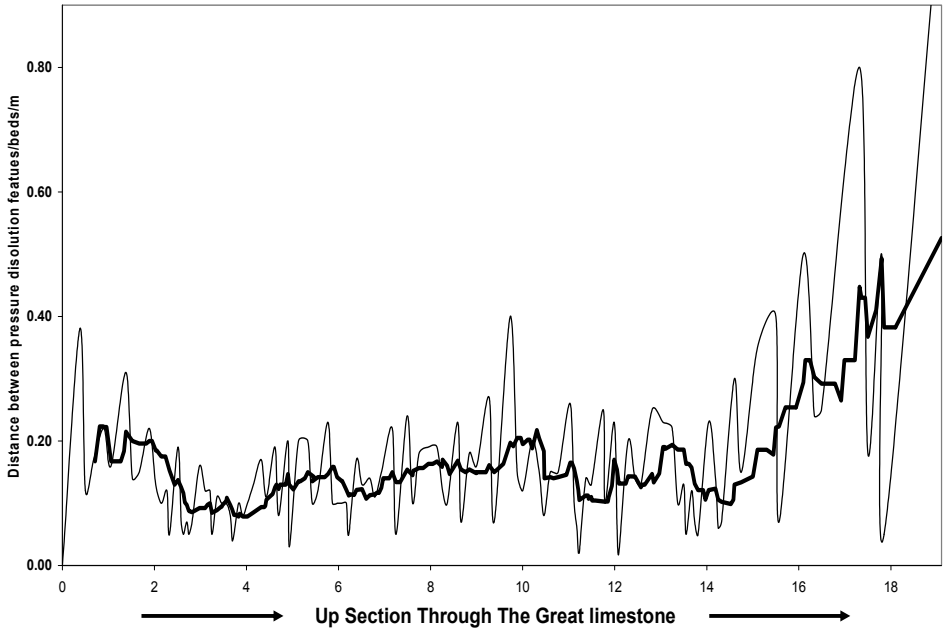

Figure 9.2. Distance between pressure dissolution features and/or bedding planes together with 12 period moving average trend line.

It is generally assumed that clay minerals exert a direct control on the formation of pressure-dissolution features and there is also evidence that differential cementation and differences in competency between adjoining layers due to compositional and facies changes are important too (Simpson, 1985; Bathurst, 1991). In the case of the Great Limestone, there is little change in composition/facies up through the limestone unit, so this is unlikely to be a major contribution to the presence of pressure dissolution features, but variations in the clay content of the limestone probably are. It is difficult to assess whether differences in cementation or compaction are important. The role of clay in the formation of fitted fabric, pressure-dissolution seams, stylolites and stylolite swarms is still unclear, as in certain circumstances clay also inhibits the formation of these structures by hampering cementation or enhancing pore-water flow (Bathurst, 1991). Certainly within the Great Limestone, the presence of clay appears to be intrinsic to the formation of these structures and, therefore, it may be expected that there will be a relationship between the percentage total acid

insoluble material and the distance between pressure-dissolution features and/or beds.

If the existence of pressure-dissolution features within the Great Limestone is related to clay content, then this relationship would suggest that, as terrigenous material (acid insoluble material) increases, then the distance between the pressure-dissolution structures and bedding planes would be expected to decrease; i.e., a negative relationship should exist. Conversely, it may be expected that as the 'cleanness' of the limestone increases (as the input of terrigenous material decreases and/or carbonate productivity increases) the distance between pressure-dissolution structures and bedding planes should increase, i.e. a positive relationship will exist between calcium carbonate and pressure-dissolution features.

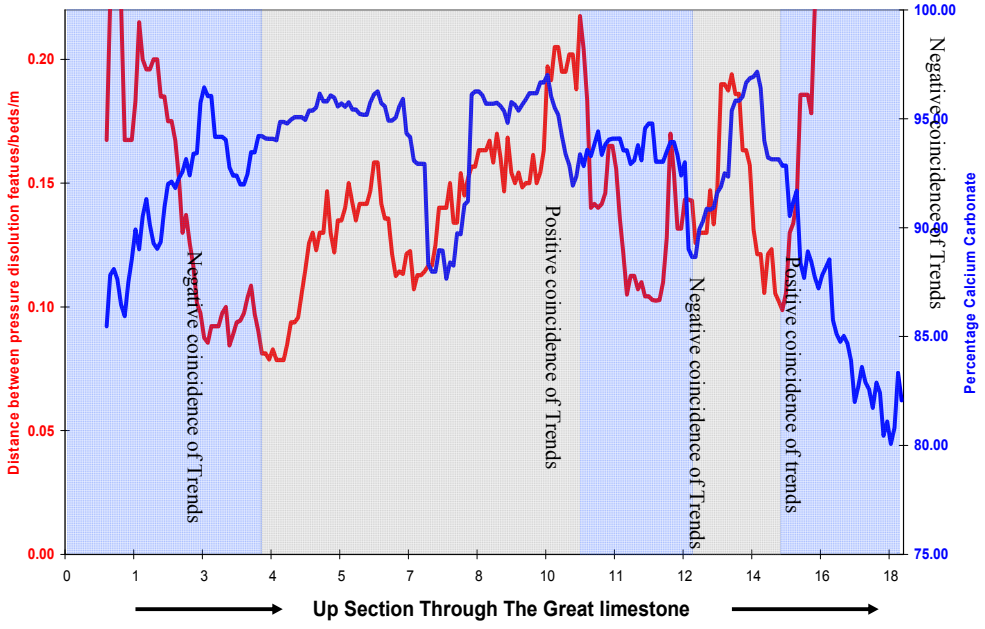

Figure 9.3. The 12 period moving average trend lines for distance to pressure-dissolution features and/or bedding planes (red line) and the percentage calcium carbonate (blue line) 'pushed together'. Note the positive (grey area fill) and negative (blue area fill) coincidence of trends.

Figure 9.3 shows the relationship between percentage calcium carbonate and the distance between pressure-dissolution features and bedding planes together with the 12 period moving average trend lines for both plots and this

figure shows that there is in fact strong positive coincidence of trends between approximately 4 metres to 10.5 metres and 12 metres to 14.5 metres above the bottom of the Great Limestone, although there are some 'lags'. As discussed above, this coincidence of trends would suggest that as calcium carbonate production increases, due to a decrease in terrestrial material, then the distance between pressure-dissolution features and bedding planes increases. Below 4 metres, between 10.5 metres to approximately 12 metres and above 14.5 metres (i.e. within the 'Tumbler Beds') there are generally negative coincidences. This suggests another mechanism or threshold exists in these areas controlling the propagation of pressure-dissolution features and calcium carbonate production. Interestingly, a greatest distance between bedding planes and pressure-dissolution features exists within the Tumbler Beds, even though here the percentage insoluble material is at a maximum. It may be; therefore, that there is a threshold above which increases in terrigenous/insoluble material, inhibits the development of pressure dissolution.

Even though it is difficult to analyse statistically the degree of diagenesis that has occurred within the Great Limestone, the Petrography section (Chapter 5) described the presence of pressure-dissolution 'micro-swarm' areas in some sections of the limestone. These are multiple, millimetre-spaced micro-stylolites seen only in thin section (see Bathurst, 1991 for a discussion). The above discussions with regard to the distances between pressure-dissolution features and bedding planes have not taken into account these 'swarm areas' due to the difficulty in recognition in the field. It is also possible that later diagenesis of the Great Limestone may have resulted in the loss of some of these 'micro-swarm' areas, which would have distorted the results. Even so, micro-swarms are usually associated with bedding planes and stylolite locations; therefore, further analysis of these would not be expected to change the discussion above.

On a bed-by-bed scale, the relationship between many of the trace elements and bedding planes has been discussed in Chapter 8 and the positions of stylolites was also noted. Stylolites can be seen within many of the beds and in

certain cases the positions of the stylolites can be seen to be associated with changes in the trace elements.

9.4 Conclusion

Bed changes within the Great Limestone are highlighted by mud/shale horizons, many of which are only millimetres thick and contain many stylolites. Bedding planes within the Great Limestone are regarded as forming at a time of increased mud/terrigenous material deposition. The stylolites, within recognised beds, have also formed due to increases in mud deposition. The possibility therefore exists for the positions of stylolites within beds to be poorly formed bedding planes of a higher frequency.

10.0 Summary of conclusions.

10.1. Introduction

The results of fieldwork and laboratory work presented in this thesis have been carried out to determine the effects of environmental factors, primarily driven by climate and eustasy, together with local tectonics on the formation of Yoredale-Type cycles (cyclothems) within the Viséan and early Namurian of the Carboniferous of north east England. The evidence has been provided through a 'top down' approach, i.e. from a discussion of the large scale global changes through the Asbian to the early Namurian, down to the small-scale of the geochemistry and petrography of one such cyclothem, the Great Limestone Cyclothem of the northern Pennines (Alston Block), as well as an assessment of previous research.

The global environmental changes during the Carboniferous, a pivotal time in the Earth's history, included the proliferation of land plants, leading to increased rates of continental weathering and storage of organic carbon leading to a drawdown of atmospheric CO_2 and cooling. The Carboniferous climate was entering icehouse conditions, from the Asbian onwards, with glaciations and sea-level oscillations, and during this time many of the changes in temperature, palaeoceanography, ice volume and nutrient supply (etc), as well as carbon cycling/storage, were recorded in the bedding architecture, composition and geochemistry of the marine Yoredale carbonates.

The cyclicity which so dominates Carboniferous sedimentary successions was largely produced by glacioeustatic changes in sea level as a result of the effects of orbital forcing and variations in solar irradiance on ice-volume. Local controls, such as tectonics and autocyclic processes, would also have affected deposition. The mid-Carboniferous strata of northern England are characterised by mixed clastic–carbonate cycles (Yoredale cyclothems), attributed in this research to the short eccentricity Milankovitch rhythm. In a typical cycle, transgressive normal-marine shelf carbonates are succeeded by marine shales, then highstand prodelta mudstones and delta front-delta top sandstones with local coals. The study of the Great Limestone Cyclothem reveals that within the

transgressive carbonates, the beds, average 75 centimetres in thickness and are defined by thin shale partings or thicker mudrock layers. The beds form at least two thinning-upward to thickening-upward bed-sets with individual beds and the bed-sets being correlated across the region. Oxygen isotope and strontium trace element data also reveal patterns of increasing and decreasing values through the limestone, which broadly correspond to the bed-thickness cycles. The beds are interpreted as millennial-scale cycles, the result of high-frequency, arid–humid climatic fluctuations. The bed-sets are interpreted as being driven by even lower frequency rhythm of either obliquity or precession, the response to orbitally-driven arid–humid climatic changes and sea-level rhythms. It is postulated that millennial-scale climatic changes, which are a well-known feature of the Quaternary and are here inferred for the Carboniferous, may also have been responsible for the deposition of the beds that are a characteristic feature of many marine sedimentary successions in the geological record.

10.2. Summary of conclusions.

- The Carboniferous sedimentary history of northern England is strongly influenced by a sequence of events which can be traced back to at least the Cambrian: the Closing of the Iapetus Ocean and the resulting Caledonian Mountain building events, faulting and the emplacement of post-Caledonian granite plutons were instrumental in the formation of a series of east-west oriented block and trough/basin structures in the North of England.

- The submergence of the Alston and Askrigg Blocks in the late Asbian in the form of a shallow epeiric sea resulted in marine carbonate conditions prevailing with terrigenous sediment encroaching on to the northern margins of the Alston Block only by the end of the Asbian. By the Brigantian and into the early Namurian the marine transgressions extended over the whole of the Mid-Northumberland Basin and deposition of major cyclothems occurred.

- The bedding planes of the Great Limestone are generally sharp and planar; however, some can be seen to have undergone differential compaction resulting in undulating surfaces, and pressure dissolution features are also common throughout.

- 2½ bed-sets, consisting of around 10 beds, are visible within Fischer Plots of the Great Limestone and consist of thinning-upward and thickening-upward beds. The individual beds of the limestone and their thicknesses are correlatable over much of the platform, suggesting that the same depositional conditions were operating over the whole platform.

- Thickness variations of the Scar to the Little cyclothems, across the Alston Block, reflect localised differential settlement and probably uplift on the block as well as a longer term flexing of the block in a west to east and north to south direction, creating rhythmic alternations of areas of maximum cyclothem thickness. The thicknesses of limestones in the cyclothems are generally constant, with localised thinning; however the thicknesses of the siliciclastics can be seen to change greatly.

- The facies and microfacies of the Great Limestone are typical of a shallow-marine environment, i.e. outer shoreface/transition to offshore environment. Three biostromes exist within the Great Limestone; the *Chaetetes* Band, the Brunton Band and the Frosterley band. The *Chaetetes* Band mainly consists of the sclerosponge *Chaetetes depressus*. The Brunton Band consists of the alga *Calcifolium bruntonense* sp. Nov and the Frosterley band is a lenticular coralline biostrome, or biostromes, characterised by abundant remains of simple rugose corals, particularly *Dibunophyllum bipartitum* (McCoy).

- Apart from the biostromes there is no observable change in the proportions of the various bioclastic elements throughout the Great Limestone. All samples are similar bioclastic wackestones to packstones with a range of

skeletal fragments. Evidence does not suggest that the bioclasts have been transported over large distances.

- Isopachous and drusy calcite spar cements are visible within skeletal fragments which are attributed to marine phreatic conditions where the fragments were left uncovered by sediment for long periods of time. Neomorphic spar is visible within some thin-sections suggesting dissolution of grains and skeletal parts during burial diagenesis.

- The Great Limestone is classified as a wackestone to packstone and the microfacies is described as a bioclastic crinoid, bryozoan, brachiopod packstone with foraminifers. Analysis of thin sections revealed moderate to poor sorting, fragmentation of larger grains and alignment and imbrication of grains at the top of beds suggestive of storm and wave action.

- Analysis of the bioclast/grain contents and facies of the Great Limestone would suggest that the limestone is generally autochthonous. The presence of some fossils in growth position such as corals, brachiopods and *Chaetetes* is indicative of long periods without major storm disruption and is suggestive of low-energy environments, possibly below fair-weather wave base.

- Multivariate analysis would suggest that the communities were, in general, stable, with palaeoenvironmental conditions, in particular water depth and energy conditions, varying little during deposition of the Great Limestone.

- Both the trace elements and isotopic data for the Great Limestone demonstrate that, inevitably, diagenetic alteration has occurred which has resulted in the resetting of the initial values. An attempt has been made to show that the $\delta^{13}C$ and $\delta^{18}O$ trends do in fact track an original pattern, namely that of the bed-thickness pattern.

- Fischer Plots are used in this research for comparison of bed thickness patterns from many localities. The use of Fischer Plots has been questioned; therefore RUNS analysis was carried out to assess the acceptability of the plots with regard to randomness. The z scores do indicate that the Fischer Plot patterns may be due to random events. Overall the Fischer Plots for various locations show that the factors controlling deposition of the beds in the Great Limestone are operating over a large area in a uniform way, to give individual beds of similar thickness. The deposition of the individual beds, however, was probably taking place over a quite random time-frame as indicated by the z-scores), although on the millennial-scale.

- The $\delta^{13}C$ values are comparable to ancient limestones and only slightly more negative than modern marine calcite. The $\delta^{18}O$ values on the other hand are very negative with an average of -10.4‰ and the most negative value of -13.6‰. These very negative values are nearly an order of magnitude less than modern marine carbonates, which would suggest that these values have been reset by a meteoric diagenetic fluid or through recrystallisation at a higher temperature.

- Time Series Analysis has been carried out on the $\delta^{13}C$ and $\delta^{18}O$ data using time frames for the deposition of the Great Limestone of 34 kyr, 45 kyr and 100 kyr. The Time Series do suggest that periodicity of the bed-sets is in the range of the obliquity and precession rhythms with beds being deposited in periods of sub-Milankovitch millennial time-scale.

- Bed changes within the Great Limestone are highlighted by mud/shale horizons, many of which are only millimetres thick and contain many stylolites. Bedding planes within the Great Limestone are regarded as forming at a time of increased mud/terrigenous material deposition. The stylolites, within recognised beds, have also formed due to increases in mud deposition. The possibility therefore exists for the positions of stylolites within beds to be poorly formed bedding planes of a higher frequency.

Appendices

	1	2	3	4	5	6	7	8	9	10	11	12	13	14	15	16	17	18	19	20	21	22	23	24	25	26	27	28	29	30
Marine															1			2	5			1								
Gap																					5									
Sandstone		**3**	**15**			8	14		14		5	8		10		5	4	6		36	39	5	4	16	12	25	1	11	10	
Marine																			22											
Gap																					2									
Mudstone	**8**	**12**	**2**	10			6			4	7	10	3	15					3	9				8	1	2	5			5
Marine																									1					
Gap																														
Coal	**2**				1	1	1	1	1	1		1		1	1				1		1									
Sandstone	**4**	**13**	**8**	8	17	7		12	20	5	3	25	7	3	13	8	6	13	5		6		28	25		17	7	19	20	18
Marine																			6			28								
Gap																					3	8								
Mudstone	**8**			14	6	5	6			8	4		4		4	4	8	5	5				4		15	7	13			
Marine																1	1	1	1											
Gap																														
Coal	**1**	**1**	**0**		1	1	1	1	0	2	1				1								1							1
Marine																														
Gap																														
Sandstone	**6**		**7**	5	43	38		11		20	20		1		8	4	3	1			3	2	4		10		6	19	18	14
Marine																														
Gap															5							5			3					
Mudstone	**15**	**14**	**15**	8	3	5		5	7	4	3					6	6	4			7		3				7	4	6	4
Marine																					1									
Coal								0	2				1			1	1	1												
Gap																						2								
Sandstone				6				19							7	18	4	4					3							
Marine																4														
Gap																														
Mudstone				34				3					1		2		7	4				2	6							
Marine																														
Gap																						4								
Coal															1															
Marine															3															
Gap																														
Sandstone													7				4	2												
Marine																														
Gap																														
Mudstone													12				6	3												
Marine																	2													
Gap																		3												
Coal																														
Gap																														
Sandstone													10																	
Gap																														
Mudstone													1																	
Marine																														

Table 9.1 Measurements of clastics from cross sections from Hodge (1965)

	31	32	33	34	35	36	37	38	39	40	41	42	43	44	45	46	47	48	49	50	51	52	53	54	55	56	57	58	59	60
Marine					1	1		1	2		1	1			1	1	1	1	1	1	1	1				1				
Gap																														
Sandstone	9		6	7		2	4	1	1	3	2	1		1	1	3	1	1	1	5	2	2	5	4	4	1	4	5		26
Marine					4																									
Gap								6																						
Mudstone	2	6			3				1	5			12	12		1					2		3					4	2	
Marine																							1		7					
Gap									4												10									
Coal										1		1	1		0			1	1							1	1		1	2
Sandstone	3	2	41			5	7		11	1	12	8	6	8	3	1	3	3	4	5	13	5	4	3	13	5	6	18	7	3
Marine				34	10			5		1						1		1	1	1										
Gap					4	4									5	2	6	3			4									
Mudstone	3	1	6	5	1		1	1	2		7		7	7					2		2		6	2	5		29	3		7
Marine			1								1												1							
Gap				3						5																				
Coal				1	1								1	1							1	1				1			1	1
Marine					1																									
Gap																						6								
Sandstone	13	7	5	4	3	11	8	1	27		52	2	5	3	2	1	3	5	6	8	9		4	4	2	16		4	1	14
Marine							1					1							1											1
Gap				11		10									3						6			8						
Mudstone	5	2	10			1	1	3	1	2			6	6			2	3			2	2	9		7	6		21		
Marine			1																			1	1		2					
Coal	1				1	1	1	1	1			1			1	1		1		1		1								
Gap																														
Sandstone	6	2			7	4	2	25		4		2			3	4	10	3	6	10		10		3		2			9	
Marine																														
Gap						10	2	15				6				5			2	18		2								
Mudstone	4	2			3				1	4					4			3	3			1		10				17		
Marine										1														1		6				
Gap	5				7													2												
Coal										1									1											
Marine																														
Gap																														
Sandstone		3					2		1	42		3			6	6			15			2								
Marine												1			1															
Gap							2		3			9				9						8								
Mudstone															12			4	3											
Marine																														
Gap																			6											
Coal																														
Gap																														
Sandstone		7																4												
Gap																		8												
Mudstone		6																												

Table 9.1 Measurements of clastics from cross sections from Hodge (1965) continued

	61	62	63	64	65	66	67	70	71	75	76	77	78	79	81	84	100	102	103	104	105	106	109
Marine															1								
Gap												15											
Sandstone	2	5		9	3	7	14	3	6	1	1		22	8		4						12	
Marine														1									
Gap									3														
Mudstone	9	6	11	2	2	8	3			1	1		1	11							2		
Marine																							4
Gap																							
Coal			1						2	0	0	2	1		1		1	2	1	1		4	1
Sandstone	16	19	3	7	2	6	3	2	3	7		30		6	4	7			11	9	5		6
Marine														1									
Gap																							
Mudstone	17	14	7	10	1				5		2	1	2	9	5	31	2	6	9			4	19
Marine														1	1								
Gap																							
Coal							1		1			1					1		3	2	2		
Marine																							
Gap																							
Sandstone			3	18	7	10	13	4	3	3				8	23	14		5	5		6	4	46
Marine														1	1							8	
Gap																							
Mudstone			5	7	2	4		3	12			15		5			2	2	4	29	9		38
Marine									2		1				8					2	2		
Coal								1		1								3					
Gap																							
Sandstone					5	1	3	6				17		7		11	12	8	7	6		24	
Marine																							
Gap																							
Mudstone					4	3		4		12	2	26				12	9	19	57	50	9		
Marine										3				3	6					10		5	
Gap																							
Coal							1				1						2				1		
Marine																		4					
Gap																							
Sandstone					7	13	6	7		18	5				3		10	23				3	
Marine																							
Gap																							
Mudstone					1	6	13	3		15	7						5	50			4		
Marine															4						2		
Gap																							
Coal											1												
Gap																							
Sandstone					1			1									3				2	40	

Table 9.1 Measurements of clastics from cross sections from Hodge (1965) continued

No From Map	Name	Easting	Northing
1	Harton BH	437500	564700
2	Chopwell BH	414380	557430
3	Roddymoor BH	415130	536350
4	Elstob Bh	395106	546351
5	Ramshaw Shaft	395000	547220
6	Whiteheaps Shaft	394670	546610
7	Jeffries Mine Taylors Shaft	396580	548240
8	Jeffries Mine Jemmies Shaft	395270	542390
9	Jeffries Engine Shaft	396020	547810
10	Shildon Shaft	396300	550900
11	Stotsfield Burn Mine	394367	542452
12	Stotsfield Burn Mine	394548	542462
13	Boltsburn Mine Stony Hill	392750	542170
14	Boltsburn Mine NE Shaft	394680	543480
15	Stanhope Burn	398742	542569
16	Rogerly Gill	401376	537750
17	Fine Plantation and Rogerly	401470	537963
18	Cow Burn	399375	537316
19	Harehope Gill	403288	535626
20	Harehopegill Mine	403422	535303
21	Wager Burn	401250	534500
22	Howden Burn	400000	533500
23	Cornish Hush	400000	532500
24	Pickestone Brow Shaft	394800	529400
25	Hudeshope Beck	393975	529982
26	Skears Mine East Rise	395700	523080
27	Skears Mine Great Rise	395800	523510
28	Skears Mine F Vein	393900	528100
29	Skears Mine D Rise	393800	527900
30	Skears Low Level And Coldberry	393800	528500
31	Howgill	394586	527060
32	Snaisgill Syke	395258	526878
33	West Grain	390500	534250
34	Green Sike	391326	533952
35	Brapergill Sike	390800	532500
36	Rowantreegill Sike	391500	532000
37	Pike Law Hush	390000	531500
38	Redgill Sike	386000	532300
39	Harthope Beck	386000	532600
40	West Beck	385500	524250
41	Aller Cleugh	387500	539500
42	Sedling Burn	387100	541500
43	Sedling Mine	386000	541100
44	Burtree Pasture Engine Shed	383000	541800
45	Snodberry Cleugh	383500	543200
46	Cowhorse Hush	382900	542300
47	Wellhope Burn	382000	541200
48	Wellheads Hush	383000	540400
49	Sally Grain	381000	539000
50	Scraith Burn	380600	538200
51	Dry Sike	379800	537000
52	Ashgill Beck	381300	534900
53	Swinhope No 1	383000	545100
54	Swinhope No 2	383500	545600
55	Swinhope No 3	383000	546100
56	Swinhope No 4	382500	545500
57	Coalcleugh Exposures	380100	545100
58	ESp's Vein	384390	550670
59	Whitfield Hall Grounds Waterfall	378000	556500
60	Blagill Burn	374400	548200
61	Blagill Mine	374400	547400
62	Thorngill West	373500	547400
63	Rotherhope Fell Mine	372300	542000
64	East Cross Fell Mines	370500	535200
65	Dun Fell Hush	371500	531900
66	Dunfell Boreholes 4	372100	531900
67	Dunfell Boreholes 5	372500	531900
70	Silverband Mine Henrake Vein	370480	531830
71	Clargill Burn	373200	549700
75	Faugh Cleugh	363500	553500
76	Croglin Water	360200	548100
77	Little Bleaberry Gill	356000	551000
78	East Beck	395500	523500
79	Selset	392000	521000
81	Rowton Sike	387000	521000

Table 9.2 locations for cross sections in Table 9.1

No From Map	Name	Easting	Northing
84	Thorpe Scar	409650	514500
100	Havannah and Blacksike Pit	359500	557400
102	Denton Fell BH	361500	562000
103	Reaygarth Colliery	365000	564000
104	Chineley Burn	375500	564700
105	Brockenheugh BH	385900	566000
106	Fallowfield Sinking	392900	568500
109	Brinkburn Estate	411800	598200

Table 9.2 2 locations for cross sections in Table 9.1 continued

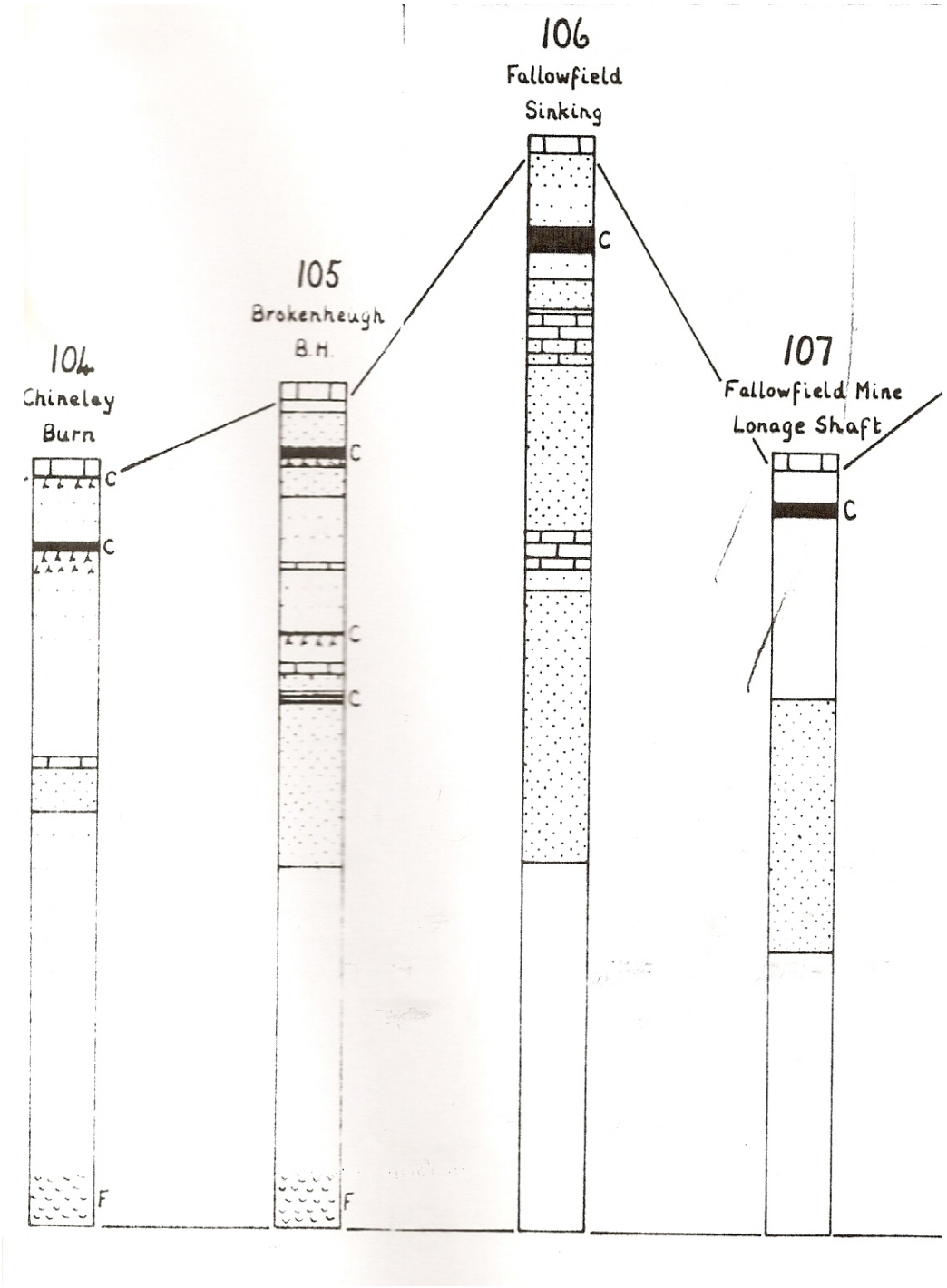

Typical cross sections from Hodge (1965)

Easting	Northing	Limestone thickness	Easting	Northing	Limestone thickness	Easting	Northing	Limestone thickness	Easting	Northing	Limestone thickness
366000	564750	13	376375	543875	20	386875	544750	20	394625	543625	20
370875	565750	14	375375	544250	19	386625	545500	20	395500	544250	21
385750	567250	15	373875	544750	18	383750	545500	20	396125	544625	20
388750	569000	14	377750	544875	20	382500	545500	19	394875	547125	16
392750	567250	14	379250	543875	19	383125	546125	19	395875	547750	22
393500	567750	12	377250	545250	20	382375	546500	20	392625	549750	17
393750	568000	11	377000	546250	19	380250	546750	18	402500	541000	20
393000	568375	12	379750	546875	19	385000	548625	18	362500	536375	12
393750	570500	14	377500	548250	19	384750	546750	18	367000	537000	15
439663	565629	21	374250	547500	16	391250	541125	19	370000	532375	18
359000	559000	12	373125	547625	20	392625	542250	19	369375	533250	19
358750	552875	13	380500	541250	16	394750	541500	18	370250	532125	21
369750	551375	18	382125	540375	18	394625	541875	18	371750	531875	20
376750	550125	18	385500	540125	18	396375	541375	20	370750	533750	20
376750	552000	19	388900	540625	18	398500	540875	21	379000	535500	10
372625	550000	19	386000	541250	18	398750	540250	24	378000	536250	4
384250	550625	20	385750	541750	19	398750	540375	23	379250	537375	20
383875	552250	22	384750	542250	18	398750	540500	21	377500	539125	18
395875	550875	18	382875	543000	18	398750	541000	20	379500	538875	20
404375	557250	22	381500	544000	18	398750	541375	21	386500	531250	18
361500	547500	12	383125	545000	21	395250	542250	23	388000	531375	20
364250	543000	11	385625	544500	20	395000	542375	23	388875	530875	20
364625	541750	12	386750	544375	20	394625	542375	23	385875	532000	20
370750	540000	13	388625	543625	20	390875	543000	21	385750	532500	20
378750	541875	18	389250	544250	20	390125	543250	22	385000	533375	8
375750	543000	19	387000	545125	20	394375	543500	20	384750	533500	11

Table 9.3 thickness of Great Limestone from isopach maps by Hodge (1965)

Easting	Northing	Limestone thickness	Easting	Northing	Limestone thickness	Easting	Northing	Limestone thickness	Easting	Northing	Limestone thickness
384875	533625	14	387000	539875	18	397250	537625	21	401375	537750	23
384750	533750	18	387750	539500	18	397750	537875	21	402875	537125	21
384375	534125	16	388750	539000	12	398000	538000	22	402375	537250	21
388125	534125	20	387500	539000	13	397500	539750	22	415000	536000	19
380125	536000	18	387875	539125	21	398625	538375	23	380750	524625	21
380250	535875	10	388750	538875	19	399000	538250	22	381875	524750	13
380375	536500	17	382500	537625	20	400000	536750	23	382000	524750	16
380500	536000	14	391375	530250	21	399375	537250	24	390000	521875	17
380750	536000	10	391000	530625	19	399250	537875	23	394250	522875	12
381000	535750	14	391375	531375	21	399875	539500	22	396750	523250	19
381375	535500	15	390875	531875	20	399750	539625	20	395000	526875	18
381500	535375	17	394750	530000	18	399250	540000	25	394625	527625	18
382000	535500	18	396375	530125	22	399500	535000	21	394375	527750	20
382500	536125	18	393500	530500	18	400250	532625	18	393875	528000	20
384250	535750	22	392500	534250	21	400750	535000	21	393750	528625	21
384125	536375	21	392875	534500	20	401625	535250	21	392000	529125	18
388000	536125	18	392000	534250	19	402125	535625	21	393500	529250	18
387000	536500	18	391375	534250	16	403250	535125	21	42520	523750	13
386000	536625	18	391500	534500	12	401625	536000	22	382375	512125	12
386000	537000	18	395125	535125	20	403000	536375	22	382500	513125	27
385000	537250	18	393750	537000	21	403125	536250	21	382250	516750	33
384125	537125	18	394625	537250	22	400375	536500	22	385875	513750	23
381000	536750	19	392375	539000	21	400125	537000	23	384750	515000	19
386625	539750	20	391000	539000	22	401000	538000	24	383625	519875	22
386875	539125	15	395500	539375	20	402125	537250	23	390375	512250	11
387375	539000	16	395875	539375	19	401625	537500	21	396250	512000	13

Table 9.3 thickness of Great Limestone from isopach maps by Hodge (1965) continued

Easting	Northing	Limestone thickness	Easting	Northing	Limestone thickness	Easting	Northing	Limestone thickness	Easting	Northing	Limestone thickness
398875	510750	18	377200	552000	19	394670	546610	0	397960	502570	22
397250	512875	14	384190	552400	22	395000	547220	17	398030	502430	22
396250	513125	11	384390	550670	20	395270	542390	0	398230	503000	20
397125	513375	14	385150	548760	18	396020	547810	22	398670	502550	22
401500	514125	26	382490	547510	20	396580	548240	0	402160	503230	18
403500	515250	17	386020	545340	0	396300	550900	0	404600	502400	22
409250	514625	25	385800	544560	20	392800	549500	17	414290	500550	14
412250	513500	17	386820	545290	20	380500	535500	17	424670	507050	9
414250	517750	11	382440	544490	20	391380	531260	19	386380	495510	21
370300	531700	18	381560	543310	18	393800	527900	20	387060	497080	23
371700	536700	20	383000	541800	19	393900	528100	20	389750	496430	23
373200	549100	18	386000	541100	18	396300	530100	22	393110	494700	16
373400	547400	18	388170	538900	18	394800	529400	18	396430	495160	20
375800	544500	19	389000	540500	18	393700	530300	0	400980	497020	18
375000	545600	17	389600	544100	20	415130	536350	19	404700	493000	23
376600	545000	19	392180	541750	0	414380	557430	21	406300	492900	22
377600	544600	20	392750	542170	0	377780	500310	24	407500	491900	19
378500	544700	20	394680	543480	20	383200	499100	29	378620	487710	23
375600	542500	19	395640	544230	21	388560	503620	22	384280	473460	29
377500	543000	19	396340	544580	0	389750	502020	27	387440	471240	10
378200	543500	19	393400	542900	0	391180	501180	24	346130	546600	18
380100	545100	19	386100	537120	18	393700	501500	22	386040	545390	20
380400	546600	18	386200	536800	18	394000	503000	22	406200	527300	16
380300	546900	19	388800	537900	18	394200	501420	21	386040	545390	19
377900	546610	19	400400	534900	18	395970	503640	20	398900	514200	11
377000	550000	18	403200	535300	20	396000	502000	24	386040	545390	21

Table 9.3 thickness of Great Limestone from isopach maps by Hodge (1965) continued

Easting	Northing	Limestone thickness
359360	564393	17
393990	567740	12
403170	577040	14
341200	544400	17
386000	565700	15
341150	544340	18
370560	532580	18
369690	533530	18
439663	565629	22
413200	567100	14
399860	527500	18
390100	526900	14
403280	515080	15
392950	570100	14
376200	566700	11
452500	525500	20
403170	577040	14
396500	522500	18

Table 9.3 thickness of Great Limestone from isopach maps by Hodge (1965) continued

Location	EAST	NORTH	Scar Limestone	Slaty Hazel	Other Probably Shale	Five Yard Limestone	Six Fathom Hazle	Other Probably Shale	Three Yard Liomestone	Nattrass Gill Hazle	Other Probably Shale	Four Fathom Limestone	Quarry Haxle	Other probably shale	Iron Post Limestone	Tuft	Other Probably Shale	Great/Main Limestone	All Sandstones	Shale	Chert	Little Limestone	Pattinson Sill	White Sill	Firestone	All Sandstones	Shale
Silverband Mine	370300	531700				3	18	3	2.7	11	14	7	3	11	0	3	6	18	13	14							
Middle tongue Beck	370400	532400	12		9	3	18	3	2.7	11	14	7	3	11													
East Cross Fell Mine	371700	536700	11	7	11	6	11	9	2.7	12	11	8	5	9	0	5	4	20	17	8		3	2		12	13	20
Holyfield Mine	373200	549100										7	5	13	1	3	5	18	4	15							
Blagill Mines	373400	547400													1	2	4	18	9	13		2	5	1	9	14	26
Galligill Sike Mine	375800	544500										7	6	9				19	6	15		2	2	4	10	16	19
Hudgill Burn Mine	375000	545600	11	4	4	2	15	1	4.3	4	19	7	6	10	1	4	6	17	4	14							
Nentsberry Haggs Mine West	376600	545000	17	7	3	5	11	3	2.7	5	21	7	9	12	1	3	7	19	7	12		3	4	3	10	17	25
Brownley Hill Mine	377600	544600										7	9	11	0	5	3	20	12	10							
Guddamgill Mine	378500	544700													1	3	5	20	9	12		2	4	4	13	21	30
Bentyfield Mine	375600	542500				5	7	6	4.3	10	22							19	9	10		2	2	1	2	5	28
Dowgang Mine	377500	543000										7	9	12	0	3	7	19	9	10		4	1		4	4	30
Middlecleugh Mines	378900	542500																				2	5		4	8	28
Rampgill mine	378200	543500	13	10	6	3	6	7	2.4	6	20	6	9	12	0	3	5	19	6	12		6	4	4	12	20	24
Coalcleugh	380100	545100																19	8	14		2	6	2	6	13	18
Barneycraig East	380400	546600										7	7	17				18	6	12							
Scaithole Mine	380300	546900													1	2	3	19	6	12		3	4	3	5	12	24
Wellhope Shaft	377900	546610																19	7	12							
Mohopehead Mine	377000	550000													1	2	4	18	4	13		2	6	2	6	14	29
Longcleugh Mine	377200	552000	17	6	5	6	0	11	2.7	13	4							19	8	11							

Table 9.4 Thickness of Scar to Little Cyclothems from Memoir of the British Geologica Survey (Dunham 1990)

Location	EAST	NORTH	Scar Limestone	Slaty Hazel	Other Probably Shale	Five Yard Limestone	Six Fathom Hazle	Other Probably Shale	Three Yard Lionestone	Nattrass Gill Hazle	Other Probably Shale	Four Fathom Limestone	Quarry Haxle	Other probably shale	Iron Post Limestone	Tuft	Other Probably Shale	Great/Main Limestone	All Sandstones	Shale	Chert	Little Limestone	Pattinson Sill	White Sill	Firestone	All Sandstones	Shale
Holmes Linn S	38419	55240																2	1	1							
Esp's Plantation Shaft	384390	550670																20	12	14							
St Peters Mine	385150	548760							3	7	18	7	7	19				18	6	15							
Swinhopehead Shaft	382490	547510																20	6	17							
Allenhead's	386020	545340	10	9	5	5	8	3	3	16	12	6	10	12	1	1	5	20	8	13		4	3	5	10	18	22
Plantation Shaft	385800	544560																20	7	20		3	4	9	10	23	12
Low UG Shaft	386820	545290																20	6	10		3	6	9	9	24	19
High UG Shaft	382440	544490																20	5	11		2	7	7	11	25	18
Killhopehead Mine	381560	543310										6	10	12				18	9	9		2	1	2	12	15	30
Burtree Pasture Mine	383000	541800	11	5	13	5	9	6	4.9	9	6	6	5	13				19	5	12		3	2		10	12	15
Sedling Mine West	386000	541100	11	11	9	5	12	2	3	20	10	6	7	12				18	6	12							
Levelgate Mine	388170	538900																18	22	7							
Middlehope Mines	389000	540500																18	24	8							
Groverake Mine	389600	544100										6	10	11				20	6	11		3	4	1	12	17	20
Boltsburn Mine West	392180	541750																	10	9		2	2	1	14	17	21
Boltsburn Mine West	392750	542170																	12	13							
Boltsburn Mine East	394680	543480																20	23	4		3	4	2	12	17	20
Boltsburn Mine East 2	395640	544230																21	17	7		3	3	1	15	19	23
Boltsburn Mine East 3	396340	544580																	3	11							

Table 9.4 Thickness of Scar to Little Cyclothems from Memoir of the British Geologica Survey (Dunham 1990) continued

Location	EAST	NORTH	Scar Limestone	Slaty Hazel	Other Probably Shale	Five Yard Limestone	Six Fathom Hazle	Other Probably Shale	Three Yard Lionestone	Nattrass Gill Hazle	Other Probably Shale	Four Fathom Limestone	Quarry Haxle	Other probably shale	Iron Post Limestone	Tuft	Other Probably Shale	Great/Main Limestone	All Sandstones	Shale	Chert	Little Limestone	Pattinson Sill	White Sill	Firestone	All Sandstones	Shale
Fulwood Mine	393400	542900																	6	12		4	7		10	17	19
Carrick's Mine, Carr's	386100	537120																18	9	9							
Blackdene Mine	386800	539000	9	16	3	2	6	1	2.7	7	18	6	11	8	0	3	4										
Dawson's Shaft	386200	536800																18	6	10							
Greenlaws Mine	388800	537900	7	12	7	7	11	5	3.4	10	18	6	4	9	1	9	3	18	9	11		2	3		9	12	25
Slitt Shaft	390580	539200	9	7	13	4	10	6	2.7	12	10																
Rigg BH	391450	538950	9	15	6	3	2	9	2.7	11	20																
Cammock Eals Mine	393500	538300	11	13	10	6	5	4	1.8	9	21																
Rookhope	393340	524780	9	7	17	5	6	8	1.8	9	20	6	7	13	1	8	4										
Bollihope	400400	534900																18	19	6							
Ettersgill	389000	529000	7	9	8	4	12	2																			
Harehope Gill	403200	535300																20	18	4		6	9		5	14	10
Whiteheaps Engine Shaft	394670	546610																	28	4		4	1	7	11	19	28
Ramshaw Shaft	395000	547220																17	27	6		2		5	11	16	28
Jemmy's Shaft	395270	542390																	20	4		3		7	9	16	26
Jeffries Shaft	396020	547810													2	3	4	22	16	4		4	3	9	15	26	23
Taylor's Shaft	396580	548240																	7	6		4	3	4	11	19	28
Shildon Mine	396300	550900																	11	8		4	25		8	33	32
Beldon Mine	392800	549500																17	13	11		3	8	5	8	21	18
Ashgillhead Mine	380500	535500							2.7	4	22	7	4	13				17	13	8		1	1		12	13	13

Table 9.4 Thickness of Scar to Little Cyclothems from Memoir of the British Geologica Survey (Dunham 1990) continued

Location	EAST	NORTH	Scar Limestone	Slaty Hazel	Other Probably Shale	Five Yard Limestone	Six Fathom Hazle	Other Probably Shale	Three Yard Limestone	Nattrass Gill Hazle	Other Probably Shale	Four Fathom Limestone	Quarry Haxle	Other probably shale	Iron Post Limestone	Tuft	Other Probably Shale	Great/Main Limestone	All Sandstones	Shale	Chert	Little Limestone	Pattinson Sill	White Sill	Firestone	All Sandstones	Shale
Flushiemere (No.2) Shaft	391380	531260																19	13	7							
Skears D2 Vein	393800	527900										7	10	5	1	2		20	22	3		2			19	19	11
Skears F Vein	393900	528100													1	2	5	20	23	2							
Manorgill North Sump	396300	530100													1	3	6	22	20	4		1	3	7	5	15	27
Pikestone Brow Mine	394800	529400																18	20	4							
Parkin Hush Mine	393700	530300																	11	9							
Roddymoor BH	415130	536350	9	1	14				3.4	26	12	5	6	16	1	1	6	19	13	9		1		2	7	9	20
Chopwell BH	414380	557430																21	8	12		4	3	22	4	29	18
Woodlands Borehole	309080	527700																									
Deep Gill	377780	500310																24									
Great Sleddale Beck	383200	499100																29									
Starting Gill Shaft	388560	503620																22			9						
East Gill	389750	502020																27			2						
Swinner Gill	391180	501180																24			4						
Lownathwaite Mine	393700	501500																22			5						
Blakethwaite Mine	394000	503000																22			6						
Friarfold Hush	394200	501420																21			4						
LittlePunchard Gill	395970	503640																20			6						
Brandy Bottle Incline	396000	502000																24			5						
Surrender Mine	397960	502570																22			5						
Wetshaw Fourth Whim	398030	502430																22			5						
Stodart Hush	398230	503000																20			5						

Table 9.4 Thickness of Scar to Little Cyclothems from Memoir of the British Geologica Survey (Dunham 1990) continued

Location	EAST	NORTH	Scar Limestone	Slaty Hazel	Other Probably Shale	Five Yard Limestone	Six Fathom Hazle	Other Probably Shale	Three Yard Liomestone	Nattrass Gill Hazle	Other Probably Shale	Four Fathom Limestone	Quarry Haxle	Other probably shale	Iron Post Limestone	Tuft	Other Probably Shale	Great/Main Limestone	All Sandstones	Shale	Chert	Little Limestone	Pattinson Sill	White Sill	Firestone	All Sandstones	Shale
Blackside Vein at Danby	398670	502550																22			5					
Slei (furn) Level	402160	503230																18			6					
Hurst Mines	404600	502400																22			5					
Church Gill	414290	500550																14			4					
Chantry Borehole	424670	507050																9								
Fossdale Gill	386380	495510																21			2					
Greenseat Beck	389750	496430																23			2					
Oxnop No 2 Borehole	393110	494700																16			3					
Summer Lodge Beck	396430	495160																20			2					
Browner Gill	400980	497020																18			2					
Redmire Quarry	404700	493000																23			1					
Preston Moor Shafts	406300	492900																22								
Keld Heads Mine	407500	491900																19								
Blea Grin Gill	378620	487710																23								
Pen-y-ghent	384280	473460																29								
Fountains Fell	387440	471240																10								
Grainy Gill	387060	497080																23			1					

Table 9.4 Thickness of Scar to Little Cyclothems from Memoir of the British Geologica Survey (Dunham 1990) continued

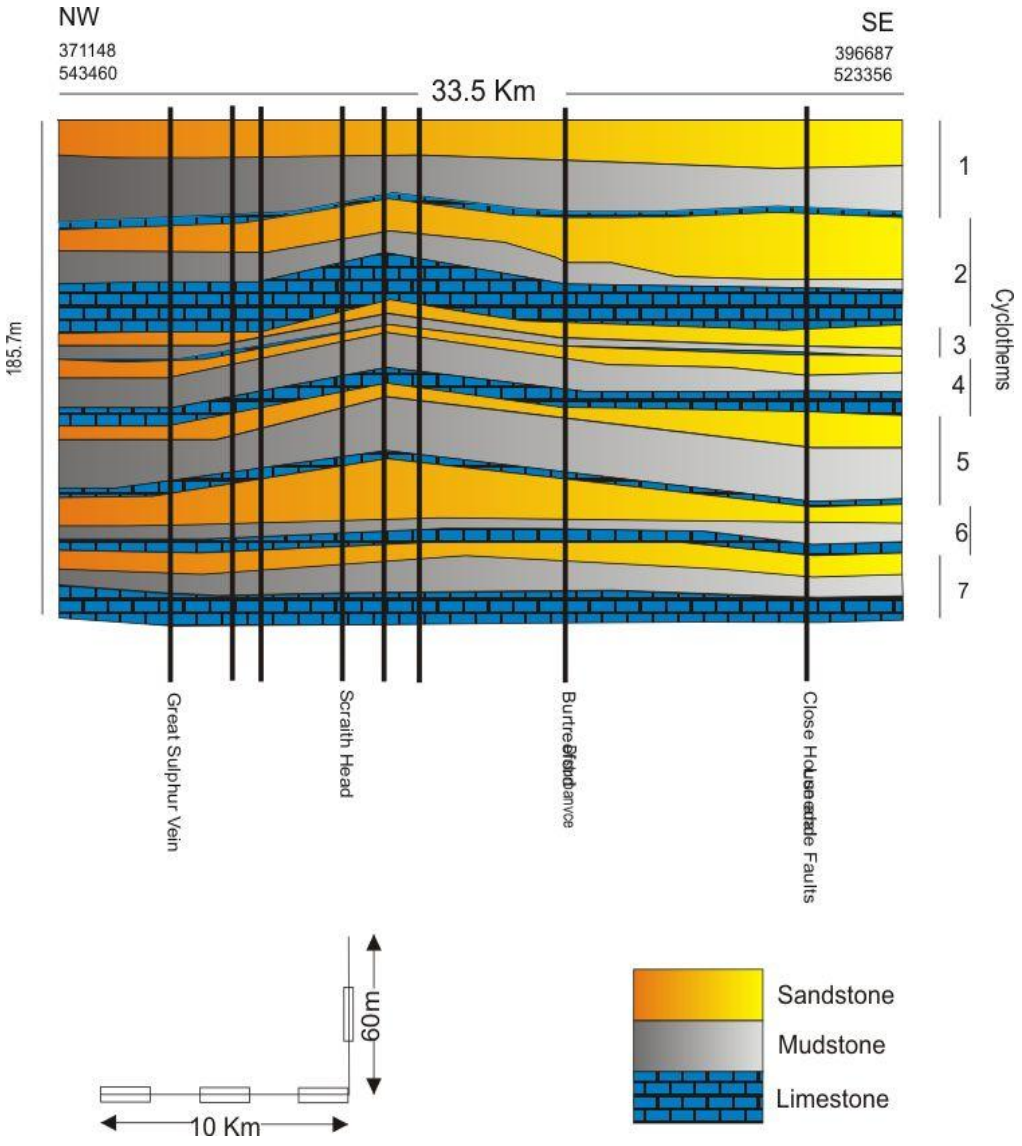

Appendix B Section line 1

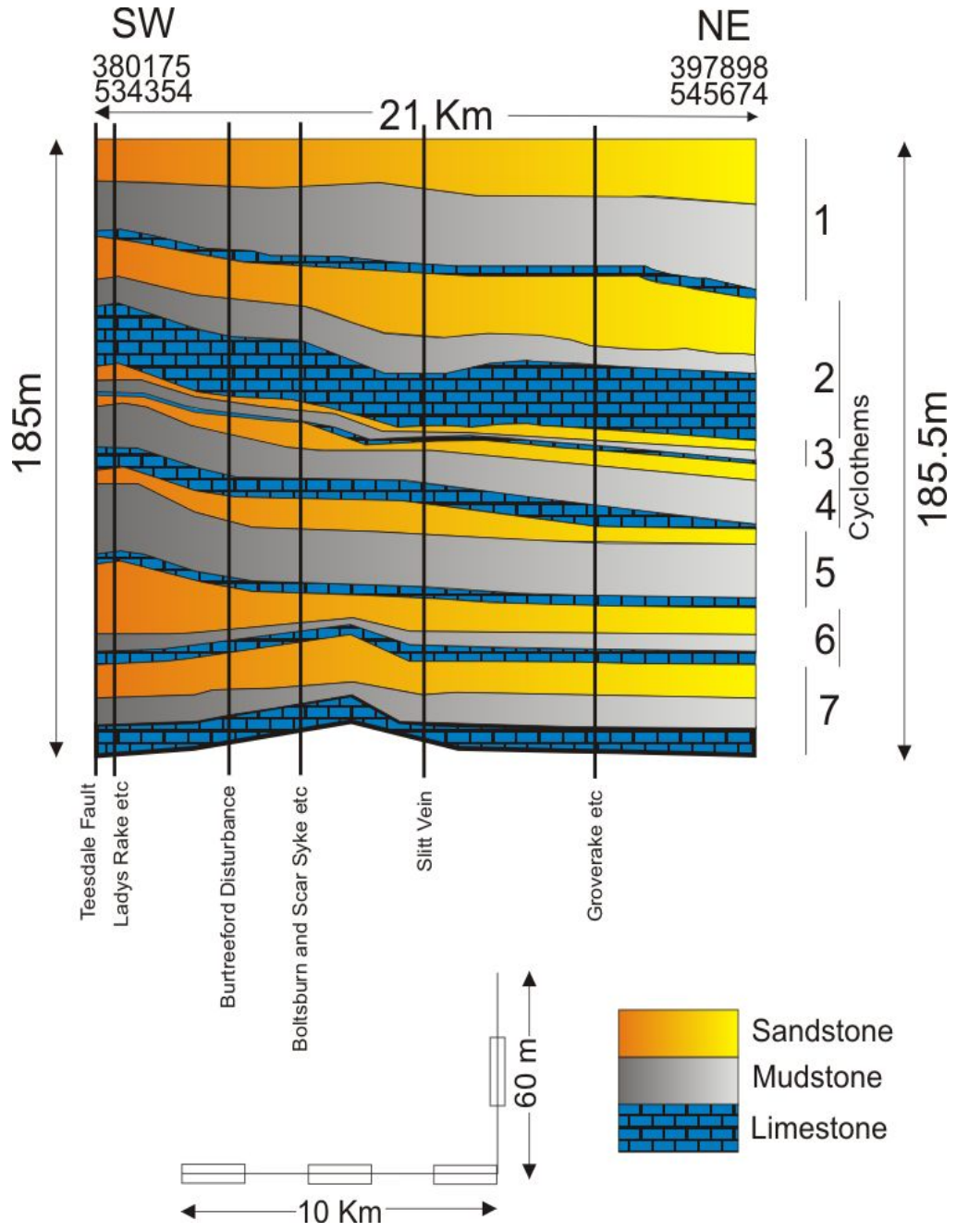

Appendix B Section line 2

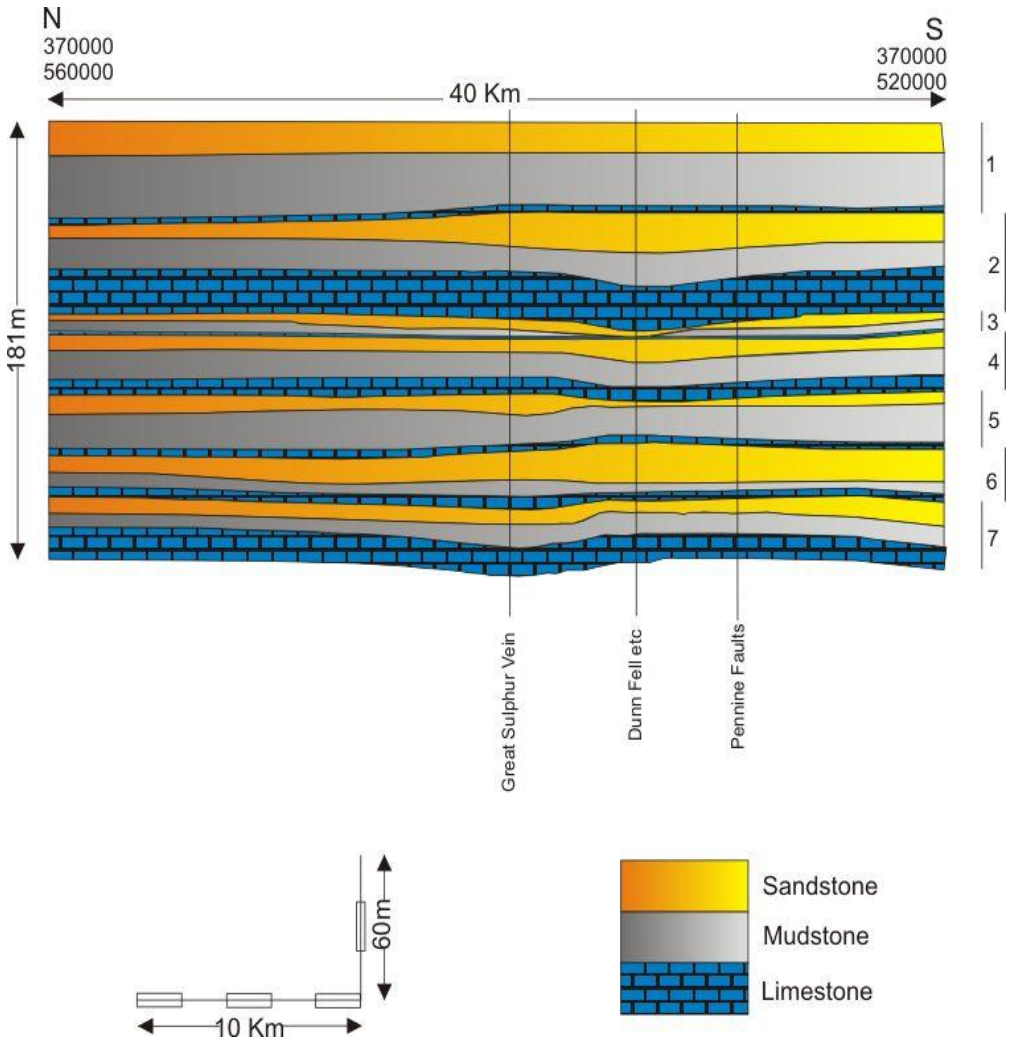

Appendix B Section line 3

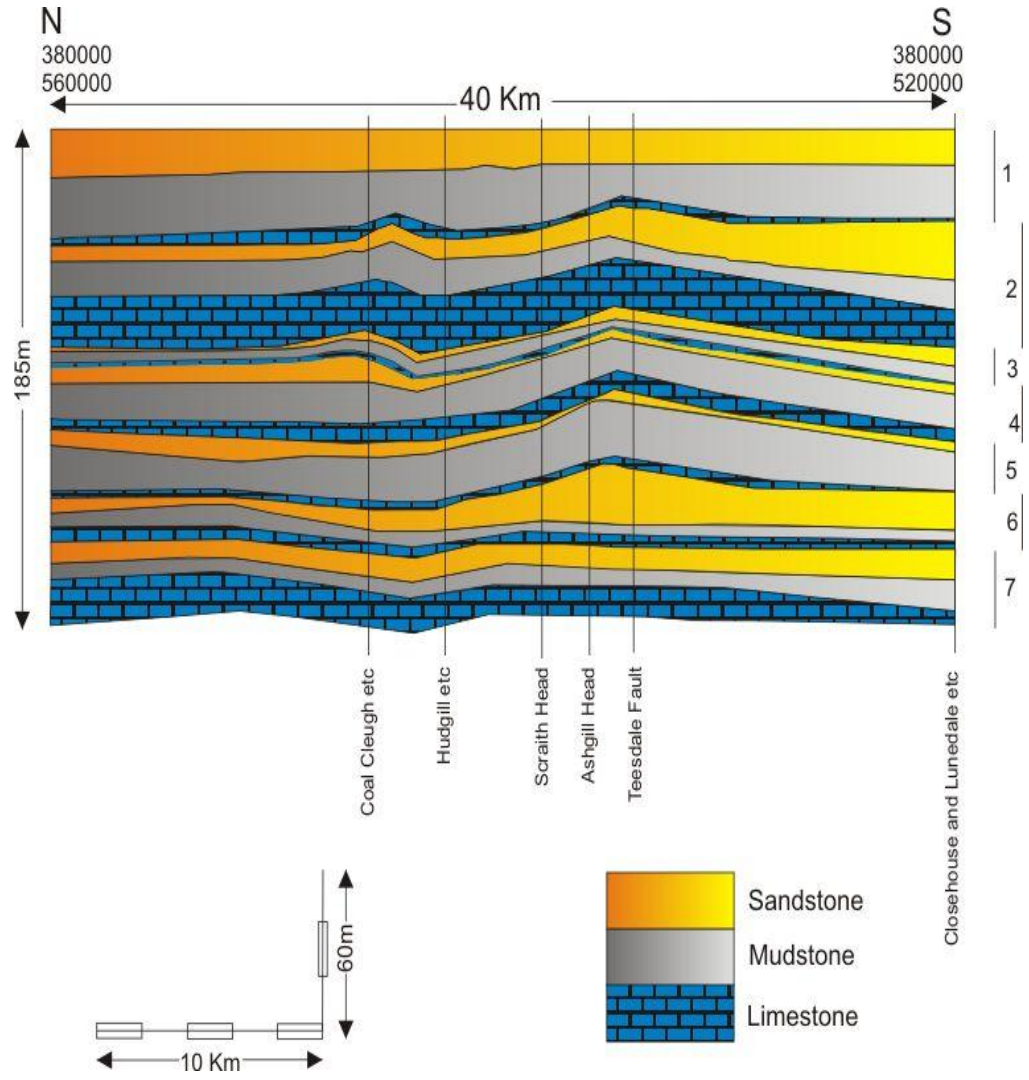

Appendix B Section line 4

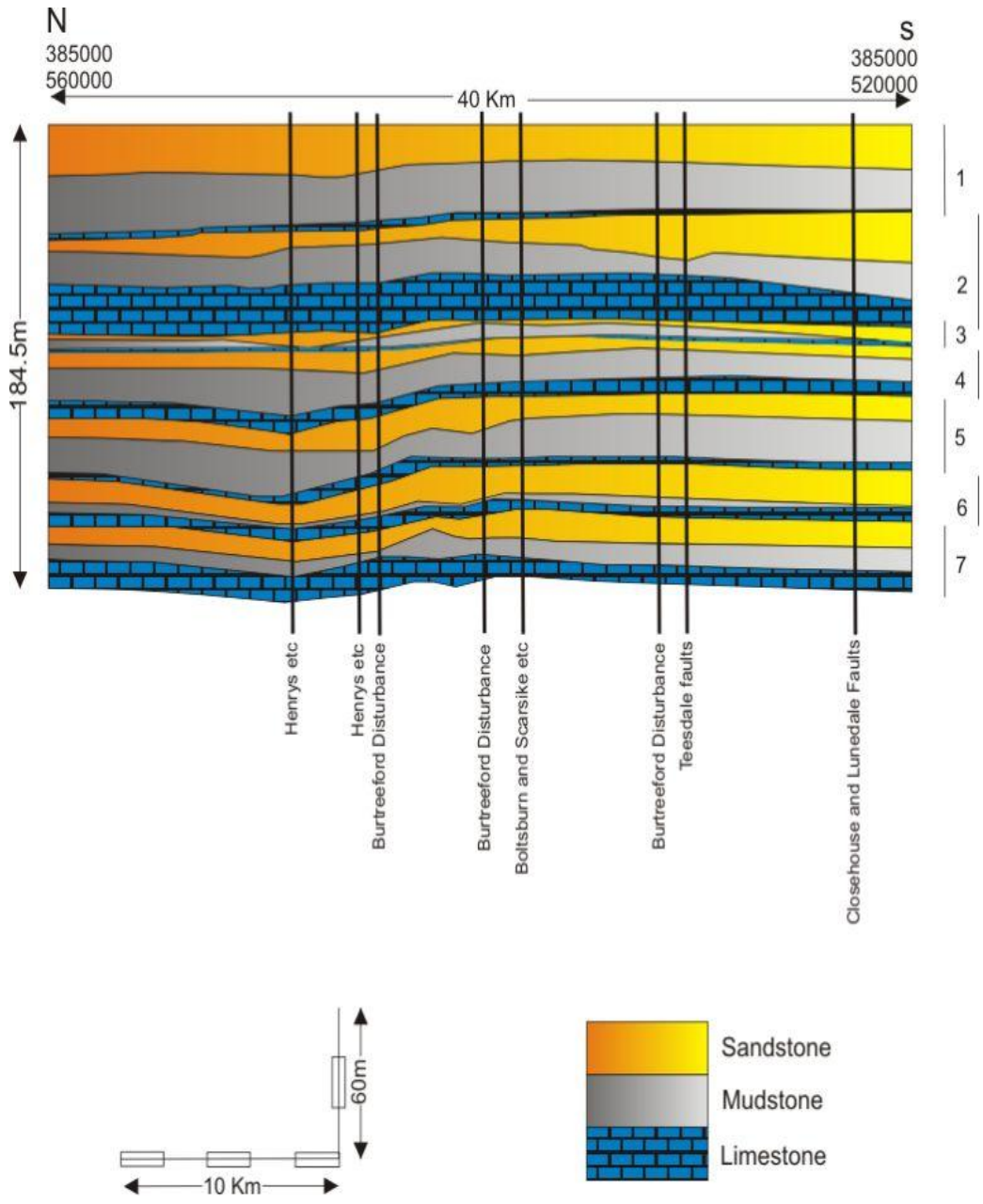

Appendix B Section line 5

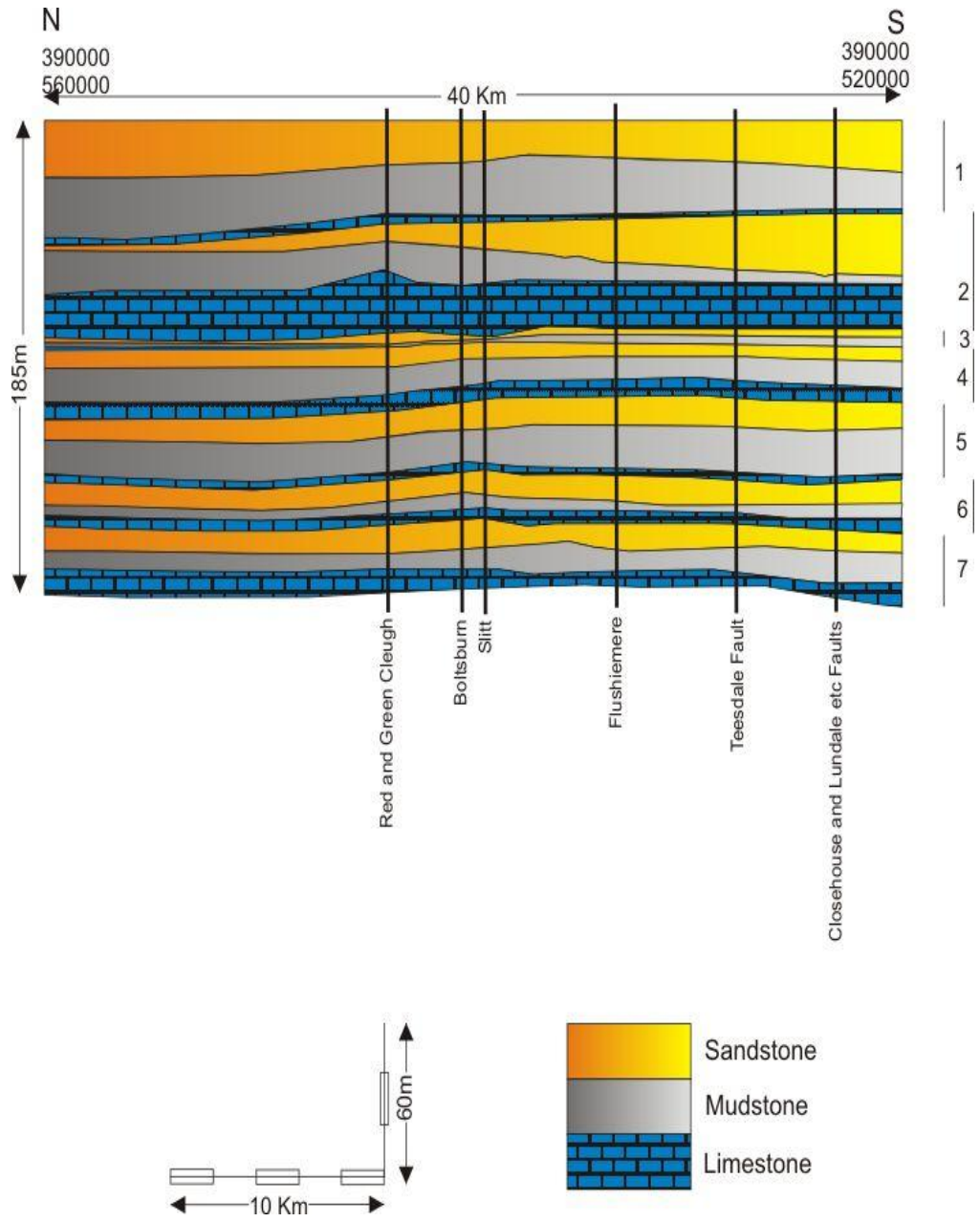

Appendix B Section line 6

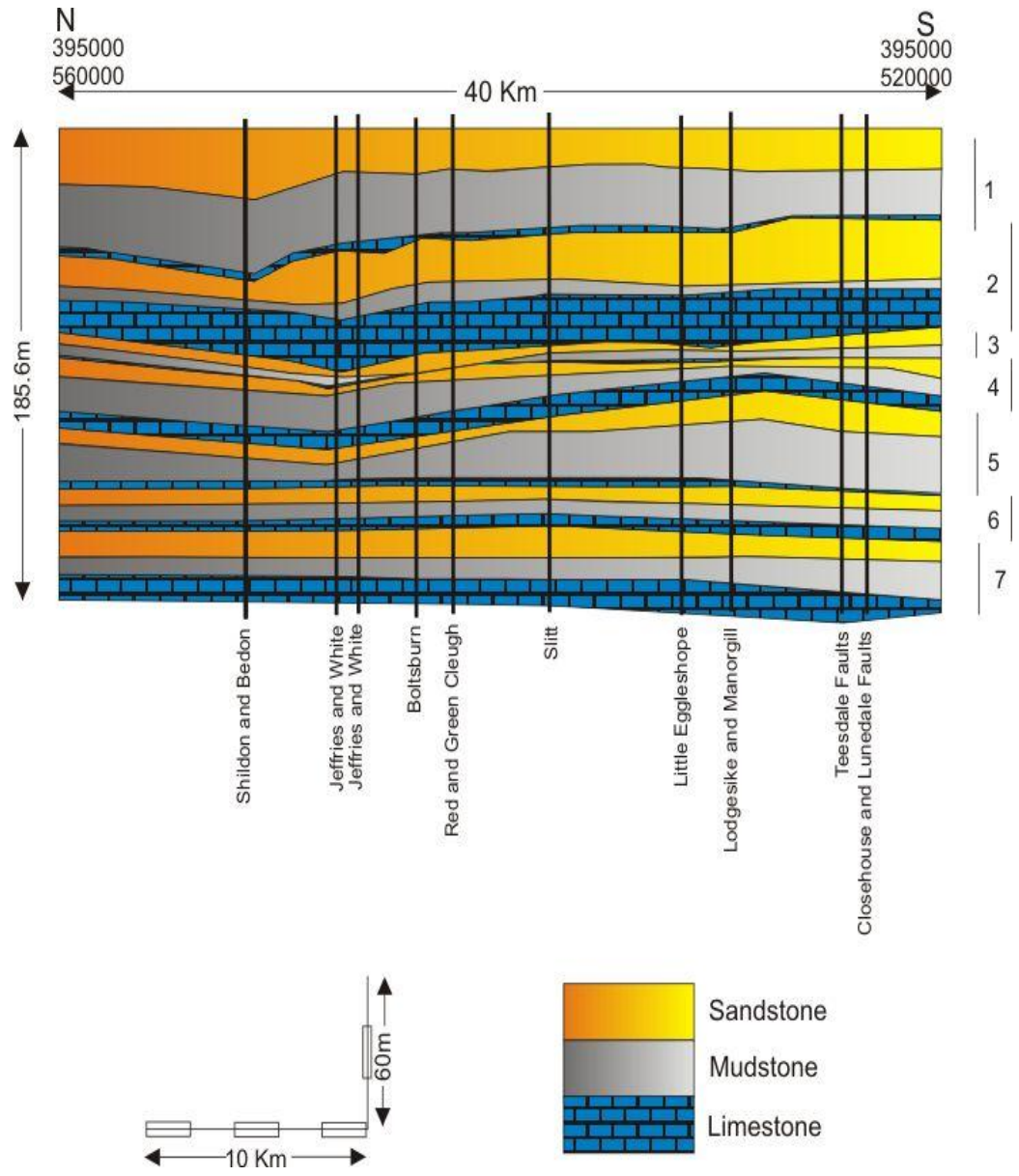

Appendix B Section line 7

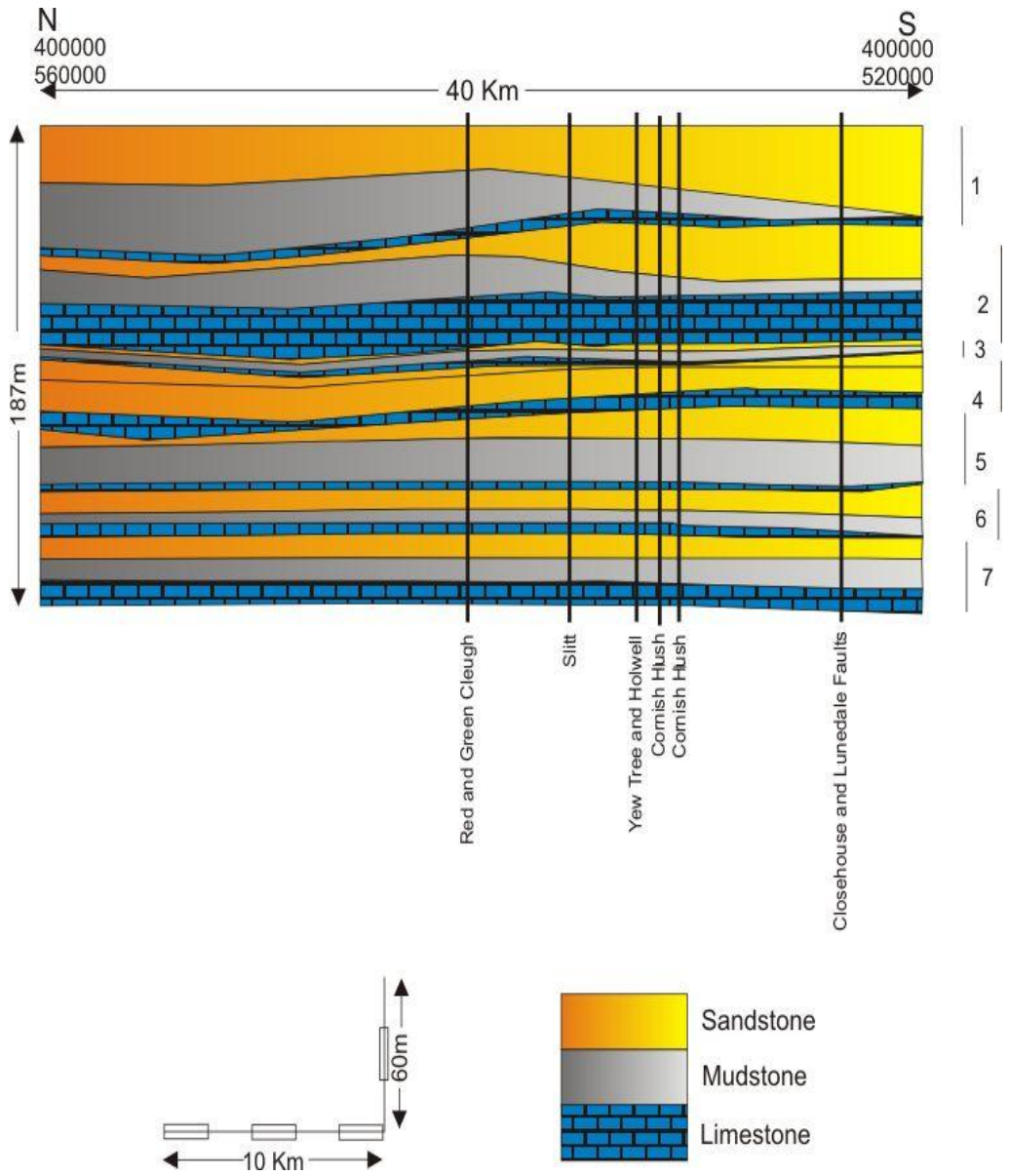

Appendix B Section line 8

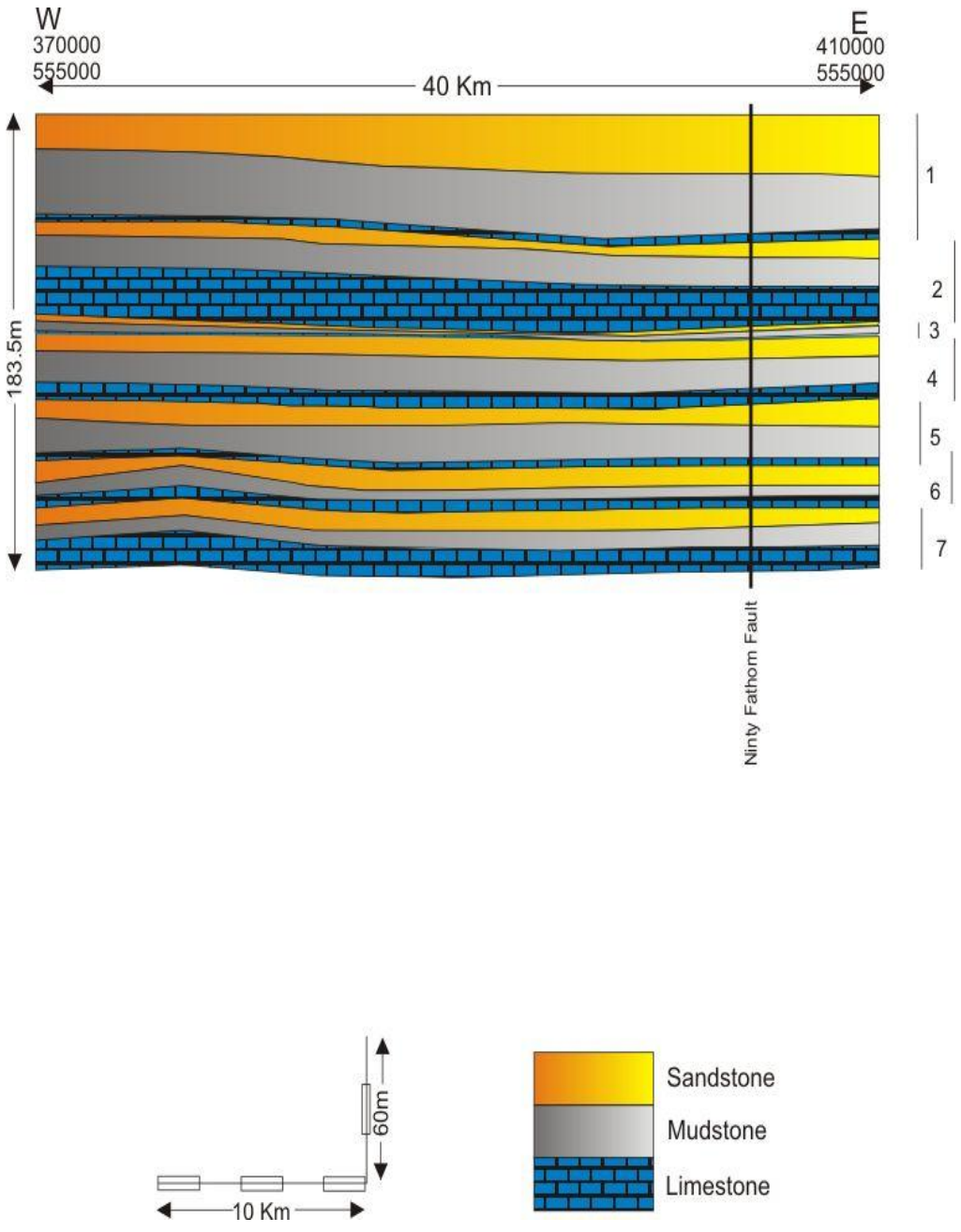

Appendix B Section line 9

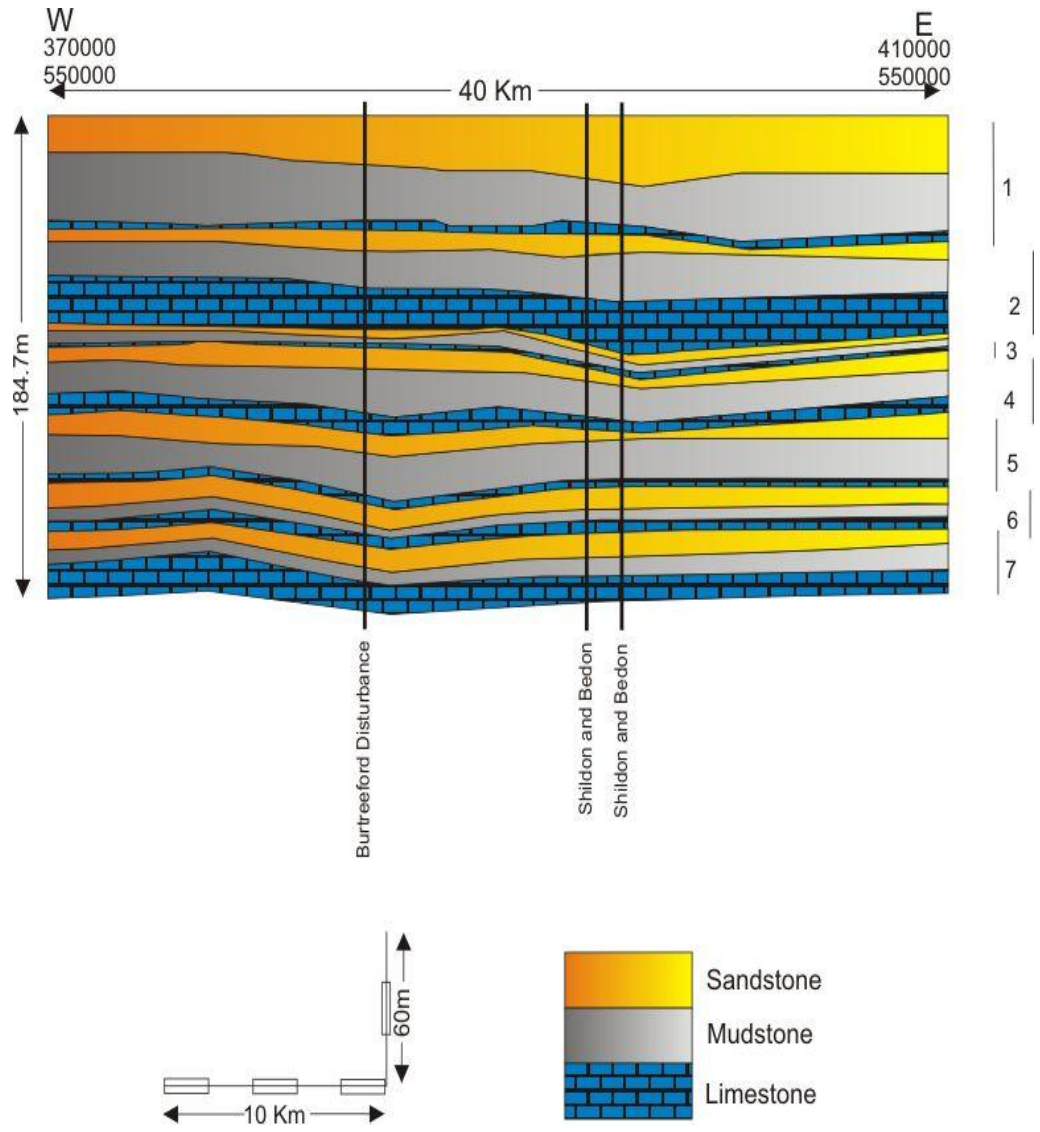

Appendix B Section line 10

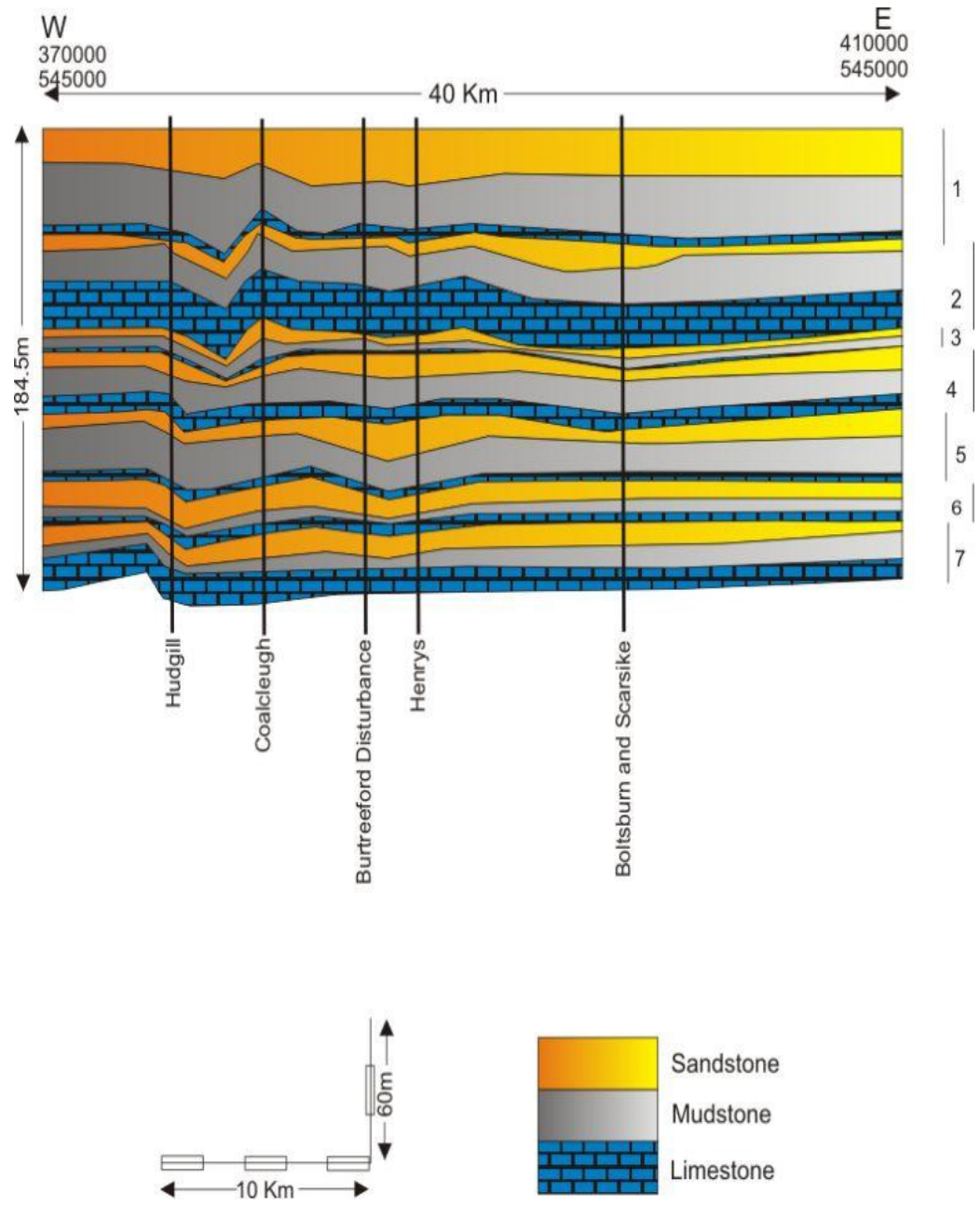

Appendix B Section line 11

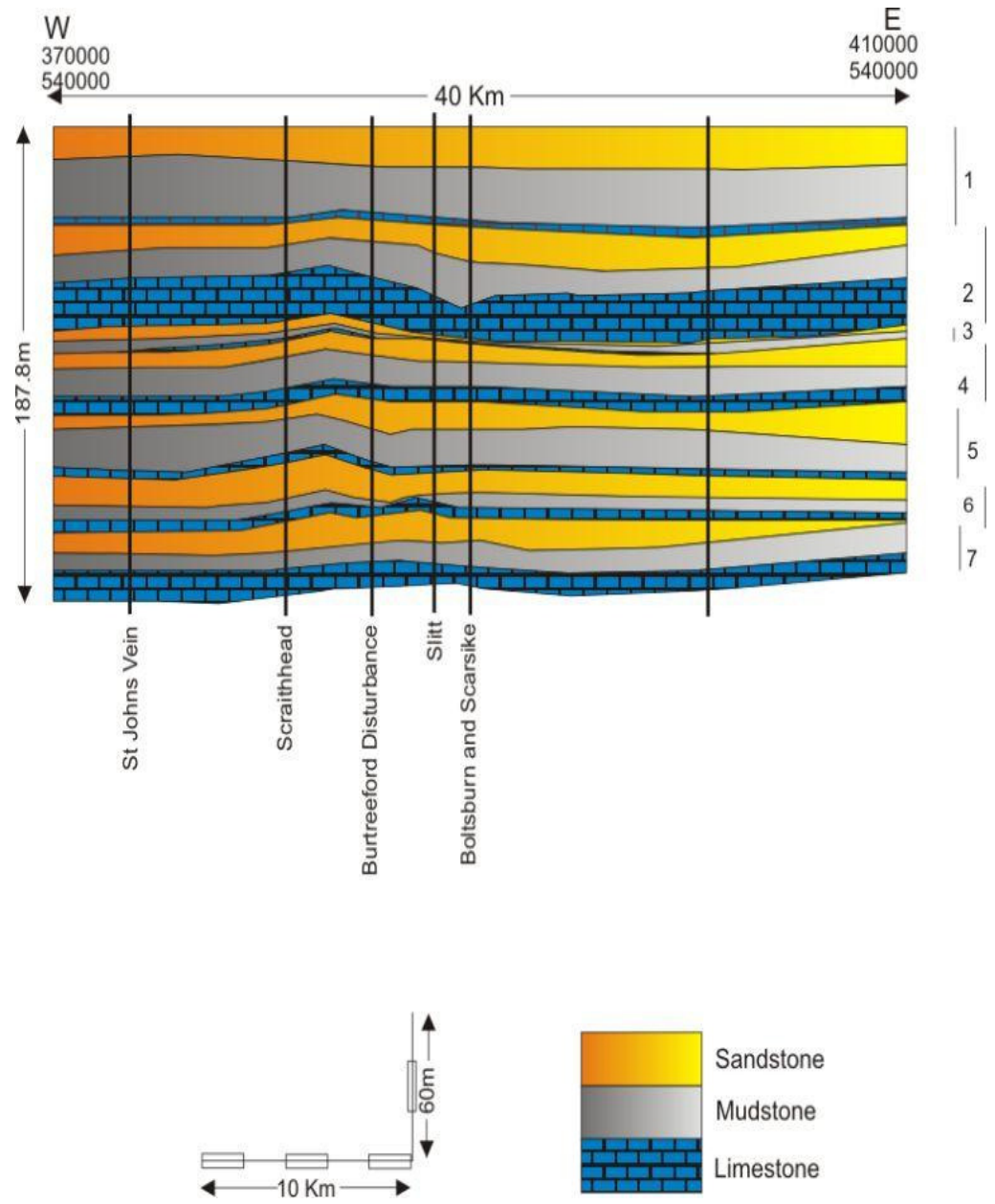

Appendix B Section line 12

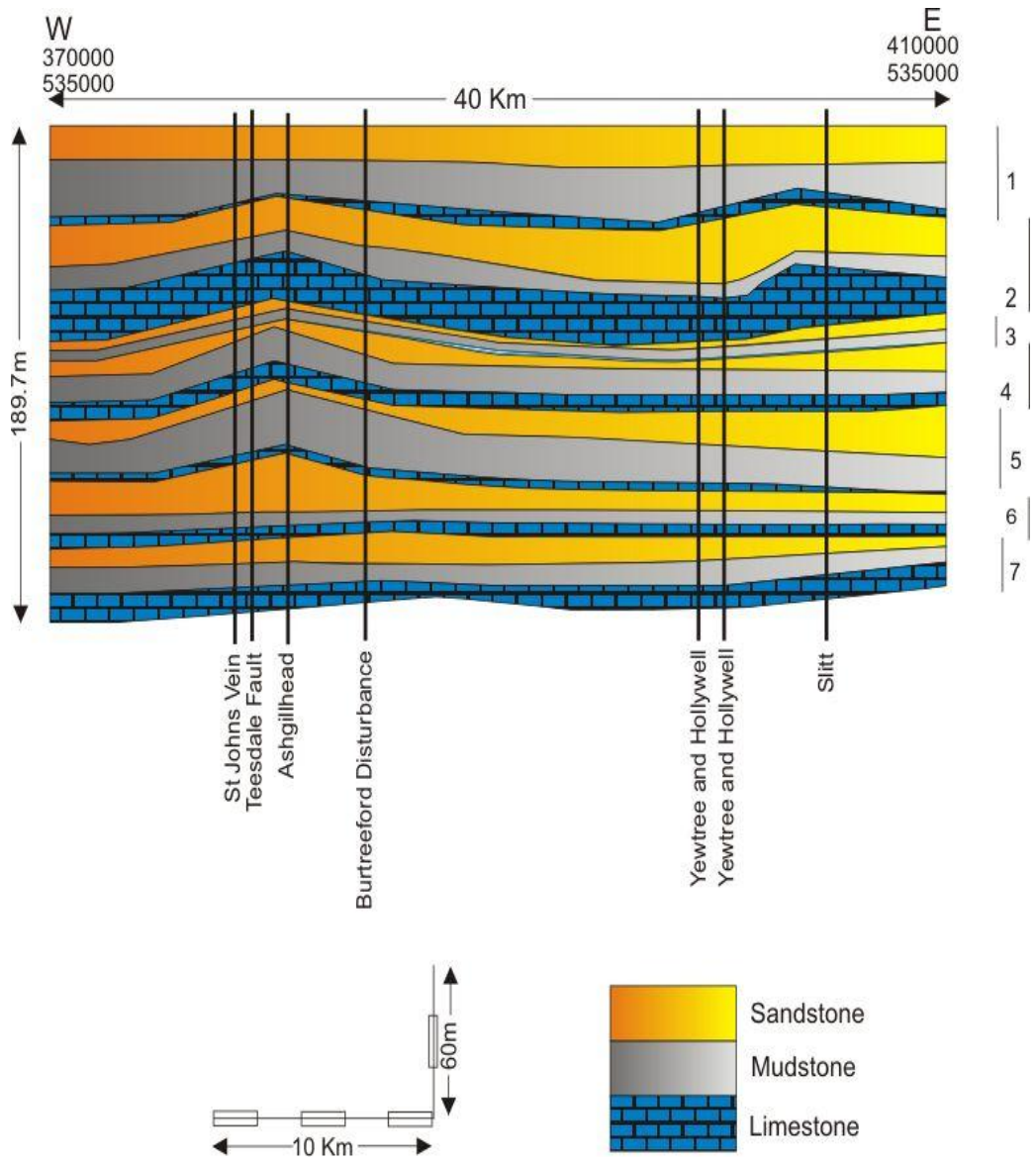

Appendix B Section line 13

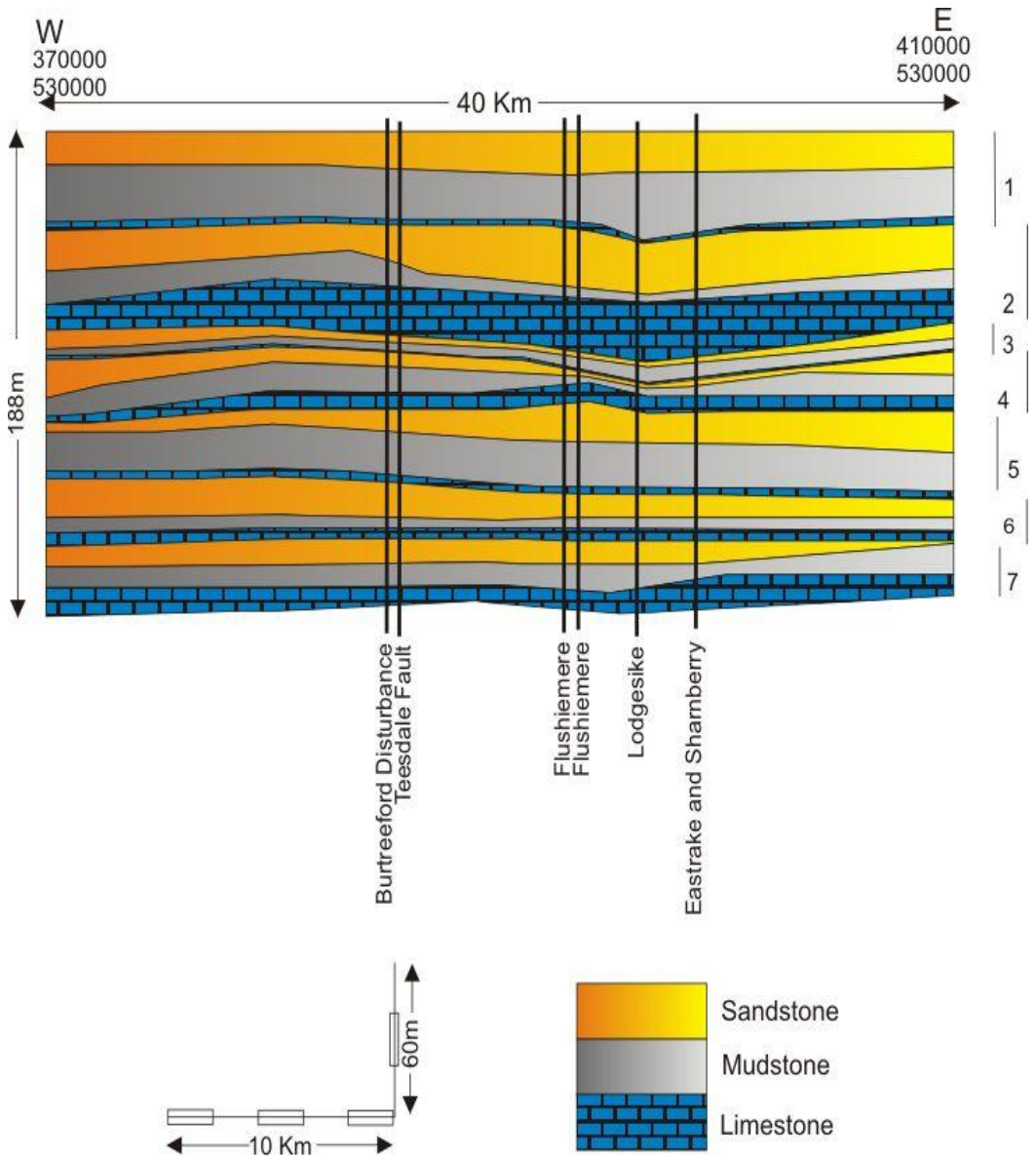

Appendix B Section line 14

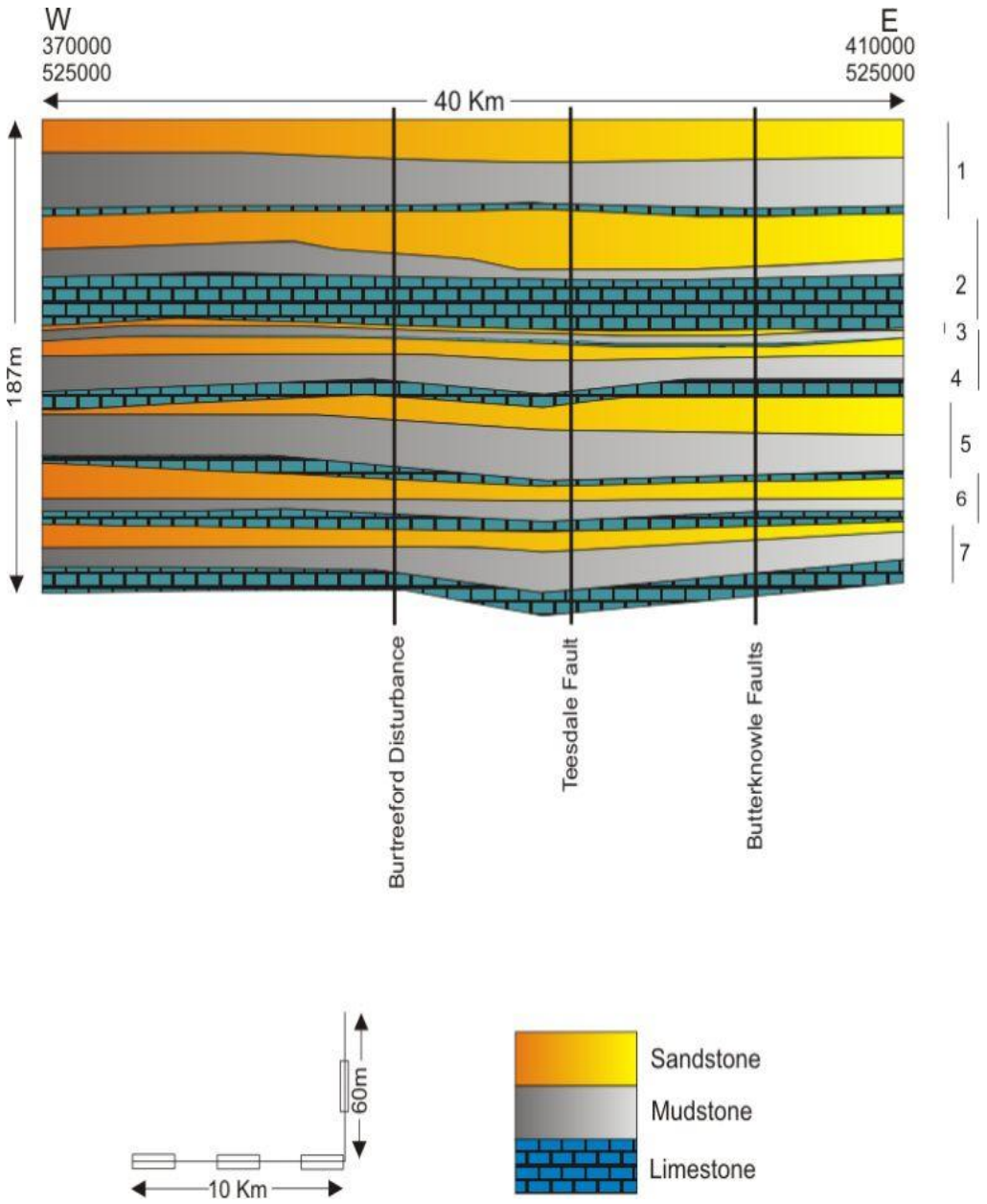

Appendix B Section line 15

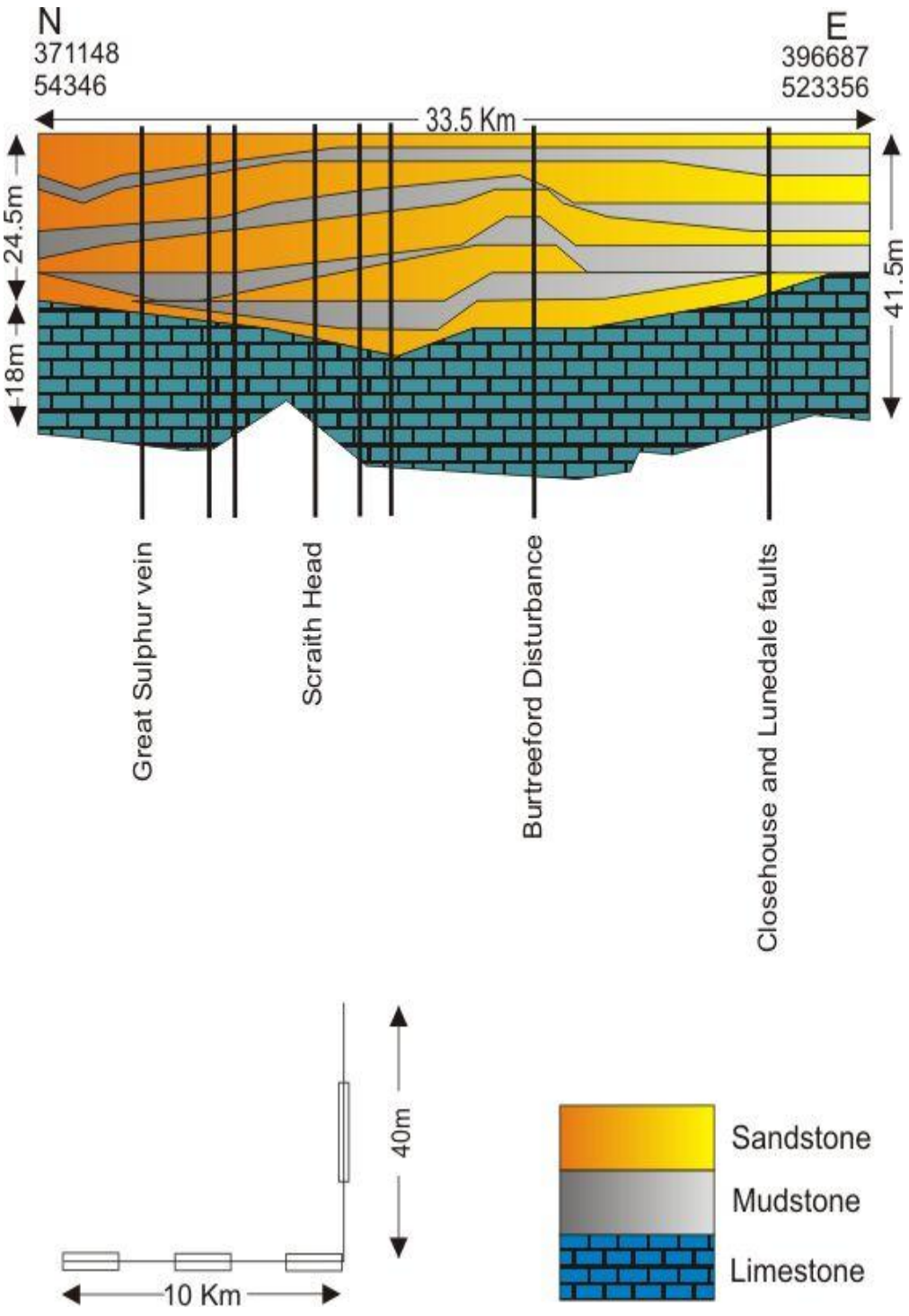

Appendix B Section line 16

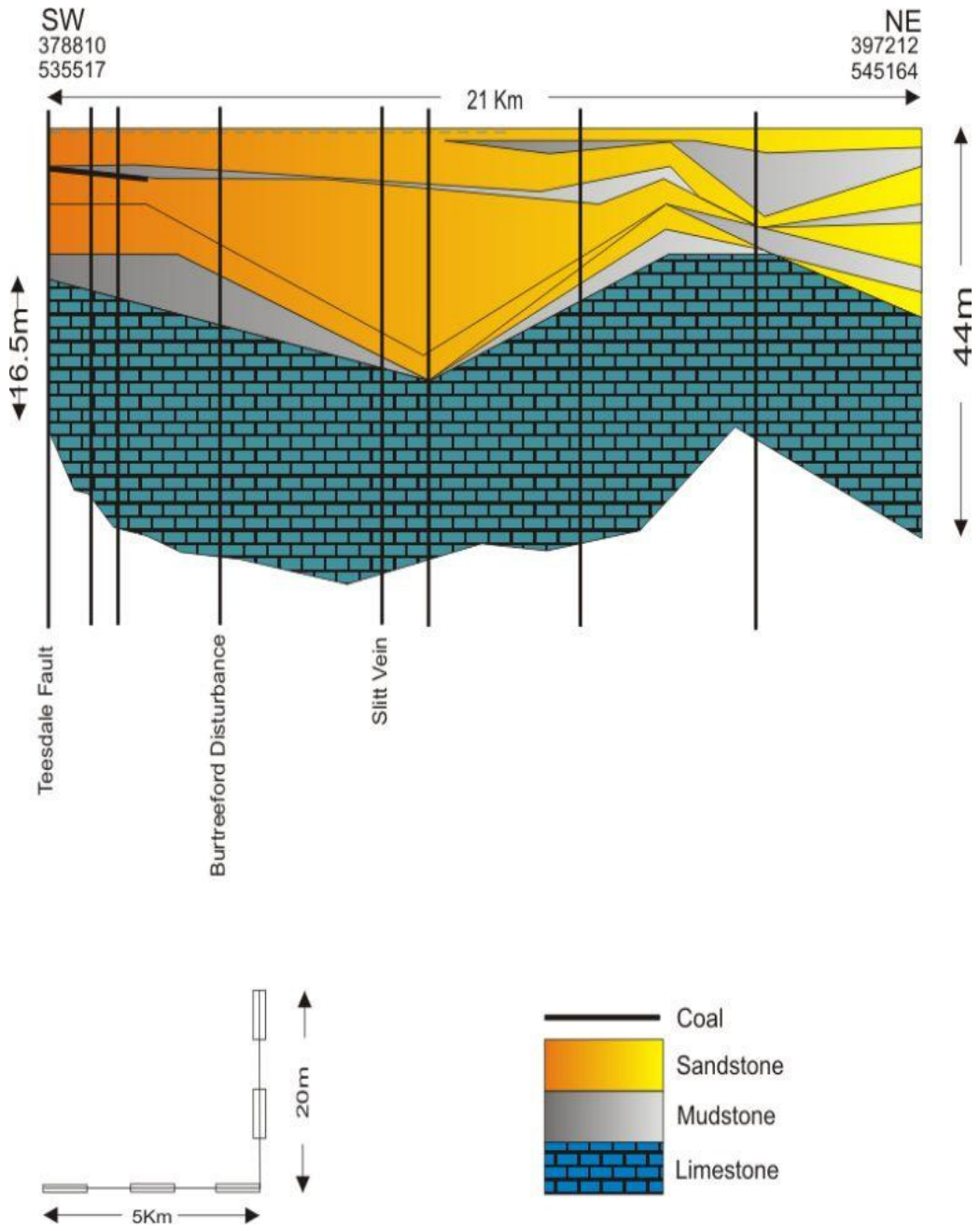

Appendix B Section line 17

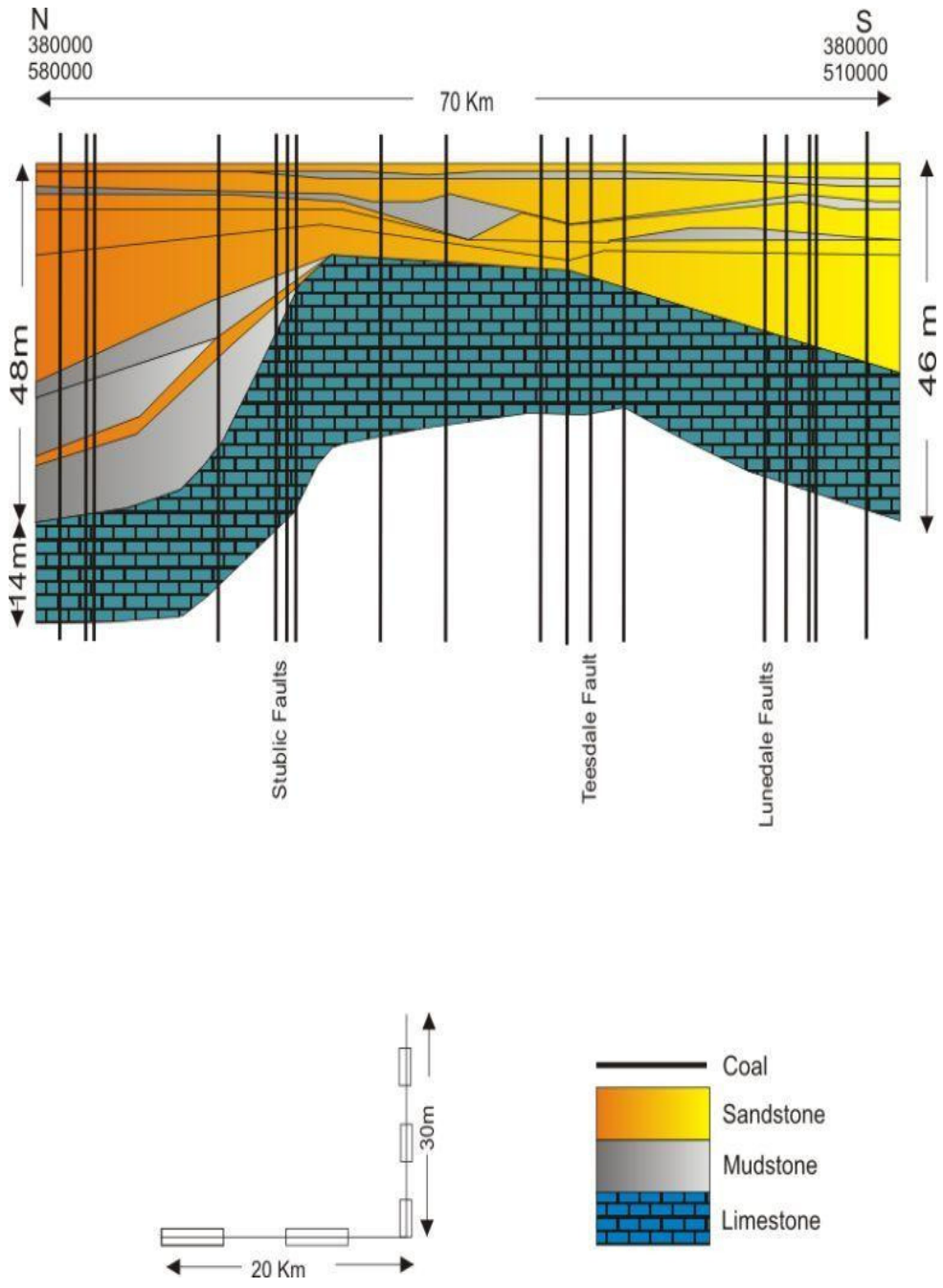

Appendix B Section line 18

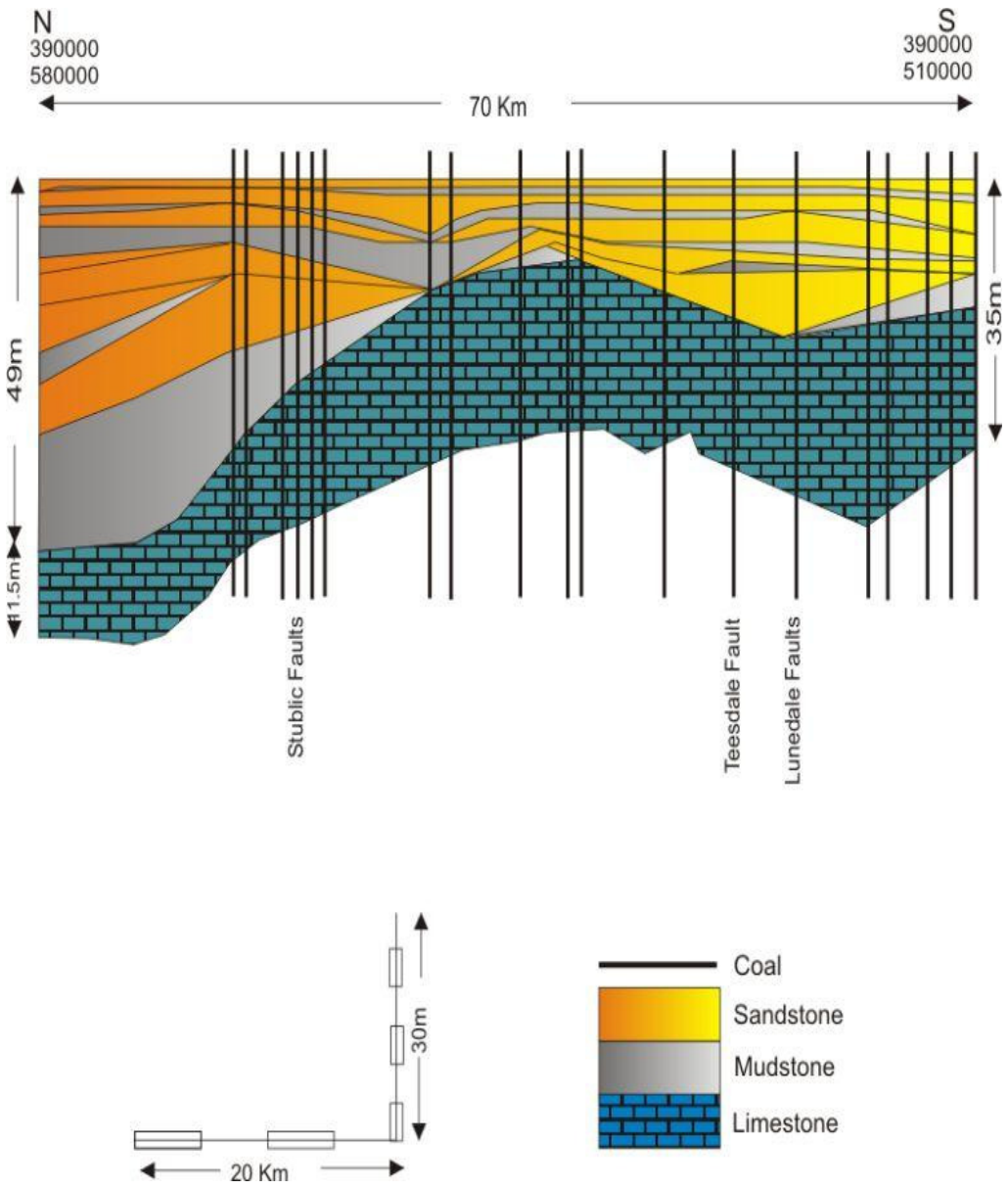

Appendix B Section line 19

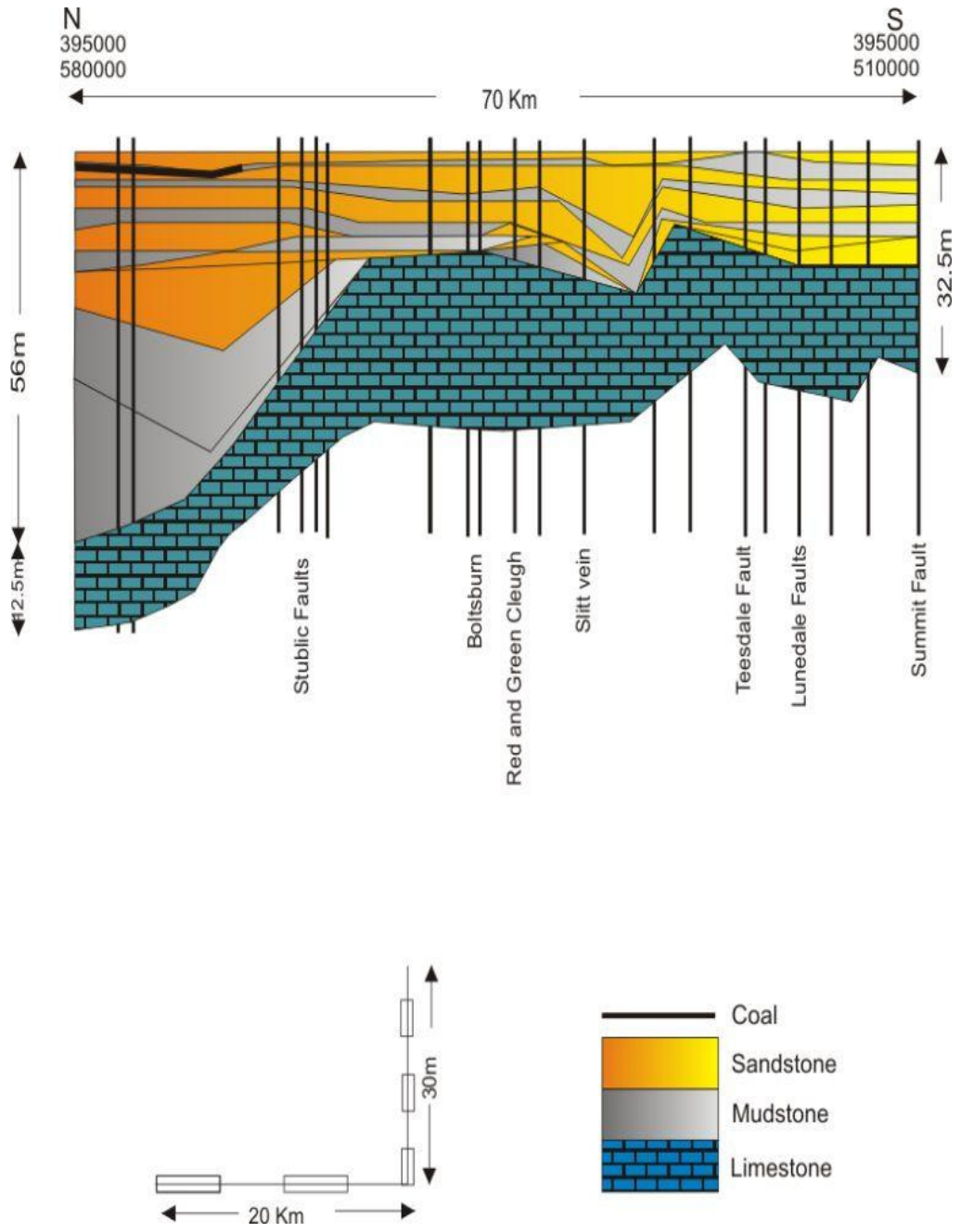

Appendix B Section line 20

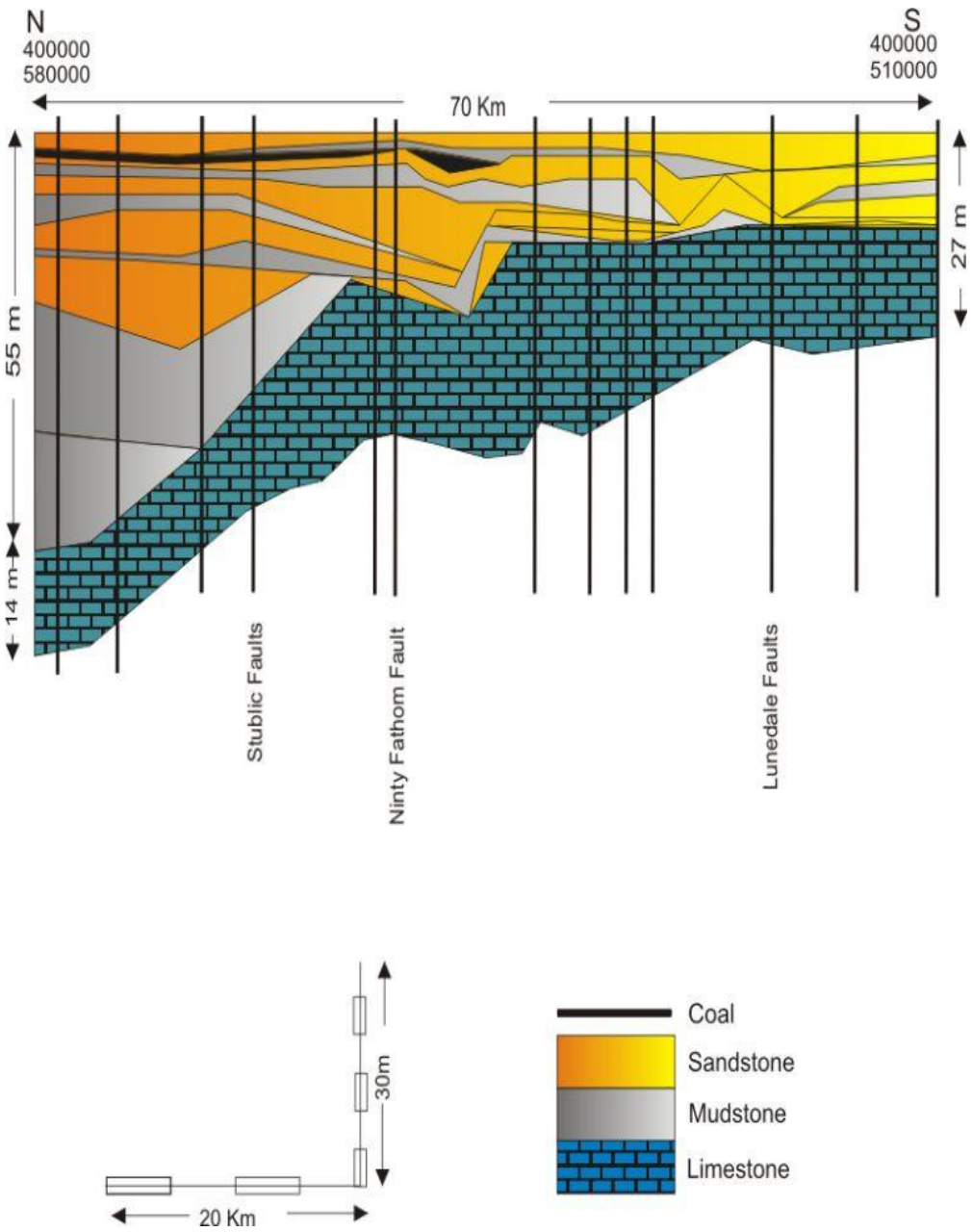

Appendix B Section line 21

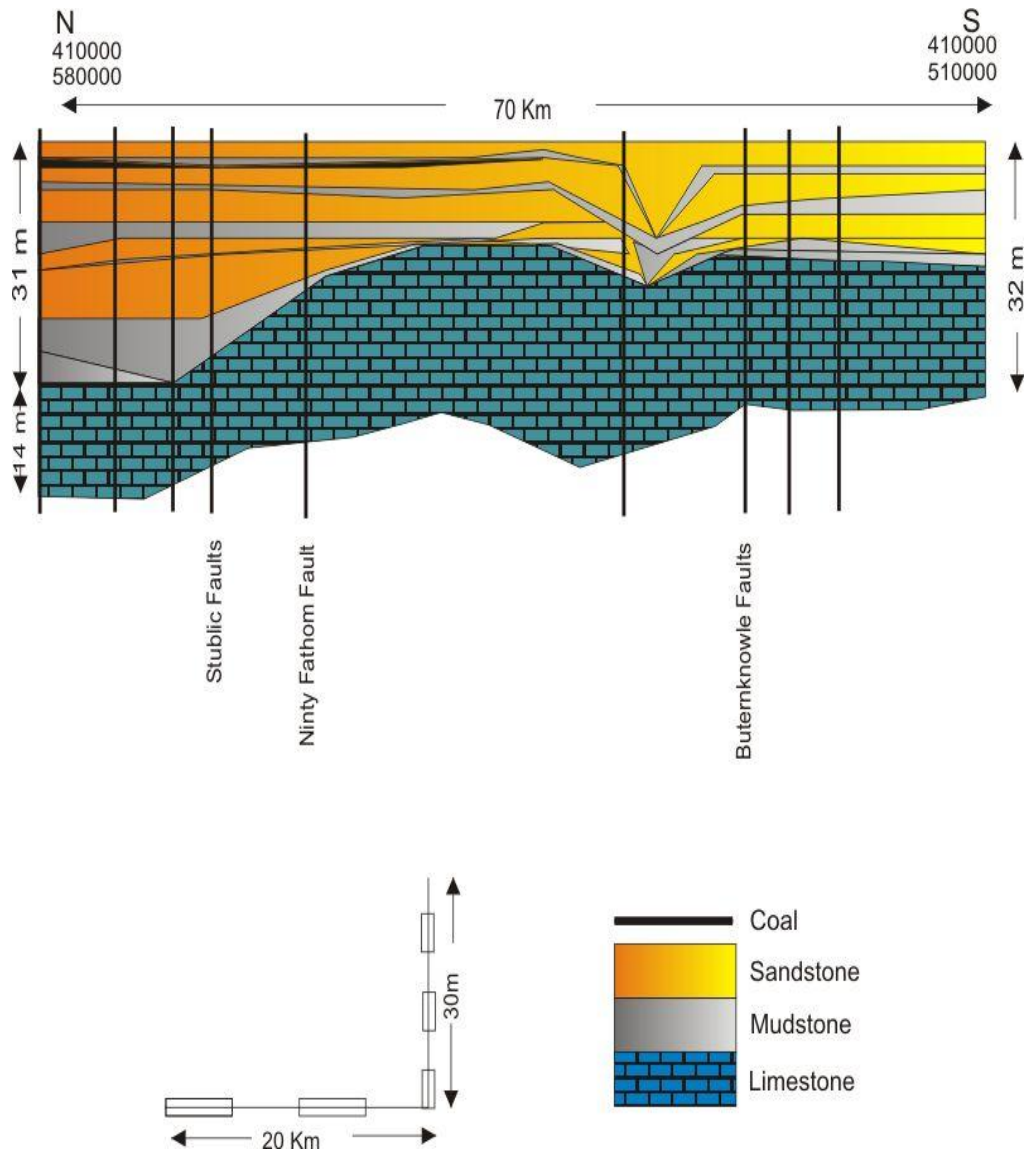

Appendix B Section line 22

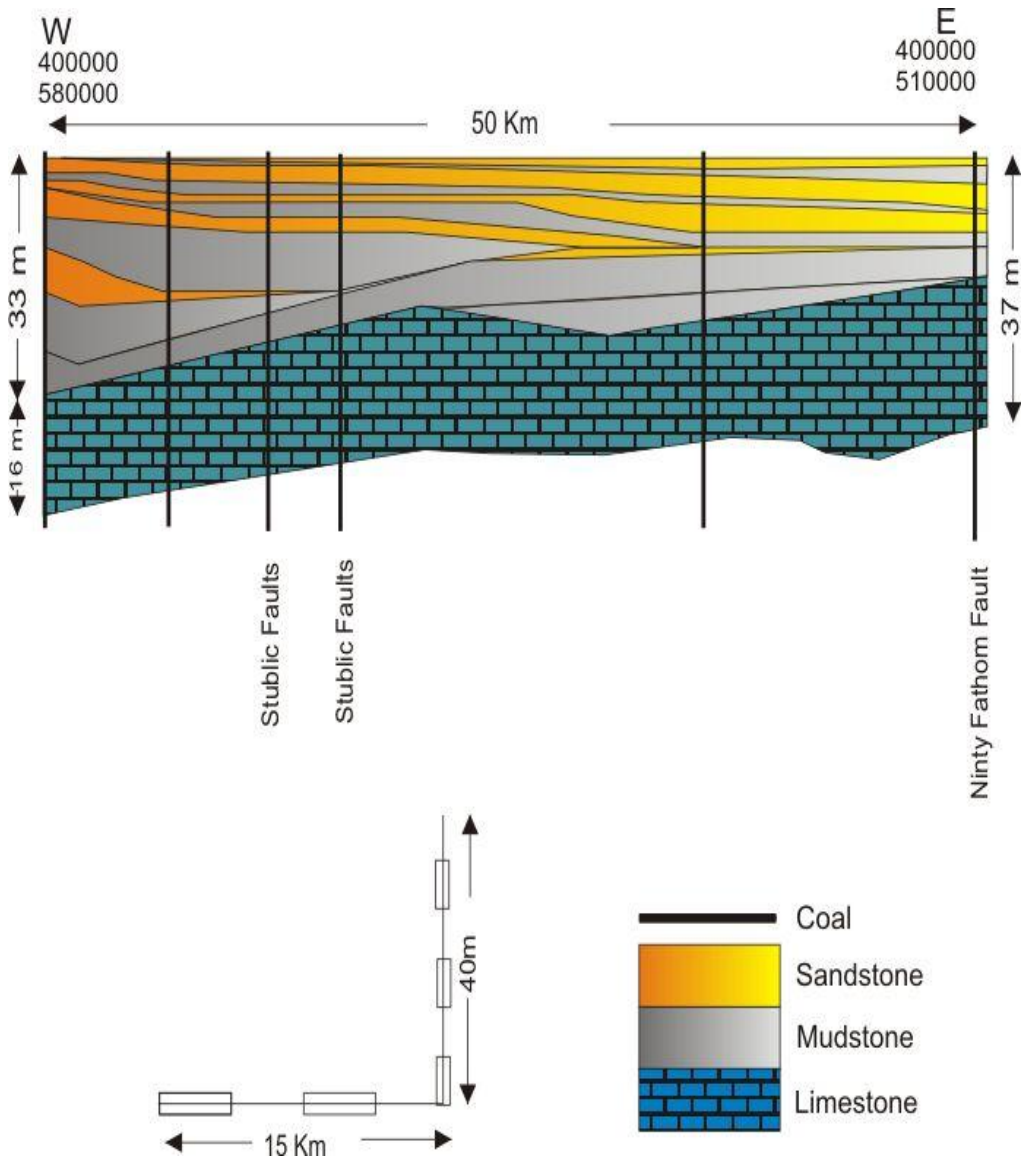

Appendix B Section line 23

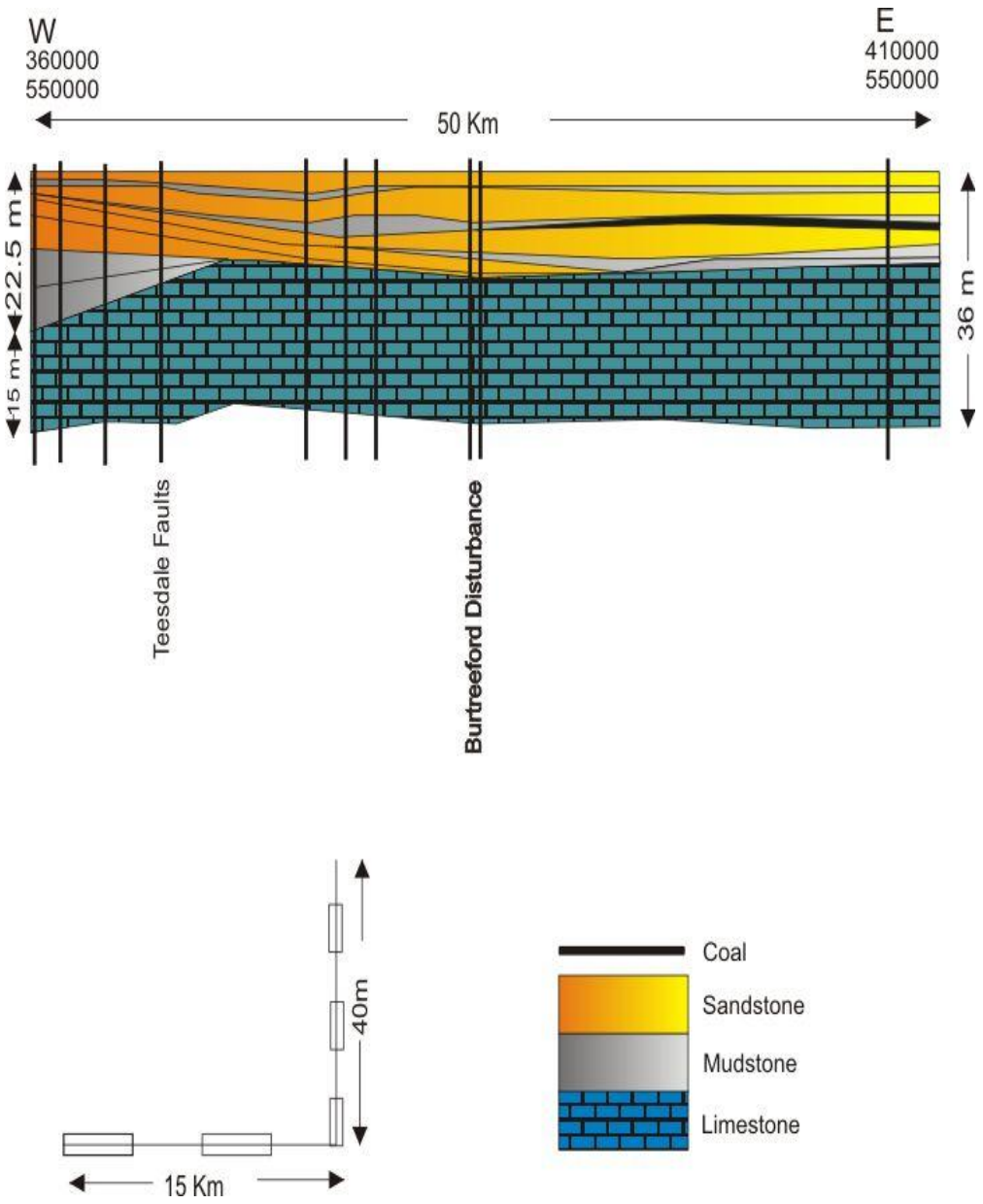

Appendix B Section line 24

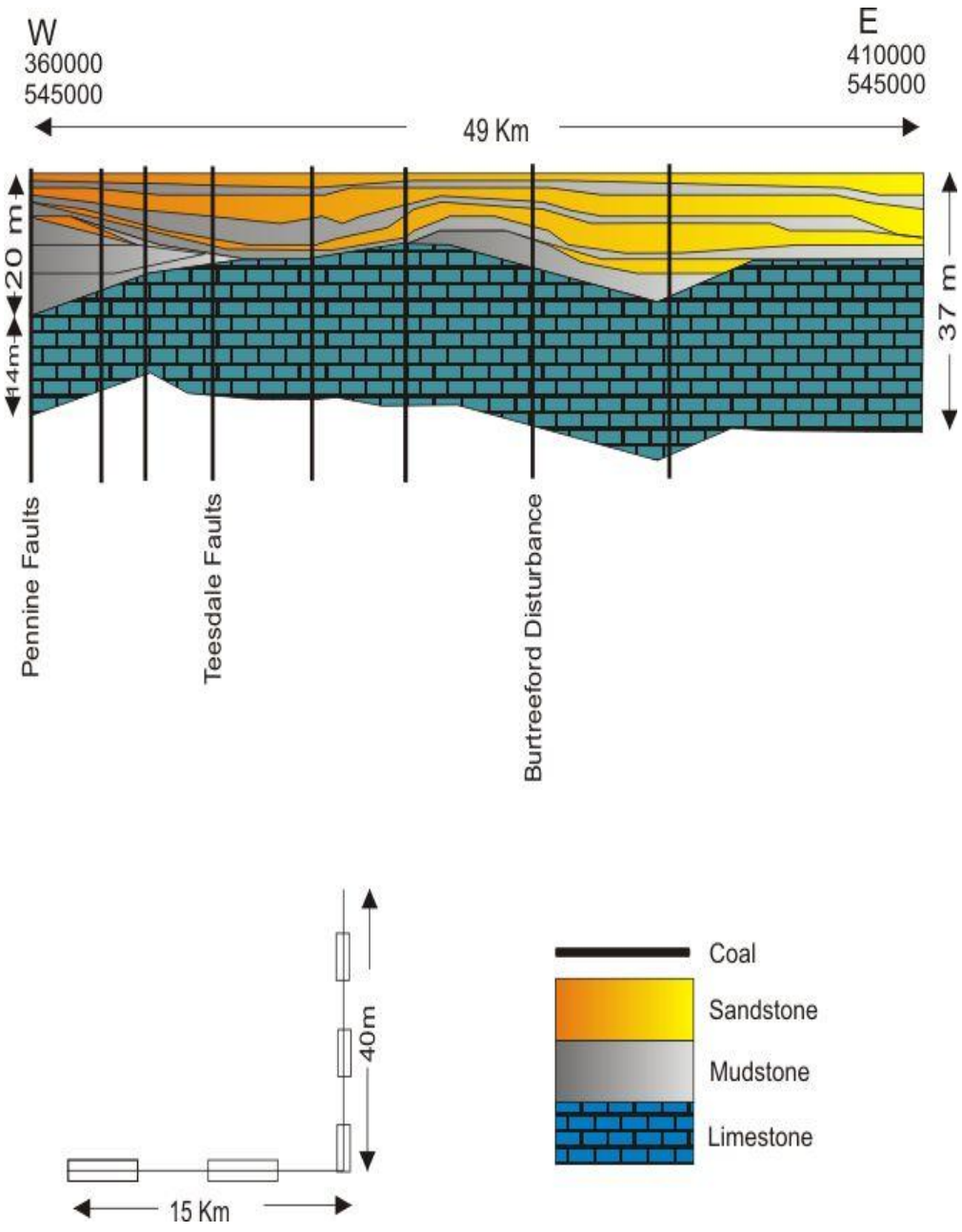

Appendix B Section line 25

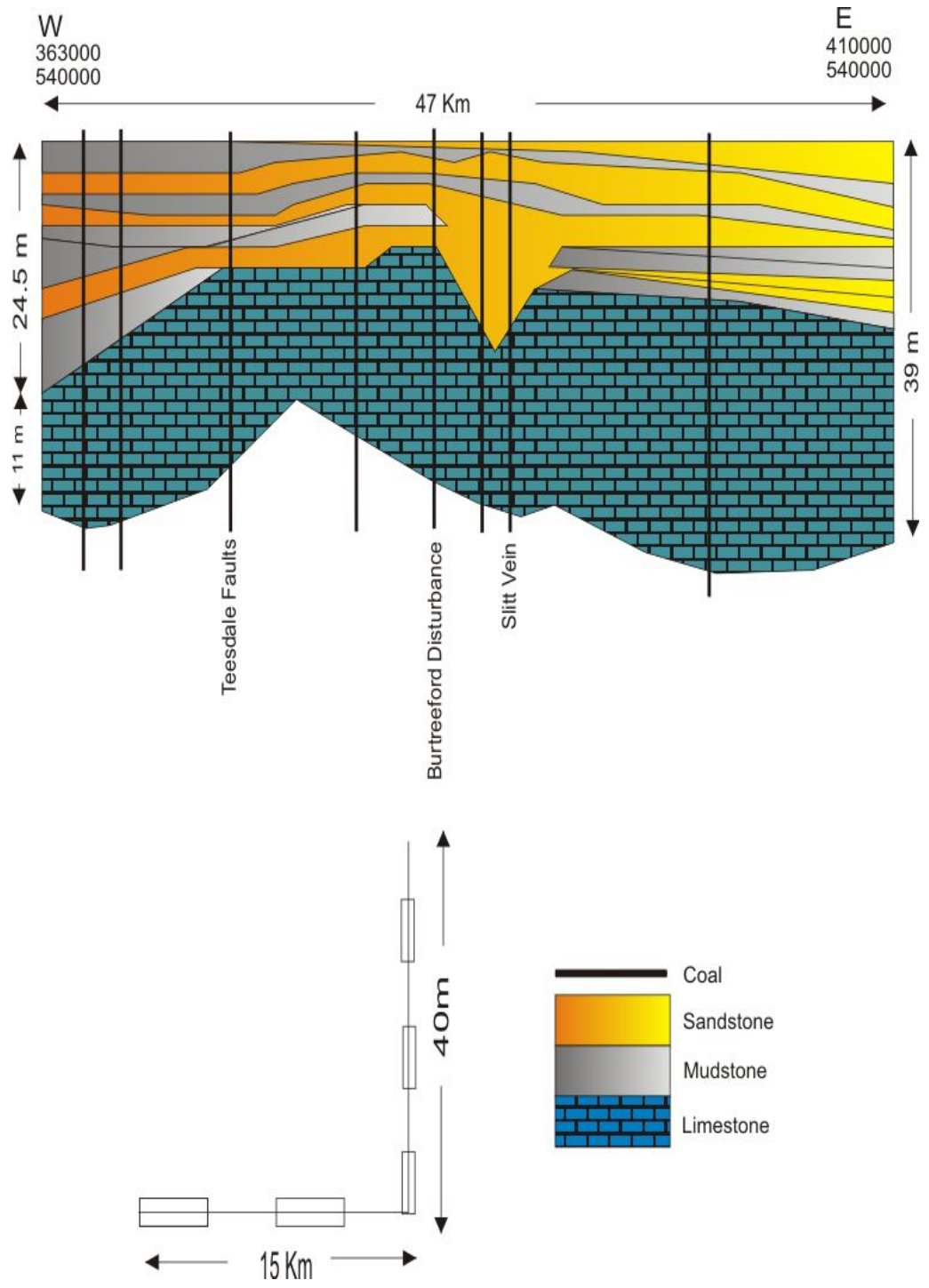

Appendix B Section line 26

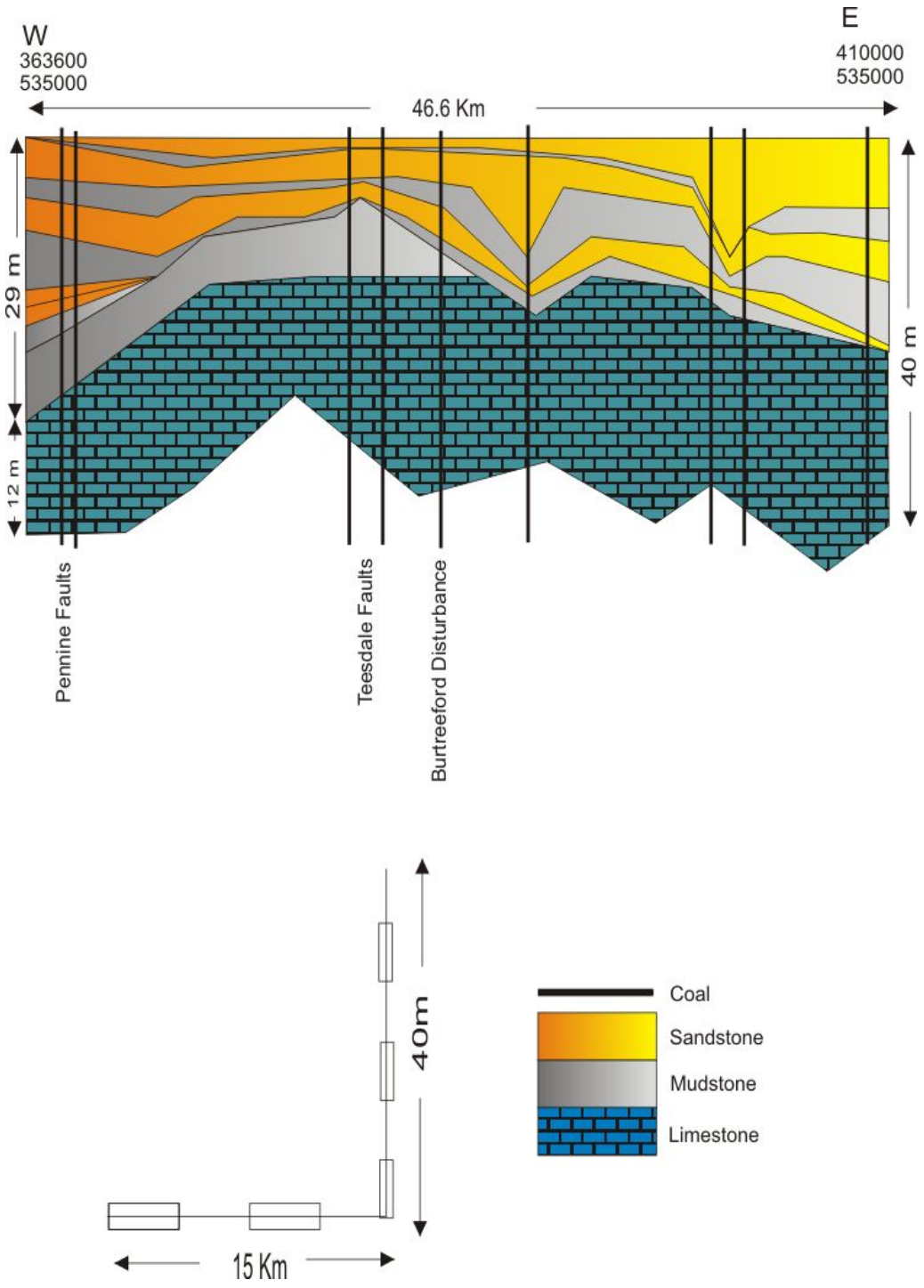

Appendix B Section line 27

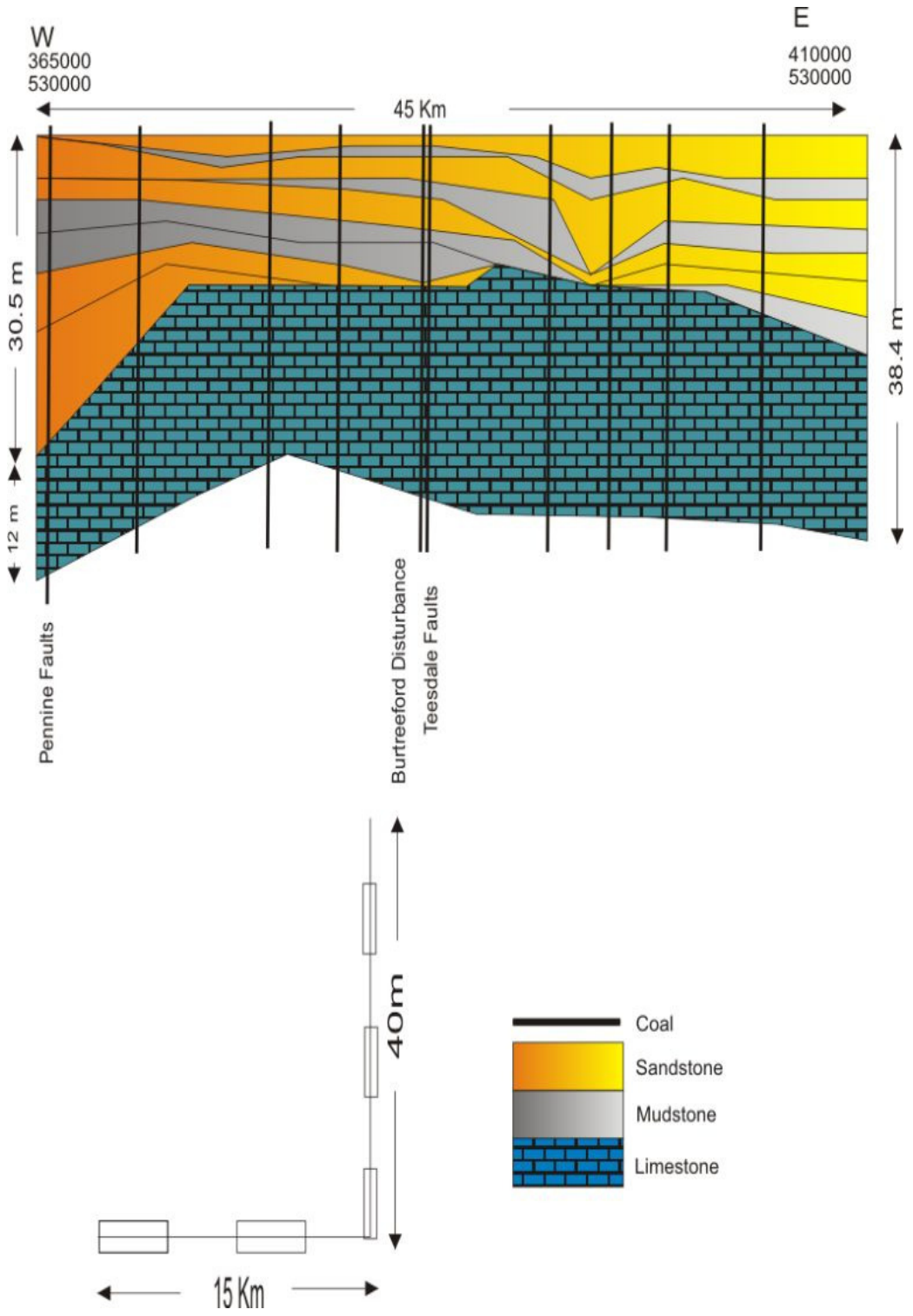

Appendix B Section line 28

Appendix C

Thickness variations within section lines 1 to 15

C.0 Introduction

These statistics are to be read in conjunction with chapter 4.0, thickness variations of Carboniferous Cyclothems and the Great limestone, and section lines within Appendix B. The section line statistics illustrates how total and unit sectional areas change throughout the block in both a west to east and a north to south direction.

The following tables are colour enhanced showing the section line statistics. The light grey cells are the calculated area in km^2 of the individual lithological units e.g. in the case of the Little Cyclothem, the calculated area of the limestone unit in section line 1 is 0.07 km^2, the calculated area of the Mudstone unit in section line 1 is 0.60 km^2 and the calculated area of the Sandstone unit in section line 1 is 0.50 km^2, giving a total area of the Little Cyclothem of 1.17 km^2.

The light orange cells are the calculated percentage that the individual lithological units are of each cyclothem e.g. in the case of the Little Cyclothem, the limestone is 6.19 percent of the cyclothem, the mudstone is 51.45 percent of the cyclothem and the sandstone is 42.35 percent of the cyclothem.

The blue cells are the percentage that the lithological unit in each cyclothem is of all similar lithological units in the section line e.g. in the case of the Little Cyclothem, the limestone is 5.21 percent of all limestones in section line 1, the mudstone is 24.13 percent of all mudstones in section line 1 and the sandstone is 21.85 percent of all sandstones in section line 1.

C.1 Section Line 1 Statistics

Section line 1 is 33.5 km long and commences at 371148 543460 and runs in a south-east to north-west direction following the line of the Teesdale Faults, Leehouse Well, Scar End and Sir John's veins and finishes at 396687 523356.

Cyclothem	Area of limestone in the cyclothem		Area of mudstone in the cyclothem		Area of sandstone in the cyclothem		Total Area of cyclothem
	Percent of Cyclothem	Percent of Limestone in section	Percent of Cyclothem	Percent of mudstone in section	Percent of Cyclothem	Percent of sandstone in section	Percentage of All Beds
Little	0.07		0.60		0.50		1.17
	6.19	5.21	51.45	24.13	42.35	21.85	19.01
Great	0.56		0.26		0.52		1.34
	41.94	40.31	19.30	10.34	38.76	22.85	21.73
Iron Post	0.01		0.11		0.17		0.29
	3.47	0.72	37.66	4.33	58.87	7.45	4.67
Four Fathom	0.21		0.38		0.17		0.76
	27.91	15.17	49.57	15.03	22.53	7.51	12.29
Three Yard	0.10		0.61		0.23		0.94
	10.50	7.07	65.38	24.56	24.12	9.97	15.23
Five Yard	0.14		0.17		0.45		0.76
	18.95	10.27	21.88	6.62	59.17	19.68	12.26
Scar	0.30		0.38		0.24	0.91	
	32.41	21.25	41.00	14.99	26.60	10.69	14.82
Totals	**1.40**		**2.50**		**2.28**		**6.17**

C.2 Section Line 2 Statistics

Section line 2 is 21 km long and commences at 380175 534354 and runs in a south-west to north-east direction and finishes at 397898 545674.

Cyclothem	Area of limestone in the cyclothem		Area of mudstone in the cyclothem		Area of sandstone in the cyclothem		Total Area of cyclothem
	Percent of Cyclothem	Percent of Limestone in section	Percent of Cyclothem	Percent of mudstone in section	Percent of Cyclothem	Percent of sandstone in section	Percentage of All Beds
Little	0.06		0.37		0.28		0.71
	7.83	7.28	52.48	30.73	39.69	23.21	22.26
Great	0.33		0.14		0.31		0.78
	42.02	42.83	18.44	11.83	39.54	25.32	24.38
Iron Post	0.02		0.04		0.04		0.10
	18.88	2.58	38.89	3.35	42.23	3.63	3.27
Four Fathom	0.11		0.18		0.11		0.40
	28.18	14.61	44.52	14.52	27.30	8.89	12.40
Three Yard	0.05		0.27		0.13		0.45
	11.82	6.90	59.82	21.98	28.36	10.41	13.97
Five Yard	0.07		0.07		0.16		0.30
	23.27	9.12	23.17	5.71	53.56	13.19	9.37
Scar	0.13		0.14		0.19		0.46
	27.81	16.68	31.46	11.88	40.73	15.35	14.35
Totals	**0.76**		**1.21**		**1.21**		**3.19**

C.3 Section Line 3 Statistics

Section line 3 is 40 km long and commences at 370000 560000 and runs in a south to north direction and finishes at 370000 520000.

Cyclothem	Area of limestone in the cyclothem		Area of mudstone in the cyclothem		Area of sandstone in the cyclothem		Total Area of cyclothem
	Percent of Cyclothem	Percent of Limestone in section	Percent of Cyclothem	Percent of mudstone in section	Percent of Cyclothem	Percent of sandstone in section	Percentage of All Beds
Little	0.11		0.95		0.52		1.57
	6.79	**5.41**	**60.23**	**31.39**	**32.98**	**22.35**	**21.50**
Great	0.75		0.48		0.44		1.67
	44.77	**37.79**	**28.94**	**15.99**	**26.29**	**18.90**	**22.80**
Iron Post	0.09		0.10		0.15		0.33
	26.77	**4.53**	**28.57**	**3.16**	**44.65**	**6.43**	**4.57**
Four Fathom	0.28		0.44		0.27		0.99
	28.11	**14.05**	**44.71**	**14.63**	**27.18**	**11.57**	**13.50**
Three Yard	0.12		0.58		0.23		0.93
	13.47	**6.33**	**62.12**	**19.09**	**24.41**	**9.76**	**12.68**
Five Yard	0.16		0.18		0.47		0.82
	19.33	**8.00**	**22.63**	**6.13**	**58.04**	**20.45**	**11.18**
Scar	0.47		0.29		0.24		1.01
	46.89	**23.90**	**28.80**	**9.61**	**24.30**	**10.55**	**13.77**
Totals	**1.97**		**3.01**		**2.32**		**7.31**

C.4 Section Line 4 Statistics

Section line 4 is 40 km long and commences at 380000 560000 and runs in a north to south direction and finishes at 380000 520000.

Cyclothem	Area of limestone in the cyclothem		Area of mudstone in the cyclothem		Area of sandstone in the cyclothem		Total Area of cyclothem
	Percent of Cyclothem	Percent of Limestone in section	Percent of Cyclothem	Percent of mudstone in section	Percent of Cyclothem	Percent of sandstone in section	Percentage of All Beds
Little	0.09		0.83		0.59		1.51
	5.75	**4.64**	**55.30**	**20.62**	**38.95**	**25.39**	**20.62**
Great	0.73		0.41		0.43		1.58
	46.59	**39.34**	**25.92**	**21.59**	**27.49**	**18.76**	**21.59**
Iron Post	0.03		0.19		0.13		0.35
	9.12	**1.73**	**53.19**	**4.84**	**37.69**	**5.77**	**4.84**
Four Fathom	0.25		0.54		0.20		0.99
	25.59	**13.55**	**54.22**	**13.53**	**20.19**	**8.64**	**13.53**
Three Yard	0.11		0.69		0.18		0.98
	10.89	**5.69**	**70.35**	**13.36**	**18.76**	**7.92**	**13.36**
Five Yard	0.17		0.21		0.44		0.81
	21.30	**9.29**	**25.29**	**11.15**	**53.41**	**18.83**	**11.15**
Scar	0.48		0.27		0.34		1.09
	44.17	**25.76**	**24.65**	**14.91**	**31.18**	**14.70**	**7.31**
Totals	**1.87**		**3.13**		**2.31**		**7.31**

C.5 Section Line 5 Statistics

Section line 5 is 40 km long and commences at 385000 560000 and runs in a north to south direction and finishes at 385000 520000.

Cyclothem	Area of limestone in the cyclothem		Area of mudstone in the cyclothem		Area of sandstone in the cyclothem		Total Area of cyclothem
	Percent of Cyclothem	Percent of Limestone in section	Percent of Cyclothem	Percent of mudstone in section	Percent of Cyclothem	Percent of sandstone in section	Percentage of All Beds
Little	0.09		0.79		0.69		1.57
	5.46	**4.90**	**50.45**	**27.16**	**44.10**	**25.44**	**21.25**
Great	0.71		0.49		0.45		1.65
	43.18	**40.68**	**29.67**	**16.78**	**27.15**	**16.45**	**22.32**
Iron Post	0.02		0.14		0.12		0.29
	7.92	**1.31**	**50.04**	**4.95**	**42.04**	**4.45**	**3.90**
Four Fathom	0.25		0.49		0.24		0.98
	25.24	**14.11**	**49.80**	**16.71**	**24.96**	**8.98**	**13.25**
Three Yard	0.13		0.61		0.38		1.12
	11.25	**7.18**	**54.79**	**20.98**	**33.96**	**13.94**	**15.12**
Five Yard	0.19		0.09		0.46		0.74
	25.08	**10.68**	**12.71**	**3.25**	**62.21**	**17.04**	**10.09**
Scar	0.37		0.30		0.37		1.04
	35.61	**21.15**	**28.56**	**10.18**	**35.84**	**13.69**	**14.07**
Totals	**1.75**		**2.92**		**2.72**		**7.38**

C.6 Section Line 6 Statistics

Section line 6 is 40 km long and commences at 390000 560000 and runs in a north to south direction and finishes at 390000 520000.

Cyclothem	Area of limestone in the cyclothem		Area of mudstone in the cyclothem		Area of sandstone in the cyclothem		Total Area of cyclothem
	Percent of Cyclothem	Percent of Limestone in section	Percent of Cyclothem	Percent of mudstone in section	Percent of Cyclothem	Percent of sandstone in section	Percentage of All Beds
Little	0.08		0.84		0.71		1.64
	5.16	**4.96**	**51.44**	**28.97**	**43.40**	**26.21**	**22.37**
Great	0.74		0.41		0.51		1.67
	44.60	**43.69**	**24.70**	**14.17**	**30.70**	**18.88**	**22.77**
Iron Post	0.02		0.09		0.08		0.18
	11.07	**1.20**	**47.78**	**3.03**	**41.16**	**2.80**	**2.52**
Four Fathom	0.25		0.43		0.27		0.95
	26.60	**14.86**	**45.31**	**14.82**	**28.08**	**9.85**	**12.99**
Three Yard	0.12		0.62		0.41		1.15
	10.03	**6.77**	**53.83**	**21.27**	**36.14**	**15.31**	**15.69**
Five Yard	0.18		0.17		0.36		0.71
	24.86	**10.32**	**24.61**	**5.98**	**50.53**	**13.17**	**9.65**
Scar	0.31		0.34		0.37		1.02
	30.22	**18.20**	**33.34**	**11.75**	**36.44**	**13.78**	**14.00**
Totals	**1.70**		**2.90**		**2.71**		**7.31**

C.7 Section Line 7 Statistics

Section line 7 is 40 km long and commences at 395000 560000 and runs in a north to south direction and finishes at 395000 520000.

Cyclothem	Area of limestone in the cyclothem		Area of mudstone in the cyclothem		Area of sandstone in the cyclothem		Total Area of cyclothem
	Percent of Cyclothem	Percent of Limestone in section	Percent of Cyclothem	Percent of mudstone in section	Percent of Cyclothem	Percent of sandstone in section	Percentage of All Beds
Little	0.10		0.95		0.74		1.79
	5.73	**5.57**	**53.02**	**32.52**	**41.24**	**26.78**	**23.81**
Great	0.73		0.19		0.72		1.63
	44.48	**39.35**	**11.67**	**6.52**	**43.85**	**25.92**	**21.68**
Iron Post	0.02		0.14		0.15		0.31
	5.37	**0.89**	**44.84**	**4.71**	**49.79**	**5.54**	**4.08**
Four Fathom	0.28		0.39		0.19		0.86
	32.83	**15.32**	**45.58**	**13.43**	**21.59**	**6.73**	**11.44**
Three Yard	0.10		0.64		0.30		1.04
	9.64	**5.46**	**61.23**	**21.87**	**29.12**	**11.01**	**13.87**
Five Yard	0.19		0.24		0.26		0.69
	27.05	**10.15**	**34.98**	**8.28**	**37.97**	**9.52**	**9.19**
Scar	0.43		0.37		0.40		1.20
	35.76	**23.26**	**30.86**	**12.67**	**33.38**	**14.50**	**15.94**
Totals	**1.84**		**2.92**		**2.76**		**7.53**

C.8 Section Line 8 Statistics

Section line 8 is 40 km long and commences at 400000 560000 and runs in a north to south direction and finishes at 400000 520000.

Cyclothem	Area of limestone in the cyclothem		Area of mudstone in the cyclothem		Area of sandstone in the cyclothem		Total Area of cyclothem
	Percent of Cyclothem	Percent of Limestone in section	Percent of Cyclothem	Percent of mudstonet in section	Percent of Cyclothem	Percent of sandstone in section	Percentage of All Beds
Little	0.14		0.69		0.94		1.76
	7.96	**7.72**	**38.91**	**23.70**	**53.13**	**34.79**	**23.81**
Great	0.75		0.42		0.49		1.66
	45.18	**41.32**	**25.08**	**14.41**	**29.74**	**18.37**	**22.46**
Iron Post	0.06		0.13		0.08		0.27
	23.38	**3.54**	**48.75**	**4.63**	**27.87**	**2.85**	**3.71**
Four Fathom	0.24		0.45		0.15		0.83
	28.82	**13.24**	**53.45**	**15.42**	**17.74**	**5.50**	**11.28**
Three Yard	0.11		0.63		0.33		1.08
	10.05	**5.94**	**58.85**	**21.87**	**31.10**	**12.43**	**14.53**
Five Yard	0.16		0.20		0.34		0.70
	22.67	**8.76**	**28.80**	**6.99**	**48.53**	**12.66**	**9.49**
Scar	0.35		0.38		0.36		1.09
	32.49	**19.48**	**34.45**	**12.98**	**33.06**	**13.39**	**14.73**
Totals	**1.82**		**2.89**		**2.69**		**7.40**

C.9 Section Line 9 Statistics

Section line 9 is 40 km long and commences at 370000 555000 and runs in a west to east south direction and finishes at 410000 555000.

Cyclothem	Area of limestone in the cyclothem		Area of mudstone in the cyclothem		Area of sandstone in the cyclothem		Total Area of cyclothem
	Percent of Cyclothem	Percent of Limestone in section	Percent of Cyclothem	Percent of mudstonet in section	Percent of Cyclothem	Percent of sandstone in section	Percentage of All Beds
Little	0.12		0.97		0.67		1.76
	6.73	**7.07**	**55.09**	**31.73**	**38.17**	**30.19**	**25.29**
Great	0.76		0.48		0.23		1.48
	51.62	**45.37**	**32.59**	**15.72**	**15.80**	**10.46**	**21.18**
Iron Post	0.02		0.09		0.07		0.19
	11.29	**1.25**	**48.74**	**2.97**	**39.97**	**3.34**	**2.67**
Four Fathom	0.03		0.52		0.31		0.85
	3.05	**1.55**	**60.67**	**16.93**	**36.28**	**13.91**	**12.26**
Three Yard	0.12		0.52		0.32		0.96
	12.03	**6.87**	**54.49**	**17.06**	**33.48**	**14.40**	**13.75**
Five Yard	0.19		0.20		0.31		0.70
	26.68	**11.05**	**29.17**	**6.63**	**44.15**	**13.78**	**9.98**
Scar	0.45		0.27		0.31		1.03
	43.55	**26.84**	**26.50**	**8.96**	**29.95**	**13.91**	**14.85**
Totals	**1.68**		**3.06**		**2.23**		**6.96**

C.10 Section Line 10 Statistics

Section line 10 is 40 km long and commences at 370000 550000 and runs in a west to east direction and finishes at 410000 550000.

Cyclothem	Area of limestone in the cyclothem		Area of mudstone in the cyclothem		Area of sandstone in the cyclothem		Total Area of cyclothem
	Percent of Cyclothem	Percent of Limestone in section	Percent of Cyclothem	Percent of mudstone in section	Percent of Cyclothem	Percent of sandstone in section	Percentage of All Beds
Little	0.12		0.91		0.79		1.82
	6.36	**6.32**	**50.05**	**28.75**	**43.59**	**33.29**	**24.65**
Great	0.69		0.56		0.26		1.52
	45.63	**37.80**	**37.14**	**17.80**	**17.23**	**10.97**	**20.56**
Iron Post	0.04		0.15		0.11		0.30
	14.79	**2.46**	**47.80**	**4.59**	**37.41**	**4.78**	**4.12**
Four Fathom	0.24		0.52		0.28		1.04
	23.21	**13.19**	**50.15**	**16.48**	**26.64**	**11.64**	**14.10**
Three Yard	0.12		0.58		0.29		1.00
	12.16	**6.64**	**58.34**	**18.41**	**29.49**	**12.37**	**13.54**
Five Yard	0.18		0.18		0.32		0.67
	26.25	**9.65**	**26.07**	**5.54**	**47.68**	**13.47**	**9.12**
Scar	0.44		0.27		0.32		1.03
	42.74	**23.95**	**26.00**	**8.43**	**31.26**	**13.47**	**13.91**
Totals	**1.83**		**3.16**		**2.38**		**7.38**

C.11 Section Line 11 Statistics

Section line 11 is 40 km long and commences at 370000 545000 and runs in a west to east direction and finishes at 410000 545000.

Cyclothem	Area of limestone in the cyclothem		Area of mudstone in the cyclothem		Area of sandstone in the cyclothem		Total Area of cyclothem
	Percent of Cyclothem	Percent of Limestone in section	Percent of Cyclothem	Percent of mudstone in section	Percent of Cyclothem	Percent of sandstone in section	Percentage of All Beds
Little	0.14		0.89		0.74		1.77
	8.00	**8.90**	**50.03**	**29.00**	**41.97**	**34.82**	**26.11**
Great	0.73		0.54		0.27		1.55
	47.15	**45.79**	**35.20**	**17.82**	**17.64**	**12.78**	**22.80**
Iron Post	0.04		0.15		0.15		0.34
	11.43	**2.43**	**42.98**	**4.76**	**45.59**	**7.22**	**4.99**
Four Fathom	0.00		0.45		0.27		0.72
	0.00	**0.00**	**61.93**	**14.62**	**38.07**	**12.86**	**10.63**
Three Yard	0.13		0.57		0.00		0.70
	18.61	**8.23**	**81.39**	**18.76**	**0.00**	**0.00**	**10.38**
Five Yard	0.15		0.17		0.36		0.69
	22.45	**9.71**	**25.04**	**5.64**	**52.51**	**16.94**	**10.15**
Scar	0.40		0.29		0.33		1.01
	39.23	**24.94**	**28.36**	**9.40**	**32.41**	**15.37**	**14.93**
Totals	**1.59**		**3.06**		**2.14**		**6.79**

C.12 Section Line 12 Statistics

Section line 12 is 40 km long and commences at 370000 540000 and runs in a west to east direction and finishes at 410000 540000.

Cyclothem	Area of limestone in the cyclothem		Area of mudstone in the cyclothem		Area of sandstone in the cyclothem		Total Area of cyclothem
	Percent of Cyclothem	Percent of Limestone in section	Percent of Cyclothem	Percent of mudstone in section	Percent of Cyclothem	Percent of sandstone in section	Percentage of All Beds
Little	0.12		0.88		0.60		1.60
	7.71	**6.89**	**54.67**	**29.61**	**37.62**	**23.23**	**21.81**
Great	0.75		0.41		0.49		1.64
	45.45	**41.56**	**24.94**	**13.83**	**29.61**	**18.72**	**22.33**
Iron Post	0.01		0.12		0.10		0.22
	4.02	**0.50**	**51.43**	**3.89**	**44.54**	**3.84**	**3.05**
Four Fathom	0.26		0.43		0.28		0.97
	26.75	**14.47**	**44.27**	**14.51**	**28.98**	**10.83**	**13.20**
Three Yard	0.11		0.59		0.34		1.04
	10.78	**6.24**	**56.27**	**19.76**	**32.95**	**13.20**	**14.14**
Five Yard	0.16		0.20		0.41		0.77
	21.18	**9.12**	**25.37**	**6.62**	**53.46**	**15.91**	**10.51**
Scar	0.38		0.35		0.37		1.10
	34.63	**21.23**	**31.72**	**11.79**	**33.65**	**14.26**	**14.97**
Totals	**1.79**		**2.96**		**2.60**		**7.35**

C.13 Section Line 13 Statistics

Section line 13 is 40 km long and commences at 370000 535000 and runs in a west to east direction and finishes at 410000 535000.

Cyclothem	Area of limestone in the cyclothem		Area of mudstone in the cyclothem		Area of sandstone in the cyclothem		Total Area of cyclothem
	Percent of Cyclothem	Percent of Limestone in section	Percent of Cyclothem	Percent of mudstone in section	Percent of Cyclothem	Percent of sandstone in section	Percentage of All Beds
Little	0.15		0.68		0.57		1.40
	10.63	**8.35**	**48.67**	**24.66**	**40.70**	**20.15**	**18.99**
Great	0.72		0.32		0.65		1.69
	42.82	**40.75**	**18.67**	**11.45**	**38.51**	**23.08**	**22.99**
Iron Post	0.01		0.16		0.14		0.30
	2.84	**0.48**	**52.33**	**5.72**	**44.83**	**4.79**	**4.10**
Four Fathom	0.25		0.41		0.25		0.91
	27.46	**14.13**	**44.69**	**14.83**	**27.85**	**9.03**	**12.43**
Three Yard	0.10		0.65		0.40		1.15
	9.11	**5.91**	**56.36**	**23.56**	**34.53**	**14.11**	**15.67**
Five Yard	0.19		0.21		0.45		0.85
	22.51	**10.79**	**24.32**	**7.52**	**53.17**	**16.06**	**11.58**
Scar	0.35		0.34		0.36		1.05
	33.23	**19.58**	**32.30**	**12.27**	**34.47**	**12.80**	**14.24**
Totals	**1.78**		**2.76**		**2.82**		**7.35**

C.14 Section Line 14 Statistics

Section line 14 is 40 km long and commences at 370000 530000 and runs in a west to east direction and finishes at 410000 530000.

Cyclothem	Area of limestone in the cyclothem		Area of mudstone in the cyclothem		Area of sandstone in the cyclothem		Total Area of cyclothem
	Percent of Cyclothem	Percent of Limestone in section	Percent of Cyclothem	Percent of mudstone in section	Percent of Cyclothem	Percent of sandstone in section	Percentage of All Beds
Little	0.09		0.81		0.58		1.49
	6.17	**4.90**	**54.56**	**29.40**	**39.27**	**20.44**	**19.86**
Great	0.72		0.29		0.71		1.71
	41.93	**38.25**	**16.79**	**10.38**	**41.28**	**24.65**	**22.79**
Iron Post	0.18		0.16		0.15		0.49
	36.31	**9.50**	**32.49**	**5.76**	**31.20**	**5.34**	**6.54**
Four Fathom	0.24		0.32		0.22		0.78
	29.99	**12.55**	**41.41**	**11.75**	**28.60**	**7.84**	**10.46**
Three Yard	0.11		0.66		0.41		1.18
	9.58	**6.04**	**55.48**	**23.72**	**34.94**	**14.43**	**15.76**
Five Yard	0.17		0.18		0.46		0.81
	21.45	**9.33**	**22.53**	**6.64**	**56.02**	**15.95**	**10.87**
Scar	0.36		0.34		0.32		1.03
	35.35	**19.43**	**33.12**	**12.34**	**31.53**	**11.35**	**13.73**
Totals	**1.87**		**2.76**		**2.86**		**7.50**

C.15 Section Line 15 Statistics

Section line 15 is 40 km long and commences at 370000 525000 and runs in a west to east direction and finishes at 410000 525000.

Cyclothem	Area of limestone in the cyclothem		Area of mudstone in the cyclothem		Area of sandstone in the cyclothem		Total Area of cyclothem
	Percent of Cyclothem	Percent of Limestone in section	Percent of Cyclothem	Percent of mudstone in section	Percent of Cyclothem	Percent of sandstone in section	Percentage of All Beds
Little	0.10		0.76		0.60		1.46
	6.88	**5.42**	**52.13**	**25.46**	**40.99**	**22.74**	**19.53**
Great	0.78		0.29		0.72		1.78
	43.52	**41.76**	**16.07**	**9.57**	**40.42**	**27.33**	**23.81**
Iron Post	0.02		0.14		0.07		0.22
	8.03	**0.97**	**60.60**	**4.52**	**31.37**	**2.66**	**2.98**
Four Fathom	0.25		0.44		0.25		0.94
	26.41	**13.32**	**46.88**	**14.68**	**26.71**	**9.50**	**12.52**
Three Yard	0.15		0.69		0.38		1.22
	12.42	**8.13**	**56.49**	**22.95**	**31.09**	**14.34**	**16.24**
Five Yard	0.22		0.23		0.34		0.78
	27.54	**11.61**	**29.06**	**7.60**	**43.41**	**12.90**	**10.46**
Scar	0.35		0.46		0.28		1.08
	32.27	**18.80**	**42.07**	**15.21**	**25.66**	**10.54**	**14.46**
Totals	**1.86**		**3.00**		**2.64**		**7.50**

Sample and Bed No	gastropods	brachiopod	crinoids	corals	bryozoans	ostracods	Forams
8 Post 1	2	36	48	0	5	2	67
9 Post 1	2	32	31	0	7	1	80
10 Post 1	15	50	108	0	50	1	98
11 Post 1	2	25	26	0	8	4	124
12 Post 1	3	23	56	0	21	1	90
13 Post 1	1	39	60	1	4	1	76
14 Post 1	1	27	62	0	11	2	94
1 Post 2	3	57	50	3	8	7	86
2 Post 2	1	55	69	0	13	3	84
3 Post 2	1	46	43	0	9	4	70
4 Post 2	4	67	42	1	9	1	79
5 Post 2	6	45	53	0	6	1	46
6 Post 2	1	55	54	0	12	1	53
7 Post 2	2	18	38	0	28	1	91
15 Post 3	0	31	52	0	35	1	121
16 Post 3	1	22	53	0	20	9	133
18 Post 3	7	9	87	0	31	5	85
20 Post 3	0	9	42	0	41	0	135
22 Post 4	2	14	43	0	37	1	112
23 Post 4	2	16	72	0	50	0	98
24 Post 5	3	24	81	1	58	1	73
27 Post 5	0	48	109	0	38	0	68
31 Post 6	0	22	98	4	36	0	88
36 Post 7	0	26	79	0	40	2	76
39 Post 8	1	6	43	0	17	2	52
43 Post 8	1	11	103	1	63	0	41
45 Post 8	0	24	56	1	48	4	66
48 Post 9	1	31	39	8	85	1	66
50 Post 9	1	39	116	1	55	1	57
51 Post 9	0	37	148	0	35	0	51
56 Post 10	0	56	81	3	42	2	60
63Post 11	1	31	144	0	44	1	45
67Post 12	3	14	73	6	88	0	83
72Post 12	0	47	52	0	18	1	56
73Post 13	1	20	85	0	60	0	46
74Post 13	2	27	97	0	51	4	27
75Post 13	3	3	89	0	40	1	36
76Post 13	0	73	84	0	51	1	23
77Post 14	2	76	21	0	17	7	21
78Post 14	0	68	38	0	46	5	47
79Post 15	0	93	38	4	28	1	22
80Post 15	1	62	45	3	24	2	42
81Post 15	10	37	75	0	32	0	64
82 Post 15	0	41	83	0	46	0	61
83 Post 15	0	75	94	0	51	0	29
86 Post 16	1	101	69	5	36	4	45
91 Post 17	0	56	98	3	36	0	52
94 Post 17	1	35	71	0	49	0	90
96 Post 17	1	35	66	0	45	5	95
100Post 17	3	36	66	5	61	0	54
106Post 18	1	40	121	2	59	0	40
110Post 18	0	64	143	3	30	0	27
114Post 18	0	42	42	0	38	0	145
117Post 19	0	25	62	0	49	0	130
121Post 20	1	51	25	0	63	5	130
125Post 20	1	22	50	0	50	4	141
128Post 21	0	5	77	0	51	0	135
138Post 23	2	10	84	0	48	0	126
140Post 23	0	6	77	0	52	0	135
143Post 23	0	12	83	0	48	0	118
144Post 23	0	20	90	0	63	0	95
149Post 25	0	31	160	0	79	0	22

Table 5.1 initial results of point counting 62 thin sections from Hudeshope Beck near Middleton in Teesdale. (O. S. 394784, 527610 and O. S. 394916, 527276)

	Algae				Foraminifera								
Thin Section No.	Palaeoberesellids	Calcifolium	Fasciella	Girvanella	Archaediscus	Calcispheres	Earlandia	Endothyra	Endothyranopsis	Eostaffella	Palaeotextularia	Tetrataxis	Total forams
10	1	0	1	0	5	18	0	20	12	41	2	0	98
12	0	0	3	0	37	24	0	21	25	16	2	0	124
1	1	0	0	0	24	9	0	38	0	11	2	2	86
4	2	0	1	0	39	4	0	26	0	5	2	3	79
15	0	0	7	0	44	24	1	17	18	13	2	2	121
16	0	0	14	0	67	49	0	5	7	3	0	1	133
18	0	0	11	0	21	9	0	7	35	3	8	1	85
20	0	0	8	0	77	24	0	6	8	10	10	0	135
22	0	0	30	0	45	36	1	11	6	11	1	1	112
23	0	0	2	0	39	24	1	14	11	3	4	2	98
24	0	0	1	1	45	12	0	4	6	3	3	0	73
27	5	0	1	0	55	5	0	0	1	1	0	6	68
31	0	0	10	0	61	7	0	9	4	3	0	4	88
36	0	51	5	1	19	17	0	21	10	6	1	2	76
39	1	150	3	1	21	18	1	9	1	2	0	0	52
43	1	35	15	0	30	3	0	2	3	3	0	0	41
45	1	70	6	1	30	21	0	5	0	7	1	2	66
48	0	18	15	1	23	12	0	10	6	12	2	1	66
50	1	0	1	0	27	4	0	17	4	5	0	0	57
51	4	1	0	0	29	7	0	7	0	7	1	1	51
56	0	30	16	0	13	13	1	10	9	11	1	2	60
63	3	5	7	0	23	8	0	7	6	1	0	1	45
67	3	0	7	2	23	11	2	24	1	19	1	2	83
72	0	101	10	8	11	21	2	15	2	2	0	3	56
74	0	75	12	0	0	8	0	3	8	6	1	1	27
76	0	56	8	0	1	7	0	1	9	0	1	4	23
81	5	9	22	0	21	4	3	27	1	9	0	0	64
83	0	0	8	0	24	0	0	3	0	1	0	1	29
86	0	13	16	0	10	20	0	9	0	5	1	0	45
91	5	6	15	0	9	0	0	21	9	8	1	4	52
94	3	10	13	1	27	12	2	28	0	21	0	0	90
96	5	7	5	2	29	11	5	35	1	14	1	0	95
100	2	13	42	0	6	11	0	17	0	18	1	1	54
106	3	0	5	0	27	3	0	5	0	2	0	3	40
110	0	0	2	0	19	2	0	4	0	1	0	1	27
114	2	0	4	0	11	8	0	44	9	71	0	2	145
117	5	0	0	0	11	13	0	38	7	56	3	2	130
121	0	0	0	0	17	8	0	23	8	70	5	0	130
125	1	0	1	0	47	16	0	12	10	54	2	0	141
128	0	0	0	0	15	3	1	50	5	55	5	1	135
138	0	0	0	0	0	0	0	45	1	75	5	0	126
140	0	0	0	0	0	3	1	46	5	74	5	1	135
143	0	0	0	0	0	0	0	63	1	48	5	1	118
144	0	0	0	0	0	0	0	61	3	31	0	0	95
149	0	0	0	0	0	0	0	5	2	15	0	0	22

Table 5.2 results of point counting 45 thin sections from Hudeshope Beck near Middleton in Teesdale. (O. S. 394784, 527610 and O. S. 394916, 527276)

Sample No	Sample Height	$\delta^{13}C$	$\delta^{18}O$	Sample No	Sample Height	$\delta^{13}C$	$\delta^{18}O$	Sample No	Sample Height	$\delta^{13}C$	$\delta^{18}O$
8	0.00	-0.3	-9.4	52	6.08	1.0	-10.2	100	12.29	1.7	-10.4
9	0.10	-0.3	-7.8	53	6.24	1.6	-9.1	101	12.30	1.3	-12.5
10	0.22	0.1	-8.3	54	6.34	0.9	-11.1	102	12.44	1.9	-10.5
11	0.30	0.0	-8.5	55	6.35	0.8	-12.3	103	12.60	1.2	-11.6
12	0.40	0.3	-8.1	56	6.51	1.7	-9.9	104	12.64	1.8	-11.5
13	0.45	0.8	-8.9	57	6.60	1.4	-10.5	105	12.65	1.7	-12.0
1	0.51	0.8	-10.2	58	6.68	0.8	-12.2	106	12.81	1.4	-11.9
2	0.61	0.9	-9.7	59	6.70	0.8	-12.2	107	12.85	0.2	-11.1
3	0.71	0.9	-9.3	60	6.83	1.9	-8.8	108	12.97	1.6	-11.1
4	0.81	1.0	-8.5	61	6.97	-0.3	-10.0	109	13.09	1.1	-11.8
5	0.89	0.5	-9.8	62	7.03	0.1	-9.9	110	13.10	1.4	-11.8
6	0.96	0.4	-9.1	63	7.25	0.4	-12.2	113	13.61	1.6	-8.0
7	1.06	0.7	-10.1	64	7.34	0.9	-11.4	114	13.81	1.1	-7.9
15	1.07	0.6	-10.9	65	7.49	1.3	-11.1	115	13.92	1.3	-10.4
16	1.27	1.0	-11.4	66	7.61	1.6	-9.1	116	13.97	0.2	-13.1
17	1.34	0.8	-11.0	67	7.62	1.4	-9.4	117	14.19	1.3	-8.1
18	1.52	0.6	-9.1	68	7.75	1.6	-8.3	118	14.52	1.3	-9.9
19	1.67	0.0	-10.3	69	7.84	1.7	-9.2	120	14.60	1.5	-11.6
20	1.82	0.8	-11.8	70	8.04	-0.3	-10.5	121	14.75	1.3	-8.9
22	1.95	0.1	-12.2	71	8.05	1.4	-9.1	122	15.00	1.4	-8.6
23	2.05	0.8	-9.0	72	8.25	1.8	-9.2	123	15.10	1.5	-10.3
24	2.03	0.8	-9.4	73	8.26	1.6	-10.3	124	15.15	1.3	-9.6
25	2.24	0.9	-10.2	74	8.41	1.4	-11.0	125	15.30	1.2	-8.2
26	2.44	1.2	-9.3	75	8.66	1.4	-9.8	126	15.45	0.8	-12.1
27	2.51	0.5	-12.5	76	8.76	1.2	-10.2	127	15.57	0.6	-12.7
28	2.66	0.8	-12.0	77	8.99	1.2	-10.6	128	15.71	1.6	-8.1
30	3.02	0.7	-11.8	78	9.00	1.2	-10.7	129	15.84	1.1	-9.1
31	3.21	0.9	-12.4	79	9.20	1.2	-10.6	130	15.94	1.0	-9.4
32	3.36	0.8	-12.8	80	9.45	1.4	-10.9	131	16.10	0.1	-11.0
33	3.56	1.5	-10.1	81	9.80	1.5	-11.0	132	16.14	1.0	-9.0
34	3.57	1.5	-11.5	82	10.00	1.3	-10.3	133	16.24	0.9	-9.5
35	3.77	1.6	-9.4	83	10.01	1.3	-11.4	134	16.34	0.8	-11.1
36	3.92	1.6	-10.7	84	10.21	1.8	-9.9	136	16.64	0.3	-12.5
37	3.98	1.6	-10.2	85	10.31	1.6	-10.4	137	16.79	1.1	-9.6
38	4.15	1.7	-10.6	86	10.46	1.6	-10.4	138	16.92	0.9	-9.0
39	4.39	1.8	-10.5	87	10.47	1.5	-12.2	139	16.99	0.2	-12.0
40	4.57	1.8	-8.7	88	10.67	1.6	-10.0	140	17.16	1.5	-9.0
41	4.62	1.5	-9.5	89	10.77	0.4	-10.0	141	17.22	1.0	-9.7
42	4.70	1.6	-9.1	90	10.95	1.2	-11.6	142	17.32	-0.7	-12.3
43	4.73	1.0	-11.6	91	11.07	1.2	-11.2	143	17.36	0.1	-11.9
44	5.02	0.9	-12.2	92	11.21	1.7	-8.7	144	17.44	0.8	-10.4
45	5.17	1.0	-11.9	93	11.42	0.9	-12.3	145	17.50	0.6	-10.9
46	5.27	1.3	-10.8	94	11.43	1.6	-10.4	146	17.80	1.0	-10.1
47	5.47	1.3	-10.2	95	11.58	1.6	-7.8	147	17.85	0.9	-10.9
48	5.77	1.4	-10.3	96	11.79	1.0	-10.5	148	18.09	0.9	-8.3
49	5.87	1.5	-10.5	97	11.94	1.1	-10.0	149	18.95	-0.7	-13.6
50	5.97	0.8	-12.2	98	11.99	1.2	-10.5				
51	6.07	1.2	-11.2	99	12.09	1.6	-12.1				

Table 7.1 Table of results $\delta^{13}C$ and $\delta^{18}O$ analysis

Height Above Base	Sample Number	Al	Fe	Mg	Mn	Si	Zn	Pb	Ba	Sr	S	Na	CaCO3	MgCO3	Soluble Material	Insoluble Residue
0.0	8	257.8	6097.7	19148.6	671.5				30.2	1776.1			74.4	6.6	81.0	19.0
0.1	9	149.0	2970.5	14960.4	413.4	205.5			16.6	916.0			79.1	5.2	84.3	15.7
0.2	10	103.6	2973.2	19384.4	362.2	103.2	37.0	5.0	12.0	1163.4	3784.0	166.5	92.2	6.7	99.0	1.0
0.3	11	150.8	2642.6	17820.2	341.7	172.7	44.5	4.5	15.7	1220.0	3768.9	174.4	92.7	6.2	98.9	1.1
0.4	12	57.0	1671.4	11251.1	305.2				16.9	1301.6			81.9	3.9	85.8	14.3
0.5	13	66.0	592.0	5703.4	145.4				15.6	1711.3			83.6	2.0	85.6	14.4
0.5	14	91.7	535.8	5234.9	144.5				19.3	2353.4			75.1	1.8	76.9	23.1
0.5	1	360.5	1230.6	12465.8	215.2	522.9	49.0	12.6	35.0	2123.2	3913.8	141.4	98.0	4.3	107.3	
0.6	2	282.1	775.5	3116.9	210.4	403.0	41.5		46.0	1027.8			79.6	3.4	83.0	17.0
0.7	3	360.8	835.4	7868.0	188.4	502.0	44.3	12.3	16.4	1424.9	3698.2	97.6	98.3	2.7	101.0	
0.8	4	346.9	1339.7	8037.4	246.4	522.2	57.2	7.7	27.0	1270.3	3495.6	116.5	97.8	2.8	100.6	
0.9	5	282.1	775.5	3116.9	210.4	403.0	41.5		46.0	1027.8			81.8	1.1	82.9	17.1
1.0	6	243.3	595.4	3413.9	206.9	341.9	20.7		27.4	1136.7			82.2	1.2	83.4	16.6
1.1	7	162.3	524.2	4392.2	187.3				15.5	1416.2			81.2	1.5	82.8	17.3
1.1	15	627.5	992.8	7540.5	258.8	807.7	180.6	8.0	19.6	1465.3	3974.8	203.5	97.0	2.6	99.6	0.4
1.3	16	168.3	708.0	3562.7	325.9	230.2	40.3		21.3	1278.3	1530.2	58.9	94.4	1.2	95.6	4.4
1.3	17	271.3	1402.5	9933.8	316.0	383.3	41.1	3.9	11.8	1391.3	3153.4	109.3	88.8	3.5	92.2	7.8
1.5	18	150.4	2383.5	14419.5	436.9	192.4	65.7	7.7	4.9	1091.7	3308.9	148.9	93.2	5.0	98.2	1.8
1.7	19	192.3	2089.1	12408.0	440.8	319.6	43.8	0.9	7.5	1261.3	3429.9	103.3	98.4	4.3	102.7	
1.8	20	194.3	1119.8	20270.7	269.2	251.9	40.0	6.1	9.6	1379.9	2608.3	62.5	86.5	7.0	93.5	6.5
1.9	21															
2.0	22	314.2	1711.2	38818.3	342.7	460.0	40.1	5.4	20.9	2092.2	1276.1	76.0	79.6	13.5	93.1	6.9
2.0	23	136.4	412.7	10539.6	206.0	171.8	255.5		12.7	1589.1	1554.9	318.4	92.2	3.7	95.8	4.2
2.1	24	231.3	398.7	4279.4	215.7	315.5	46.6	3.5	9.1	1199.3	3204.8	91.4	98.0	1.5	103.1	
2.2	25	263.5	984.7	6715.1	350.4	402.6	49.6		11.4	1309.1	3138.5	103.6	98.0	2.3	104.5	
2.4	26	117.3	702.8	3946.4	263.6	194.6	37.3		11.3	1239.5	1514.5	33.4	94.8	1.4	96.1	3.9
2.5	27	175.8	908.3	3760.9	297.3	254.1	61.1		12.2	1404.0	3055.5	97.0	97.8	1.3	99.1	0.9
2.7	28	362.8	1664.6	4992.4	385.4	538.9	97.3	4.2	22.9	1238.5	2932.3	132.6	93.6	1.7	95.4	4.6
2.8	29															
3.0	30	137.5	1344.7	4544.1	394.2	218.8	75.5		12.8	1206.8	1501.3	87.6	90.5	1.6	92.1	7.9
3.2	31	242.9	838.7	7561.8	284.2	308.6	48.2	1.3	81.9	1619.3	2955.6	107.0	94.2	2.6	96.8	3.2
3.4	32	198.5	1211.9	4769.0	433.4	288.8	38.9	3.9	51.9	1315.5	1517.6	27.9	91.3	1.7	92.9	7.1
3.6	33	92.8	295.5	3916.7	142.2	122.0	33.5		11.7	1317.1	1571.9	55.2	94.0	1.4	95.3	4.7
3.6	34	124.7	252.2	3418.3	157.0	147.5	43.5		10.3	1362.5	3019.7	76.8	97.4	1.2	98.6	1.4
3.8	35	146.9	472.1	6182.9	194.0	223.9	35.9		10.7	1395.0	1537.0	66.8	93.7	2.1	95.8	4.2
3.9	36	146.7	284.1	2980.5	140.8	196.6	31.0		9.2	1089.8	1500.0	29.0	91.0	1.0	92.0	8.0
4.0	37	91.0	345.3	3673.2	182.5	122.7	44.9		8.2	1275.1	3078.4	103.0	98.2	1.3	99.5	0.5
4.2	38	96.3	356.8	3020.4	198.0	123.6	38.5		12.6	1115.0	1579.3	43.6	94.5	1.1	95.5	4.5
4.4	39	315.4	351.0	4198.9	181.0	437.3	40.8		14.6	1428.8	2179.9	92.8	98.0	1.5	123.7	
4.6	40	155.4	368.8	3537.6	237.1	233.6	87.5		9.6	1265.0	1582.6	111.9	94.3	1.2	95.6	4.5
4.6	41	142.2	402.8	3451.5	135.4	201.5	35.2		11.6	1242.2	1676.8	81.5	96.2	1.2	97.4	2.6
4.7	42	313.0	581.6	3435.4	165.5	442.6	41.8	0.5	22.8	1318.5	3048.7	123.9	96.4	1.2	97.6	2.4
4.7	43	197.1	547.4	3201.9	247.2	274.8	32.2		13.5	1135.5	1616.8	35.0	95.4	1.1	96.5	3.5
5.0	44	162.6	837.2	5906.6	264.2	220.2	44.1		9.1	1163.8	2927.8	78.5	95.5	2.1	97.5	2.5
5.2	45	216.9	1125.6	7735.6	338.0	301.5	40.5		9.1	1189.6	2983.6	69.1	96.4	2.7	99.1	0.9
5.3	46	107.4	1343.3	13530.5	278.1	158.3	45.5	7.8	9.4	1216.1	2965.4	94.7	94.6	4.7	99.3	0.7
5.5	47	94.7	1510.5	7598.0	303.7	169.9	30.1		8.0	1112.7	1563.7	36.9	94.2	2.6	96.9	3.1
5.8	48	135.4	520.8	2798.2	207.2	180.3	45.8		7.9	1126.5	3092.4	117.0	98.0	1.0	102.0	
5.9	49	64.0	276.7	2799.9	165.8	87.0	36.5		13.7	1067.5	1814.1	45.6	98.0	1.0	102.1	
6.0	50	163.9	577.4	2364.6	209.8	227.0	33.5		13.8	1612.3	1630.4	29.7	93.0	0.8	93.8	6.2
6.1	51	344.6	530.0	3330.6	164.5	446.2	41.7		28.3	1204.8	3025.3	99.9	95.5	1.2	96.7	3.3
6.1	52	415.4	1177.6	3194.3	281.4	590.8	37.6		142.8	1351.5	1724.9	44.2	90.7	1.1	91.8	8.2
6.2	53	212.9	518.7	4239.8	146.7	312.6	40.3		28.2	1517.4	3128.9	99.0	98.1	1.5	99.6	0.4
6.3	54	206.3	348.5	3753.9	152.0	271.4	39.7		21.4	1237.7	3217.3	76.9	98.0	1.3	102.8	
6.4	55	500.6	3168.5	18960.4	559.6	780.4	33.2		41.6	1162.9	1529.3	74.5	83.2	6.6	89.8	10.2
6.5	56	326.2	601.5	7659.3	173.5	459.4	30.1		12.7	1398.8	1679.0	43.5	92.9	2.7	95.6	4.4
6.6	57	169.6	1003.6	13559.4	225.5	240.6	30.4		13.3	1503.0	1561.5	45.4	88.3	4.7	93.0	7.1
6.7	58	188.2	812.6	4437.1	420.9	247.6	44.0	3.4	23.3	1283.1	3035.9	79.2	96.6	1.5	98.2	1.8
6.7	59	204.0													0.2	
6.8	60	251.2												58.8	564.2	

Table 8.1 Trace element analysis results

Height Above Base	Sample Number	Al	Fe	Mg	Mn	Si	Zn	Pb	Ba	Sr	S	Na	CaCO3	MgCO3	Soluble Material	Insoluble Residue
7.0	61	190.1	559.8	4179.7	207.9	278.9	31.7		9.3	1307.9	1782.5	29.9	95.8	1.5	97.3	2.7
7.0	62	179.0	1196.1	8683.7	518.3	257.7	35.6		12.8	1668.5	2324.1	67.6	98.0	3.0	126.3	
7.3	63	467.0	1223.6	5258.4	258.6	653.9	48.3		45.6	1245.4	1738.3	61.8	92.1	1.8	94.0	6.1
7.3	64	402.8	733.9	2658.3	251.5	556.4	52.9	7.3	26.2	1565.7	3083.5	75.8	97.1	0.9	98.0	2.0
7.5	65	146.9	402.7	3443.0	134.4	213.7	35.4		11.7	1235.4	1821.4	62.9	96.4	1.2	97.6	2.4
7.6	66	351.5	732.9	4129.3	169.2	473.9	38.9		194.3	1414.2	3255.3	131.5	99.1	1.4	100.6	
7.6	67	684.5	710.6	3570.3	173.3	1000.7	30.9		73.2	1374.1	1811.6	36.8	92.4	1.2	93.7	6.3
7.8	68	237.2	490.7	4158.0	163.9	342.5	41.0		55.3	1530.0	3266.5	165.8	98.0	1.4	102.1	
7.8	69	353.8	655.4	4247.2	140.4	510.0	41.3		75.2	1618.8	3180.2	130.7	97.3	1.5	98.7	1.3
8.0	70	178.1	392.8	5755.2	140.4	228.7	33.7		12.0	1581.1	1915.5	55.7	94.2	2.0	96.2	3.8
8.1	71	235.1	417.6	4178.2	163.2	327.1	58.4		69.5	1608.9	1805.3	100.3	94.6	1.5	96.0	4.0
8.3	72	153.1	307.5	5563.1	132.2	190.7	52.8		14.4	1661.2	4051.4	202.8		1.9	126.6	
8.3	73	557.5	612.4	2289.7	123.9	766.4	46.7		22.5	1239.1	2932.1	101.3	92.6	0.8	93.4	6.6
8.4	74	236.0	629.3	2325.9	152.8	330.4	33.5		22.6	954.6	1740.5	10.1	94.6	0.8	95.4	4.6
8.7	75	160.5	507.2	4050.4	221.3	222.5	38.8	0.8	16.3	1083.7	3096.8	124.6	99.1	1.4	100.5	
8.8	76	132.2	495.3	2693.4	221.1	189.1	33.3		12.8	1014.6	1789.6	56.2	97.1	0.9	98.1	1.9
9.0	77	117.9	480.4	2801.2	177.6	156.6	37.6		12.9	953.3	3082.2	108.3	97.3	1.0	98.3	1.8
9.0	78	126.0	734.0	8510.8	170.8	181.5	39.2		9.6	1154.3	1760.2	66.0	95.9	3.0	98.8	1.2
9.2	79	110.8	331.9	3546.0	171.4	130.4	40.1		10.1	1093.0	3160.8	100.5	96.6	1.2	97.9	2.1
9.5	80	99.4	663.2	7861.5	221.8	123.7	50.1		17.5	1092.2	3174.4	133.7	96.1	2.7	98.8	1.2
9.8	81	1068.2	1065.7	3363.8	200.7	1555.2	39.9		17.1	1201.9	1824.7	72.0	90.1	1.2	91.2	8.8
10.0	82	825.1	1045.8	3146.2	146.7	1150.5	36.2		81.6	1447.6	1930.7	56.4	89.4	1.1	90.5	9.5
10.0	83	494.1	1087.5	2941.4	156.5	731.0	35.9		24.9	1313.3	1887.9	56.7	92.2	1.0	93.3	6.8
10.2	84	154.9	477.6	2650.5	125.2	245.0	32.3		11.8	1404.1	1856.3	32.6	94.0	0.9	95.0	5.1
10.3	85	230.9	420.6	2892.7	120.4	322.9	39.3		8.4	1215.7	3199.3	109.4	98.4	1.0	99.5	0.6
10.5	86	97.6	388.8	4097.2	110.0	121.6	41.2		7.4	1240.8	3187.6	88.9	97.3	1.4	98.7	1.3
10.5	87	167.3	661.5	8683.0	121.0	220.0	41.0		12.4	1274.3	1743.3	48.8	91.6	3.0	94.6	5.4
10.7	88	229.2	414.9	3871.5	113.0	369.0	43.7		7.6	1196.0	3208.0	113.0	98.0	1.3	99.3	0.7
10.8	89	160.1	999.8	8384.8	193.1	243.7	44.6		20.8	1241.1	1668.7	65.6	85.8	2.9	88.7	11.3
11.0	90	146.6	628.4	7364.8	175.9	195.3	36.8		14.9	1289.9	1842.6	34.3	93.1	2.6	95.7	4.3
11.1	91	144.3	486.6	2850.7	134.7	183.2	44.2		11.5	1281.3	3110.2	84.8	94.5	1.0	95.4	4.6
11.2	92	184.9	365.9	3466.5	128.1	267.0	34.2		17.9	1305.0	1868.9	67.7	94.6	1.2	95.8	4.2
11.4	93	626.2	1470.8	7765.0	180.2	912.4	47.2		37.9	1393.2	1902.6	88.9	92.6	2.7	95.3	4.7
11.4	94	151.5	357.0	3547.2	111.6	205.4	39.3		12.7	1257.9	3356.6	111.8	98.0	1.2	101.5	
11.6	95	200.7	412.0	4456.7	85.5	308.1	62.6		17.9	1585.4	2008.0	91.6	94.2	1.6	95.8	4.2
11.8	96	1000.3	1605.5	6688.3	570.3	1349.9	75.8	0.5	128.5	1507.3	1834.8	112.1	85.7	2.3	88.1	12.0
11.9	97	154.7	424.9	4754.1	103.2	217.3	64.5		13.7	1600.2	3212.3	122.4	96.9	1.7	98.5	1.5
12.0	98	214.9	766.4	8331.6	129.8	315.7	50.3	5.7	66.0	1543.5	3199.9	120.7	96.1	2.9	99.0	1.0
12.1	99	301.3	654.6	12210.7	108.6	397.3	128.9		21.6	1458.3	1803.1	152.3	89.1	4.2	93.3	6.7
12.3	100	121.6	426.0	3607.1	79.8	163.5	30.6		13.8	1379.9	1942.9	12.6	96.0	1.3	97.3	2.8
12.3	101	428.6	938.5	12546.9	192.5	644.0	39.4		30.1	1142.7	1347.4	52.0	65.2	4.4	69.5	30.5
12.4	102	294.5	617.0	12124.7	93.4	439.8	31.6		13.1	1692.5	1925.6	15.6	91.7	4.2	95.9	4.1
12.6	103	110.2	403.8	9125.2	113.7	144.4	45.7		14.4	1730.8	3126.6	89.0	94.5	3.2	97.7	2.3
12.6	104	192.6	661.5	9732.7	80.7	243.8	61.8	1.1	15.3	1389.9	3173.4	117.6	93.0	3.4	96.4	3.6
12.7	105	261.6	400.4	2893.7	109.9	321.5	41.2		18.5	1453.8	2021.7	45.6	95.5	1.0	96.5	3.5
12.8	106	383.3	627.3	3135.6	193.4	533.0	50.4		46.1	1652.6	3269.0	102.7	96.5	1.1	97.6	2.4
12.9	107	443.5	712.6	2981.8	89.1	620.8	45.6		15.9	1573.5	3328.8	142.2	96.9	1.0	97.9	2.1
13.0	108	182.2	625.5	4718.0	123.7	248.4	42.1	1.2	26.7	1343.0	3308.4	102.8	97.8	1.6	99.5	0.5
13.1	109	351.6	620.8	6021.3	116.5	451.3	49.0		27.5	1564.2	3363.5	109.0	97.9	2.1	100.0	0.0
13.1	110	272.6	441.0	6414.9	135.0	331.5	33.3		21.1	1295.1	2055.3	50.3	94.6	2.2	96.8	3.2
13.3	111															
13.5	112															
13.6	113	187.8	291.7	4391.1	76.1	257.4	38.0		14.8	1218.0	3364.4	114.1	97.5	1.5	99.0	1.0
13.8	114	340.7	416.5	5516.6	118.8	487.6	40.4		19.6	1389.6	3592.7	134.3	98.0	1.9	105.0	
13.9	115	1860.9	762.1	4216.1	189.8	2808.6	51.5	0.1	68.2	2157.2	3325.5	186.6	94.0	1.5	95.5	4.5
14.0	116	3063.2	3000.4	18928.1	92.6	4662.8	66.9	18.9	69.5	2045.1	3350.1	315.3	82.0	6.6	88.6	11.4
14.2	117	1003.6	1156.1	9003.3	151.6	1573.3	47.9		46.9	1800.2	3424.3	158.0	94.2	3.1	97.3	2.7
14.5	118	1454.4	1930.1	3480.8	97.2	2354.3	68.1		375.2	2134.8	3489.0	220.7	91.4	1.2	92.6	7.4
14.6	119															
14.6	120	5295.8	2260.4	9492.2	82.8	8168.2	34.1		124.0	2040.4	3267.9	268.5	83.6	3.3	86.9	13.1

Table 8.1 Trace element analysis results continued

Height Above Base	Sample Number	Al	Fe	Mg	Mn	Si	Zn	Pb	Ba	Sr	S	Na	CaCO3	MgCO3	Soluble Material	Insoluble Residue
14.8	121	708.9	938.8	5795.7	75.4	1103.9	38.3		100.2	2172.1	4204.5	223.4	95.0	2.0	97.0	3.0
15.0	122	820.8	1357.5	5760.1	124.4	1294.2	32.2		146.6	1932.0	2870.2	68.6	95.3	2.0	97.3	2.7
15.1	123	2475.5	5452.1	23211.0	102.8	3807.6	28.5	2.0	61.3	1493.2	6760.7	128.0	71.6	8.1	79.7	20.3
15.2	124	2404.5	2278.9	3320.6	102.3	3836.8	40.6	6.6	52.1	1797.1	3254.9	175.9	88.5	1.2	89.6	10.4
15.3	125	462.9	903.8	4973.2	92.0	732.0	31.0		166.8	1872.1	2122.6	56.3	91.7	1.7	93.4	6.6
15.5	126	4060.3	2510.8	3228.3	83.1	6079.0	43.0	12.0	94.4	2199.0	3469.8	340.0	84.7	1.1	85.8	14.2
15.6	127	3380.9	2122.1	2619.4	69.4	5139.7	35.6		32.7	1907.7	2080.9	96.7	83.2	0.9	84.1	15.9
15.7	128	547.1	894.4	5154.4	85.6	893.4	31.5		40.3	1743.0	2113.5	33.5	93.3	1.8	95.0	5.0
15.8	129	582.2	1657.2	4263.5	104.9	904.5	38.0		56.9	2213.4	3450.5	120.6	95.0	1.5	96.5	3.5
15.9	130	1203.7	2619.5	6799.3	132.4	1915.4	38.7	7.9	53.1	1919.2	3361.7	114.9	92.0	2.4	94.4	5.6
16.1	131	3061.0	11730.1	27536.9	130.2	4786.6	37.2	62.1	53.7	1374.8	5858.2	242.2	53.2	9.6	62.7	37.3
16.1	132	1276.4	3307.5	3436.9	116.6	2039.0	39.5		18.5	1538.3	2021.4	43.7	87.9	1.2	89.1	11.0
16.2	133	1908.5	4162.5	3794.0	144.5	3130.9	50.9	18.7	69.4	1780.7	3381.9	119.3	91.4	1.3	92.7	7.3
16.3	134	5038.8	6883.8	3070.1	103.6	7996.4	47.4	24.1	60.5	1667.3	2994.4	214.2	74.6	1.1	75.6	24.4
	135															
16.6	136	3283.5	7222.0	2285.4	110.0	5018.2	46.8	1.1	43.9	1418.3	1699.7	81.3	67.6	0.8	68.3	31.7
16.8	137	1470.4	3808.5	6437.5	172.3	2304.6	47.9	21.2	34.8	1474.4	3228.0	139.2	89.2	2.2	91.5	8.5
16.9	138	635.4	1080.8	4312.1	121.6	973.0	30.8		70.2	1797.2	2166.7	35.5	92.0	1.5	93.5	6.5
17.0	139	1120.5	2815.2	5479.7	135.2	1647.3	28.7		66.0	1329.6	2150.8	43.0	86.2	1.9	88.1	11.9
17.2	140	568.7	1267.6	5053.6	121.1	820.9	28.4		46.6	1510.4	3278.5	25.3	91.7	1.8	93.5	6.5
17.2	141	1750.6	4014.3	23379.7	254.3	2602.3	41.2	24.4	86.6	1624.4	3059.4	149.9	83.6	8.1	91.7	8.3
17.3	142	1924.5	7613.4	39414.6	171.9	2923.7	26.6	6.5	61.9	1378.6	1926.0	52.0	64.7	13.7	78.3	21.7
17.4	143	2973.4	8962.0	13157.8	186.0	4490.5	41.3	43.5	340.6	1664.0	5189.8	271.8	83.3	4.6	87.8	12.2
17.4	144	3003.0	6470.4	3081.9	158.8	4532.0	35.0	27.9		1486.7	3363.7	218.5	71.7	1.1	72.7	27.3
17.5	145	1907.8	5915.7	22893.3	194.8	2824.8	34.9	4.8	79.9	1585.5	1934.7	92.1	70.8	7.9	78.7	21.3
17.8	146	1214.3	2168.0	3440.2	155.8	1720.7	29.6		104.7	1702.0	2193.6	44.4	88.3	1.2	89.5	10.5
17.9	147	1367.8	2805.4	2566.1	256.7	1980.8	29.8		38.2	1414.9	2031.9	31.6	86.2	0.9	87.1	12.9
18.1	148	310.6	1261.2	4570.6	743.0	444.7	31.3		27.2	1102.6	2289.3	63.0	95.1	1.6	96.7	3.4
19.1	149	3906.8	22566.2	21130.3	982.4	5902.9	30.8		117.1	1923.5	6614.9	54.6	75.5	7.3	82.8	17.2

Table 8.1 Trace element analysis results continued

Sample_No/Name	Weight	Total_Carbon_(TC)	Total Inorganic Carbon _(TIC wt%)	Total Organic Carbon _(TOC_wt%)	Sulphur_(wt%)	Nitrogen_(wt%)	Organic Carbon/Nitrogen
JG1B	0.3002	11.52	11.14	0.38	0.01282	0.03478	10.9258
JG2B	0.3009	11.65	11.58	0.07	0.0152	0.01973	3.5479
JG3B	0.3005	11.71	11.64	0.07	0.00769	0.01842	3.8002
JG4B	0.2999	11.55	11.44	0.11	0.00766	0.02043	5.3842
JG5B	0.3004	11.65	11.56	0.09	0.00872	0.01972	4.5639
JG6B	0.2999	11.44	11.29	0.15	0.00344	0.02141	7.0061
JG7B	0.3008	11.57	11.53	0.04	0.00664	0.01641	2.4375
JG8B	0.3	11.15	11.61		0.00555	0.02264	
JG9B	0.3005	11.64	11.5	0.14		0.01838	7.617
JG10B	0.3004	11.43	11.23	0.2	0.00658	0.02326	8.5985
JG11B	0.3002	11.41	11.16	0.25	0.00661	0.02418	10.3391
JG12B	0.3004	11.37	11.31	0.06	0.00663	0.02055	2.9197
JG13B	0.3005	11.64	11.58	0.06	0.00555	0.01692	3.5461
JG14B	0.3	11.7	11.62	0.08	0.00871	0.01781	4.4919
JG15B	0.3002	11.79	11.64	0.15	0.00766	0.01791	8.3752
JG16B	0.2995	11.63	11.38	0.25	0.00661	0.02369	10.553
JG17B	0.3018	11.65	11.35	0.3	0.00871	0.02149	13.96
JG18B	0.3007	11.77	11.57	0.2	0.00662	0.01742	11.4811
JG19B	0.3012	11.83	11.73	0.1	0.00451	0.0196	5.102
JG20B	0.3011	11.65	11.3	0.35	0.00555	0.03052	11.4679
JG21B	0.3017	11.67	11.35	0.32	0.00556	0.02476	12.9241
JG22B	0.2998	11.8	11.68	0.12	0.00555	0.02086	5.7526
JG23B	0.3008	11.81	11.66	0.15	0.00763	0.01837	8.1655
JG24B	0.3016	11.78	11.62	0.16	0.0045	0.01852	8.6393
JG25B	0.3004	11.69	11.37	0.32	0.00874		
JG26B	0.3	11.57	10.85	0.72	0.00974		
JG27B	0.3004	11.69	11.58	0.11	0.00662	0.01876	5.8635
JG28B	0.3002	11.51	11.17	0.34	0.00872	0.02705	12.5693
JG29B	0.3019	11.79	11.68	0.11	0.00769	0.01957	5.6208
JG30B	0.2998	11.86	11.75	0.11	0.00656	0.01728	6.3657
JG31B	0.2998	11.72	11.52	0.2	0.00132	0.0216	9.2593
JG32B	0.3	11.85	11.56	0.29	0.00662	0.02249	12.8946
JG33B	0.3015	11.91	11.72	0.19	0.00554	0.01941	9.7888
JG34B	0.3013	11.89	11.7	0.19	0.00765	0.0189	10.0529
JG35B	0.3001	11.88	11.69	0.19	0.00449	0.01891	10.0476
JG36B	0.3001	11.75	11.68	0.07	0.00448	0.01632	4.2892
JG37B	0.3009	11.81	11.63	0.18	0.00451	0.01818	9.901
JG38B	0.2996	11.88	11.68	0.2	0.00026	0.01678	11.919
JG39B	0.3013	11.86	11.94		0.00345		
JG40B	0.3	11.96	11.77	0.19	0.00554		
JG41B	0.3008	11.9	11.86	0.04		0.02883	1.3874
JG42B	0.3007	11.65	11.28	0.37		0.0268	13.806
JG43B	0.3003	12.03	11.85	0.18		0.02714	6.6323
JG44B	0.3011	11.85	11.89			0.02828	
JG45B	0.3008	11.85	11.76	0.09		0.02728	3.2991
JG46B	0.3008	12.07	11.87	0.2		0.02805	7.1301
JG47B	0.2998	12.57	11.34	1.23	0.00131	0.05095	24.1413
JG48B	0.2998	11.93	11.78	0.15	0.00027	0.02657	5.6455
JG49B	0.301	11.86	11.64	0.22		0.02671	8.2366
JG50B	0.301	11.83	11.72	0.11		0.02536	4.3375
JG51B	0.3012	11.81	11.73	0.08	0.00026	0.02671	2.9951
JG52B	0.301	11.84	11.69	0.15	0.00131	0.02767	5.421
JG53B	0.3008	11.97	11.22	0.75	0.00027	0.04053	18.5048
JG54B	0.2993	11.63	11.51	0.12		0.0288	4.1667
JG55B	0.3013	11.66	11.66		0.00452	0.02954	
JG56B	0.2999	11.49	11.31	0.18	0.00344	0.03113	5.7822
JG57B	0.3009	11.46	11.38	0.08	0.00452	0.03182	2.5141
JG58B	0.3012	11.61	11.39	0.22		0.03011	7.3065
JG59B	0.3007	11.68	11.08	0.6	0.0056	0.03911	15.3413
JG60B	0.3012	11.8	11.77	0.03		0.02502	1.199
JG61B	0.3004	11.73	11.49	0.24	0.00025	0.02771	8.6611
JG62B	0.3019	11.56	11.35	0.21	0.00131	0.02646	7.9365
JG63B	0.3008	11.77	11.72	0.05		0.02493	2.0056
JG64B	0.3018	11.75	11.67	0.08		0.02564	3.1201
JG65B	0.3018	11.77	11.63	0.14		0.03086	4.5366

Table 8.2 CSN analysis results

Sample_No/Name	Weight	Total_Carbon_(TC)	Total Inorganic Carbon _(TIC wt%)	Total Organic Carbon _(TOC_wt%)	Sulphur_(wt%)	Nitrogen_(wt%)	Organic Carbon/Nitrogen
JG66B	0.3001	11.78	11.69	0.09		0.02789	3.227
JG67B	0.3004	11.78	11.73	0.05		0.02613	1.9135
JG68B	0.3014	11.81	11.82			0.03003	
JG69B	0.3015	11.93	11.69	0.24		0.03584	6.6964
JG70B	0.2998	11.55	11.25	0.3	0.00237	0.03693	8.1235
JG71B	0.3004	11.92	11.5	0.42	0.00025	0.03607	11.644
JG72B	0.3011	11.93	11.79	0.14	0.00237	0.02809	4.984
JG73B	0.3012	11.46	11.4	0.06		0.02648	2.2659
JG74B	0.3008	11.37	11.32	0.05		0.0257	1.9455
JG75B	0.2996	11.57	11.41	0.16		0.03115	5.1364
JG76B	0.3016	11.5	11.25	0.25	0.00132	0.0257	9.7276
JG77B	0.3004	11.68	11.55	0.13		0.02783	4.6712
JG78B	0.3006	11.8	11.7	0.1		0.02634	3.7965
JG79B	0.3008	11.77	11.71	0.06		0.02621	2.2892
JG80B	0.3005	11.77	11.69	0.08		0.02783	2.8746
JG81B	0.3008	11.56	11.68			0.02788	
JG82B	0.2996	11.82	11.71	0.11		0.02784	3.9511
JG83B	0.3009	11.81	11.69	0.12		0.02884	4.1609
JG84B	0.3	11.76	11.57	0.19		0.02754	6.8991
JG85B	0.3012	11.71	11.32	0.39	0.00107	0.03353	11.6314
JG86B	0.3014	11.84	11.63	0.21		0.02984	7.0375
JG87B	0.3014	11.86	11.7	0.16		0.02777	5.7616
JG88B	0.2995	11.8	11.72	0.08		0.02697	2.9663
JG89B	0.3014	11.82	11.75	0.07		0.02821	2.4814
JG90B	0.3008	11.82	11.71	0.11		0.03257	3.3773
JG91B	0.3013	11.72	11.16	0.56		0.04822	11.6134
JG92B	0.2999	11.94	11.73	0.21		0.02905	7.2289
JG93B	0.2997	11.89	11.76	0.13		0.02863	4.5407
JG94B	0.3016	11.68	11.59	0.09		0.02769	3.2503
JG95B	0.3	11.79	11.54	0.25		0.03073	8.1354
JG96B	0.3001	11.89	11.68	0.21		0.02723	7.7121
JG97B	0.2997	11.94	11.77	0.17	0.00106	0.03029	5.6124
JG98B	0.3002	11.55	11.27	0.28		0.03046	9.1924
JG99B	0.299	12.03	11.71	0.32		0.03178	10.0692
JG100B	0.3012	11.94	11.44	0.5	0.00212	0.04117	12.1448
JG101B	0.301	12.08	11.65	0.43		0.03475	12.3741
JG102B	0.3009	12.02	11.74	0.28	0.00211	0.03254	8.6048
JG103B	0.2996	12.03	11.68	0.35	0.00106	0.03059	11.4416
JG104B	0.3014	12	11.73	0.27		0.03171	8.5147
JG105B	0.2992	10.72	10.38	0.34	0.00212	0.03347	10.1584
JG106B	0.3006	12.32	11.06	1.26	0.00212	0.05904	21.3415
JG107B	0.3009	11.92	11.77	0.15		0.03101	4.8371
JG108B	0.2996	11.93	11.63	0.3		0.03512	8.5421
JG109B	0.3004	11.96	11.69	0.27	0.00107	0.03751	7.1981
JG110B	0.3009	11.99	11.7	0.29		0.04119	7.0405
JG111B	0.3007	11.94	11.77	0.17	0.00317	0.03648	4.6601
JG112B	0.3018	11.63	11.38	0.25	0.00424	0.03545	7.0522
JG113B	0.3004	11.33	10.9	0.43	0.00107	0.03804	11.3039
JG114B	0.3014	11.81	11.75	0.06		0.03288	1.8248
JG115B	0.3007	11.84	11.75	0.09	0.00106	0.03653	2.4637
JG116B	0.3014	11.79	11.54	0.25		0.03569	7.0048
JG117B	0.3008	11.81	11.65	0.16		0.03368	4.7506
JG118B	0.3001	11.84	11.74	0.1		0.03222	3.1037
JG119B	0.2994	11.86	11.73	0.13	0.00106	0.03434	3.7857
JG120B	0.3003	11.87	11.72	0.15		0.03164	4.7408
JG121B	0.2999	11.89	11.75	0.14	0.00343	0.02585	5.4159
JG122B	0.2999	11.84	11.73	0.11	0.00344	0.027	4.0741
JG123B	0.301	11.72	11.55	0.17		0.02527	6.7273
JG124B	0.3019	11.69	11.62	0.07		0.02822	2.4805
JG125B	0.3012	11.77	11.78			0.0254	
JG126B	0.3014	11.74	11.8			0.02705	
JG127B	0.3001	11.79	11.83		0.00025	0.02692	
JG128B	0.3014	11.79	11.81			0.02537	
JG129B	0.3015	11.77	11.8		0.00025	0.02447	

Table 8.2 CSN analysis results continued

Sample_No/Name	Weight	Total_Carbon_(TC)	Total Inorganic Carbon _(TIC wt%)	Total Organic Carbon _(TOC_wt%)	Sulphur_(wt%)	Nitrogen_(wt%)	Organic Carbon/Nitrogen
JG130B	0.2996	11.64	11.69			0.02693	
JG131B	0.3007	11.72	11.7	0.02	0.00131	0.02767	0.7228
JG132B	0.3005	11.71	11.72		0.00239	0.02943	
JG133B	0.3011	11.73	11.74			0.02459	
JG134B	0.3005	11.82	11.78	0.04		0.02694	1.4848
JG135B	0.2997	11.74	11.8			0.0235	
JG136B	0.3012	11.79	11.77	0.02	0.00026	0.02489	0.8035
JG137B	0.2995	11.77	11.77			0.02489	
JG138B	0.3008	11.73	11.65	0.08		0.02862	2.7952
JG139B	0.3013	11.68	11.7			0.02604	
JG140B	0.2998	11.75	11.72	0.03		0.02656	1.1295
JG141B	0.3004	11.67	11.74		0.00131	0.02823	
JG142B	0.3006	11.31	11.55			0.02762	
JG143B	0.3	11.59	11.46	0.13		0.03395	3.8292
JG144B	0.3001	11.63	11.52	0.11	0.0013	0.03117	3.529
JG145B	0.3007	11.64	11.53	0.11	0.00554	0.03182	3.4569
JG146B	0.3	11.6	11.52	0.08	0.00342	0.05477	1.4607
JG147B	0.2997	11.27	11.14	0.13	0.00341	0.03002	4.3304
JG148B	0.3012	11.7	11.46	0.24	0.00238	0.03242	7.4028
JG149B	0.3002	11.56	11.41	0.15	0.00549	0.03667	4.0905
JG150B	0.2997	11.46	11.37	0.09		0.02718	3.3113
JG151B	0.3006	11.45	11.3	0.15	0.00238	0.0342	4.386
JG152B	0.301	11.26	11.11	0.15	0.00237	0.02794	5.3686
JG153B	0.2999	11.52	11.41	0.11	0.00132	0.02634	4.1762
JG154B	0.2995	10.75	10.24	0.51	0.01497	0.04553	11.2014
JG155B	0.3008	11.32	10.91	0.41	0.00557	0.02846	14.4062
JG156B		11.58			0.00555	0.01838	
JG157B	0.2993	11.63	11.42	0.21	0.0013	0.01593	13.1827
JG158B	0.3006	11.54	11.41	0.13		0.02278	5.7068
JG159B	0.3016	11.4	11.42			0.04718	
JG160B	0.2997	11.55	11.39	0.16	0.00025	0.08569	1.8672

Table 8.2 CSN analysis results continued

Height Above Base	Distances Between Stylolites/Beds	Height Above Base	Distances Between Stylolites/Beds	Height Above Base	Distances Between Stylolites/Beds
0	0	5.17	0.12	10.95	0.13
0.4	0.38	5.4	0.23	11.21	0.25
0.51	0.17	5.47	0.1	11.42	0.23
0.81	0.22	5.6	0.1	11.43	0.1
1.06	0.31	5.7	0.1	11.53	0.06
1.27	0.18	5.77	0.1	11.58	0.02
1.34	0.14	5.87	0.05	11.79	0.2
1.82	0.48	6.07	0.17	11.94	0.14
1.95	0.1	6.15	0.13	11.99	0.13
2.05	0.1	6.24	0.12	12.29	0.25
2.24	0.12	6.35	0.11	12.44	0.23
2.25	0.05	6.51	0.15	12.72	0.22
2.44	0.19	6.7	0.22	12.81	0.1
2.51	0.07	6.83	0.05	12.97	0.13
2.56	0.05	7.03	0.24	13.09	0.05
2.66	0.07	7.14	0.1	13.1	0.12
2.68	0.05	7.34	0.18	13.19	0.07
2.82	0.16	7.49	0.19	13.25	0.05
2.96	0.12	7.75	0.19	13.5	0.23
3.02	0.12	7.84	0.15	13.61	0.14
3.13	0.05	8.04	0.1	13.67	0.06
3.21	0.1	8.18	0.23	13.81	0.07
3.36	0.1	8.36	0.18	13.97	0.3
3.41	0.08	8.66	0.27	14.19	0.15
3.45	0.04	8.76	0.07	14.52	0.35
3.56	0.05	9	0.4	15	0.4
3.57	0.1	9.2	0.15	15.45	0.5
3.68	0.08	9.45	0.2	16.24	0.8
3.77	0.1	9.6	0.15	16.79	0.5
3.92	0.17	9.68	0.08	17.5	0.8
3.98	0.11	9.8	0.15	17.8	0.2
4.15	0.19	10	0.15	18.1	0.28
4.39	0.07	10.21	0.26	18.22	0.2
4.52	0.2	10.31	0.1	18.62	0.4
4.57	0.03	10.46	0.06	18.74	0.12
4.73	0.2	10.47	0.02	19.09	0.35
4.95	0.2	10.67	0.2	19.56	1.1
5.02	0.1	10.77	0.14		

Fischer Plots

Fischer Plots have been used in this study for a comparison of bed thickness data between outcrops in the search for any bed patterns through the Great limestone. Following Fischer's 1964 paper, bed thickness analysis has been carried out by way of a simple graphical method of showing cumulative deviation of bed thickness relative to the average bed thickness. Fischer Plots of metre-scale shallowing-upward cycles have been used to interpret long-term changes in accommodation space and for interpreting relative sea-level changes through time. However, such interpretations can only be made for cycles that shallow up to sea level with subaerial exposure. Fischer Plots track the cumulative departure from mean cycle thickness and therefore, the plot shape is sensitive to the mean thickness.

Fischer Plots have been widely used in sequence stratigraphic studies to identify long-term cycle thickness patterns, which reflect particular systems tracts. However, there has been much discussion and even controversy with regard to their use (Drummond and Wilkinson, 1993: Saddler *et al*., 1993; Boss and Rasmussen, 1995: Burgess *et al*., 2001: Murray *et al*., 1996: Burgess, 2006; Bosence *et al*., 2009). If several different sections are analysed and similar patterns are found in the plots which can be correlated then this goes a long way to confirm their validity. The Fischer Plot of bed thickness for Middleton in Teesdale Chapter 3 (Fig. 3.26) has been compared with Fischer Plots from other sections in Weardale (Fairbairn, 1978) in Chapter 3 (Fig. 3.27), and similarly shaped plots were found. Even though the beds of the Great Limestone are not thought to have filled the available accommodation space (there is little indication of subaerial exposure, however, see Chapter 3, section 3.6.8), the principle behind Fischer plots as a means of displaying patterns and trends is still thought to be useful.

Apart from providing a visual display of data, Fischer Plots can be analysed statistically (Sadler *et al*. 1993). In this regard it has been suggested that 50 is the minimum number of cycles/beds that can give a meaningful plot. Statistical analysis involves determining whether the Fischer Plot is showing a

random or ordered arrangement of the beds/cycles through the succession. Plots which are too short may not have any interpretive value (Day, 1997: Husinec *et al*., 2008).

The number of beds in the Great Limestone at the Middleton in Teesdale locality is only 25; since this is less than 50, a Fischer Plot may not be very meaningful and it may not be possible to confirm statistically that the pattern is non-random. Nevertheless, as discussed above, the Middleton in Teesdale Fischer Plot is extremely similar to plots from several other locations in Weardale, suggesting that the pattern itself extends over the Alston Block.

Runs Analysis

As discussed, to assess the Fischer Plot further, Runs Analysis can be used to test the data for randomness. Runs analysis is used to assess whether the pattern in the plot has arisen by pure chance, i.e. it assesses whether there are signs of randomness in the length of the run and frequency of the runs. The most commonly used methods for Runs Analysis of bed thickness patterns are the assessment of runs about the median (RAM) and runs up and down (RUD) (Murray *et al*., 1996). RAM can be used to examine groupings of thick and thin beds and codes beds thinner than the median as zero and those thicker as one; the numbers of ones and zeros are then counted to give the number of runs. RUD highlights any local trends in upward-thickening and upward-thinning beds. Considering one data point (bed), the thickness of the next point/bed is assessed and if it is thicker than the first it is coded as one, otherwise it is coded as zero; the number of runs of ones and of zeros is then counted, to give the number of runs. The total number of runs and the distance from the mean value of runs is then calculated as a z-score which can be looked up in tables of area under the tails of the standard normal distribution (Sadler *et al*., 1993).

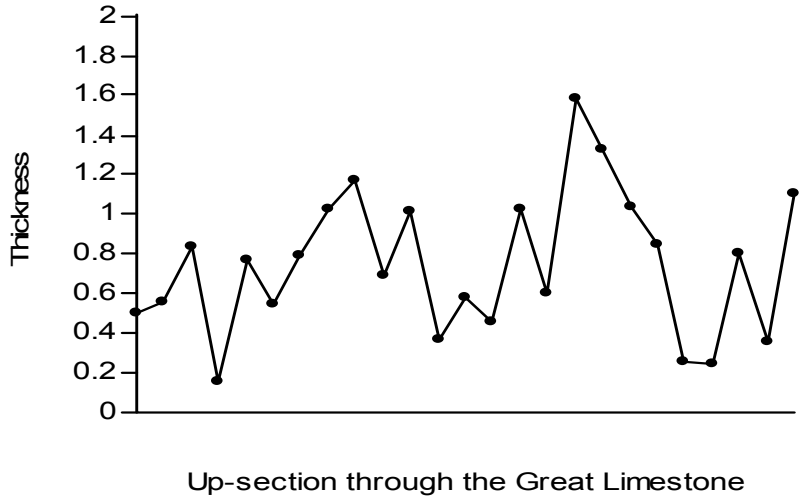

Figure 1 Plot of bed thickness throughout the Great Limestone

	RAM	RUD
N_1 (number of thick cycles)	13	12
N_2 (Number of thin cycles)	12	13
Number of Runs	16	18
Z-Score	+1.03	+1.85

Table 1 Results of RUNS analysis for Middleton in Teesdale beds

Figure 1 is a plot of bed thickness changes up through the Great Limestone at Middleton in Teesdale and is used for the calculation of RAM and RUD. The results of the RUNS analysis in Table 1 shows z-values of 1.03 (RAM) and 1.85 (RUD), both of which suggest that the pattern is due to chance and is not from an ordered periodic forcing. Sadler *et al*. (1993) showed that z-scores between -2.1 and +2.1 are within the random field; Bosence *et al.* (2009) regarded the range as -1.8 to +1.8.

Conclusion

Fischer Plots are used in this research for comparison of bed thickness patterns from many localities. The use of Fischer Plots for the Great Limestone beds can be questioned since there are generally around 25 data points used, when a minimum of 50 points is recommended. However, the patterns in all Fischer Plots of the Great Limestone from Weardale are similar, but the z scores indicate a random pattern. Overall then, this shows that the factors controlling deposition of the beds in the Great Limestone are operating over a large area in a uniform way, to give individual beds of a similar thickness, but the time-frame of bed deposition through the limestone is quite random.

References

Adams, A. E., Al-Zahrani, **M. S.** (2000) Palaeoberesellids (Dasycladaceans) from the Upper Jurassic Arab-D reservoir, Saudi Arabia. *Palaeontology,* **43,** 591-597.

Adams, A. E., Horbury, A. D., Ramsay, A. T. S. (1992). Significance of Palaeoberesellids (Chlorophyta) in Dinantian sedimentation, UK. *Lethaia,* **25.** 375-382.

Aguirre, J., Riding, R. (2005) Dasycladalean Algal Biodiversity Compared with Global Variations in Temperature and Sea Level over the Past 350 Myr. *Palaios.* **20.** 581-588.

Ainsworth, R. B., Crowley, S. F. (1994) Wave-dominated nearshore sedimentation and 'forced' regression: post-abandonment facies, Great Limestone Cyclothem, Stainmore, UK. *Journal of the Geological Society, London*. **151.** 681-695.

Algeo, T. J., Berner, R. A., Maynard, J. B., Scheckler, S. E. (1995) Late Devonian oceanic anoxic events and biotic crisis "Rooted" in the evolution of vascular land plants. *GSA Today,* **5,** 64-66.

Alibert, A., Kinsley, l., Fallon, S. J., McCulloch, M. T., Berkelmans, R., McAllister, F. (2003). Source of trace element variability in Great Barrier Reef corals affected by the Burdekin flood plumes. *Geochimica et Cosmochimica Acta.* **67**, 231-248.

Al-Hashimi, W., S. (1976). Significance of strontium distribution in some carbonate rocks in the Carboniferous of northern England. *Journal of Sedimentary Petrology*. **46**, 369-376.

Allison, P. A., Wright, V. P. (2005) Switching off the carbonate factory: A-tidality, stratification and brackish wedges in epeiric seas. *Sedimentary Geology.* **179.** 175-184.

Amorosi, A., Colalongo, M.L., Dinelli, E., Lucchini, F., Vaiani, S.C. (2007). Cyclic variations in sediment provenance from late Pleistocene deposits of the eastern Po Plain, Italy. In: Arribas, J., Critelli, S., Johnsson, M.J. (Eds.), Sedimentary Provenance and Petrogenesis: Perspectives from Petrography and Geochemistry. Geology Society of America Special Paper, vol. 420, pp. 13–24.

Amorosi, A., Colalongo, M. L. (2005). The linkage between alluvial and coeval nearshore marine successions: evidence from the Late Quaternary record of the Po River Plain, Italy. In: Blum, M.D., Marriott, S.B., Leclair, S.F. (Eds.), Fluvial Sedimentology VII. Special Publication, vol. 35. International Association of Sedimentologists, 257–275.

Amorosi, A., Centineo, M.C., Colalongo, M.L., Fiorini, F. (2005). Millennial-scale depositional cycles from the Holocene of the Po Plain, Italy. *Marine Geology* **222– 223**, 7–18.

Amorosi, A., Colalongo, M.L., Fiorini, F., Fusco, F., Pasini, G., Vaiani, S.C., Sarti, G. (2004). Palaeogeographic and palaeoclimatic evolution of the Po Plain from 150-ky core records. *Global and Planetary Change* **40**, 55–78.

Amorosi, A., Centineo, M.C., Colalongo, M.L. Pasini, G., Sarti, G., Vaiani, S.C. (2003). Facies architecture and Latest Pleistocene–Holocene depositional history of the Po Delta (Comacchio area). Italy. *The Journal of Geology* **111**, 39–56.

Amorosi, A., Colalongo, M.L., Pasini, G., Preti, D. (1999). Sedimentary response to Late Quaternary sea-level changes in the Romagna coastal plain (northern Italy). *Sedimentology* **46**, 99–121.

Amorosi, A., Colalongo, M.L., Fusco, F., Pasini, G., Fiorini, F. (1999). Glacio-eustatic control of continental-shallow marine cyclicity from Late Quaternary deposits of the southeastern Po Plain (Northern Italy). *Quaternary Research* **52**, 1–13.

Amorosi, A., Marchi, N. (1999). High-resolution sequence stratigraphy from piezocone tests: an example from the Late Quaternary deposits of the SE Po Plain. *Sedimentary Geology* **128**, 69–83.

Anderson , J. L., Arthur, M. A. (1983) Stable isotopes of oxygen and carbon and their application to sedimentologic and palaeoenvironmental problems. *In* Arthur, M. A., Anderson, T. F., Kaplan, I. R., Veizer, J., Land, L. S., eds., Stable isotopes in sedimentary geology: Society of Economic palaeontologists and Mineralogists Short Course no 10, pp 1-151.

Aretz, M. (2010) Rugose corals from the upper Viséan (carboniferous) of the Jerada Massif (NE Morocco): taxonomy, biostratigraphy, facies and palaeobiogeography. *Paläontologische Zeitschrift* doi: 10.1007/s12542-009-0046-0.

Arrigo, K. R., G. L. Van Dijken. (2003) Phytoplankton dynamics within 37 Antarctic coastal polynyas. *Journal of Geophysical Research*. **108**, 27-1 to 27-18

Arrigo, K. R., D. Lubin, G. L. van Dijken, O. Holm-Hansen, Morrow, **E.** (2003) The impact of a deep ozone hole on Southern Ocean primary production. *Journal of Geophysical Research.* **108**, 23-1 to 23-19

Armstrong, H. A., Brasier, M. D. (2005). Microfossils, pp, 296, Blackwell Publishing, Oxford.

Armstrong, H. A., Purnell, M. A. (1987). Dinantian conodont biostratigraphy of the Northumberland Trough. *Journal of Micropalaeontology,* **6**, 97-112.

Baccelle L., Bosellini A. (1965): Diagrammi per la stima visiva della composizione percentuale nelle rocce sedimentarie. Ann. Univ. Ferrara (N.S.) sez. **9**, 4: 59-62.

Baldwin, B. (1971). Ways of deciphering compacted sediments. *Journal of. Sedimentary Petrology*. **41**, 293-301.

Bartolini, A., Pillet, B., Mattioli, E., Hunziker, J., C. (2002). Shallow-platform palaeoenvironmental conditions recorded in deep-shelf sediments: C and O stable isotopes in Upper Jurassic sections of southern Germany (Oxfordian-Kimmeridgian). *Sedimentary Geology*. **31**, 1-24

Bathurst, R. G. C. (1991). Pressure-dissolution and limestone bedding: the influence of stratified cementation: In Cycles and Events in Stratigraphy Ed**.** Einsele, G. Ricken, W. Seilacher A. Chapter 3, Diagenetic Overprint. Springer-Verlag Berlin**.**

Bathurst, R. G. C. (1987). Diagenetically enhanced bedding in argillaceous platform limestones: stratified cementation and selective compaction. *Sedimentology*. **34**. 749-778.

Bausch, W. M. (1968) Clay content and calcite crystal size of limestones. *Sedimentology*. **10**. 71-75.

Bayon, G., German, C. R., Burton, K. W., Nesbitt, R. W., Rogers, N. (2004). Sedimentary Fe–Mn oxyhydroxides as paleoceanographic archives and the role of aeolian flux in regulating oceanic dissolved REE. *Earth and Planetary Science Letters*. **224.** 477-492.

Beadle, H. L. (1980). Mining and Smelting in Teesdale. *Cleveland Industrial Archaeological Society Research Report*. **3**.

Bennett, C. (2008) A review of the Carboniferous colonisation of non-marine environments by ostracods. *Palaeobiodiversity and Palaeoenvironments*. **88.** 37-46.

Berner, R., A. (1994) 3GEOCARB II: A revised model of atmospheric CO_2 over Phanerozoic time: *American Journal of Science.* **294,** 56-91.

Berner, R., A. (1978). Equilibrium kinetics, and the precipitation of magnesian calcite from seawater. *American Journal of Science.* **278**, 1435-1477.

Berner, R., A. (1975). The role of magnesium in the crystal growth of calcite and aragonite from seawater. *Geochimica et Cosmochimica Acta.* **39**, 489-504.

Bless, M. J. M., Bouckaert, J., Paproth, E. (1987) In European Environments. Ed. Miller, J. Adams, A. E., Wright, V. P. John Wiley and Sons Ltd.

Bosence, D., Procter, D. E., Aurell, M., Kahla, A. B. Boudagher-Fadel, M., Casaglia, F., Cirilli, S., Mehdie, M., Nieto, L., Rey, J., Scherreiks, R., Soussi, M., Waltham, D. (2009) A dominant tectonic signal in high- frequency, peritidal carbonate cycles? A regional analysis of Liassic platforms from western Tethys. *Journal of sedimentary research,* **79**, 389-415

Boss, S. K., Rasmussen, K. A. (1995) Misuse of Fischer plots as sea-level curves. *Geology*, **23**, 221-224.

Bott, M. H. P. (1987). Subsidence mechanisms of Carboniferous basins in northern England. In: *European Dinantian Environments* (J. Miller, A.E. Adams, V.P. Wright, eds.). John Wiley and Sons, 21-32.

Bott, M. H. P. (1984). Subsidence mechanisms of Carboniferous basins of UK. In: *First Meeting on European Dinantian environments* (A.E. Adams, T.P. Burchette, J. Miller, R.D. Maughn, V.P. Wright, eds.). Open University Press, Berkshire, 96.

Bott, M. H. P., Swinburn, P. M., Long, R. E. (1984). Deep structure and origin of the Northumberland and Stainmore Basins. *Proceedings of the Yorkshire Geological Society*, **44**, 479-495.

Bott, M. H. P., Johnson, G. A. L. (1967). The controlling mechanism of Carboniferous cyclic sedimentation. *Quarterly Journal of the Geological Society of London*, 122(488), 421-441.

Brand, U. Legrand-Blain, M. Streel, M. (2004). Biochemostratigraphy of the Devonian-Carboniferous boundary global stratotype section and point, Griotte Formation, La Serre, Montagne Noire, France. *Palaeogeography, Palaeoclimatology, Palaeoecology*. **205.** 337-357

Brand, U., Legrand-Blain, M. (1993) Paleoecology and biogeochemistry of brachiopods from the Devonian-Carboniferous boundary interval of the Griotte Formation, La Serre, Montagne Noire, France. *Annales de la Societe Geologique de Belgique.* **115.** 497-505.

Brand, U., Veizer, J. (1980) Chemical diagenesis of a multicomponent carbonate system-1: Trace elements. *Journal of Sedimentary Petrology, **50,*** 1219-1236.

Brenchley, P. J., Harper, D. A. T. (1998) palaeoecology: Ecosystems, Environments and Evolution. Routtledge.

Bruckschen, P., Oesmann, S., Veizer, J. (1999). Isotope stratigraphy of the European Carboniferous: proxy signals for ocean chemistry, climate and tectonics. *Chemical Geology*, **161**, 127-163.

Bruckschen, P., Veizer, J. (1997). Oxygen and carbon isotope composition of Dinantian brachiopods: Palaeoenvironmental implications for the Lower Carboniferous of western Europe. *Palaeogeography, Palaeoclimatology, Palaeoecology.* **132**, 243-264.

Burgess, P. M. (2006). The signal and the noise: forward modelling of allocyclic and autocyclic processes influencing peritidal carbonate stacking patterns. *Journal of Sedimentary Research.* **76.** 962-977.

Burgess, P. M., Wright, V. P., Emery, D. (2001) Numerical forward modelling of peritidal carbonate parasequence development: implications for outcrop interpretation. *Basin Research*, **13**, 1-16.

Burgess, I. C. Holliday, D. W. (1979). Geology of the country around Brough-under-Stainmore. Memoir for 1:50000 Geological Sheet 31 and parts of sheets 25 and 30. *British Geological Survey*. pp131.

Burgess, I. C., Mitchell, M. (1976). Viséan lower Yoredale limestones on the Alston and Askrigg Blocks, and the base of the D 2 zone in northern England. *Proceedings of the Yorksire Geological Society.* **40**, 613-630

Cabrera, S. C., Slitter, W. V., Jarvis, I. (1999) Integrated foraminiferal biostratigraphy and chemostratigraphy of the Querecual formation (Cretaceous), Eastern Venezuela. *Journal of Foraminiferal Research.* **29.** 487-499

Calver, M. A. (1969). Distribution of Westphalian marine faunas in northern England and adjoining areas. Proceedings of the Yorkshire Geological Society. **37,** 1-72.

Cain, J. D. C. (1968) Aspects of the depositional environments and palaeoecology of crinoidal limestones. *Scottish Journal Geology.* **4.** 191-208.

Caputo, M. V., Crowell, J. C. (1985). Migration of glacial centers across Gondwana during Paleozoic Era. *Geological Society of America Bulletin*, **96**, 1020-1036.

Carpenter, S., J. Lohmann, K., C. Holden, P. Walter, L., M. Huston, T., J. Halliday, A., N. (1991) $\delta^{18}O$ values, $^{87}Sr/^{86}Sr$ and Sr/Mg ratios of late Devonian abiotic marine calcite: Implications for the composition of ancient seawater. *Geochimica et Cosmochimica.***55.** 1991-1010.

Cherns, L., Wright, V. P. (2000**).** Missing molluscs as evidence of large-scale, early skeletal aragonite dissolution in a Silurian sea. *Geology*. **28**. 791-794.

Chao, W. C., Chen, B. (2001). The origin of monsoons. *Journal of the Atmospheric Sciences*, **58**, 3497-3507.

Cimino, G., Duce, G. D., Kadonaga, L. K., Rotundo, G., Sisani, A., Stabiloe, G., Tirozzi, B., Whiticar, M. (1999) Time Series Analaysis of geological data. *Chemical geology.* **161.** 253-270.

Clark, P.U.,Webb, P.S., Keigwin, L.D., (Eds) (1999). Mechanisms of global climate change at millennial time scales. Geophysical Monograph, American Geophysical Union, 112.

Cliff, R. A., Drewery, S. E., Leeder, M. R. (1991). Sourcelands for the Carboniferous Pennine river system; constraints from sedimentary evidence and U-Pb geochronology using zircon and monazite. In: *Developments in sedimentary provenance studies* (A.C. Morton, S.P. Todd and P.D.W. Haughton, eds.). *Geological Society Special Publication*, **57**, 137-159.

Cobb, W. R. (1969). Penetration of calcium carbonate substrates by the boring sponge, *Cliona*. *American Zoologist,* **9**, 783-790.

Coe, A. E., Bosence, D. W. J., Church, K. D., Flint, S. S., Howell, J. A., Wilson, R. C. L. (2003) The Sedimentary record of sea-level change (Edited by Coe, A. E.) The Open University, Cambridge University Press. Cambridge. pp 287.

Coggins, D., Fairless, K. J. (1984). The Bronze Age settlement of Bracken Rigg, Upper Teesdale, Co. Durham. *Durham Archaeological Journal.* **1**. 5-21.

Coleman, J. M., Prior, D. B. (1982), Deltaic environments, in P. A. Scholle, D. R. Spearing, eds., Sandstone depositional environments: AAPG Memoir **31**, 39–178.

Coleman, J. M., L. D. Wright. (1975), Modern river deltas: Variability of processes and sand bodies, in M. L. Broussard, ed., Deltas: Models for exploration: Houston, Texas, Houston Geological Society, p. 99–149.

Coleman, J. M., Gagliano, S. M., Smith, W. G. (1964), Minor sedimentary structures in a prograding distributary: Marine Geology, v. 1, p. 240–258.

Coleman, J. M., Gagliano, S. M. (1964), Cyclic sedimentation in the Mississippi River delta plain: *Gulf Coast Association of Geological Societies Transactions*, v. **14**, 67–80.

Conil, R., Longerstaey, P. J., Ramsbottom, W. H. C. (1980). Matériaux pour l'étude micropaléontologique du Dinantien de Grande-Bretagne. Mémoires de L'Institut Géologique de L'Université de Louvain 30, 187 pp.

Cossey, P. J. (1997) Hexaphyllia: a spiny Heterocoral from Lower Carboniferous reef limestones in Derbyshire, England. *Palaeontology,* **40.** 1031-1059.

Cossey, P. J., Mundy, D. J. C. (1990). Tetrataxis, a loosely attached limpet-like foraminifera from the Upper Paleozoic. *Lethaia*, **23**. 311-322,

Cozar, P. (2005). Early Serpukhovian (Late Mississippian) microflora from the Guadiato area (southwestern Spain). *Geological Journal.* **40.** 405-424.

Cozar, P., Somerville, H. E. A., Somerville, I. D. (2005) Foraminifera, calcareous algae and rugose corals in Brigantian (Late Viséan) limestones in NE Ireland. *Proceedings of the Yorkshire Geological Society.* **55.** 287-300.

Cozar, P., Rodr□guez, S. (2004). Pendleian (early Serpukhovian) marine carbonates from SW Spain: Sedimentology, biostratigraphy and depositional model. *Geological Journal.* **39.** 25-47.

Cozar, P., Somerville, I. D. (2004) New algal and foraminiferal assemblages and evidence for recognition of the Asbian-Brigantian boundary in northern England. *Proceedings of the Yorkshire Geological Society.* **55.** 43-65

Cozar, P., Vachard, D. (2004). Morphological adaptations of the Late Mississippian problematic algae Calcifolium to fluctuating environments, *Lethaia*, **37**. 351-363.

Cozar, P., Somerville, I. D., Aretz, M., Herbig, D. G. (2004) Biostratigraphical dating of Upper Viséan limestones (NW Ireland) using foraminiferans, calcareous algae and rugose corals.

Cozar, P. (2003): Foraminiferal taphofacies in the Mississippian rocks of the Guadiato Area, SW Spain. *Facies*. **49**. 1-18

Craig, H. (1965) the measurement of oxygen isotope paleotemperatures. In *Stable Isotopes in Oceanographic studies and Paleotemperatures* (Ed. By E. Tongiorgi) pp. 1-24. Spoleto, July 26-27, Consigio Nazionale delle Richerche, Laboratorio di Geologia Nucleare, Pisa.

Creaney, S. (1980). Petrographic texture and vitrinite reflectance variations on the Alston Block, north-east England. *Proceedings of the Yorkshire Geological Society*, **42**, 553-580.

Crowell, J. C. (1983), Ice ages recorded on Gondwanan continents: *Geological Society of South Africa Transactions*, **86**. 237–263.

Crowell, J. C. (1978). Gondwanan glaciation, cyclothems, continental positioning, and climate change. *American Journal of Science*, **278**, 1345-1372.

Crowley, T. J., Baum, S. K. (1991). Estimating Carboniferous sea-level fluctuations from Gondwanan ice extent. *Geology*, **19**(10), 975-977.

Crowley, T. J., Mengel, J. G., Short, D. A. (1987). Gondwanaland's seasonal cycle. *Nature,* **329**(6142), 803-807.

Cumings, E. R. (1932). Reefs or bioherms? *Bulletin of the Geological Society of America*. **43**, 331– 352.

Currie, E. D. (1954) Scottish Carboniferous Goniatites *Transactions of the Royal Society Edinburgh*. **62**. 527-602.

Cutler, A. H., Flessa, K. W. (1995), Bioerosion, dissolution and precipitation as taphonomic agents at high and low latitudes: *Senckenbergiana Maritime*, **25**, 115–121.

Dakyns J. R., Tiddeman, R. H., Russell, R., Clough, C. T., Strahan, A. (1891). The geology of the country around Mallerstang with parts of Wensleydale, Swaledale and Arkendale. *Memoir of the Geological Survey of Great Britain,* pp 213

Day, P. I. (1997) the Fischer diagram in the depth domain: a tool for sequence stratigraphy, *Journal of sedimentary research,* **67**, 982-984.

Dehairs, F. R., Stroobants, N., Goeyens, L. (1991). Suspended Barite as a tracer of biological activity in the Southern Ocean. *Marine Chemistry*. **35,** 399-410.

Dehairs, F., Goeyens, L. Stroobants, N. Bernard, P. Goyet, C. Poisson, A. Chesselet, R. (1990) On suspended barite and the oxygen minimum in the southern ocean. *Global Biogeochemical Cycles,* **4,** 85 – 102.

Dehairs, F. Chesselet, R. Jedwab, J. (1980). Discrete suspended particles of barite and the barium cycle in the open ocean. *Earth Planet Sciences.* **49,** 528- 550.

Denton, G. H. (2000) Does an asymmetric thermohaline-ice-sheet oscillator drive 100,000 yr glacial cycles. *Journal of Quaternary Science*. **15**. 301-318.

Dettman, D. L., Kohn, M. J., Quade, J., Ryerson, F. J., Ojha, T. P., Hamidullah, S. (2001). Seasonal stable isotope evidence for a strong Asian monsoon throughout the past 10.7m.y. *Geology (Boulder)*, **29**, 31-34.

Dickins, J. M. (1996) Problems of a late Palaeozoic glaciations in Australia and subsequent climate in the Permian. *Palaeogeographic, Palaeoclimatology, Palaeoecology.* **125,** 185-197

Diester-haass, L., Meyers, P. A., Rothe, P. (1992) Neogene-Quaternary history of the Benguela current and associated upwelling on the southwest African margin (DSDP Sites 362 and 532). In C. P. Summerhayes, W. L. Prell, K. C. Emeis (Editors), Evolution of Upwelling Systems Since the Early Miocene. The Geological Society, Bath, pp 331-342.

Dietzel, M., Gussone, N., Eisenhauer, A. (2004). Co-precipitation of Sr^{2+} and Ba^{2+} with aragonite by membrane diffusion of CO_2 between 10 and 50^0 C. *Chemical Geology*, **203**, 139-151.

Driscoll, E. G. (1970) Selective bivalve destruction in marine environments, a field study: *Journal of Sedimentary Petrology.***40**. 895-905.

Drummond, C. N., Wilkinson, B. H. (1993) A periodic accumulation of cyclic peritidal carbonate. *Geology*, **21**. 1023-1026.

Dunham, K. (1990) geology of the Northern Pennine Orefield. Volume 1 Tyne to Stainmore. Economic memoir of the British Geological Survey. London HMSO pp 299.

Dunham, R.J. (1962). Classification of carbonate rocks according to depositional texture. In: *Classification of Carbonate Rocks* (W.E. Ham, ed.). *American Association of Petroleum Geologists Memoir,* **1**, 108-121.

Dunham, K. C.,(1950). Lower Carboniferous sedimentation in the northern Pennines (England). Reportt. 18th International Geological Congress, Pt. 4, 46–63.

Dunham, K. C. (1948) Geology of the Northern pennine orefield (1st Edition) Volume 1 Tyne to Stainmore. *Memoire of the Geological Survey of Great Britain.* pp 357.

Dymond, J., Collier, R. (1996). Particulate Barium fluxes and their relationship to biological productivity. *Deep-Sea Research.* **43,** 1283-1308.

Dymond, J., Suess, E., Lyle, M. (1992). Barium in deep-sea sediment: a geochemical proxy for paleoproductivity. Paleoceanography
7, 163–181.

Eagle, M., A. Paytan, K., R. Arrigo, G. Van Dijken. Murray, R. W. (2003). A comparison between excess barium and barite as indicators of carbon export. *Paleoceanography,* **18.** 21-13 to 21-13.

Elliott, G. F. (1988) A new alga from the Carboniferous Frosterly Marble of Northern England. *Palaeontology.* **31**. 741-745.

Elliott, T. (1976). Sedimentary sequences from the Upper Limestone Group of Northumberland. *Scottish Journal of Geology*, **12**, 115-124.

Elliott, T. (1976)b. Upper Carboniferous sedimentary cycles produced by river-dominated, elongate deltas. *Journal of the Geological Society of London*, **132**, 199-208.

Elliott, T. (1976)c. The morphology, magnitude and regime of a Carboniferous fluvial-distributary channel. *Journal of Sedimentary Petrology*, **46**, 70-76.

Elliott, T. (1975). The sedimentary history of a delta lobe from a Yoredale (Carboniferous) cyclothems. *Proceedings of the Yorkshire Geological Society*, **40**, 505-536.

Elliott, T. (1974). Interdistributary bay sequences and their genesis. *Sedimentology*, **21**, 611-622.

Epstein, S., Buchsbaum, R., Lowenstam, H. A., Urey, H. C. (1953) Revised carbonate-water isotopic temperature scale. *Geological Society of America.* **64**. 1315-1326.

Fairburn, R. A. (2001) The stratigraphy of the Namurian Great/Main Limestone on the Alston Block, Stainmore Trough and Askrigg Block of northern England. *Proceedings Yorkshire Geological Society,* **53**, 265–274.

Fairbairn, R. A. (1999). Palaeocurrent direction and velocity in the Great/Main Limestone on the Alston and Askrigg blocks of northern England. *Proceedings of the Yorkshire Geological Society*, **52**, 353-359.

Fairbairn, R. A. (1990) The stratigraphy of the Namurian Great/Main Limestone on the Alston Block, Stainmore Trough and Askrigg Block of northern England. *Proceedings of the Yorkshire Geological Society*, **53,** 265-274

Fairbairn, R.A. (1980). The Great Limestone (Namurian) of south Northumberland. Proceedings Yorkshire Geological Society 43, 159–167.

Fairbairn, R. A. (1978). Lateral persistence of beds within the Great Limestone (Namurian, E_1) of Weardale. *Proceedings of the Yorkshire Geological Society*, **41**, 533-544.

Falcon-Lang, H. J. (2000). Fire ecology of the Carboniferous tropical zone. *Palaeogeography, Palaeoclimatology, Palaeoecology*, **164**, 339-355.

Ferguson, J. (1984) The methane content of some Carboniferous limestones from the northern Pennines and its relationship to mineralization. *Proceedings of the Yorkshire Geological Society*, **45**, 67-69.

Fewtrell, M. D., Ramsbottom, W. H. C., Strank, A. R. S. (1981). Carboniferous. In Stratigraphical Atlas of Fossil Foraminifera. British Micropalaeontological Series. D. G. Jenkins, J. W. Murray (eds). 1981. Chichester: Ellis Horwood. 310 pp.

Fewtrell, M. D., Ramsbottom, W. H. C., Strank, A. R. E. (1981): Carboniferous Foraminifera. In: Jenkyns, D. G., Murray, J. W. (eds.): Stratigraphical atlas of fossil foraminifera. British Micropaleontology Society Series, 15-69, Chichester.

Fischer, A. G. (1964). The Lofer Cyclothems of the Alpine Triassic. *Kansas Geological Survey Bulletin*. **169**, 107-149

Flügel, E. (2004). Microfacies of Carbonate Rocks: Analysis, Interpretation and Application, pp, 976. Springer, Berlin Heidelberg New York.

Folk, R. L. (1965) Recrystallisation in Ancient Limestones. In: *Dolomitisation and Limestone Diagenesis: A symposium.* (L.C. Prey, R.C. Murray, eds.). *Society of Economic Palaeontologists and Mineralogists Special Publications*, **13**, 14-48.

Folk, R. L. (1962) Spectral subdivision of limestone types. In: *Classification of Carbonate Rocks* (W.E. Ham, ed.). *American Association of Petroleum Geologists Memoir*, **1**, 62-84.

Folk, R. L. (1959) practical petrographic classification of limestones. *Bulletin of the American Association of Petrologists*, **43**. 1-38.

Forster, W. (1821). A treatise on a section of strata from Newcastle-on-Tyne to the mountain of Cross Fell in Cumberland: with remarks on mineral veins in General. 2nd edition (Alston).

Forster, W. (1809). A treatise on a section of strata from Newcastle-on-Tyne to the mountain of Cross Fell in Cumberland: with remarks on mineral veins in General. 1st edition (Alston).

Forster, W. (1809). A Treatise on a Section of Strata, commencing near Newcastle upon Tyne, and concluding on The West Side of the Mountain of Cross-Fell. With Remarks on Mineral Veins in General, and Engraved Figures of Some of the different Species of those Productions. To which are added Tables of the Strata in Yorkshire and Derbyshire Newcastle. Preston and Heaton i-vi ii, 156pp.

Foukal, P., Frohlich, C., Spruit, H., Wigley, T. M. L. (2006) Variations in solar luminosity and their effect on the Earth's climate. *Nature*, **443**, 161–166.

Foucault, F, Melieres, F. (2000). Palaeoclimatic cyclicity in central Mediterranean Pliocene sediments: the mineralogical signal. *Palaeogeography, Palaeoclimatology, Palaeoecology.* **158.** 311-323.

Fraser, A. J., Gawthorpe, R. L. (1990.) Tectono-stratigraphic development and hydrocarbon habitat of the Carboniferous in northern England. In: *Proceedings of Tectonic events responsible for Britain's oil and gas reserves* (R.F.P. Hardman, J. Brooks, eds.). *Geological Society Special Publication*. **55**, 49-86.

Fraser, A. J., Nash, D. F., Steele, R. P., Ebdon, C. C. (1990). A regional assessment of the intra-Carboniferous play of northern England. In: *Classic Petroleum Provinces* (J. Brooks, ed.). *Geological Society Special Publication*, **50**, 417-440.

Frakes, L. A., Francis, J. E., Syktus, J. I. (1992): Climate modes of the Phanerozoic: The history of the Earths climate over the past 600 million years. Cambridge University Press, Cambridge, 274p

Frank, D. T., Arthur, M. A., Dean, W. E. (1999) Diagenesis of lower Cretaceous pelagic carbonates, north Atlantic: paleoceanographic signals obscured. *Journal of Foraminiferal Research.* **29**, 340-351.

Frey R. W., Seilacher A. (1980). Uniformity in marine invertebrate ichnology. *Lethaia* **13***,* 183–207.

Froehlich, K., Grabczak, J., Rozanski, K. (1988) \deuterium and oxygen-18 in the Baltic Sea *Chemical Geology*. **72**. 77-83.

Gallagher, S. J., Holdgate, G. (2000) the palaeogeographic and palaeoenvironmental evolution of a Palaeogene mixed carbonate-siliciclastic cool-water succession in the Otway Basin, Southeast Australia. *Palaeogeography, Palaeoclimatology, Palaeoecology.* **156.** 19-50.

Gallagher, S. J. (1998). Controls on the distribution of calcareous Foraminifera in the Lower Carboniferous of Ireland. *Marine Micropaleontology.* **34.** 187-211.

Gallagher, S. J., Somerville, I. D. (1997) Late Dinatian (Lower Carboniferous) platform carbonate stratigraphy of Buttevant area North Co. Cork, Ireland. *Geological Journal.* **32.** 313-335

Garwood, E.J. (1913). The Lower Carboniferous succession in the north-west of England. *Quarterly Journal of the Geological Society of London,* **68**, 449-586.

Gawthorpe, R. L., Gutteridge, P., Leeder, M. R. (1989). Late Devonian and Dinantian basin evolution in northern England and North Wales. In: *The role of tectonics in Devonian and Carboniferous sedimentation in the British Isles* (R.S. Arthurton, P. Gutteridge, S.C. Nolan, eds.). *Occasional Publication of the Yorkshire Geological Society*, **6,** 1-23.

Gawthorpe, R. L. (1987). Tectono-sedimentary evolution of the Bowland Basin, N England, during the Dinantian. *Journal of the Geological Society of London*, **144**, 59-71.

George, G. T. (2000). Characterisation and high resolution sequence stratigraphy of storm-dominated braid delta and shoreface sequences from the Basal Grit Group (Namurian) of the South Wales Variscan peripheral foreland basin. *Marine and Petroleum Geology*, **17**, 445-475.

George, T. N., Johnson, G. A. L., Mitchell, M., Prentice, J. E., Ramsbottom, W. H. C., Sevastopulo, G. D., Wilson, R. B. (1976). A correlation of Dinantian rocks in the British Isles. *Geological Society Special Publication*, **7**, pp 87.

George, T. N. (1958). Lower Carboniferous palaeogeography of the British Isles. *Proceedings of the Yorkshire Geological Society,* **31**, 227–318

Goldhammer, R. K. (1997). Compaction and decompaction algorithms for sedimentary carbonates. *Journal of Sedimentary Research*. **67**, 26-35.

Goldhammer, R. K., Oswald, E. J., Dunn, P. A. (1994). High-frequency glacio-eustatic cyclicity in the Middle Pennsylvanian of the Paradox Basin: an evaluation of Milankovitch forcing. In: de Boer, P.L., Smith, D.G. (Eds.), Orbital Forcing and

Cyclic Sequences. *International Association of Sedimentologists Special Publication*, **19**, pp. 243–293.

González, C. R. (1990) Development of the late Palaeozoic glaciations of the South American Gondwana in western Argentina. *Palaeogeographic, Palaeoclimatology, Palaeoecology.* **79,** 275-287.

Grossman, E. L. (1994). The carbon and oxygen isotope record during the evolution of Pangea; Carboniferous to Triassic. In: *Pangea; paleoclimate, tectonics, and sedimentation during accretion, zenith and breakup of a supercontinent* (G.D. Klein, ed.). *Special Paper - Geological Society of America*, **288**, 207-228.

Grossman, E. L. Mii, H-S., Yancey, T. E. (1993) Stable isotopes in late Pennsylvanian brachiopods from the United States: Implications for Carboniferous paleoceanography. *Geological Society of America Bulletin.* **105**. 1284-1296.

Gunn, W. (1895). The geology of part of Northumberland, including the country between Wooler and Coldstream. *Memoirs of the Geological Survey of Great Britain*, pp97.

Gutteridge, P. (1990) Comments on Saccaminopsis affinities. *Lethaia*, **23.** 222-222.

Hallett, D. (1970) Foraminifera and Algae from the Yoredale 'Series' (Viséan-Namurian) of Northern England. Proceedings of the 6th International carboniferous Congress. Sheffield. Volume III. pp. 18-86.

Hammer, Ø., Harper, D. A. T. (2005). Paleontological data analysis, pp 351, Blackwell Science Publishers, Oxford.

Hammer, Ø., Harper, D.A.T., P. D. Ryan. (2001). PAST: Paleontological Statistics Software Package for Education and Data Analysis. Palaeontologia Electronica 4(1): 9 pp.

Hance, l., Muchez, Ph., Hou, H. F., Wu, X. (1997) Biostratigraphy, Sedimentology and sequence stratigraphy of the Tournaisian-Viséan transitional strata in South China (Guangxi). *Geological Journal.* **32.** 337-357.

Harland, W. B., Cox, A. V., Lewellyn, P. G., Pickton, C. A. G., Smith, A. G., Walters, R. (1982). *Geological Time Scale*. Cambridge University Press, pp131.

Haynes, J. R. (1981). Foraminifera, Wiley, Chichester, 433pp.

Heckel, P. H. (1994). Evaluation of evidence for glacio-eustatic control over marine Pennsylvanian cyclothems in North America and consideration of possible tectonic events. In: *Tectonic and eustatic controls on sedimentary cycles* (J.M. Dennison, F.R. Ettensohn, eds.). *Concepts in sedimentology and palaeontology*, **4**, 65-87.

Heckel, P. H. (1986). Sea-level curve for Pennsylvanian eustatic marine transgressive–regressive depositional cycles along the mid-continent outcrop belt, North America. *Geology* **14**, 330–334.

Hedges, J. I., Hu, F. S., Deol, A. H., Hartnett, H. E., Tsamakis, E., Keil, R. G. (1999) Sedimentary organic matter preservation: a test for selective degradation under oxic conditions. *American Journal of Science.* **299.** 529-555.

Hennebert, M., Lees, A. (1991) Environmental gradients in carbonate sediments and rocks detected by correspondence analysis: examples from the Recent of Norway and the Dinatian of Southwest England. *Sedimentology.* **38.** 623-642.

Hennebert, M., Lees, A. (1985) Optimized similarity matrices applied to the study of carbonate rocks. *Geological Journal.* **20.** 123-131.

Herkat, M. (2007) Application of correspondence analysis to palaeobathymetric reconstruction of Cenomanian and Turonian (Cretaceous) rocks of Eastern Algeria. *Palaeogeography, Palaeoclimatology, Palaeoecology*. **254**. 583-605.

Hillgartner, H., Strasser, A. (2003) Quantification of high-frequency sea-level fluctuations in shallow-water carbonates: an example from the Berriasian–Valanginian (French Jura). *Palaeogeography, Palaeoclimatology, Palaeoecology*. **200**. 43-63.

Hirst, M. (2003). Analysis of marine sediments collected in Cooks Bay, Mo'orea, French Polynesia. Investigating the environment: research for environmental management. Senior Research Seminar. Environmental Sciences Group Major. University of California, Berkeley,

Hodge, B. L., Dunham, K. C. (1991). Clastics, coals, palaeodistributaries and mineralisation in the Namurian Great Limestone Cyclothem, Northern Pennines and Northumberland Trough. *Proceedings Yorkshire Geological Society* **48**, 323–337.

Hodge, B.L., Dunham, K.C. (1991). Clastics, coals, palaeodistributaries and mineralisation in the Namurian Great Limestone Cyclothem, Northern Pennines and Northumberland Trough. Proceedings Yorkshire Geological Society **48**, 323–337

Hodge, B. L. (1965). The Great Cyclothem of Northern England. *Unpublished PhD. University of Durham.*

Holliday D. W., Burgess I. C., Frost D. V. (1975). A recorrelation of the Yoredale limestones (Upper Visean) of the Alston Block with those of the Northumberland Trough. *Proceedings of the Yorkshire Geological Society.* **40,** 319–334.

Horbury, A. D., Adams, A. E. (1996). Microfacies associations in Asbian carbonates: an example from the Urswick Limestone Formation of the southern Lake District, northern England. In: Strogen, P., Somerville, I. D., Jones, G. Li (Eds), Recent advances in Carboniferous Geology, *Geological Society Special* Publication. 1**07**, 221-237.

Horbury, A. D. (1992). A Late Dinantian peloid cementstone-palaeoberesellid build-up from North Lancashire, England. *Sedimentary Geology*. **79,** 117-137.

Horbury, A.D. (1989). The relative roles of tectonics and eustasy in the deposition of the Urswick Limestone in south Cumbria and north Lancashire. *Yorkshire Geological Society Occasional Publication* **6**, 153–169.

Hori, K., Saito, Y., Zhao, Q., Wang, P. (2002). Architecture and evolution of the tide-dominated Changjiang (Yangtze) River delta, China. *Sedimentary Geology* **146**, 249-264.

Howson, M. R., Pethybridge, A. D., House, W. A. (1987) Synthesis and distribution coefficients of low-magnesium calcites. *Chemical Geology.* **64**. 79-87.

Hubbard, J. A. E. B. (1970) Sedimentological factors affecting the distribution and growth of Viséan caninioid corals in north west Ireland. *Palaeontology.* **13.** 191-209.

Hudson, R. G. S. (1924). On the rhythmic succession of the Yoredale Series in Wensleydale. *Proceedings of the Yorkshire Geological Society*, **18**, 125-135.

Huls, M., Zahn, R. (2000). Millennial–scale sea-surface temperature variability in the western tropical North Atlantic from planktonic foraminiferal census counts. Paleoceanography **15**, 659-678.

Husinec, A., Basch, D., Rose, B., Read, J. R. (2008) FISCHERPLOTS: An Excel spreadsheet for computing Fischer Plots of accommodation change in cyclic carbonate successions in both the time and depth domains. *Computers and Geoscience*. **34.** 269-277.

Hutchings, T. M. (1898). The contact-rocks of the Great Whin Sill. *Geological Magazine*. **35**, 69-82 and 123-131.

Hutchinson, W. (1794). In *The history and antiquities of the County Palatine of Durham.***3.**

Irwin, M. L. (1965) General theory of epeiric clear water sedimentation. *Bulletin of the American Association of Petroleum Geologists*, **49**, 445-459.

Jarvis, I., Murphy, A., M., Gale, A., S. (2001). Geochemistry of pelagic and hemipelagic carbonates: criteria for identifying systems tracts and sea-level changes. *Journal of the Geological Society, London.* **158**, 658-696.

Jenkyns, H, C., Jones, C, E., Grocke, D, R., Hesselbo, S, P., Parkinson, D, N. (2002). Chemostratigraphy of the Jurassic System: applications, limitations and implications for palaeoceanography. *Journal of the Geological Society, London*. **159**, 351-378.

Jerram, D. A., Cheadle, M. J. (2000) On the cluster analysis of grains and crystals in rocks. *American Mineralogist,* **85**, 47–67

Johnson, G. A. L., Dunham, K. C. (2001). Emplacement of the Great Whin Dolerite Complex and the Little Whin Sill in relation to the structure of northern England. *Proceedings of the Yorkshire Geological Society*. **53**, 177-186.

Johnson, G. A. L., Nudds, J. R. (1996) Carboniferous biostratigraphy of the Rookhope Borehole Co. Durham. *Transactions of the Royal Society of Edinburgh: Earth Sciences.* **86.** 181-226**.**

Johnson, G. A. L. (1995) (Ed.) Robson's Geology of north east England. *Transactions of the Natural History Society of Northumberland.*

Johnson, G. A. L. (1984). Subsidence and sedimentation in the Northumberland Trough. *Proceedings of the Yorkshire Geological Society,* **45**, 71-83.

Johnson, G. A. L. (1982). Geographical change in Britain during the Carboniferous period. *Proceedings of the Yorkshire Geological Society.* **44**, 181-203.

Johnson, G. A. L. (1981). Geographical evolution from Laurasia to Pangaea. *Proceedings of the Yorkshire Geological Society.* **43**, 221-252.

Johnson, G. A. L. (1967). Basement Control of Carboniferous Sedimentation in Northern England. *Proceedings of the Yorkshire Geological Society,* **36**, 175–94

Johnson, G. A. L. (1960). Palaeogeography of the Northern Pennines and part of North Eastern England during the deposition of carboniferous cyclothemic deposits. Reprint from the report of the *International geological Congress*, XX1, Norden 1960 Part X11. Copenhagen 1960.

Johnson, G. A. L. (1959) The Carboniferous stratigraphy of the Roman Wall District in western Northumberland. *Proceedings of the Yorkshire Geological Society*, **32**, 83-130.

Johnson, G. A. L. (1958). Biostromes in the Namurian Great Limestone of northern England. *Palaeontology,* **1**, 147-157.

Kasten, S., Haese, Ralf, R., Zabel, M., Ruhlemann, C., Schulz, H. D. (2001). Barium peaks at glacial terminations in sediments of the equatorial Atlantic Ocean—relics of deglacial productivity pulses?. Chemical Geology **175**. 635-651.

Keller, G., Berner, Z., Thierry, A., Stueben, D. (2004) Cenomanian-Turonian and $\delta^{13}C$ and $\delta^{18}O$, sea level and salinity variations at Pueblo, Colorado. *Palaeoclimatology, Palaeoclimatology, Palaeoecology*. **211**. 19-43.

Kimbell, G. S., Young, B., Millward, D., Crowley, Q. G. (2010) The North pennine batholiths (Weardale Granite) of northern England: new data on its age and form. *Proceedings of the Yorkshire Geological Society*, **58**, 107-128..

King, B., McAllister, F., Wolankski, E., Done, T., Spagnol, S. (2001). River plume dynamics in the central Great Barrier Reef. In: E. Wolankski, Editor, Coral Reef Processes: Physics-Biology links in the Great Barrier Reef (2001), CRC Press. 145-159.

Langhorne B. Smith, Jr., Read, J. F. (2000) Rapid onset of late Paleozoic glaciation on Gondwana: Evidence from Upper Mississippian strata of the Midcontinent, United States. *Geology*. **28**. 279-282

Lea, D. W., Mashiotta, T. A., Spero, H. J. (1999). Controls on magnesium and strontium uptake in planktonic foraminifera determined by live culturing. *Geochimica et Cosmochimica Acta.* **63**, 2369-2379.

Leeder, M. R., Fairhead, D., Lee, A., Stuart, G., Clemmey, H., El-Haddaheh, Green, C. (1989). Sedimentary and tectonic evolution of the Northumberland Basin. In. The role of tectonics in Devonian and Carboniferous sedimentation in the British Isles (R.S. Arthurton, P. Gutteridge, S.C. Nolan, eds.). *Publication of the Yorkshire Geological Society*, **6**, 207-223.

Leeder, M. R. (1988). Recent developments in Carboniferous geology; a critical review with implications for the British Isles and N.W. Europe. *Proceedings of the Geologists' Association*, **99**, 73-100.

Leeder, M. R. (1987). Tectonic and palaeogeographic models for Lower Carboniferous Europe. In: *European Dinantian Environments* (J.A. Miller, A.E. Adams, V.P Wright, eds.). John Wiley and Sons, 1-20.

Leeder, M. R., Strudwick, A. E. (1987). Delta–marine interaction: a discussion of sedimentary models for Yoredale type cyclicity in the Dinantian of northern England. In: Miller, J., Adams, A.E.,Wright, V.P. (Eds.), European Dinantian Environments. John Wiley and Sons, Chichester, pp. 115–130.

Leeder, M. R. (1982). Upper Palaeozoic basins of the British Isles; Caledonide inheritance versus Hercynian plate margin processes. *Journal of the Geological Society of London*, **139**, 479-491.

Leeder, M. R. (1975). Lower Border Group (Tournaisian) stromatolites from the Northumberland Basin. *Scottish Journal of Geology*, **11**, 207-226.

Leeder, M. R. (1974) The origin of the Northumberland Basin. *Scottish Journal of Geology*, **10**, 283-296.

Lemon, K. (2006) The Climatic, eustatic and tectonic controls on Mid Carboniferous (Viséan and Namurian) strata of Northumbria, England. Unpublished PhD thesis, University of Durham.

Libes, S. M. (1992). An introduction to Marine Biogeochemistry: John Wiley and Sons Inc. Singapore. pp 734.

Loeblich, A. R. Tappan, H. (1964) Protista 2. In Moore, R. C. : *Treatise on Invertebrate Paleontology* , 1–900. Lawrence, Kansas.

Longiaru S. (1987). Visual comparators for estimating the degree of sorting from plane and thin sections. *J. Sed. Petrol.*, 57, 791-794.

Lukasik, J. J., James, N. P., McGowran, B., Bone, Y. (2000) An epeiric ramp: low-energy, cool-water carbonate facies in a Tertiary inland sea, Murray Basin, South Australia. *Sedimentology*. 47, 851-881

McArthur, J. M., Donovan, D. T., Thirlwall, M. F., Fouke, B. W., Mattey, D. (2000). Strontium isotope profile of the early Toarcian (Jurassic) ocean anoxic event, the duration of ammonite biozones, and belemnite palaeotemperatures. *Earth and Planetary Science Letters*. **179**, 269-285.

McConnaughey, T. (1989) ^{13}C and ^{18}O isotope disequilibrium in biological carbonates, II. In vitro simulation of Kinetic isotope effects. *Geochem Cosmochim Acta*. **53.** 163-171.

McManus, J., Berelson, W., M., Klinkhammer, G., P., Johnson, K., S., Coale, K., H., Anderson, R., F., Kumar, N., Burdige, D., J., Hammond, D., E., Brumsack, H., J., McCorkle, D., C., Rushdi, A. (1998). Geochemistry of barium in marine sediments: implications and its use as a paleoproxy. *Geochimica et Cosmochimica Acta.* **62**, 3453-3473.

MacEachern, J., A., Pemberton, S., G., Gingras, M., K., Bann, K., L. (2007). The Ichnofacies Paradyn: A fifty-year retrospective. In Ed W Miller, III. Trace fossils, concepts, problems and prospects. Amsterdam. Elsevier.

Mackie, E. A. V., leng, J. M., Lloyd, J. M., Arrowsmith, C. (2005) Bulk organic $\delta^{13}C$ and C/N ratios as palaeosalinity indicators within a Scottish isolation basin. *Journal of Quaternary Science.* **20.** 303-312.

Madi, A., Bourque, P. A., Mamet, B. L. (1996): Depth-related ecological zonation of a Carboniferous carbonate ramp: Upper Viséan of Béchar Basin, Western Algeria. *Facies*, **35**, 58-80.

Maliva, R. G. (1998). Skeletal aragonite neomorphism - quantitative modelling of a two-water diagenetic system. *Sedimentary Geology*. **121**, 179-190.

Mamet, B., Zhu, Z. (2005). Carboniferous and Permian algal microflora, Tarim Basin (China). *Geologica Belgica.* **8**. 3-13.

Marr, J. E. (1921). The rigidity of north-west Yorkshire. *Naturalist, Hull, 63-72.*

Mason, B. (1966). Principles of Geochemistry. pp 329. John Wiley and Sons inc. New York.

Mathew, A. E., Woods, A. J., Oliver, C. (1991) Spots before the eyes: New comparison charts for visual percentage estimation in archaeological material. – In: Middleton, A., Freestone, j. (eds): Recent developments in ceramic petrology. British Museum Occasional Paper, **81**, 221-264

Matías, R., Molina, José Miguel, Löser, H., Navarro, V., Ruiz-Ortiz, P. A. (2009) Coral biostromes of the Middle Jurassic from the Subbetic (Betic Cordillera, southern Spain): facies, coral taxonomy, taphonomy, and palaeoecology. *Facies,* **55.** 575-593.

Mawson, M., Tucker, M. E. (2009) High-frequency cyclicity (Milankovitch and millennial-scale) in slope-apron carbonates: Zechstein (Upper Permian), North-east England. *Sedimentology*, **56**, 1905-1936.

Maynard, J. R., Leeder, M. R. (1992). On the periodicity and magnitude of Late Carboniferous glacio-eustatic sea-level changes. Journal. Geological Society London **149**, 303–311.

Melezhik, V., A., Gorokhov, I., M., Fallick, A., E., Gjelle, S. (2001). Strontium and carbon isotope geochemistry applied to dating of carbonate sedimentation: an example from high-grade rocks of the Norwegian Caledonides. *Precambrian Research.* **108**, 267-292.

Menning, M., Weyer, D., Drozdzewski, G., van Amerom, H.W.J., Wendt, I. (1999). A Carboniferous time scale 2000; discussion and use of geological parameters as time indicators from Central and Western Europe. *Geologisches Jahrbuch. Reihe A: Allgemeine und Regionale Geologie BR Deutschland und Nachbargebiete, Tektonik, Stratigraphie, Palaeontologie*, **156**, 3-44.

Meyers, P. A. (1994) preservation of elemental and isotopic identification of sedimentary organic matter. *Chemical Geology*. **114.** 289-302.

Meyers, P. A., Takemura, K. Horie, S. (1993) A reinterpretation of Lake Quaternary sediment chronology of lake Biwa, Japan, from correlation with marine glacial-interglacial cycles. *Quaternary Research.* **39**. 154-162.

Meyers, P. A. (1992) Organic matter variations in sediments from DSDP Sites 362 and 532: Evidence of upwelling changes associated with the Bengguela Current In C.P. Summerhayes, W. L. Prell, K. C. Emeis (Editors), Evolution of Upwelling Systems Since the Early Miocene. *The Geological Society.* Bath, pp. 323-329.

Menning, M., Weyer, D., Drozdzewski, G. Van Amerom, H. W. J., Wendt, I. (2000) A Carboniferous Time Scale 2000: Discussion and use of Geological parameters as time indicators from central and western Europe. *Geologisches Jahrbuch,* **156**, 3–44

Mii, Horng-Sheng., Grossman, E.L., Yancey, T.E., Chuvashov, B., Egorov, A. (2001). Isotopic records of brachiopod shells from the Russian Platform – evidence for the onset of mid-Carboniferous glaciation. *Chemical Geology*. **175**,133-147.

Mii, Horng-Sheng., Grossman, E.L., Yancey, T.E. (1999). Carboniferous isotope stratigraphies of North America: Implications for Carboniferous palaeoceanography and Mississippian glaciation. *Geological Society of America Bulletin*. **111,** 960- 973

Miller, H. (1887). The Geology of the country around Otterburn and Elsdon. *Memoirs of the Geological Survey of Great Britain,* pp147.

Milligan G. W., M. C. (1985). An examination of procedures for determining the number of clusters in a data set. Psychometrika, pages 159–159

Milliman, J. D. (1974). Marine Carbonates. pp 375. Springer-Verlag New York.

Moore, D. (1959). Role of deltas in the formation of some British lower Carboniferous cyclothems. *Journal of Geology*, **67**, 522-539.

Moore, D. (1958). The Yoredale series of upper Wensleydale and adjacent parts of north-west Yorkshire. *Proceedings of the Yorkshire Geological Society*, **31**, 91-146.

Morse, J,. Arvidson, R. S. (2002). The dissolution kinetics of major sedimentary carbonate minerals. *Earth Science Reviews*. **58**, 51-84.

Morse, J., W. Wang, Q. Tsio, M., Y. (1997) Influences of temperature and Mg:Ca ratio on $CaCO_3$ *Geology***. 25**. 85-87.

Morse, J., W., Mackenzie, F., T. (1990). Geochemistry of Sedimentary Carbonates. Developments in Sedimentology 48. pp 707, Elsevier Publishers New York.

Murray, C. J., Lowe, D. R., Graham, S. A., Martinez, P. A., Zeng, J., Carroll, A. R., Cox, R., Hendrix, M., Heubeck, C., Miller, D. Moxon, I. W., Sobel, E., Wendebourg, J., Williams, T. (1996). Statistical analysis of bed-thickness patterns

in a turbidite section from the Great valley Sequence, Cache Creek, Northern California. *Journal of Sedimentary Research.* **66.** 900-908

Nakrem, H. A. (1994) Middle Carboniferous to Early Permian bryozoans from Spitsbergen. *Acta Palaeontologica Polonica.* **39**. 45-116.

Nakrem, H. A., Blaźejowski, B., Gaździcki, A. (2009). Lower Permian bryozoans from southern and central Spitsbergen, Svalbard. *Acta palaeontologica Polonica.* **54.** 677-698.

Nielsen, P., Flipkens, V., Groessens, E., Swennen, R. (2000) Sedimentology and diagenesis of the Dinantian succession in the Vinalmont Borehole. *Geologica Belgica,* **3.** 369-393.

Noren, A. J., Bierman, P. R., Steig, E. J., Andrea Lini , A., Southon, J. (2002). Millennial-scale storminess variability in the north-eastern United States during the Holocene epoch. Nature **419**, 821-824.

Nudds, J. D., Day, A. (1977) The effects of clastic sedimentation on a fasciculate rugose coral from the Lower Carboniferous of Northern England. *Bolet□n de la Real Sociedad Espanola de Historia natural, SecciÓn Geologica,* **91,** 93-97.

Oomori, T., Kaneshima, H., Maezato, Y. (1987) Distribution coefficient of Mg^{2+} ions between calcite and solution at 10-50^{0}C. *Mar. Chem*. **20**. 237-336

Perrier, R., Quiblier, J. (1974) Thickness changes in sedimentary layers during compaction history; methods for quantitive evaluation. *American Association of Petrolium Geologists*. **58**. 507-520

Pettijohn, F. J. (1973) Sedimentary Rocks, 3rd edition. Elsevier, Amsterdam, 844 pp.

Phillips, J. (1836). Illustrations of the Geology of Yorkshire. Part II. The Mountain Limestone District, London.

Phillips, J. (1836). On the Classification of the Carboniferous Limestone Series; Northumbrian Type Geological Magazine (Decade III) , **4**: 117-120

Podani, J., Miklos, I. (2002) Resemblance coefficients and the horseshoe effect in Principal Coordinates analysis. *Ecology.* **83.** 3331-3343.

Poncet, Jacques (1989) New data about the taxonomic position of *Saccaminopsis. Lethaia,* **22**,425-429.

Porta, G. D., Kenter, J. A. M., Bahamonde, J. R. (2004) Depositional facies and strata geometry of an Upper Carboniferous prograding and aggrading high-relief carbonate platform (Cantabrian Mountains, N. Spain) *Sedimentology.* **51**. 267-295.

Popp, B. N., Anderson, T. F., Sandberg. P. A. (1986). Textural, elemental and isotopic variations among constituents in middle Devonian limestone. North America. *Journal of Sedimentary Petrology.* **56**, 715-727.

Potter, E. M., Esat, T. M., Schellmann, G., Radtke, U., Lambeck, K., McCulloch, M. T. (2004). Suborbital-period sea-level oscillations during marine isotope substages 5a and 5c. Earth and Planetary Science Letters **225**, 191-204.

Pytkowicz, R., M. (1973). Calcium carbonate retention in supersaturated seawater. *American Journal of Science.* **273**, 515-522.

Pytkowicz, R., M. (1965). Rates of inorganic calcium carbonate nucleation. *Journal of Geology.* **73**, 196-199.

Rachold, V., Brumsack, H. J. (2001). Inorganic geochemistry of Albian sediments from the Lower Saxony Basin NW Germany: palaeoenvironmental constraints and orbital cycles. *Palaeogeography, Palaeoclimatology, Palaeoecology*. **174,** 121-143.

Railsback, L. B. (1990) Influence of changing deep ocean circulation on the Phanerozoic oxygen isotope record. *Geochimica et Cosmochimica Acta.* **54**. 1501-1509.

Ramsbottom, W. H. C. (1979) Rates of transgression and regression in the Carboniferous of N. W. Europe. *Journal of Geology.* **136**. 147-153.

Ramsbottom, W. H. C., Calver, M. A., Eagar, R. M. C., Hodson, F., Holliday, D. W., Stubblefield, C. J., Wilson, R. B. (1978)**.** A correlation of Silesian rocks in the British Isles. *Geological Society Special Publication*, **10**, pp81.

Ramsbottom, W. H. C. (1978). Correlation of the Scottish Upper Limestone Group (Namurian) with that of the north of England. *Scottish Journal of Geolology,* **13**, 327–30.

Ramsbottom, W. H. C. (1977). Major cycles of transgression and regression (mesothems) in the Namurian. *Proceedings of the Yorks. geological Society,* **41**, 261–91.

Ramsbottom, W. H. C. (1973). Transgressions and regressions in the Dinantian: a new synthesis of British Dinantian stratigraphy. *Proceedings of the Yorks. geological Society,* **39**, 567–607.

Ramsbottom, W. H. C. (1969). The Namurian of Britain. *6th International. Congessr of Carboniferous. Stratagraphic Géolologist,* **1**, 219–32, (*Sheffield* 1967).

Raymond, A., Kelley, P. H., Lutken, C. B. (1989), Polar glaciers and life at the equator: the history of Dinantian and Namurian (Carboniferous) climate: *Geology*, **17**. 408-411.

Read, J. F. (1998): Phanerozoic carbonate ramps from greenhouse, transitional and ice-house worlds: clues from field and modelling studies. - In: Wright, V. P., Burchette, T. P. (eds.): Carbonate ramps. - Geological. Society London, Special Publication, **149**, 104-135

Redfern, R. (2000). Origins: The evolution of continents, oceans and life. pp. 360, Cassell and Co, London.

Reynolds, A. D. (1992). Storm, wave and tide-dominated sedimentation in the Dinantian Middle Limestone Group, Northumbrian Basin. *Proceedings of the Yorkshire Geological Society*, **49**, 135-148.

Reynolds, A. D. (1992). Storm, wave and tide dominated sedimentation in the Dinantian Middle Limestone Group, Northumbrian Basin. *Proceedings of the Yorkshire Geological Society*. **49.** 135-148

Richter, F. M., Liang, Y. (1993). The rate and consequences of Sr diagenesis in deep-sea carbonates. *Earth and Planetary Science Letters*. **117**, 553-565.

Richter, F. M., DePaolo, D. J. (1987). Numerical models for diagenesis and the Neogene Sr isotope evolution of seawater from DSDP site 590B. *Earth and Planetary Science Letters*. **83**, 27-38.

Ricken, W. (1991). Variations of sedimentation rates in rhythmically bedded sediments. Distinction between depositional types. In Einsele, G., Ricken, W., Seilacher, A. eds. Cycles and events in stratigraphy. Berlin: Springer.

Ridd, M. F., Walker, D. B., Jones, J. M. (1970) A deep Borehole at Harton on the margin of the Northumbrian Trough. *Proceedings of the Yorkshire Geological Society,* **38**. 75-103.

Rinna, J., Warning, B., Meyers, P. A., Brumsack, H. J., Rullkotter, J. (2002). Combined organic and inorganic geochemical reconstruction of paleodepositional conditions of a Pliocene sapropel from the eastern Mediterranean Sea. *Geochimica et Cosmochimica Acta*. **66.** 1969-1986.

Robaszynski, F., Gale, A. S., Juignet, P., Amedro, F., Hardenbol, J. (1998). Sequence Stratigraphy in the Upper Cretaceous series of the Anglo-Paris Basin: Exemplified by the Cenomanian stage. In: Graciansky, P., C., D., Hardenbol, J., Jacquin, T. Vail, P., R. (eds.). *Mesozoic and Cenozoic Sequence Stratigraphy of European Basins.* SEPM Special Publications, **60,** 363-386.

Rohling, E. J. (2000). Paleosalinity: confidence limits and future applications. *Marine Geology* **163**, 1-11.

Ross, C. A., Ross, J. R. P. (1988) Late Palaeozoic transgressive-regressive deposition. *The Society of Economic Palaeontologists and Mineralogists Special Publication.* **42,** 227-247.

Ross, C.A., Ross, J.R.P. (1987). Late Paleozoic transgressive–regressive deposition. In: Wilgus, C.K., Hastings, B.S., Kendall, C.G.St.C., Posamentier, H.W., Ross, C.A., Van Wagoner, J.C. (Eds.), Sea-Level Changes: an Integrated Approach. Special Publication, **42**. Society of Economic Paleontologists and Mineralogists, pp. 227–248.

Rowley, D. B., Raymond, A., Parrish, J. T., Lottes, A. L., Scotese, C.R., Ziegler, A. M., (1985), Carboniferous paleogeographic, phytogeographic, and paleoclimatic reconstructions: International. Journal of Coal Geology, **5**. 7-42.

Saager, P. M., De Baar, H. J. W., Burkill, P.H. (2004). Manganese and iron in Indian Ocean waters. *Geochimica et Cosmochimica Acta.* **53.** 2259–2267.

Sadler, P. M., Osleger, D. A., Montañez, I. P. (1993) On the labelling, length and objective basis of Fischer Plots. *Journal of Sedimentary Petrology*.**63.** 360-368.

Sakai, S., Kano, A. (2001) Original oxygen isotope composition of planktic foraminifera preserved in diagenetically altered Pleistocene shallow-water carbonates. *Marine Geology*. **172**. 197-204.

Saltzman, R. S. (2003) Late Paleozoic ice age: Oceanic gateway or pCO_2? *Geological Society of America*. **31**. 151-154.

Sarntheim, M., Kennett, J.P., Allen, J.R.M., Beer, J., Grootes, P., Laj, C., McManus, J., Ramesh, R., SCOR-IMAGES Working Group 117, 2002. Decadal-to-millennial scale climate variability — chronology and mechanisms: summary and recommendations. *Quaternary Science Reviews* **21**, 1121–1128

Schieber, J., Southard, J., Thaisen, K. (2007), Accretion of mudstone beds from migrating floccule ripples: *Science,* **318**, 1760-1764.

Schieber, J., Krinsley, D., Riciputi, L. (2000), Diagenetic origin of quartz silt in mudstones and implications for silica cycling: *Nature,* **406**, 981-985.

Schieber, J. (1987), Storm-dominated epicontinental clastic sedimentation of the Mid-Proterozoic Newland Formation, Montana: *Sedimentology* , **36**, 203-219.

Schulz, M., Mudelsee, M. (2002) REDFIT: estimating red-noise spectra directly from unevenly spaced paleoclimatic time series: *Computers and Geosciences*. **28**, p. 421-426.

Scoffin, T. P., Bradshaw, C. (2000). The taphonomic significance of endoliths in dead versus live coral-skeletons. Palaios **15**, 248–254.

Scoffin, T. P. (1992) Taphonomy of coral reefs: a review. *Coral Reefs*. **11**. 57-77.

Scoffin, T. P. (1987). An Introduction to Carbonate Sediments and Rocks. Blackie Publication Co, New York. 274 pp.

Scotese, C. R. "Paleomap Project" University of Texas at Arlington: website http//www.scotese.com. November 2008.

Scotese, C. R., McKerrow, W. S. (1990). Revised world maps and introduction. In: *Palaeozoic palaeogeography and biogeography* (W.S. McKerrow, C.R. Scotese, eds.). *Memoir of the Geological Society of London*, **12**, 1-21

Scrutton, C. T. (2000). Discussion of palaeocurrent direction and velocity in the Great/Main Limestone on the Alston and Askrigg Blocks of northern England 'proceedings, Volume 52, part 4, pp353-359, 1999. *Proceedings of the Yorkshire Geological Society,* **53.** 73-74.

Scrutton, C. T. (1999). Palaeozoic corals: their evolution and palaeoecology. *Geology Today.* **15**. 184-193.

Scrutton, C. T. (1998) The Palaeozoic corals, I: origins and relationships. *Proceedings of the Yorkshire Geological Society,* **51.** 177-208.

Scrutton, C. T. (1998) The Palaeozoic corals, II: structure, variation and palaeoecology. *Proceedings of the Yorkshire Geological Society,* **52.** 1-57.

Sedgwick, A. (1835). Description of a series of longitudinal and transverse sections through a portion of the Carboniferous chain between Penigent and Kirby Stephen. *Transactions of the Geological Society of London.* **2**. 69-101.

Sedgwick, A. (1829). On the association of trap rocks with the mountain limestone formation of High Teesdale. *Transactions Cambridge Philosophical society ,***2**. 139.

Seilacher, A. (1967) Bathymetry of trace fossils. *Marine Geology.* **5.** 413-428.

Shackleton, H. J. (1977) Carbon-13 in *Uvigerina*: tropical rainforest history and the equatorial Pacific carbonate dissolution cycle in*:* Anderson, N. R., Malahoff, A. (Eds). *The fate of fossil fuel CO_2 in the oceans.* Plenum, New York, PP 401-421.

Shotton, F. W. (1935) the stratigraphy and tectonics of the Cross Fell Inlier. *Quartery Journal of the Geological Society London.* **91**. 639-700.

Simpson, J. (1985). Stylolite-controlled layering in an homogeneous limestone: pseudo-bedding produced by burial diagenesis. *Sedimentology*. **32**, 495-505.

Skompski, S. (1986) Upper Viséan calcareous algae from the Lublin Coal Basin. *Acta Geologica Polonica.* **36**, 251–280

Smith, L.B., Read, J.F. (2001). Discrimination of local and global effects on Upper Mississippian stratigraphy, Illinois Basin, U.S.A. Journal of Sedimentary Research **71**, 985–1002.

Smith, L. B., Read, J. F. (2000). Rapid onset of late Paleozoic glaciation on Gondwana; evidence fro Upper Mississippian strat of the Midcontinent, United States. *Geology (Boulder),* **28**, 279-282.

Smith, L. B., Read, J. F. (1999). Application of high-resolution sequence stratigraphy to tidally influenced Upper Mississippian carbonates, Illinois Basin. In: *Advances in carbonate sequence stratigraphy; application to reservoirs, outcrops and models* (P.M. Harris, A.H. Saller, J.A. Simo, Eds). *Special Publication - Society for Sedimentary Geology*, **63**, 107-126.

Smith, L.B., Read, J.F. (2000). Rapid onset of late Palaeozoic glaciation on Gondwana: evidence from Upper Mississippian strata of the Mid-continent, U.S.A. Geology **28**, 279–282.

Sneath, P. H. A., Sokal, R. R. (1973). Numerical taxonomy — the principles and practice of numerical classification. (W. H. Freeman: San Francisco.)

Somerville, I. D. (2008) Biostratigraphic zonation and correlation of Mississippian rocks in Western Europe: some case studies in the late Viséan/Serpukhovian. *Geological Journal.* **43.** 209-240.

Somerville, I. D., Cozar, P. (2006) A new Mississippian problematicum from Ireland and Britain: comparison with the problematicum Draffania. *Lethaia.* **39.** 49-56.

Sopwith, T. (1833). *An account of the mining district of Alston Moor, Weardale and Teesdale in Cumberland and Durham*. Alnwick.

Sopwith, T. (1829). *Geological sections at Holyfield, Hudgill Cross vein and Silverband Leas Mines in Alston Moor and Teesdale*. Newcastle.

Soreghan, G. S., Soreghan, M. J. (2002) Atmospheric dust and algal dominance in the late Palaeozoic. *Journal of Sedimentary Research.* **72.** 457-461.

Spence, G.H., Tucker, M. (1999) Modeling carbonate microfacies in the context of high-frequency dynamic relative sea-level and environmental changes. *Journal of Sedimentary Research* **69.** 947-961.

Spence, G.H., Arnaud-Vanneau, A., Arnaud, H. (1996), The sequence stratigraphic significance of environmental relays detected in limestones using computer optimised Jaccard's similarity coefficient matrices (abstract): Fifth Cretaceous International Symposium, Freiburg, Saxony, Sept 16–24, Abstract Volume, p. 158.

Steuber, T., Veizer, J. (2002). Phanerozoic record of plate tectonic control of seawater chemistry and carbonate sedimentation. *Geological Society of America*. **30.** 1123-1126.

Stephens, N. (2002). Sedimentology and Diagenesis of the Upper Devonian of the Canning Basin, WA. *Unpublished PhD Thesis, University of California at Davis.*

Stephenson, M. H., Millward, D., Leng, M. J., Vane, C. H. (2008) Palaeoecological and possible evolutionary effects of early Namurian (Serpukhovian), Carboniferous) glacioeustatic cyclicity. *Journal of the Geological Society, London.* **165.** 993-1005.

Stoll, H. M., Schrag, D. P. (2001). Sr/Ca variations in Cretaceous carbonates: relation to productivity and sea-level changes. *Palaeogeography, Palaeoclimatology, Palaeoecology.* **168**, 311-336.

Stoll, H. M., Schrag, D. P. (1996). Evidence for glacial control of rapid sea-level changes in the early Cretaceous. *Science.* **272**, 1771-1774

Trotter, F. M. (1952) Sedimentation facies in the Namurian of northwest England and adjoining areas, *Liverpool Manchester Geological Journal,* **1** , pp. 77–112

Trotter, F. M. Hollingworth, S. E. (1932). The Geology of the Brampton District. *Memoir of the Geological Survey of Great Britain, England and Wales*, Sheet 18.

Trotter, F. M. Hollingworth, S. E. (1928). The Alston Block. *Geological. Magazine.* **65.** 433-448.

Tucker, M. E., Gallagher, J., Leng, M. J. (2009). Are beds in shelf carbonates millennial-scale cycles? An example from the mid-Carboniferous of northern England. *Sedimentary Geology.* **214.** 19-34.

Tucker, M.E. (2003). Mixed clastic-carbonate cycles and sequences: Quaternary of Egypt and Carboniferous of England. *Geologica Croatica* **56**, 19–37.

Tucker, M. E. (1993). Carbonate diagenesis and sequence stratigraphy. In: Wright, V. P. (Editor.), Sedimentology Review, vol. 1. Blackwell Science, Oxford, pp. 51–72.

Tucker, M. E., Wright, V. P. (1990). Carbonate Sedimentology, pp, 482, Blackwell Science Publishers, Oxford.

Tucker, M. E. (1986). Formerly aragonitic limestones associated with tillites in the late Proterozoic of Death Valley, California. *Journal of Sedimentary Petrology*. **56**, 818-830.

Turner, B. R., Robson, D. A., Dearman, W. R., Jones, J. M., Magraw, D., Smith, F. W. (1995). Structure: In: *Robson's Geology of north east England* (G.A.L. Johnson, ed.). *Transactions of the Natural History Society of Northumberland,* 331-343.

Turner J. S. (1956). Some faunal bands in the upper Visean and early Namurian of the Askrigg Block. *Liverpool Manchester Geological Journal*, **1**, 410–419.

Turner J. S. (1955). Upper Yoredales and Millstone Grit relations in the Stainmore Coalfield. *Geological. Magazine,* **92***,* 350.

Turner, J. S. (1935). Structural geology of Stainmore, Westmorland, and notes on the late-Palaeozoic (late-Variscan) tectonics of the north of England. *Proceedings of the geological Association.***46,** 121-151.

Van der Zwan C. J., Boulter, M. C., Hubbard, R. N. L. B. (1985). Climatic change during the Lower Carboniferous in Euramerica, based on multivariate statistical analysis of palynological data. *Palaeogeography, Palaeoclimatology, Palaeoecology*, **52**, 1-20.

Van Der Zwan, C. J. (1981) Palynology, Phytogeography and Climate of the Lower Carboniferous. *Palaeogeography, Palaeoclimatology, Palaeoecology.* **33**, 279-310.

Varker, W. J. (1968). Conodont distribution in Yoredale Limestone (D2-E,) of the North of England. *Transactions of the Leeds Geological Association* **7**, 275-290.

Vaughan, A. (1905). The palaeontological sequence in the Carboniferous Limestone of the Bristol area. *Quarterly Journal of the Geological Society of London,* **61***,* 181-307.

Veevers, J. J., Powell, M. (1987) Late Paleozoic glacial episodes in Gondwanaland reflected in transgressive-regressive depositional sequences in Euramerica. *Geological Society of America Bulletin*. **98**. 475-487.

Veizer, J., Ala, D., Azmy, K., Bruckschen, P., Buhl, D., Bruhn, F., Carden, G. A. F., Diener, A., Ebneth, S., Godderis, Y., Jasper, T., Korte, C., Pawellek, F., Podlaha, O. G., Strauss, H. (1999). $^{87}Sr/^{86}Sr$, $\delta^{13}C$ and $\delta^{18}O$ evolution of Phanerozoic seawater. *Chemical Geology*. **161**, 59-88.

Veizer, J., Bruckschen, P., Pawellek, F., Diener, A., Podlaha, O., G., Carden, G., A., F., Jasper, T., Korte, C., Strauss, H., Azmy, K., Ala, D. (1997). Oxygen isotope evolution of Phanerozoic seawater. *Palaeogeography, Palaeoclimatology, Palaeoecology.* **132**, 159-172.

Veizer, J. (1984). Trace elements and isotopes in sedimentary carbonates. *In* Reeder, R. J., ed., Carbonates: Mineralogy and Chemistry. *Mineral Society of America, Reviews in Mineralogy*. **11**, 265-299.

Versteegh, G. J. M., Servais, T., Streng, M., Munnecke, A., Vachard, D. (2009) A discussion and proposal concerning the use of the term Calcispheres. *Palaeontology***. 52.** 343-348.

Wagner, G. H., Konig, R. H., Smith, D. A., Steele, K. F., Zachry, Jr. D. L. (1979). Geochemistry of Carboniferous limestone units in northwest Arkansas. *Chemical Geology*. **25**, 293-313.

Walkden, G. M. (1987). Sedimentary and diagenetic styles in mid-Dinantian carbonates of Britain. In: Miller, J., Adams, A.E., Wright, V.P. (Eds.), European Dinantian Environments. John Wiley and Sons, Chichester, pp. 131–155.

Wanless, A. R., Shepherd, F. P. (1936). Sea level and climatic changes related to late Paleozoic cycles. *Bulletin of the Geological Society of America*, **47**, 1177-1206.

Waters, C. N., Davies, S. J. (2006) Carboniferous: extensional basins, advancing deltas and coal swamps. In: Brenchley, P. J.; Rawson, P. F., (eds.) *The geology of England and Wales.* London, England, Geological Society of London, 173-223.

Wehausen, R., Brumsack, H. J. (1999) Cyclic variations in the chemical composition of eastern Mediterranean Pliocene sediments: A key to understanding sapropel formation. *Marine Geology*. **153.** 161-176.

Weissert, H., Lini, A., Follmi, K. B., Kuhn, O. (1998). Correlation of early Cretaceous carbon isotope stratigraphy and platform drowning events: a possible link? *Palaeogeography, Palaeoclimatology, Palaeoecology.* **137,** 189-203.

Wells, M. R., Allison, P. A., Piggott, M. D., Pain, C. C., Hampson, G. J., Oliveira. (2005) Large sea, small tides: the Late carboniferous seaway of NW Europe. *Journal of the Geological Society of London.* **162.** 417-420.

Wells, A. J. (1960) Cyclic sedimentation: a review. *Geological Magazine*. **97**. 389-403.

Wells, A. J. (1957) The stratigraphy and structure of the Middleton Tyas-Sleightholme anticline, north Yorkshire. *Proceedings of the geological Association.* **68**. 231-254

Wilson, R. B. (1989). A study of the Dinantian marine macrofossils of central Scotland. *Transactions of the Royal Society of Edinburgh: Earth Sciences*, **80**, 91–126.

Wilson, J. L. (1975) Carbonate facies in geologic history. New York. Springer. 471 pp

Wilson, J. L. (1974) Characteristics of carbonate-platform margins. American Association of Petroleum Geology Bulletin, **58**, 810-824.

Wilson, R. B. (1967). A study of some Namurian marine faunas of central Scotland. *Transactions of the Royal Society of Edinburgh*, **66**, 445–490.

Winch, H. J. (1817). Observations on the geology of Northumberland and Durham. *Transcripts of the Geological Society London.* **4.** 1-7.

Wolff, T., Grieger, B., Hale, W., Dürkoop, A., Mulitza, S., Pätzold, J., Wefer, G. (1999) On the reconstruction of Paleosalinities. In: Fischer, G., Weffer, G. (Eds), Use of proxies in Paleoceanography: examples from the south Atlantic, Springer-Verlag, Berlin, pp. 207-228.

Wolfenden, E. B. (1958) Palaeoecology of the carboniferous reef complex and shelf limestones in northwest Derbyshire, England. *Bulletin of the geological society of America,* **69.** 871-898.

Wright, P., Cherns, L., Hodges, P. (2003). Missing Molluscs: Field testing taphonomic loss in the Mesozoic through early large-scale aragonite dissolution. *Geology*. **3,**. 211-214.

Wright, V. P., Vanstone, S. D. (2001). Onset of late Palaeozoic glacio-eustasy and the evolving climates of low latitude areas: a synthesis of current understanding. *Journal of the Geological Society of London*, **158**, 579-582.

Wright, V. P. (1986). Facies sequences on a carbonate ramp; the Carboniferous limestone of South Wales. *Sedimentology*, **33**, 221-241.

Wright, V. P. (1990). Equatorial aridity and climatic oscillations during the Early Carboniferous, southern Britain. *Journal of the Geological Society of London*, **147**, 359-363.

Wright, V. P. (1992). Paleosol recognition; a guide to early diagenesis in terrestrial settings. In: *Diagenesis, III. Developments in Sedimentology, 47* (K.F. Wolf, G.V. Chilingarian, eds.). 591-619.

Wright, V. P., Vanstone S. D., Robinson, D. (1991). Ferrolysis in Arundian alluvial Palaeosols, evidence of a shift in the Early Carboniferous monsoonal system. *Journal of the Geological Society of London*, **148**, 9-12.

Wright, V. P., Marriott, S. B. (1993). The sequence stratigraphy of fluvial depositional systems: the role of floodplain sediment storage. *Sedimentary Geology*, **86**, 203-210.

Wright, V. P., Vanstone, S. D. (2001). Onset of late Palaeozoic glacio-eustasy and the evolving climates of low latitude areas: a synthesis of current understanding. *Journal of the Geological Society of London*, **158**, 579-582.

Yang, W., Mazzullo, S. J., Teal, C. S. (2002): Lateral and vertical variations in sedimentation rates of Holocene subtidal platform carbonate sediments, Belize.– Abstract, GSA Annual Meeting, Denver, 2002.

Yang, W., Mazzullo, S. J., Teal, C. S. (2004): Sediments, Facies Tracts, and Variations in Sedimentation Rates of Holocene Platform Carbonate Sediments and Associated Deposits, Northern Belize-Implications for "Representative" Sedimentation Rates. *Journal of Sedimentary Research*. ***74;*** 498-512